University of Cincinnati

Date: 6/30/2021

I, Sobiya George, hereby submit this original work as part of the requirements for the degree of Doctor of Philosophy in Chemistry.

It is entitled:

Towards Achieving Higher Product Selectivity by Controlling Photoreactivity

Student's name: **Sobiya George**

This work and its defense approved by:

Committee chair: Anna Gudmundsdottir, Ph.D.

Committee member: Ruxandra Dima, Ph.D.

Committee member: James Mack, Ph.D.

39327

Towards Achieving Higher Product Selectivity by Controlling Photoreactivity

A dissertation submitted to the
Graduate School
of the University of Cincinnati
in partial fulfillment of the
requirements for the degree of

Doctor of Philosophy

in the Department of Chemistry
of the College of Arts and Sciences

by Sobiya George

MSc. Chemistry, Sam Houston State University, Texas,

August 2016

Committee Chair: Anna D. Gudmundsdottir, Ph.D.

Abstract

The outline of this dissertation is achieving higher selectivity by controlling the photoreactivity. We report the selective formation of the targeted photoproducts by controlling the photoreactivity of 2-hydroxy chalcone derivatives as well as different types of organic azides. In addition, we explored the photoreactivity under continuous flow method and in cryogenic matrices as well.

Below is a summary of the research projects explored and studied in this dissertation,

- The triplet reactivity of the 2-hydroxy chalcones forms flavanones. Flavanone formation takes places via the excited state intramolecular proton transfer (ESIPT) at the triplet excited state. The triplet reactivity of 2-hydroxy chalcones is selective under diluted concentration and continuous flow method. The bimolecular reactivity of 2-hydroxy chalcones is favored under higher concentrations which competes with the ESIPT and forms a secondary photoproduct via intramolecular hydrogen atom abstraction.

- Selective intramolecular sensitization of gamma azides over Intramolecular gamma hydrogen atom abstraction. The intramolecular sensitization in gamma azides will be selective when the (π-π) * triplet excited ketone is more stabilized. The EDA (electron donor acceptor) complexation with the TTMSS [Tris(trimethyl)silyl silane] stabilizes the (π-π) * triplet excited ketone and favors the intramolecular sensitization and facilitates the formation of the indole type N-heterocycles with much higher yield. This is a most

feasible photochemical synthesis of N-heterocycles under mild conditions without the heavy metal catalysts.

- The stability of triplet vinylnitrenes from isoxazoles under cryogenic temperature. These triplet vinylnitrenes are flexible at cryogenic temperatures and forms the corresponding ketenimine. The flexibility of the vinylic double bond facilitates the intersystem crossing of the triplet vinylnitrenes to form the products. The stability of the triplet vinyl nitrenes at cryogenic temperatures can be increased by limiting the rotation around the vinylic bond.

Dedication

This thesis is dedicated to my parents, my husband, my brother, sister, and all my dear friends who have supported me through my duration of graduate school.

Acknowledgements

I would like to offer my sincere thanks to my supervisor, Prof. Anna. D. Gudmundsdottir for her guidance and immense support throughout my PhD career. Thank you for your trust and encouragement which motivated me to work harder and achieve my goal. I also would like to thank my committee members Prof. James Mack and Prof. Dima Ruxandra for their encouragement and valuable suggestions which helped me to widen my research from various perspectives and improve as a scientist.

I also would like to thank some of the chemistry department staff who were really helpful in getting my research work done. The first important person would be Dr. Jeanette. A. Krause who did the X-Ray crystallographic analysis to all of my photoproducts. It would have been impossible to finish my projects without her support. I also would like to thank Dr. Larry Sallans and Dr. Stephen F. Macha who did the HRMS analysis for most of my compounds and trained me to do the GCMS analysis. I also would like to thank Dr. Alexander I. Greenwood who helped me with the NMR analysis. I owe my sincere thanks to Robert T. Voorhees for designing all the LED set-ups which I needed to do the product studies and to Rudy W. Thomas for helping me in designing my flow reactor.

Further I would like to thank the department of chemistry, University of Cincinnati for giving me an opportunity to pursue my PhD degree. I also would like to thank the National Science Foundation (NSA), USA for the research funding. I also acknowledge the Ohio Supercomputing Centre (OSC) for the support in getting my calculations done.

I also would like to thank the members and the senior members of Prof. Gudmundsdottir' s research group for all the help and support they have given me throughout my PhD career. Special thanks to Dr. Karthik. S., Dr. Dushanee. S., and Dr. Kosala. H. who helped me a lot in the beginning days and gave me a better understanding of photochemistry and also trained me to do all the instrumental analysis.

Finally, I would like to thank my parents, brother, sister, and my dear husband for all the love and support they are giving me throughout. I would not have achieved my goal without their continuous love and support especially my dad who always supported me and encouraged my decisions. Without them I would not have come this far and pursue my dream. Also, my dear friends who were always stood with me during the difficult times in this journey and supported me in many ways. They all made this journey so comfortable and a memorable one. I love them all with my heart.

Table of Contents

List of Figures

List of Schemes

Chapter 1 Introduction

1. Introduction to photochemistry

Organic photochemistry based synthetic routes are continuously being developed in modern day organic synthesis. The photochemical and photophysical changes in an organic molecule is initiated by the electronic excitation upon absorption of light. In order for an electronic excitation to take place, the energy of the absorbed light should match with the energy difference between the ground and the excited state of the molecule [1]. In general, most of the organic molecules absorbs the UV-Vis light and undergo electronic excitation. The photophysical and photochemical changes takes place in a molecule upon excitation of an electron can be better explained by using a Jablonski diagram [2] (Figure 1).

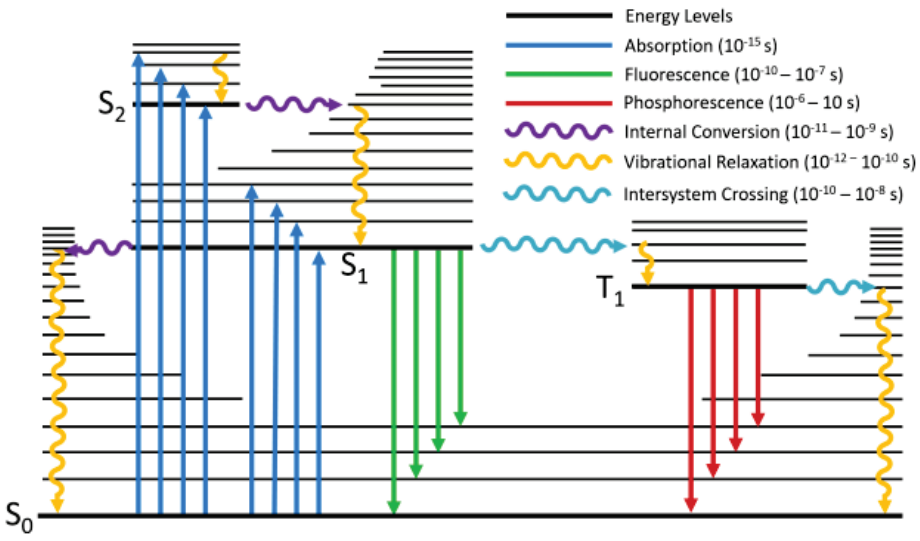

Figure 1. Jablonski diagram

Upon absorption of a photon with an appropriate energy, the outer shell electron of the molecule will be excited to its higher singlet state which is shown by the blue lines in the diagram. From the higher singlet excited state, it can undergo internal conversion (yellow lines) and relaxes back to the lowest singlet excited state (S_1) and from there it can intersystem crosses to the triplet excited state. The molecule at the higher singlet or triplet excited state can follow mainly two pathways to lose the absorbed energy such as photophysical pathway and photo chemical pathway.

In photo chemical pathway the excited molecule may undergo a unimolecular or bimolecular rearrangement to lose the excess energy and form new stable products with the lower energy. In photophysical pathway the molecule from the lowest excited singlet or triplet state relaxes back to the ground state while emitting the excess energy as light. The relaxation from the singlet excited state to the ground state is termed as fluorescence (green lines) which is a spin allowed process and the relaxation from the lowest triplet excited state to the ground state is called phosphorescence (red lines) which is a spin forbidden process [3].

The above-mentioned photochemical processes take place in a very short time scale, so that normally transient spectroscopy is used to detect the corresponding short-lived intermediates. There are various types of transient spectroscopy is used in the identification of short-lived intermediates such as laser flash photolysis, cryogenic matrix UV or IR and EPR.

2. Identification of reactive intermediates

I. Laser flash Photolysis

Laser flash photolysis is a technique used to identify the short-lived reactive intermediates [4]. Using this technique, the intermediates which has the lifetime in nano to femtosecond range can be detected either using a transient UV or Transient IR spectroscopy. In this method initially a laser pulse with the particular wavelength will be used to excite the molecule, and the transient absorption of the reactive intermediates will be captured and multiplied by the photomultiplier tube and the multiplied transient absorption will be collected with respective to time and wavelength (Figure 2).

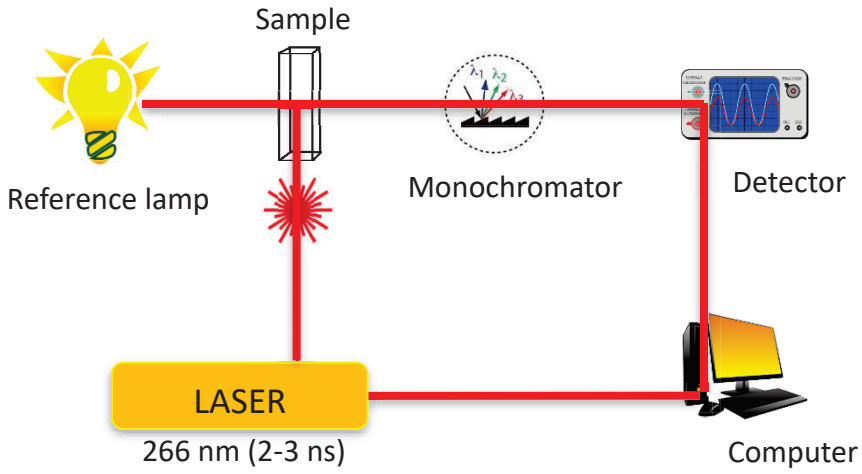

Figure 2. Schematic diagram of laser flash photolysis

The change in transient absorption with time can be best fitted as the mono or bi exponential fit to calculate the lifetime of either the decay or the growth of the corresponding intermediate (Figure 3). In addition to this, the transient UV collected can be compared with the

TD-DFT calculated UV-vis spectra of the suspected intermediates to find out the corresponding intermediate from which the transient absorption is generated (Figure 4).

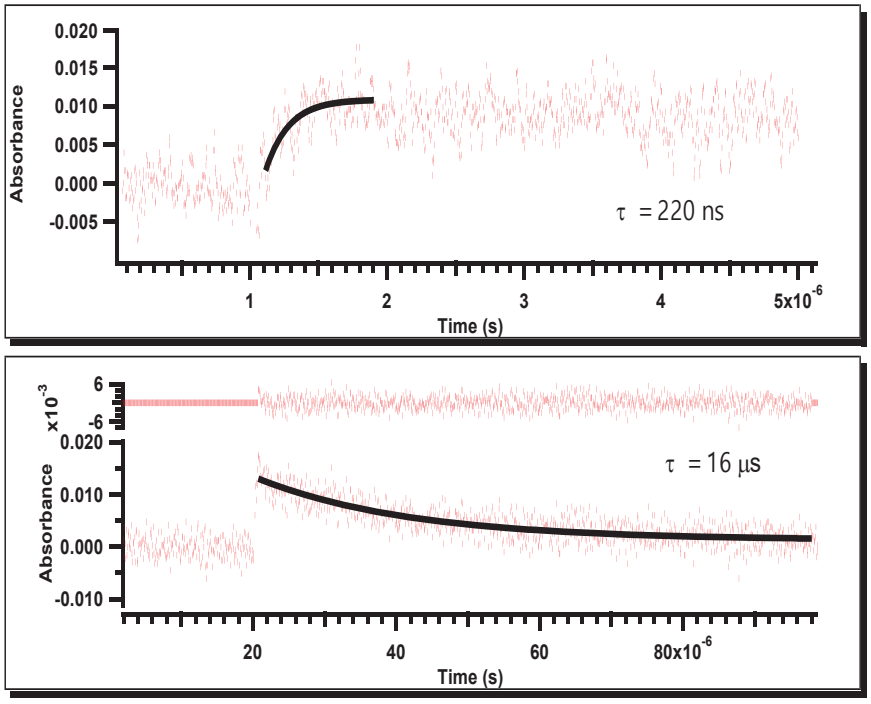

Figure 3. Kinetics of Laser flash photolysis

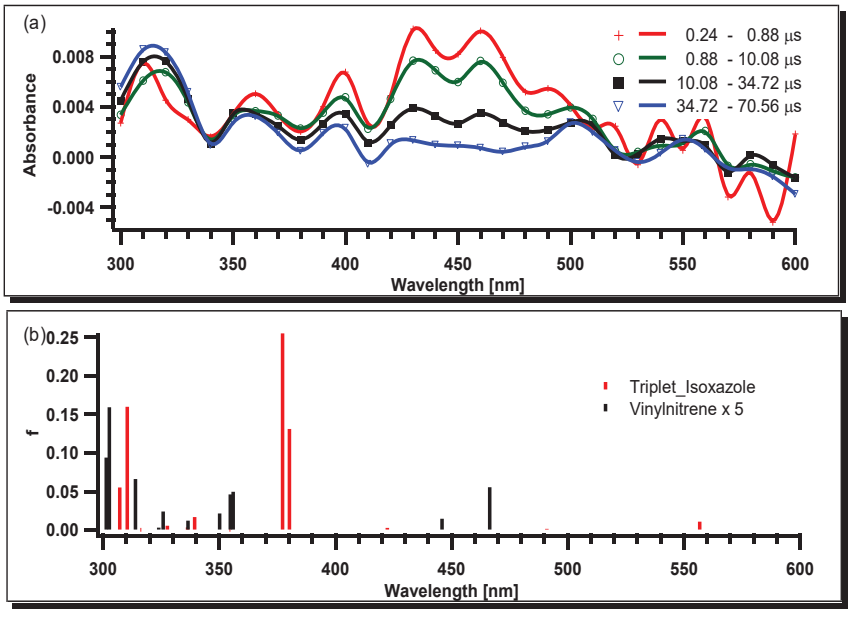

Figure 4. Transient UV and the TD-DFT calculated UV

II. Cryogenic matrix analysis

Matrix isolation is a technique that is being used to isolate the reactive intermediates at cryogenic temperatures [5]. The principle of the matrix isolation technique is explained in the Figure 5. In this method normally the reactive intermediates are trapped inside of an inert host material which forms rigid matrix at cryogenic temperatures. Inside of this rigid matrix the diffusion of the reactive intermediates is prevented thus the intermolecular reactions can no longer takes place so that it can be detected using a spectroscopic method. Normally we use either argon or liquid nitrogen as the host material since they can form the rigid glassy matrix at temperatures lower than 77 K.

The trapped molecule inside the glassy matrix will be irradiated and either the UV spectrum or the IR spectrum of the corresponding intermediate will be collected at different time intervals. The experimentally obtained spectra will be compared and matched with the TD-DFT calculated spectra in order to find out the corresponding intermediate.

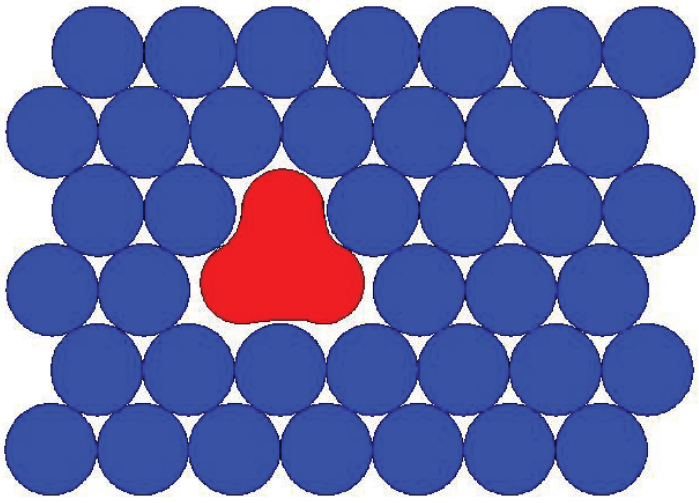

Figure 5. Molecule trapped in a matrix

3. Flow chemistry

The process of performing a chemical reaction in a continuous stream is called flow chemistry [6]. Application of continuous flow method in photochemistry facilitates the scale up of photochemical reactions for industrial purposes. The following figure is the schematic representation of a typical flow reactor [7] (Figure 6).

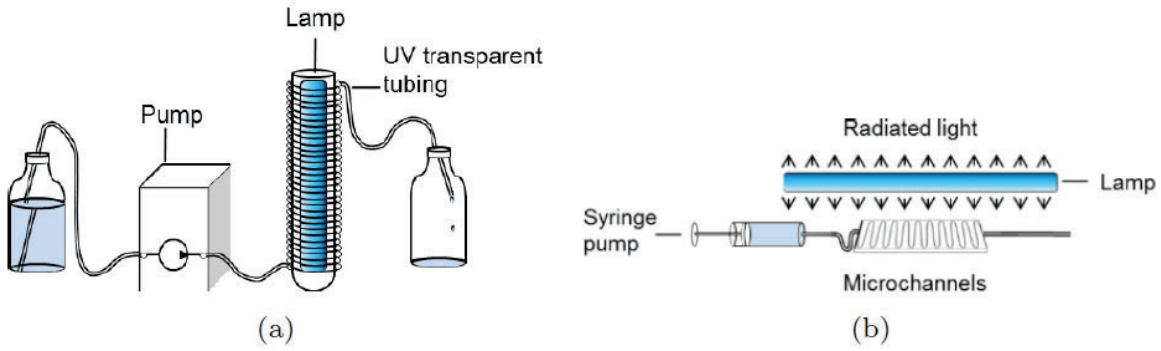

Figure 6. Schematic diagram of a typical flow diagram

The major advantage of applying continuous flow in photochemical reactions is the larger surface area and the narrow liquid radius. In general, photochemical reactions rely on efficient irradiation. One of the critical issues in scaling up a photochemical reaction in a batch reactor is maintaining uniform irradiation throughout the reactor.

In batch reactors due to the larger liquid radius the light penetration will be decreasing towards the center of the radius, thus resulting in a gradient of irradiation which might causes the secondary photoreactions [8] (Figure 7). Applying flow method would be ideal to overcome this issue. The narrow tubing of the flow reactors with the smaller liquid radius facilitates the uniform irradiation throughout the reactor thus the secondary photoreactions can be prevented, and the selectivity will be higher when compared to batch reactors [9,10,11,12] .

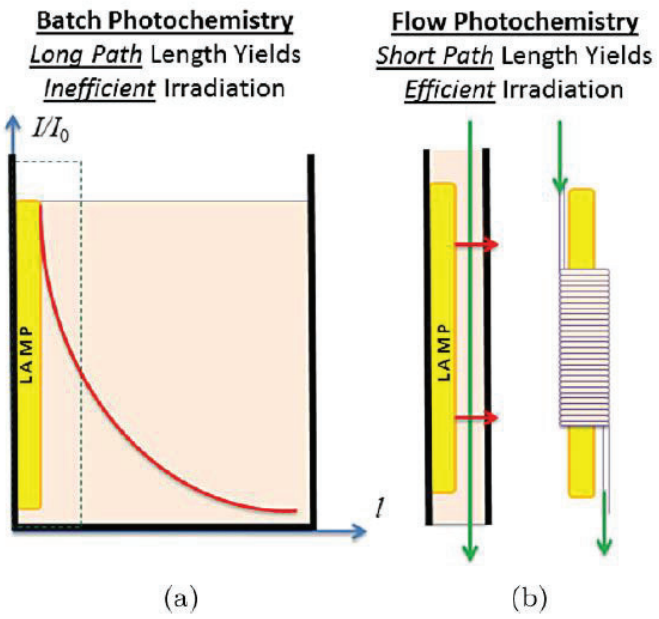

Figure 7. Schematic illustration of light penetration in both batch and the flow reactors. (Copied from Ref. 12. Copyright c_ 2014 The Chemical Society of Japan andWiley-VCH Verlag GmbH & Co. KGaA, Weinheim)

In addition to the light penetration, in flow reactors the scaling up of a photoreaction becomes feasible by the continuous introduction of the reactants. This phenomenon is very much useful to perform the photocatalysis in a larger scale. Furthermore, the enhanced mass and heat transfer provides additional safety to the method so that highly explosive reactions can be carried out in flow reactors in a quiet larger scale [13,14, 15,16,17] .

The application of flow method in a photochemical reaction was first reported in 1959 in the synthesis of vitamin D using a spiral glass reactor [18]. As Noel and co-workers reported, there are certain factors needs to be considered when designing a flow reactor such as the light source, the solvent and the reactants [11]. The light source can be placed either inside or the outside of the reaction zone. When designing a photo flow reactor, one of the important thing to consider is that the tubing should be UV transparent [9]. Generally, perfluoro alkoxy alkanes (PFA) which transmits

up to 96% of UV light and 91 % of visible light and fluorinated ethylene propylene (FEP) are used in a typical Photoflow reactor. In addition to the higher transmittance of light, they also show good amount of resistance to acids and bases [19].

The reactants are pumped down to the reaction zone continuously from the mixing zone via an HPLC pump. The mixing zone consists of multiple coils of tubing which provides larger surface area for the reaction to take place. The irradiation source of a Photoflow reactor can be placed either inside or outside of the reaction zone. Generally low-pressure mercury arc lamp, compact fluorescence lamp (CFL), and light emitting diodes are used as the irradiation source. The common organic solvents which are being used in the photochemical synthesis are used in the flow reactors such as MeCN, MeOH, C_6H_{12}, and $CHCl_3$ [20].

4. Reference:

1. Fagnoni, M., Modern Molecular Photochemistry of Organic Molecules. By Nicholas J. Turro, V. Ramamurthy and Juan C. Scaiano. *Angewandte Chemie International Edition* **2010,** *49* (38), 6709-6710.
2. Jablonski, A., Efficiency of Anti-Stokes Fluorescence in Dyes. *Nature* **1933,** *131* (3319), 839-840.
3. Srinivasan, R., Molecular Photochemistry. *Journal of the American Chemical Society* **1966,** *88* (15), 3682-3682.
4. Scaiano, J. C., In *Reactive Intermediate Chemistry*, Moss, R. A., Platz, M. S., Jones Jr., M. , Ed. John Wiley & Sons: Inc.: Hoboken, New Jersey, 2004.
5. Whittle, E.; Dows, D. A.; Pimentel, G. C., Matrix Isolation Method for the Experimental Study of Unstable Species. *The Journal of Chemical Physics* **1954,** *22* (11), 1943-1943.
6. Wirth, T., Microreactors in Organic Synthesis and Catalysis. Wiley-VCH: Weinheim, 2008.
7. Protti, S.; Ravelli, D.; Fagnoni, M., Design Consideration of Continuous-Flow Photoreactors. In *Photochemical Processes in Continuous-Flow Reactors*, WORLD SCIENTIFIC (EUROPE): 2016; pp 1-36.
8. Coyle, E. E.; Oelgemöller, M., Micro-photochemistry: photochemistry in microstructured reactors. The new photochemistry of the future? *Photochemical & Photobiological Sciences* **2008,** *7* (11), 1313-1322.
9. Knowles, J. P.; Elliott, L. D.; Booker-Milburn, K. I., Flow photochemistry: Old light through new windows. *Beilstein Journal of Organic Chemistry* **2012,** *8*, 2025-2052.
10. Schuster, E. M.; Wipf, P., Photochemical Flow Reactions. *Israel Journal of Chemistry* **2014,** *54* (4), 361-370.
11. Su, Y.; Straathof, N. J.; Hessel, V.; Noël, T., Photochemical transformations accelerated in continuous-flow reactors: basic concepts and applications. *Chemistry* **2014,** *20* (34), 10562-89.
12. Garlets, Z. J.; Nguyen, J. D.; Stephenson, C. R., The Development of Visible-Light Photoredox Catalysis in Flow. *Isr J Chem* **2014,** *54* (4), 351-360.
13. Finelli, F. G.; Miranda, L. S. M.; de Souza, R. O. M. A., Expanding the toolbox of asymmetric organocatalysis by continuous-flow process. *Chemical Communications* **2015,** *51* (18), 3708-3722.
14. Ley, S. V.; Fitzpatrick, D. E.; Myers, R. M.; Battilocchio, C.; Ingham, R. J., Machine-Assisted Organic Synthesis. *Angewandte Chemie International Edition* **2015,** *54* (35), 10122-10136.
15. Wegner, J.; Ceylan, S.; Kirschning, A., Flow Chemistry – A Key Enabling Technology for (Multistep) Organic Synthesis. *Advanced Synthesis & Catalysis* **2012,** *354* (1), 17-57.
16. Wiles, C.; Watts, P., Continuous Flow Reactors, a Tool for the Modern Synthetic Chemist. *European Journal of Organic Chemistry* **2008,** *2008* (10), 1655-1671.
17. Yoshida, J.; Kim, H.; Nagaki, A., Green and sustainable chemical synthesis using flow microreactors. *ChemSusChem* **2011,** *4* (3), 331-40.
18. Henley, E. J.; Barr, N. F., Ionizing Radiation Applied to Chemical Processes and to Food and Drug Processing. In *Advances in Chemical Engineering*, Drew, T. B.; Hoopes, J. W., Eds. Academic Press: 1956; Vol. 1, pp 369-425.
19. Gutierrez, A. C.; Jamison, T. F., Scalable and Robust Synthesis of CpRu(MeCN)3PF6 via Continuous Flow Photochemistry. *Journal of Flow Chemistry JFC* **2012,** *1* (1), 24-27.
20. Welton, C. R. a. T., Solvents and Solvent Effects in Organic Chemistry. 4 ed.; Wiley-VCH: Weinheim, 2011.

Chapter 2

Taming the Triplet Reactivity of 2,4-dihydroxy Chalcones to Yield Flavanone Selectively

Sobiya George, Geethika K. Weragoda, Jeanette A. Krause, and Anna D. Gudmundsdottir*

† Department of Chemistry, University of Cincinnati, Cincinnati, Ohio 45221-0172, United States

Abstract

Irradiation (365 nm LED) of dilute argon-statured acetonitrile solution of *cis*-**1** or *trans*-**1** yields *cis-trans* isomerization and flavone **1P**, and prolonged irradiation selectively gave flavone **1P**, whereas irradiation of *cis*-**1** or *trans*-**1** in oxygen-saturated acetonitrile results only in *cis-trans* isomerization. Irradiating more concentrated acetonitrile solutions of *cis*-**1** or *trans*-**1** gave a mixture of **1P** and **1b**, with higher concentrations favoring **1b** over **1P**. Addition, of TTMSSS to the photoreactions also favored formation of **1b**. In contrast, irradiation of *trans*-**1** in argon-saturated solution flown through PTFE tube, while being exposed to 365 nm LED light, selectively formed **1P**. In mTHF *cis*-**1** shows phosphorescence upon excitation, but not *trans*-**1**. Laser flash photolysis of *cis*-**1** in acetonitrile yields a transient absorption with l_{max} at 340 nm, that is assigned to keto-tautomer E-**4**. In contrast *trans*-**1** does not yield any transient absorption on nano-second timescale. It was proposed that flavanone **1P** is formed from the electrocyclic ring closure of keto-tautomer E-**4**, which is formed from the triplet excited state of *cis*-**1**, whereas the *cis-trans* isomerization takes place on the singlet excited states of *cis*-**1** and *trans*-**1**. In more concentrated solution the T_1 of *cis*-**1** decays by H atom abstraction of phenolic protons to form **1b**, and thus by carrying out the reaction in flow the formation of **1b** is prevented. DFT-calculations were used to further support the proposed mechanism.

1. Introduction

Photoenolization is the light initiated keto-enol tautomerization process followed by the excited state intramolecular proton transfer (ESIPT) [1, 2]. Generally, ESIPT occurs in molecules with a strong intramolecular H bond between two electronegative heteroatoms, forming a H-bonded ring structure. o-Hydroxyacetophenone derivatives have been reported to undergo ESIPT in their singlet excited state to form the corresponding keto tautomers (Scheme 1) [3,4, 5]. Photoenols are high-energy ground state intermediates that are highly reactive and has been widely used in applications such as synthesizing complex natural products and pharmaceutical drugs and initiating release from photoremovable protecting groups [6, 7, 8].

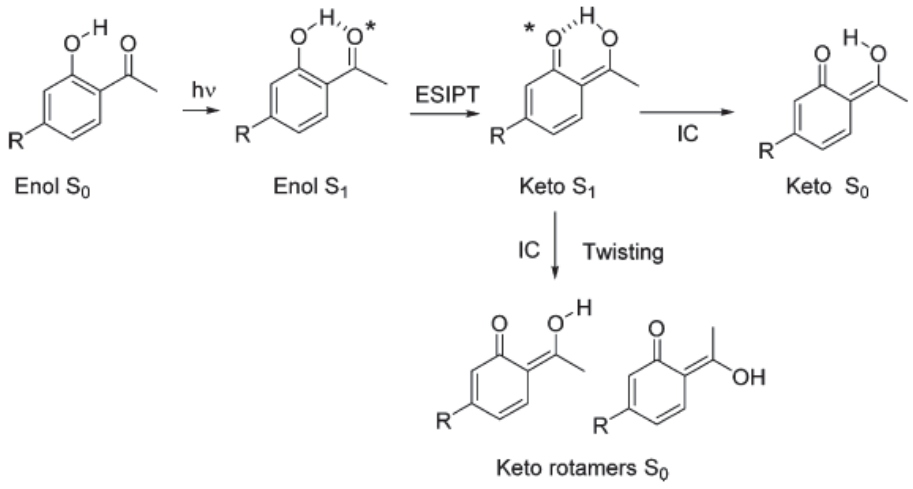

Scheme 1. ESIPT of o-Hydroxyacetophenone derivatives

Flavanones are a type of flavonoids which are phytochemical with multiple benefits to human health such as anti-inflammatory, anti-diabetic and antioxidant [9,]. In addition to their health benefits recent studies have shown that they can be used to treat the cancer cells [10].

Thus, the synthesis of flavanones has always been an interesting topic in the research field. Flavanones are naturally synthesized in plants via enzymatic cyclization of 2-hydroxy chalcones in which the chalcone isomerase is the enzyme that involves in the cyclization [11].

Photocyclization of 2-hydroxychalcones is one of the most sustainable method reported so far to synthesize flavanones [12, 13, 14]. Though there are reported studies which describes the photochemical cyclization and the mechanism which explains the photochemical cyclization of flavanones, however the in detailed mechanism with the support of spectroscopic evidence is little known so far. To synthesize flavanones in an industrial scale with much higher yields, it is important to understand the mechanism of the photocyclization of 2- hydroxy chalcones in detail.

One of the critical problems in the photochemical synthesis of flavanones from 2-hydroxy chalcones is that the presence of phenolic hydrogen. The abstractable phenolic hydrogen causes secondary photoreactions thus the selectivity of the method becomes questionable. Matsushima and Hirao reported in their studies that the photochemical cyclization is efficient in polar aprotic solvents whereas in apolar solvent and in protic solvents the efficiency was nil [13]. In addition to this Kageyama et al. have reported that upon UV irradiation in polar aprotic solvents 2-hydroxy chalcones underwent photocyclization to give the corresponding flavanones selectively, but protic solvents disturbed the formation of a cyclic intramolecular hydrogen bonding and strongly retarded the photocyclization [14].

In this project we have studied the photoreactivity of 2-hydroxy chalcones in polar aprotic and polar protic solvent and found out that the photoreactivity of 2-hydroxy chalcones is

concentration dependent as well as solvent dependent. Further we used Laser flash photolysis and TD-DFT calculations to support the proposed mechanism.

2. Product studies in aprotic solvents

We demonstrated that irradiating (λ_{max} 365 ± 5 nm LED) *trans*-**1** selectively forms photoproduct **1P**. In more details, diluted solution of *trans*-**1** (< 1.5 mM) in argon- and oxygen-saturated acetonitrile were irradiated, and the progress of the reaction was monitored using ^{1}H-NMR spectroscopy. Initially, irradiation in argon-saturated acetonitrile resulted in the formation of *cis*-**1** and photoproduct **1P**. Further irradiation depleted the ^{1}H NMR bands due *trans*-**1**, whereas the ^{1}H NMR bands corresponding to the *cis*-**1** initially increased and then decreased. After 115 h irradiation, ^{1}H-NMR spectra of the reaction mixture showed selective formation of photoproduct **1P** and full depletion of *trans*-**1** and *cis*-**1** (Figure *8*). In contrast, irradiation in oxygen-saturated acetonitrile resulted only in *cis*-*trans* isomerization (Figure S112).

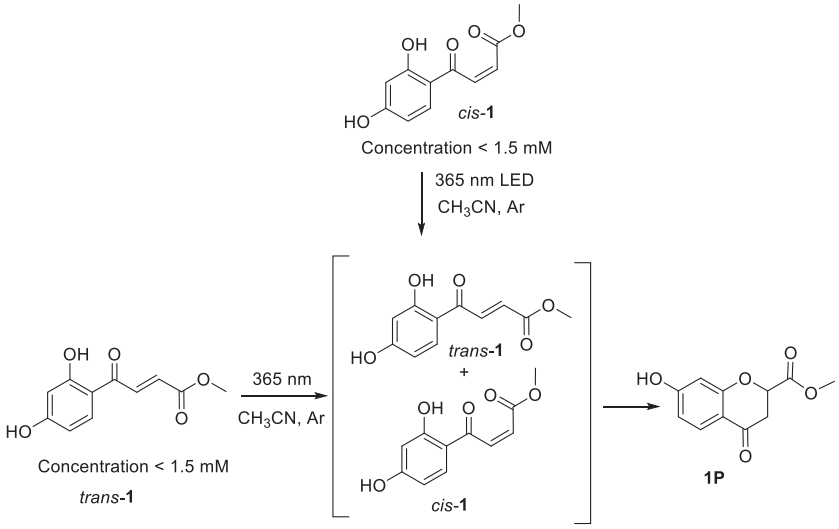

Scheme 2**.** Formation of **1P** upon irradiation of trans-**1** and cis-**1** dilute acetonitrile solution with 365 nm LED.

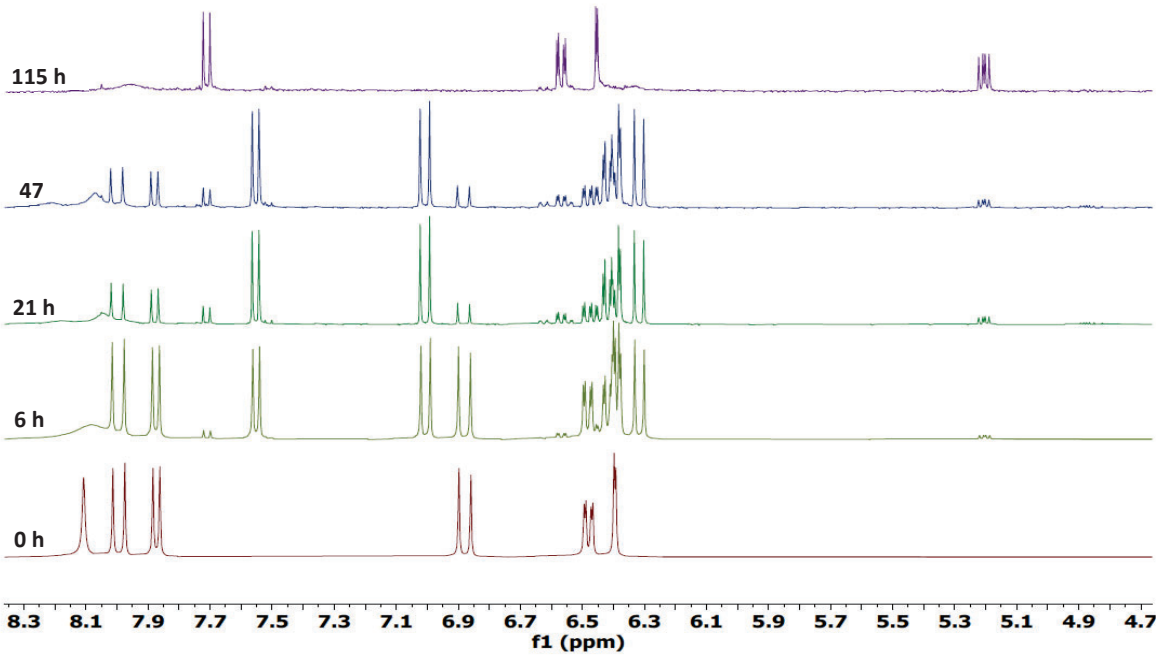

Figure 8. ^{1}H-NMR spectra of the reaction mixture upon irritating (365 nm LED) trans-**1** in dilute solution argon-saturated acetonitrile-d

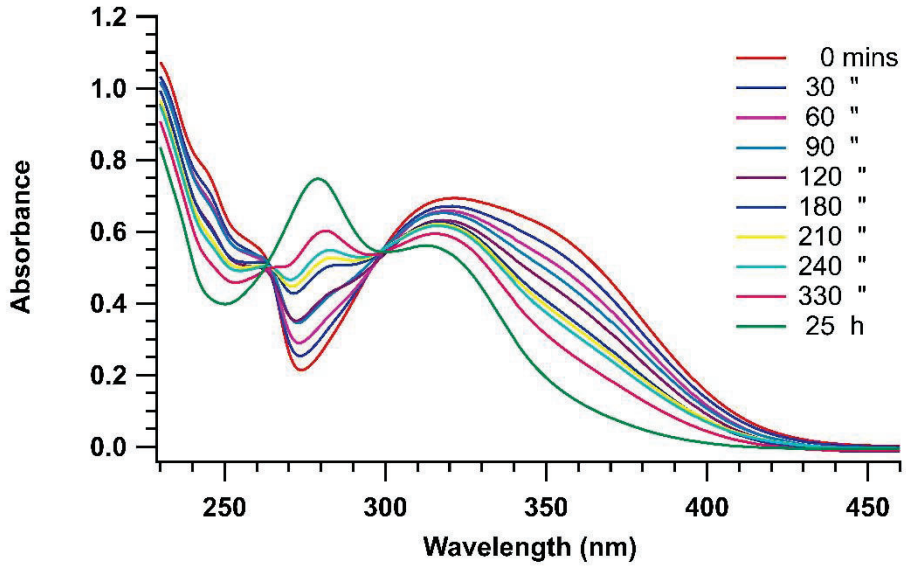

Figure 9. UV-Vis absorption spectra as a function of irradiation of trans-**1** in dilute argon-saturated acetonitrile.

Similarly, results were obtained when *cis*-**1** (< 1.5 mM) was irradiated in argon (Figure S101) and oxygen-saturated acetonitrile (Figure S107).

Because oxygen quenches formation of photoproduct **1P** from both *trans*-**1** and *cis*-**1**, it is reasonable to assume that the flavanone-**1P** is formed from a triplet excited state. As irradiation in oxygen-saturated acetonitrile does not quench the *cis-trans* isomerization of **1**, it is also reasonable to assume that the isomerization is a singlet state reactivity. Furthermore, because only *cis*-**1** and not *trans*-**1** is phosphorescent, we propose that upon irradiation of *trans*-**1** in dilute acetonitrile it is converted into *cis*-**1**, and that *cis*-**1** undergoes photoenolization as displayed in Scheme *3*. In more details, upon irradiation the singlet excited state (S_1) of *cis*-**1** is formed and it intersystem crosses to its triplet configuration of **1**, which abstracts a hydrogen atom from *ortho* hydroxyl moiety and forms triplet 1,4 biradical **2Br**. Presumably, **2Br** intersystem crosses to photoenols Z-**4** and E-**4**. The Z-isomer is expected to be short lived as it is set up to undergo 1,5 H-shift in Z-**4** to regeneration of **1**, whereas the E-isomer can undergo electrocyclic ring closure to form the enol conformer **5** of flavanone **1a.**

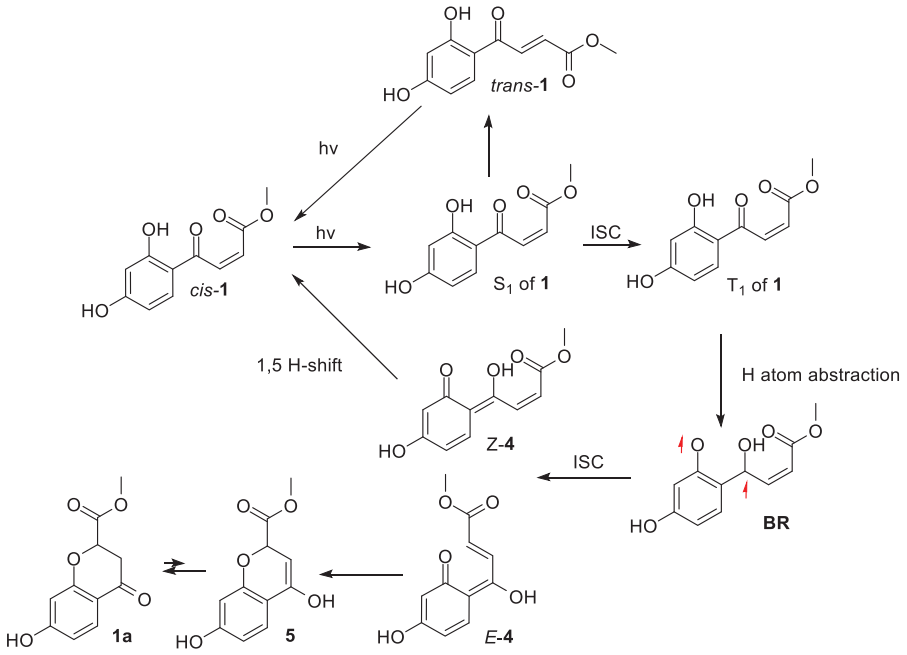

Scheme 3**.** Proposed mechanism for forming flavanone **1a** from **1**

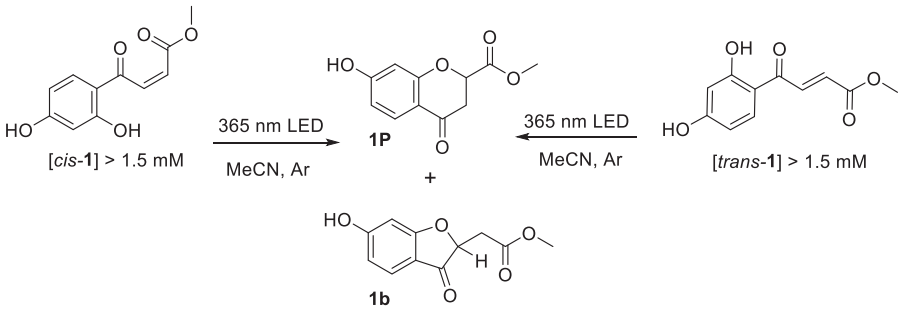

Scheme 4**.** Formation of **1P** and **1b** upon irradiation (λ_{max} ~ 365 ± 5 nm LED) of concentrated acetonitrile solution of trans-**1** or cis-**1**.

Intriguingly, irradiation of more concentrated solution (>1.5 mM) of *trans*-**1** and *cis*-**1** in argon-saturated acetonitrile does not yield selective formation of **1P**, but a mixture of **1P** and **1b** (Scheme *4*). Similarly, to product studies in dilute solution, ^{1}H NMR spectroscopy shows *cis-trans* isomerization taking place initially and then the formation of 1p and 1b were observed.

To explore further the effect of concentration on the photoreactivity, several solutions of *trans*-**1** at different concentration were irradiated. The ratio between **1P** and **1b** changes as a function of the concentration, with **1b** being favored at higher concentrations (Figure S*124*). Similar results were obtained for *cis*-**1**, higher concentrations favored formation of **1b** (Figure S*117*).

Based on the fact, that the photochemistry of *trans*-**1** and *cis*-**1** is concentration dependent, it is reasonable to expect formation of **1b** to require bimolecular reactivity. Furthermore, because phenolic hydrogen atoms are easily abstractable by triplet ketone,[15,16] we propose that **1b** is formed (Scheme *5*) from triplet ketone (T_1) of *cis*-**1** abstracting a phenolic hydrogen from the ground state (S_0) of **1** to form phenoxy radical **6** and ketyl radical **7**.[4,17,18,15] These resulting radicals can both cyclize to form product **1b**.

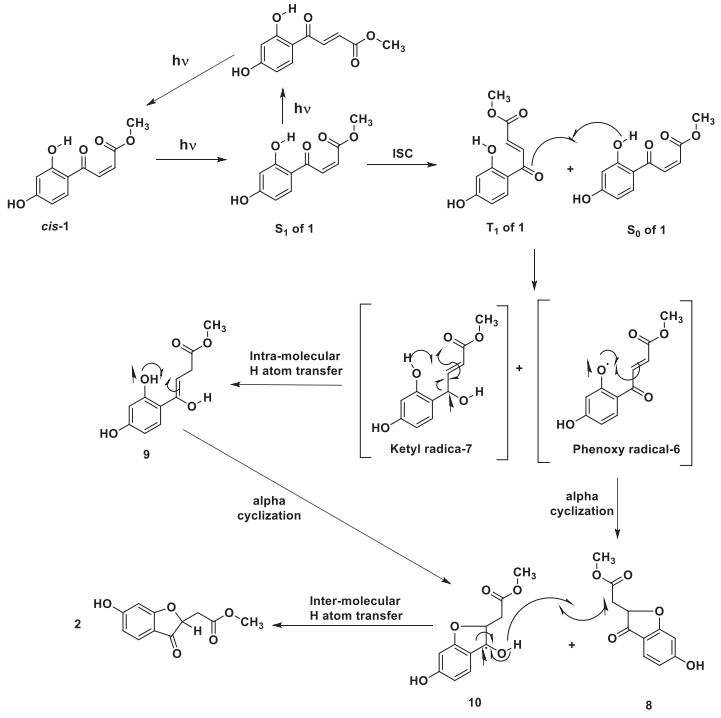

Scheme 5. Proposed mechanism for the bimolecular reactivity

To further support the notion that product **1b** is initiated from T_1 of *cis*-**1** abstracting phenolic H atom, we carried out trapping studies using tris trimethylsilyl silane (TTMSS), which is an excellent source of abstractable H atoms. [19,20,21] Irradiation in the presence of TTMSS changes the product ratio to favor product **1b** (Figure 5), and even dilute solution of *trans*-**1** (< 1.5 mM) yielded **1b**, which selectively form **1a** in the absence of TTMSS (Figure S*135*).

The reactivity of *trans*-**1** under continuous flow irradiation using 365 nm LED was explored. A series of 50 mL solutions of *trans*-**1** in CH_3CN with varying concentrations (0.45 mM, 0.9 mM, 1.8 mM, and 2.7 mM) were prepared and placed in a round bottom flask and sealed with a rubber cap and the solution was degassed by purging with argon for 20 minutes. Each solution was continuously pumped through the flow system using a peristaltic pump with the flow rate of 0.3 mL min^{-1} while being irradiated with LED placed inside the multiple coils of the flow system tubing. After certain time of irradiation under the continuous flow (18 h for 0.45 mM, 66 h for 0.9 mM, 72 h for 1.8 mM and 92 h for 2.7 mM) each solution was evaporated separately, and the crude reaction mixture was dissolved in CD_3CN and the ^{1}H-NMR spectra of each solution analyzed, to show that the major product is **1P** (Figure S*134*).

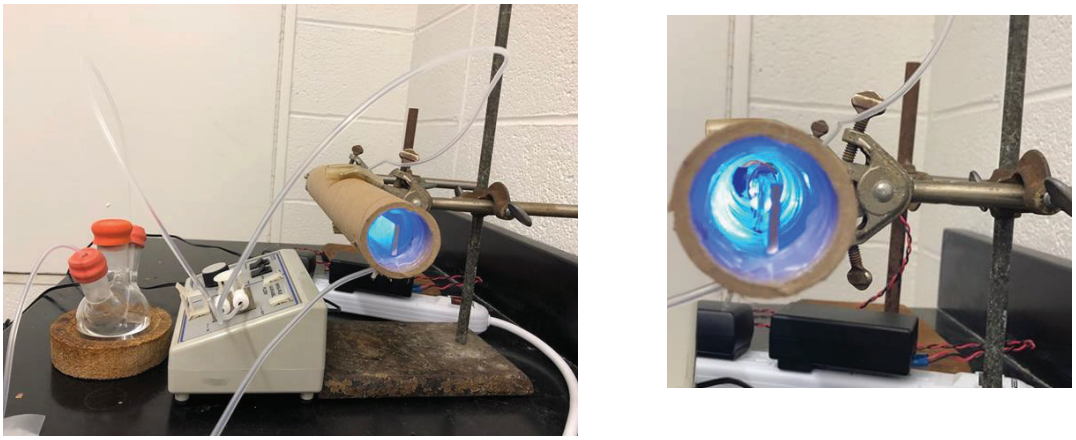

Figure 10. Image of the flow system

3. Product studies in protic solvents

The product studies of *trans*-**1** and *cis*-**1** was carried out in a protic solvent methanol.[22] Upon dissolving *cis*-**1** in methanol it converts completely into **1b** in the dark . In contrast, product **1b** is formed significantly slower from *trans*-**1** in the absence of irradiation, whereas upon irradiation the rate is increased dramatically (Figure *11*).

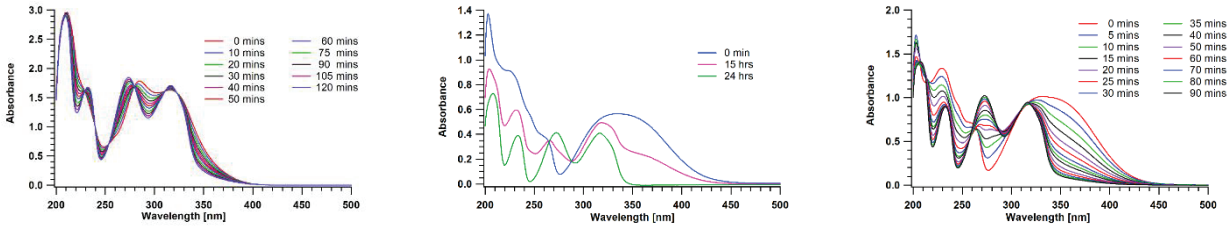

Figure 11**.** UV-Vis absorption monitoring of methanol solution of a) cis-**1** converting into **1b** in methanol in the dark, b) trans-**1** converting into **1b** upon irradiation with 365 nm LED

The above data demonstrated that the *cis*-**1** forms **1b** in the dark almost as efficiently as *trans*-**1** forms **1b** upon irradiation. Because *cis*-**1** to form **1b** in the dark, methanol must be sufficient catalyst for the cyclization to take place. Donnelly et al. proposed that the phenolic protons can protonate the double bond, and the resulting phenoxide anion would attack the alpha carbon atom to form **1b**. [23,24]

4. Laser flash photolysis

We carried out laser flash photolysis of *cis*- and *trans*-**1** (Excimer laser, 308 nm, 17 ns) to characterize the excited state and intermediates responsible for the flavanone **1a** formation. Laser flash photolysis of *cis*-**1** in argon-saturated acetonitrile resulted in a broad transient absorption with λ_{max} at 340 nm (Figure *13*). The absorption is formed within the time resolution of the laser flash instrument. Analysis of the kinetics in argon- and oxygen-saturated acetonitrile at 340 nm (Figure *12*) show that the decay can be fitted as a mono exponential function to yield a rate constant of 9.0×10^4 s^{-1} (τ = 111 µs), and a residual absorption that only decays on second timescale. In oxygen-saturated acetonitrile the yield of the transient absorption was slightly reduced, indicating that the transient absorption is due to a singlet intermediate which is formed from a triplet precursor. Based on comparison to TD-DFT calculations the transient is assigned to E-**4**, which shows major electronic transitions at 343 (*f* = 0.5285) nm and 558 (*f* = 0.0723) nm (Figure *13*). We assign the residual absorption to absorption of the photoproduct formation.

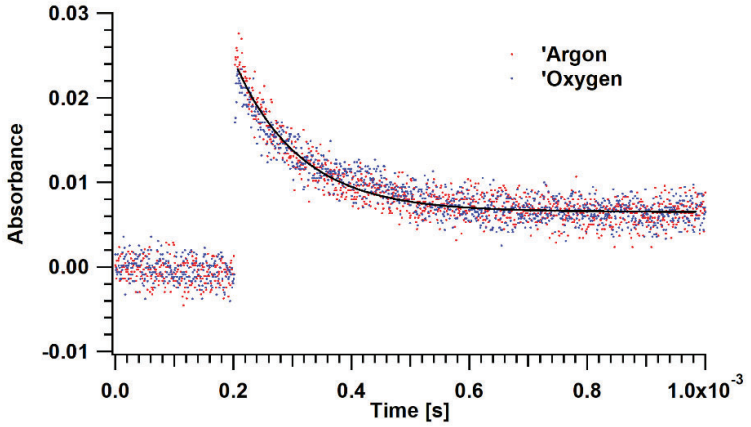

Figure 12. Kinetic traces obtained at 340 nm in argon- and oxygen-saturated acetonitrile from laser flash photolysis of cis-**1**

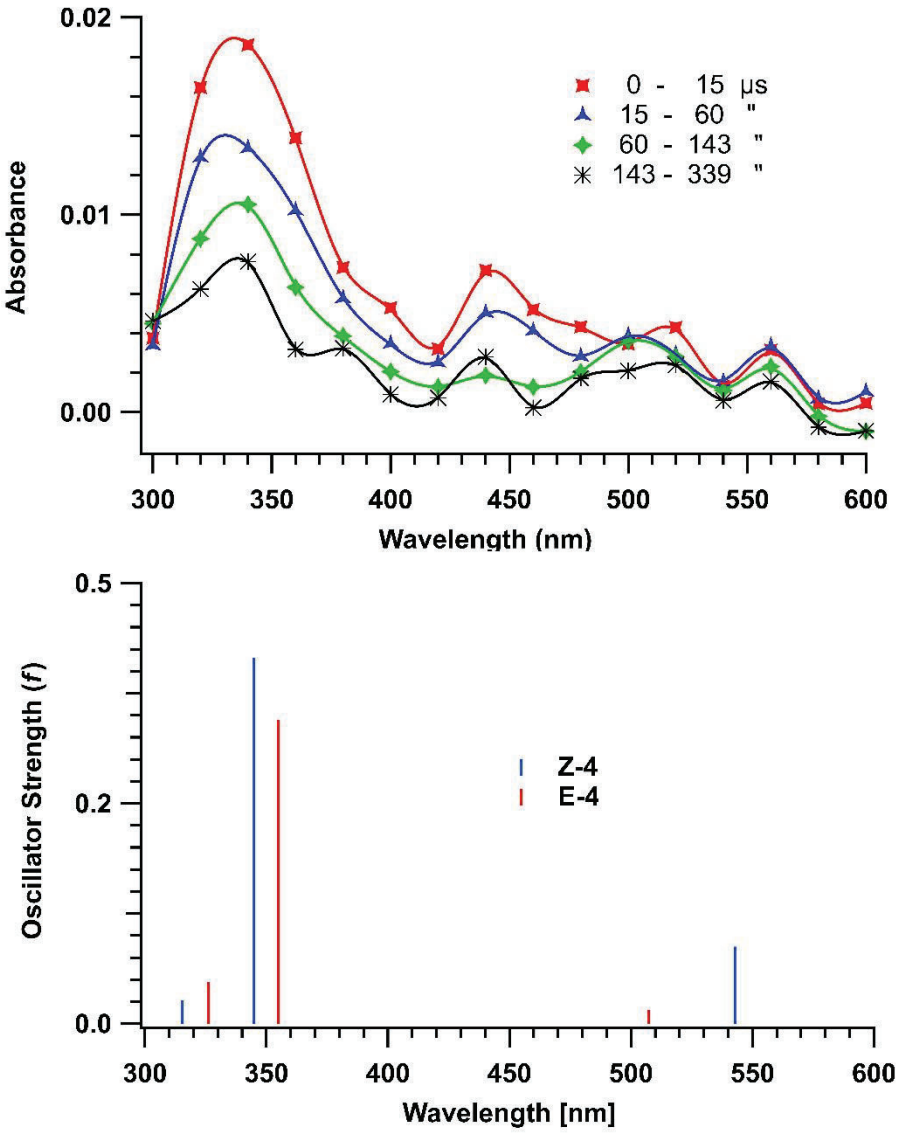

Figure 13. Laser flash photolysis of cis-**1** in argon-saturated acetonitrile solution and TD-DFT calculated electronic transition for E-**4** and Z-**4**

In contrast, laser flash photolysis of the *trans*-**1** in acetonitrile did not results in any transient absorption, thus further supporting that the *trans*-**1** undergoes only singlet reactivity, which fits with it not displaying any phosphorescence.

Finally, we did laser flash photolysis of *cis*-**1** at higher concentration and observed only the residual absorption due to product formation, presumably because T_1 of *cis*-**1** is efficiently quenched by H atom abstraction and formation of E-**4** is not observed. Similarly, in the presence of TTMSS the transient absorbance corresponding to the *E*-enol **4** was reduced. This is due to reduction in the growth of 1,4-biradical **2** which is the precursor of *E*-enol **4.** It can be conformed from the results that the TTMSS quenches the triplet ketone T_1 which is the precursor of 1,4-biradical **2** thus, resulting in the reduction of growth of 1,4 biradical-**2**.

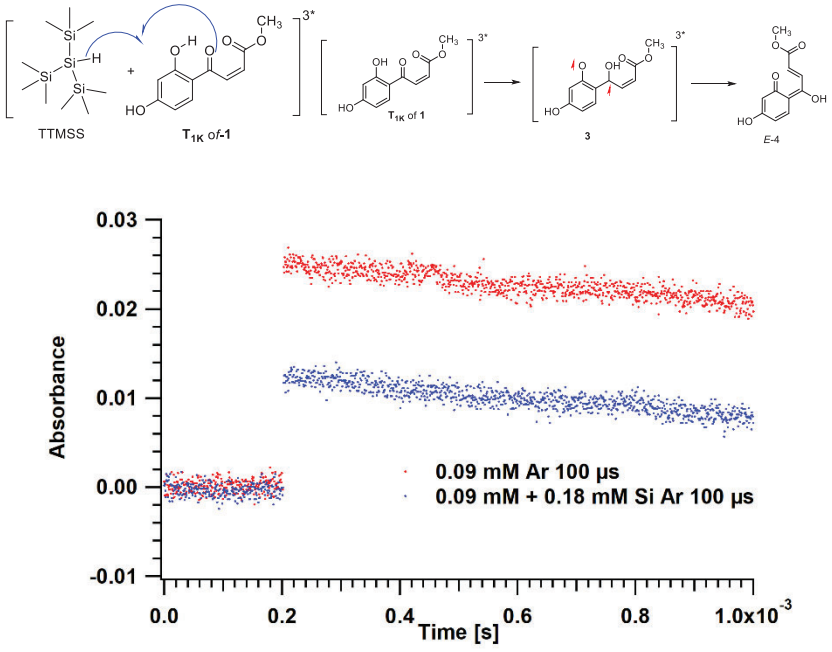

Figure 14. Kinetic traces obtained under argon saturated acetonitrile of cis-**1** with and without TTMSS.

5. Quantum Mechanical Calculations

I. Mechanism for the flavanone (1a) formation

To support the mechanism in Scheme 4, the stationary points on the singlet and triplet surface of *trans*- and *cis*-**1** were calculated using Gaussian16 at the B3LYP level of theory and with the 6-31+G (d) basis set.[25,26,27]

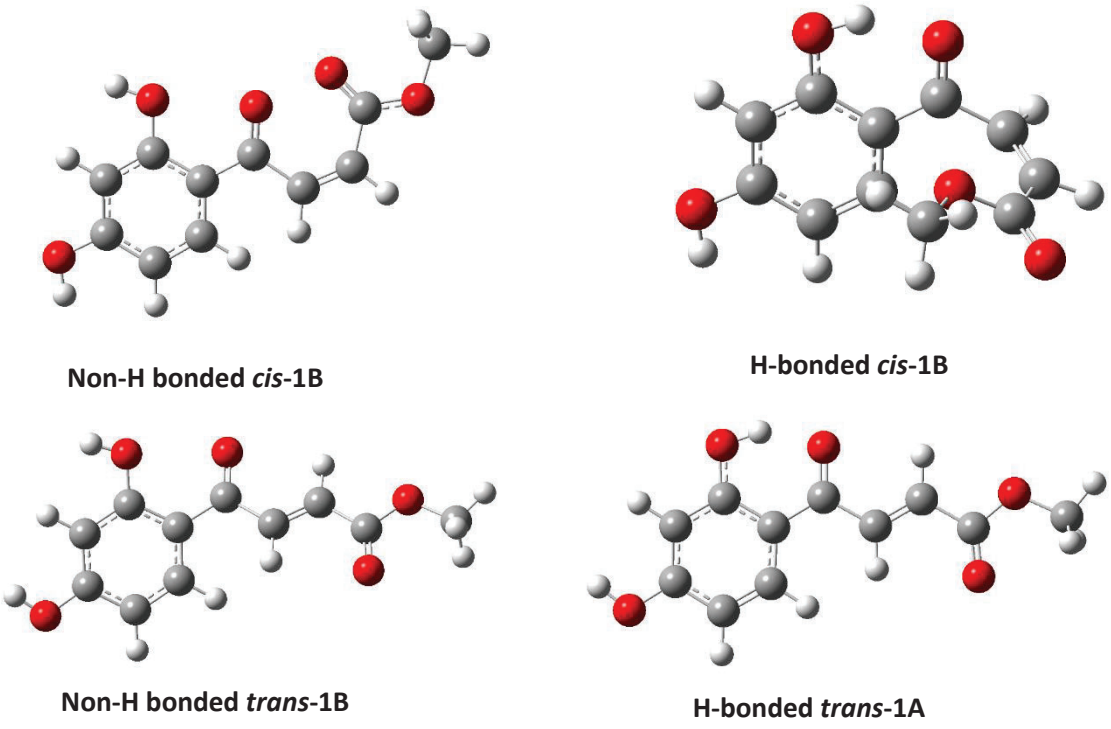

Figure 15. Optimized S_0 structure of H bonded and non-H bonded conformers of cis-**1** and trans-**1**

The optimized structure of the ground state (S_0) of *cis*-**1** and *trans*-**1** are displayed in (Figure *15*)**.** The minimal energy conformers *trans*-**1A** and *cis*-**1A** have intramolecular H-atom bonding between the *ortho*-hydroxy group and the ketones and it should be noted that these structures

are similar to the crystal structures of *cis*- and *trans*-**1**. We also optimized conformers B of *cis*-**1** and *trans*-**1** without intramolecular H-bonding. Gas phase calculations predicts that the A conformers of *cis*-**1** and *trans*-**1** are stabilized over its non-H bonded conformers by 14 kcal mol^{-1}.

TD-DFT calculations were performed on the optimized structure of *cis*- and *trans*-**1** to locate their first singlet and triplet excited states (S_1 and T_1) of *trans*-**1A** at 80 and 58 kcal mol^{-1} above its S_0**,** whereas for conformer *trans*-**1B** the S_1 and T_1 were placed at 70 and 59 kcal mol^{-1}. In comparison, TD-DFT calculation located the S_1 and T_1 of *cis*-**1A** at 87 and 71 kcal mol^{-1} above its S_0 and for *cis*-**1B** the S_1 and T_1 are 87 and 71 kcal mol^{-1} above their **S_0** (**Error! Reference source not found.**).

The optimized structure of *trans*-**1B**, a conformer without intramolecular H bond was located at 52 kcal mol^{-1} above the S_0 of *trans*-**1B**. It was not possible to optimize the structure of T_1 of *trans*-**1A** as it yielded biradical *trans*-**2BrA**. In contrast, the optimized structure of T_1 of *cis*-**1A** and *cis*-**1B** were located 54 and 41 kcal mol^{-1} above S_0 of *cis*-**1A** and *cis*-**1B**, respectively.

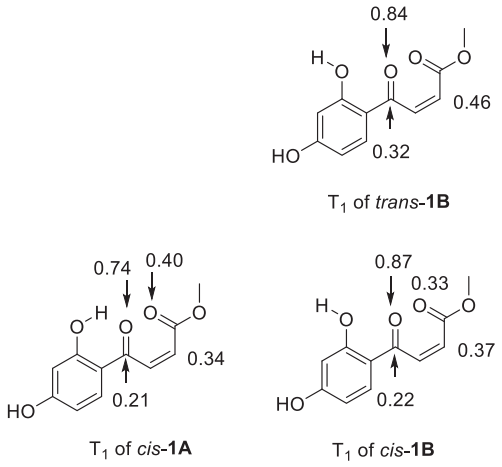

Scheme 6. Calculated spin densities of T_1 of *cis*-**1** and *trans*-**1**

Several conformers of triplet 1,4 biradicals **2Br** were optimized (Scheme *7*). The lowest energy conformer with keto and ketyl oxygen in E alignment was located at 51 kcal mol^{-1} above the S_0 of **1A,** whereas the lowest energy conformer in Z alignment has intramolecular H bonding between the keto and ketyl oxygen. Spin density calculation for the biradical **2Br** shows that the unpaired electrons are centered on the *o*-hydroxy and ketyl carbon atoms.

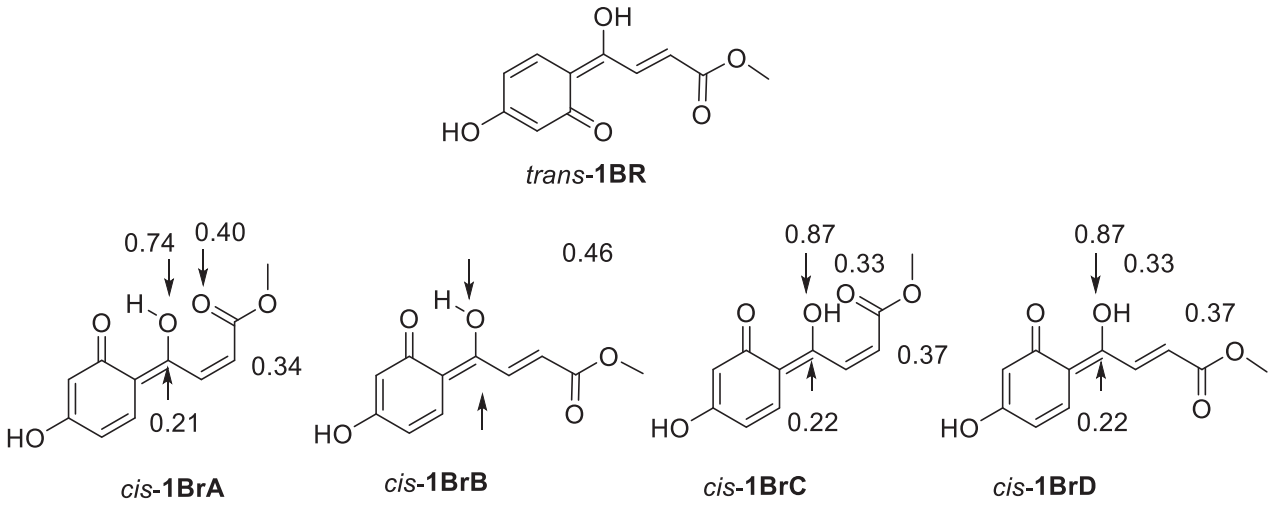

Scheme 7.Optimized conformers of triplet 1,4 biradicals **2Br**

The optimized structure of photoenols *E*-**4** and *Z*-**4** were located at 6 and 26 kcal/mol above the S_0 of **1**. However, we were unable to optimize the hydrogen bonded Z-enol since it converts to *cis*-**1**. Thus, the calculation support further that Z-**4** is not detected in the laser flash photolysis as it decays efficiently to reform the starting material.

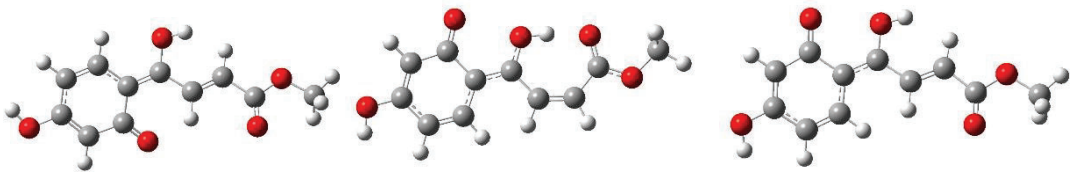

Figure 16. Optimized structures of the ground state conformer of **1a**

We calculated the transition state barrier for hydrogen atom shift from T_1 of **1a** is 1.5 kcal mol^{-1}. Thus, hydrogen atom transfer to form **2** is highly feasible.

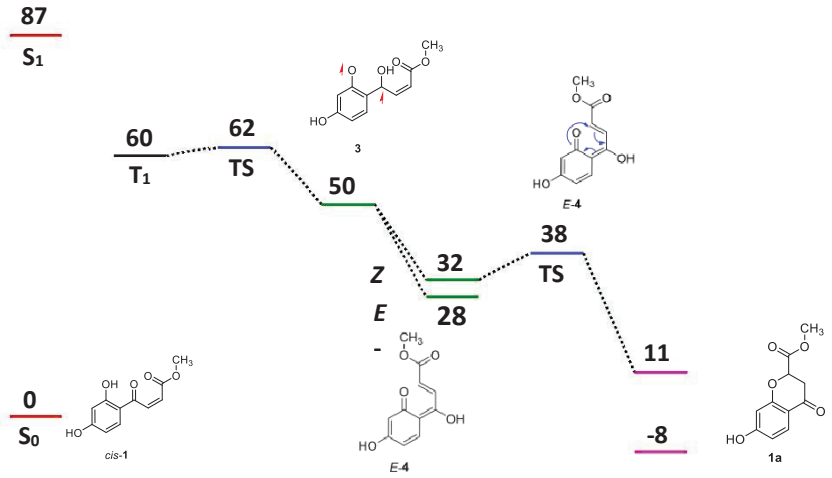

Figure 17. Calculated stationary points on the singlet and triplet energy surfaces of **1**. Calculated energies are in Kcal mol^{-1}.

II. Mechanism for the 5-ring (1b) formation

To support the mechanism in **Scheme 6**, the stationary points on the singlet and triplet surface of 1 were calculated using *Gaussian16* at the B3LYP level of theory and with the 6-31+G (d) basis set [25,26,27].

We calculated the transition state barrier for the intermolecular H atom abstraction of ground state molecule of *cis*-**1** by the $\mathbf{T_{1k}}$ and which is 11.9 Kcal mol^{-1}**.** Thus, it shows that the intermolecular H abstraction is feasible. The optimized energy of the ketyl radical **7** and the phenoxy radical **6** places its energy at 64.9 Kcal mol^{-1} above its $\mathbf{S_0}$ respectively.

The calculated transition state barrier for the alpha cyclization of the phenoxy radical **6** to form the radical **8** is 10.2 Kcalmol^{-1}. The transition state barrier of the intramolecular H atom transfer in ketyl radical **7** to form the radical **9** is 16.3 Kcal mol^{-1}. The calculated transition state barrier for the alpha cyclization of radical **9** to form the cyclized radical **10** is at 13.2 Kcal mol^{-1}. The optimized energies of radical **8, 9** and **10** is 56.0 Kcal mol^{-1}, 66.2 Kcal mol^{-1}, and 58.3 Kcal mol^{-1} respectively. The calculated transition state barrier of the intermolecular H abstraction from radical **10** by the radical **8** is 9.2 Kcal mol^{-1}. All the calculated values of the stationary points and the transition state barriers also support that the proposed mechanism for the formation of **1b** is feasible.

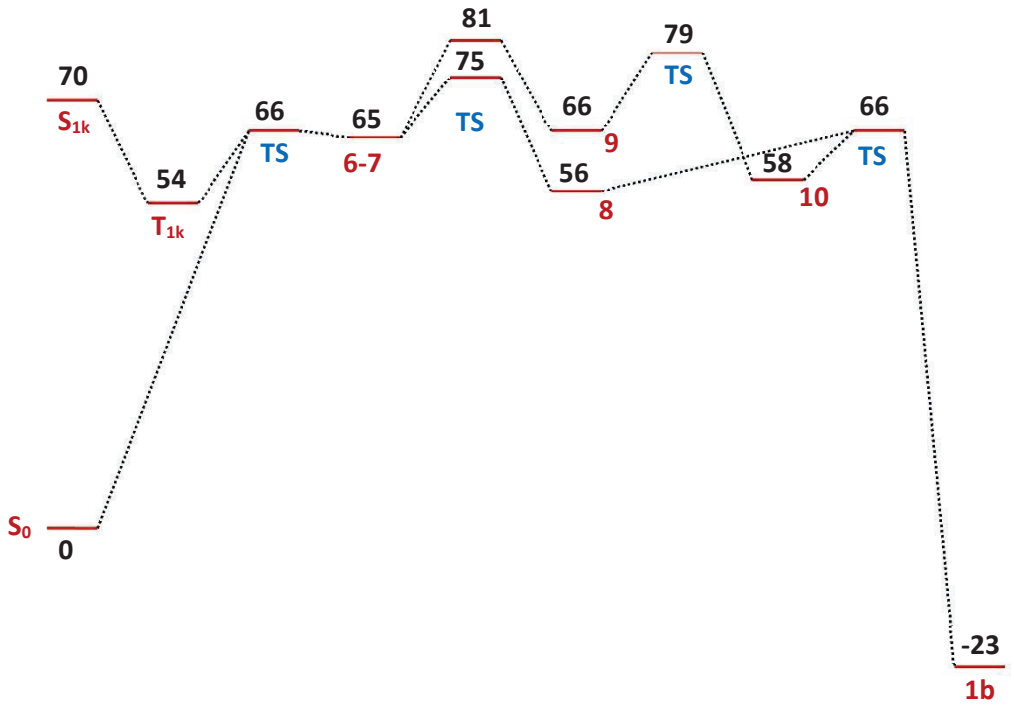

Figure 18. Calculated stationary points on the singlet and triplet energy surface of **1**.

6. Discussion

Photochemistry of 2-hydroxychalcone-**1** is concentration dependent as well as solvent dependent where the irradiation in diluted aprotic solution (< 1.5 mM) yields the selective formation of the flavanone **1a** and the irradiation in concentrated solution yields both photoproducts **1a** and **1b** with photoproduct **1b** being favored in high concentrations. In addition, irradiation of **1** in protic solvents yields the selective formation of the photoproduct **1b** regardless of the concentration. This is in agreement with what Kageyama et al. have reported that upon UV irradiation in polar aprotic solvents 2-hydroxy chalcones underwent photocyclization to give the corresponding flavanones selectively, but protic solvents disturbed the formation of a cyclic intramolecular hydrogen bonding and strongly retarded the photocyclization [14].

In aprotic solution, the cis-**1** intersystem crosses to its triplet surface and forms the 1,4-biradical **2** which intersystem cross and forms the keto tautomer **5** which is the precursor of the flavanone **1a**. However, in high concentrations, the increased intermolecular interactions resulting in a secondary photoreaction and forms the photoproduct **1b**. The acidic phenolic hydrogen of the cis-**1** quenches the triplet ketone $\mathbf{T_{1k}}$ and forms the ketyl radical **6** and phenoxy radical **7** which then rearranges to form the photoproduct **1b**. The ratio of photoproduct **1b** to **1a** increased proportionally with increased concentration of the acidic phenolic hydrogen. This is an agreement with the triplet carbonyl quenching reported by Scaiano et al. in the presence of phenolic hydrogen [4]. Furthermore, the trapping studies with TTMSS also supports that the formation of **1b** in high concentrated aprotic solvent is due to the intermolecular H atom abstraction**.**

In protic solvents we see ground state reactivity of the cis-**1** is which readily undergoes alpha cyclisation and forms the product **1b**. This is in agreement with Lindsay et al**.** reported that in 1:1 MeCN: H_2O the alpha cyclisation of 2-hydroxychalcones prevails over beta cyclization and gives the five membered heterocyclic rings as the major product [28].

The rate of formation of product **1b** is slow in trans in comparison to cis since the transition state barrier for the formation of **1b** from trans is higher than the cis. Upon irradiation of trans-1 in MeOH, the rate of formation of product 1b increases since the trans-1 undergoes cis-trans isomerization, thus the cis-1 readily cyclizes and forms **1b**.

7. Summary and Conclusion

The triplet reactivity of *cis*-**1** is responsible for forming **1a**, and at lower concentration its T1 undergoes intramolecular H atom abstraction to form **2BR** that decays by intersystem crossing to *E*-**4** and *Z*-**4**, with the latter one being unstable as it reforms the starting material. The *E*-**4** undergoes electrocyclic ring closure to yield product **1a**. In contrast, at higher concentration intermolecular H atom abstraction of phenolic proton can compete to form ketyl radicals that yield product **1b**. Similarly, in the presence of other abstractable H atom sources such as TTMSS *cis*-**1** and *trans*-**2** yield product **1b**.

Thus, to selectively form flavanones form chalcone derivatives, they have to undergo triplet reactivity to form E photoenols. Furthermore, because chalcones have phenolic proton it is critical to design reaction conditions where intermolecular H atom abstraction does not compete

with the intramolecular H atom abstraction to form photoenols. Similarly, the solvent has to be non-protic to not cause ground state reactivity to compete with photoenol formation.

8. Experimental

i. Preparation of starting material *cis*- and *trans*- methyl-β-(2,4-dihydrobenzoyl)acrylate (1)

Preparation of trans and cis β-(2,4-dihydrobenzoyl)acrylic acid

The preparation of *trans*- and *cis*-β-(2,4-dihydrobenzoyl)acrylic acid was achieved by modifying the method reported by Barr *et al*.[29] Powdered aluminum chloride (15.00 g, 0.1125 mol) was slowly added over 30 minutes to resorcinol (4.500 g, 0.041 mol) and maleic anhydride (6.00 g, 0.061 mol) in stirred ethylene chloride (150 mL) at –10 °C. The reaction mixture was stirred at room temperature overnight and warmed to 80 °C for 1 h, filtered and the crude dissolved in ice cold water and the reaction quenched by adding 12 M HCl (15 mL). The product that precipitated was filtered and washed with water (150 mL) to get a mixture of pure *cis* isomer of 2,4-dihydroxybenzoylacrylic acid (1a) (yellow color solid, 5.80 g, 0.0279 mol, 68.0% yield) and the pure trans isomer of 2,4-dihydroxybenzoylacrylic acid (1a) (yellow color solid, 0.6138 g, 0.0029 mol, 7.2% yield). The products were characterized with NMR and IR spectroscopy and these spectra are in agreement with those published.[30,31]

cis-β-(2,4-dihydroxybenzoyl)acrylic acid. Mp: 150-154 °C (lit.:[31] 154 °C). IR (solid): ν_{max} 3443, 3269, 1695, 1624, 1584, 1502, 1447, 1328, 1237 cm^{-1}. ^{1}H NMR (400 MHz, CD_3CN) δ 12.13 (s, 1H), 8.18 (s, 1H), 7.58 (d, *J* = 8.8 Hz, 1H), 7.01 (d, *J* = 12.2 Hz, 1H), 6.42 (dd, *J* = 8.8, 2.4 Hz, 1H), 6.37 (d, *J* = 2.4 Hz, 1H), 6.29 (d, *J* = 12.2 Hz, 1H). ^{13}C NMR (101 MHz, CD_3CN) δ 197.01, 165.0, 164.7, 164.5, 138.5, 135.9, 133.7, 126.1, 112.7, 108.1, 107.8, 102.5, 102.4 ppm.

trans-β-(2,4-dihydroxybenzoyl)acrylic acid**.** Mp: 204-206 °C (lit.: 206-208 °C),[29] IR (solid): ν_{max} 3567, 3469, 3066, 1695, 1629, 1581, 1505, 1422, 1343, 1298 cm^{-1}. ^{1}H NMR (400 MHz, Acetonitrile-d_3) δ 12.76 (s, 1H), 8.19 (s, 1H), 7.97 (d, *J* = 15.4 Hz, 1H), 7.87 (d, *J* = 8.9 Hz, 1H), 6.83 (d, *J* = 15.4 Hz, 1H), 6.48 (dd, *J* = 8.9, 2.4 Hz, 1H), 6.39 (d, *J* = 2.4 Hz, 1H) ppm. ^{13}C NMR (101 MHz, CD_3CN) δ 191.1, 166.2, 165.2, 165.19, 135.9, 133.1, 131.0, 113.0, 108.1, 102.5 ppm.

Preparation of *cis*- and *trans*-methyl-β-(2,4-dihydrobenzoyl)acrylate (*cis*-1, *trans*-1).

Cis-β-(2,4-dihydroxybenzoyl)acrylic acid (3.022 g, 0.0144 mol) was heated in methanol (150 mL) containing catalytic amount of sulfuric acid for 12 h. The product was extracted with diethyl ether (3 x 100 mL) and the solvent was removed under reduced pressure to give a mixture of crude *trans*- and *cis*-isomers of methyl-β-(2,4-dihydrobenzoylacrylate (**1**) (orange color oil, 3.0729 g, 0.0138 mol, 95.83% yields). The residue was purified on a silica column eluted with ethyl acetate/hexane (2:3) mixture to yield pure *trans*-**1** as a yellow color solid (1.2911 g, 5.8 mmol 42.02 % yields) and pure *cis*-**1** as a white solid (0.5164 g, 2.3 mmol, 16.67% yields). *cis*-**1** and *trans*-**1** were characterized using ^{1}H and ^{13}C NMR and IR spectroscopy. Their IR and NMR spectra of *trans*-**1** fit with those in the literature.[29]

(4-(2,4-dihydroxy-phenyl)-4-oxo-*trans*-crotonic acid methyl ester (*trans*-1). Mp: 158-160 °C (lit.: [29] 158 °C). IR (solid): ν_{max} 3222, 1727, 1701, 1655, 1612, 1592, 1506, 1438, 1392, 1352, 1322, 1286, 1233, 1178, 1132, 1024, 1001 cm^{-1}. ^{1}H NMR (400 MHz, CD_3CN) δ 12.76 (s, 1H), 8.12 (s, 1H), 8.00 (d, *J* = 15.4 Hz, 1H), 7.88 (d, *J* = 9.0 Hz, 1H), 6.88 (d, *J* = 15.4 Hz, 1H), 6.48 (dd, *J* = 8.9, 2.4 Hz, 1H), 6.40 (d, *J* = 2.4 Hz, 1H), 3.82 (s, 3H) ppm. ^{13}C NMR (101 MHz, CD_3CN) δ 191.7, 167.8, 166.9, 166.2, 136.7, 134.2, 132.1, 114.2, 109.6, 103.8, 52.6 ppm.

(4-(2,4-dihydroxy-phenyl)-4-oxo-*cis*-crotonic acid methyl ester (*cis*-1). Mp: 152-154 °C. IR (solid) ν_{max} 3312, 1717, 1697, 1632, 1594, 1501, 1448, 1438, 1395, 1319, 1274, 1236, 1183, 1163, 1132, 1019 cm^{-1}. ^{1}H NMR (400 MHz, CD_3CN) δ 12.15 (s, 1H), 7.99 (s, 1H), 7.55 (d, *J* = 8.8 Hz, 1H), 7.01 (d, *J* = 12.1 Hz, 1H), 6.46 – 6.28 (m, 3H), 3.64 (s, 3H) ppm. ^{13}C NMR (101 MHz, CD_3CN) δ 197.9, 166.3, 166.1, 165.9, 139.8, 134.7, 126.8, 113.8, 109.1, 103.6, 52.1 ppm.

ii. Product Studies

a. Photoreactivity of dilute acetonitrile-d3 solution of *cis*-1 and *trans*-1 (~1.1 mM)

The photoreactivity of dilute concentration of *cis*-**1** and *trans*-**1** was monitored using ^{1}H-NMR spectroscopy, a stock-solutions of *cis*-**1** and *trans*-**1** (1.13 mM) were prepared by dissolving 1 mg of **1** in 4 mL of acetonitrile-d3. Typically, 0.6 mL of the stock solution of *cis*-**1** or *trans*-**1** were transferred into NMR tubes, which were capped with rubber caps, purged with argon gas for 5 min. The samples were irradiated with LED (λ_{max} ~ 365 nm) and the progress of the reaction was monitored as a function of time. After 115 h (*trans*-**1**) and 110 h (*cis*-**1**) of irradiation the peaks corresponding to the starting material was completely depleted and the peaks corresponding to the photoproduct **1P** was observed.

b. Photoreactivity of concentrated acetonitrile-d3 solution of *cis*-1 and *trans*-1 (4.52 mM)

The photoreactivity of *cis*-**1** and *trans*-**1** in concentrated acetonitrile-d3 solution was monitored using ^{1}H-NMR spectroscopy, the stock solutions of *cis*-**1** and *trans*-**1** (4.52 mM) were prepared by dissolving 4 mg of **1** in 4 mL of acetonitrile-d3. Typically, 0.6 mL of the stock solution of *cis*-**1** and *trans*-**1** were transferred into the NMR tubes, which were capped with rubber caps, and purged with argon gas for 5 min. The samples were irradiated with LED (λ_{max} ~ 365 nm) and the progress of the reaction is monitored as a function of time. After 200 h (*trans*-**1**) and 210 h (*cis*-**1**) of irradiation ^{1}H NMR spectra of the reactions mixture of both showed the presence of *cis*-**1**, *trans*-**1**, **1P**, and **1b**. The reaction did not go to the completion at the time when the irradiation was stopped for both *cis*-**1** and *trans*-**1**. UV-Vis monitoring of the photoreactivity of *cis*-1 and *trans*-1 in CH_3CN

iii. Preparatory Photoreactions of *trans*-1

To isolate the photoproduct *trans*-**1** (300.5 mg, 1.35 mmol) was dissolved in 100.0 mL of acetonitrile (13.5 mM) in a volumetric flask and the flask is sealed with a rubber stopper and purged with argon for 30 min. The sample was irradiated with LED (λ_{max} ~ 365 nm) for 5 days. The solution was evaporated under air stream and the photoproduct was purified using the flash column eluted with ethyl acetate/hexane (2:3) mixture to yield pure methyl 7-hydroxy-4-oxochromane-2-carboxylate **1P** as a pale white color solid (78.2 mg, 0.35 mmol, 25.9 % yields) and pure 2-(6-hydroxy-2,3-dihydrobezofuran-3-yl)-acetic acid methyl ester **1b** as white color solid (112.7 mg, 0.51 mmol, 37.4 % yields). The pure **1P** and **1b** were characterized using ^{1}H and ^{13}C NMR and IR spectroscopy.

Methyl 7-hydroxy-4-oxochromane-2-carboxylate 1a. mp 117-120 °C (lit.:[29] 117-118 °C). IR (solid): ν_{max} 3149, 2959, 2919, 1737, 1647, 1598, 1570, 1460, 1403, 1381, 1341, 1273, 1248, 1219, 1154, 1126 cm^{-1}. ^{1}H NMR (400 MHz, CD_3CN) δ 7.96 (s, 1H), 7.71 (d, *J* = 8.7 Hz, 1H), 6.57 (dd, *J* = 8.6, 2.3 Hz, 1H), 6.45 (d, *J* = 2.2 Hz, 1H), 5.20 (dd, *J* = 8.1, 5.2 Hz, 1H), 3.74 (s, 3H), 3.00 (dd, *J* = 17.1, 5.2 Hz, 1H), 2.91 (dd, *J* = 17.1, 8.2 Hz, 1H). ^{13}C NMR (101 MHz, CD_3CN) δ 188.1, 169.1, 163.2, 159.4, 128.3, 115.5, 110.4, 102.5, 72.96, 54.3, 38.3. ppm

2-(6-hydroxy-2,3-dihydrobenzofuran-3-yl)acetic acid methyl ester (1b). mp 110-115 °C. IR (solid): ν_{max} 3324, 3066, 2999, 1717, 1692, 1613, 1499, 1446, 1392, 1375, 1327, 1225, 1202, 1154, 1107, 1095 cm^{-1}. ^{1}H NMR (400 MHz, CD_3CN) δ 8.14 (s, 1H), 7.51 (d, *J* = 8.5 Hz, 1H), 6.62 (dd, *J* = 8.5, 2.0 Hz, 1H), 6.53 (d, *J* = 2.0 Hz, 1H), 4.88 (dd, *J* = 7.4, 3.9 Hz, 1H), 3.66 (s, 4H), 3.02 (dd, *J* = 17.1, 3.9 Hz, 1H), 2.81 (dd, *J* = 17.1, 7.4 Hz, 1H). ^{13}C NMR (101 MHz, CD_3CN) δ 197.2, 172.9, 169.7, 166.0, 125.8, 113.8, 111.3, 96.8, 81.4, 50.1, 33.2.

iv. Concentration dependent photoreactivity

To study the effect of concentration on the photoreactivity, different concentrations of the trans-**1** and cis-**1** were prepared by dissolving 2 mg, 5 mg, 10 mg, 20 mg, 30 mg, and 50 mg of each in 15 mL CH_3CN in a test tube separately to yield the concentration of 0.6 mM, 1.5 mM, 3.0 mM, 6.0 mM, 9.0 mM, and 15.0 mM, respectively. Each test tube containing the above different concentration of solution was degassed by bubbling argon through the solution for 10 min, capped with a rubber stopper and sealed with a piece of parafilm tape.

Resulting solutions were irradiated separately using 365 nm LED. After certain period of time, the irradiation was stopped [*cis*-**1** (0.6 mM after 2 days, 1.5 mM after 5 days, 3.0 mM after 8 days, 6.0 mM after 12 days, 9.0 mM after 12 days and 15.0 mM after 14 days), *trans*-**1** (0.6 mM after 5 days, 1.5 mM after 5 days, 3.0 mM after 14 days, 6.0 mM after 14 days, 9.0 mM after 14 days and 15.0 mM after 14 days)] and CH_3CN solution was evaporated under air stream and the remaining crude from each concentration was dissolved in deuterated CD_3CN and the ^{1}H-NMR of each concentration was compared and the percentages of products **1a** and **1b** were calculated from the integration of the signals at 5.20 and 4.88 ppm.

v. Silyl Trapping

The quenching studies was performed using tris(trimethylsilyl)silane [TTMSS] for three different concentrations of *trans*-**1**. To the 0.6 mM solution of *trans*-**1**, 6 µL TTMSS (1:4 equivalent) was added and the resulting solution was degassed by bubbling argon through the solution for 10 minutes, capped with a rubber stopper and sealed with a piece of parafilm tape.

Similarly, the 1.5 mM solution of *trans*-1 was mixed with 7.5 µL of TTMSS (1:2 equivalent) and 3.0 mM solution was mixed with 15.0 µL of TTMSS (1:2 equivalent) and degassed. All these three solutions were irradiated separately using 365 nm LED for certain amount of time [(0.6 mM for 42 h), (1.5 mM for 90 h), (3.0 mM for 90 h)] and then the irradiation was stopped, and the resulting solutions were air dried, and the crudes were dissolved in deuterated CD_3CN and the ^1H NMR was checked for each solution. The percentage of the product **1b** in the presence of TTMSS was calculated from the integration and compared with the percentage of **1b** in the absence of TTMSS for the same concentrated solution of *trans*-**1**.

vi. Irradiation in Protic solvents

To identify the photoreactivity of *trans*-**1** in protic solvents, 0.6 mM and 3.0 mM of *trans*-**1** were prepared by dissolving 2 mg and 10 mg of *trans*-**1** in 15 mL of MeOH in a test tube. The solution was degassed by bubbling argon through the solution for 10 minutes, capped with a rubber stopper and sealed with a piece of parafilm tape. The resulting solution was irradiated for a certain amount of time and then the irradiation was stopped, the solvent is evaporated, and the crude was dissolved in CD_3CN and the ^1H NMR of the reaction mixture obtained, it showed the complete conversion of *trans*-**1** into product **1b** in both 0.6 mM and 3.0 mM solution.

vii. UV-Vis monitoring of the photoreactivity of *cis*-1 and *trans*-1 in MeOH

a. Reactivity of *cis*-1 and *trans*-1 in methanol solutions in the dark

To monitor the reactivity of *cis*-**1** (4.5 µM) and *trans*-**1** (4.5 µM) in MeOH using UV-Vis absorption spectroscopy, typically, ~ 2.5 mL of the stock solutions of both were placed in 10 mm × 10 mm × 48 mm quartz cuvettes separately, and they capped with rubber caps and purged with argon for 5 min. The samples were kept in dark, and the UV-Vis absorption spectra were collected using JASCO V-750 spectrophotometer as a function of time. The UV absorption spectra of the *cis*-**1** was converted from the absorption spectra of the starting material to the product **1b** after 120 mins in the dark, with six isosbestic points at 229 nm, 239 nm, 253.5 nm, 279.5 nm, 311 nm, and 323 nm. The UV absorption spectra of the *trans*-**1** was converted from the absorption spectra of the starting material to the product **1b** after 24 h in the dark.

b. Photoreactivity of *trans*-1 in methanol solutions upon irradiation at 365 nm

To monitor the reactivity of *trans*-**1** (4.5 µM) upon irradiation in MeOH using UV-Vis absorption spectroscopy, typically, ~ 2.5 mL of the stock solutions of both were placed in 10 mm × 10 mm × 48 mm quartz cuvettes separately, and they capped with rubber caps and purged with argon for 5 min. The sample was irradiated with LED (λ_{max} ~ 365 nm) and and the UV-Vis absorption spectra were collected using JASCO V-750 spectrophotometer as a function of time. The UV absorption spectra of the *trans*-**1** was converted from the absorption spectra of the starting material to the product **1b** after 90 mins of irradiation, with an isosbestic point at 310 nm.

viii. Laser Flash Photolysis Studies

Excimer laser (308 nm, 17 ns) was used to acquire transient UV-Vis and corresponding kinetic traces.[32] Spectroscopic grade acetonitrile was used to prepare stock solutions of 2-hydroxychalcones *cis*-**1**, and *trans*-**1** such that UV absorption of the solutions at 308 nm between 0.3 and 0.8. The stock solution of 250 mL was taken in a volumetric flask and flowed through the quartz cuvette continuously with the help of a peristaltic pump. Throughout the experiment, argon or oxygen was flowed continuously in the solution.

ix. Quantum Modelling

All geometries were optimized with density functional theory (DFT) using Gaussian16 [33] at the B3LYP level of theory with the 6-31+G(d) basis set.[25,26] Energies of excited singlet and triplet states and UV-Vis spectra of optimized ground states were computed using TD-DFT.[34,35] We analyzed the second derivative of the energy with respect to the internal coordinates to satisfy all transition states having one imaginary vibrational frequency. Intrinsic reaction coordinate (IRC) calculations verified the located transition states corresponded to the respective reactant and the products.[36,37] The calculations were carried out at the Ohio Supercomputer.

x. Phosphorescence

mTHF solutions of *trans*-**1** (0.06 M) and *cis*-**1** (0.06 M) were prepared and cooled to 77 K and their phosphorescence spectra obtained using a Phosphorimeter, which has been described

previously.[38] The samples were excited with 280 nm light and the emission spectra were recorded between 300 nm and 800 nm.

xi. X-ray crystallographic analysis.

X-ray crystallographic experiments were performed at UC.

a. X-ray crystallographic analysis of *cis*-**1**

Crystals were obtained from ethyl acetate-hexane (2:3). For X-ray examination and data collection, a suitable colorless rod-shaped crystal, approximate dimensions 0.253 x 0.084 x 0.052 mm, was mounted in a loop with Paratone-N oil and transferred to the goniostat bathed in a cold stream.

Intensity data were collected at 150K on a Bruker D8 Venture Mo-I□S Photon-II diffractometer, λ=0.71073Å. For data collection frames were measured in shutterless mode. The data frames were processed using the program SAINT. The data were corrected for decay, Lorentz and polarization effects as well as absorption and beam corrections based on the numerical technique.

The structure was solved by a combination of direct methods in SHELXTL and the difference Fourier technique and refined by full-matrix least squares on F^2. Non-hydrogen atoms were refined with anisotropic displacement parameters. Hydroxyl H-atoms were located directly from the difference map and the coordinates refined. All remaining H-atoms were calculated and treated with a riding model. The refinement converged with crystallographic agreement factors of R1=3.34%, wR2=8.96% for 2329 reflections with I>2σ(I) (R1=3.69%, wR2=9.32% for all data) and 152 variable parameters.

b. X-ray crystallographic analysis of *trans*-**1**

Crystals were obtained from ethyl acetate-hexane (2:3). For X-ray examination and data collection, a suitable yellow plate-shaped crystal, approximate dimensions 0.201 x 0.100 x 0.073 mm, was mounted in a loop with Paratone-N oil and transferred to the goniostat bathed in a cold stream.

Intensity data were collected at 150K on a Bruker D8 Venture Mo-I□S Photon-II diffractometer, λ=0.71073Å. For data collection frames were measured in shutterless mode. The data frames were processed using the program SAINT. The data were corrected for decay, Lorentz and polarization effects as well as absorption and beam corrections based on the numerical technique.

The structure was solved by a combination of direct methods in SHELXTL and the difference Fourier technique and refined by full-matrix least squares on F^2. Non-hydrogen atoms were refined with anisotropic displacement parameters. Hydroxyl H-atoms were located directly from the difference map and the coordinates refined. All remaining H-atoms were calculated and treated with a riding model. The refinement converged with crystallographic agreement factors of R1=3.38%, wR2=9.31% for 2262 reflections with I>2σ(I) (R1=3.82%, wR2=9.76% for all data) and 152 variable parameters.

c. X-ray crystallographic analysis of **1P**

Crystals were obtained from ethyl acetate For X-ray examination and data collection, a suitable colorless blade-shaped crystal, approximate dimensions 0.075 x 0.035 x 0.016 mm, was mounted in a loop with Paratone-N oil and transferred to the goniostat bathed in a cold stream.

Intensity data were collected at 150K on a Bruker PHOTON-II detector at Beamline 12.2.1 at the Advanced Light Source (Lawrence Berkeley National Laboratory) using synchrotron radiation tuned to λ=0.7288Å. For data collection frames were measured in shutterless mode. The data frames were collected using the program APEX3 and processed using the program SAINT routine within APEX3. The data were corrected for absorption and beam corrections based on the multi-scan technique as implemented in SADABS.

The structure was solved by a combination of direct methods and the difference Fourier technique as implemented in the SHELX suite of programs and refined by full-matrix least squares on F^2 for reflections out to 0.85Å resolution. Non-hydrogen atoms were refined with anisotropic displacement parameters. The hydroxyl H-atom was located directly from the difference map and the coordinate refinement. Remaining H-atom positions were calculated and treated with a riding model. The H-atom isotropic displacement parameters were defined as $a*U_{eq}$ (a=1.5 for OH and methyl, 1.2 for all others) of the adjacent atom. The refinement converged with crystallographic agreement factors of R1=6.71%, wR2=16.21% for 1363 reflections with I>2σ(I) (R1=8.25%, wR2=17.04% for all data) and 149 variable parameters.

d. X-ray crystallographic analysis of **1b**

For X-ray examination and data collection, a suitable **colorless** plate-shaped crystal, approximate dimensions 0.138 x 0.061 x 0.042 mm, was mounted in a loop with Paratone-N oil and transferred to the goniostat bathed in a cold stream.

Intensity data were collected at 150K on a Bruker D8 Venture Mo-I□S Photon-II diffractometer, λ=0.71073Å. For data collection frames were measured in shutterless mode. The data frames were processed using the program SAINT. The data were corrected for decay, Lorentz and polarization effects as well as absorption and beam corrections based on the numerical technique.

The structure was solved by a combination of direct methods in SHELXTL and the difference Fourier technique and refined by full-matrix least squares on F^2 for reflections out to 0.80Å resolution. Non-hydrogen atoms were refined with anisotropic displacement parameters. All H-atoms were located directly from the difference map and the coordinates and displacement parameter refined. The refinement converged with crystallographic agreement factors of R1=3.84%, wR2=8.18% for 1601 reflections with I>2σ(I) (R1=5.49%, wR2=9.17% for all data) and 185 variable parameters.

9. References

(1) Klán, P.; Wirz, J.; Gudmundsdottir, A. D. 2012.

(2) Sammes, P. G. *Tetrahedron* **1976**, *32*, 405.

(3) Guerin, B.; Johnston, L. J. *Canadian Journal of Chemistry* **1989**, *67*, 473.

(4) Das, P. K.; Encinas, M. V.; Scaiano, J. C. *Journal of the American Chemical Society* **1981**, *103*, 4154.

(5) Muthukrishnan, S.; Sankaranarayanan, J.; Pace, T. C. S.; Konosonoks, A.; DeMichiei, M. E.; Meese, M. J.; Bohne, C.; Gudmundsdottir, A. D. *The Journal of Organic Chemistry* **2010**, *75*, 1393.

(6) Haag, R.; Wirz, J.; Wagner, P. J. *Helvetica Chimica Acta* **1977**, *60*, 2595.

(7) Sankaranarayanan, J.; Muthukrishnan, S.; Gudmundsdóttir, A. *Advances in Physical Organic Chemistry - ADVAN PHYS ORGAN CHEM* **2009**, *43*, 39.

(8) Herrmann, A. *Photochemical & Photobiological Sciences* **2012**, *11*, 446.

(9) Falcone Ferreyra, M. L.; Rius, S.; Casati, P. *Frontiers in Plant Science* **2012**, *3*.

(10) Evans, B. E.; Rittle, K. E.; Bock, M. G.; DiPardo, R. M.; Freidinger, R. M.; Whitter, W. L.; Lundell, G. F.; Veber, D. F.; Anderson, P. S.; Chang, R. S. L.; Lotti, V. J.; Cerino, D. J.; Chen, T. B.; Kling, P. J.; Kunkel, K. A.; Springer, J. P.; Hirshfield, J. *Journal of Medicinal Chemistry* **1988**, *31*, 2235.

(11) Nibbs, A. E.; Scheidt, K. A. *European journal of organic chemistry* **2012**, *2012*, 449.

(12) Stermitz, F. R.; Adamovics, J. A.; Geigert, J. *Tetrahedron* **1975**, *31*, 1593.

(13) Matsushima, R.; Hirao, I. *Bulletin of the Chemical Society of Japan* **1980**, *53*, 518.

(14) Matsushima, R.; Kageyama, H. *Journal of the Chemical Society, Perkin Transactions 2* **1985**, 743.

(15) Leigh, W. J.; Lathioor, E. C.; St. Pierre, M. J. *Journal of the American Chemical Society* **1996**, *118*, 12339.

(16) Lathioor, E. C.; Leigh, W. J. *Photochemistry and Photobiology* **2006**, *82*, 291.

(17) Samanta, S.; Mishra, B. K.; Pace, T. C. S.; Sathyamurthy, N.; Bohne, C.; Moorthy, J. N. *The Journal of Organic Chemistry* **2006**, *71*, 4453.

(18) Galian, R. E.; Litwinienko, G.; Pérez-Prieto, J.; Ingold, K. U. *Journal of the American Chemical Society* **2007**, *129*, 9280.

(19) Lalevée, J.; Allonas, X.; Fouassier, J. P. *The Journal of Organic Chemistry* **2007**, *72*, 6434.

(20) Lalevée, J.; Blanchard, N.; El-Roz, M.; Graff, B.; Allonas, X.; Fouassier, J. P. *Macromolecules* **2008**, *41*, 4180.

(21) Klima, R. F.; Jadhav, A. V.; Singh, P. N. D.; Chang, M.; Vanos, C.; Sankaranarayanan, J.; Vu, M.; Ibrahim, N.; Ross, E.; McCloskey, S.; Murthy, R. S.; Krause, J. A.; Ault, B. S.; Gudmundsdóttir, A. D. *J. Org. Chem.* **2007**, *72*, 6372.

(22) Kaneda, K.; Arai, T. *Organic & Biomolecular Chemistry* **2003**, *1*, 2041.

(23) Furlong, J. J. P.; Nudelman, N. S. *Journal of the Chemical Society, Perkin Transactions 2* **1985**, 633.

(24) Donnelly, J. A.; Doran, H. J. *Tetrahedron* **1975**, *31*, 1565.

(25) Becke, A. D. *The Journal of Chemical Physics* **1993**, *98*, 5648.

(26) Parr, R. G.; Yang, W. *Density-functional theory of atoms and molecules*; Oxford University Press: Oxford, 1994.

(27) Stratmann, R. E.; Scuseria, G. E.; Frisch, M. J. *The Journal of Chemical Physics* **1998**, *109*, 8218.

(28) Adams, C. J.; Main, L. *Tetrahedron* **1992**, *48*, 9929.

(29) Barr, K. P.; Dean, F. M.; Locksley, H. D. *Journal of the Chemical Society (Resumed)* **1959**, 2425.

(30) Ashcroft, S. J.; Thorne, M. P. *Canadian Journal of Chemistry* **1972**, *50*, 3478.

(31) Konieczny, M.; Korngut, S. *Arch. Immunol. Ther. Exp.* **1975**, *23*, 809.

(32) Muthukrishnan, S.; Sankaranarayanan, J.; Klima, R. F.; Pace, T. C. S.; Bohne, C.; Gudmundsdottir, A. D. *Org. Lett.* **2009**, *11*, 2345.

(33) Frisch, M. J.; Trucks, G. W.; Schlegel, H. B.; Scuseria, G. E.; Robb, M. A.; Cheeseman, J. R.; Scalmani, G.; Barone, V.; Petersson, G. A.; Nakatsuji, H.; Li, X.; Caricato, M.; Marenich, A. V.; Bloino, J.; Janesko, B. G.; Gomperts, R.; Mennucci, B.; Hratchian, H. P.; Ortiz, J. V.; Izmaylov, A. F.; Sonnenberg, J. L.; Williams; Ding, F.; Lipparini, F.; Egidi, F.; Goings, J.; Peng, B.; Petrone, A.; Henderson, T.; Ranasinghe, D.; Zakrzewski, V. G.; Gao, J.; Rega, N.; Zheng, G.; Liang, W.; Hada, M.; Ehara, M.; Toyota, K.; Fukuda, R.; Hasegawa, J.; Ishida, M.; Nakajima, T.; Honda, Y.; Kitao, O.; Nakai, H.; Vreven, T.; Throssell, K.; Montgomery Jr., J. A.; Peralta, J. E.; Ogliaro, F.; Bearpark, M. J.; Heyd, J. J.; Brothers, E. N.; Kudin, K. N.; Staroverov, V. N.; Keith, T. A.; Kobayashi, R.; Normand, J.; Raghavachari, K.; Rendell, A. P.; Burant, J. C.; Iyengar, S. S.; Tomasi, J.; Cossi, M.; Millam, J. M.; Klene, M.; Adamo, C.; Cammi, R.; Ochterski, J. W.; Martin, R. L.; Morokuma, K.; Farkas, O.; Foresman, J. B.; Fox, D. J. Wallingford, CT, 2016.

(34) Bauernschmitt, R.; Ahlrichs, R. *Chemical Physics Letters* **1996**, *256*, 454.

(35) Foresman, J. B.; Head-Gordon, M.; Pople, J. A.; Frisch, M. J. *The Journal of Physical Chemistry* **1992**, *96*, 135.

(36) Gonzalez, C.; Schlegel, H. B. *The Journal of Chemical Physics* **1989**, *90*, 2154.

(37) Gonzalez, C.; Schlegel, H. B. *The Journal of Physical Chemistry* **1990**, *94*, 5523.

(38) Ranaweera, R. A. A. U.; Scott, T.; Li, Q.; Rajam, S.; Duncan, A.; Li, R.; Evans, A.; Bohne, C.; Toscano, J. P.; Ault, B. S.; Gudmundsdottir, A. D. *The Journal of Physical Chemistry A* **2014**, *118*, 10433.

Chapter 3

Visible light mediated synthesis of N-Heterocycles via intramolecular reductive cyclization of triplet alkyl nitrenes

Sobiya George, Jeanette A. Krause, and Anna D. Gudmundsdottir*

[†] Department of Chemistry, University of Cincinnati, Cincinnati, Ohio 45221-0172, United States

Abstract

Organoazides, in particular alkyl azides, are widely used as versatile synthetic intermediates to construct nitrogen-containing molecules owing to their unique reactivity. The limited use of nitrogen radicals in synthesis is mainly due to the lack of methods for selectively yielding nitrogen centered radicals. In this work we have demonstrated that the combination of visible light and the tris(trimethylsilyl) silane promote the reductive cyclization of triplet alkyl nitrene. Triplet excited state of the azido chromophore can be formed upon irradiation of gamma azido aryl ketones, the aryl ketone moiety serves a built-in intramolecular triplet sensitizer, which undergoes intramolecular energy transfer to azide moiety. The triplet alkyl nitrene intermediates are formed from the triplet azides, by expelling the nitrogen molecule. In competition with the energy transfer to form triplet alkyl nitrenes, the gamma-azido undergo alpha-cleavage to form benzoyl and azido alkyl radical. Interestingly, in the presence of TTMSS we observed the selective formation of N-heterocycle which is formed via the intermolecular H atom abstraction of triplet alkyl nitrene from TTMSS. Thus, these alkyl nitrenes have the potential to make five-membered heterocyclic derivatives in synthetic applications with much higher yields. We used transient

spectroscopy, trapping studies, cryogenic matrix isolation and density functional theory (DFT) calculations to characterize the triplet alkyl nitrene and to support the proposed mechanism.

1. Introduction

Nitrenes have the potential to be used to make new C-N bond in synthetic applications since they can be the source of nitrogen radicals. However, the use of nitrogen centered radical in synthetic applications is limited since the selective formation of nitrenes is very difficult as they and their precursors are highly reactive [1]. Direct photolysis of the alkyl, aryl, and vinyl azides form singlet nitrene that are highly reactive and tend to undergo unimolecular rearrangements, rather than intersystem cross to their triplet surface and form triplet alkyl nitrenes. [2]. Typically, selective formation of triplet nitrenes can be achieved by the irradiation of azides in the presence of a triplet sensitizer (Scheme 8) [3,4]. However, one of the limitations of relaying of intramolecular sensitization to form triplet alkyl nitrene, is that the photoreactivity of the triplet sensitizer can compete with energy transfer.

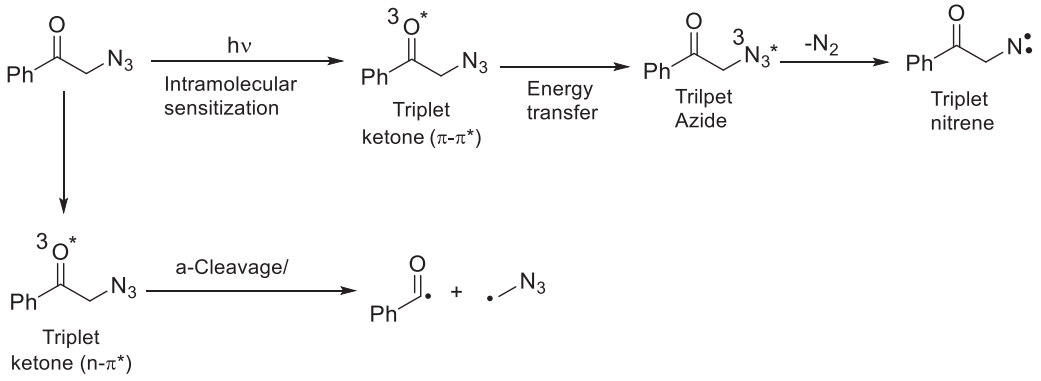

Scheme 8. Selective formation of triplet alkyl nitrenes from α-azido acetophenones

Triplet sensitization can be either intermolecular or intramolecular in which the energy is transferred from the triplet excited ketone to the azido moiety and forms the triplet excited azide. The expulsion of nitrogen molecule from the azide group generates the triplet alkyl nitrene. For aryl azido derivatives irradiation above 300 nm ensures the excitation of only the ketone chromophore not the azido chromophore [5, 6]. Selective formation of triplet alkyl nitrene can be achieved using this method, but energy transfer competes with other photoreactivity of the aryl ketone such as alpha cleavage or intermolecular H atom abstraction by the triplet ketone.

The energy transfer to from a triplet azido moiety is favored for triplet ketones with the (π-π^*) configuration whereas triplet ketone with (n- π^*) configuration undergo alpha cleavage and H atom abstraction in competition with energy transfer [7, 8]. For triplet excited ketones with(π-π^*) configuration, the energy transfer will be dominated over alpha cleavage, and whereas triplet ketones with (n- π^*) configuration, alpha cleavage can compete with energy transfer [9].

Photolysis of gamma azido butyrophenones can be used to generate the 1,5 nitrogen-carbon biradicals which has the potential to make five membered heterocyclic derivatives in synthetic applications. In gamma azides, the alpha cleavage resulting in the formation of benzoyl radical and an azido propyl radical whereas the intermolecular H atom abstraction resulting in the formation of ketyl iminyl radical. The expel of nitrogen molecule from the ketyl iminyl radical will result in the formation of imine radical. The intramolecular cyclization of the imine radical leads to the formation of product **2** [10].

Triplet alkyl nitrenes do not generally abstracts a H atom from the solvent but can cyclize to form heterocyclic products. In comparison, the triplet aryl ketones can abstract H atom intramolecular in alkyl azide to and form a different heterocyclic product [11]. Thus, the irradiation of gamma azides can lead to the formation of two types of N-heterocycles; thus, it is important to explore the conditions which favors the formation of each to have the selective formation of one particular product, so that it can be beneficial in synthetic aspects.

Muthukrishnan *et al*. reported that, when the energy gap between the (n,π) and (π,π) configuration of the triplet aryl ketone is large enough, then it would be possible to get a selective reactivity only from the lowest triplet excited ketone. When the energy gap between the two energy states is small, it can be expected that both configuration of the aryl ketones can react [12]. The substituent group attached to the benzene plays a major role in altering the energy gap between both the (n,π) and (π,π) configuration of the triplet aryl ketone [13]. Generally, when an electron donating group is attached the (π-π*) state of the triplet ketone will be stabilized and thus it will have a lower energy.

The purpose of our work is to find a better condition for selective reactivity of gamma azido butyrophenone derivatives, thus it can be applicable in synthetic reactions to make the N-heterocycles with much higher yields, and in a more sustainable way. So, we synthesized two gamma azido butyrophenone derivatives in which one has a para- methoxy substituent and the other is the p-bromo substituent. In p-methoxy substituted butyrophenones the lowest energy triplet ketone T_{1K} has the (π-π*) configuration, whereas in p-bromo substituted butyrophenones the lowest energy triplet ketone has (n, π*) and (π,π*) configuration. Product studies showed that the irradiation of azide **1a** yields mainly photoproduct **2a** and a small amount of

acetophenone. However, the irradiation of **1b** yields mainly the photoproduct **2b** and 3-(4-bromophenyl)-1H-pyrrole and a small amount of acetophenone. Interestingly in the presence of TTMSS both the azides **1a** and **1b** resulted in the selective formation photoproduct **2a** and **2b,** respectively.

2. Product studies

I. Product studies of 1a

Argon saturated MeOH solution of **1a** (9.2 mM) was irradiated using 340 nm LED for. After 18 h of irradiation the solvent was evaporated, and the crude mixture was analyzed using ^{1}H-NMR spectroscopy. After 18 h of irradiation, ^{1}H-NMR spectra of the reaction mixture showed the formation of the photoproduct **2a** and acetophenone in major amount together with the small percentage of unreacted starting material and the formation of unknown photoproducts (Figure S163).

Further, argon saturated MeOH solution of **1a** (15.4 mM) was added with 100 uL of Tris(trimethylsilyl)silane (TTMSS) and the solution was irradiated using 340 nm LED (Scheme 9.). The progress of the reaction was monitored using ^{1}H-NMR spectroscopy. After 7 h of irradiation, ^{1}H-NMR spectra of the reaction mixture showed that **1a** was depleted completely and the photoproduct **2a** was formed selectively (Figure 19).

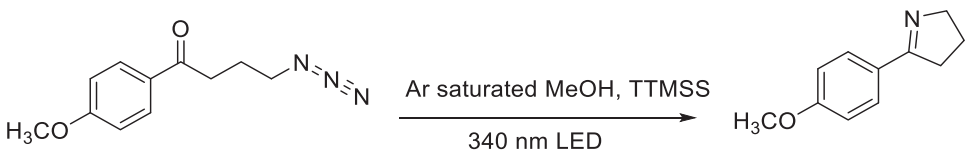

Scheme 9. Irradiation of argon saturated 1a in MeOH using 340 nm LED

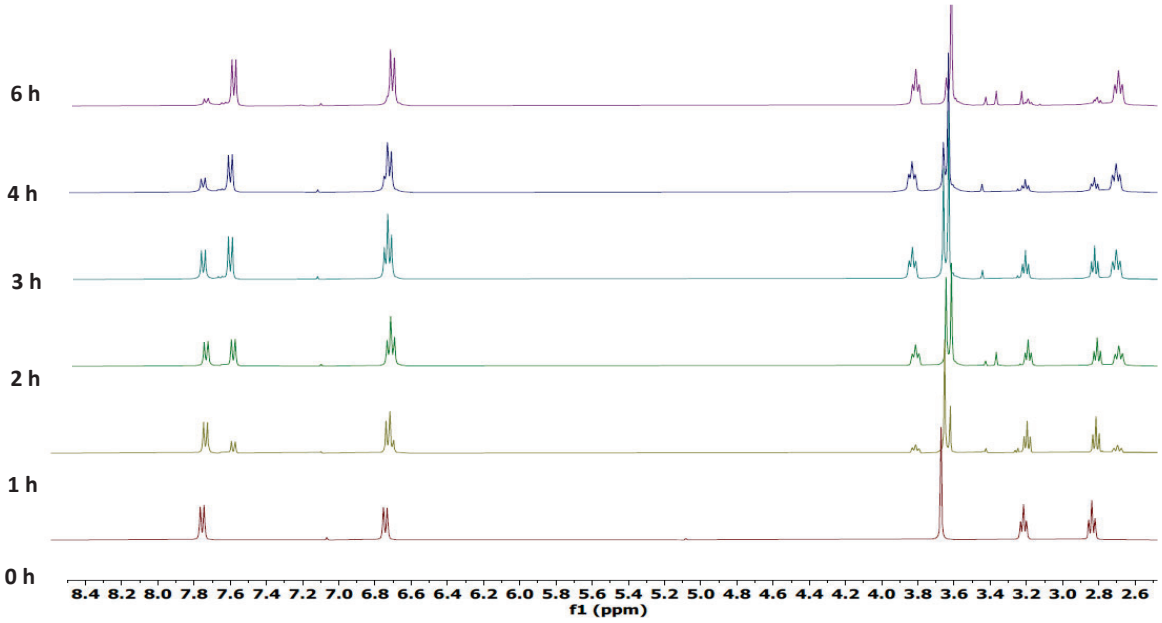

Figure 19. ^{1}H-NMR spectra showing the progress of the reaction of 1a with 100 mL TTMSS in argon saturated MeOH upon irradiation at 340 nm

To explain the formation of photoproduct **2a** from azide **1a**, we proposed the mechanism shown in Scheme 10. Upon irradiation the ground state of azide **1a** gets excited to the singlet excited state of the ketone $\mathbf{S_{1K}}$, which intersystem crosses to its triplet configuration $\mathbf{T_{1K}}$. Intramolecular energy transfer from the $\mathbf{T_{1K}}$ to the azide chromophore results in the formation of triple azide $\mathbf{T_{1A}}$. Triplet alkyl nitrene **1aN** is formed from $\mathbf{T_{1A}}$ via the release of N_2 molecule. Triplet alkyl nitrene **1aN** abstracts a H atom from TTMSS and forms the imine radical **5**. Imine radical-**5** presumably undergoes intramolecular cyclization and forms the radical **6**. The H atom abstraction by radical**6** from TTMSS followed by water elimination resulting in the formation of the photoproduct **2a**. We propose the similar mechanism for the formation of **2b** from **1b.**

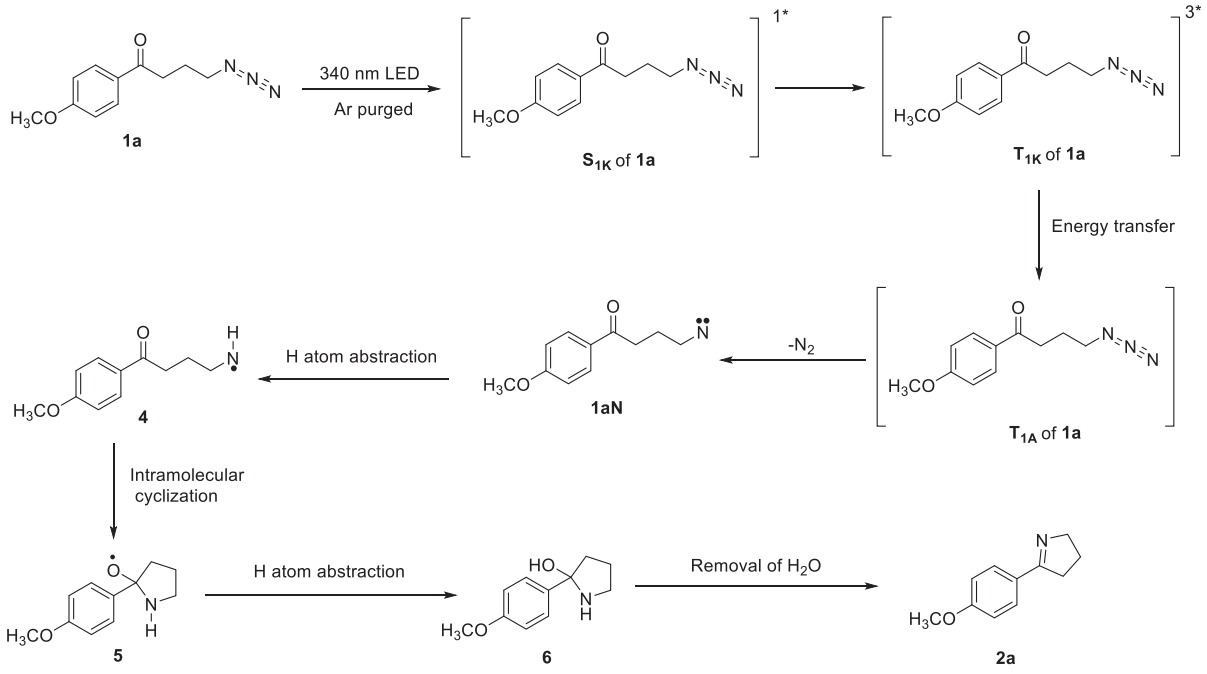

Scheme 10. Proposed mechanism for the formation of photoproduct **2a** from **1a**

II. Product studies of 1b

Similarly, argon saturated MeOH solution of **1b** (11.4 mM) was irradiated using 340 nm LED for. After 18 h of irradiation the solvent was evaporated, and the crude mixture was analyzed using ^{1}H-NMR spectroscopy. After 18 h of irradiation, ^{1}H-NMR spectra of the reaction mixture showed the formation of the photoproduct **2b** and 3-(4-bromophenyl)-1H-pyrrole in major amount and a small amount of acetophenone (Figure S164).

Further, the irradiation of argon saturated MeOH solution (19 mM) of bromo substituted gamma azide **1b** in the presence of TTMSS was carried out. The progress of the reaction was

monitored using ^{1}H-NMR spectroscopy. After 4 h of irradiation, ^{1}H-NMR spectra of the reaction mixture showed that **1a** was depleted completely and the photoproduct **2b** was formed selectively (Figure 20).

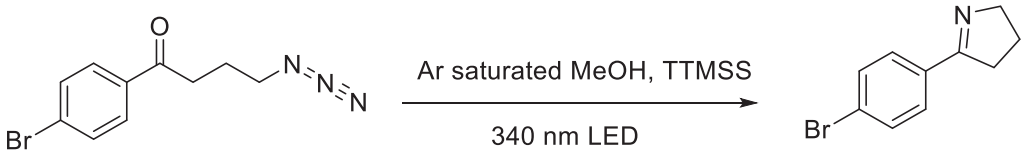

Scheme 11. Irradiation of argon saturated **1b** in MeOH using 340 nm LED

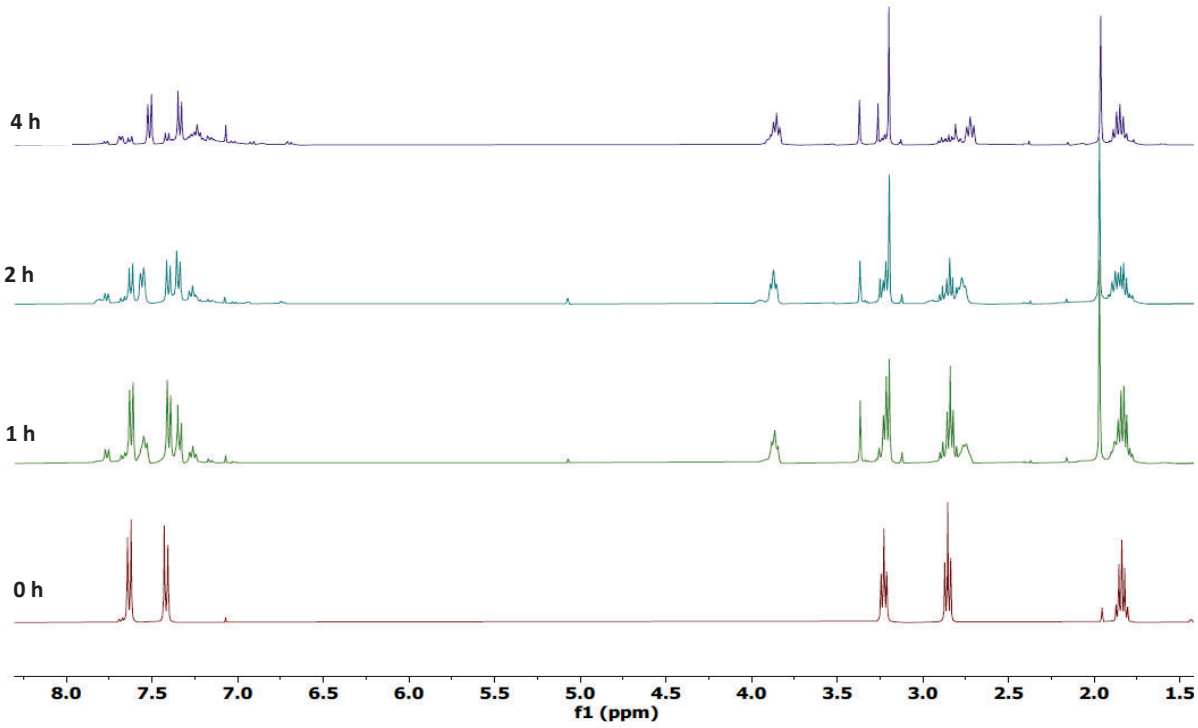

Figure 20. ^{1}H-NMR spectra showing the progress of the reaction of **1b** with 100 μL TTMSS in argon saturated MeOH upon irradiation at 340 nm

We proposed the similar mechanism **Error! Reference source not found.** to explain the f ormation of photoproduct **2b** from **1b.** Upon irradiation the ground state azide molecule will get excited to the singlet excited state and forms the singlet ketone **S_1K**. From the singlet excited

state, the singlet ketone **S_1K** intersystem crosses to its triplet state and forms the triplet ketone **T_1K**. At the triplet excited state, the intramolecular energy transfer from the **T_1K** to the azide group results in the formation of triple azide **T_1A**.

Triplet nitrene **3b** will be formed from the triplet azide **T_1A** via the release of N_2 Molecule. Triplet nitrene **3b** abstracts a H atom from TTMSS and forms the imine radical-**5b**. The ground state imine radical-**5b** undergoes intramolecular cyclization and forms the ring-radical**-6b**. The H atom abstraction by radical-**6b** from TTMSS followed by water elimination resulting in the formation of the photoproduct **2b**.

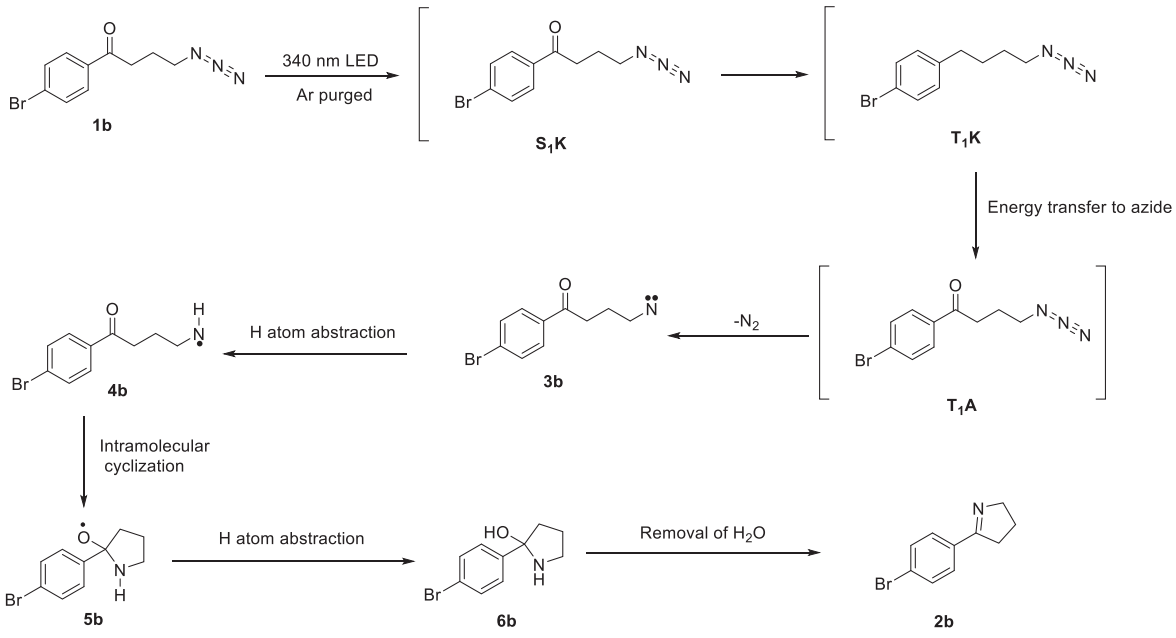

Scheme 12. Proposed mechanism for the formation of photoproduct **2b** from **1b**

3. Quantum Mechanical Calculations

I. Mechanism for the formation of 2a from 1a

To support the mechanism in **Scheme 4**, the stationary points on the singlet and triplet surface of **1a** were calculated using *Gaussian16* at the B3LYP level of theory and with the 6-31+G (d) basis set.

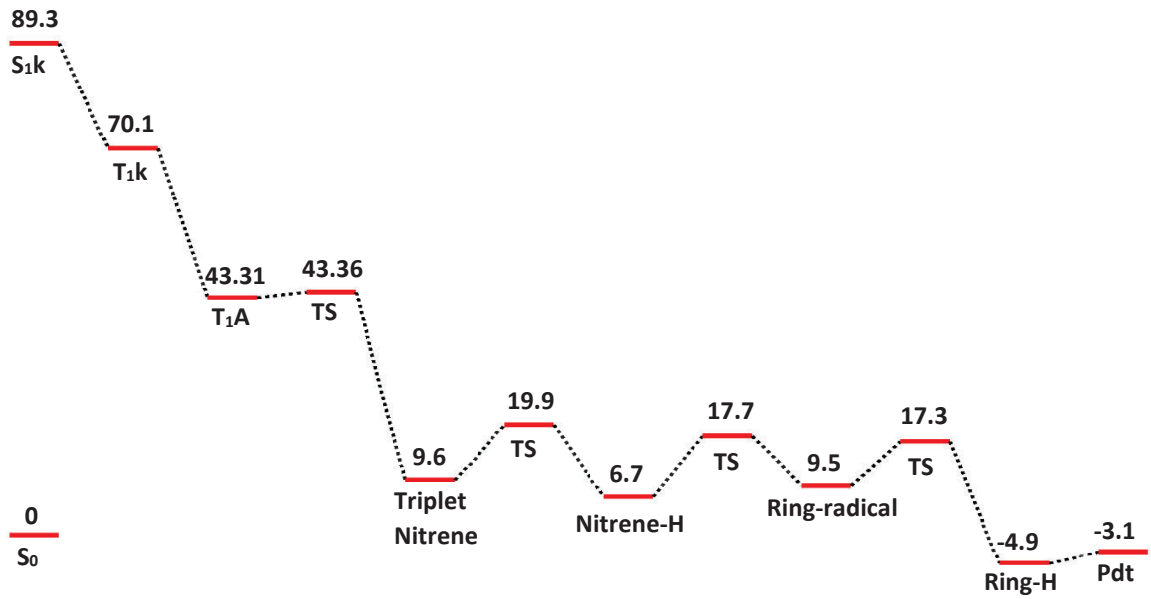

Figure 21. Calculated stationary points on the singlet and triplet energy surfaces of 1a. Calculated energies are in Kcal mol^{-1}.

TD-DFT calculation of the optimized structure of **1a** places the energies of $\mathbf{S_{1K}}$ and $\mathbf{T_{1K}}$ at 89.3 Kcal mol^{-1} and 70.1 Kcal mol^{-1} respectively above its S_0. Optimized structure of $\mathbf{T_{1A}}$ of **1a** is located at 43.3 kcal mol^{-1} above its S_0. We calculated the transition state barrier for alkyl nitrene **1aN** formation from $\mathbf{T_{1A}}$ **of 1a** and found that it is 0.05 kcal mol^{-1}. The optimized structure of triplet alkyl nitrene **1aN** located at 9.6 kcal mol^{-1} above the S_0 of **1a**.

We propose that alkyl nitrene **1aN** abstracts a H atom from the TTMSS and forms the iminyl radical **4**. The calculated transition state barrier for the H atom abstraction from TTMSS is 10.3 kcal mol^{-1} depicting that the process may be feasible. The optimized structure of iminyl radical **4** located 6.7 kcal mol^{-1} above its S_0 of **1a**. We also calculated the transition state barrier for the intramolecular cyclization of iminyl radical **4** which is 11 kcal mol^{-1}. The optimized structure of radical **5** is located 9.5 kcal mol^{-1} above the S_0 of **1a**. The calculated transition barrier for the hydrogen atom abstraction by the oxygen atom of radical **5** from TTMSS is 7.8 kcal mol^{-1} depicting the process maybe feasible. The optimized structure of radical **6** and the photoproduct **2a** located 4.9 kcal mol^{-1} and 3.1 kcal mol^{-1} below the S_0 of **1a**.

II. Mechanism for the formation of 2b from 1b

To support the mechanism in **Error! Reference source not found.**, the stationary points on the s inglet and triplet surface of **1a** were calculated (**Error! Reference source not found.**) using *Gaussian16* at the B3LYP level of theory and with the 6-31+G (d) basis set[14,15,16]

Optimization of the singlet ketone $\mathbf{S_1k}$ and triplet ketone $\mathbf{T_1k}$ places its energy at 86.4 Kcal mol^{-1} and 70.4 Kcal mol^{-1} respectively above its S_0. Optimized triplet azide $\mathbf{T_1A}$ located at 43.39 kcal mol^{-1} above its S_0. We calculated the transition state barrier for nitrene **3** formation from $\mathbf{T_1A}$ and it is 0.06 kcal mol^{-1}. The optimized triplet nitrene 3b located at 9.9 kcal mol^{-1} above its S_0.

The nitrene **3** abstracts a H atom from the TTMSS and forms the iminyl radical **4b**. The transition state barrier for the H atom abstraction from TTMSS is 9.8 kcal mol^{-1} depicting strong

feasibility of the process. The optimized iminyl radical **4b** located 6.7 kcal mol^{-1} above its S_0. We also calculated the transition state barrier for the intramolecular cyclization of iminyl radical **4b** which is 9.3 kcal mol^{-1}. The optimized ring radical **5b** is located 7.2 kcal mol^{-1} above its S_0. The calculated transition barrier for the hydrogen atom abstraction by the oxygen atom of radical **5b** from TTMSS is 7.1 kcal mol^{-1} depicting strong feasibility of the process. The optimized ring **6b** and the photoproduct **2b** located -6.0 kcal mol^{-1} and -4.3 kcal mol^{-1} below its S_0.

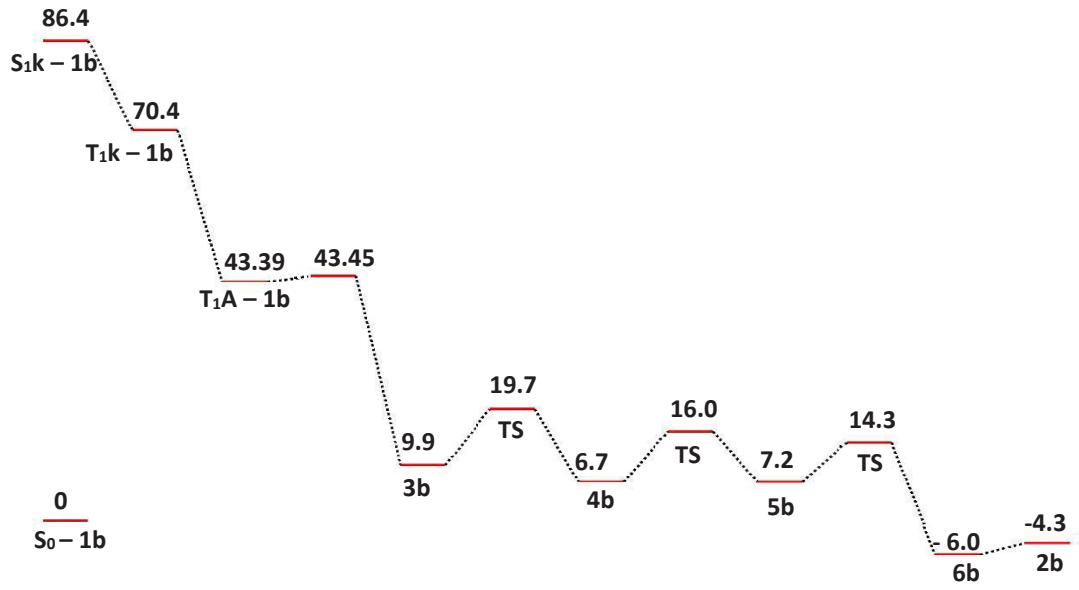

Figure 22. Calculated stationary points on the singlet and triplet energy surfaces of 1a. Calculated energies are in Kcal mol^{-1}.

4. Laser flash photolysis

1. 1a

We use laser flash photolysis (Yag laser (266 nm, 4000 ns) to determine the excited states and intermediates responsible for the formation of **2a**. Laser flash photolysis of **1a** in argon-saturated acetonitrile resulted in a broad transient absorption with λ_{max} at 390 nm (Figure 6).'

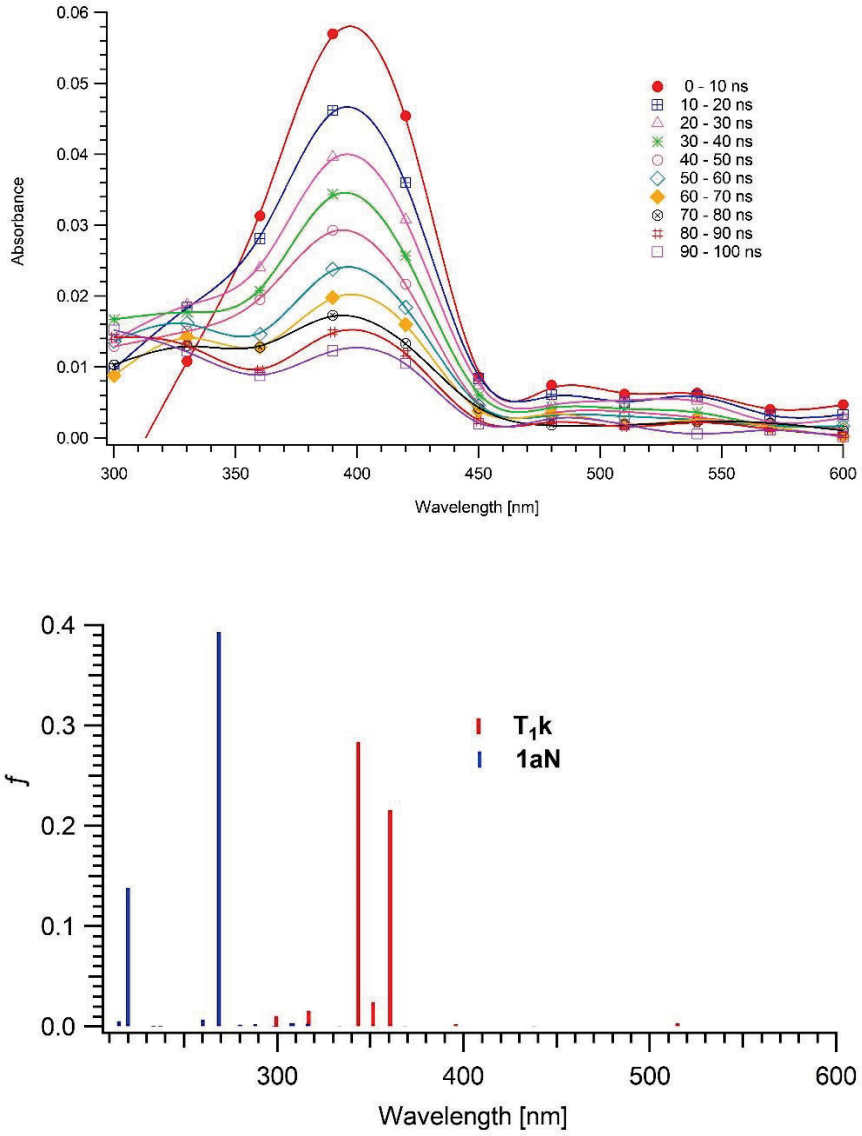

Figure 23. a) Transient UV obtained by laser flash photolysis of 1a and b) the TD-DFT calculated UVs of T_{1K} of **1a**, alkyl nitrene **1aN**.

Comparison of the calculated TD-DFT UV absorption with the obtained transient UV absorption spectra clearly indicates that the transient absorption is due to T_{1K} of **1a** and the triplet alkyl nitrene **1aN**. The TD-DFT calculated UV of T_{1K} of **1a** shows strong absorption at wavelength at 300 nm (*f* = 0.011), 317 nm (*f* = 0.016), 343 nm (*f* = 0.284), 352 nm (*f* = 0.024) and 360 nm *f* = (0.215). The calculated UV of the triplet alkyl nitrene **1aN** shows the strong absorptions at 220 nm (*f* = 0.1385), 269 nm (*f* = 0.3932), 307 nm (*f* = 0.035), 308 nm (*f* = 0.036), and 316 nm (*f* = 0.028).

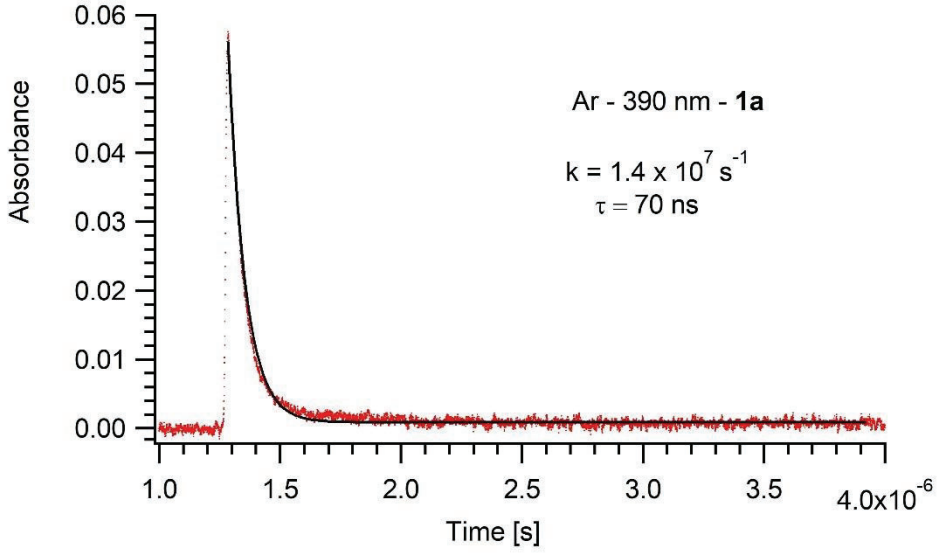

Figure 24. Kinetic traces at 390 nm are obtained in argon-saturated acetonitrile by doing laser flash photolysis of **1a** resulting in the decay of **T_{1K}** of **1a.**

Analysis of the kinetics in argon saturated acetonitrile at 390 nm (Figure 7) shows that at shorter timescales, the decay is best fitted as a mono exponential function to yield a rate constant of 1.43×10^7 s^{-1} (τ = 70 ns). Based on the calculated UV we attribute this decay to T_{1K} of

1a. In addition to this, a decay was obtained at 320 nm (Figure 8) with a rate constant of 2.15 × 10^6 s^{-1} (τ = 465 ns) and it has not been assigned to any particular intermediate but can be assigned to the radicals formed in the reaction.

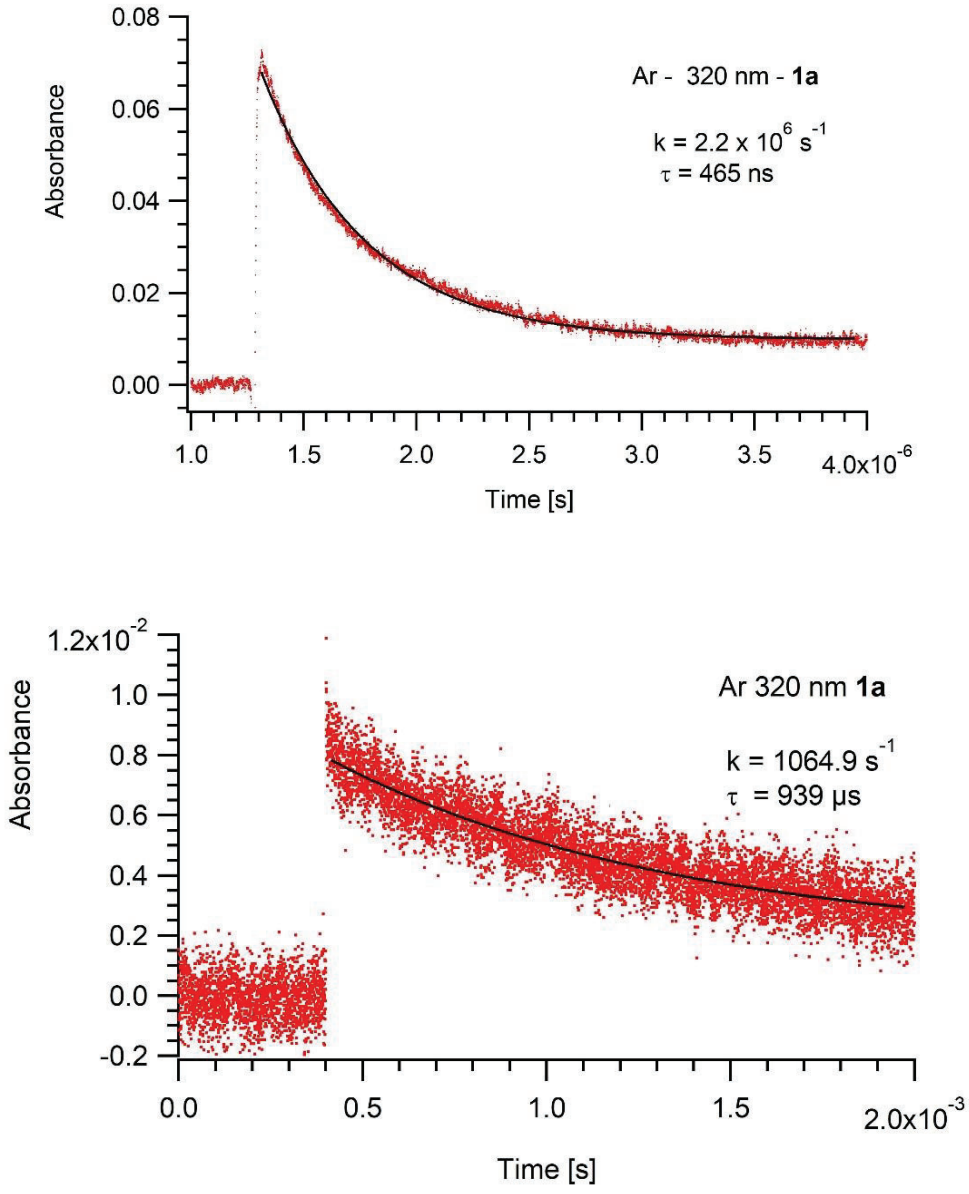

Figure 25. Kinetic traces obtained from doing laser flash photolysis of **1a** in argon saturated acetonitrile at 320 nm a) 4000 ns and b) 2 ms timescales**.**

2. 1b

Laser flash photolysis of **1b** in argon-saturated acetonitrile resulted in a transient absorption with λ_{max} at 320 nm (Figure 9).' Comparison of the calculated TD-DFT UV absorption with the obtained transient UV absorption spectra clearly indicates that the transient absorption is due to T_{1K} of **1b** and the triplet alkyl nitrene **1bN**. The calculated UV of the triplet ketone shows strong absorption at wavelength 292 nm (*f* = 0.254), 298 nm (*f* = 0.034), 335 nm (*f* = 0.004), and 340 nm (*f* = 0.002). The calculated UV of the triplet alkyl nitrene **1bN** shows strong absorption at wavelength 262 nm (*f* = 0.0205), 265 nm (*f* = 0.0086), 266 nm (*f* = 0.3466), 276 nm (*f* = 0.0316), 304 nm (*f* = 0.0046) and 311 nm (*f* = 0.033).

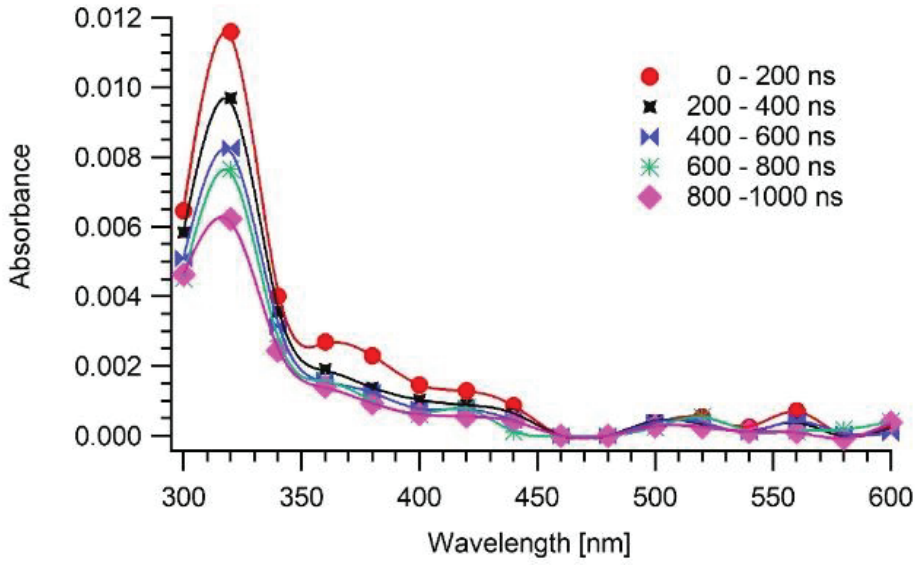

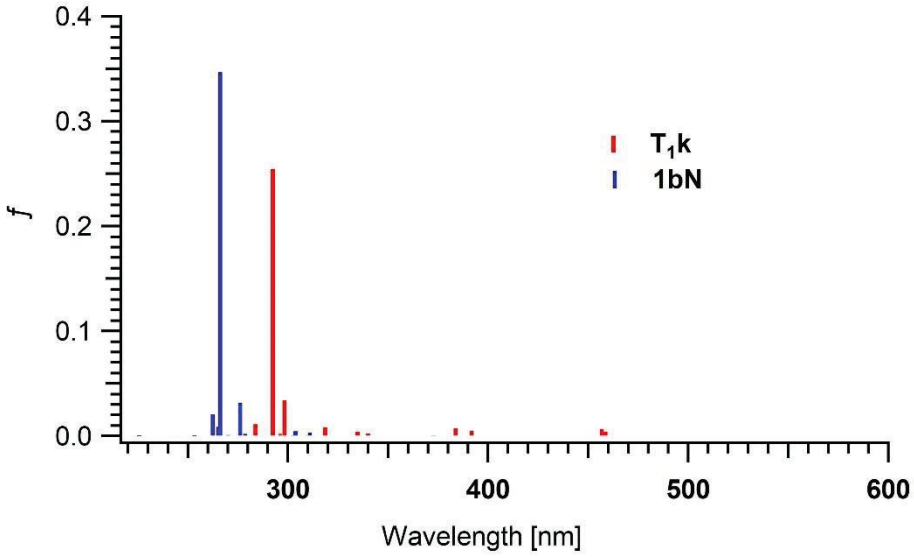

Figure 26. a) Transient UV absorption spectra obtained by laser flash photolysis of 1b and b) the TD-DFT calculated UV absorption spectra of T_1k of **1b**, and alkyl nitrene **1bN**.

Analysis of the kinetics in argon saturated acetonitrile at 320 nm (Figure 27) shows that at shorter timescales, the decay is best fitted as a mono exponential function to yield a rate constant of $2.0126 \times 10^6\ s^{-1}$ (τ = 497 ns). Based on the calculated UV, the shorter timescale decay is attributed to the triplet ketone T_{1k} and to some other radicals formed in the reaction. At longer timescales, the decay is best fitted as a mono exponential function to yield a rate constant of $1659.8\ S^{-1}$ (τ = 602 μs). The longer timescale decay is attribute to the triplet alkyl nitrene **1bN**.

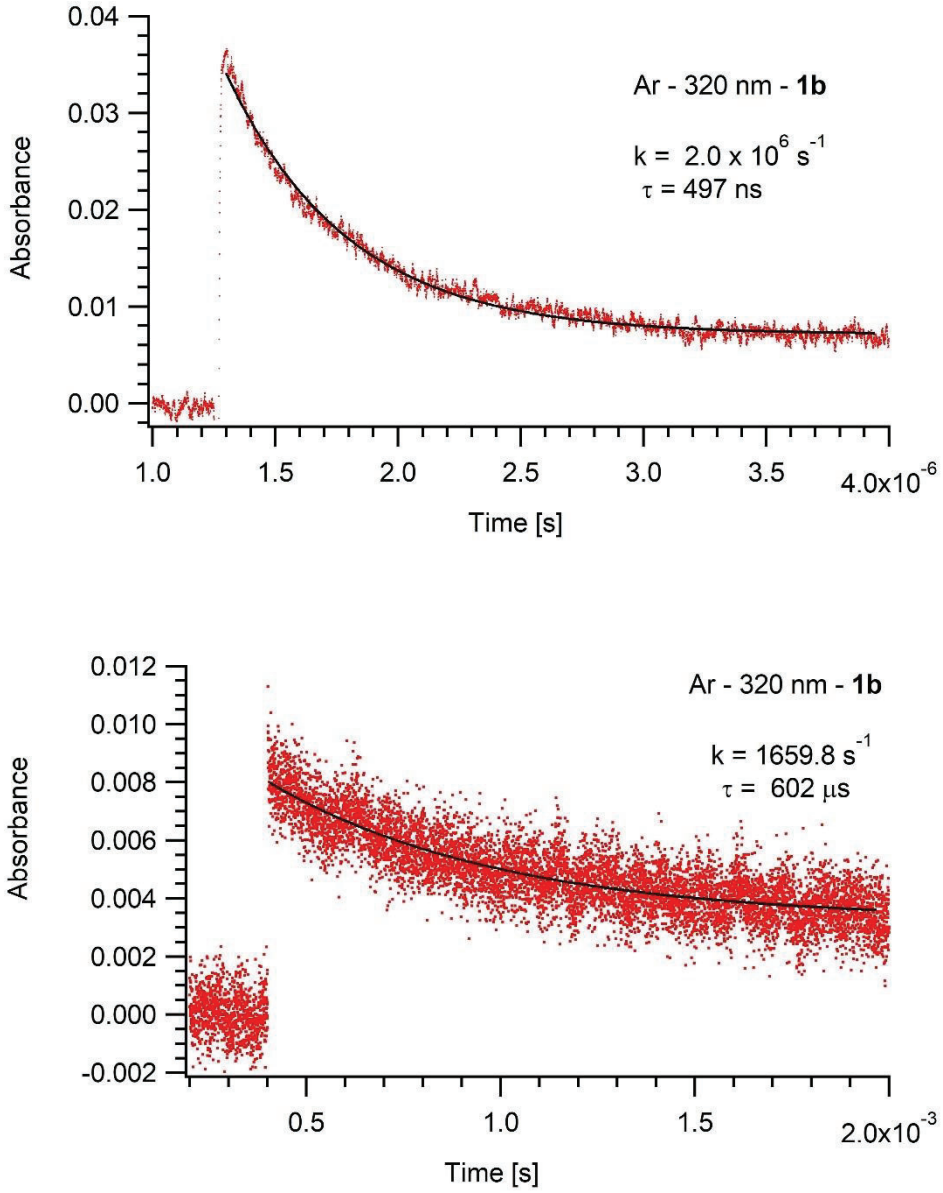

Figure 27. Kinetic traces are obtained in argon saturated acetonitrile of **1b** at 320 nm resulting in the decay of a) $\mathbf{T_1k}$ at shorter time scale and triplet nitrene b) **1bN** at longer time scale.

5. Quenching studies of 1a and 1b with TTMSS and Isoprene

I. Quenching studies of **1a**

To support our proposed mechanism that the H atom abstraction by the triplet nitrene leads to the formation of the heterocyclic product, we performed the quenching studies of **1a** at 390 nm and 320 nm with Isoprene and TTMSS [Tris(trimethylsilyl)silane]. The quenching studies with TTMSS at 390 nm showed that the lifetime of the triplet ketone is not affected by the increasing concentration of the quencher (Fig 11). The control studies of quenching with isoprene showed the reduction in lifetime of the triplet ketone with the increasing concentration of the quencher. The quenching studies at 390 nm confirms that it is not the triplet ketone but the triplet nitrene which absorbs the H atom and leads to the formation of the photoproduct **2a**.

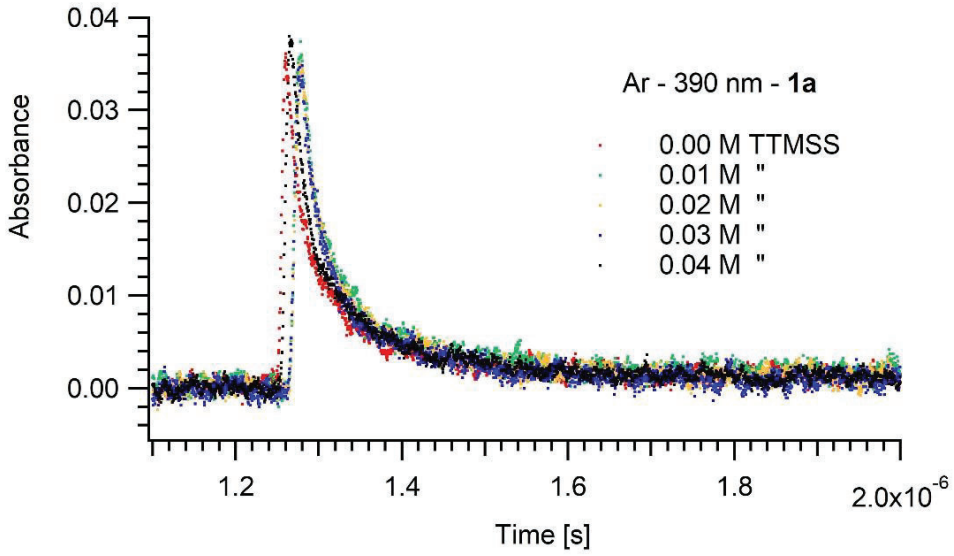

Figure 28. 390 nm kinetic traces of argon saturated acetonitrile solution of 1a with the increasing concentration of TTMSS

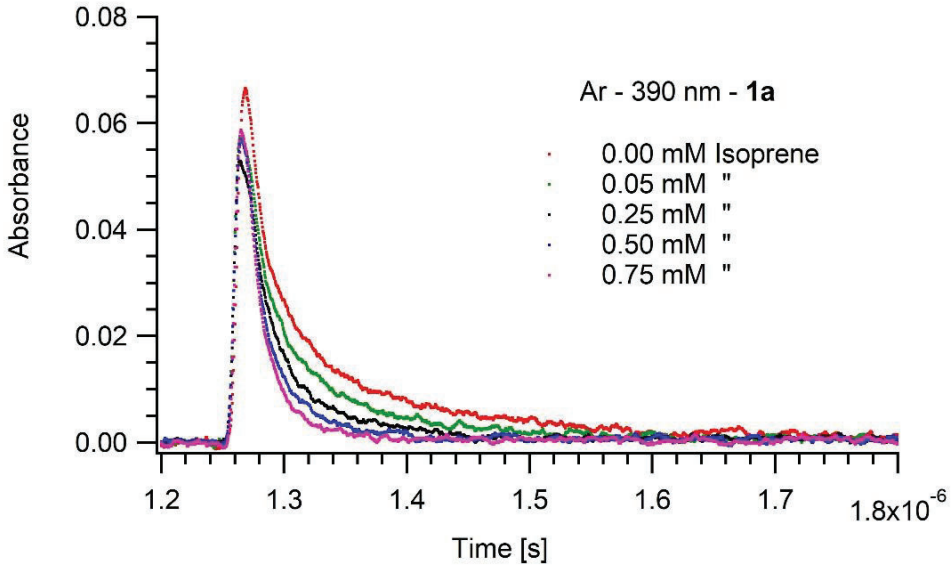

Figure 29. 390 nm kinetic traces of argon saturated acetonitrile solution of 1a with the increasing concentration of Isoprene

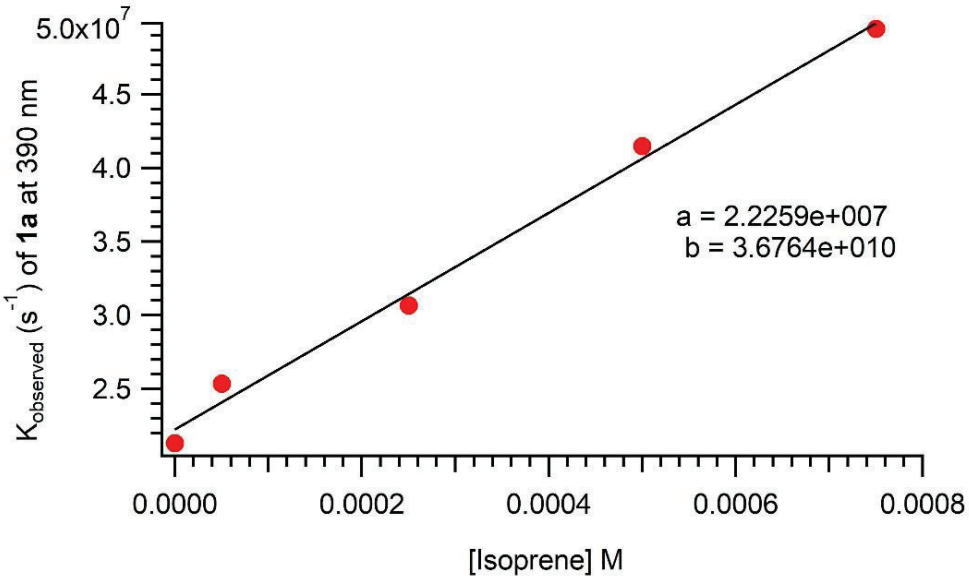

Figure 30. Plot of Kobs at 390 nm of 1a Vs Concentration of Isoprene

But the results obtained for the quenching studies at 320 nm is different than what we observed at 390 nm. The lifetime of the intermediate that we observed at 320 nm which is the ketyl radical is reduced with the increasing concentration of both TTMSS and Isoprene.

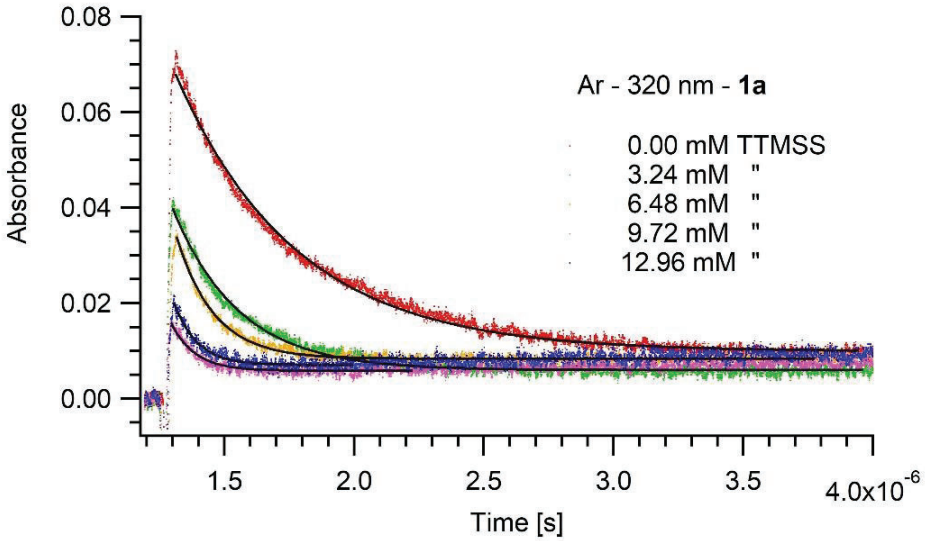

Figure 31. 320 nm kinetic traces of argon saturated acetonitrile solution of 1a with the increasing concentration of TTMSS

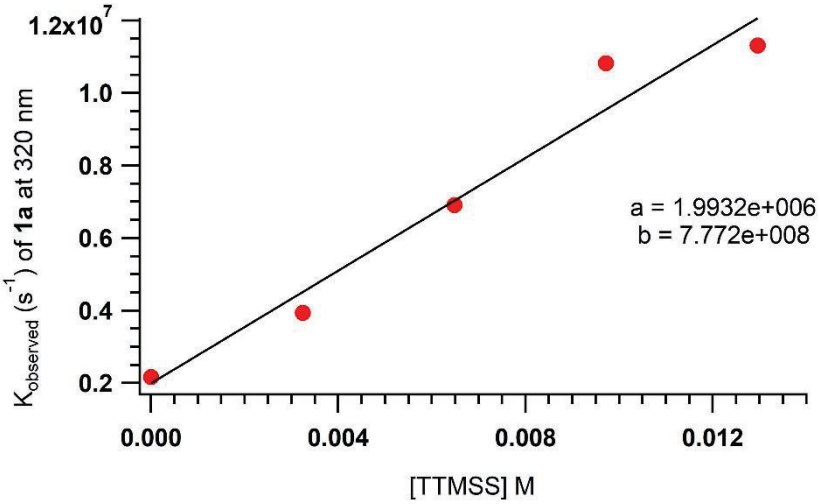

Figure 32. Plot of Kobs at 320 nm of 1a Vs Concentration of TTMSS

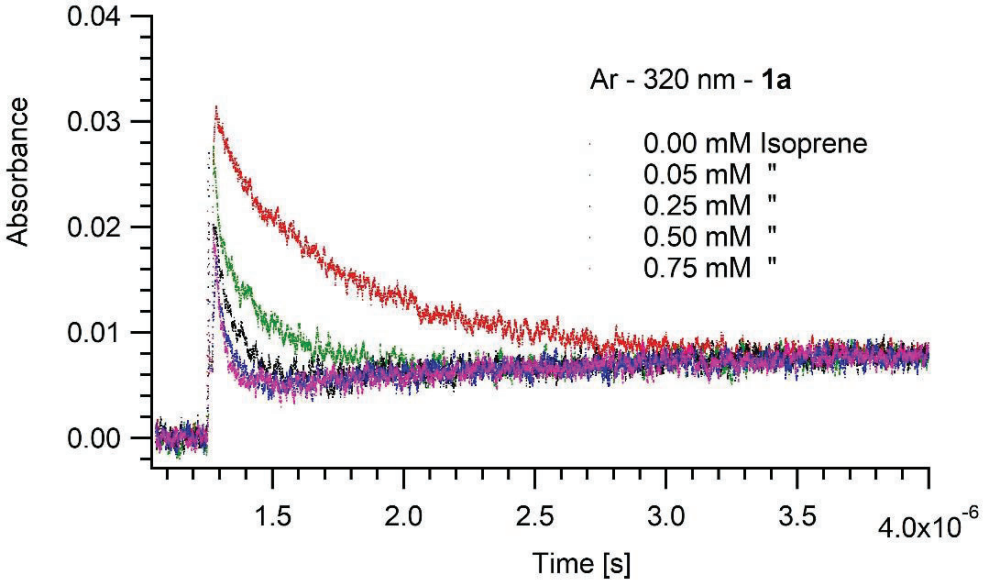

Figure 33. 320 nm kinetic traces of argon saturated acetonitrile solution of 1a with the increasing concentration of Isoprene

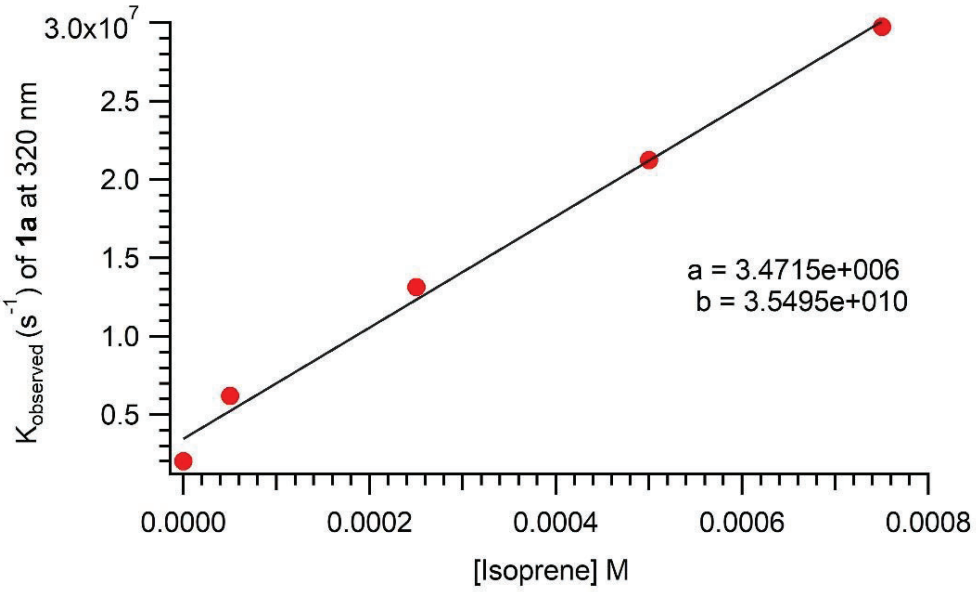

Figure 34. Plot of Kobs at 320 nm of 1a Vs Concentration of Isoprene

II. Quenching studies of **1b**

we performed the quenching studies of **1b** at 320 nm with Isoprene and TTMSS [Tris(trimethylsilyl)silane]. The quenching studies with TTMSS at 320 nm showed that the lifetime of the triplet ketone is reduced with the increasing concentration of the quencher (Fig 11). The control studies of quenching with isoprene also showed the reduction in lifetime of the triplet ketone. The quenching studies of **1b** at 320 nm shows that the triplet ketone abstracts the H atom in the presence of a hydrogen donor which resulting in the reduction of the lifetime with the increasing concentration of TTMSS.

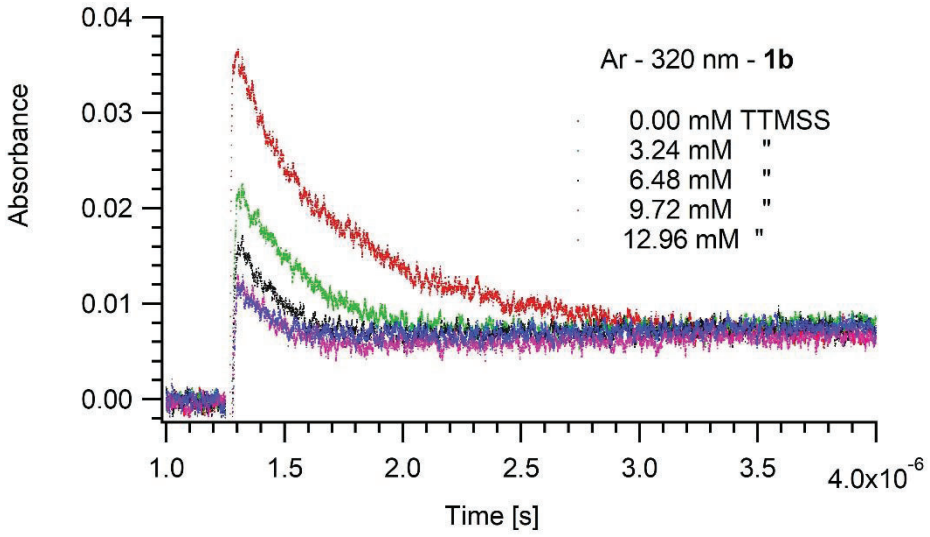

Figure 35. 320 nm kinetic traces of argon saturated acetonitrile solution of 1b with the increasing concentration of TTMSS

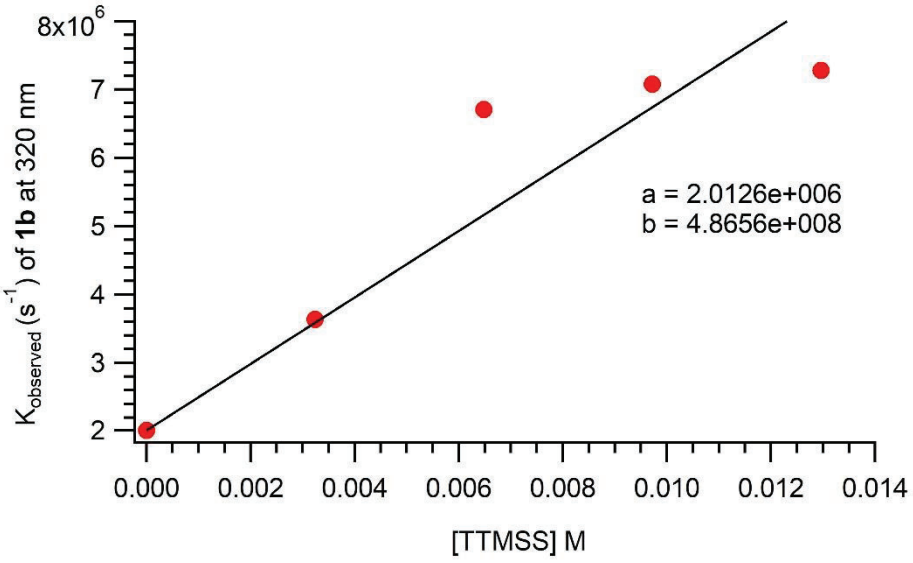

Figure 36. Plot of Kobs at 320 nm of 1b Vs Concentration of TTMSS

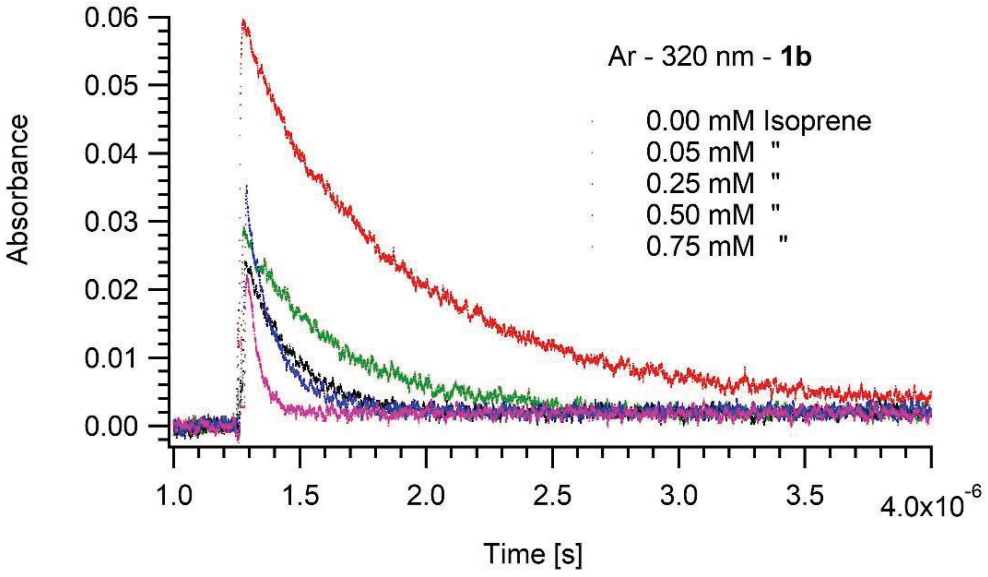

Figure 37. 320 nm kinetic traces of argon saturated acetonitrile solution of 1b with the increasing concentration of Isoprene

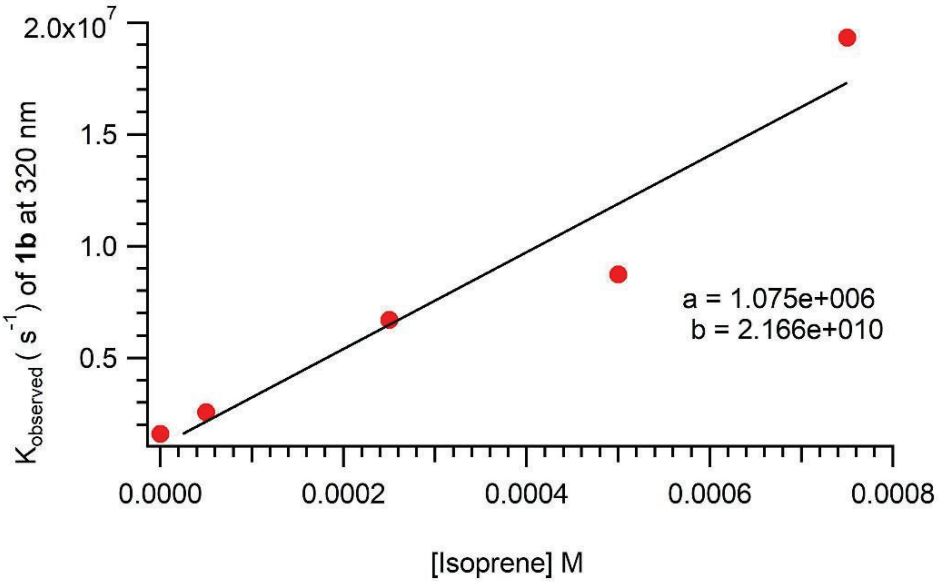

Figure 38. Plot of Kobs at 320 nm of 1b Vs Concentration of Isoprene

6. Phosphorescence

The phosphorescence spectrum of **1a** was obtained at 77 K by irradiating the glassy matrix of mTHF solution (0.15 M) of **1a** at 268 nm and the emission spectrum is collected from 300 nm to 800 nm. The emission band observed for azide **1a** does not have the well resolved vibrational band indicating that T_1k of **1b** has greater extent of (π, π*) character. The onset of the emission band at 390 nm was used to determine the [0,0] emission of T_K of **1**, which corresponds to an energy of 73.4 kcal/mol.

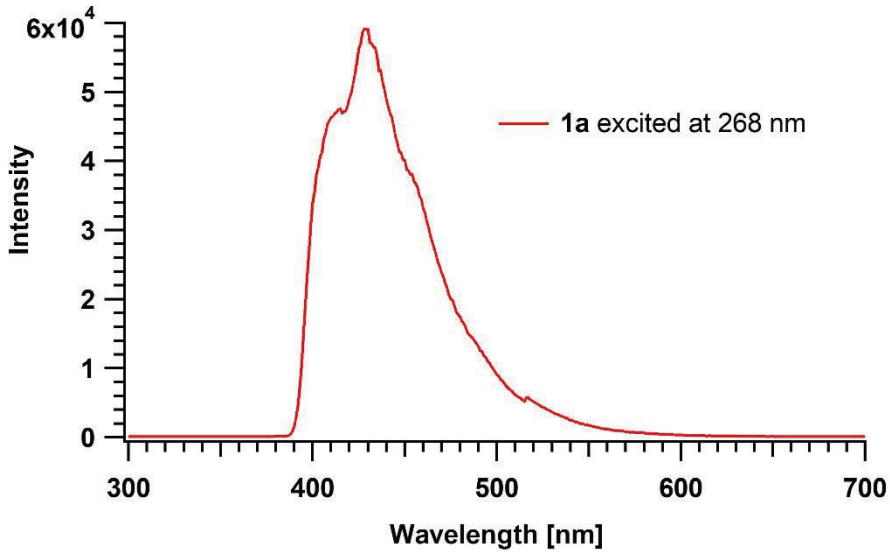

Figure 39. Phosphorescence obtained from irradiating 1a in frozen mTHF glassy matrix at 77 K.

The phosphorescence spectrum of **1b** was obtained at 77 K by irradiating the glassy matrix of mTHF solution (0.19 M) of **1b** at 250 nm. The emission band observed for azide **1b** does not have the well resolved vibrational bands typically observed for triplet ketones with (n, π*) configuration, indicating that T_1k of **1b** has greater extent of (π, π*) character. The onset of the

emission band at 390 nm was used to determine the [0,0] emission of T_1k of **1b**, which corresponds to an energy of 73.4 kcal/mol.

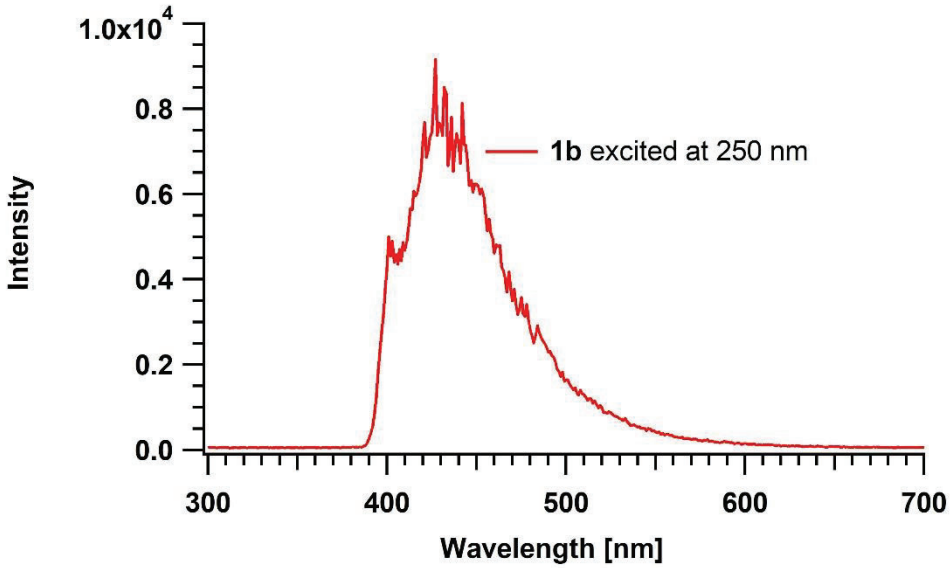

Figure 40. Phosphorescence obtained from irradiating **1b** in frozen mTHF glassy matrix at 77 K.

7. Cryogenic matrix analysis

Solution of azide **1a** (1.5 µM) was prepared using mTHF solvent and the sample was loaded in liquid N_2 at 77 K to form the glassy matrix. The glassy matrix of compound **1a** was Irradiated using Xenon lamp and the absorption spectrum was collected between 200nm to 800nm. The irradiation resulted in new broad absorption band which has two isosbestic points at 232 nm and 291 nm, evidently due to the photobleaching occurred because of high ground state absorption of **1a** between 230 nm and 292 nm.

The absorption band has λ_{max} at 228 nm, and a small weak absorption with the λ_{max} at 294 nm. The intensity of these bands was increased slowly with the continuous irradiation of the glassy matrix. Comparison of absorption spectrum measured at 77 K with the calculated UV/Vis spectrum of triplet nitrene of **1a** shows good agreement hence we assign the UV/Vis spectrum obtained at 77 K in mTHF matrix, to the corresponding triplet nitrene of **1a**.

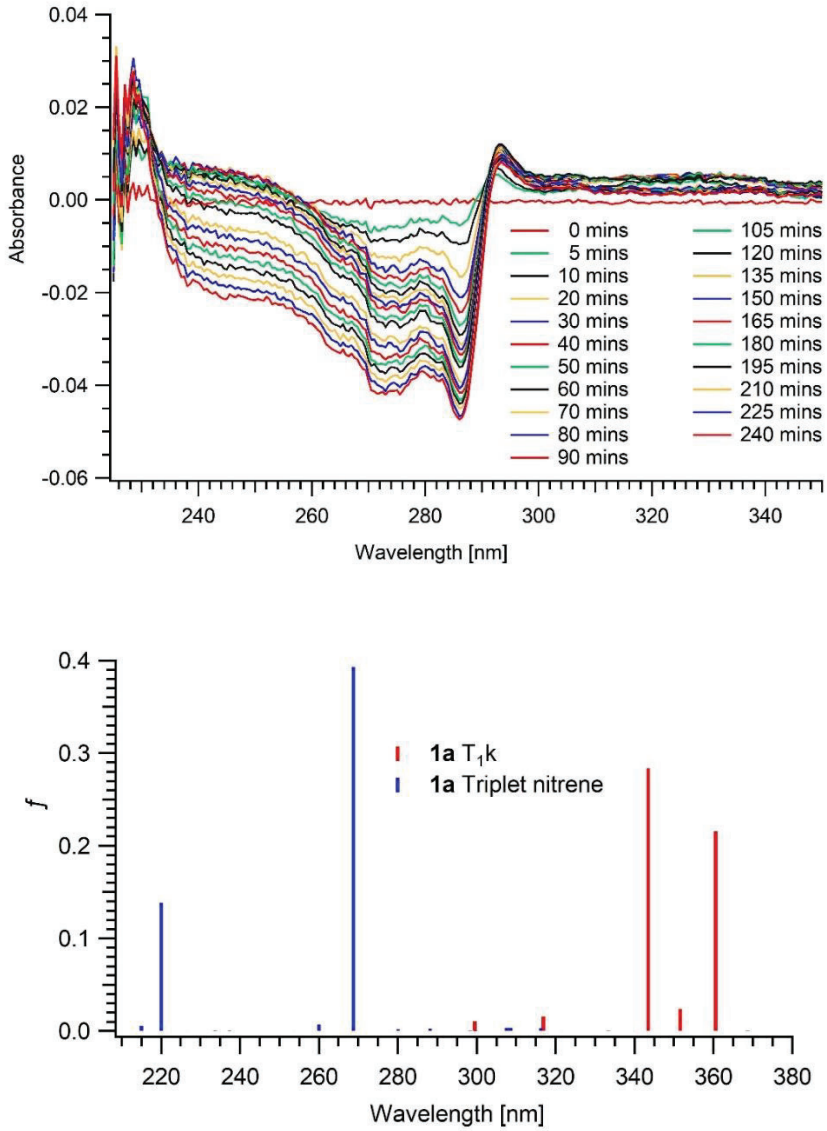

Figure 41. a) Cryogenic UV obtained for 77 K mTHF matrix of **1a** and b) the TD-DFT calculated UV absorption of T_1k and 1aN**.**

Similarly, the azide **1b** was also prepared by dissolving it in mTHF and the sample (2.6 µM) was then loaded in cryogenic unit filled with liquid N_2 which resulted in the formation of the glassy matrix of **1b**. The irradiation of the glassy matrix of **1b** using Xenon lamp resulted in the growth of weak absorption bands in the UV between 274-280 nm and a broad absorption between 300-350 nm which is centered around 322 nm.

We also noticed the depletion in absorbance between 230-274 nm. Comparison of absorption spectrum measured at 77 K and calculated TD-DFT UV absorption triplet alky nitrene of 1bN shows good agreement hence we assign the UV/Vis spectrum obtained at 77 K in mTHF matrix, to the triplet nitrene of 1bN.

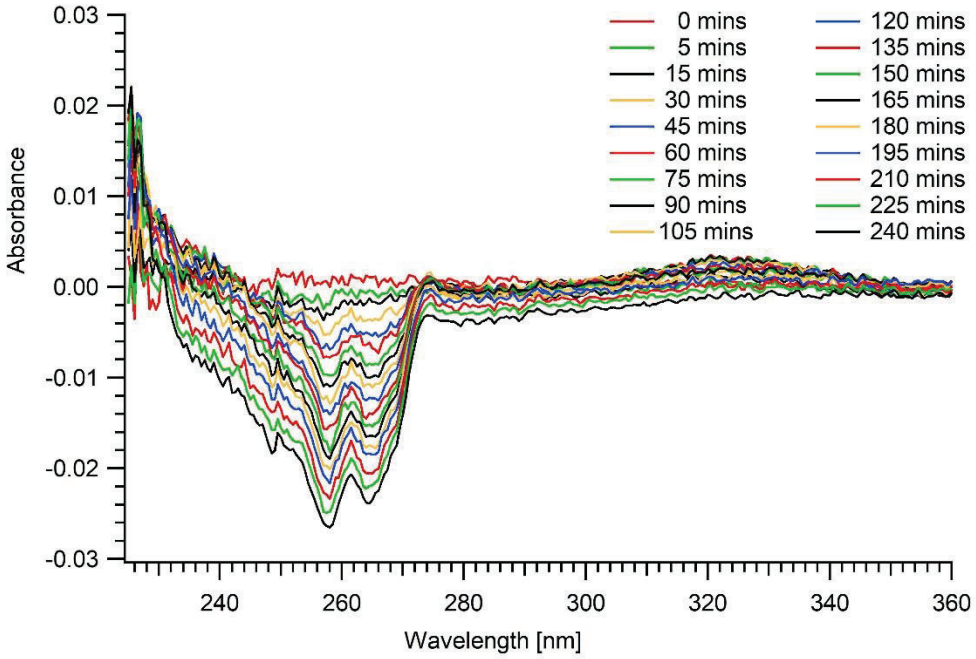

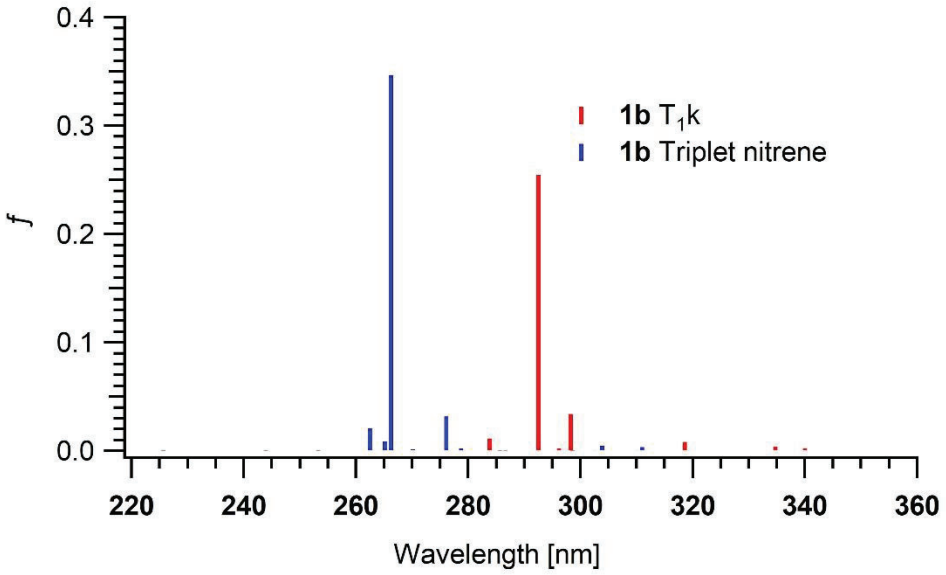

Figure 42. Cryogenic UV and the calculated UV of **1b**

8. Control experiment with TTMSS in the absence of irradiation

Finally, to confirm that the H abstraction by the triplet nitrene which only leads to the formation of the photoproduct we did a small control experiment. Argon saturated solution of methoxy gamma azide (15.4 mM) was taken in two test tubes and added with TTMSS and one was kept in dark for an hour and the other one was irradiated at 340 nm for an hour. Proton NMR of the two reaction mixtures were taken and analyzed. The formation of the heterocyclic product was observed in the one which was irradiated at 340 nm and no product formation is seen in the one which kept under dark. This control experiment clearly confirms that the TTMSS reacts with the triplet nitrene and leads to the formation of the photoproduct.

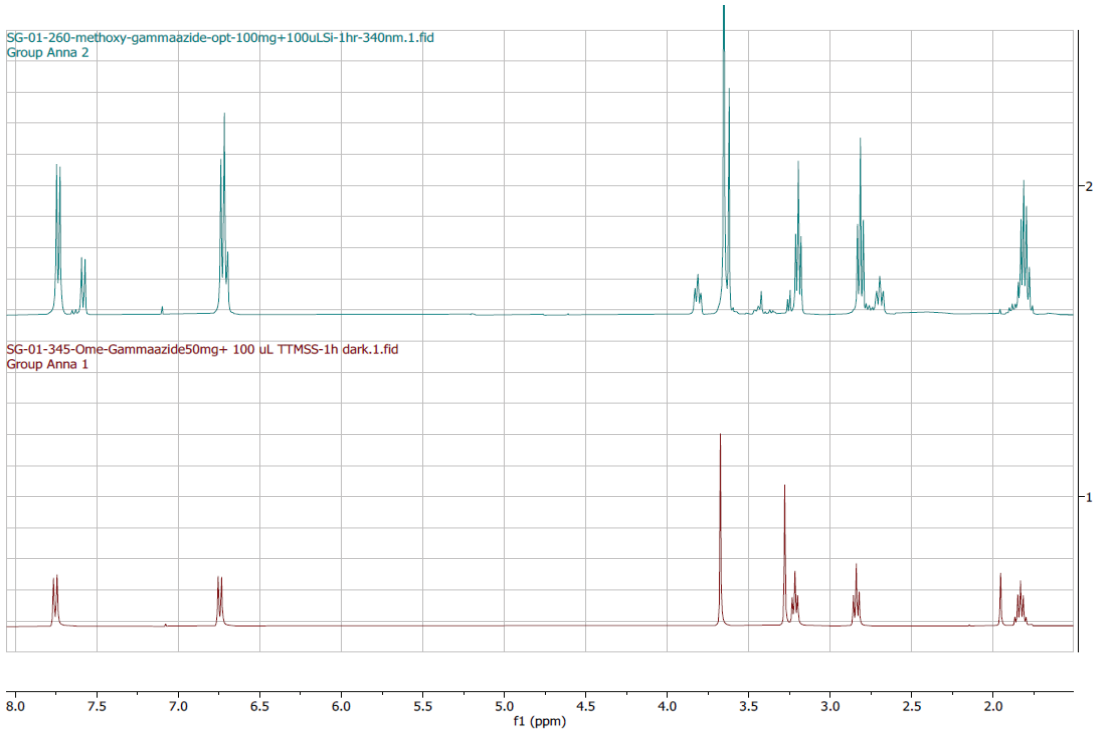

Figure 43. 1H-NMR spectra of **1a** after irradiation at 340 nm for 1 h with and without TTMSS

9. Discussion

TD-DFT calculations shows that in methoxy gamma azide the lowest excited triplet ketone has the (π-π*) configuration. Thus, the intramolecular sensitization is favored and resulting in the formation of photoproduct A in much higher yields when compared to B and C. However, there is a small percentage of formation of B and C is observed. This is due to the smaller energy gap between the T_1k and T_2k of the methoxy azide, and thus they are degenerated. So, in addition to the T_1k it is possible to get the reactivity from the T_2k state as well.

Whereas in bromo gamma azide the lowest triplet ketone has the (n-π*) configuration according to the TD-DFT calculations, thus the gamma hydrogen abstraction is preferred over

intramolecular sensitization and resulting in the formation of the photoproducts **B** and **C** in much higher yields and smaller amounts of the formation of photoproduct **A** also observed. The TD-DFT calculated energy values of T_1K and T_2K are close enough and thus these two energy states are degenerated and resulting in the reactivity from both states. But in both cases the major reactivity is from the lowest T_1K.

In the presence of TTMSS we see the selective reactivity from the ketone with the (π-π*) configuration of both the azides regardless of the lowest energy ketone. So, we believe that the TTMSS forms a complex with the triplet excited ketone upon irradiation. The complexation between the TTMSS and the excited ketone should stabilize the (π-π*) state of the ketone and thus lowers its energy. This stabilization resulting in the increase of the energy gap between the T_1K and T_2K and thus the two states can no longer be degenerated thus resulting in the selective reaction from the (π-π*) state. So, in the presence of TTMSS the intramolecular sensitization is preferred over gamma-H atom abstraction in gamma azides.

According to the kinetics obtained for gamma methoxy azide, the triplet ketone of methoxy gamma azide has the lifetime of 70 ns and the triplet alkyl nitrene has the lifetime of 939 μs. The triplet alkyl nitrene of bromo azide 1bN has the lifetime of 602 μs.

The cryogenic matrix UV irradiation of both the azides resulted in a weaker absorption bands which indicates that the triplet alkyl nitrene of both theses azides are not stable and highly reactive.

10. Experimental Procedure

I. Synthesis of 4-azido-1-(4-methoxyphenyl) butanone (1a)

3-Azido-1-(4-methoxyphenyl) propanone (**1a**) was synthesized following a procedure similar to a method described by Singh et al. The commercially available 3-chloro-1-(4-methoxyphenyl) propanone (1.50 g, 7.08 mmol, 1.0 equiv) was dissolved in DMF (20 mL) and solid NaN3 (1.84 g, 28.32 mmol, 4.0 equiv) was added and heated up to 50 °C and stirred for overnight. After completion of the reaction the reaction mixture was diluted with dichloromethane (150 mL) and washed with water (120 mL). The organic layer was separated and dried with Na_2SO4 and concentrated in vacuo which resulted in (1.41 g, 6.44 mmol, 91 % yield) of pale-yellow color crude product. The crude product was purified via column chromatography using eluent of ethyl acetate-hexane (2:8) solvent system. The column separation of the crude product yielded the pure **1a** as a white color solid (1.17 g, 5.34 mmol 83 % column yield). Similar procedure was followed for the synthesis of bromo substituted 3-azido-1-(4-phenyl) propanone (**1b**).

1a: ^{1}H NMR (400 MHz, Chloroform-*d*) δ 7.95 (d, *J* = 8.5 Hz, 1H), 6.94 (d, *J* = 8.5 Hz, 1H), 3.87 (s, 1H), 3.41 (t, *J* = 6.6 Hz, 1H), 3.03 (t, *J* = 7.1 Hz, 1H), 2.04 (q, *J* = 6.8 Hz, 1H).
^{13}C NMR (101 MHz, $CDCl_3$) δ 197.5, 163.6, 130.3, 129.8, 113.8, 77.4, 77.1, 76.7, 55.5, 51.0, 34.8, 23.5.

1b: ^{1}H NMR (400 MHz, Chloroform-*d*) δ 7.82 (d, *J* = 8.2 Hz, 1H), 7.61 (d, *J* = 8.2 Hz, 1H), 3.42 (t, *J* = 6.5 Hz, 1H), 3.05 (t, *J* = 7.0 Hz, 1H), 2.03 (p, *J* = 6.8 Hz, 1H).
^{13}C NMR (101 MHz, $CDCl_3$) δ 197.9, 135.4, 132.0, 129.5, 128.4, 77.4, 77.1, 76.8, 50.8, 35.1, 23.2, 11.9.

II. Product studies without TTMSS

1a)

A solution of **1a** was prepared by dissolving (30.2 mg, 0.138 mmol) of **1a** in 15 mL MeOH in a Pyrex test tube. The resulting solution was degassed by bubbling argon gas through the solution for 10 minutes, sealed with a rubber cap and parafilm. The argon purged solution was then irradiated for 18 h using 340 nm LED. The irradiated solution was air dried, and the ^{1}H NMR analysis of the resulting crude mixture showed the formation of **2a**, acetophenone, and the unreacted starting material **1a** in the ratio of 1.0: 0.48: 0.12. The integration was based on the NMR signals at 4.04 ppm for product **2a**, 3.64 ppm for acetophenone, and 3.42 ppm for **1a**. The reaction was not particularly selective and residual nmr signals show that additional products were formed, but in lesser yields than product **2a** and acetophenone.

^{1}H NMR (400 MHz, $CDCl_3$) δ 7.95 (ddd, *J* = 8.8, 6.9, 1.6 Hz, 1H), 7.88 – 7.84 (m, 0H), 7.83 – 7.78 (m, 1H), 6.94 (ddt, *J* = 9.1, 7.0, 2.6 Hz, 3H), 5.48 – 5.37 (m, 0H), 4.04 (tt, *J* = 7.2, 2.0 Hz, 1H), 3.94 – 3.79 (m, 5H), 3.64 (s, 0H), 3.42 (t, *J* = 6.6 Hz, 0H), 3.04 (td, *J* = 7.1, 4.5 Hz, 1H), 2.93 (ddd, *J* = 10.3, 5.4, 2.0 Hz, 1H), 2.41 – 2.30 (m, 0H), 2.25 (p, *J* = 7.1 Hz, 0H), 2.13 – 1.98 (m, 1H).

1b)

A solution of **1b** was prepared by dissolving (30 mL, 0.171 mmol) of **1b** in 15 mL MeOH in a Pyrex test tube. The resulting solution was degassed by bubbling argon gas through the solution for 10 minutes, sealed with a rubber cap and parafilm. The argon purged solution was then

irradiated for 18 h using 340 nm LED. The irradiated solution was air dried and ^{1}H NMR analysis of the resulting crude mixture showed the formation of **2b**, the H-abstracted product, acetophenone, and the unreacted starting material **1b** in the ratio of 1.0: 0.29: 0.08: 0.19. The integration was based on the NMR signals at 4.04 ppm for product **2a**, 3.64 ppm for acetophenone, and 3.42 ppm for **1a**. The reaction was not particularly selective and residual nmr signals show that additional products were formed, but in lesser yields than product 2b, H-abstracted product and acetophenone.

^{1}H NMR (400 MHz, $CDCl_3$) δ 9.02 (s, 0H), 7.97 – 7.78 (m, 2H), 7.72 – 7.42 (m, 3H), 7.44 – 7.32 (m, 1H), 7.36 – 7.18 (m, 1H), 6.91 (q, *J* = 2.4 Hz, 0H), 6.55 (qd, *J* = 3.8, 1.6 Hz, 0H), 6.32 (dq, *J* = 5.9, 2.7 Hz, 0H), 4.84 (dd, *J* = 8.1, 4.9 Hz, 0H), 4.24 (t, *J* = 7.6 Hz, 0H), 4.14 (dddd, *J* = 10.9, 8.8, 5.4, 2.8 Hz, 1H), 3.92 (td, *J* = 7.2, 3.6 Hz, 0H), 3.51 (s, 0H), 3.47 (t, *J* = 6.6 Hz, 1H), 3.39 (dt, *J* = 7.4, 4.8 Hz, 0H), 3.21 – 3.03 (m, 2H), 2.97 (dt, *J* = 11.8, 6.9 Hz, 0H), 2.82 (td, *J* = 7.2, 4.3 Hz, 0H), 2.78 – 2.54 (m, 0H), 2.24 – 2.13 (m, 1H), 2.15 – 1.98 (m, 1H).

III. Product studies with TTMSS

a) Isolation of the photoproduct

A solution of **1a** was prepared by dissolving (300.4 mg, 1.37 mmol) of **1a** in 15 mL MeOH in a Pyrex test tube and mixed with tris(trimethylsilyl)silane-TTMSS (300 µL). The resulting solution was degassed by bubbling argon gas through the solution for 10 minutes, sealed with a rubber cap and parafilm. The solution was then irradiated for 20 h using 340 nm LED. The solution was air dried and ^{1}H NMR analysis of the resulting crude mixture showed complete decomposition of

1a and formation of a single major product **2a.** The crude was then purified on a silica column eluted with 10 % ethyl acetate in hexane to obtain (**2a**) as a pure white solid (211 mg, 1.21 mmol, 88 % yield). Similarly, the photoproduct **2b** was also isolated.

2-(4-methoxyphenyl)-1-pyrroline:

^{1}H NMR (400 MHz, $CDCl_3$) δ 7.80 (d, *J* = 8.8 Hz, 2H), 6.96 – 6.89 (m, 2H), 4.03 (td, *J* = 7.3, 1.9 Hz, 2H), 3.85 (s, 3H), 2.97 – 2.87 (m, 2H), 2.02 (p, *J* = 7.8 Hz, 2H) ppm.

^{13}C NMR (101 MHz, $CDCl_3$) δ 171.5, 161.3, 129.2, 127.5, 113.7, 77.3, 77.0, 76.7, 61.4, 55.3, 34.9, 22.8 ppm.

5-(4-bromophenyl)-3,4-dihydro-2H-pyrrole:

^{1}H NMR (400 MHz, $CDCl_3$) δ 7.71 (d, *J* = 8.5 Hz, 1H), 7.54 (d, *J* = 8.5 Hz, 1H), 4.06 (td, *J* = 7.3, 3.8 Hz, 1H), 2.96 – 2.86 (m, 1H), 2.04 (q, *J* = 7.8 Hz, 1H) ppm.

^{13}C NMR (101 MHz, $CDCl_3$) δ 172.3, 133.5, 131.6, 129.1, 124.8, 77.4, 77.0, 76.7, 61.7, 34.9, 22.7, ppm.

b) ^{1}H-NMR Monitoring of the photoreaction with time in the presence of TTMSS

Several batches of solution of **1a** were prepared in Pyrex test tube by dissolving 50 mg of **1a** in 15 mL of MeOH (15.4 mM) and each sample was added with 100 µL of Tris(trimethylsilyl)silane (TTMSS). The resulting solution was degassed by bubbling argon gas through the solution for 10 minutes, sealed with a rubber cap and parafilm. The solution was then irradiated using 340 nm LED and the irradiation was stopped after 1h, 2h, 3h,4h, and 6h for different batches and the resulting irradiated solution was dried and dissolved in deuterated CDCl3 and the ^{1}H-NMR

spectrum of each solution was analyzed. After 6 h of irradiation, ^{1}H-NMR spectra of the reaction mixture showed that **1a** was depleted completely and the photoproduct **2a** was formed selectively. Similarly, the photoreaction of **1b** was also monitored for different batches of MeOH solution (19 mM) in Pyrex test tube at different time intervals by irradiating the solution using 340 nm LED.

IV. Phosphorescence

mTHF solutions of **1a** (0.15 M) and **1b** (0.19 M) were prepared and cooled to 77 K and their phosphorescence spectra obtained using a Phosphorimeter, which has been described previously.[17] The samples were excited with 280 nm light and the emission spectra were recorded between 300 nm and 800 nm.

V. Laser flash photolysis

Yag laser (266 nm, 4000 ns) was used to acquire transient UV-Vis and corresponding kinetic traces.[10] Spectroscopic grade acetonitrile was used to prepare stock solutions of **1a**, and **1b** such that UV absorption of the solutions at 266 nm between 0.3 and 0.8. The stock solution of 250 mL was taken in a volumetric flask and flowed through the quartz cuvette continuously with the help of a peristaltic pump. Throughout the experiment, argon or oxygen was flowed continuously in the solution.

VI. Cryogenic UV

Cryogenic UV-Vis spectroscopy was performed using a conventional set up.[18] A stock solution of gamma azide **1a** (1.5 μM) and **1b** (2.6 μM) in anhydrous mTHF was prepared with a maximum absorbance at below 0.6. 2 mL of the corresponding sample was placed in a temperature resistant 10 mm X 10 mm cuvette and argon gas was purged through the solution for 2 mins and the cuvette was capped and sealed with a piece of Teflon tape. Then, the cuvette was inserted in a cryostat. Liquid nitrogen was poured into the cryostat until the temperature reached 77 K and glassy mTHF matrix was formed. UV-Vis spectra before irradiation was recorded as baseline in the JASCO V-750 UV-Vis spectrophotometer. The matrix was irradiated with Xenon lamp and difference spectra were recorded at different time intervals.

VII. Quantum Modelling

All geometries were optimized with density functional theory (DFT) using Gaussian16 [19] at the B3LYP level of theory with the 6-31+G(d) basis set.[14, 15] Energies of excited singlet and triplet states and UV-Vis spectra of optimized ground states were computed using TD-DFT.[20, 21] We analyzed the second derivative of the energy with respect to the internal coordinates to satisfy all transition states having one imaginary vibrational frequency. Intrinsic reaction coordinate (IRC) calculations verified the located transition states corresponded to the respective reactant and the products.[22, 23] The calculations were carried out at the Ohio Supercomputer.

11. References:

1. Bucher, G., *Photochemical Reactivity of Azides. In CRC Handbook of Organic Photochemistry and Photobiology*. 2nd ed ed.; Horspool, W., Lenci, F., Eds.; CRC Press: Boca Raton, FL, 2004; p 32.
2. Gritsan, N.; Platz, M., Photochemistry of Azides: The Azide/Nitrene Interface. 2010; pp 311-372.
3. Mandel, S. M.; Krause Bauer, J. A.; Gudmundsdottir, A. D., Photolysis of α-Azidoacetophenones: Trapping of Triplet Alkyl Nitrenes in Solution. *Organic Letters* **2001,** *3* (4), 523-526.
4. Singh, P. N. D.; Mandel, S. M.; Sankaranarayanan, J.; Muthukrishnan, S.; Chang, M.; Robinson, R. M.; Lahti, P. M.; Ault, B. S.; Gudmundsdóttir, A. D., Selective Formation of Triplet Alkyl Nitrenes from Photolysis of β-Azido-Propiophenone and Their Reactivity. *Journal of the American Chemical Society* **2007,** *129* (51), 16263-16272.
5. Mandel, S. M.; Singh, P. N. D.; Muthukrishnan, S.; Chang, M.; Krause, J. A.; Gudmundsdóttir, A. D., Solid-State Photolysis of α-Azidoacetophenones. *Organic Letters* **2006,** *8* (19), 4207-4210.
6. Klima, R. F.; Gudmundsdóttir, A. D., Intermolecular triplet-sensitized photolysis of alkyl azides: Trapping of triplet alkyl nitrenes. *Journal of Photochemistry and Photobiology A: Chemistry* **2004,** *162* (2), 239-247.
7. Klima, R. F.; Jadhav, A. V.; Singh, P. N. D.; Chang, M.; Vanos, C.; Sankaranarayanan, J.; Vu, M.; Ibrahim, N.; Ross, E.; McCloskey, S.; Murthy, R. S.; Krause, J. A.; Ault, B. S.; Gudmundsdóttir, A. D., Photoinduced C–N Bond Cleavage in 2-Azido-1,3-diphenyl-propan-1-one Derivatives: Photorelease of Hydrazoic Acid. *The Journal of Organic Chemistry* **2007,** *72* (17), 6372-6381.
8. Wagner, P. J., *In Rearrangements in Ground and Excited States*. Academic Press: : New York,, 1980; Vol. 42-3, p 381.
9. Ranaweera, R. A. A. U.; Zhao, Y.; Muthukrishnan, S.; Keller, C.; Gudmundsdottir, A. D., Competition Between Azido Cleavage and Triplet Nitrene Formation in Azidomethylacetophenones. *Australian Journal of Chemistry* **2010,** *63* (12), 1645-1655.
10. Muthukrishnan, S.; Sankaranarayanan, J.; Klima, R. F.; Pace, T. C. S.; Bohne, C.; Gudmundsdottir, A. D., Intramolecular H-Atom Abstraction in γ-Azido-Butyrophenones: Formation of 1,5 Ketyl Iminyl Radicals. *Organic Letters* **2009,** *11* (11), 2345-2348.
11. Sankaranarayanan, J.; Rajam, S.; Hadad, C. M.; Gudmundsdottir, A. D., The ability of triplet nitrenes to abstract hydrogen atoms. *Journal of Physical Organic Chemistry* **2010,** *23* (4), 370-375.
12. Muthukrishnan, S.; Mandel, S.; Hackett, J.; Singh, P.; Hadad, C.; Krause, J.; Gudmundsdóttir, A., Competition between α-Cleavage and Energy Transfer in α-Azidoacetophenones. *The Journal of organic chemistry* **2007,** *72*, 2757-68.
13. Wagner, P. J.; Kemppainen, A. E.; Schott, H. N., Effects of ring substituents on the type II photoreactions of phenyl ketones. How interactions between nearby excited triplets affect chemical reactivity. *Journal of the American Chemical Society* **1973,** *95* (17), 5604-5614.
14. Becke, A. D., Density-functional thermochemistry. III. The role of exact exchange. *The Journal of Chemical Physics* **1993,** *98* (7), 5648-5652.
15. Parr, R. G.; Yang, W., *Density-functional theory of atoms and molecules*. Oxford University Press: Oxford, 1994.
16. Stratmann, R. E.; Scuseria, G. E.; Frisch, M. J., An efficient implementation of time-dependent density-functional theory for the calculation of excitation energies of large molecules. *The Journal of Chemical Physics* **1998,** *109* (19), 8218-8224.

17. Ranaweera, R. A. A. U.; Scott, T.; Li, Q.; Rajam, S.; Duncan, A.; Li, R.; Evans, A.; Bohne, C.; Toscano, J. P.; Ault, B. S.; Gudmundsdottir, A. D., Trans–Cis Isomerization of Vinylketones through Triplet 1,2-Biradicals. *The Journal of Physical Chemistry A* **2014,** *118* (45), 10433-10447.
18. Banerjee, U.; Karney, W. L.; Ault, B. S.; Gudmundsdottir, A. D., Photolysis of 5-Azido-3-Phenylisoxazole at Cryogenic Temperature: Formation and Direct Detection of a Nitrosoalkene. *Molecules* **2020,** *25* (3), 543.
19. Frisch, M. J.; Trucks, G. W.; Schlegel, H. B.; Scuseria, G. E.; Robb, M. A.; Cheeseman, J. R.; Scalmani, G.; Barone, V.; Petersson, G. A.; Nakatsuji, H.; Li, X.; Caricato, M.; Marenich, A. V.; Bloino, J.; Janesko, B. G.; Gomperts, R.; Mennucci, B.; Hratchian, H. P.; Ortiz, J. V.; Izmaylov, A. F.; Sonnenberg, J. L.; Williams; Ding, F.; Lipparini, F.; Egidi, F.; Goings, J.; Peng, B.; Petrone, A.; Henderson, T.; Ranasinghe, D.; Zakrzewski, V. G.; Gao, J.; Rega, N.; Zheng, G.; Liang, W.; Hada, M.; Ehara, M.; Toyota, K.; Fukuda, R.; Hasegawa, J.; Ishida, M.; Nakajima, T.; Honda, Y.; Kitao, O.; Nakai, H.; Vreven, T.; Throssell, K.; Montgomery Jr., J. A.; Peralta, J. E.; Ogliaro, F.; Bearpark, M. J.; Heyd, J. J.; Brothers, E. N.; Kudin, K. N.; Staroverov, V. N.; Keith, T. A.; Kobayashi, R.; Normand, J.; Raghavachari, K.; Rendell, A. P.; Burant, J. C.; Iyengar, S. S.; Tomasi, J.; Cossi, M.; Millam, J. M.; Klene, M.; Adamo, C.; Cammi, R.; Ochterski, J. W.; Martin, R. L.; Morokuma, K.; Farkas, O.; Foresman, J. B.; Fox, D. J. *Gaussian 16 Rev. C.01*, Wallingford, CT, 2016.
20. Bauernschmitt, R.; Ahlrichs, R., Treatment of electronic excitations within the adiabatic approximation of time dependent density functional theory. *Chemical Physics Letters* **1996,** *256* (4), 454-464.
21. Foresman, J. B.; Head-Gordon, M.; Pople, J. A.; Frisch, M. J., Toward a systematic molecular orbital theory for excited states. *The Journal of Physical Chemistry* **1992,** *96* (1), 135-149.
22. Gonzalez, C.; Schlegel, H. B., An improved algorithm for reaction path following. *The Journal of Chemical Physics* **1989,** *90* (4), 2154-2161.
23. Gonzalez, C.; Schlegel, H. B., Reaction path following in mass-weighted internal coordinates. *The Journal of Physical Chemistry* **1990,** *94* (14), 5523-5527.

Chapter: 4

Understanding the reactivity of isoxazoles derivatives 1 and 2 in solution and cryogenic matrix

Abstract

Nitrenes are important class of electron-deficient intermediates that have either a triplet or singlet configuration. Short-lived singlet nitrenes generally decay by intramolecular reactivity. In comparison, triplet nitrenes are long lived, and less reactive as they require intersystem crossing to form products. There is general interest in triplet nitrenes as high spin units because of their potential use as building blocks for high-spin assemblies[1,2,3]. Triplet vinyl nitrenes are generally shorter lived-in comparison to the triplet alky and aryl nitrenes and they are mainly used in the formation of new C-N bonds in synthetic applications [4,5,6] .

We studied the photochemistry of two isoxazole derivatives, **1** and **2** in solution and in cryogenic matrix. Photolysis of **1** did not yield any new products in argon saturated MeOH, but the photolysis of **2** in argon saturated MeOH resulted in the formation of a ketenimine derivative. However, the laser flash photolysis of **1** and **2** shows the formation of triplet vinyl nitrene in argon saturated acetonitrile thus the triplet vinyl nitrene ^{3}**1N** must decay by intersystem crossing to reform the starting material.

In cryogenic matrices the vinylnitrenes ^{3}**1N** and ^{3}**2N** form the corresponding ketenimines **1k** and **2K** respectively. Therefore, we propose these vinylnitrenes ^{3}**1N** and ^{3}**2N** are flexible enough to intersystem cross to form ketenimines **1K** and **2K**. We used transient spectroscopy,

cryogenic matrix isolation and density functional theory (DFT) calculations to characterize the triplet vinyl nitrenes ^{3}**1N** and ^{3}**2N** and ketenimines **1K** and **2K** to support the proposed mechanism.

1. Introduction

Nitrenes are reactive intermediates which can be generated upon irradiation of azides. Based on the type of azide from which they are generated, nitrenes can be categorized as aryl nitrene, alkyl nitrene and vinyl nitrene. In addition to this, based on the electronic configuration nitrenes can be categorized as triplet nitrenes and singlet nitrenes. In general, singlet nitrenes are very reactive and short lived. In comparison to the singlet nitrenes triplet nitrenes are longer lived.

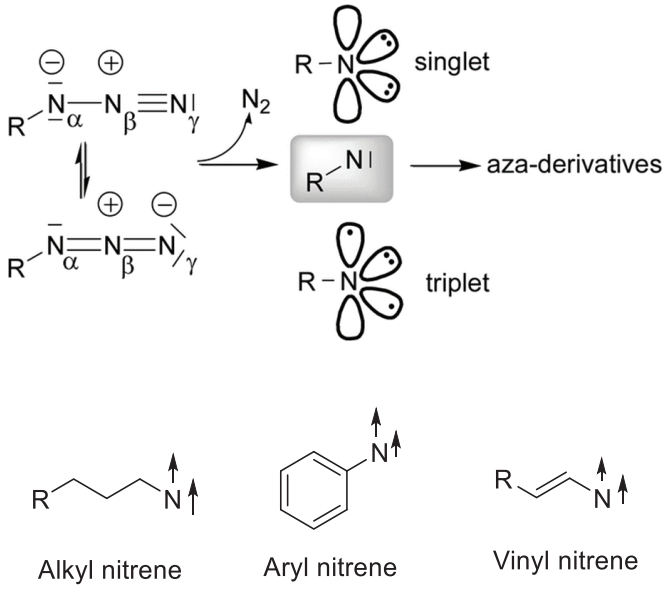

Figure 44. Types of triplet nitrenes

Among the triplet nitrenes, triplet vinyl nitrenes are shorter-lived intermediates in comparison to the triplet alkyl nitrenes and triplet aryl nitrenes. Triplet alkyl and aryl nitrenes are long-lived in solution as they decay by dimerization, and thus their lifetime is generally a few microseconds in solution. Triplet vinylnitrenes can be generated upon irradiation of viny azide or isoxazoles or azirines in the presence of a triplet sensitizer (Scheme *13*)[7] . However, in cryogenic matrices upon irradiation of isoxazoles and azirines the formation of the corresponding ketenimines was reported not the vinyl nitrenes even though the ketenimine is formed via the triplet vinyl nitrene intermediate. The detection of triplet vinyl nitrenes at cryogenic matrices using EPR and IR was not reported since they are not stable at cryogenic temperature [8,9,10,11].

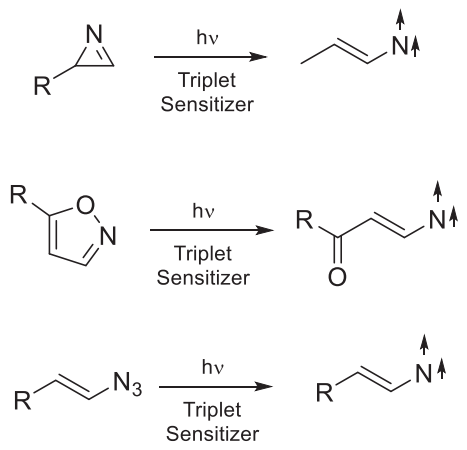

Scheme 13. Different precursors to form triplet vinylnitrenes

Our group reported the first detection of triplet vinylnitrene in solution by performing laser flash photolysis of (3-methyl-2H-azirin-2-yl) phenylmethanone **1**(Scheme 14) [11]. However, in cryogenic matrices upon irradiation of the same azirines and isoxazoles interestingly the corresponding ketenimine was detected, not the vinylnitrene, even though the ketenimines are suspected to be formed from the triplet vinyl nitrenes (Scheme 15).

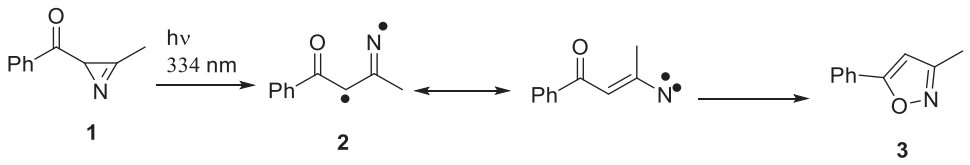

Scheme 14. Proposed mechanism for vinylnitrene formation

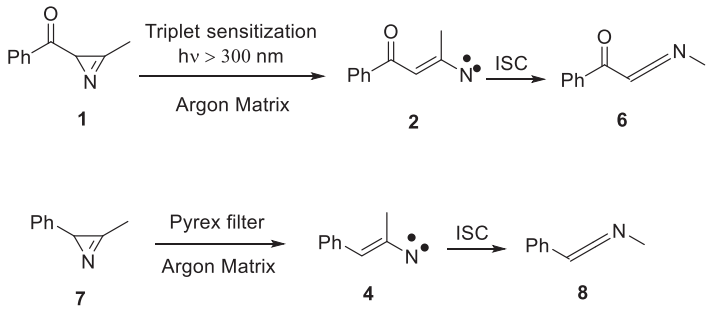

Scheme 15. Irradiation of azirines in cryogenic matrix

It was proposed that the rotation around the vinylic double bond facilitates intersystem crossing of the triplet vinylnitrenes to form products. The calculated rotational barrier of the triplet vinylnitrenes in Scheme *16*, further supports our hypothesis as the barrier is less than 11 kcal/mol (Scheme 16)**.**

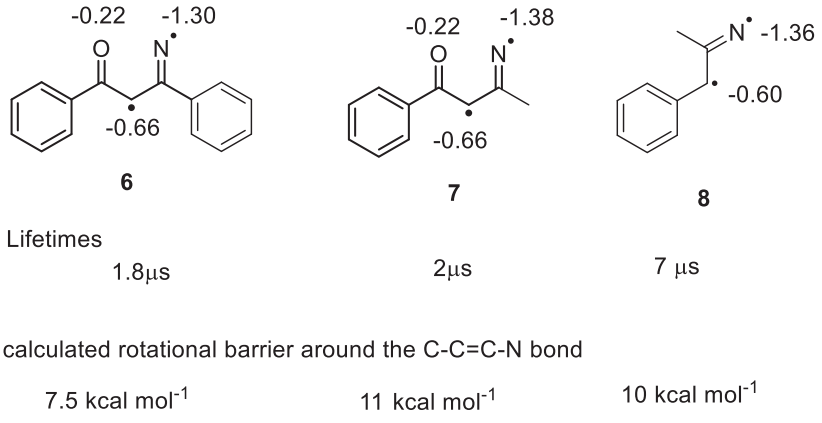

Scheme 16. Calculated rotational barrier of stable vinyl azides

To address this issue Sarkar et al. from our group studied the physical properties and reactivity of triplet vinylnitrenes formed from 2-azido-1,4-naphthoquinone (Scheme 17), which is rigid as the vinyl moiety is incorporated into a cyclic ring. In their study they were able to detect the triplet vinylnitrene for the first time in cryogenic matrix using IR and ESR spectroscopy [12]. In addition to this, we were able to detect other stable triplet vinylnitrene in cryogenic matrix in our group studies [13,14] (Scheme 18).

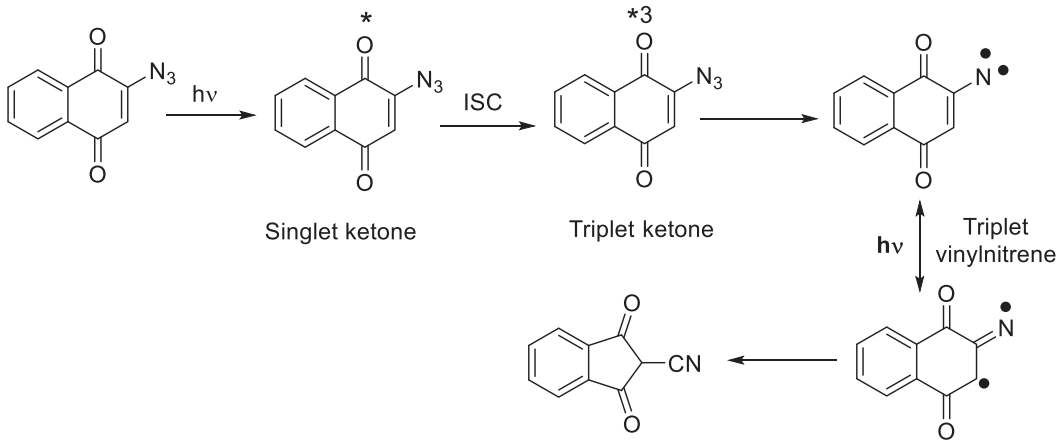

Scheme 17. Proposed mechanism for the formation of triplet vinylnitrene from rigid azide in cryogenic matrix

The stability of this triplet vinylnitrene is attributed to the rigidity of the vinylic double bond which restricts the rotation around the double bond and thus prevents the intersystem crossing of triplet vinyl nitrenes to form the products. Thus, we can conclude that the flexibility of the triplet vinyl nitrenes can be controlled by the rigidity of the vinylic double bond. Thus, our next question is how much of a rigidity is required to prevent intersystem crossing.

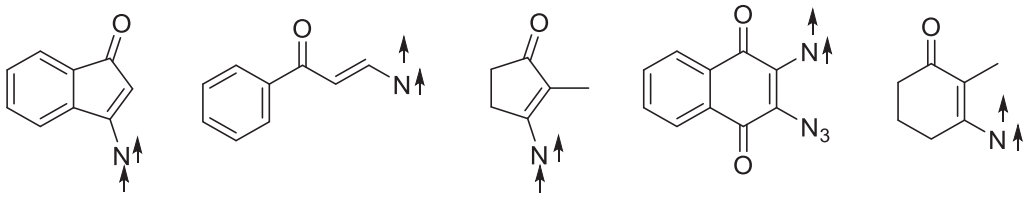

Scheme 18. Stable Triplet nitrenes reported in our group

In this study we explored the photoreactivity of 3-phenyl-4-H-cyclopent[c]isoxazole **1** (Scheme 19) and 3-phenylcyclohexisoxazole **2 (**Scheme 20**)** in solution and cryogenic matrices. We detected the corresponding triplet vinyl nitrenes **^{3}1N** and **^{3}2N** from isoxazoles **1** and **2** respectively in solution, but in cryogenic matrix we detected the corresponding ketenimines **1K** and **2K** and not the corresponding triplet vinylnitrenes. From our studies we figured it out that the triplet vinyl nitrenes from isoxazoles **1** and **2** intersystem cross to form the corresponding ketenimine **1K** and **2K** in the cryogenic matrix.

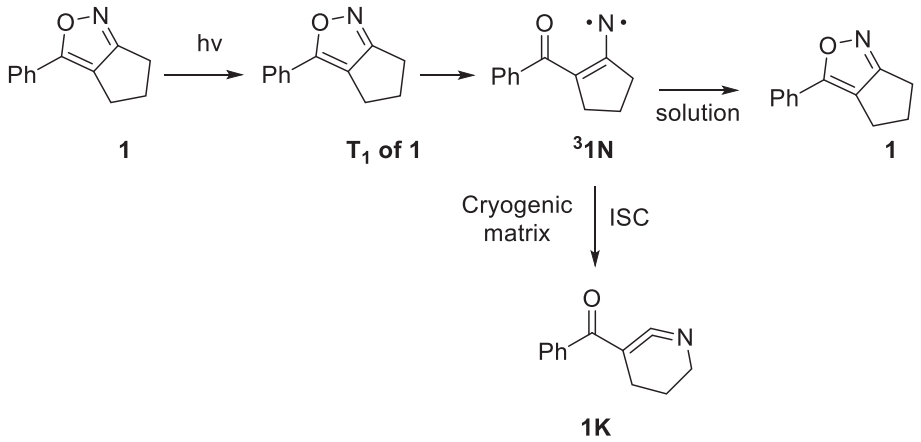

Scheme 19. Photoreactivity of isoxazole-**1** in solution and in cryogenic matrix

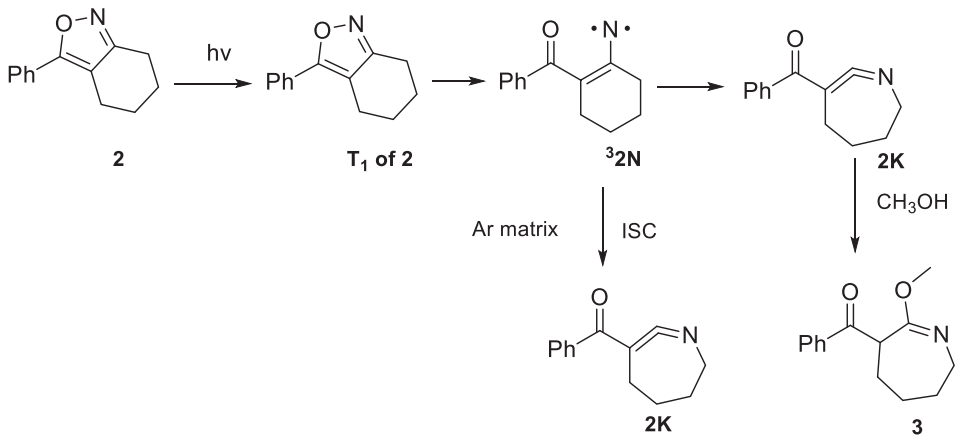

Scheme 20. Photoreactivity of isoxazole-**1** in solution and in cryogenic matrix

2. Product studies

Irradiation of isoxazole **1** in argon saturated MeOH did not produce any new products. Irradiation of Isoxazole **2** (3.34 mM) in argon saturated MeOH using mercury arc lamp for 48 h resulted in the formation of the MeOH trapped ketenimine **3 (**Figure S189**)**. In addition, photolyzed sample of **2** in argon saturated MeOH was analyzed using GCMS (Figure S194).

Further, Isoxazole **2** was irradiated using 254 nm light and UV/Vis's spectra were measured as a function of irradiation time in argon and oxygen-saturated acetonitrile. Similar differences were observed in both argon and oxygen-saturated samples. After 1 hour of irradiation the argon-saturated sample was kept in dark for 30 more minutes and the UV/vis spectra was monitored, and no changes were observed.

Photolyzed sample of **2** in argon-saturated and oxygen-saturated acetonitrile was analyzed using GCMS. The newly formed photoproducts were identified with further analysis of the ^{1}H NMR and FT-IR spectra of photolysis mixture. The formation of azirine **7** is observed in dry solvent

and in polar protic and in moist solvents we observe trapping and hydrolysis of azirine, respectively.

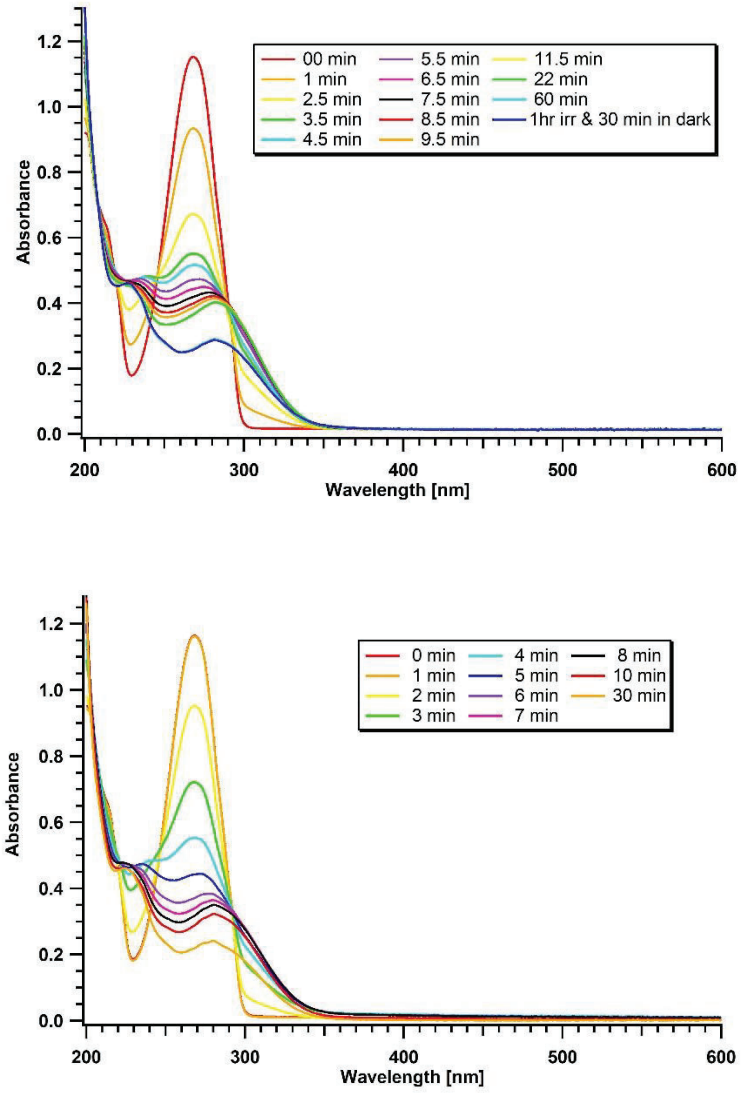

Figure 45. UV/ Vis analysis of **2** with time upon irradiation at 254 nm a) in argon saturated CH_3CN b) in oxygen saturated CH_3CN

3. Cryogenic matrix UV-vis absorption Spectroscopy

Solution of isoxazole **1** (9 µM) was prepared using mTHF solvent and the sample was loaded in liquid N_2 at 77 K to form the glassy matrix. The glassy matrix of compound **1** was Irradiated using Xenon lamp and the absorption spectrum was measured between 200 nm to 800 nm.

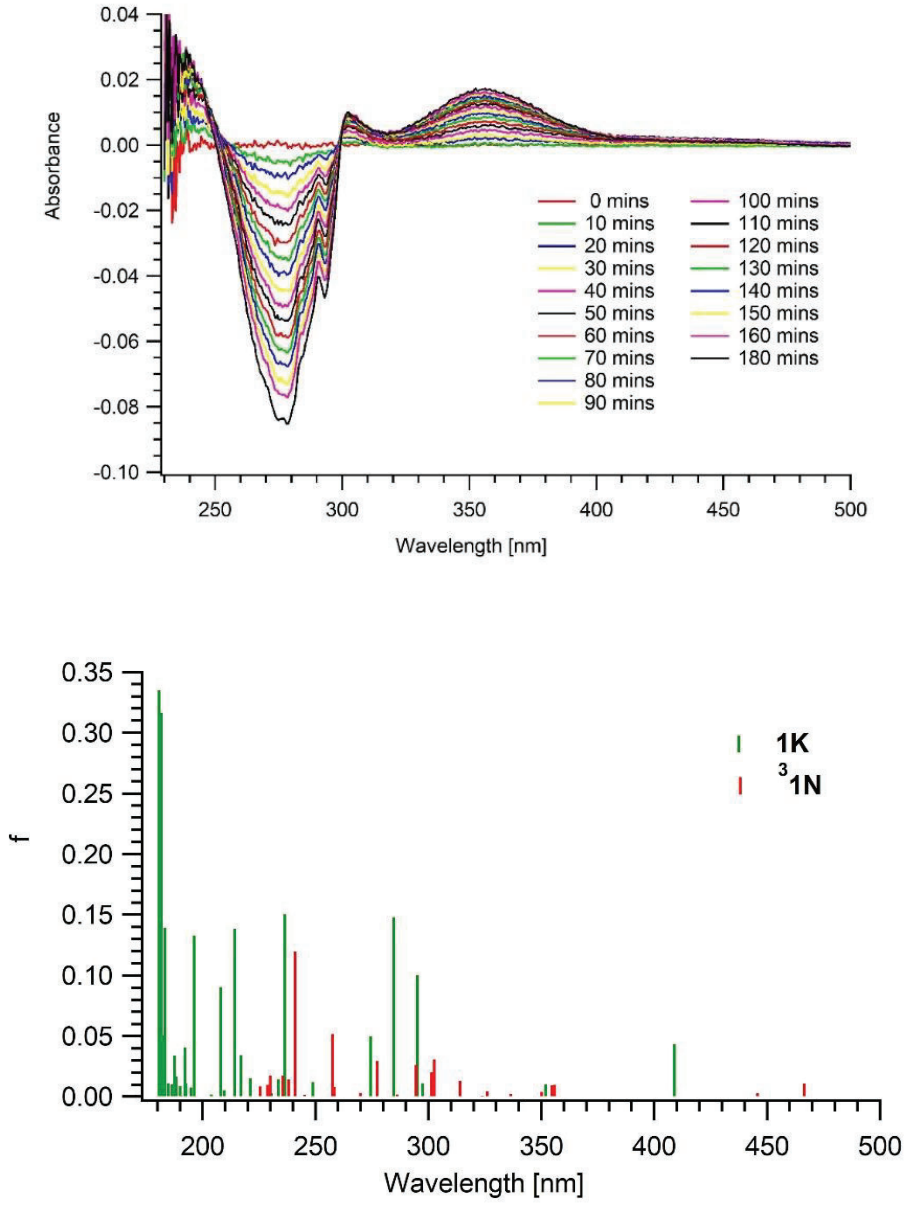

Figure 46. Cryogenic UV-Vis spectrum of **1** and the TD-DFT calculated UV of **1**

Irradiation of the mTHF matrix resulted in new broad absorption band which has two isosbestic points at 251 nm and 294 nm, evidently due to the photobleaching of the starting material a negative absorption was observed between 251 nm and 294 nm. The absorption has λ_{max} at 234 nm, and another intense absorption band with λ_{max} at 300 nm, and a broad absorption centered at 358 nm. The intensity of these bands was increased with the continuous irradiation of the glassy matrix. Comparison of absorption spectrum measured at 77 K with the TD-DFT calculated UV/Vis spectrum of ketenimine shows good agreement hence we assign the UV/Vis spectrum obtained at 77 K in mTHF matrix, to the corresponding ketenimine of **1**.

Similarly, a solution of isoxazole-**2** (25 μM) in mTHF was also loaded in cryogenic unit filled with liquid N_2 which resulted in the formation of the glassy matrix. The irradiation of the glassy matrix of **2** using Xenon lamp resulted in the growth of absorption bands in the UV between 225 -255 nm and 300 - 440 nm. In comparison the absorbance between 250 - 350 nm was depleted upon irradiation. Comparison of absorption spectrum measured at 77 K and the TD-DFT calculated UV/Vis spectrum of ketenimine **2K** shows good agreement hence we assign the UV/Vis spectrum obtained at 77 K in mTHF matrix, to the ketenimine **2K**.

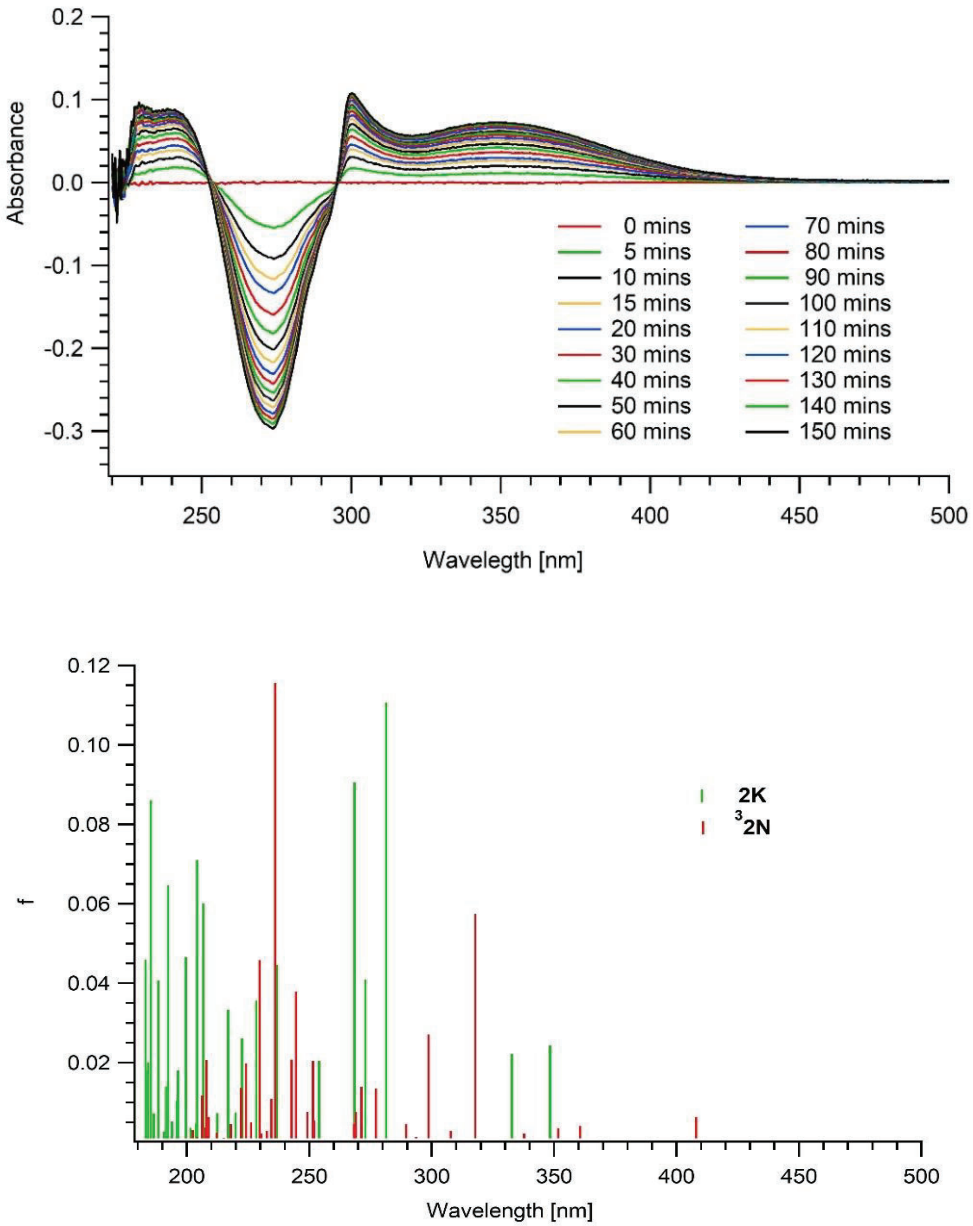

Figure 47. Comparison of Absorption spectra obtained by irradiating **2** in glassy MTHF matrix at 77 K (Figure 3a) vs calculated UV/Vis spectrum of lowest energy conformer of triplet vinyl nitrene ^{3}**6 (Figure 3b)**.

4. Cryogenic Matrix IR spectroscopy

To further characterize the reactivity of vinylnitrenes ^{3}**1N** and ^{3}**2N**, we attempted to detect them directly in argon matrices. Irradiation of isoxazole **1** in argon matrices resulted in depletion of some bands. Concurrently, with the depletion of these bands, new bands were formed. We assign these bands to ketenimine **1K** based on comparison to its calculated IR bands.

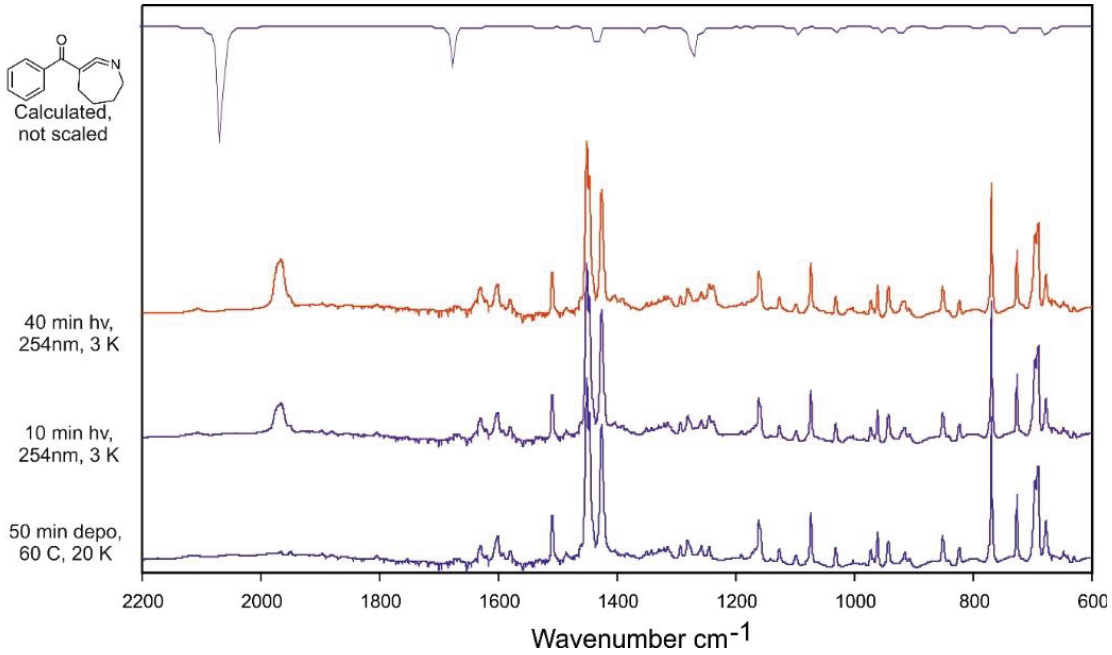

Figure 48. Matrix IR spectrum and the TD-DFT calculated IR spectrum of 1

In a separate experiment Isoxazole **2** was deposited into an argon matrix at 20 K by heating it to 60 °C. The argon matrix was irradiated directly with a 254 nm light for total of 40 min with recording infrared spectra at different time intervals. IR spectra showed that irradiation of **2** in argon matrices led to the growth of new set of absorption bands around 1977, 1618 and 1246

cm^{-1}. The intensities of these new bands increased with similar rate upon further irradiation. They are assigned to ketenimine **2K** based on comparison of the calculated spectra to the observed spectra (Figure *49*). The band at 1620 cm^{-1} is assigned to the C=O stretch of the carbonyl group in ketenimine **C**, which is calculated to be at 1683 and scaling by 0.9613 places at 1618 cm^{-1}. The band formed 1980 cm^{-1} is identified as the most intense band and we assigned to the asymmetric N=C=C stretching, which is calculated to be at 2056 cm^{-1} and scaling with 0.9613 places it at 1877 cm^{-1}. Furthermore, new band at 1246 cm^{-1} is assigned to the asymmetric C-C stretching which is calculated to be at 1296 cm^{-1} and scaling by 0.9613 places it at 1246 cm^{-1}.

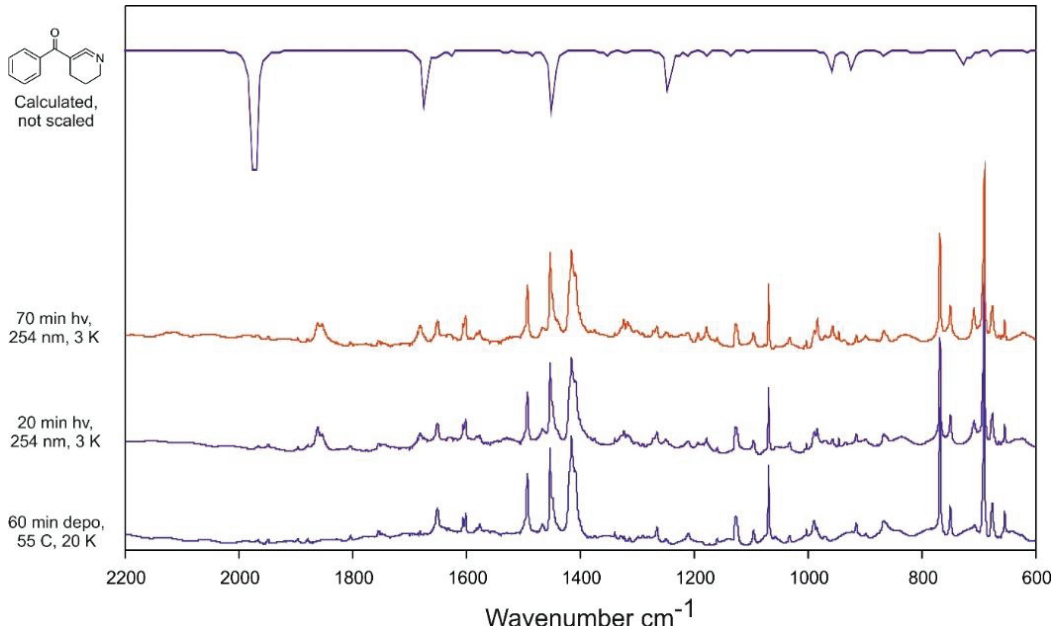

Figure 49. Matrix IR spectrum and the DFT/B3LYP/6-31G+(d) calculated IR spectrum of **1**

The matrix isolation experiment demonstrates that the photolysis of isoxazole **1** and **2** yields ketenimines **1K** and **2K**, respectively, rather than the corresponding triplet vinylnitrenes as

observed in solutions. Therefore, we propose that vinylnitrenes ^{3}**1N** and ^{3}**2N** are flexible enough to intersystem cross to form ketenimines **1K** and **2K.**

5. ESR Spectroscopy

In two separate experiments, Sublimed vapor of isoxazole **1** and **2** was deposited along with argon gas in a cooled copper rod in a vacuum of 10^{-7} mbar and 5 K. Resulted isoxazole embedded argon matrix was irradiated using Hg lamp and an ESR spectrum was recorded between 0 to 10000 G. However, no signal was observed from both ESR experiments done for compound **1** and **2.**

6. Laser Flash photolysis

I. Laser flash photolysis of isoxazole-1

Laser flash photolysis of isoxazole **1** and **2** was carried out in argon and oxygen-saturated acetonitrile to identify the excited state species and intermediates which is responsible for the product formation. Laser flash photolysis of isoxazole **1** (Edinburgh laser 266 nm, 4000 ns, 145 mJ) in argon saturated acetonitrile produced a transient spectrum with λ_{max} at 320 nm (Figure *50*). We assign this transient spectrum to triplet vinylnitrene **^{3}1N** based on its calculated absorption spectrum. The TD-DFT calculations of ^{3}**1N** in acetonitrile (method) has major electronic transitions at 466 nm (*f* = 0.0111), 445 nm (*f* = 0.0029), 355 nm (*f* = 0.0099), 314 nm (*f* = 0.0132) and 303 nm (*f* = 0.0319) which agrees well with the observed spectrum.

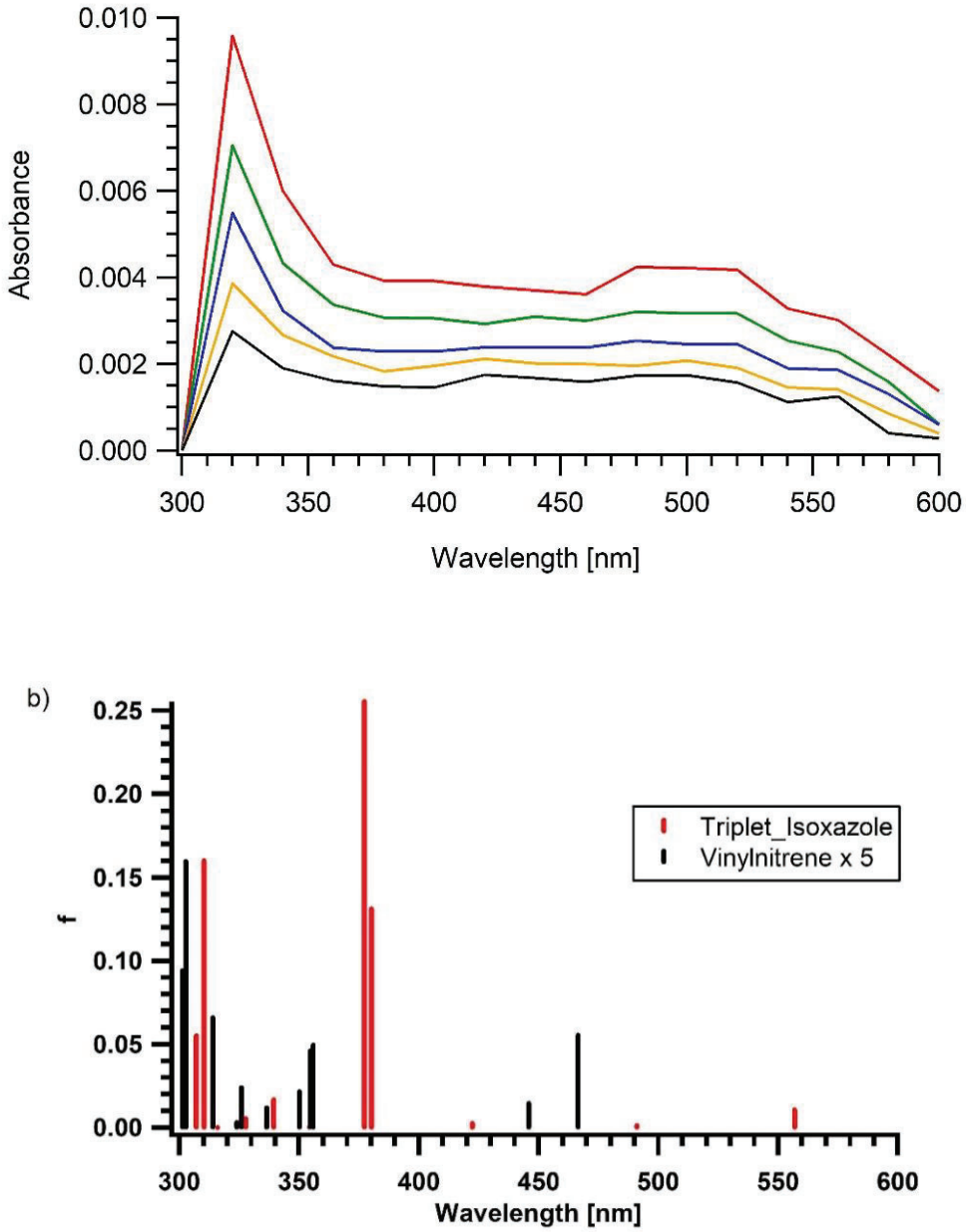

Figure 50. (a) Transient spectrum obtained from laser flash photolysis of **1** in argon-saturated acetonitrile. (b) TD-DFT calculated spectra for T_1 of **1** (red) and vinylnitrene ^{3}**1N** (black) in acetonitrile.

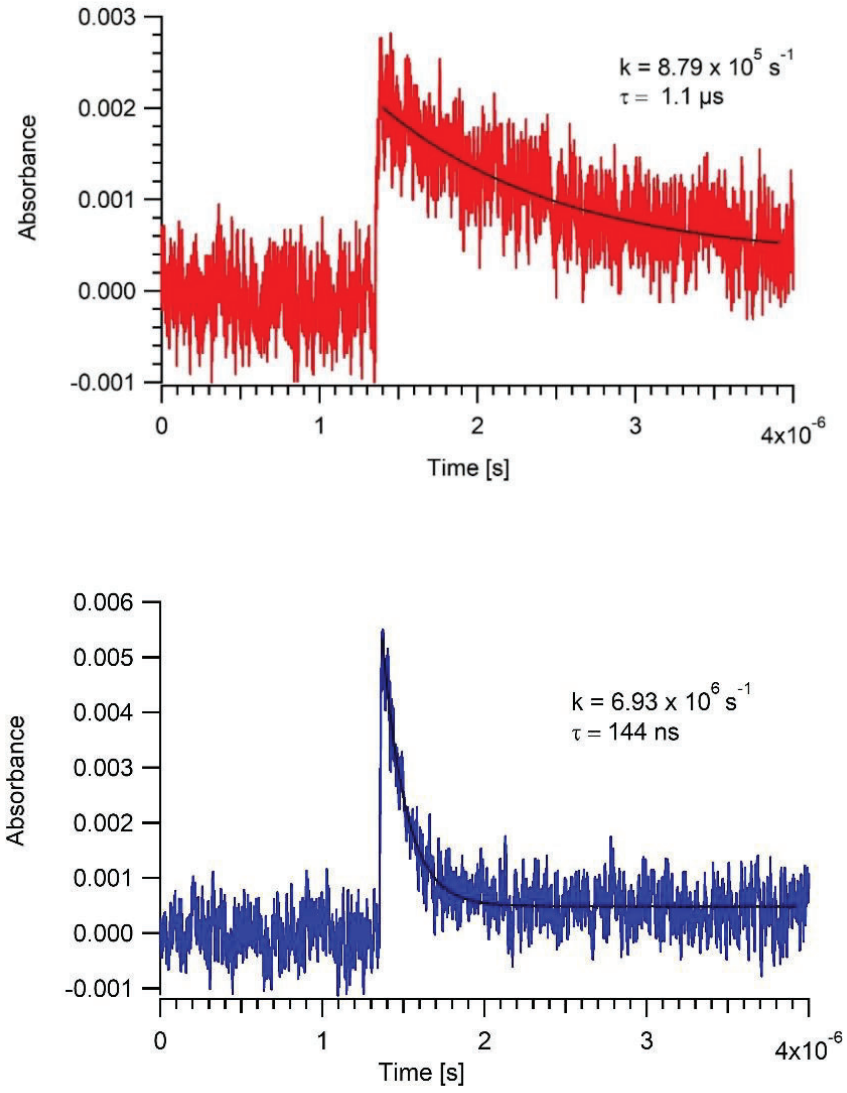

Figure 51. Kinetic traces obtained under a) argon and b) oxygen saturated acetonitrile at 450 nm for the laser flash photolysis of **1**.

Analysis of the kinetics in argon and oxygen saturated acetonitrile at 450 nm (Figure 51) further supports the assignment of the transient spectrum to triplet vinyl nitrene ^{3}**1N.** The transient absorption decay in argon saturated acetonitrile is best fitted as a mono exponential decay, which yields a decay rate constant of 8.79 x 10^{5} s^{-1} (τ = 1.1 µs). Thus, triplet vinylnitrene

^{3}**1N** has a lifetime of 1.1 µs. Further analysis of the kinetics in oxygen saturated acetonitrile is best fitted as a mono exponential decay with the rate constant of 6.93 x 10^6 s^{-1} (τ = 144 ns).

II. Laser flash photolysis of isoxazole-**2**

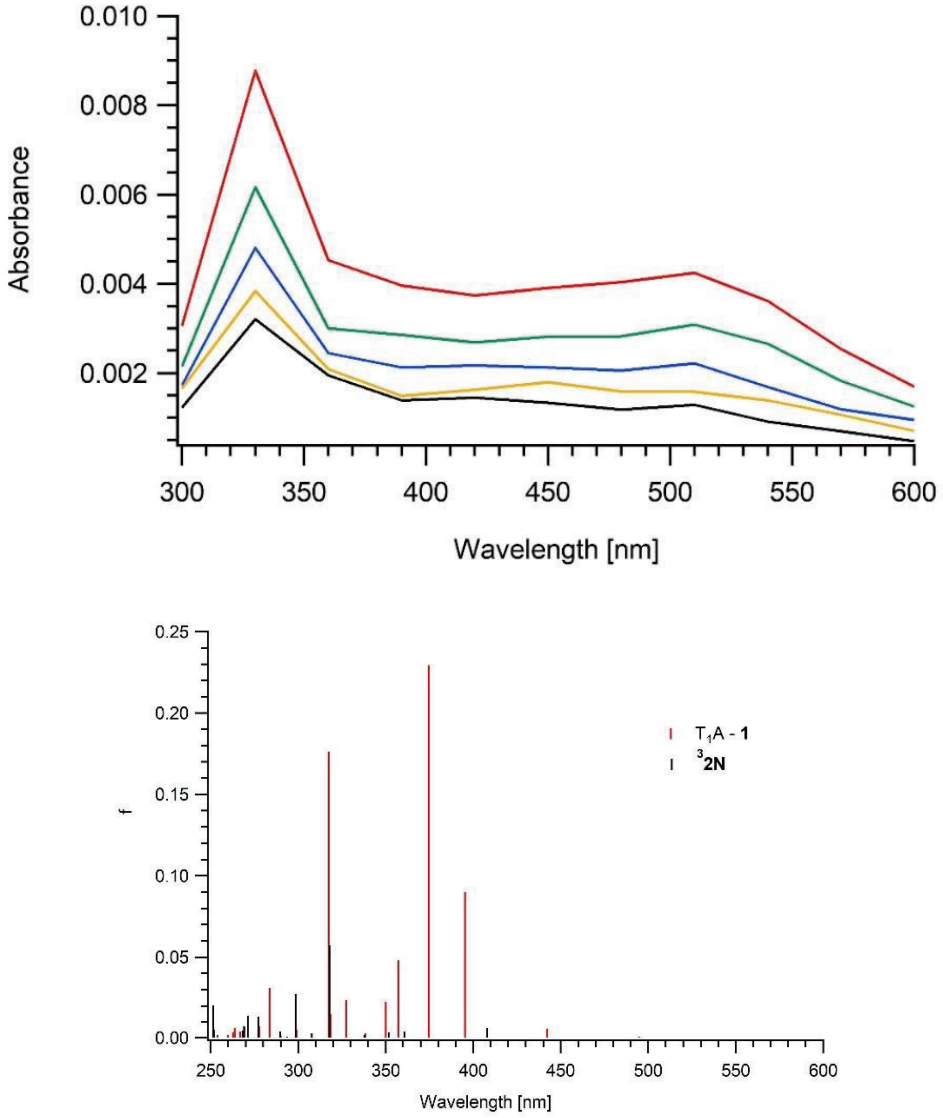

Figure 52. (a) Transient spectrum obtained from laser flash photolysis of **2** in argon saturated acetonitrile. (b) TD-DFT calculated spectra for T_1 of **2** (red) and vinylnitrene (black) in acetonitrile

Similarly, laser flash photolysis of isoxazole-**2** in argon saturated acetonitrile resulted in a broad transient absorption spectrum with a λ_{max} at 330 nm (Figure *52*). We assign this transient spectrum to triplet vinylnitrene ^{3}**2N** based on its calculated absorption spectrum. (TD-DFT) calculations of triplet vinyl nitrene ^{3}**2N** in acetonitrile has major electronic transitions at 360.7 nm (*f* = 0.004), 352 nm (*f*= 0.0035), 318 nm (*f*= 0.0574), and 298 nm (*f*= 0.0271) which agrees well with the observed spectrum.

Further analysis of the kinetics at argon saturated acetonitrile 440 nm shows a decay with a rate constant of 1.41 x 10^{6} s^{-1} (τ = 708 ns) and oxygen saturated acetonitrile shows a mono exponential decay with the rate constant of 6.58 x 10^{6} s^{-1} (τ = 152 ns) (Figure *53*). Thus, laser flash photolysis shows that both isoxazoles **1** and **2** form their triplet excited states, which decay to form vinylnitrenes ^{3}**1N** and ^{3}**2N**, respectively.

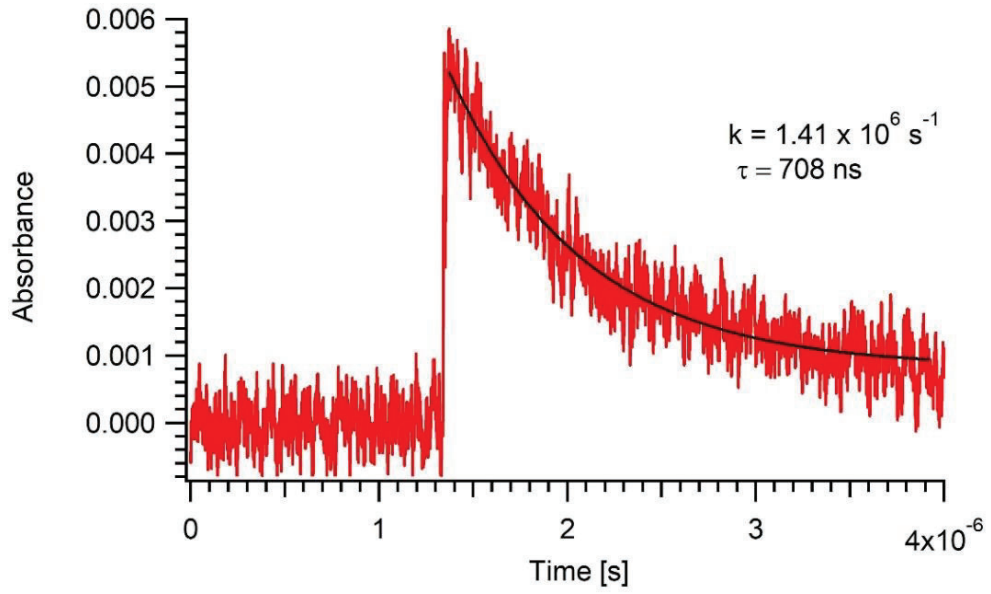

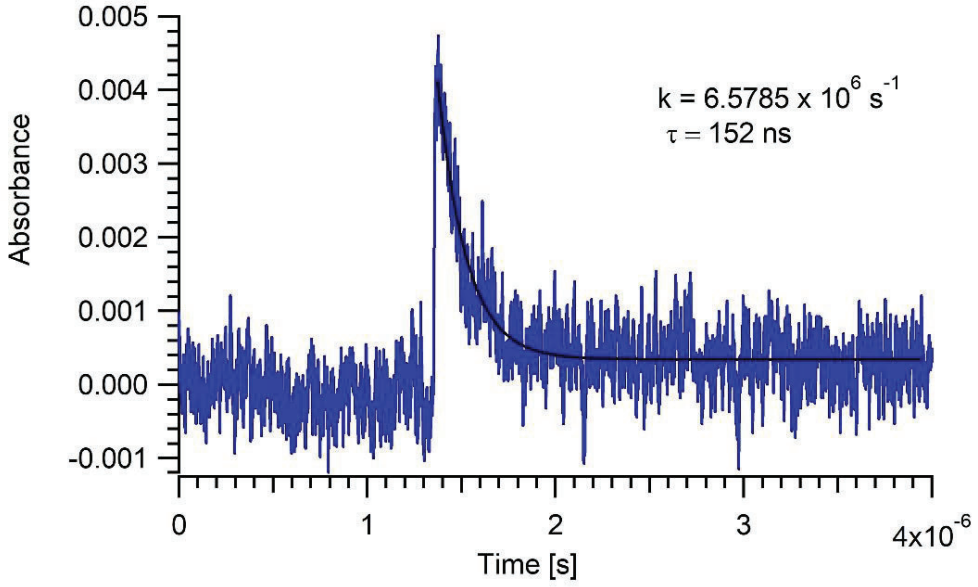

Figure 53. Kinetic traces obtained at 460 nm for the laser flash photolysis of **2** in argon saturated acetonitrile

7. Phosphorescence

The phosphorescence spectrum of **1** (10 mM) was obtained at 77 K in frozen ethanol matrices. The obtained phosphorescence spectrum of **1** is not sufficiently resolved as typically observed for (π, π*) configurations. The first vibrational band at 393 nm was assigned to the (0,0) band of the phosphorescence, which is corresponding to the energy of T_1 of **1** being 72 kcal/mol above its ground state.

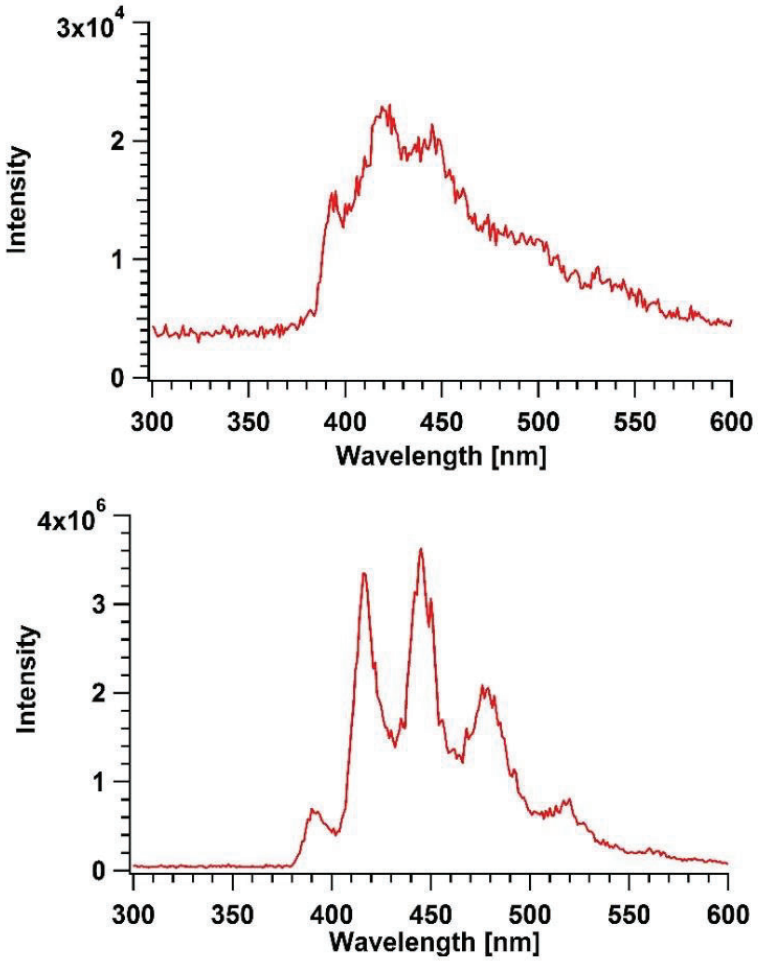

Figure 54. Phosphorescence of isoxazoles a) **1** with 275 nm irradiation and b) **2** with 254 nm irradiation

The phosphorescence spectrum of **2** (9.3 mM) was obtained in frozen methyl tetrahydrofuran (MTHF) matrices at 77 K with the excitation at 254 nm. Phosphorescence spectrum of **2** is suspected to be having contribution from (π, π^*) configuration as well as (n, π^*) configuration due to the shape of spectrum. The first vibrational band at 390 nm was assigned to the (0,0) band of the phosphorescence, which is corresponding to the energy of T_1 of **2** which is 73 kcal/mol.

8. Quantum Mechanical Calculations

To better understand the photoactivity of isoxazoles **1** and **2,** we calculated stationary points on its singlet and triplet surfaces using the B3LYP level of theory with the 6-31G+(d) basis on Gaussian09.

We optimized the ground state (S_0) of **1** and used time-dependent density functional theory (TD-DFT) to estimate the first excited singlet state of **1**(S_1) and the first and second excited triplet states (T_1 and T_2) of **1**. According to the calculations S_1 of **1** is located 104 kcal/mol above its S_0. Further, TD-DFT calculations place T_1 and T_2 of **1** at 66 and 93 kcal/mol above its S_0, respectively. The optimized energy of the T_1 of **1** is calculated to validate the values obtained from DFT calculations of T_1 of **1** and it is located at 63 kcal/mol above its S_0 and are in good agreement to TD-DFT calculations, presumably because the T_1 and S_0 of **1** have fairly similar geometries. Analysis of the calculated bond lengths in the T_1 of **1** shows the O-C and the N-C bonds are 1.40682 and 1.34948 Å and are thus elongated than the corresponding bonds in the S_0 of **1**, which are 1.36792 and 1.30865 Å, respectively.

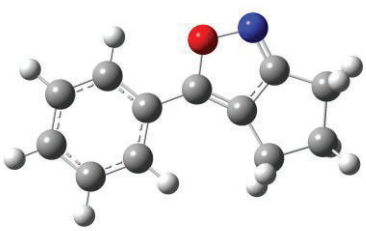

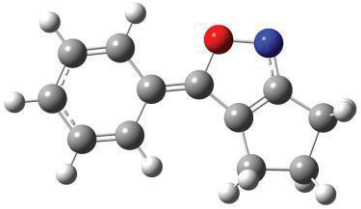

Bond	Å	Å
C-O	1.36792	1.40682
C=N	1.30865	1.34948
O-N	1.41341	1.42775
OC-CPh	1.46088	1.37401
OC-C(Cp)	1.36880	1.45597
C(Cp)-C(Cp)	1.41716	1.37112

Figure 55. Comparison of selected bond distances (Å) in the optimized structure of **1** and the T_1 of **1**.

Furthermore, the C=C bonds in the phenyl ring which is adjacent to the oxygen atom in the T_1 of **1** are no longer equivalent, as in the S_0 of **1**. These factors thus demonstrate that T_1 of **1** is best described as a triplet excited state that is delocalized throughout the isoxazole moiety and the phenyl group adjacent to the oxygen atom. The spin density calculations further support

this, as the unpaired electron density is delocalized over on both the phenyl group adjacent to the oxygen atom and the isoxazole moiety.

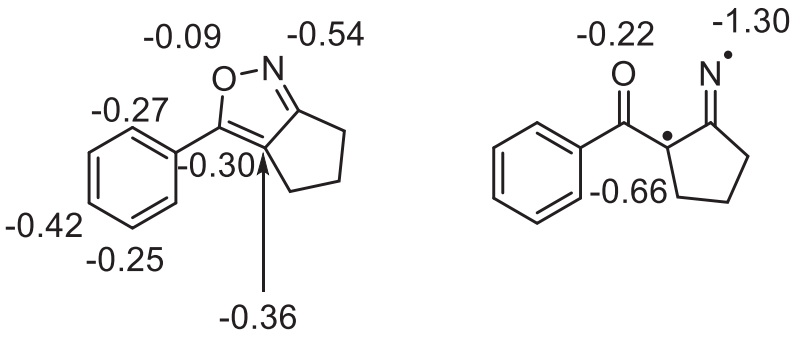

Scheme 21. Calculated spin densities of T_1 of **1** and vinylnitrene **2**.

Further, two minimum energy conformers were calculated for triplet vinylnitrene **2**, A and B. According to the calculations, conformer **2B** was slightly more stable, by 2.6 kcal/mol than the **2**A. Calculated spin density of triplet vinylnitrene **2** demonstrates that it has considerable 1,3- carbon iminyl biradical character, as the spin density is mainly located on the N and β-C atoms, -1.30 and -0.66 respectively. The calculated rotational barrier for the vinylnitrene **2** around its αC-βC bond is displayed in Figure X. Rotational barrier calculations further support that conformer **2B** is the most stable, as rotational energy between conformer **2A** and **2B**, which is ~ 4.0 kcal/mol.

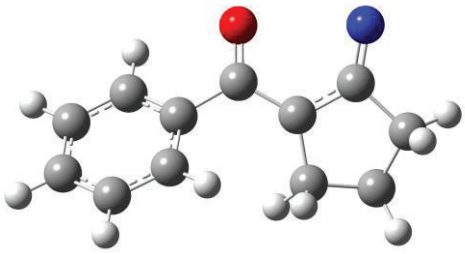

2A

0

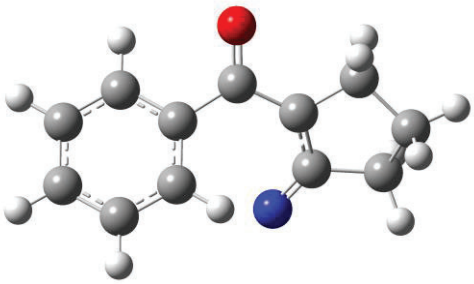

2B

-2.6 kcal/mol

Bond	Å
C=O	1.23505
CO-C(Cp)	1.46992
C(Cp)- CN	1.44672
C=N	1.28034

Figure 56. Energy comparison of the minimal energy conformers of vinylnitrene **2** A and B and selected bond lengths (Å).

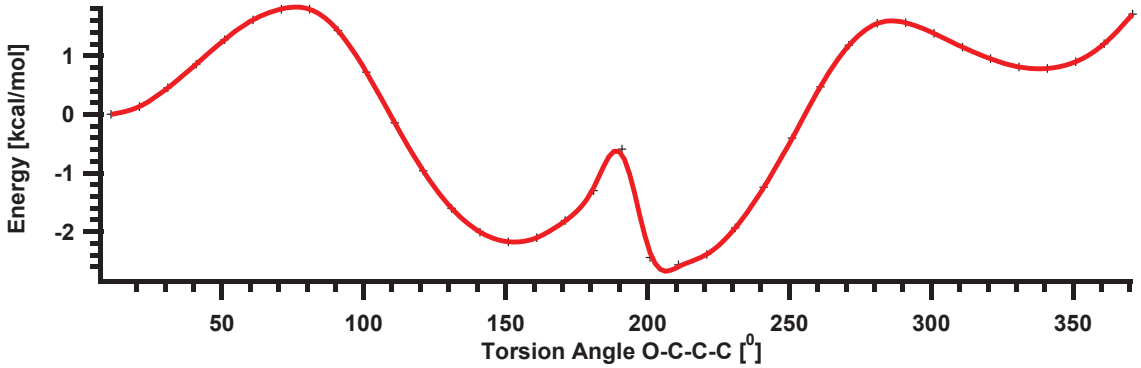

Figure 57. Calculated rotational barriers between vinylnitrene conformers **2A** and **2B**.

The calculated stationary points on the triplet surface of **1** relative to its S_0 is shown in Figure *58*. The transition state for the formation of triplet vinylnitrene **2** from the T_1 of **1** is located 7 kcal/mol above the T_1 of **1** and IRC calculations correlates this transition state with the T_1 of **1** and vinylnitrene **2**.

Although triplet vinylnitrene **2** did not produce azirine **3** in product studies, we optimized the structure of azirine **3** to determine whether its formation is energetically feasible. Azirine **3** is located 31 kcal/mol above the S_0. Thus, calculations show azirine **3** is higher in energy than the vinylnitrene **2**. Thus, the calculation shows the formation of corresponding azirine **3** from compound **1** with the UV light irradiation is not feasible.

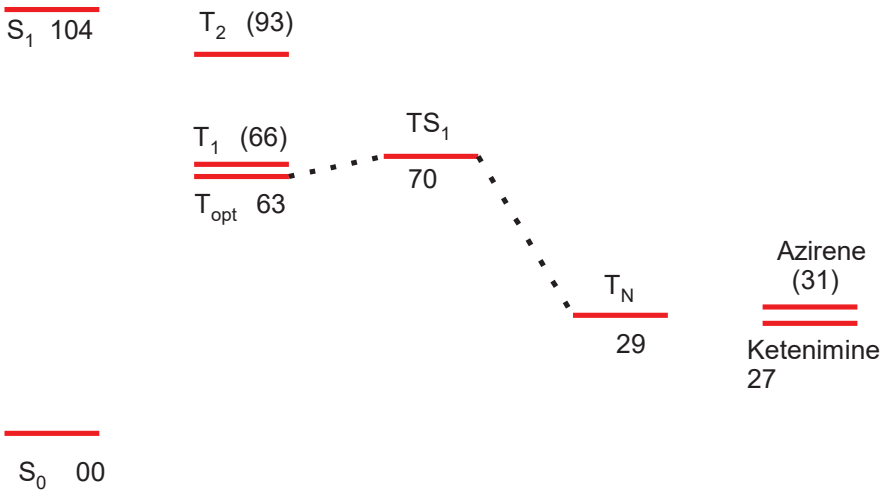

Figure 58. Calculated stationary points on the triplet surface of **1**. The energies of the S_1, T_1 and T_2 of **1** were calculated using the TD-DFT calculations, whereas the energies of S_0, T_{opt}, TS, triplet vinylnitrene and azirine were obtained by optimization calculations. Energies are in kcal/mol**.**

Similarly, the ground state of isoxazole-**2** was optimized (S_0) and used TD-DFT to estimate the first excited singlet state (S_1) and the first and second excited triplet states (T_1 and T_2). TD-DFT calculations estimate S_1 of **2** is located 105 kcal/mol above its S_0 and T_1 and T_2 of **2** at 67 and 93 kcal/mol, respectively. The T_1 of **2** was optimized and it is located at 62 kcal/mol above its S_0, which is in good agreement with TD-DFT estimations. We presume that the similar geometries of T_1 and S_0 of **2** could be the reason for the similarity of energies. bond length analysis of the optimized T_1 of **2** shows the O-C and the N-C bonds are 1.40 and 1.36 Å and they are thus elongated compared to the corresponding bonds in the S_0 of **1**, which are 1.36 and 1.31 Å, respectively (Figure 4). The C=C bonds in the phenyl ring of T_1 are no longer equivalent, as in the S_0 of **2**. The triplet excited state seems delocalized throughout the isoxazole moiety and the phenyl group according to these bond length variation analyses of S_0 and T_1 of **2**. For the verification of this observation, we performed spin density calculation on T_1 of **2**. Scheme 1 clearly demonstrate that the unpaired electron density is delocalized over on both the phenyl group and the isoxazole moiety.

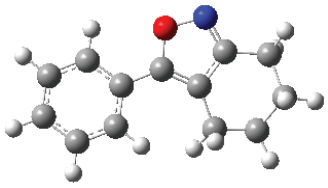

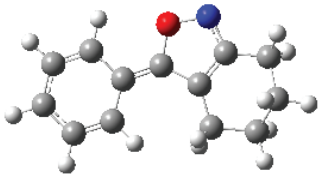

	S_0 of **5**	T_1 of **5**
Bond (Å)		
C-O	1.36	1.40
C=N	1.31	1.36
O-N	1.40	1.41
OC-CPh	1.46	1.38
OC-C(C_h)	1.37	1.47
C(C_h)-C(C_h)	1.43	1.37

Figure 59. Comparison of selected bond distances (Å) in the optimized structure of **5** and the T_1 of **5**.

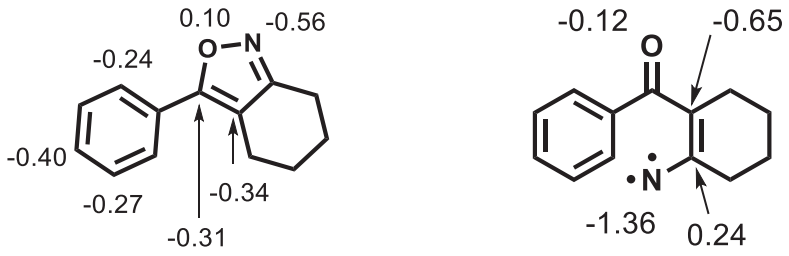

Scheme 22. Calculated spin densities of T_1 of **5** and vinylnitrene ^{3}**N2**.

In the optimization of the structure of vinylnitrene ^{3}**2N,** we were after two energy conformers, **2A** which is the lowest energy conformer and **2B** which is the conformer closest structure to starting isoxazole **2.** Calculations show that, conformer **2B** is less stable than **2A**, by ~ 4 kcal/mol. The calculated spin density of vinylnitrene ^{3}**2N** demonstrates its significant 1,3-biradical character, as the spin density is mainly located on the N and β-C atoms. (1.36 and 0.65 respectively). The calculated rotational barrier for the vinylnitrene ^{3}**2N** around its αC-βC bond is displayed in Figure 5. Rotational barrier calculations further support that conformer **2A** is the most stable, as rotational barrier between conformers **2A** and **2B**, is ~ 4 kcal/mol while the highest energy conformer is ~ 7.6 kcal/mol higher than the conformer **2A**.

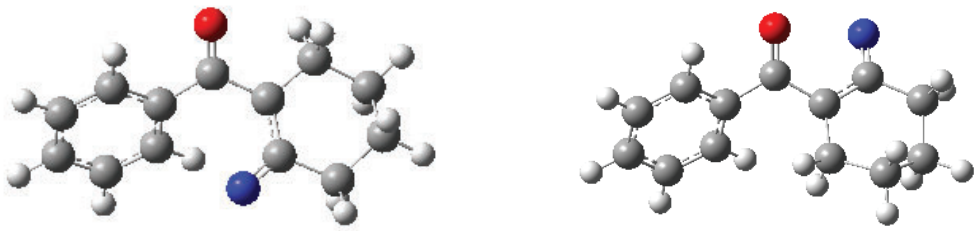

6A (0 kcal/mol) **6B** (4.2 kcal/mol)

C=O	1.23 Å
CO-C(Cp)	1.51 Å
C(Cp)- CN	1.44 Å
C=N	1.29 Å

Figure 60. Energy comparison of the minimal energy conformer 6A and the conformer 6B which is having closest structure to the isoxazole 5 of vinylnitrene and their selected bond lengths (Å).

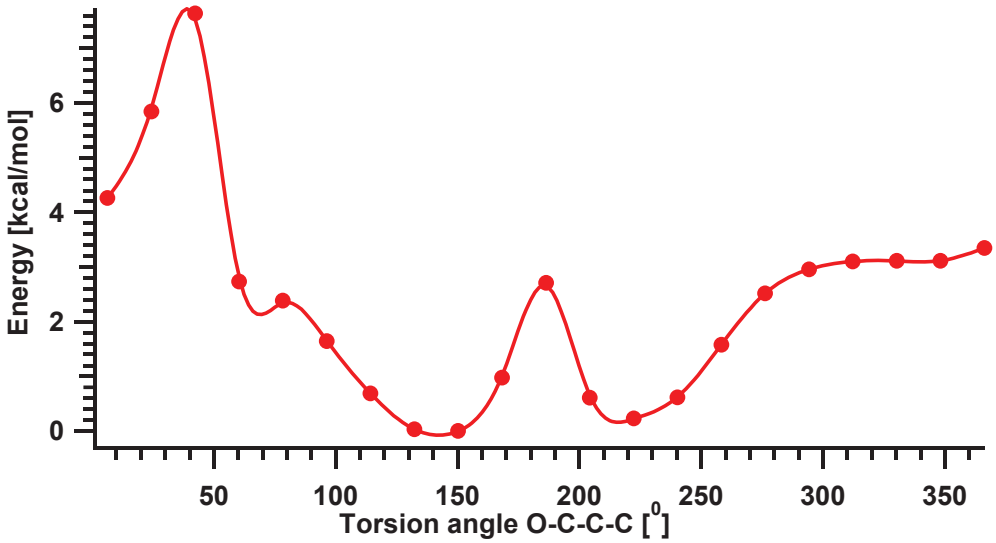

Figure 61. Calculated rotational barriers between vinylnitrene conformers **2A** and **2B**.

The calculated stationary points of **2** on the triplet surface, relative to its S_0 are shown in Figure *62*. The transition state barrier for the formation of triplet vinylnitrene ^{3}**2N** from the T_1 of **2** is located 9 kcal/mol above the T_1 of **2** and performed IRC calculation correlates this transition

state with the T_1 of **2** and vinylnitrene ^{3}**2N**. Thus, formation of vinylnitrene ^{3}**2N** from T_1 of **2** should be accessible upon excitation of **2** as long as intersystem crossing from singlet excited state of **2** is efficient.

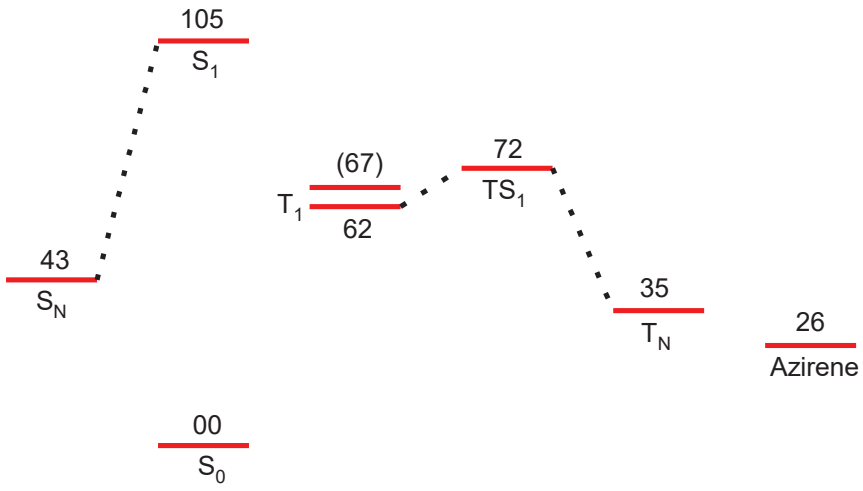

Figure 62. Calculated stationary points on the triplet surface of **2**. The energies of the S_1, T_1 and T_2 of **2** were calculated using the TD-DFT calculations, whereas the energies of S_0, T_{opt}, TS, triplet vinylnitrene (T_N) and azirine were obtained by optimization calculations. Energies are in kcal/mol.

Triplet vinylnitrene ^{3}**2N** has produce azirine **7** in product studies done in dry aprotic solvents while in undried solvent the azirine undergo trapping to from stable seven membered ring containing product **8**. Optimizations was done for the structure of azirine **7** and trapped product **8** to determine whether their formation is energetically feasible. Azirine **7** is located 9 kcal/mol below vinylnitrene ^{3}**2N.** Similarly, final trapped product **8** is 27 kcal/mol below vinylnitrene ^{3}**2N**. Thus, the calculations show that azirine **7** and trapped product **8** are lower in energy than the vinylnitrene ^{3}**2N** hence, formation of azirine **7** and trapped product formation are feasible.

9. Discussion

Product studies showed that isoxazole **1** does not yield any products when irradiated with UV light. However, 266 nm laser flash photolysis confirmed the formation of triplet vinylnitrene ^{3}**1N** with a lifetime of 865 ns. The isoxazole **2** forms the corresponding vinylnitrene ^{3}**2N** having a lifetime of 1.1 μs in solution at ambient temperature. The vinylnitrene ^{3}**1N**, and the vinylnitrene ^{3}**2N** has lifetimes of similar order thus, we have successfully demonstrated that photolysis of isoxazoles, yields short-lived triplet vinylnitrenes.

As shown in scheme 7 calculated spin densities of vinylnitrenes **2, 6, 7** and **8** are similar and demonstrates that the unpaired spin is located mainly on the N atom and the β-carbon atom giving significant 1,3-biradical character. This makes rotation around the vinylic C=C bond feasible for vinylnitrenes, where calculated rotational barriers around the vinylic C=C bond for triplet vinylnitrenes **6, 7** and **8** are only between 7.5 and 11 kcal/mol.

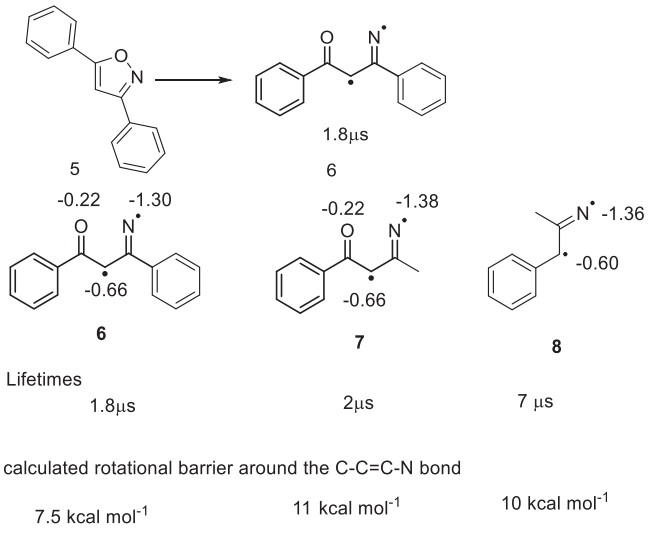

Scheme 23. Calculated spin densities of vinylnitrenes.

Recently, we have reported that irradiating a rigid vinylazide, bicyclic 2-azido-1,4-naphthoquinone **7**, with a built-in triplet sensitizer, could be used to form longer-lived vinylnitrene **8** having lifetime of 22 μs (Scheme *24*) [12]. From that study we theorized, rigidity of the molecule makes vinylnitrene **8** intersystem cross slower and thus enhances its lifetime. The significant difference between vinylnitrene **2** and **8** is that in **8** the molecule is rigid as it constructed of two infused rings, while in **2**, only the 1,3-biradical is confined to be rigid and α, β- C-C bond is flexible like in other reported vinylnitrenes **6, 7** and **8**. Thus, we proposed triplet vinylnitrenes can be stabilized by only limiting the flexibility of the vinylic C=C bond.

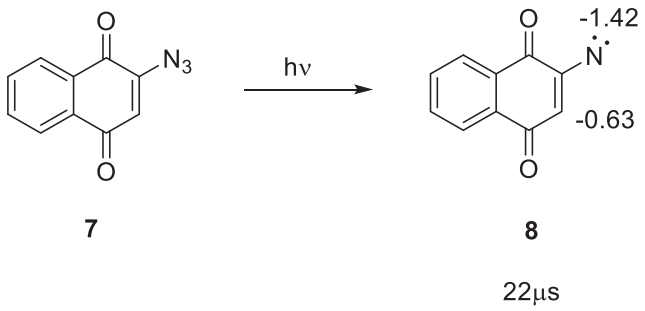

Scheme 24. Calculated spin density of rigid vinyl nitrene

Further, we have shown that isoxazole **1** forms triplet vinylnitrene as its singlet excited state must intersystem cross effectively to its triplet excited state that cleaves to form triplet vinylnitrene ^{3}**1N**, because **1** does not need a built-in sensitizer, there is no wavelength dependency in its photochemistry as reported for azirine derivatives that form triplet vinylnitrenes [15, 16, 17].

Matrix isolation of ketenimine **1K** from photolysis of **1** in argon matrices, indicates that vinylnitrene ^{3}**1N** intersystem crosses to form ketenimine **1K** as in previously reported vinylnitrenes **7** and **8**. Similarly, photolysis of 2 in argon matrices results in ketenimine **2K** rather than vinylnitrene ^{3}**2N.** We did not observe the formation of azirine and ylide from intersystem crosses of vinylnitrene ^{3}**1N** and ^{3}**2N**. This is further supported by the calculated energies as optimized energy of azirine **3** is higher than energy of vinylnitrene ^{3}**1N.** Thus, it is reasonable to expect that formed vinylnitrene ^{3}**1N** intersystem crosses back to the starting material isoxazole **1** without forming any other new photoproducts.

10. Experimental Section

I. Preparation of starting materials

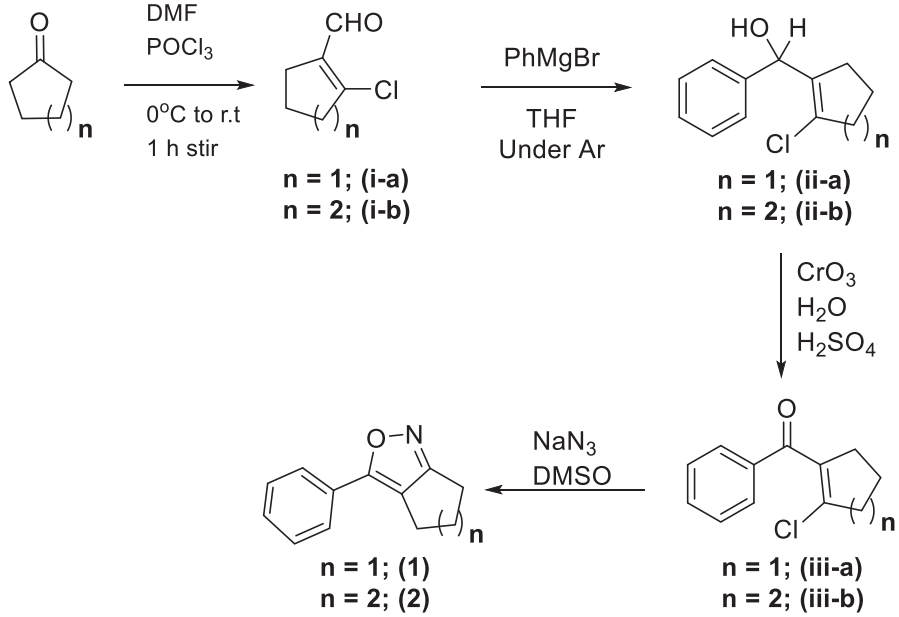

i. Synthesis of 2-chloro-1-cyclopentene-1-carboxaldehyde (i-a)2-chloro-1-cyclohexene-1-carboxaldehyde (i-b).

2-Chloro-1-cyclohexene-1-carboxaldehyde (ii-**a**) was prepared as reported by Alexander et al [18]. A solution of N, N-dimethylformamide (4.65 mL, 60 mmol) was cooled to 0°C. Phosphorous oxychloride (4.60 mL, 50 mmol) was added dropwise over a period of 10 min. The resulting white suspension was warmed to room temperature in a water bath and stirred for an additional 15 minutes. Then the mixture was cooled back to 0° C and a solution of cyclohexanone (2.94 g, 30 mmol) was added dropwise. The reaction mixture was then warmed to room temperature and stirred for 1 h. After that the mixture was poured over ice and $NaHCO_3$ was carefully added to neutralize the acids. Extract the mixture with diethyl ether (150 mL) and the organic layer was washed with water (3 x 100 mL) and brine (1 x 100mL) thoroughly, dried with $MgSO_4$, and

concentrate under pressure. Purified by column chromatographic technique using 9:1 hexane: ethyl acetate. ^{1}H NMR (400 MHz, $CDCl_3$) δ: 10.20 (s, 1H), 2.50-2.46 (m, 2H), 2.38-2.34 (m, 2H), 1.90-1.84 (m, 2H), 1.80-1.74 (m, 2H) ppm.

Similarly, 2-chloro-1-cyclopentene-1-carboxaldehyde (**i-a**) was prepared following above procedure. ^{1}H NMR (400 MHz, $CDCl_3$) d: 9.98 (s, 1H), 2.80 (t, 2H), 2.59-2.54 (m, 2H), 1.99 (quintet, 2H) ppm. IR (neat): 2955, 2829, 2854, 1680, 1615, 1335, 1245, 1092, 941, 729 cm^{-1}.

ii. Synthesis of 1-benzoyl-2-chlorocyclopent-1-ene (i-b) & 1-benzoyl-2-chlorocyclohex-1-ene(ii-b).

Compounds (ii-a and ii-b) were synthesized by following the procedure reported in the literature by Chassaing et al. with some modifications [19]. Compound (i-**b**) (1 equiv, 3.62g, 25.15 mmol) was dissolved in 10 mL THF under argon and cooled to -78^{o}C. To this solution was added slowly phenylmagnesium bromide (1.2 equiv, 3.90 mL, 1M in THF) and the solution was stirred for 10 minutes at -78 °C. Then the solution mixture was warmed to room temperature and stirred for an additional 1 hour and HCl was added until acidic to pH papers. The THF was removed under reduced pressure and the solution was extracted with diethyl ether and the extracts were dried with $MgSO_4$ and concentrated under reduced pressure to obtain (ii-**b**) (3.49 g 15.71 mmol). Crude (ii-**b**) product was proceeded to the next step without purifying. ^{1}H NMR (400 MHz, $CDCl_3$) δ 10.20 (s, 0H), 7.42 (d, *J* = 7.1 Hz, 2H), 7.35 (t, *J* = 7.5 Hz, 2H), 7.28 (d, *J* = 6.9 Hz, 1H), 2.59 (ddt, *J* = 6.3, 3.9, 2.3 Hz, 1H), 2.52 – 2.33 (m, 4H), 2.32 – 2.16 (m, 2H), 1.90 – 1.48 (m, 8H).

Similarly, compound (ii-**a**) was prepared following above procedure using (i-**a**) and proceeded to the oxidation step without purifying.

iii. Synthesis of (2-chloro-cyclopent-1-enyl)-phenyl ketone (iii-a) & of (2-chloro-cyclohex-1-enyl)-phenyl ketone (iii-b).

The synthesis of (2-chloro-cyclopent-1-enyl)-phenyl ketone (iii-**b**) was carried out by following a procedure reported by Pigge et al with some modification [20]. Crude (ii-**b**) (3.49g 15.71 mmol) was dissolved in acetone (50mL) at 0°C. CrO_3 (2 equiv) (3.14 g, 31.42 mmol) was dissolved in 10 mL H_2SO_4 acid to form a slurry, and H_2O was added to make the Jones reagent (H_2CrO_4). Formed slurry was added dropwise to the previously prepared compound (ii-**b**) acetone mixture while stirring at 0°C until the green color of the reaction mixture changed to orange. The solution was then filtered, and the solvent was neutralized with $NaHCO_3$, and the resulting solution was separated with diethyl ether (100 mL) and washed with brine (100 mL). The ether layer was dried over anhydrous $MgSO_4$, and the solvent was concentrated under reduced pressure to give (2-chloro-cyclopent-1-enyl)-phenyl ketone. H NMR (400 MHz, $CDCl_3$): 7.92 (d, 2H), 7.59 (t, 1H), 7.48 (t, 2H), 2.48 (Sept, 2H), 2.36 (Sept, 2H), 1.90-1.83 (m, 2H), 1.80-1.74 (m, 2H) ppm. IR: 3064, 3031, 2936, 1666, 1593, 1580, 1482, 1449, 1433, 1275, 1252, 740, 691 cm^{-1} [21].

Similarly, Compound (**iii-a**) was prepared following above procedure using (ii-b). ^1H NMR (400 MHz, $CDCl_3$): 7.92 (d, 2H), 7.20-7.12 (m, 3H), 2.49-2.40 (m, 4H), 1.50 (q, 2H) ppm. IR: 1653, 1616, 1595, 1451, 1321, 1283, 1072, 955, 840, 792, 713, 687, 675 cm^{-1} [22].

*iv. Synthesis of 3-phenylcyclopent[c]isoxazole (**1**) & 3-phenylcyclohex[c]isoxazole (**2**).*

Sodium azide (5 equiv) was dissolved in 10 mL DMF. Solution of (2-chloro-cyclohex-1-enyl)-

phenyl ketone (1 equiv) in 5 mL of DMSO was added dropwise to the mixture of NaN_3 and the reaction mixture was stirred at 50 °C for 72 h, monitoring by TLC. Then the reaction was diluted with diethyl ether (100 mL). The ethereal mixture was washed with water (2 x 100 mL), brine (1 x 100 mL), and water (1 x 100 mL) and dried over Na_2SO_4, filtered, and concentrate under pressure to yield a solid. Flash column chromatography purified the crude solid to a white solid of compound (**1**). ^{1}H NMR (400 MHz, $CDCl_3$): 7.74 (d, 2H), 7.47 (t, 2H), 7.40 (t, 1H), 2.80 (m, 4H), 1.83 (m, 4H) ppm; IR: 3064, 2965, 2913, 1623, 1442, 1416, 1154, 1072, 776, 697 cm^{-1} [23].

Similarly, Compound (**2**) was prepared following above procedure using (iii-a) ^{1}H NMR (400 MHz, $CDCl_3$):7.80-7.55 (m, 2H), 7.55-7.20 (m, 3H), 3.00-2.50 (m, 6H) ppm; IR: 1650, 770, 700 cm^{-1} [24].

II. Product studies in MeOH

Isoxazole **2** (3.34 mM) was irradiated in argon saturated MeOH using mercury arc lamp for 48 h in several batches and the irradiated solvents were combined and evaporated to get the crude (0.132 g,). Photolyzed sample of **2** in argon saturated MeOH was analyzed using ^{1}H-NMR. The crude was separated using column chromatography using ethyl acetate: hexane (20 %) solvent system to isolate the photo product **3** (2.3 mg). The formation of trapped ketenimine **3** is observed in MeOH.

III. Laser flash photolysis

Yag laser (266 nm, 4000 ns) was used to acquire transient UV-Vis and corresponding kinetic traces.[25] Spectroscopic grade acetonitrile was used to prepare stock solutions of isoxazoles **1**, and

2 such that UV absorption of the solutions at 266 nm between 0.3 and 0.8. The stock solution of 250 mL was taken in a volumetric flask and flowed through the quartz cuvette continuously with the help of a peristaltic pump. Throughout the experiment, argon or oxygen was flowed continuously in the solution.

IV. Cryogenic matrix UV analysis

Cryogenic UV-Vis spectroscopy was performed using a conventional set up.[26] A stock solution of gamma azide **1a** (1.5 µM) and **1b** (2.6 µM) in anhydrous mTHF was prepared with a maximum absorbance at below 0.6. 2 mL of the corresponding sample was placed in a temperature resistant 10 mm X 10 mm cuvette and argon gas was purged through the solution for 2 mins and the cuvette was capped and sealed with a piece of Teflon tape. Then, the cuvette was inserted in a cryostat. Liquid nitrogen was poured into the cryostat until the temperature reached 77 K and glassy mTHF matrix was formed. UV-Vis spectra before irradiation was recorded as baseline in the JASCO V-750 UV-Vis spectrophotometer. The matrix was irradiated with Xenon lamp and difference spectra were recorded at different time intervals.

V. Cryogenic matrix IR analysis

First, only argon was deposited at 20 K for 5 min on a Cesium Iodide (CsI) window inside the cryostat cold head. Then, isoxazole **1** was sublimed at 323 K (50 ºC) and deposited along with argon for 120 min on CsI window at 20 K. The cryostat was cooled to 9 K before irradiating the sample. The argon matrix containing isoxazole **1** was irradiated through quartz window using a Xe lamp with 300-400 nm filter, placed adjacent to the quartz window, and IR spectra were

recorded after various irradiation times. Xe lamp: JASCO, model no. SM0101.Similarly the cryogenic matrix IR spectrum of isoxazole **2** was also collected

VI. Quantum modelling

All geometries were optimized with density functional theory (DFT) using Gaussian16 [27] at the B3LYP level of theory with the 631+G(d) basis set.[28, 29] Energies of excited singlet and triplet states and UV-Vis spectra of optimized ground states were computed using TD-DFT.[30, 31] We analyzed the second derivative of the energy with respect to the internal coordinates to satisfy all transition states having one imaginary vibrational frequency. Intrinsic reaction coordinate (IRC) calculations verified the located transition states corresponded to the respective reactant and the products.[32, 33] The calculations were carried out at the Ohio Supercomputer.

VII. Phosphorescence

mTHF solutions of isoxazole **1** (0.06 M) and **2** (0.06 M) were prepared and cooled to 77 K and their phosphorescence spectra obtained using a Phosphorimeter, which has been described previously.[34] The samples were excited with 280 nm light and the emission spectra were recorded between 300 nm and 800 nm.

11. Reference

1. Tomioka, H., Triplet carbenes. In *Reactive intermediates*, Moss, R. A.; Platz, M. S. J., M., Jr., Eds. Wiley-Interscience: 2004; Vol. Chapter 9, p 375.
2. Subhan, W.; Rempala, P.; Sheridan, R. S., *J. Am. Chem. Soc.* **1998,** *120*, 11528.
3. Lahti, P. M., Magnetic properties of organic materials. Lahti, P. M., Ed. Marcel Dekker: New york, 1999; p 661.
4. Fu, J.; Zanoni, G.; Anderson, E. A.; Bi, X., α-Substituted vinyl azides: an emerging functionalized alkene. *Chemical Society Reviews* **2017,** *46* (23), 7208-7228.

5. Xie, S.; Lopez, S. A.; Ramström, O.; Yan, M.; Houk, K. N., 1,3-Dipolar Cycloaddition Reactivities of Perfluorinated Aryl Azides with Enamines and Strained Dipolarophiles. *Journal of the American Chemical Society* **2015,** *137* (8), 2958-2966.
6. Bräse, S.; Gil, C.; Knepper, K.; Zimmermann, V., Organic azides: an exploding diversity of a unique class of compounds. *Angew Chem Int Ed Engl* **2005,** *44* (33), 5188-240.
7. Banerjee, U.; Thenna-Hewa, K.; Gudmundsdottir, A. D., Triplet vinylnitrenes. In *PATAI'S Chemistry of Functional Groups*, pp 1-37.
8. Rajam, S.; Jadhav, A. V.; Li, Q.; Sarkar, S. K.; Singh, P. N. D.; Rohr, A.; Pace, T. C. S.; Li, R.; Krause, J. A.; Bohne, C.; Ault, B. S.; Gudmundsdottir, A. D., Triplet Sensitized Photolysis of a Vinyl Azide: Direct Detection of a Triplet Vinyl Azide and Nitrene. *The Journal of Organic Chemistry* **2014,** *79* (19), 9325-9334.
9. Nunes, C. M.; Reva, I.; Fausto, R., Capture of an Elusive Nitrile Ylide as an Intermediate in Isoxazole–Oxazole Photoisomerization. *The Journal of Organic Chemistry* **2013,** *78* (21), 10657-10665.
10. Nunes, C. M.; Reva, I.; Pinho e Melo, T. M. V. D.; Fausto, R., UV-Laser Photochemistry of Isoxazole Isolated in a Low-Temperature Matrix. *The Journal of Organic Chemistry* **2012,** *77* (19), 8723-8732.
11. Rajam, S.; Murthy, R. S.; Jadhav, A. V.; Li, Q.; Keller, C.; Carra, C.; Pace, T. C. S.; Bohne, C.; Ault, B. S.; Gudmundsdottir, A. D., Photolysis of (3-Methyl-2H-azirin-2-yl)-phenylmethanone: Direct Detection of a Triplet Vinylnitrene Intermediate. *The Journal of Organic Chemistry* **2011,** *76* (24), 9934-9945.
12. Sarkar, S. K.; Sawai, A.; Kanahara, K.; Wentrup, C.; Abe, M.; Gudmundsdottir, A. D., Direct Detection of a Triplet Vinylnitrene, 1,4-Naphthoquinone-2-ylnitrene, in Solution and Cryogenic Matrices. *Journal of the American Chemical Society* **2015,** *137* (12), 4207-4214.
13. Gatlin, D. M.; Karney, W. L.; Abe, M.; Ault, B. S.; Gudmundsdottir, A. D., Formation and Reactivity of Triplet Vinylnitrenes as a Function of Ring Size. *The Journal of Organic Chemistry* **2019,** *84* (14), 9215-9225.
14. Sarkar, S. K.; Osisioma, O.; Karney, W. L.; Abe, M.; Gudmundsdottir, A. D., Using Molecular Architecture to Control the Reactivity of a Triplet Vinylnitrene. *Journal of the American Chemical Society* **2016,** *138* (45), 14905-14914.
15. Inui, H.; Murata, S., Photochemistry of 2-(1-Naphthyl)-2H-azirines in Matrixes and in Solutions: Wavelength-Dependent C−C and C−N Bond Cleavage of the Azirine Ring. *Journal of the American Chemical Society* **2005,** *127* (8), 2628-2636.
16. Inui, H.; Murata, S., Mechanism of photochemical rearrangement of 2H-azirines in low-temperature matrices: Chemical evidences for the participation of vibrationally hot molecules. *Chemical Physics Letters* **2002,** *359*, 267-272.
17. Inui, H.; Murata, S., Control of CC and CN Bond Cleavage of 2H-Azirine by Means of the Excitation Wavelength: Studies in Matrices and in Solutions. *Chemistry Letters - CHEM LETT* **2001,** *30*, 832-833.
18. Komkov, A. V.; Komendantova, A. S.; Menchikov, L. G.; Chernoburova, E. I.; Volkova, Y. A.; Zavarzin, I. V., A Straightforward Approach toward Multifunctionalized Pyridazines via Imination/Electrocyclization. *Organic Letters* **2015,** *17* (15), 3734-3737.
19. Chassaing, S.; Kueny-Stotz, M.; Isorez, G.; Brouillard, R., Rapid Preparation of 3-Deoxyanthocyanidins and Novel Dicationic Derivatives: New Insight into an Old Procedure. *European Journal of Organic Chemistry* **2007,** *2007* (15), 2438-2448.
20. Pigge, F. C.; Ghasedi, F.; Zheng, Z.; Rath, N. P.; Nichols, G.; Chickos, J. S., Structural characterization of crystalline inclusion complexes formed from 1,3,5-triaroylbenzene derivatives—a new family of inclusion hosts. *Journal of the Chemical Society, Perkin Transactions 2* **2000,** (12), 2458-2464.

21. Martens, H.; Hoornaert, G.; Toppet, S., Spectral correlations for β-chlorovinyl ketones. *Tetrahedron* **1973,** *29* (24), 4241-4249.
22. Prasad, H. S.; Nagendrappa, G., Vinylsilanes in synthesis: 2-Halo-lcyclopentenyl

alkyl/aryl ketonesfrom 2-halo-l-trimethylsilylcyclopentenes. *Indian Journal Chemistry* **1997,** *36 B* (8), 691-694.

23. Shigenobu, M.; Takenaka, K.; Sasai, H., Palladium-Catalyzed Direct C□H Arylation of Isoxazoles at the 5-Position. *Angewandte Chemie International Edition* **2015,** *54* (33), 9572-9576.
24. Alberola, A.; Manuel Bañez, J.; Calvo, L.; Rodríguez Rodríguez, M. T.; Carmen Sañudo, M., Synthesis of 3-substituted 5-arylisoxazoles from α,β-unsaturated oximes. *Journal of Heterocyclic Chemistry* **1993,** *30* (2), 467-471.
25. Muthukrishnan, S.; Sankaranarayanan, J.; Klima, R. F.; Pace, T. C. S.; Bohne, C.; Gudmundsdottir, A. D., Intramolecular H-Atom Abstraction in γ-Azido-Butyrophenones: Formation of 1,5 Ketyl Iminyl Radicals. *Org. Lett.* **2009,** *11* (11), 2345-2348.
26. Banerjee, U.; Karney, W. L.; Ault, B. S.; Gudmundsdottir, A. D., Photolysis of 5-Azido-3-Phenylisoxazole at Cryogenic Temperature: Formation and Direct Detection of a Nitrosoalkene. *Molecules* **2020,** *25* (3), 543.
27. Frisch, M. J.; Trucks, G. W.; Schlegel, H. B.; Scuseria, G. E.; Robb, M. A.; Cheeseman, J. R.; Scalmani, G.; Barone, V.; Petersson, G. A.; Nakatsuji, H.; Li, X.; Caricato, M.; Marenich, A. V.; Bloino, J.; Janesko, B. G.; Gomperts, R.; Mennucci, B.; Hratchian, H. P.; Ortiz, J. V.; Izmaylov, A. F.; Sonnenberg, J. L.; Williams; Ding, F.; Lipparini, F.; Egidi, F.; Goings, J.; Peng, B.; Petrone, A.; Henderson, T.; Ranasinghe, D.; Zakrzewski, V. G.; Gao, J.; Rega, N.; Zheng, G.; Liang, W.; Hada, M.; Ehara, M.; Toyota, K.; Fukuda, R.; Hasegawa, J.; Ishida, M.; Nakajima, T.; Honda, Y.; Kitao, O.; Nakai, H.; Vreven, T.; Throssell, K.; Montgomery Jr., J. A.; Peralta, J. E.; Ogliaro, F.; Bearpark, M. J.; Heyd, J. J.; Brothers, E. N.; Kudin, K. N.; Staroverov, V. N.; Keith, T. A.; Kobayashi, R.; Normand, J.; Raghavachari, K.; Rendell, A. P.; Burant, J. C.; Iyengar, S. S.; Tomasi, J.; Cossi, M.; Millam, J. M.; Klene, M.; Adamo, C.; Cammi, R.; Ochterski, J. W.; Martin, R. L.; Morokuma, K.; Farkas, O.; Foresman, J. B.; Fox, D. J. *Gaussian 16 Rev. C.01*, Wallingford, CT, 2016.
28. Becke, A. D., Density-functional thermochemistry. III. The role of exact exchange. *The Journal of Chemical Physics* **1993,** *98* (7), 5648-5652.
29. Parr, R. G.; Yang, W., *Density-functional theory of atoms and molecules*. Oxford University Press: Oxford, 1994.
30. Bauernschmitt, R.; Ahlrichs, R., Treatment of electronic excitations within the adiabatic approximation of time dependent density functional theory. *Chemical Physics Letters* **1996,** *256* (4), 454-464.
31. Foresman, J. B.; Head-Gordon, M.; Pople, J. A.; Frisch, M. J., Toward a systematic molecular orbital theory for excited states. *The Journal of Physical Chemistry* **1992,** *96* (1), 135-149.
32. Gonzalez, C.; Schlegel, H. B., An improved algorithm for reaction path following. *The Journal of Chemical Physics* **1989,** *90* (4), 2154-2161.
33. Gonzalez, C.; Schlegel, H. B., Reaction path following in mass-weighted internal coordinates. *The Journal of Physical Chemistry* **1990,** *94* (14), 5523-5527.
34. Ranaweera, R. A. A. U.; Scott, T.; Li, Q.; Rajam, S.; Duncan, A.; Li, R.; Evans, A.; Bohne, C.; Toscano, J. P.; Ault, B. S.; Gudmundsdottir, A. D., Trans–Cis Isomerization of Vinylketones through Triplet 1,2-Biradicals. *The Journal of Physical Chemistry A* **2014,** *118* (45), 10433-10447.

Chapter 2: Supporting Information

I. X-RAY CRYSTALLOGRAPHIC ANALYSIS OF THE COMPOUNDS

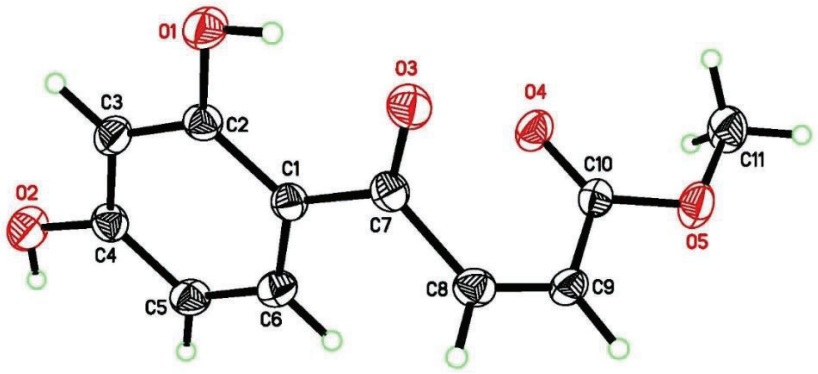

Figure S63. XRD Structure of cis-**1**

Table 1. Crystal data and structure refinement for cis-$C_{11}H_{10}O_5$.

Empirical formula	$C_{11}H_{10}O_5$	
Formula weight	222.19	
Temperature	150(2) K	
Wavelength	0.71073 Å	
Crystal system	Monoclinic	
Space group	$P2_1/c$	
Unit cell dimensions	a = 10.8195(4) Å	α = 90°
	b = 5.2850(2) Å	β = 102.3871(14) °
	c = 18.4345(8) Å	γ = 90°
Volume	1029.57(7) $Å^3$	
Z	4	
Density (calculated)	1.433 Mg/m^3	
Absorption coefficient	0.115 mm^{-1}	
F(000)	464	
Crystal size	0.253 x 0.084 x 0.052 mm^3	
θ range for data collection	3.272 to 28.278°	
Index ranges	$-14 \le h \le 14, -7 \le k \le 7, -24 \le l \le 24$	
Reflections collected	30224	
Independent reflections	2549 [R_{int} = 0.0269]	
Completeness to θ = 25.242°	99.7 %	
Absorption correction	Numerical	
Max. and min. transmission	0.862 and 0.824	
Refinement method	Full-matrix least-squares on F^2	

Data / restraints / parameters	2549 / 0 / 152
Goodness-of-fit on F^2	1.053
Final R indices [I>2σ(I)]	R1 = 0.0334, wR2 = 0.0896
R indices (all data)	R1 = 0.0369, wR2 = 0.0932
Largest diff. peak and hole	0.340 and -0.192 eÅ^{-3}

Table 2. Atomic coordinates [x10^4] and equivalent isotropic displacement parameters [Å^{2}x10^3] for cis- $C_{11}H_{10}O_5$. U(eq) is defined as one third of the trace of the orthogonalized U_{ij} tensor.

	x	y	z	U(eq)
O(1)	7932(1)	3489(2)	1605(1)	30(1)
O(2)	3869(1)	6713(2)	685(1)	33(1)
O(3)	9340(1)	5686(2)	2763(1)	27(1)
O(4)	7773(1)	5416(2)	4060(1)	27(1)
O(5)	8690(1)	7470(2)	5107(1)	30(1)
C(1)	7265(1)	7090(2)	2232(1)	21(1)
C(2)	7045(1)	5216(2)	1670(1)	22(1)
C(3)	5902(1)	5131(2)	1156(1)	25(1)
C(4)	4967(1)	6889(2)	1198(1)	24(1)
C(5)	5159(1)	8763(2)	1752(1)	25(1)
C(6)	6298(1)	8844(2)	2254(1)	24(1)
C(7)	8474(1)	7229(2)	2755(1)	21(1)
C(8)	8745(1)	9445(2)	3274(1)	24(1)
C(9)	8744(1)	9436(2)	3994(1)	23(1)
C(10)	8341(1)	7228(2)	4374(1)	21(1)
C(11)	8339(1)	5437(2)	5552(1)	33(1)
H(1)	8625(15)	3870(30)	1962(9)	44
H(2)	3357(17)	7860(30)	773(9)	49
H(3A)	5761	3878	778	30
H(5A)	4512	9953	1779	30
H(6A)	6435	10120	2625	29
H(8A)	8937	11006	3067	28
H(9A)	9014	10915	4277	28
H(11A)	8761	5684	6073	50
H(11B)	8601	3813	5377	50
H(11C)	7420	5442	5507	50

Table 3. Bond lengths [Å] and angles [°] for cis- $C_{11}H_{10}O_5$.

O(1)-C(2)	1.3479(12)	O(2)-C(4)	1.3545(12)
O(3)-C(7)	1.2399(13)	O(4)-C(10)	1.2155(13)
O(5)-C(10)	1.3282(12)	O(5)-C(11)	1.4512(14)
C(1)-C(6)	1.4057(14)	C(1)-C(2)	1.4154(14)
C(1)-C(7)	1.4507(13)	C(2)-C(3)	1.3878(14)
C(3)-C(4)	1.3882(14)	C(4)-C(5)	1.4050(15)
C(5)-C(6)	1.3735(14)	C(7)-C(8)	1.5011(14)
C(8)-C(9)	1.3277(15)	C(9)-C(10)	1.4739(14)

C(10)-O(5)-C(11)	116.91(9)	C(6)-C(1)-C(2)	118.22(9)
C(6)-C(1)-C(7)	121.21(9)	C(2)-C(1)-C(7)	120.55(9)
O(1)-C(2)-C(3)	117.67(9)	O(1)-C(2)-C(1)	121.80(9)
C(3)-C(2)-C(1)	120.52(9)	C(2)-C(3)-C(4)	119.56(9)
O(2)-C(4)-C(3)	117.10(9)	O(2)-C(4)-C(5)	121.80(9)
C(3)-C(4)-C(5)	121.10(9)	C(6)-C(5)-C(4)	118.86(9)
C(5)-C(6)-C(1)	121.74(10)	O(3)-C(7)-C(1)	123.04(9)
O(3)-C(7)-C(8)	117.52(9)	C(1)-C(7)-C(8)	119.25(9)
C(9)-C(8)-C(7)	126.33(9)	C(8)-C(9)-C(10)	122.80(9)
O(4)-C(10)-O(5)	124.33(10)	O(4)-C(10)-C(9)	124.67(9)
O(5)-C(10)-C(9)	111.00(9)		

Table 4. Anisotropic displacement parameters [$Å^2x10^3$] for cis- $C_{11}H_{10}O_5$. The anisotropic displacement factor exponent takes the form: $-2\pi^2[h^2a^{*2}U_{11}+... +2hka^*b^*U_{12}]$

	U_{11}	U_{22}	U_{33}	U_{23}	U_{13}	U_{12}
O(1)	26(1)	30(1)	30(1)	-7(1)	2(1)	9(1)
O(2)	25(1)	38(1)	33(1)	-8(1)	-2(1)	9(1)
O(3)	24(1)	29(1)	27(1)	0(1)	5(1)	4(1)
O(4)	32(1)	24(1)	24(1)	-2(1)	4(1)	-9(1)
O(5)	38(1)	32(1)	19(1)	-2(1)	3(1)	-10(1)
C(1)	22(1)	21(1)	20(1)	1(1)	6(1)	0(1)
C(2)	24(1)	21(1)	22(1)	1(1)	7(1)	3(1)
C(3)	26(1)	26(1)	23(1)	-4(1)	4(1)	3(1)
C(4)	22(1)	26(1)	23(1)	1(1)	3(1)	2(1)
C(5)	24(1)	24(1)	29(1)	-2(1)	7(1)	5(1)
C(6)	26(1)	22(1)	26(1)	-3(1)	7(1)	1(1)
C(7)	23(1)	22(1)	20(1)	2(1)	7(1)	-1(1)
C(8)	23(1)	21(1)	27(1)	1(1)	5(1)	-2(1)
C(9)	22(1)	19(1)	26(1)	-3(1)	2(1)	-4(1)

C(10)	20(1)	23(1)	20(1)	-2(1)	3(1)	-1(1)
C(11)	42(1)	36(1)	22(1)	3(1)	7(1)	-5(1)

Table 5. Torsion angles [°] for cis- $C_{11}H_{10}O_5$.

C(6)-C(1)-C(2)-O(1)	179.04(9)	C(7)-C(1)-C(2)-O(1)	0.80(15)
C(6)-C(1)-C(2)-C(3)	0.16(15)	C(7)-C(1)-C(2)-C(3)	-178.08(9)
O(1)-C(2)-C(3)-C(4)	-179.41(10)	C(1)-C(2)-C(3)-C(4)	-0.49(16)
C(2)-C(3)-C(4)-O(2)	-179.73(10)	C(2)-C(3)-C(4)-C(5)	0.22(16)
O(2)-C(4)-C(5)-C(6)	-179.67(10)	C(3)-C(4)-C(5)-C(6)	0.39(16)
C(4)-C(5)-C(6)-C(1)	-0.73(16)	C(2)-C(1)-C(6)-C(5)	0.46(15)
C(7)-C(1)-C(6)-C(5)	178.69(10)	C(6)-C(1)-C(7)-O(3)	178.46(10)
C(2)-C(1)-C(7)-O(3)	-3.36(15)	C(6)-C(1)-C(7)-C(8)	-6.72(14)
C(2)-C(1)-C(7)-C(8)	171.47(9)	O(3)-C(7)-C(8)-C(9)	-79.96(14)
C(1)-C(7)-C(8)-C(9)	104.94(12)	C(7)-C(8)-C(9)-C(10)	-6.30(16)
C(11)-O(5)-C(10)-O(4)	-1.19(16)	C(11)-O(5)-C(10)-C(9)	179.29(9)
C(8)-C(9)-C(10)-O(4)	-13.61(17)	C(8)-C(9)-C(10)-O(5)	165.91(10)

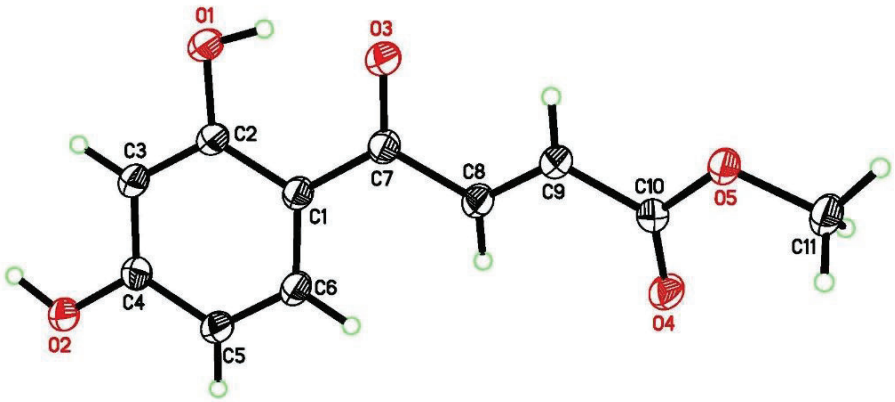

Figure S64. XRD Structure of *trans*-**1**

Table 1. Crystal data and structure refinement for trans-$C_{11}H_{10}O_5$.

Empirical formula	$C_{11}H_{10}O_5$
Formula weight	222.19
Temperature	150(2) K
Wavelength	0.71073 Å
Crystal system	Monoclinic

Space group	$P2_1/n$	
Unit cell dimensions	a = 4.7923(2) Å	α = 90°
	b = 18.9606(10) Å	β = 95.3361(18)°
	c = 11.2293(6) Å	γ = 90°
Volume	1015.93(9) $Å^3$	
Z	4	
Density (calculated)	1.453 Mg/m^3	
Absorption coefficient	0.116 mm^{-1}	
F(000)	464	
Crystal size	0.201 x 0.100 x 0.073 mm^3	
θ range for data collection	2.817 to 28.321°	
Index ranges	$-6 \le h \le 6$, $-25 \le k \le 25$, $-14 \le l \le 14$	
Reflections collected	29593	
Independent reflections	2532 [R_{int} = 0.0443]	
Completeness to θ = 25.242°	99.9 %	
Absorption correction	Numerical	
Max. and min. transmission	0.862 and 0.802	
Refinement method	Full-matrix least-squares on F^2	
Data / restraints / parameters	2532 / 0 / 152	
Goodness-of-fit on F^2	1.057	
Final R indices [I>2σ(I)]	R1 = 0.0338, wR2 = 0.0931	
R indices (all data)	R1 = 0.0382, wR2 = 0.0976	
Largest diff. peak and hole	0.350 and -0.182 $eÅ^{-3}$	

Table 2. Atomic coordinates [x10^4] and equivalent isotropic displacement parameters [$Å^2$x10^3] for trans- $C_{11}H_{10}O_5$. U(eq) is defined as one third of the trace of the orthogonalized U_{ij} tensor.

	x	y	z	U(eq)
O(1)	8693(2)	3235(1)	6816(1)	31(1)
O(2)	7324(2)	794(1)	6108(1)	27(1)
O(3)	5424(2)	4090(1)	5635(1)	28(1)
O(4)	-3050(2)	4226(1)	2689(1)	27(1)
O(5)	-1012(2)	5298(1)	2737(1)	25(1)
C(1)	4865(2)	2865(1)	5390(1)	22(1)
C(2)	7186(2)	2719(1)	6240(1)	22(1)
C(3)	7996(2)	2026(1)	6499(1)	24(1)
C(4)	6567(2)	1473(1)	5911(1)	23(1)
C(5)	4270(2)	1602(1)	5068(1)	26(1)
C(6)	3463(2)	2286(1)	4821(1)	25(1)
C(7)	4057(2)	3594(1)	5148(1)	22(1)
C(8)	1575(2)	3768(1)	4299(1)	23(1)
C(9)	1179(2)	4431(1)	3933(1)	22(1)
C(10)	-1193(2)	4627(1)	3061(1)	21(1)

C(11)	-3189(3)	5549(1)	1857(1)	30(1)
H(1)	7960(40)	3649(9)	6502(15)	47
H(2)	8910(40)	770(9)	6622(15)	41
H(3A)	9526	1933	7077	29
H(5A)	3287	1220	4674	32
H(6A)	1912	2370	4249	30
H(8A)	290	3410	4021	28
H(9A)	2449	4785	4239	27
H(11A)	-2980	6058	1747	45
H(11B)	-5030	5450	2133	45
H(11C)	-3030	5308	1094	45

Table 3. Bond lengths [Å] and angles [°] for trans- $C_{11}H_{10}O_5$.

O(1)-C(2)	1.3454(13)	O(2)-C(4)	1.3508(12)
O(3)-C(7)	1.2444(13)	O(4)-C(10)	1.2141(13)
O(5)-C(10)	1.3288(12)	O(5)-C(11)	1.4493(13)
C(1)-C(6)	1.4100(14)	C(1)-C(2)	1.4240(14)
C(1)-C(7)	1.4533(14)	C(2)-C(3)	1.3918(14)
C(3)-C(4)	1.3856(15)	C(4)-C(5)	1.4049(14)
C(5)-C(6)	1.3739(15)	C(7)-C(8)	1.4912(14)
C(8)-C(9)	1.3289(15)	C(9)-C(10)	1.4770(14)
C(10)-O(5)-C(11)	116.11(8)	C(6)-C(1)-C(2)	117.45(9)
C(6)-C(1)-C(7)	123.29(9)	C(2)-C(1)-C(7)	119.26(9)
O(1)-C(2)-C(3)	117.29(9)	O(1)-C(2)-C(1)	122.07(9)
C(3)-C(2)-C(1)	120.63(9)	C(4)-C(3)-C(2)	119.90(9)
O(2)-C(4)-C(3)	122.05(9)	O(2)-C(4)-C(5)	117.21(10)
C(3)-C(4)-C(5)	120.73(10)	C(6)-C(5)-C(4)	119.21(10)
C(5)-C(6)-C(1)	122.06(10)	O(3)-C(7)-C(1)	121.13(9)
O(3)-C(7)-C(8)	117.97(9)	C(1)-C(7)-C(8)	120.90(9)
C(9)-C(8)-C(7)	119.35(9)	C(8)-C(9)-C(10)	121.44(10)
O(4)-C(10)-O(5)	124.66(9)	O(4)-C(10)-C(9)	124.42(10)
O(5)-C(10)-C(9)	110.91(9)		

Table 4. Anisotropic displacement parameters [$Å^2x10^3$] for trans- $C_{11}H_{10}O_5$. The anisotropic displacement factor exponent takes the form: $-2\pi^2[h^2a^{*2}U_{11}+... +2hka^*b^*U_{12}]$

U_{11}	U_{22}	U_{33}	U_{23}	U_{13}	U_{12}

O(1)	32(1)	23(1)	35(1)	-1(1)	-14(1)	0(1)
O(2)	29(1)	21(1)	30(1)	0(1)	-7(1)	4(1)
O(3)	28(1)	22(1)	33(1)	-1(1)	-8(1)	-1(1)
O(4)	23(1)	24(1)	31(1)	1(1)	-6(1)	-4(1)
O(5)	25(1)	20(1)	29(1)	3(1)	-7(1)	0(1)
C(1)	20(1)	22(1)	22(1)	1(1)	-1(1)	1(1)
C(2)	21(1)	23(1)	22(1)	-1(1)	-2(1)	-1(1)
C(3)	23(1)	24(1)	23(1)	1(1)	-4(1)	2(1)
C(4)	24(1)	22(1)	22(1)	1(1)	0(1)	2(1)
C(5)	26(1)	22(1)	30(1)	-2(1)	-6(1)	-1(1)
C(6)	23(1)	25(1)	27(1)	1(1)	-6(1)	1(1)
C(7)	21(1)	22(1)	23(1)	2(1)	0(1)	0(1)
C(8)	20(1)	23(1)	26(1)	1(1)	-2(1)	0(1)
C(9)	20(1)	22(1)	24(1)	-1(1)	-2(1)	0(1)
C(10)	21(1)	20(1)	22(1)	0(1)	0(1)	1(1)
C(11)	32(1)	27(1)	30(1)	6(1)	-9(1)	1(1)

Table 5. Torsion angles [°] for trans- $C_{11}H_{10}O_5$.

C(6)-C(1)-C(2)-O(1)	178.78(10)	C(7)-C(1)-C(2)-O(1)	-1.08(16)
C(6)-C(1)-C(2)-C(3)	-0.71(16)	C(7)-C(1)-C(2)-C(3)	179.43(10)
O(1)-C(2)-C(3)-C(4)	-178.38(10)	C(1)-C(2)-C(3)-C(4)	1.14(16)
C(2)-C(3)-C(4)-O(2)	178.09(10)	C(2)-C(3)-C(4)-C(5)	-1.08(17)
O(2)-C(4)-C(5)-C(6)	-178.61(10)	C(3)-C(4)-C(5)-C(6)	0.59(17)
C(4)-C(5)-C(6)-C(1)	-0.17(18)	C(2)-C(1)-C(6)-C(5)	0.23(16)
C(7)-C(1)-C(6)-C(5)	-179.92(11)	C(6)-C(1)-C(7)-O(3)	-177.00(10)
C(2)-C(1)-C(7)-O(3)	2.85(16)	C(6)-C(1)-C(7)-C(8)	2.41(16)
C(2)-C(1)-C(7)-C(8)	-177.74(9)	O(3)-C(7)-C(8)-C(9)	11.35(15)
C(1)-C(7)-C(8)-C(9)	-168.08(10)	C(7)-C(8)-C(9)-C(10)	177.94(9)
C(11)-O(5)-C(10)-O(4)	-1.34(16)	C(11)-O(5)-C(10)-C(9)	178.42(9)
C(8)-C(9)-C(10)-O(4)	6.06(17)	C(8)-C(9)-C(10)-O(5)	-173.70(10)

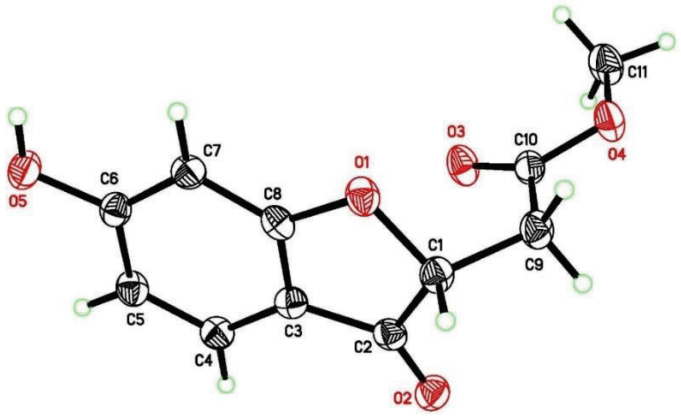

Figure S65. XRD Structure of **1b**

Table 1. Crystal data and structure refinement for $C_{11}H_{10}O_5$.

Empirical formula	$C_{11}H_{10}O_5$	
Formula weight	222.19	
Temperature	150(2) K	
Wavelength	0.71073 Å	
Crystal system	Monoclinic	
Space group	$P2_1/c$	
Unit cell dimensions	a = 10.2217(12) Å	α = 90°
	b = 5.1895(6) Å	β = 104.649(4)°
	c = 19.161(2) Å	γ = 90°
Volume	983.3(2) $Å^3$	
Z	4	
Density (calculated)	1.501 Mg/m^3	
Absorption coefficient	0.120 mm^{-1}	
F(000)	464	
Crystal size	0.138 x 0.061 x 0.042 mm^3	
θ range for data collection	3.371 to 26.382°	
Index ranges	$-12 \le h \le 12$, $-6 \le k \le 6$, $-23 \le l \le 23$	
Reflections collected	16298	
Independent reflections	2013 [R_{int} = 0.0481]	
Completeness to θ = 25.242°	99.8 %	
Absorption correction	Numerical	
Max. and min. transmission	0.862 and 0.789	
Refinement method	Full-matrix least-squares on F^2	
Data / restraints / parameters	2013 / 0 / 185	
Goodness-of-fit on F^2	1.061	
Final R indices [I>2σ(I)]	R1 = 0.0384, wR2 = 0.0818	
R indices (all data)	R1 = 0.0549, wR2 = 0.0917	
Largest diff. peak and hole	0.188 and -0.199 $eÅ^{-3}$	

Table 2. Atomic coordinates [$x10^4$] and equivalent isotropic displacement parameters [$Å^2x10^3$]

for $C_{11}H_{10}O_5$. U(eq) is defined as one third of the trace of the orthogonalized U_{ij} tensor.

	x	y	z	U(eq)
O(1)	2733(1)	410(2)	7104(1)	23(1)
O(2)	92(1)	5020(2)	6882(1)	26(1)
O(3)	2487(1)	4597(2)	5980(1)	28(1)
O(4)	1684(1)	2416(2)	4951(1)	28(1)
O(5)	5950(1)	3737(3)	9188(1)	28(1)
C(1)	1334(2)	1084(3)	6776(1)	22(1)
C(2)	1104(2)	3695(3)	7096(1)	21(1)
C(3)	2295(2)	4094(3)	7683(1)	20(1)
C(4)	2643(2)	5979(3)	8220(1)	22(1)
C(5)	3875(2)	5809(3)	8711(1)	23(1)
C(6)	4774(2)	3793(3)	8666(1)	21(1)
C(7)	4458(2)	1938(3)	8127(1)	22(1)
C(8)	3203(2)	2132(3)	7649(1)	20(1)
C(9)	1028(2)	959(4)	5967(1)	24(1)
C(10)	1826(2)	2844(3)	5648(1)	22(1)
C(11)	2451(2)	4083(4)	4594(1)	32(1)
H(5)	6450(30)	2420(50)	9120(13)	64(8)
H(1A)	763(18)	-180(40)	6938(9)	25(5)
H(4A)	2005(18)	7360(40)	8256(9)	25(5)
H(5A)	4158(18)	7030(40)	9098(10)	28(5)
H(7A)	5078(18)	600(40)	8096(9)	25(5)
H(9A)	75(19)	1310(40)	5777(10)	26(5)
H(9B)	1209(19)	-770(40)	5827(10)	31(5)
H(11B)	2230(20)	5880(50)	4655(11)	41(6)
H(11A)	3420(20)	3750(40)	4802(11)	40(6)
H(11C)	2180(20)	3680(40)	4085(12)	41(6)

Table 3. Bond lengths [Å] and angles [°] for $C_{11}H_{10}O_5$.

O(1)-C(8)	1.3672(19)	O(1)-C(1)	1.451(2)
O(2)-C(2)	1.224(2)	O(3)-C(10)	1.213(2)
O(4)-C(10)	1.325(2)	O(4)-C(11)	1.449(2)
O(5)-C(6)	1.356(2)	C(1)-C(9)	1.504(2)
C(1)-C(2)	1.530(2)	C(2)-C(3)	1.448(2)
C(3)-C(8)	1.390(2)	C(3)-C(4)	1.399(2)
C(4)-C(5)	1.371(2)	C(5)-C(6)	1.410(2)
C(6)-C(7)	1.389(2)	C(7)-C(8)	1.378(2)
C(9)-C(10)	1.499(2)		
C(8)-O(1)-C(1)	106.89(12)	C(10)-O(4)-C(11)	116.13(14)

O(1)-C(1)-C(9)	111.10(14)	O(1)-C(1)-C(2)	105.94(13)
C(9)-C(1)-C(2)	116.02(15)	O(2)-C(2)-C(3)	130.80(16)
O(2)-C(2)-C(1)	124.48(15)	C(3)-C(2)-C(1)	104.70(14)
C(8)-C(3)-C(4)	119.84(15)	C(8)-C(3)-C(2)	107.41(14)
C(4)-C(3)-C(2)	132.74(15)	C(5)-C(4)-C(3)	118.57(15)
C(4)-C(5)-C(6)	120.37(16)	O(5)-C(6)-C(7)	122.01(15)
O(5)-C(6)-C(5)	116.11(15)	C(7)-C(6)-C(5)	121.87(15)
C(8)-C(7)-C(6)	116.41(15)	O(1)-C(8)-C(7)	123.23(15)
O(1)-C(8)-C(3)	113.85(14)	C(7)-C(8)-C(3)	122.92(15)
C(10)-C(9)-C(1)	113.56(14)	O(3)-C(10)-O(4)	123.99(16)
O(3)-C(10)-C(9)	124.30(15)	O(4)-C(10)-C(9)	111.67(14)

Table 4. Anisotropic displacement parameters [$Å^2x10^3$] for $C_{11}H_{10}O_5$. The anisotropic displacement factor exponent takes the form: $-2\pi^2[h\ ^2a^{*2}U_{11}+... +2hka^*b^*U_{12}]$

	U_{11}	U_{22}	U_{33}	U_{23}	U_{13}	U_{12}
O(1)	28(1)	20(1)	21(1)	-3(1)	4(1)	1(1)
O(2)	24(1)	27(1)	26(1)	0(1)	4(1)	2(1)
O(3)	36(1)	25(1)	23(1)	-4(1)	7(1)	-10(1)
O(4)	34(1)	31(1)	18(1)	-3(1)	5(1)	-7(1)
O(5)	26(1)	29(1)	25(1)	-3(1)	-1(1)	6(1)
C(1)	23(1)	21(1)	22(1)	-1(1)	5(1)	-4(1)
C(2)	23(1)	22(1)	20(1)	2(1)	8(1)	-2(1)
C(3)	22(1)	18(1)	21(1)	3(1)	7(1)	-1(1)
C(4)	26(1)	18(1)	24(1)	0(1)	7(1)	3(1)
C(5)	28(1)	19(1)	22(1)	-4(1)	5(1)	1(1)
C(6)	22(1)	21(1)	20(1)	3(1)	4(1)	0(1)
C(7)	24(1)	19(1)	22(1)	1(1)	6(1)	4(1)
C(8)	26(1)	17(1)	18(1)	0(1)	8(1)	-2(1)
C(9)	26(1)	22(1)	24(1)	-4(1)	5(1)	-6(1)
C(10)	23(1)	22(1)	20(1)	-2(1)	3(1)	2(1)
C(11)	39(1)	37(1)	20(1)	3(1)	9(1)	-6(1)

Table 5. Torsion angles [°] for $C_{11}H_{10}O_5$.

C(8)-O(1)-C(1)-C(9)	137.09(14)	C(8)-O(1)-C(1)-C(2)	10.27(16)
O(1)-C(1)-C(2)-O(2)	170.63(15)	C(9)-C(1)-C(2)-O(2)	46.8(2)
O(1)-C(1)-C(2)-C(3)	-10.82(16)	C(9)-C(1)-C(2)-C(3)	-134.61(15)
O(2)-C(2)-C(3)-C(8)	-174.18(17)	C(1)-C(2)-C(3)-C(8)	7.40(17)

O(2)-C(2)-C(3)-C(4)	5.0(3)	C(1)-C(2)-C(3)-C(4)	-173.38(17)
C(8)-C(3)-C(4)-C(5)	-1.1(2)	C(2)-C(3)-C(4)-C(5)	179.75(17)
C(3)-C(4)-C(5)-C(6)	0.9(3)	C(4)-C(5)-C(6)-O(5)	-177.98(15)
C(4)-C(5)-C(6)-C(7)	0.6(3)	O(5)-C(6)-C(7)-C(8)	176.73(15)
C(5)-C(6)-C(7)-C(8)	-1.7(2)	C(1)-O(1)-C(8)-C(7)	173.56(15)
C(1)-O(1)-C(8)-C(3)	-6.04(18)	C(6)-C(7)-C(8)-O(1)	-178.09(14)
C(6)-C(7)-C(8)-C(3)	1.5(2)	C(4)-C(3)-C(8)-O(1)	179.51(14)
C(2)-C(3)-C(8)-O(1)	-1.16(18)	C(4)-C(3)-C(8)-C(7)	-0.1(2)
C(2)-C(3)-C(8)-C(7)	179.23(15)	O(1)-C(1)-C(9)-C(10)	-63.00(19)
C(2)-C(1)-C(9)-C(10)	58.1(2)	C(11)-O(4)-C(10)-O(3)	4.1(2)
C(11)-O(4)-C(10)-C(9)	-178.04(16)	C(1)-C(9)-C(10)-O(3)	-11.7(3)
C(1)-C(9)-C(10)-O(4)	170.50(14)		

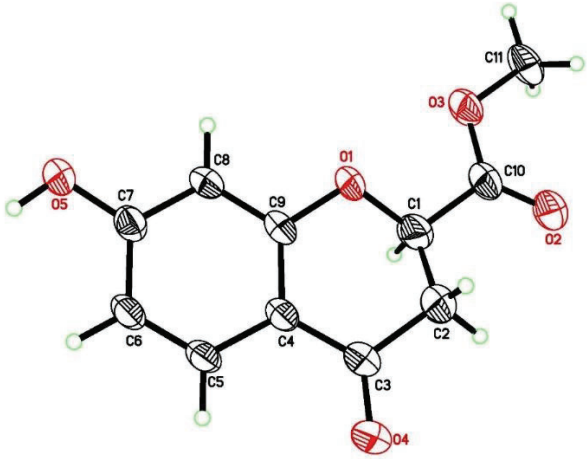

Figure S66. XRD Structure of **1P**

Table 1. Crystal data and structure refinement for $C_{11}H_{10}O_5$.

Empirical formula	$C_{11}H_{10}O_5$	
Formula weight	222.19	
Temperature	150(2) K	
Wavelength	0.7288 Å	
Crystal system	Monoclinic	
Space group	$P2_1/c$	
Unit cell dimensions	a = 10.6467(8) Å	α = 90°
	b = 12.8906(9) Å	β = 99.662(3)°
	c = 7.3638(5) Å	γ = 90°
Volume	996.29(12) $Å^3$	
Z	4	
Density (calculated)	1.481 Mg/m^3	
Absorption coefficient	0.124 mm^{-1}	
F(000)	464	

Crystal size	0.075 x 0.035 x 0.016 mm^3
θ range for data collection	1.990 to 25.384°
Index ranges	$-12 \leq h \leq 12$, $-15 \leq k \leq 15$, $-8 \leq l \leq 8$
Reflections collected	18390
Independent reflections	1701 [R_{int} = 0.0640]
Completeness to θ = 25.384°	100.0 %
Absorption correction	Semi-empirical from equivalents
Max. and min. transmission	0.746 and 0.635
Refinement method	Full-matrix least-squares on F^2
Data / restraints / parameters	1701 / 0 / 149
Goodness-of-fit on F^2	1.134
Final R indices [I>2σ(I)]	R1 = 0.0671, wR2 = 0.1621
R indices (all data)	R1 = 0.0825, wR2 = 0.1704
Largest diff. peak and hole	0.616 and -0.293 $eÅ^{-3}$

Table 2. Atomic coordinates [$x10^4$] and equivalent isotropic displacement parameters [$Å^2x10^3$] for $C_{11}H_{10}O_5$. U(eq) is defined as one third of the trace of the orthogonalized U_{ij} tensor.

	x	y	z	U(eq)
O(1)	6299(2)	4990(2)	4040(3)	33(1)
O(2)	4290(2)	7121(2)	2646(4)	46(1)
O(3)	4318(2)	5485(2)	1619(3)	40(1)
O(4)	8198(3)	7137(2)	7581(4)	57(1)
O(5)	9434(3)	2468(2)	5620(4)	46(1)
C(1)	6069(4)	6064(3)	3800(6)	48(1)
C(2)	6333(4)	6677(3)	5480(6)	52(1)
C(3)	7667(3)	6484(3)	6501(5)	41(1)
C(4)	8184(3)	5466(3)	6235(5)	29(1)
C(5)	9362(3)	5130(3)	7224(5)	32(1)
C(6)	9791(3)	4145(3)	7057(5)	34(1)
C(7)	9051(3)	3445(3)	5860(5)	33(1)
C(8)	7887(3)	3747(3)	4867(5)	31(1)
C(9)	7465(3)	4748(3)	5060(4)	28(1)
C(10)	4779(3)	6273(3)	2663(5)	37(1)
C(11)	3182(3)	5718(3)	295(5)	44(1)
H(5)	10150(50)	2350(40)	6360(70)	69
H(1A)	6698	6309	3026	58
H(2A)	5709	6498	6288	62
H(2B)	6232	7423	5168	62
H(5A)	9869	5602	8025	38
H(6A)	10585	3933	7745	40
H(8A)	7386	3273	4064	37
H(11A)	2861	5080	-345	65

H(11B)	3390	6224	-602	65
H(11C)	2527	6007	940	65

Table 3. Bond lengths [Å] and angles [°] for $C_{11}H_{10}O_5$.

O(1)-C(9)	1.374(4)	O(1)-C(1)	1.413(5)
O(2)-C(10)	1.210(4)	O(3)-C(10)	1.318(4)
O(3)-C(11)	1.452(4)	O(4)-C(3)	1.230(4)
O(5)-C(7)	1.345(4)	C(1)-C(2)	1.455(6)
C(1)-C(10)	1.508(5)	C(2)-C(3)	1.512(5)
C(3)-C(4)	1.449(5)	C(4)-C(9)	1.403(5)
C(4)-C(5)	1.409(5)	C(5)-C(6)	1.362(5)
C(6)-C(7)	1.407(5)	C(7)-C(8)	1.385(4)
C(8)-C(9)	1.381(5)		

C(9)-O(1)-C(1)	114.4(3)	C(10)-O(3)-C(11)	114.8(3)
O(1)-C(1)-C(2)	114.9(3)	O(1)-C(1)-C(10)	111.5(3)
C(2)-C(1)-C(10)	113.8(4)	C(1)-C(2)-C(3)	111.4(3)
O(4)-C(3)-C(4)	124.3(3)	O(4)-C(3)-C(2)	120.1(3)
C(4)-C(3)-C(2)	115.4(3)	C(9)-C(4)-C(5)	117.6(3)
C(9)-C(4)-C(3)	120.0(3)	C(5)-C(4)-C(3)	122.2(3)
C(6)-C(5)-C(4)	121.5(3)	C(5)-C(6)-C(7)	119.5(3)
O(5)-C(7)-C(8)	117.3(3)	O(5)-C(7)-C(6)	122.2(3)
C(8)-C(7)-C(6)	120.5(3)	C(9)-C(8)-C(7)	119.1(3)
O(1)-C(9)-C(8)	115.8(3)	O(1)-C(9)-C(4)	122.5(3)
C(8)-C(9)-C(4)	121.7(3)	O(2)-C(10)-O(3)	125.0(3)
O(2)-C(10)-C(1)	121.1(3)	O(3)-C(10)-C(1)	113.7(3)

Table 4. Anisotropic displacement parameters [$Å^2x10^3$] for $C_{11}H_{10}O_5$. The anisotropic displacement factor exponent takes the form: $-2\pi^2[h^2a^{*2}U_{11}+... +2hka^*b^*U_{12}]$

	U_{11}	U_{22}	U_{33}	U_{23}	U_{13}	U_{12}
O(1)	23(1)	36(1)	35(1)	-1(1)	-6(1)	5(1)
O(2)	36(2)	46(2)	53(2)	3(1)	-7(1)	9(1)
O(3)	30(1)	48(2)	37(1)	0(1)	-9(1)	5(1)
O(4)	41(2)	43(2)	77(2)	-16(2)	-22(2)	2(1)
O(5)	37(2)	36(2)	55(2)	-4(1)	-16(1)	7(1)
C(1)	39(2)	36(2)	61(3)	2(2)	-14(2)	3(2)
C(2)	41(2)	47(3)	61(3)	-12(2)	-12(2)	11(2)
C(3)	30(2)	41(2)	49(2)	-5(2)	-7(2)	1(2)
C(4)	22(2)	33(2)	32(2)	3(2)	1(1)	-2(1)
C(5)	23(2)	36(2)	34(2)	0(2)	-2(1)	-5(2)
C(6)	22(2)	40(2)	36(2)	3(2)	-4(1)	-1(2)

C(7)	27(2)	35(2)	34(2)	5(2)	-1(1)	1(2)
C(8)	24(2)	35(2)	30(2)	-1(2)	-2(1)	-3(1)
C(9)	19(2)	37(2)	28(2)	5(2)	1(1)	0(1)
C(10)	27(2)	44(2)	37(2)	8(2)	0(2)	3(2)
C(11)	28(2)	67(3)	31(2)	3(2)	-7(2)	5(2)

Table 5. Torsion angles [°] for $C_{11}H_{10}O_5$.

C(9)-O(1)-C(1)-C(2)	-48.9(5)	C(9)-O(1)-C(1)-C(10)	179.7(3)
O(1)-C(1)-C(2)-C(3)	53.2(5)	C(10)-C(1)-C(2)-C(3)	-176.5(4)
C(1)-C(2)-C(3)-O(4)	156.9(4)	C(1)-C(2)-C(3)-C(4)	-28.5(5)
O(4)-C(3)-C(4)-C(9)	175.7(4)	C(2)-C(3)-C(4)-C(9)	1.4(5)
O(4)-C(3)-C(4)-C(5)	0.5(6)	C(2)-C(3)-C(4)-C(5)	-173.8(4)
C(9)-C(4)-C(5)-C(6)	-0.2(5)	C(3)-C(4)-C(5)-C(6)	175.1(4)
C(4)-C(5)-C(6)-C(7)	0.6(5)	C(5)-C(6)-C(7)-O(5)	179.1(3)
C(5)-C(6)-C(7)-C(8)	-0.6(5)	O(5)-C(7)-C(8)-C(9)	-179.4(3)
C(6)-C(7)-C(8)-C(9)	0.3(5)	C(1)-O(1)-C(9)-C(8)	-161.1(3)
C(1)-O(1)-C(9)-C(4)	19.2(5)	C(7)-C(8)-C(9)-O(1)	-179.7(3)
C(7)-C(8)-C(9)-C(4)	0.0(5)	C(5)-C(4)-C(9)-O(1)	179.6(3)
C(3)-C(4)-C(9)-O(1)	4.1(5)	C(5)-C(4)-C(9)-C(8)	-0.1(5)
C(3)-C(4)-C(9)-C(8)	-175.5(3)	C(11)-O(3)-C(10)-O(2)	4.0(5)
C(11)-O(3)-C(10)-C(1)	-170.5(3)	O(1)-C(1)-C(10)-O(2)	163.3(4)
C(2)-C(1)-C(10)-O(2)	31.4(6)	O(1)-C(1)-C(10)-O(3)	-21.9(5)
C(2)-C(1)-C(10)-O(3)	-153.9(4)		

II. Spectroscopic analysis of the compounds

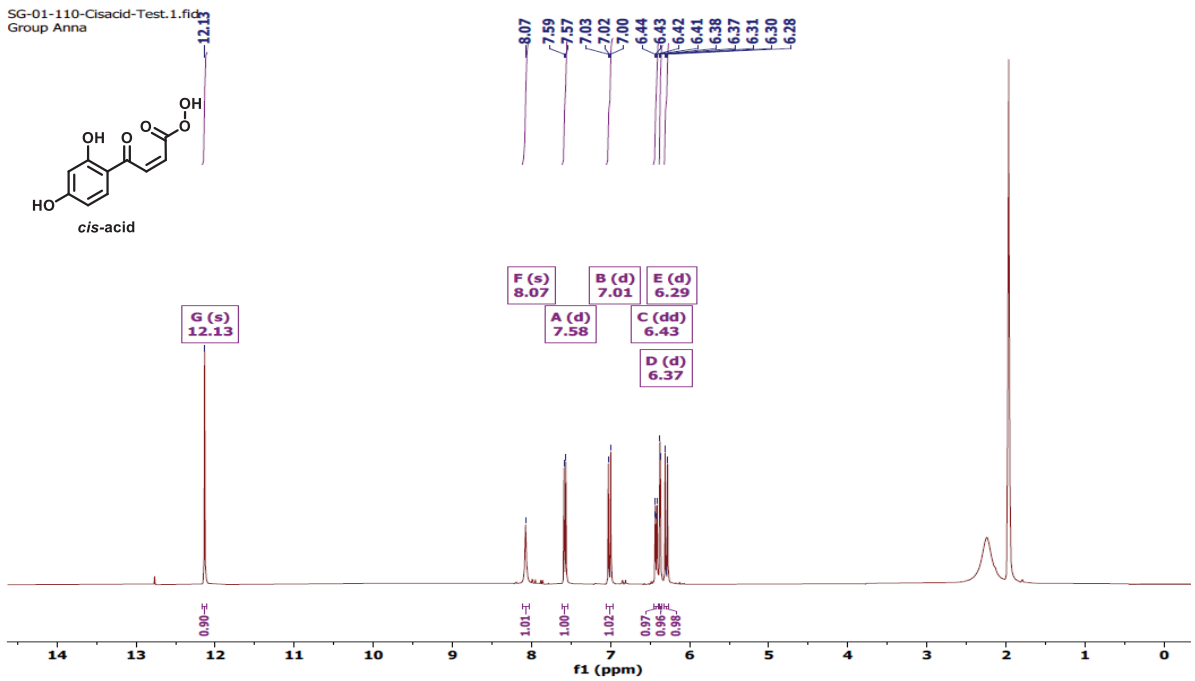

Figure S67. ^{1}H NMR spectrum of *cis* acid

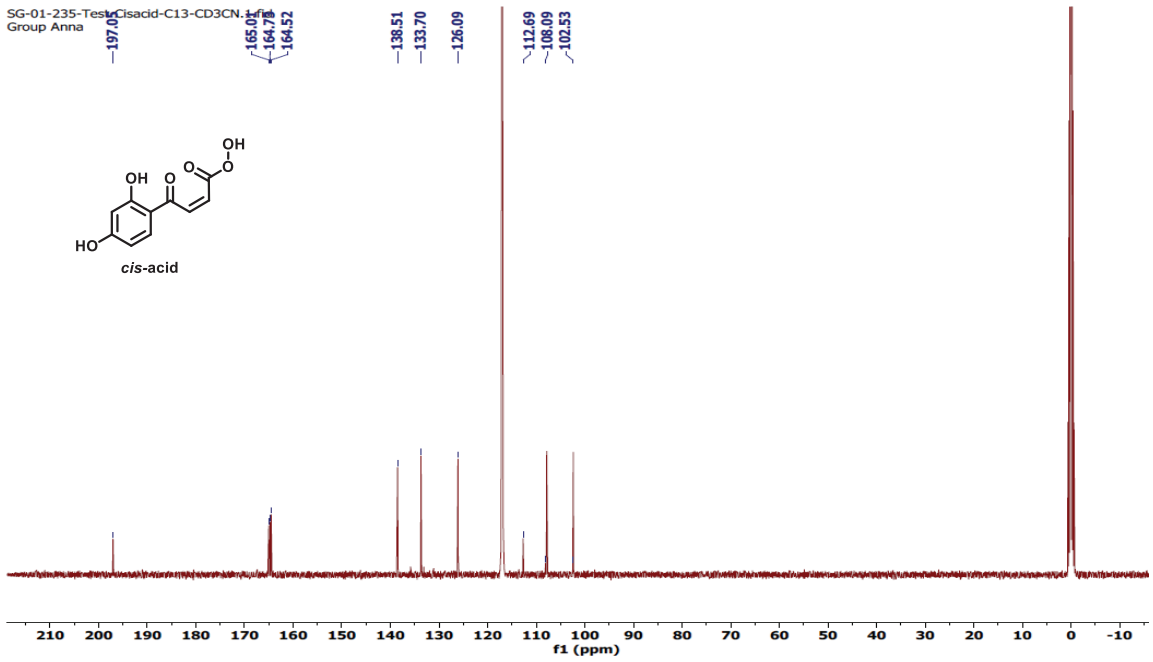

Figure S68. ^{13}C NMR spectrum of *cis* acid

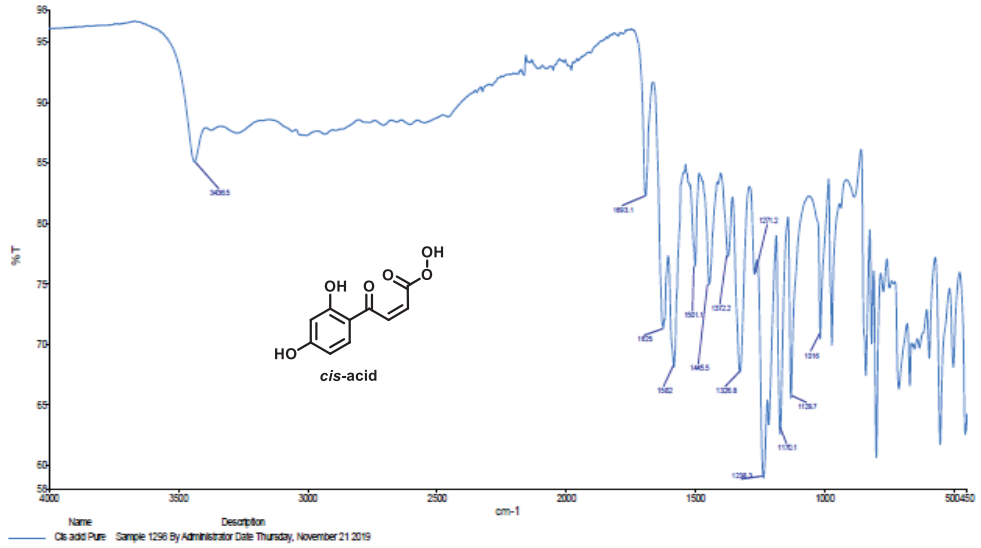

Figure S69. FTIR spectrum of *cis* acid

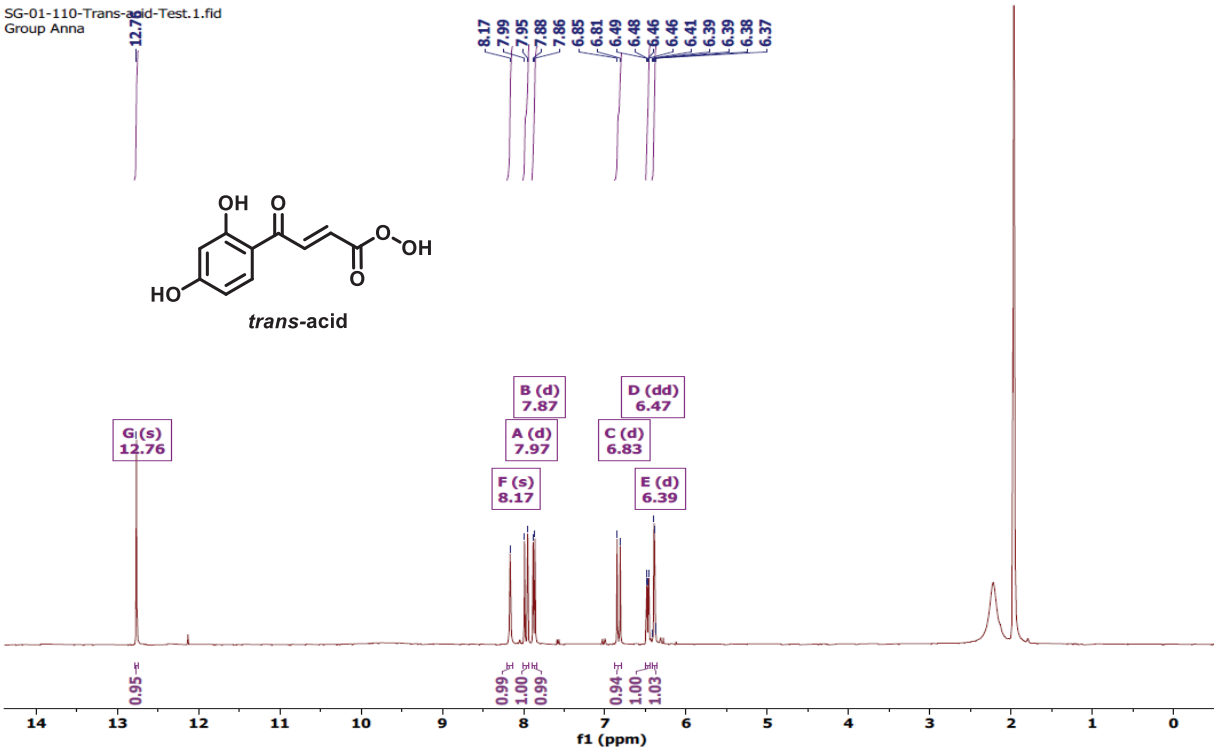

Figure S70. ^{1}H NMR spectrum of *trans* acid

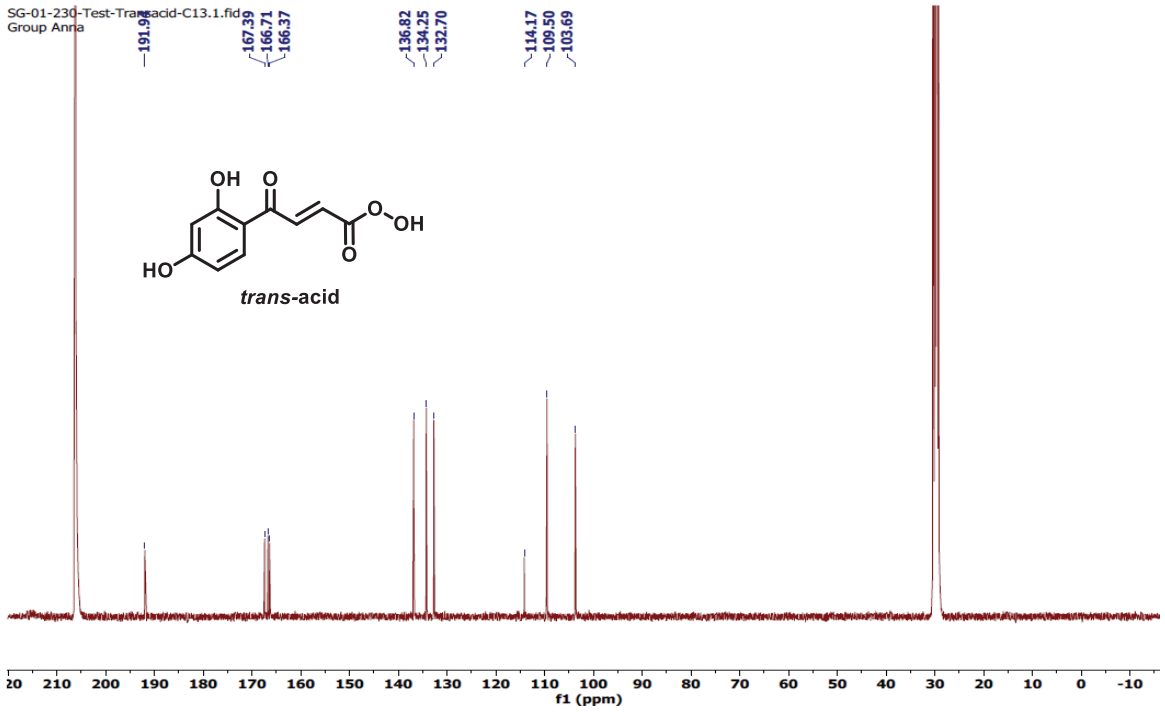

Figure S71. ^{13}C NMR spectrum of *trans* acid

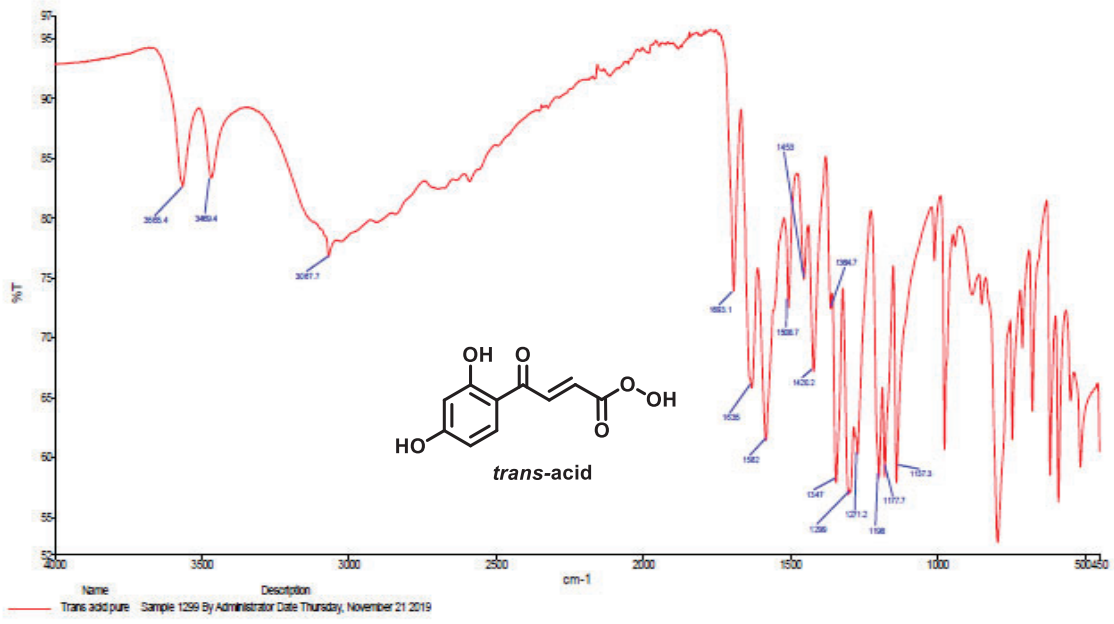

Figure S72. FTIR spectrum of *trans* acid

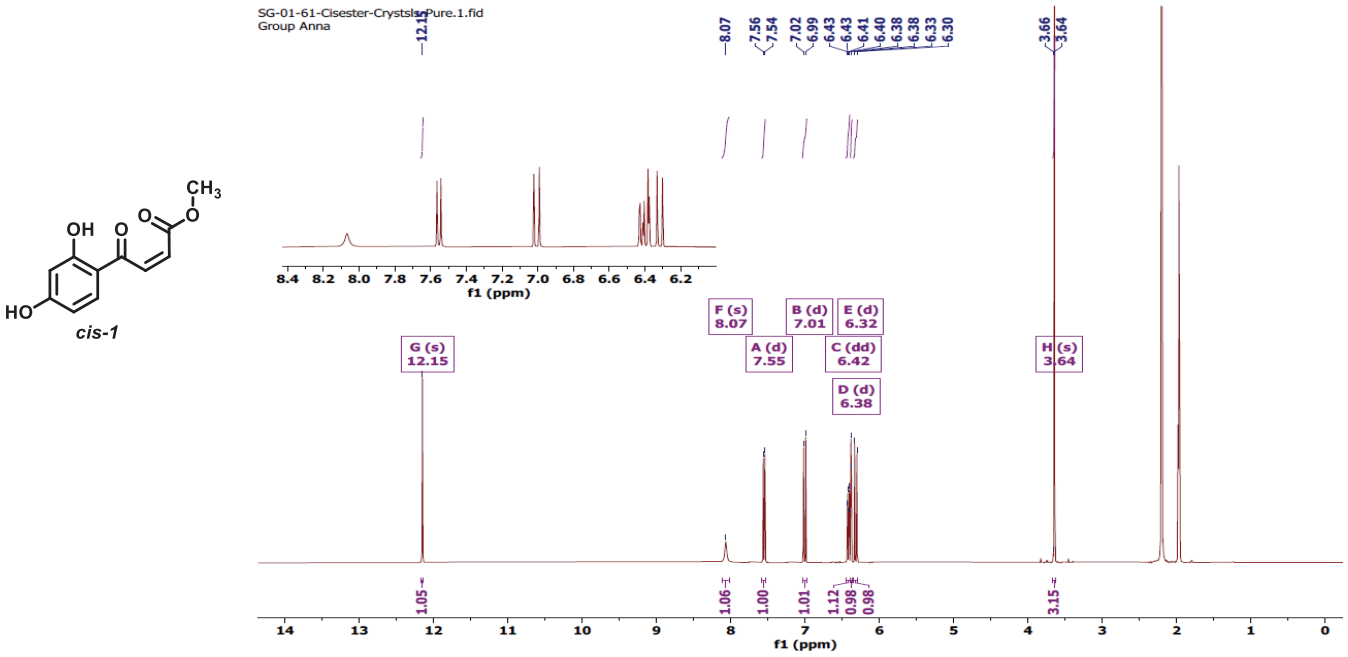

Figure S73. ^{1}H NMR spectrum of *cis*-**1**

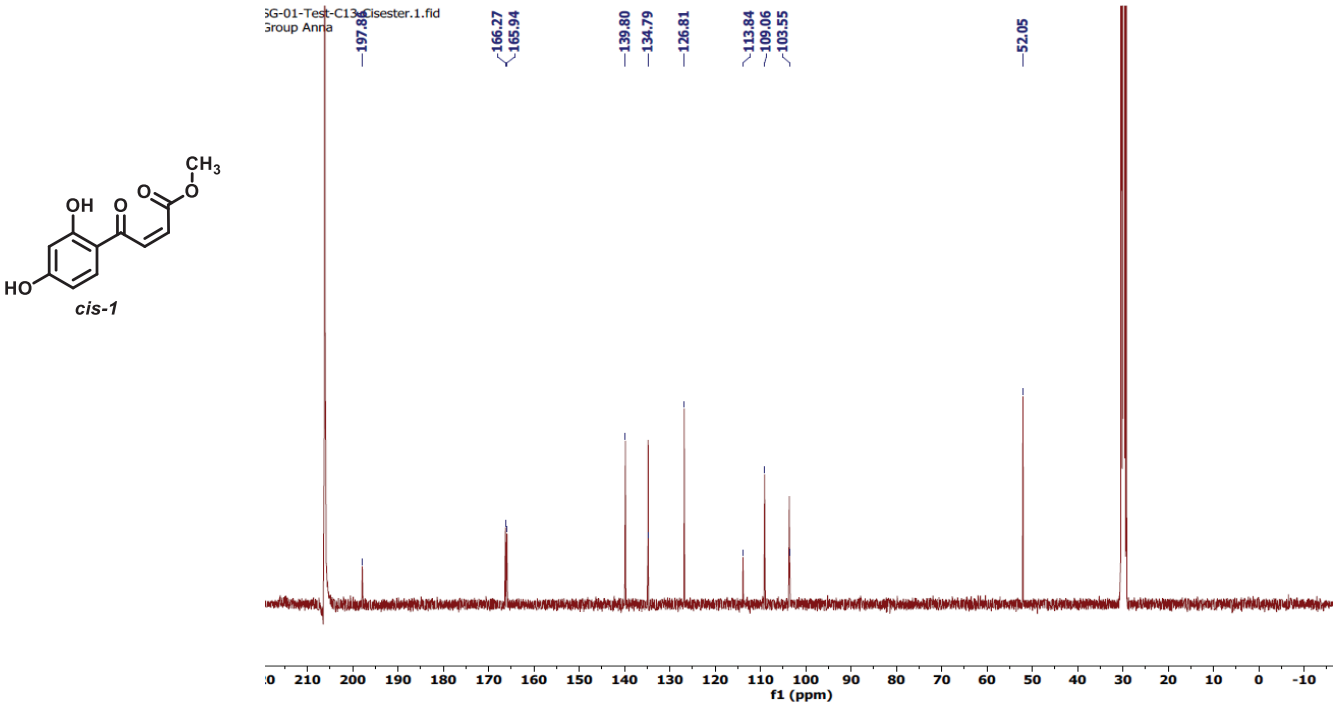

Figure S74. ^{13}C NMR spectrum of *cis*-**1**

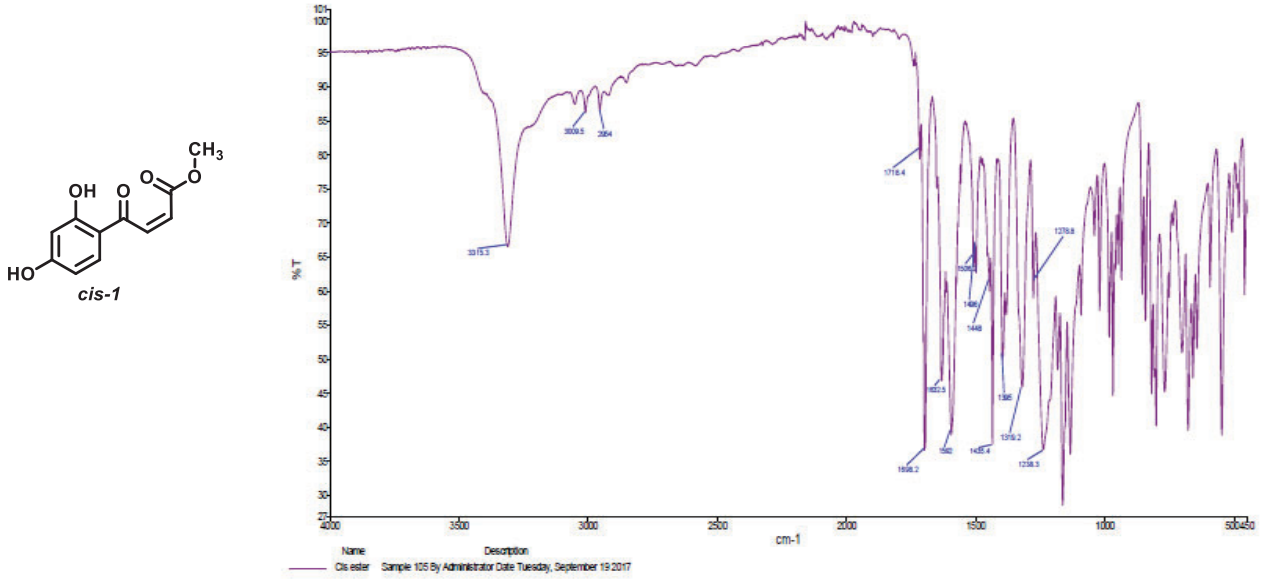

Figure S75. FTIR spectrum of *cis*-**1**

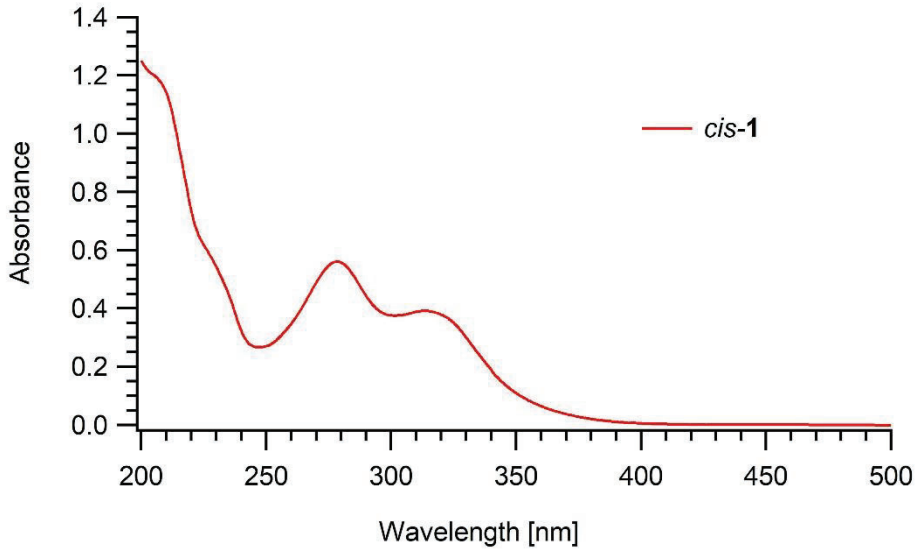

Figure S76. UV-Vis spectrum of *cis*-**1**

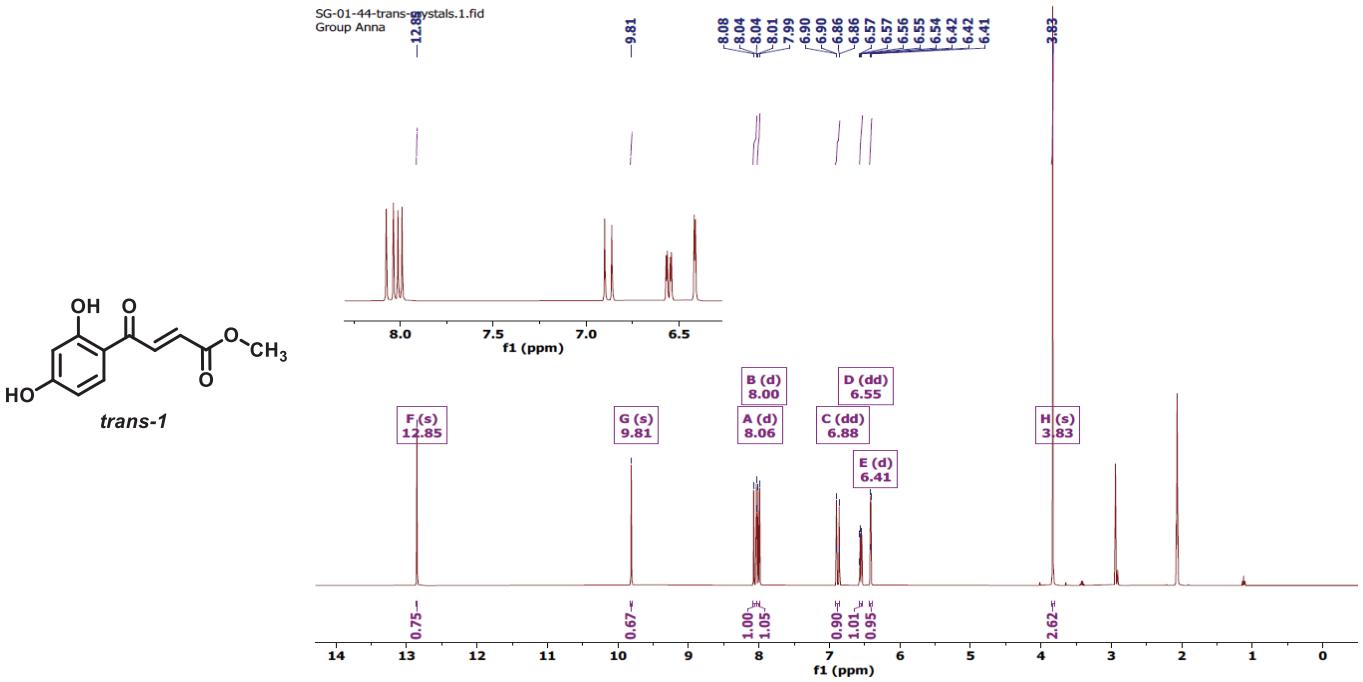

Figure S77. ^{1}H NMR spectrum of *trans*-**1**

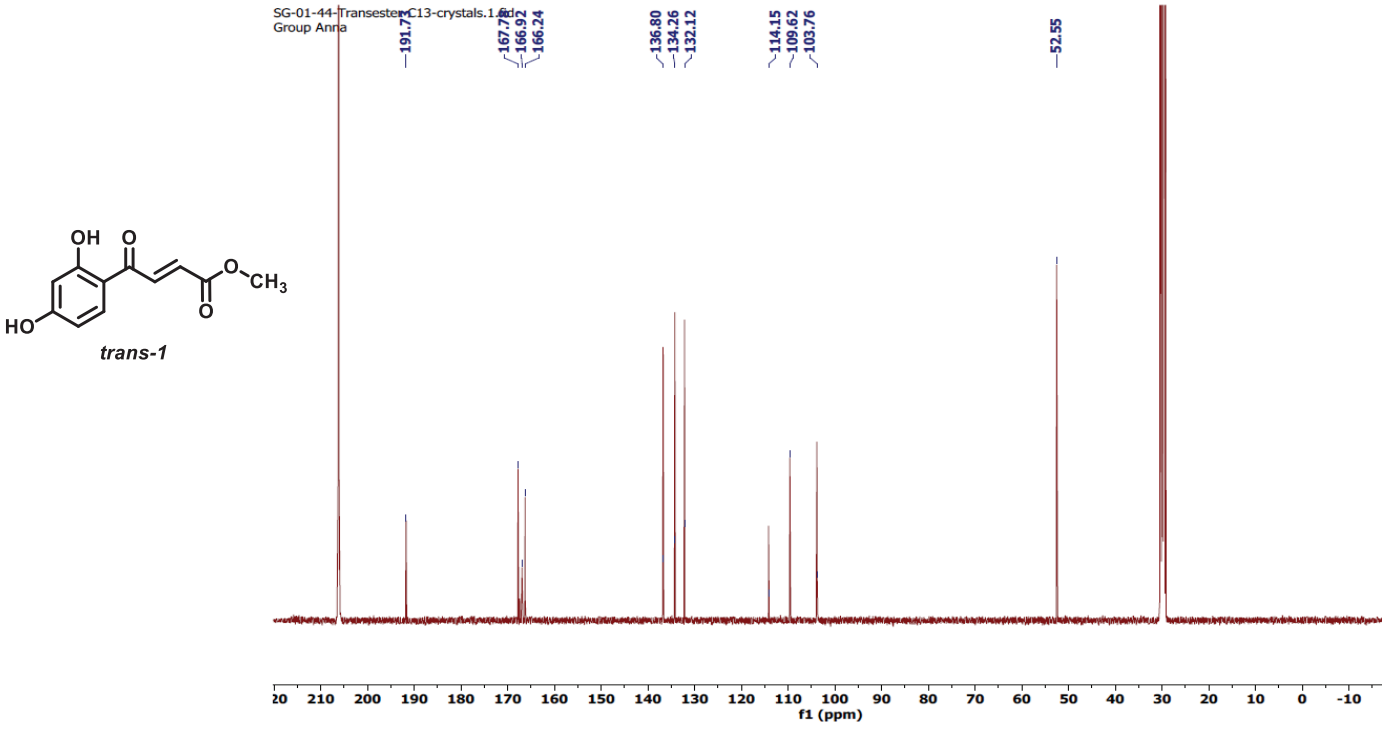

Figure S78. ^{13}C NMR spectrum of *trans*-**1**

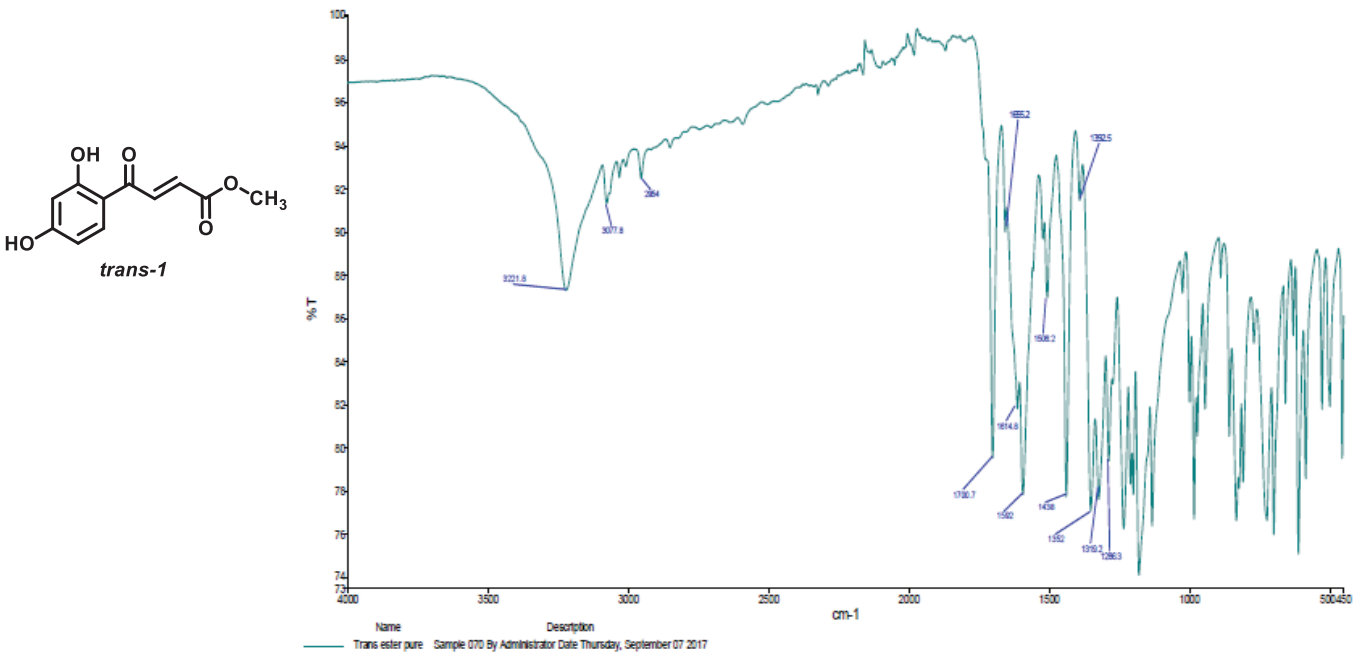

Figure S79. FTIR spectrum of *trans*-**1**

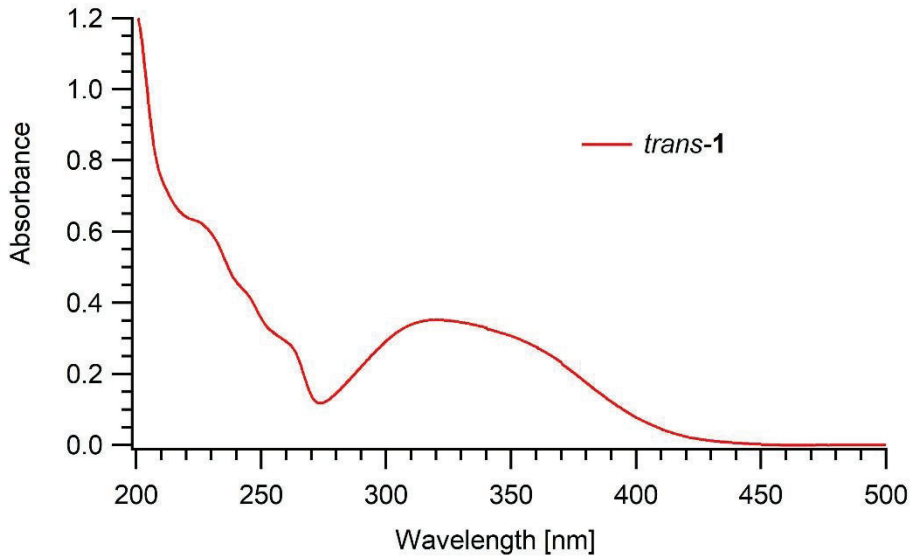

Figure S80. UV-Vis spectrum of *trans*-**1**

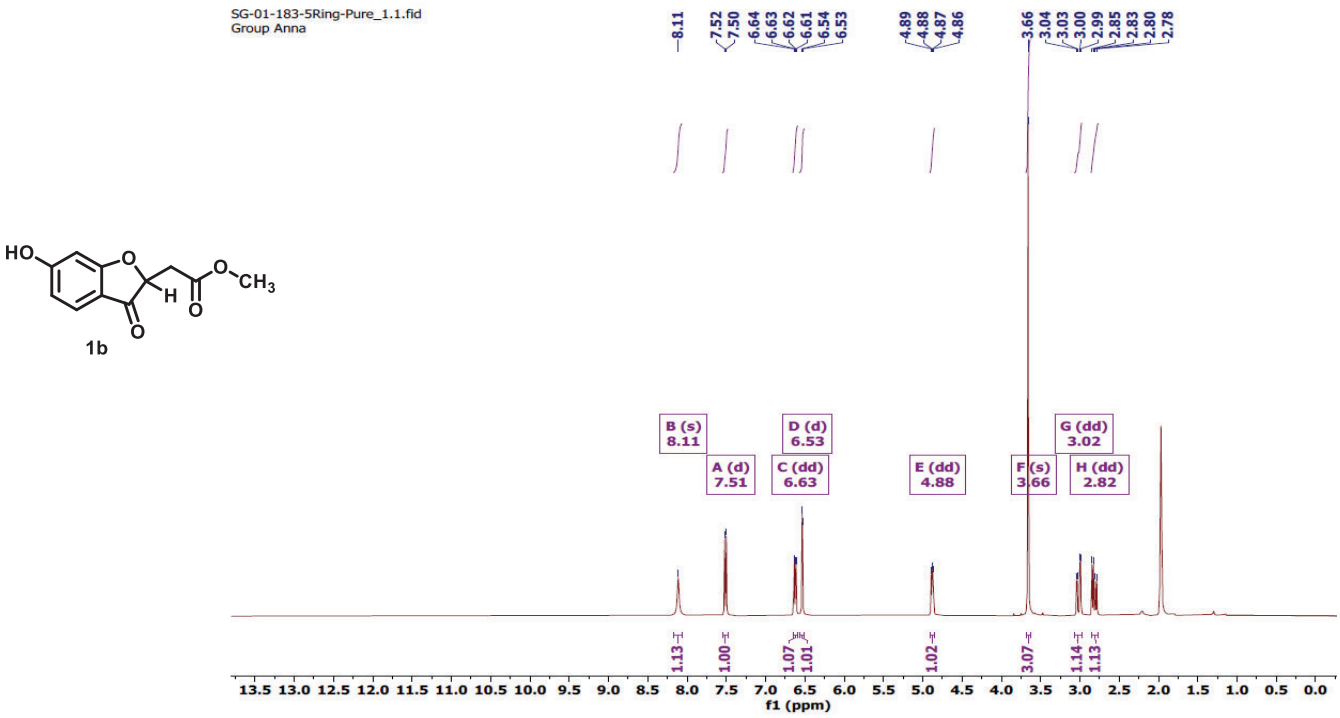

Figure S81. ^{1}H NMR spectrum of **1b**

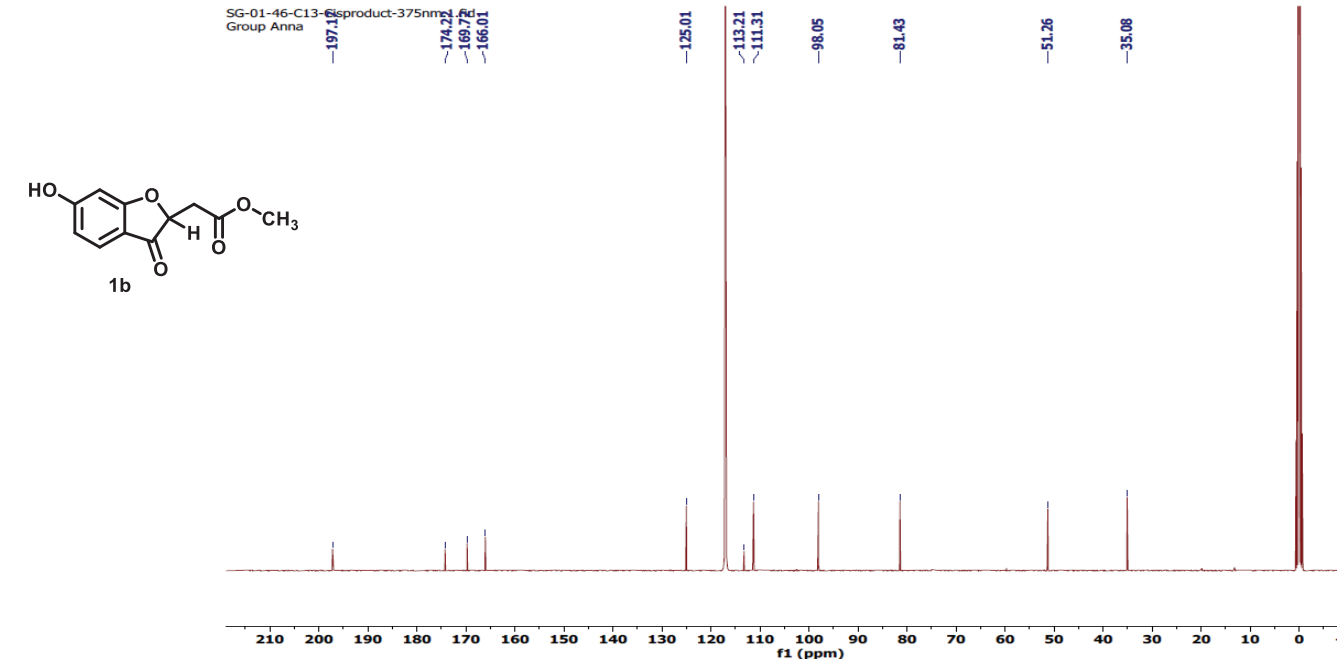

Figure S82. ^{13}C NMR spectrum of **1b**

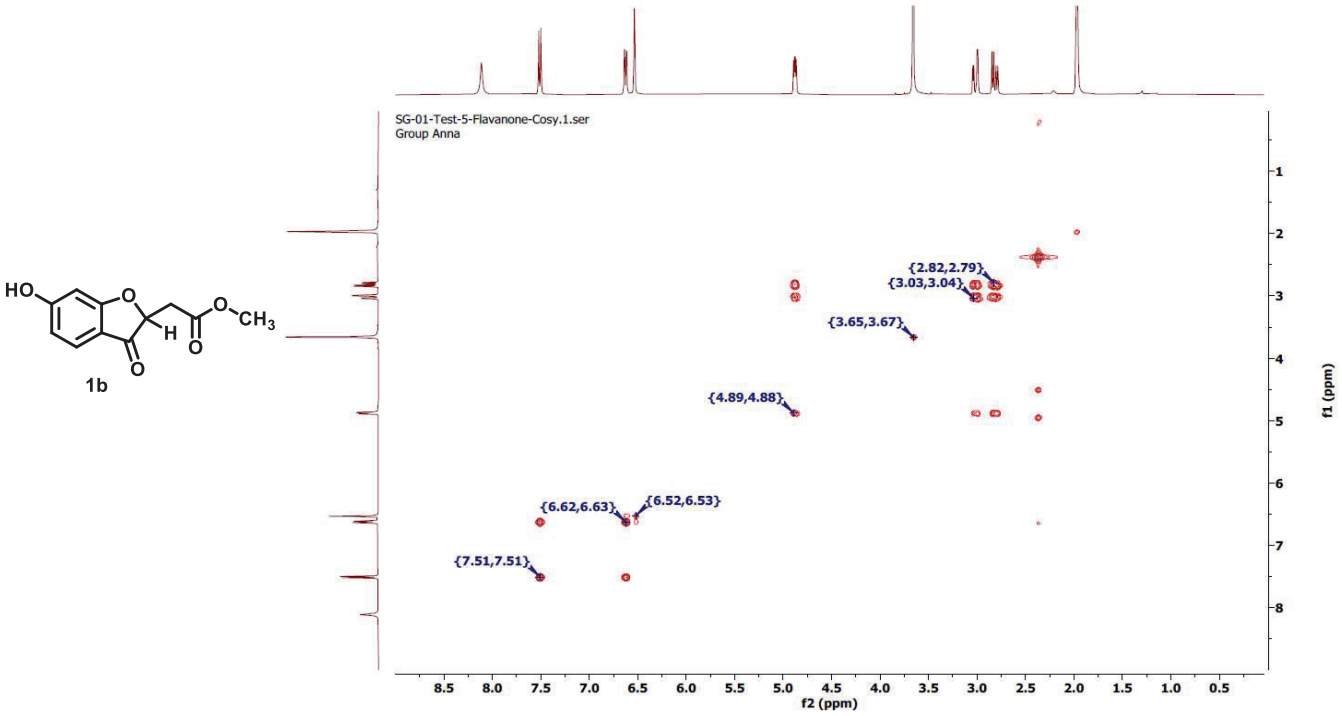

Figure S83. 2D-COSY NMR spectrum of **1b**

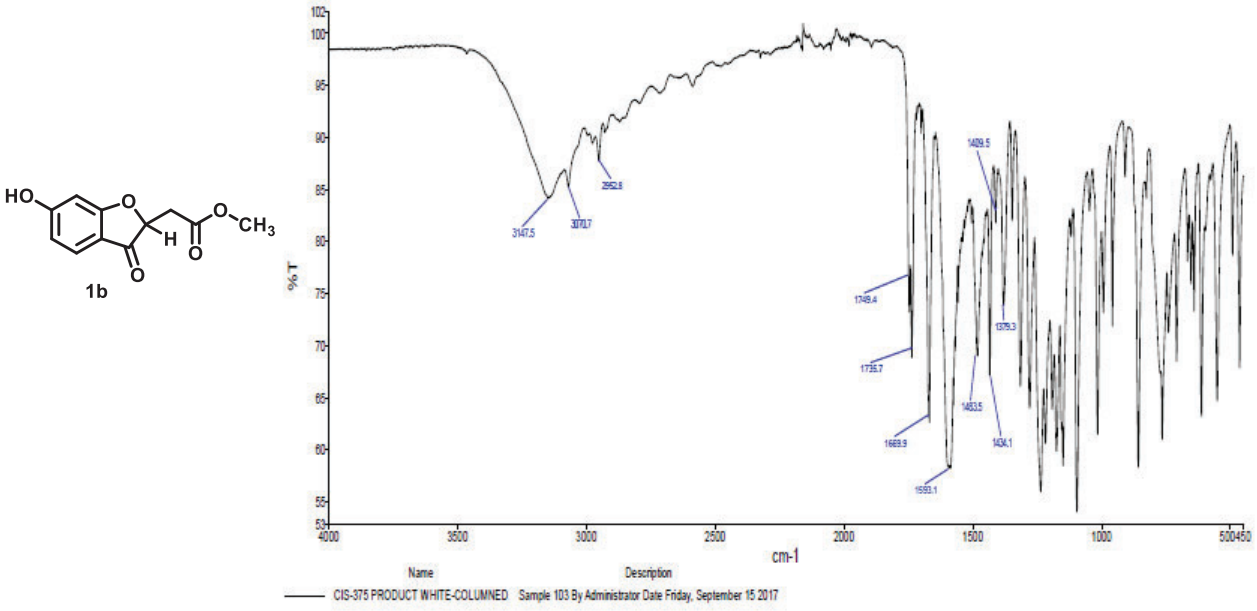

Figure S84. FTIR spectrum of **1b**

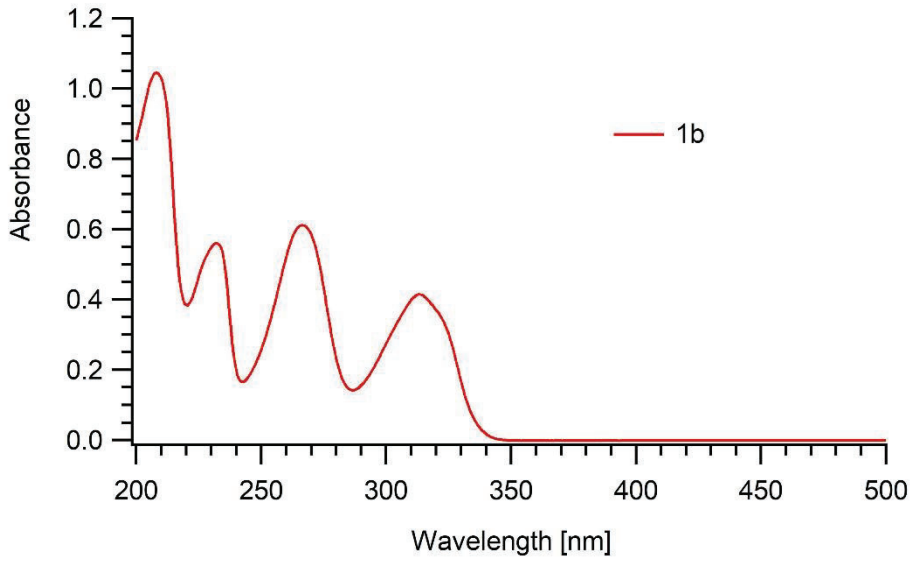

Figure S85. UV-Vis spectrum of **1b**

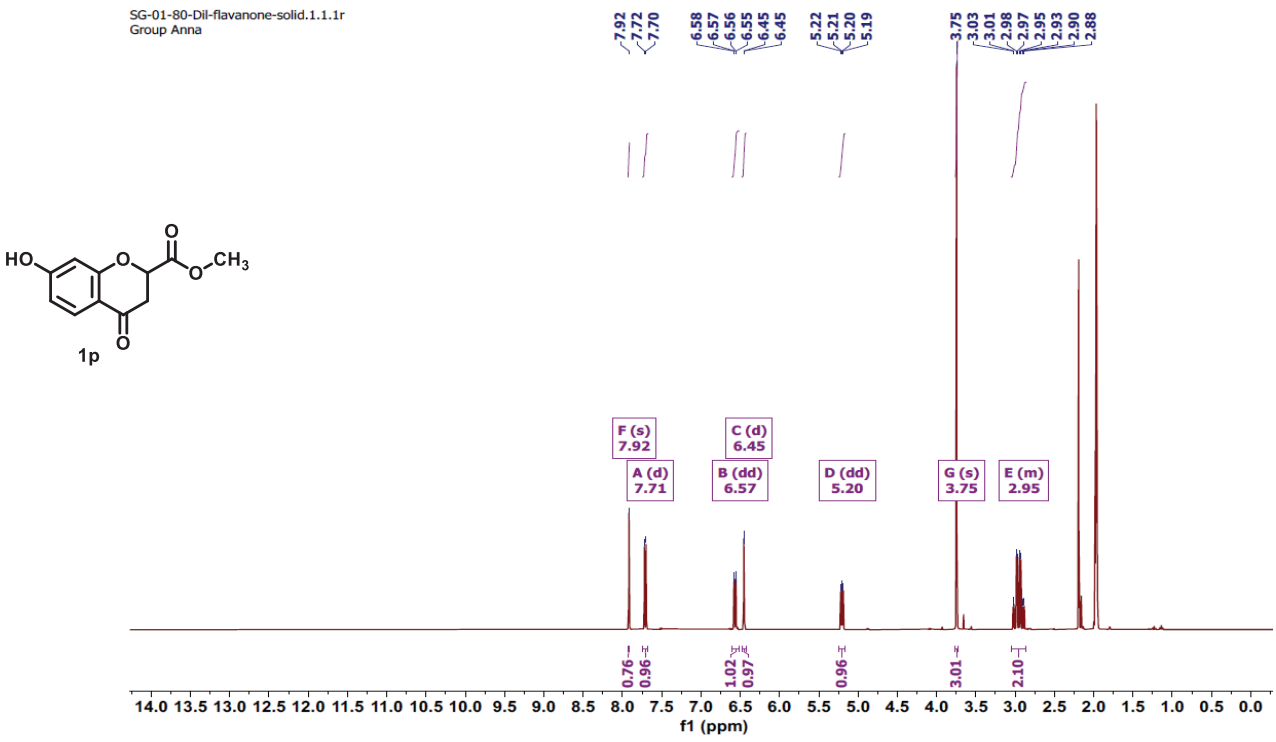

Figure S86. ^{1}H NMR spectrum of **1P**

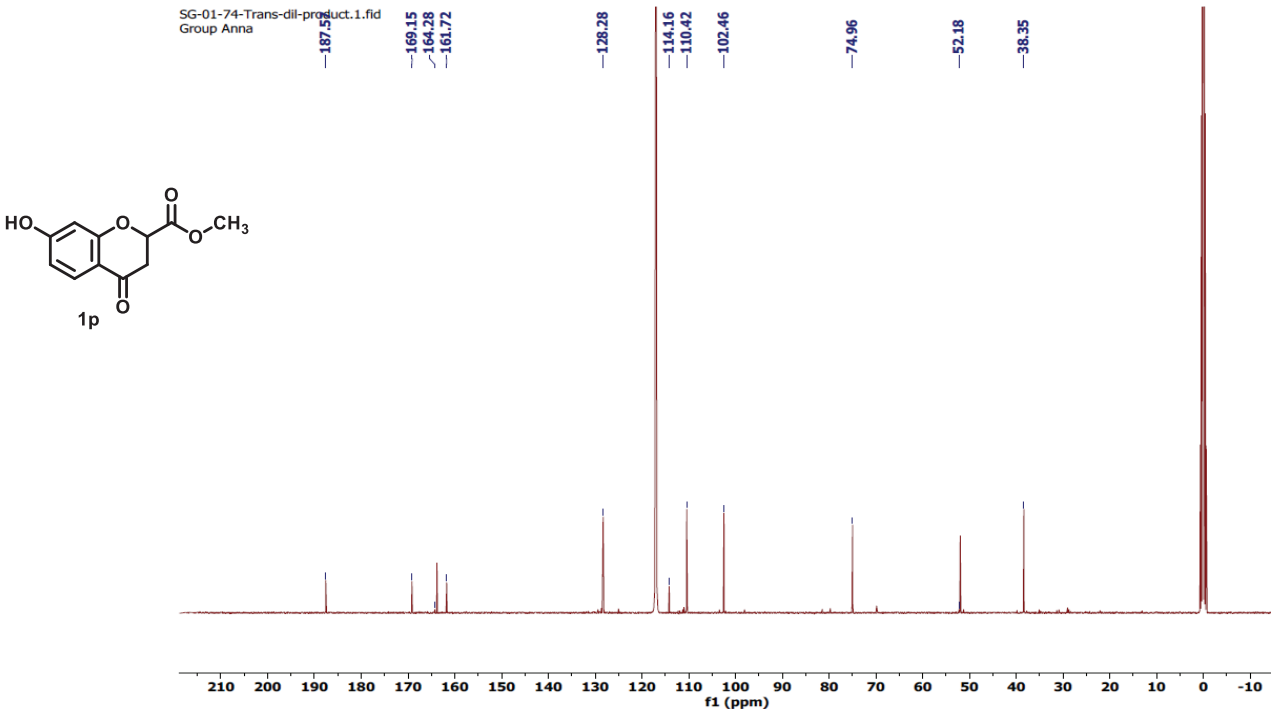

Figure S87. ^{13}C NMR spectrum of **1P**

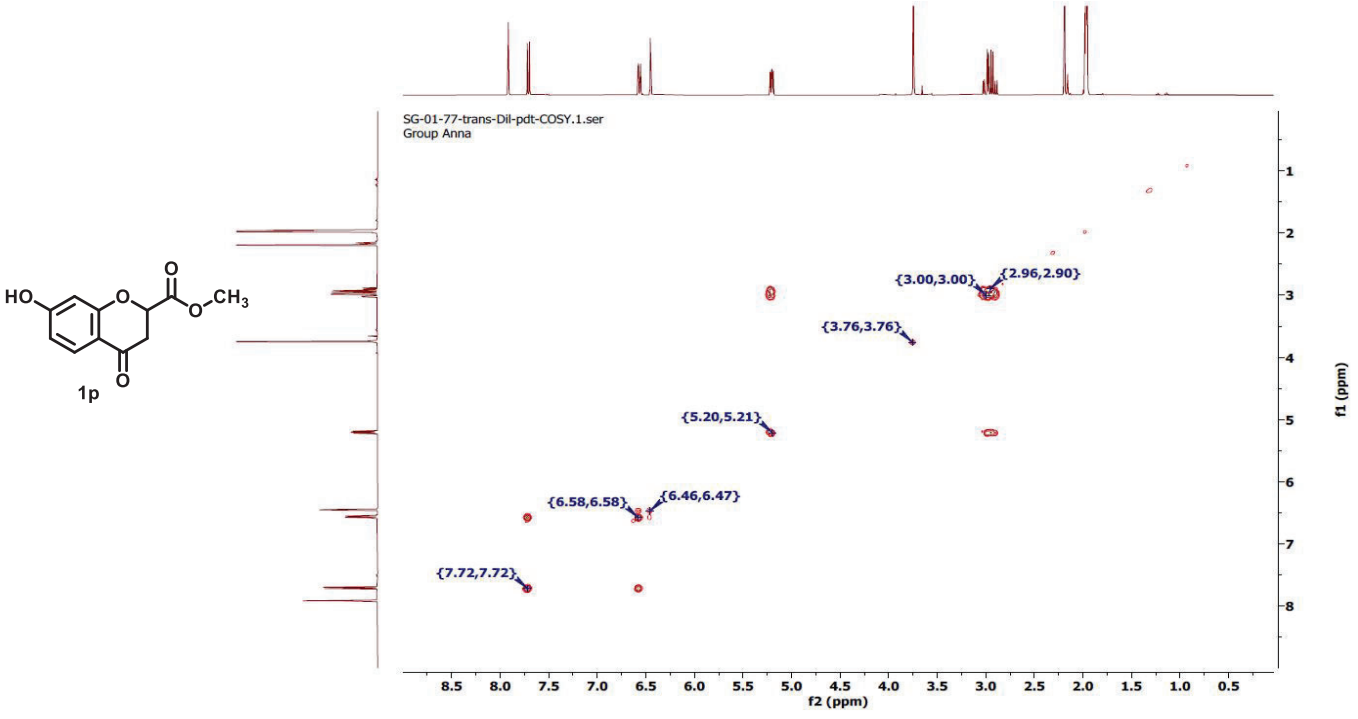

Figure S88. 2D-COSY NMR spectrum of **1P**

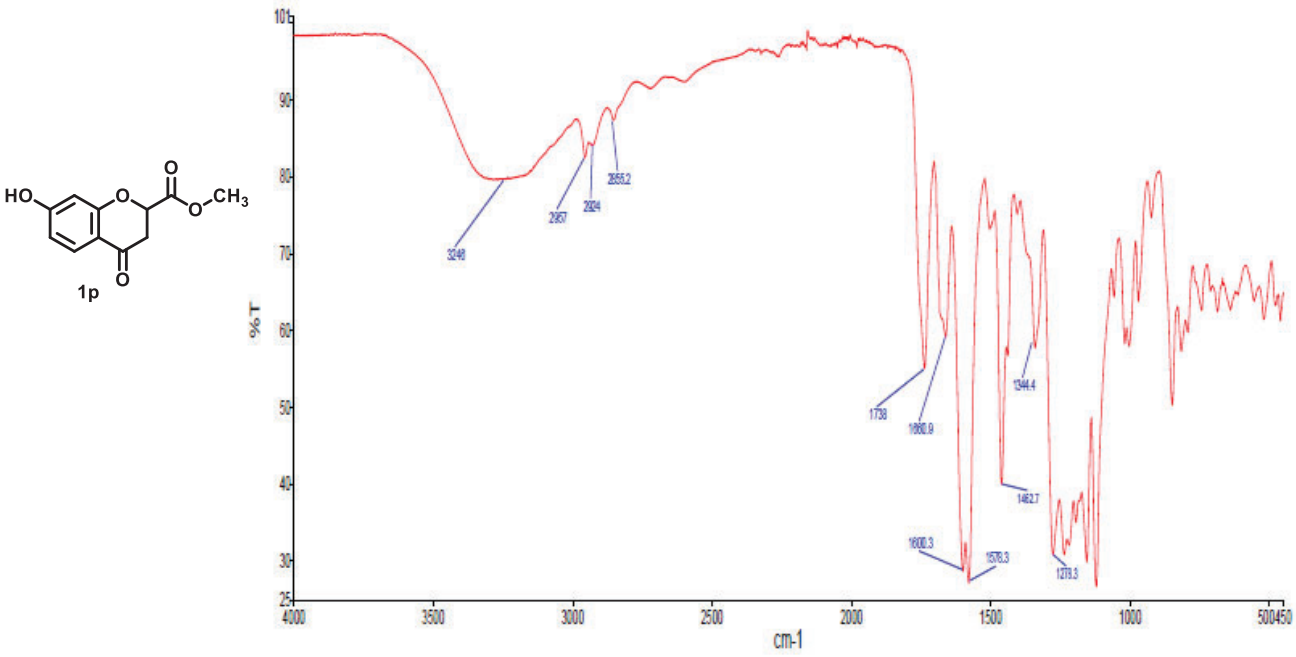

Figure S89. FTIR spectrum of **1P**

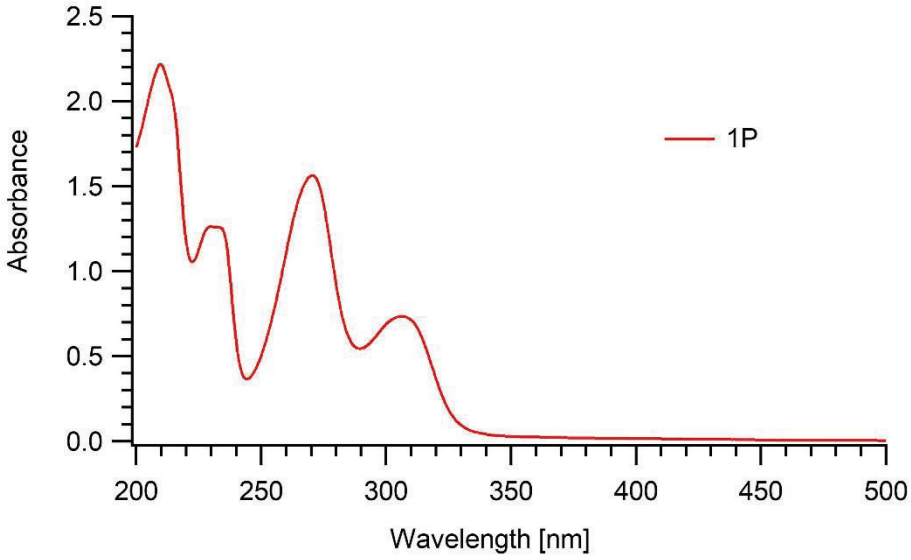

Figure S90. UV-Vis spectrum of **1P**

III. High resolution mass spectra of the compounds

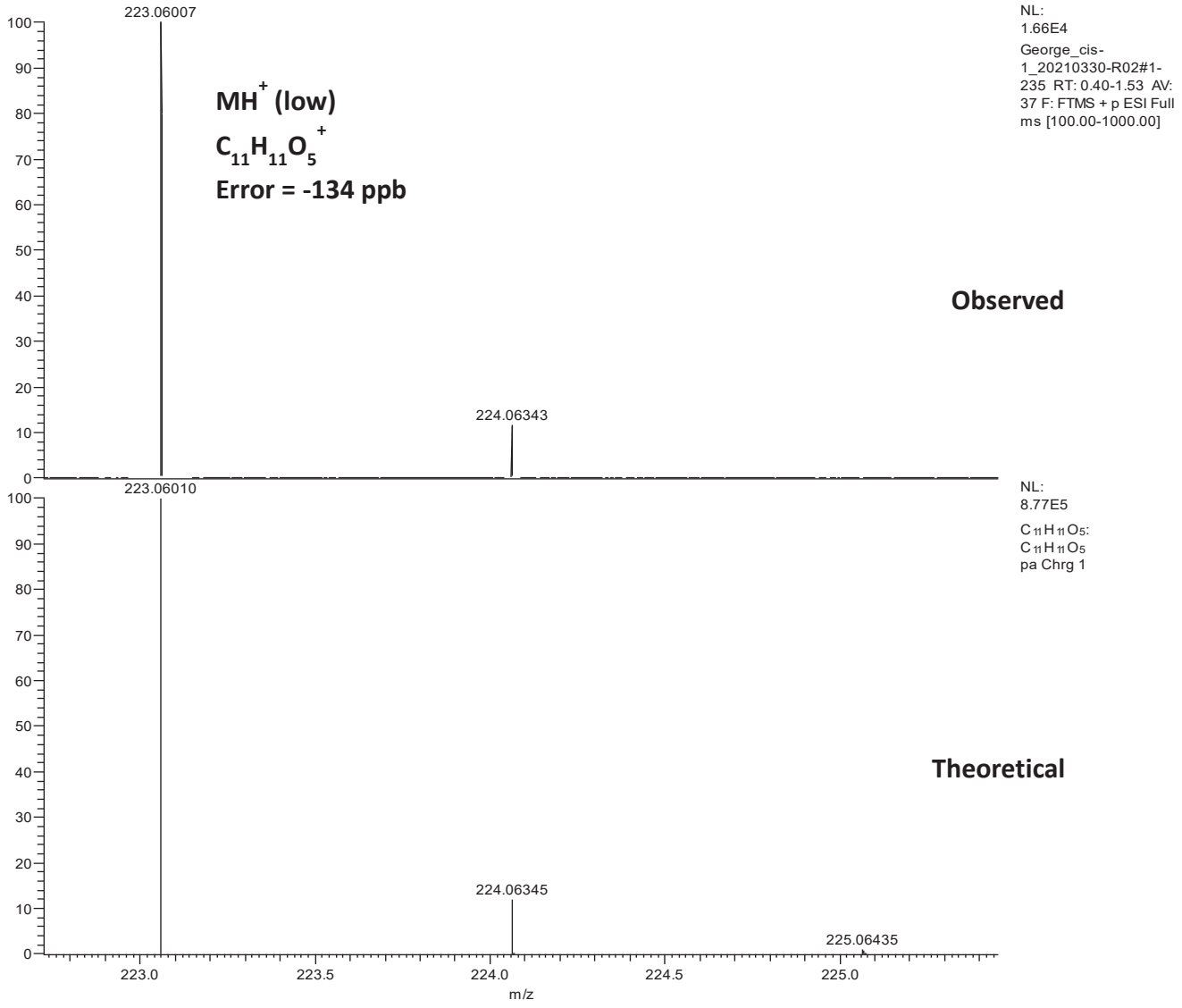

Figure S91. High resolution mass spectrum of *cis*-**1**

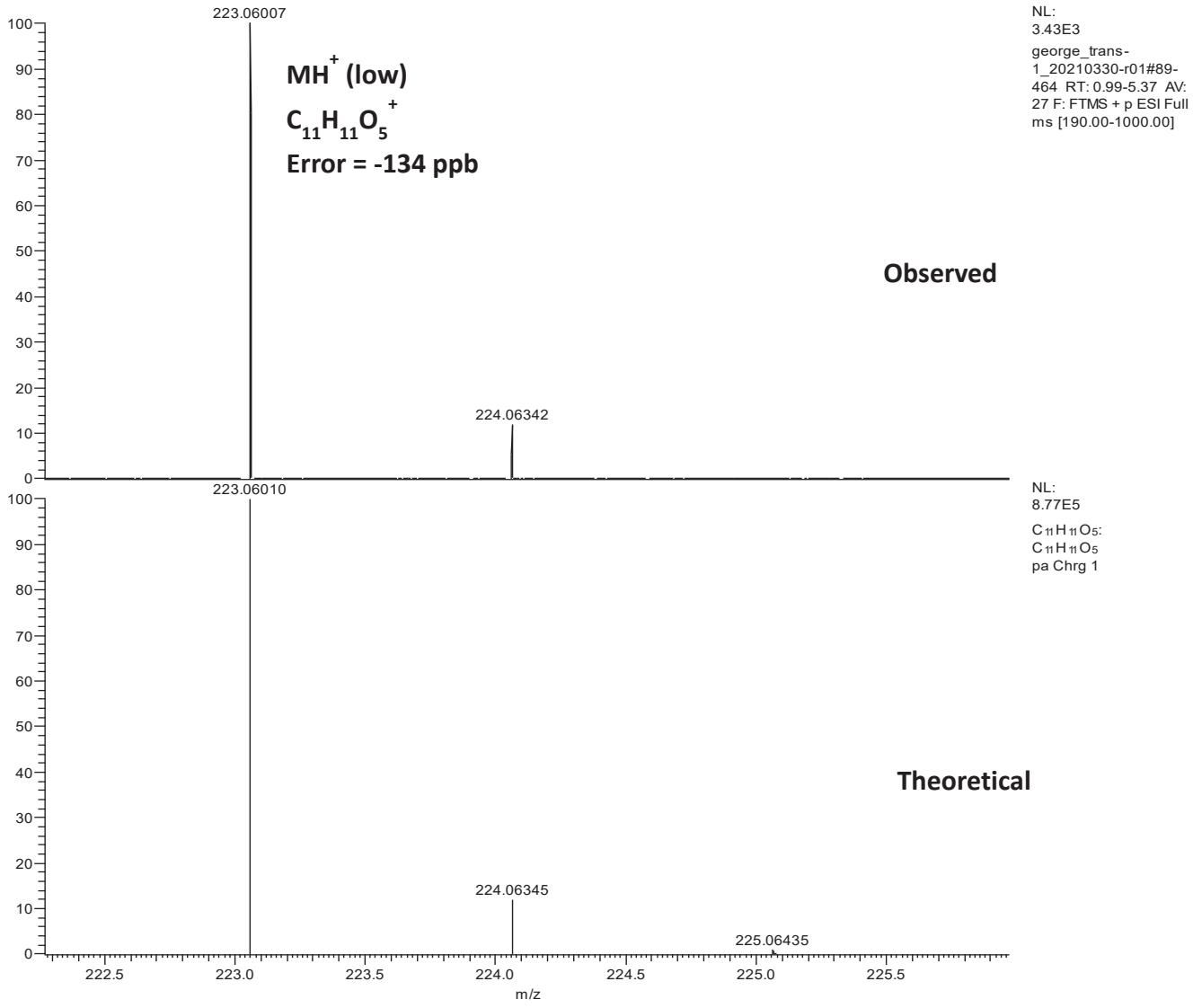

Figure S92. High resolution mass spectrum of *trans*-**1**

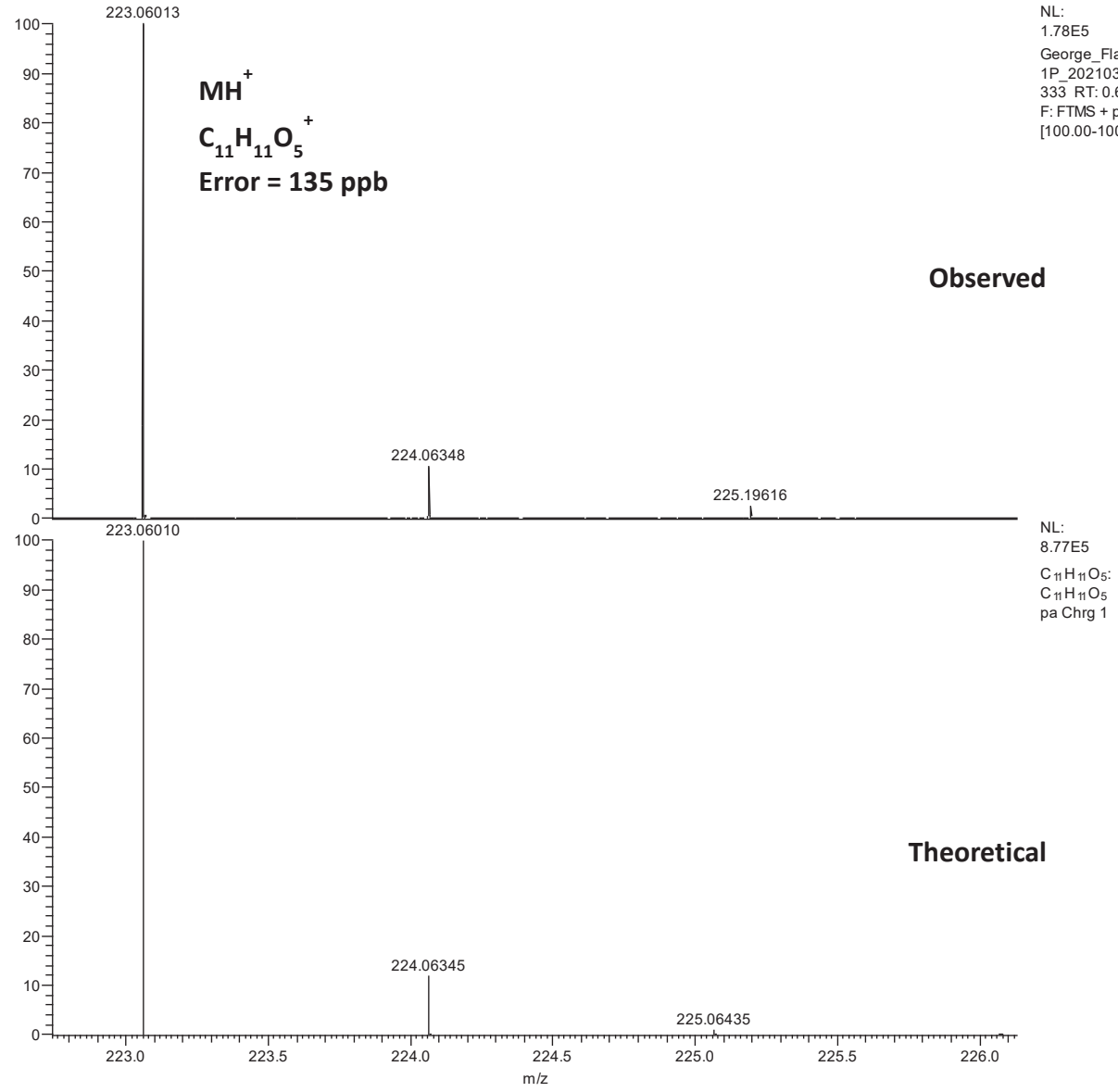

Figure S93. High resolution mass spectrum of **1P**

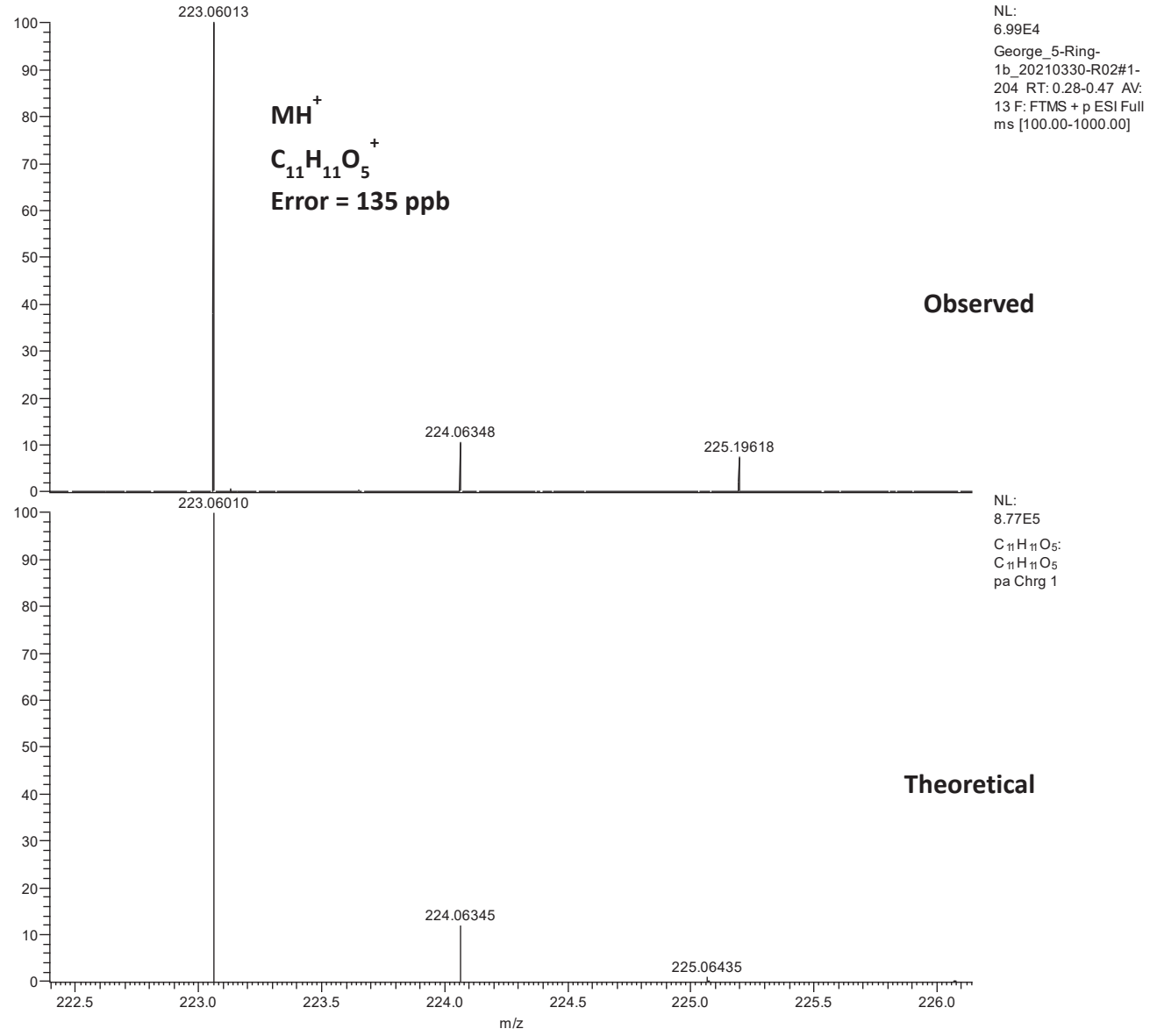

Figure S94. High resolution mass spectrum of **1b**

IV. Photoreactivity of the 2-hydroxy chalcones in diluted < 1.5 mM argon saturated acetonitrile solution

i. Photoreactivity of trans-1 monitored with time in diluted < 1.5 mM argon saturated acetonitrile solution

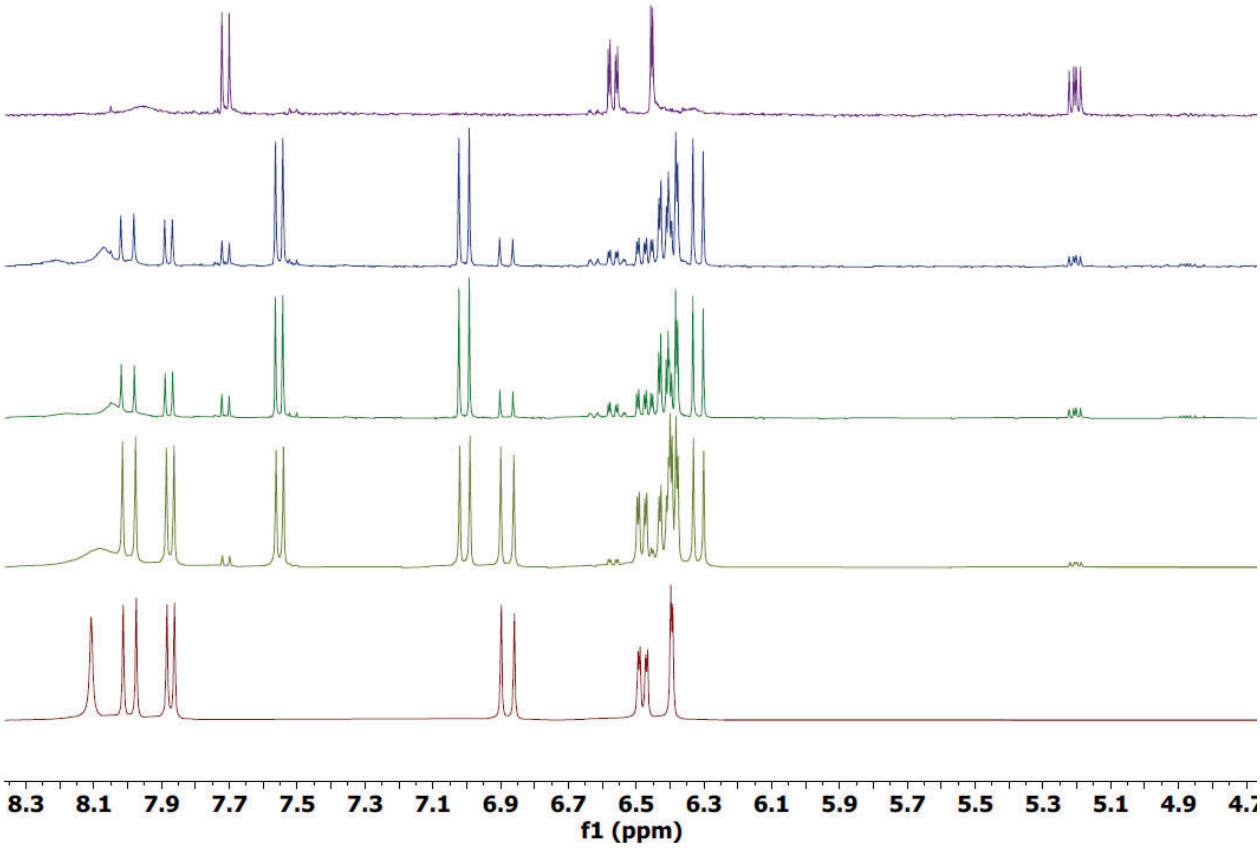

Figure S95. Overlaid ^{1}H-NMR spectra of *trans*-**1** monitored with increasing time of irradiation at 365 nm in diluted < 1.5 mM argon saturated CH_3CN solution.

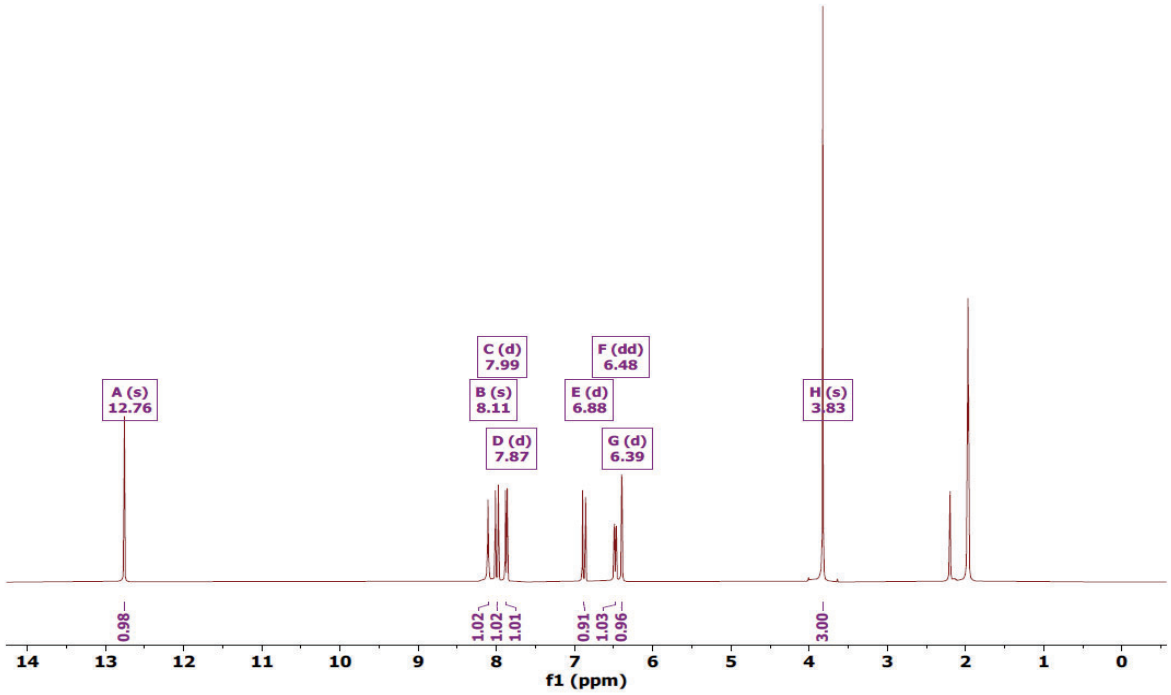

Figure S96. ^{1}H NMR spectrum of diluted argon saturated CH_3CN solution of *trans*-**1** < 1.5 mM at 0 h of irradiation.

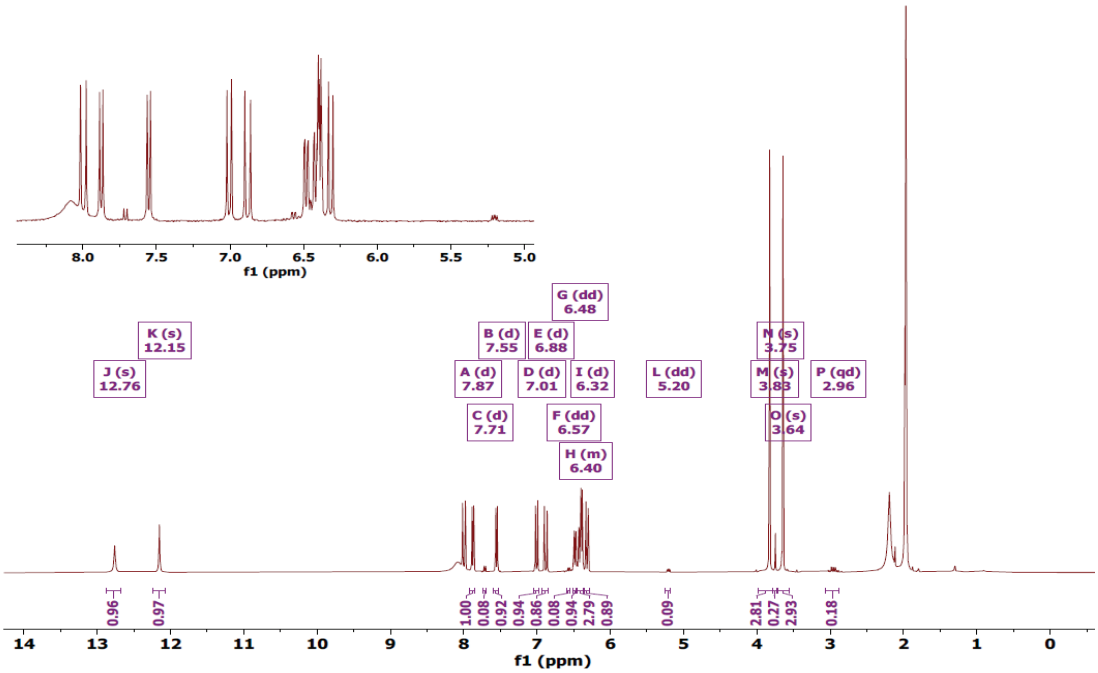

Figure S97. ^{1}H NMR spectrum of diluted argon saturated CH_3CN solution of *trans*-**1** < 1.5 mM after 6 h of irradiation.

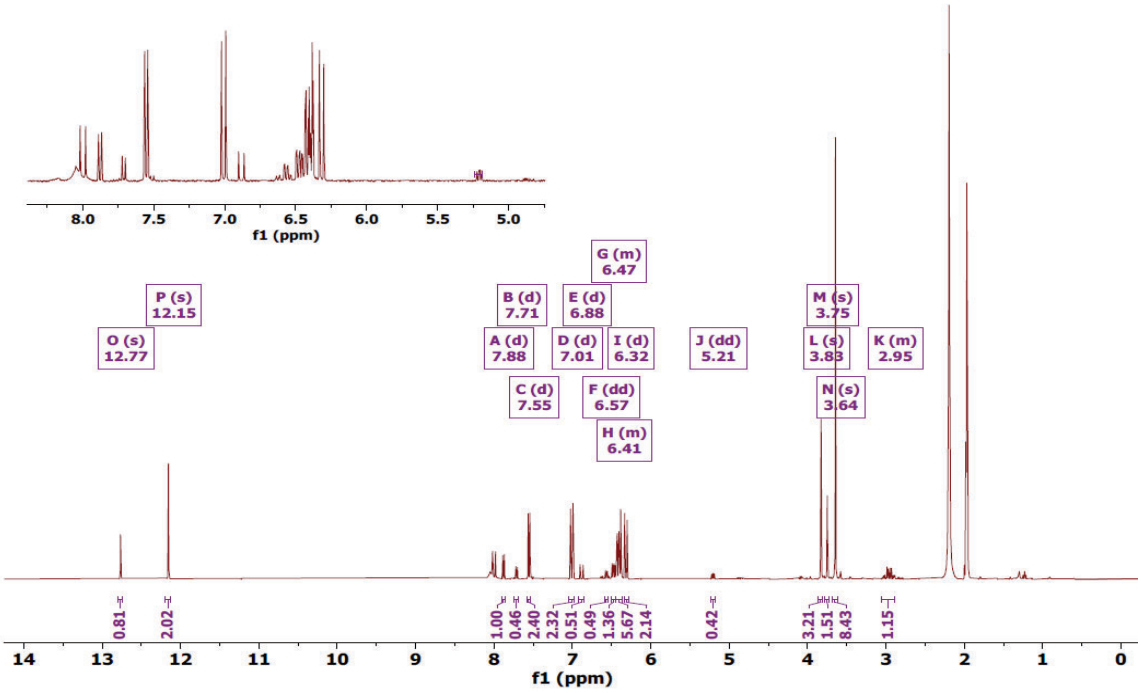

Figure S98. ^{1}H NMR spectrum of diluted argon saturated CH_3CN solution of *trans*-**1** < 1.5 mM after 21 h of irradiation.

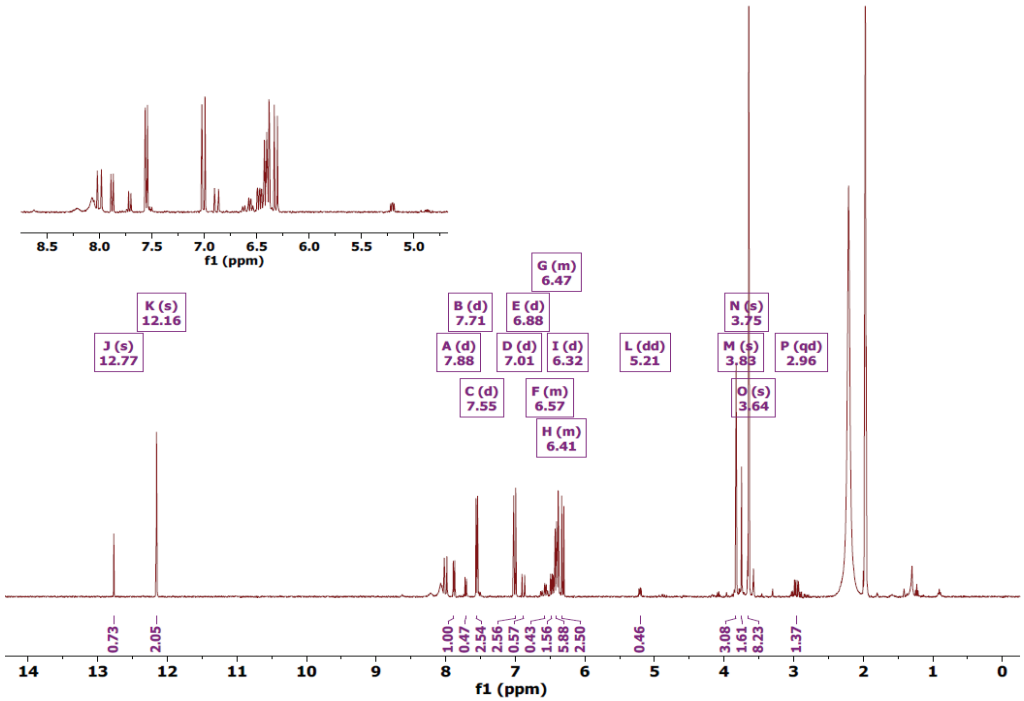

Figure S99. ^{1}H NMR spectrum of diluted argon saturated CH_3CN solution of *trans*-**1** < 1.5 mM after 47 h of irradiation.

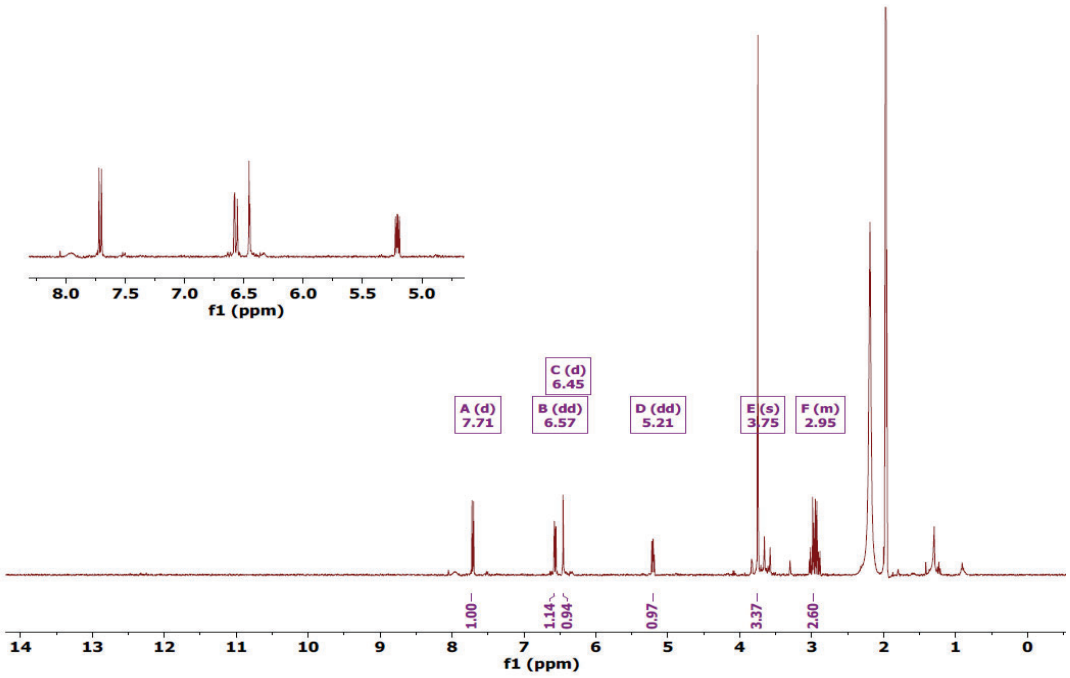

Figure S100. ^{1}H NMR spectrum of diluted argon saturated CH_3CN solution of *trans*-**1** < 1.5 mM after 115 h of irradiation.

ii. Photoreactivity of cis-1 monitored with time in diluted < 1.5 mM argon saturated acetonitrile solution

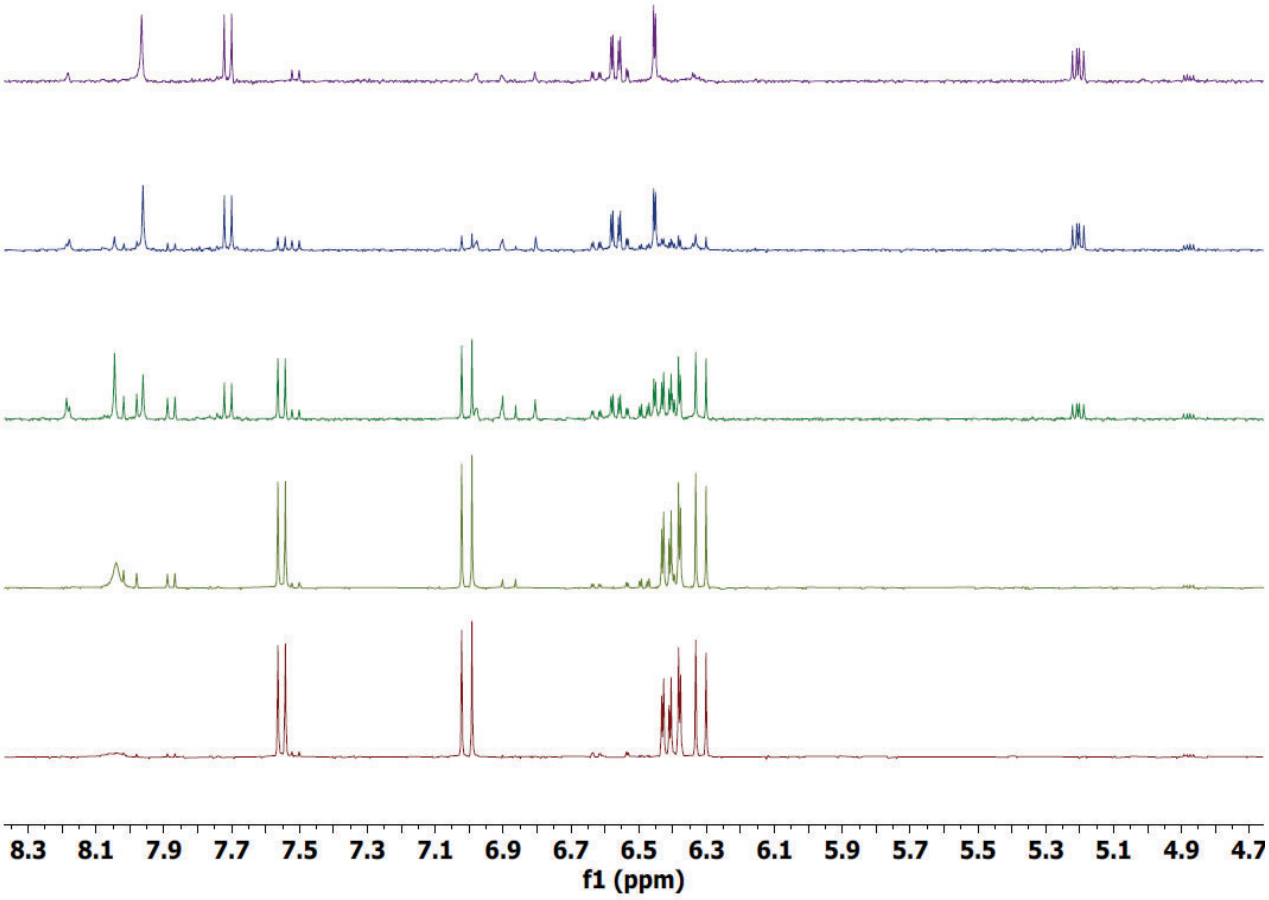

Figure S101. Overlaid ^{1}HNMR spectra of *cis*-**1** monitored with increasing time of irradiation at 365 nm in diluted < 1.5 mM argon saturated CH_3CN solution.

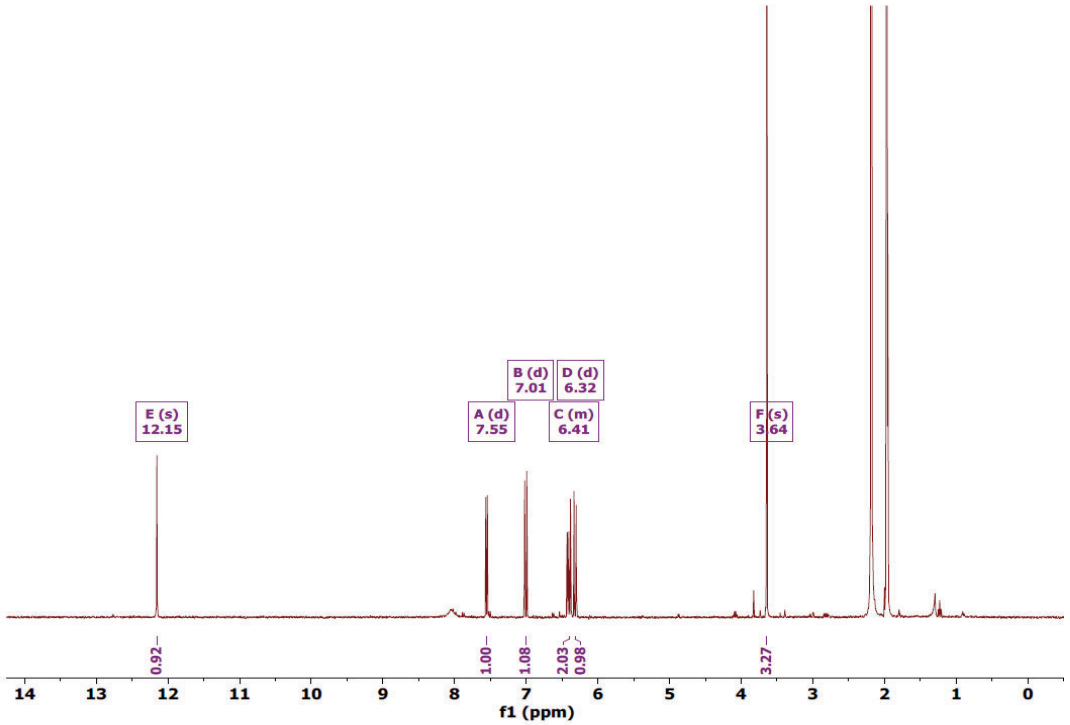

Figure S102. ^{1}H NMR spectrum of diluted argon saturated CH_3CN solution of *cis*-**1** < 1.5 mM at 0 h of irradiation.

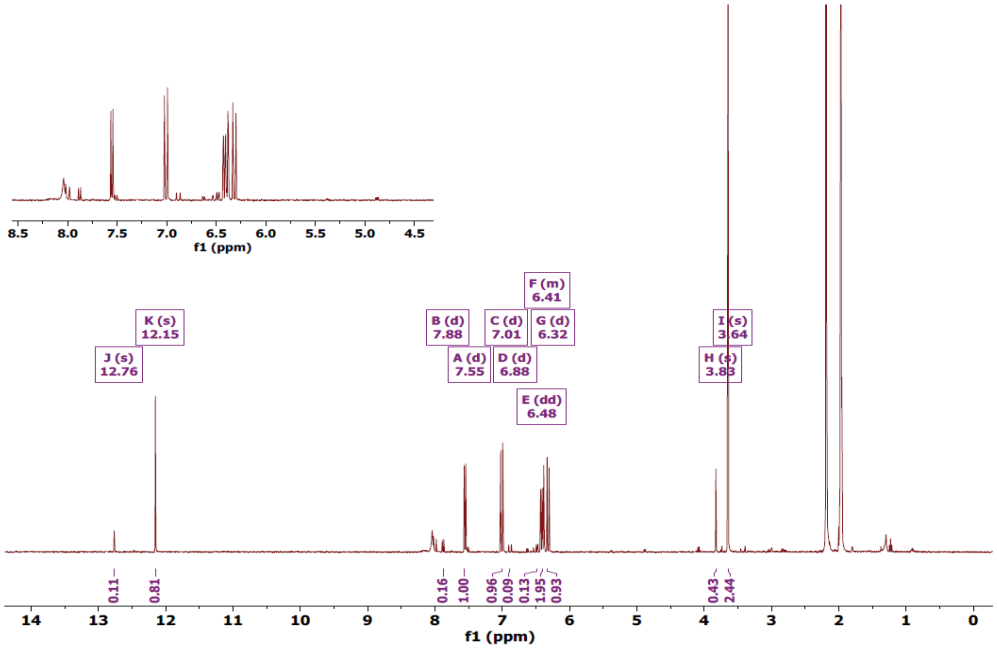

Figure S103. ^{1}H NMR spectrum of diluted argon saturated CH_3CN solution of *cis*-**1** < 1.5 mM after 1 h of irradiation.

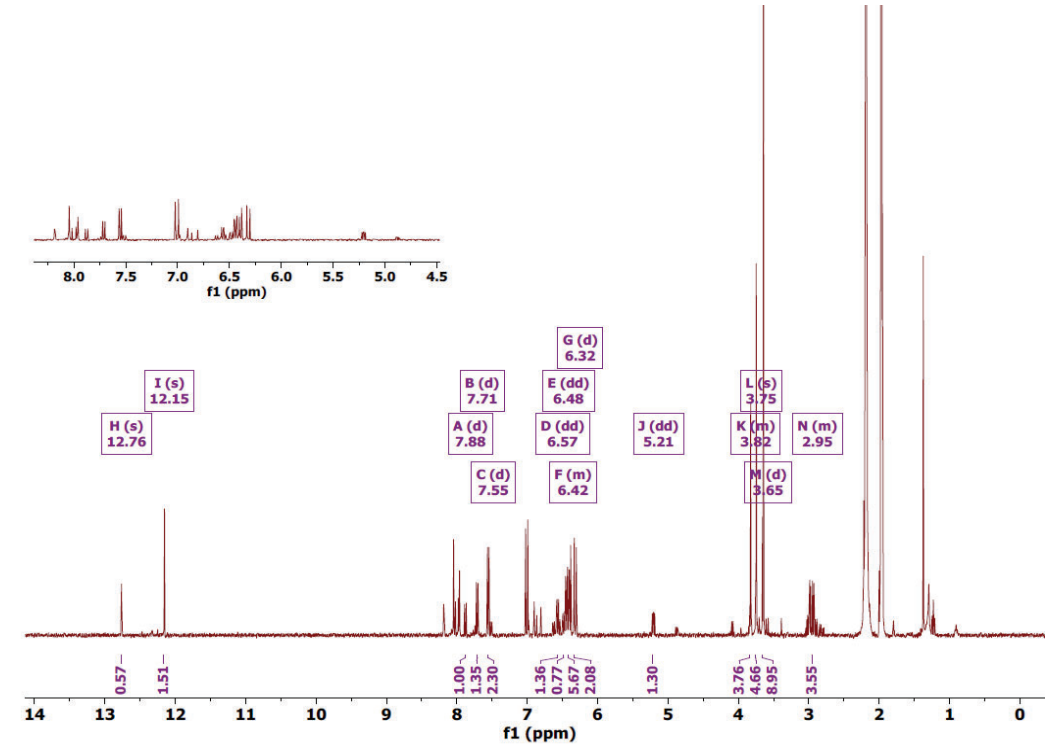

Figure S104. ^{1}H NMR spectrum of diluted argon saturated CH_3CN solution of *cis*-**1** < 1.5 mM after 67 h of irradiation.

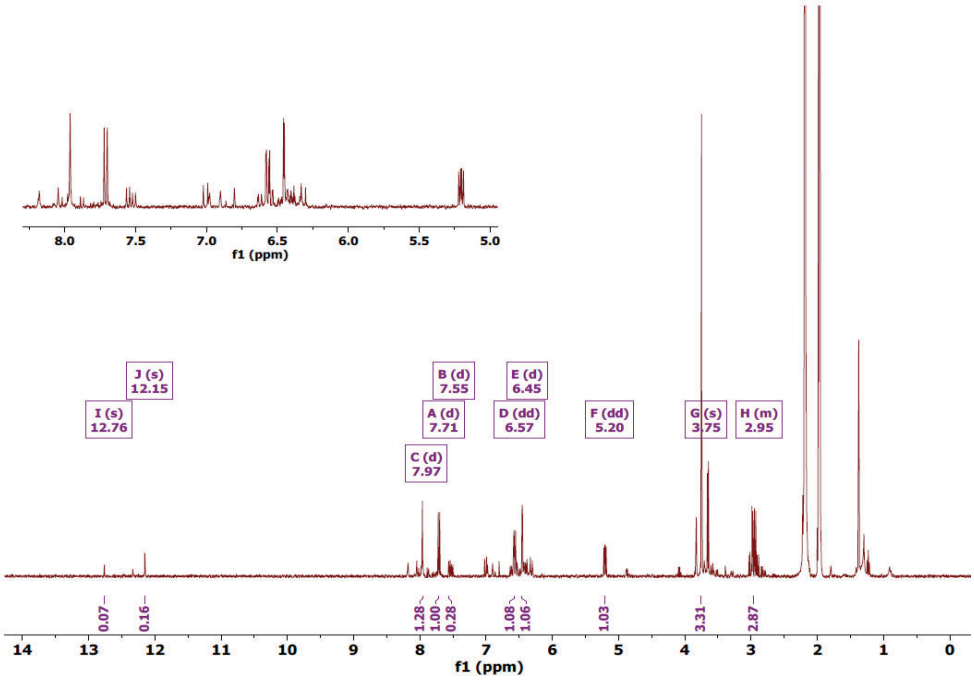

Figure S105. ^{1}H NMR spectrum of diluted argon saturated CH_3CN solution of *cis*-**1** < 1.5 mM after 90 h of irradiation.

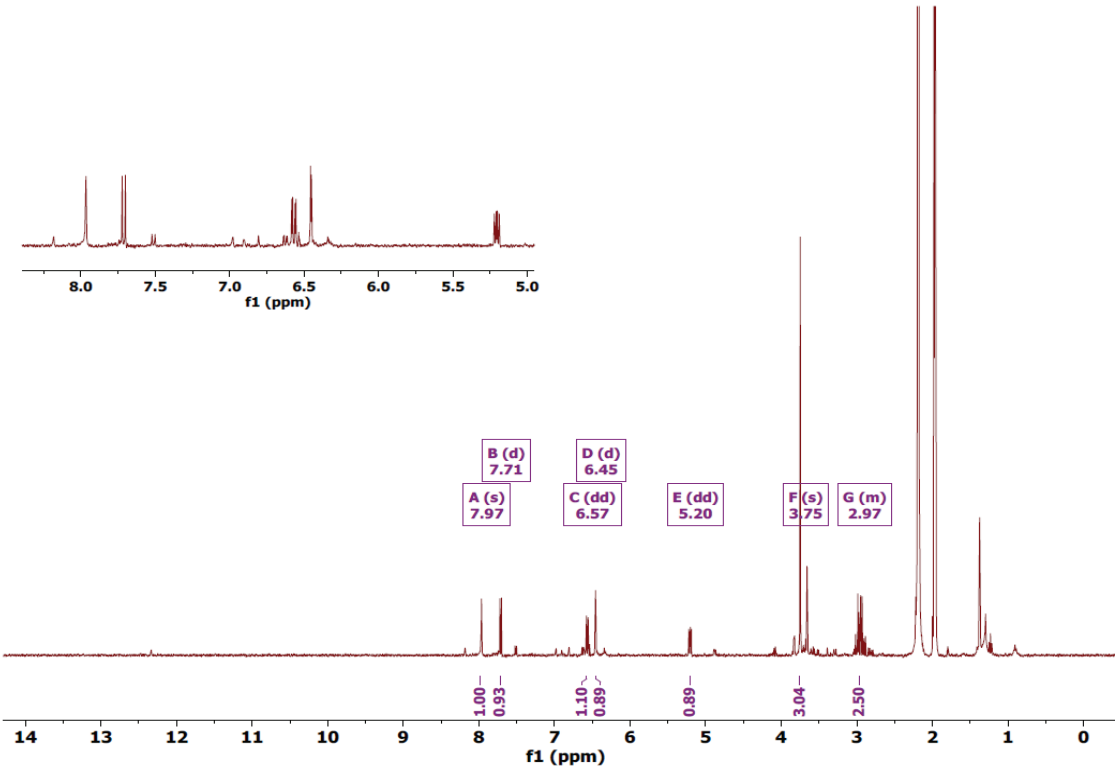

Figure S106. ^{1}H NMR spectrum of diluted argon saturated CH_3CN solution of *cis*-**1** < 1.5 mM after 110 h of irradiation.

V. Photoreactivity of the 2-hydroxy chalcones in diluted solution of < 1.5 mM oxygen saturated acetonitrile

i. Photoreactivity of cis-1 in diluted solution of < 1.5 mM oxygen saturated acetonitrile

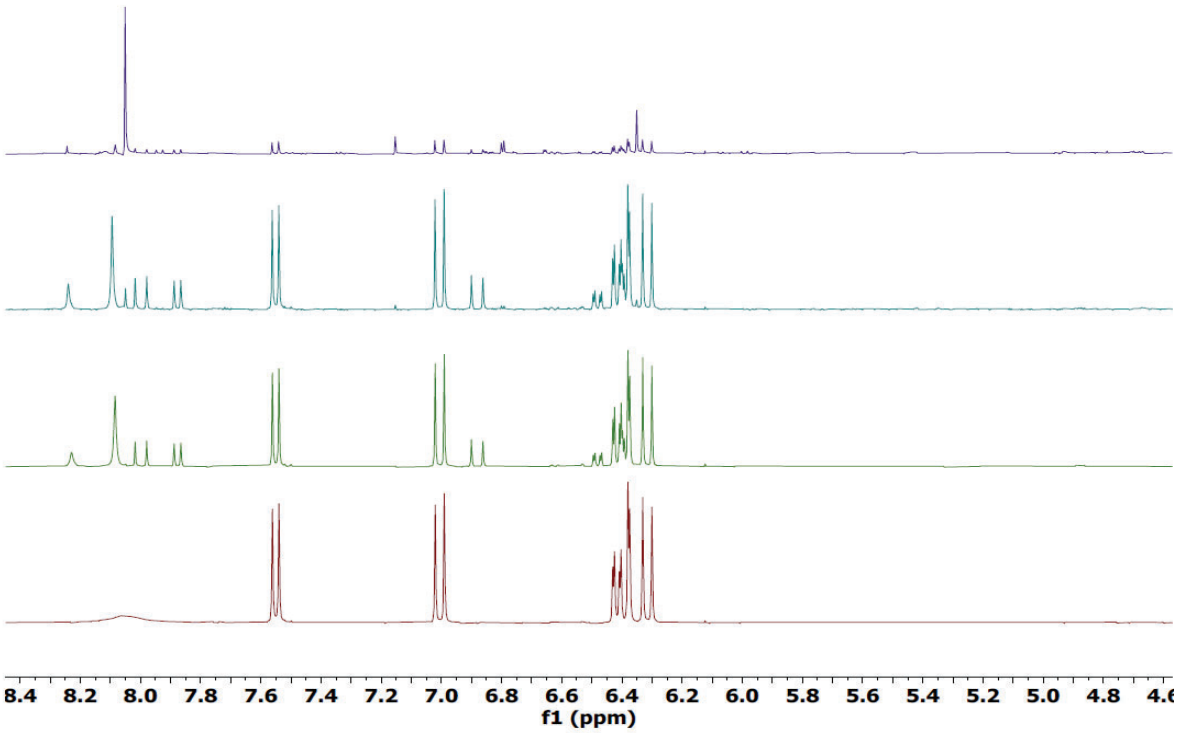

Figure S107. Overlaid ^{1}HNMR spectra of *cis*-**1** monitored with increasing time of irradiation at 365 nm in diluted solution of < 1.5 mM oxygen saturated CH_3CN

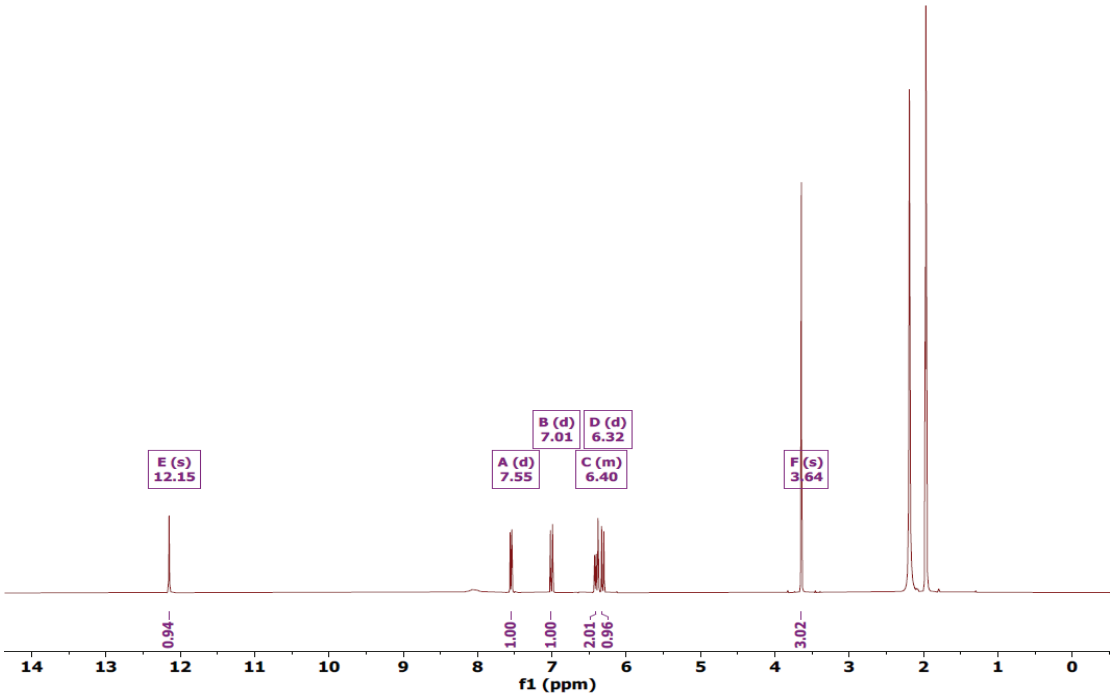

Figure S108. ^{1}H NMR spectrum of diluted < 1.5 mM oxygen saturated CH_3CN solution of *cis*-**1** at 0 h of irradiation.

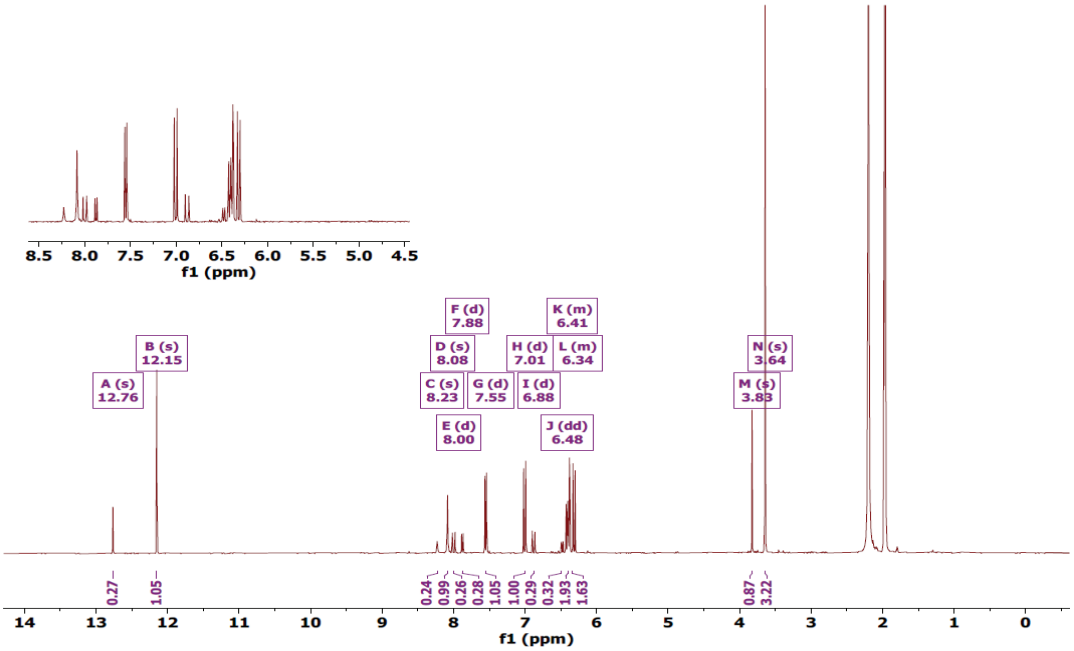

Figure S109. ^{1}H NMR spectrum of diluted < 1.5 mM oxygen saturated CH_3CN solution of *cis*-**1** after 12 h of irradiation.

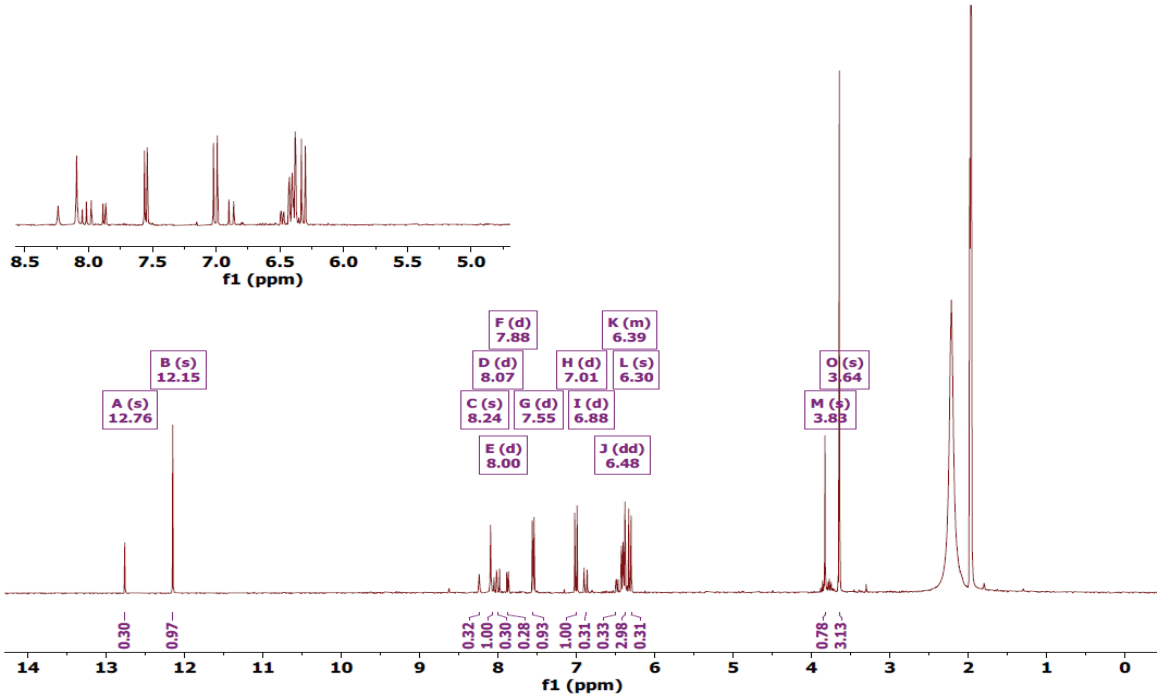

Figure S110. ^{1}H NMR spectrum of diluted < 1.5 mM oxygen saturated CH_3CN solution of *cis*-**1** after 40 h of irradiation.

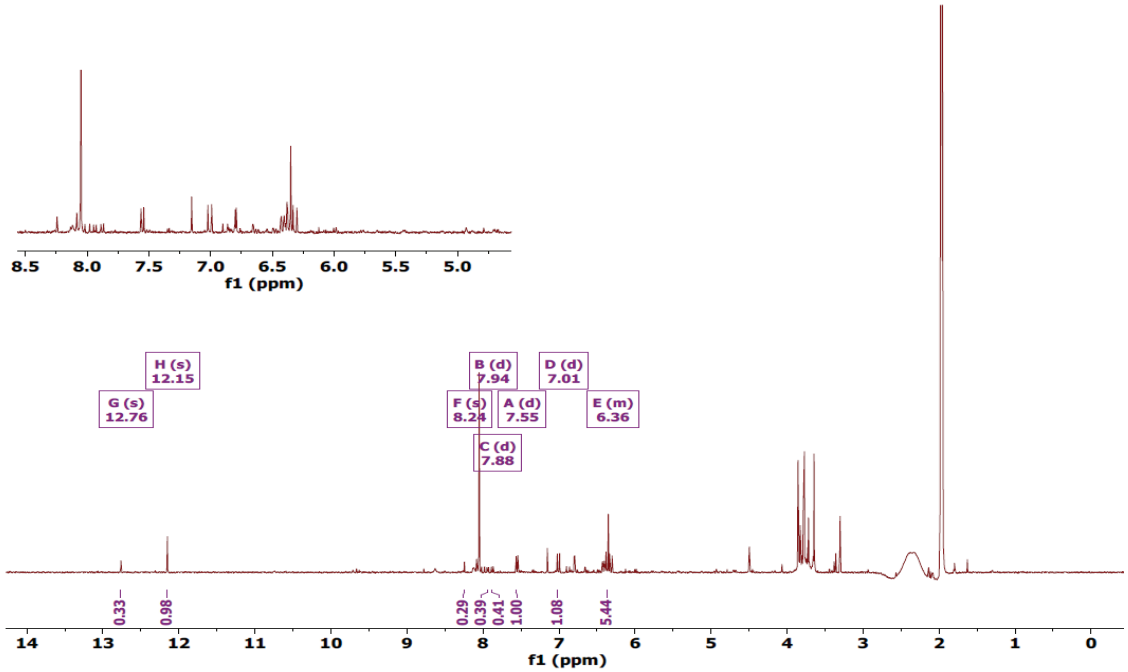

Figure S111. ^{1}H NMR spectrum of diluted < 1.5 mM oxygen saturated CH_3CN solution of *cis*-**1** after 106 h of irradiation.

ii. Photoreactivity of trans-1 in diluted solution of < 1.5 mM oxygen saturated acetonitrile

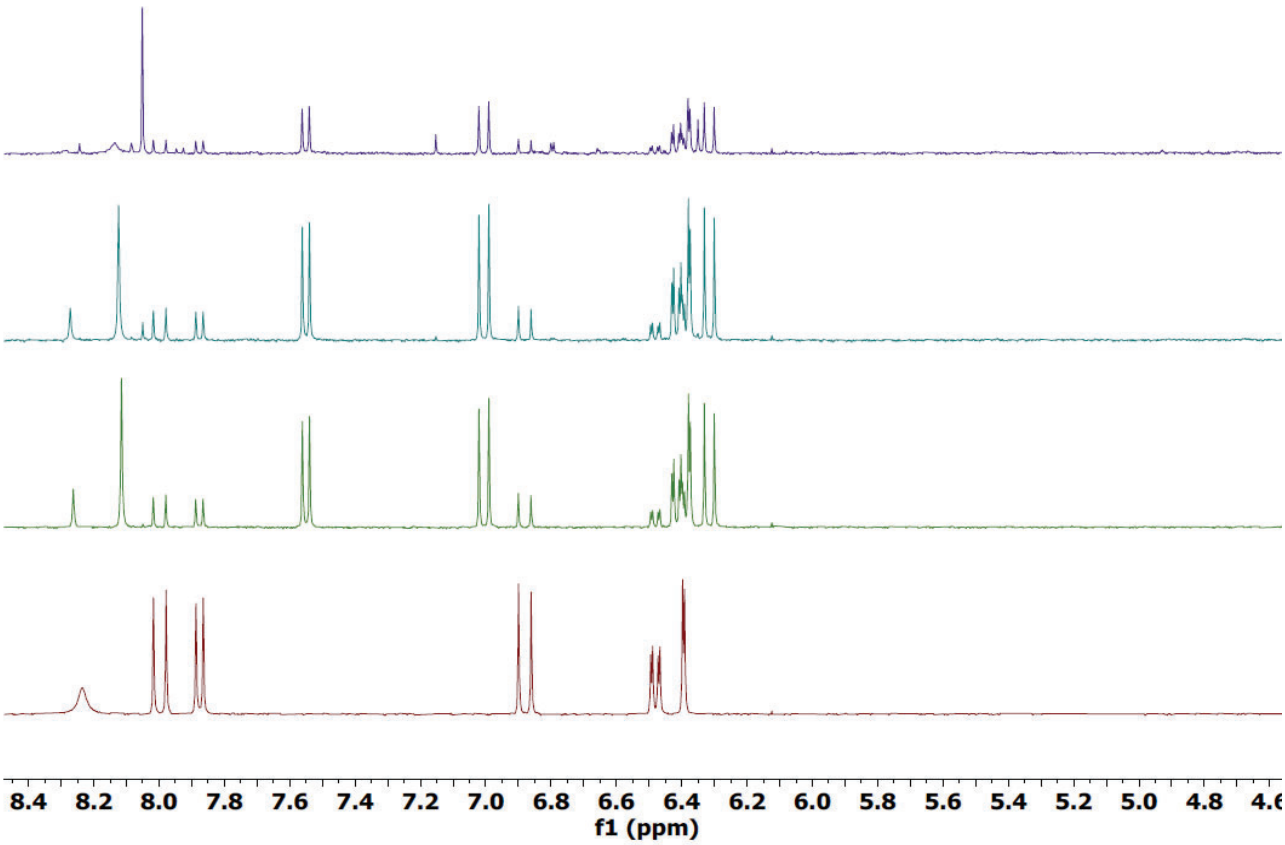

Figure S112. Overlaid ^{1}HNMR spectra of *trans*-**1** monitored with increasing time of irradiation in diluted < 1.5 mM oxygen saturated CH_3CN solution.

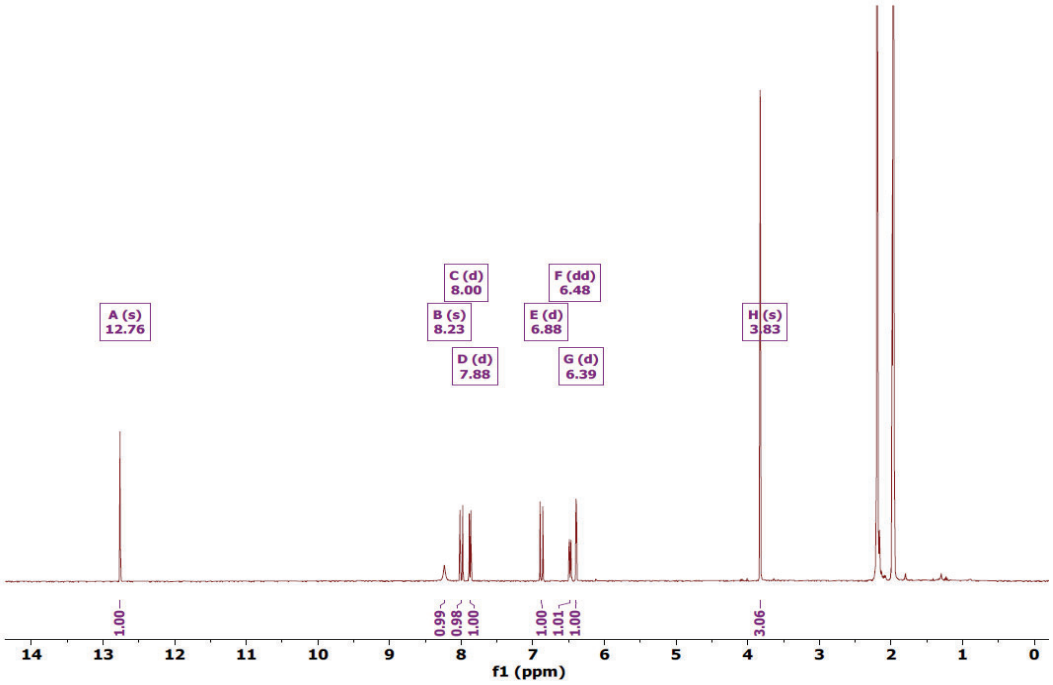

Figure S113. ^{1}H NMR spectrum of diluted < 1.5 mM oxygen saturated CH_3CN solution of *trans*-**1** at 0 h of irradiation.

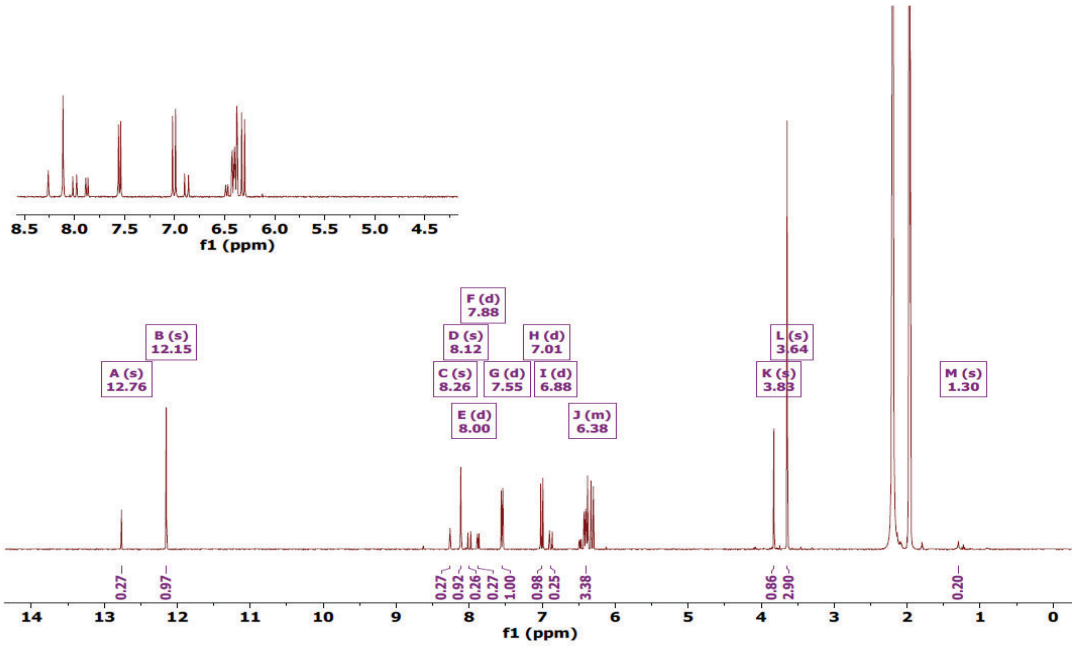

Figure S114. ^{1}H NMR spectrum of diluted < 1.5 mM oxygen saturated CH_3CN solution of *trans*-**1** after 12 h of irradiation.

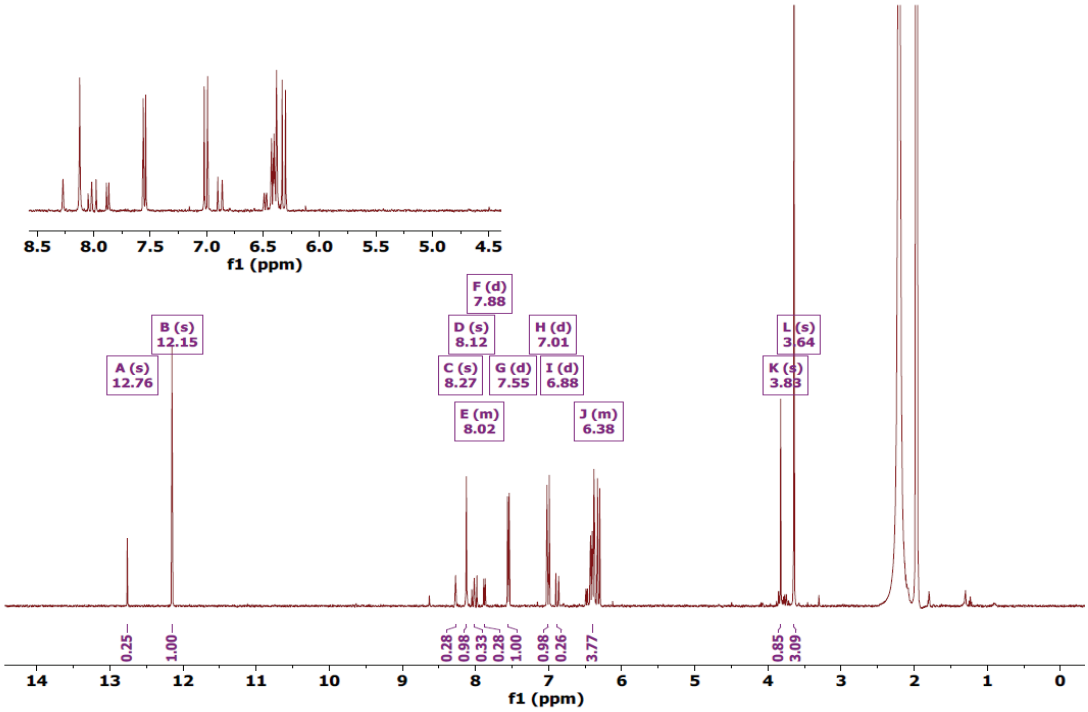

Figure S115. ^{1}H NMR spectrum of diluted < 1.5 mM oxygen saturated CH_3CN solution of *trans*-**1** after 40 h of irradiation.

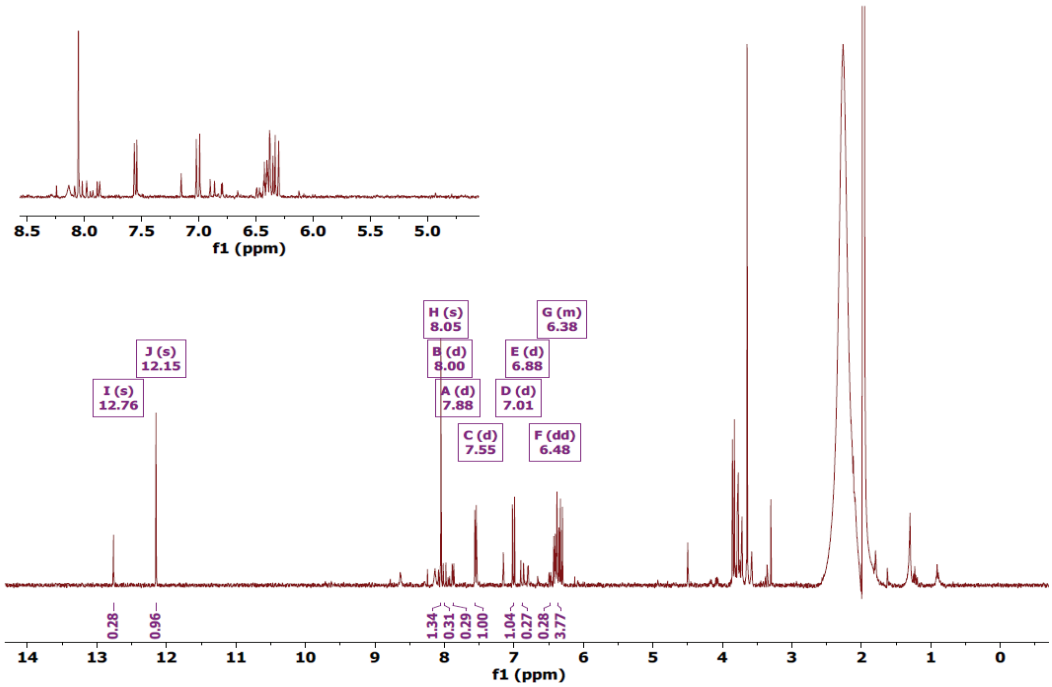

Figure S116. ^{1}H NMR spectrum of diluted < 1.5 mM oxygen saturated CH_3CN solution of *trans*-**1** after 106 h of irradiation.

VI. Concentration dependent photoreactivity of 2-hydroxychalcones in argon saturated acetonitrile

i. Concentration dependent photoreactivity of cis-1 in argon saturated acetonitrile

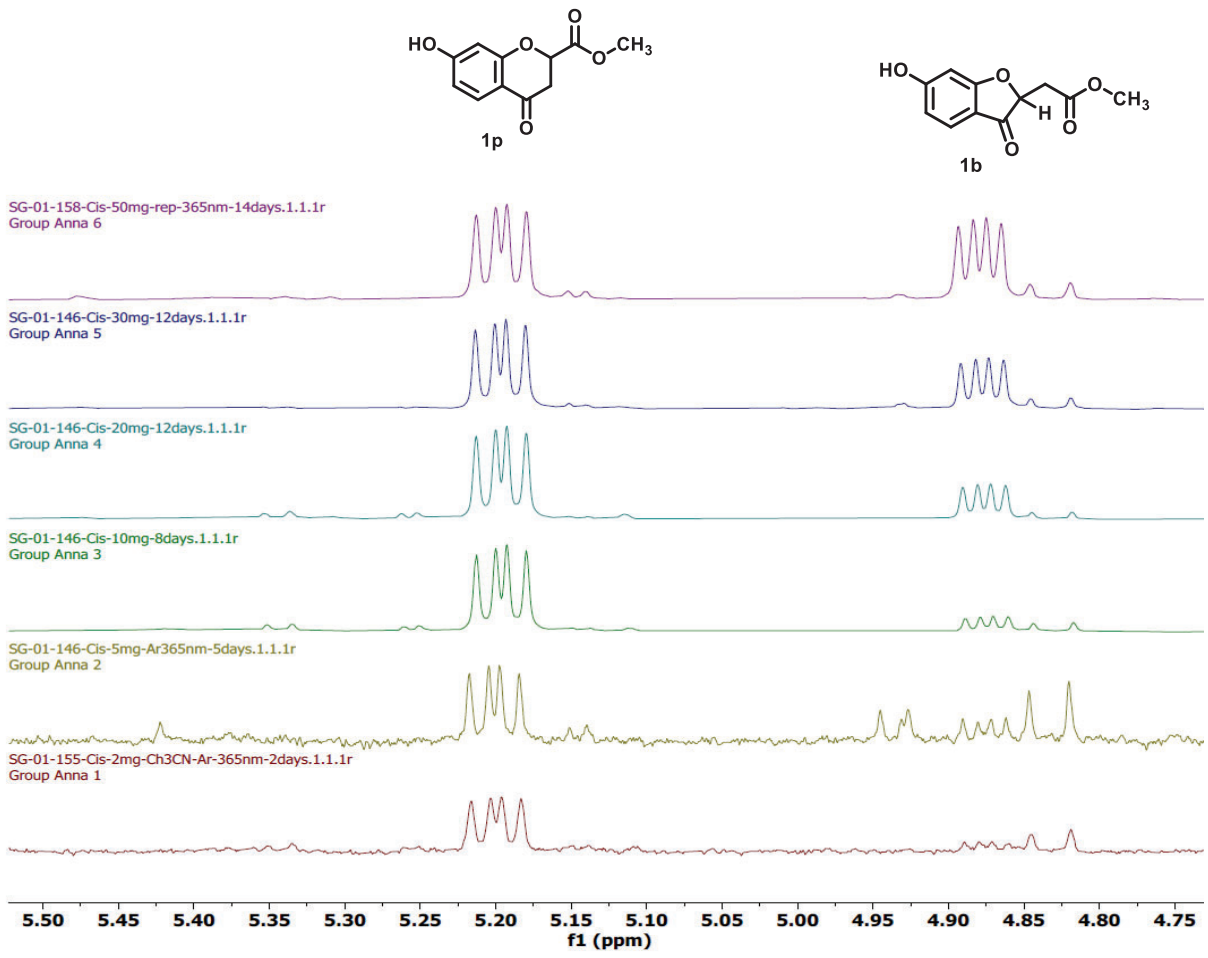

Figure S117. Overlaid ^{1}H-NMR spectra of *cis*-**1** in argon saturated acetonitrile solution with varying concentration

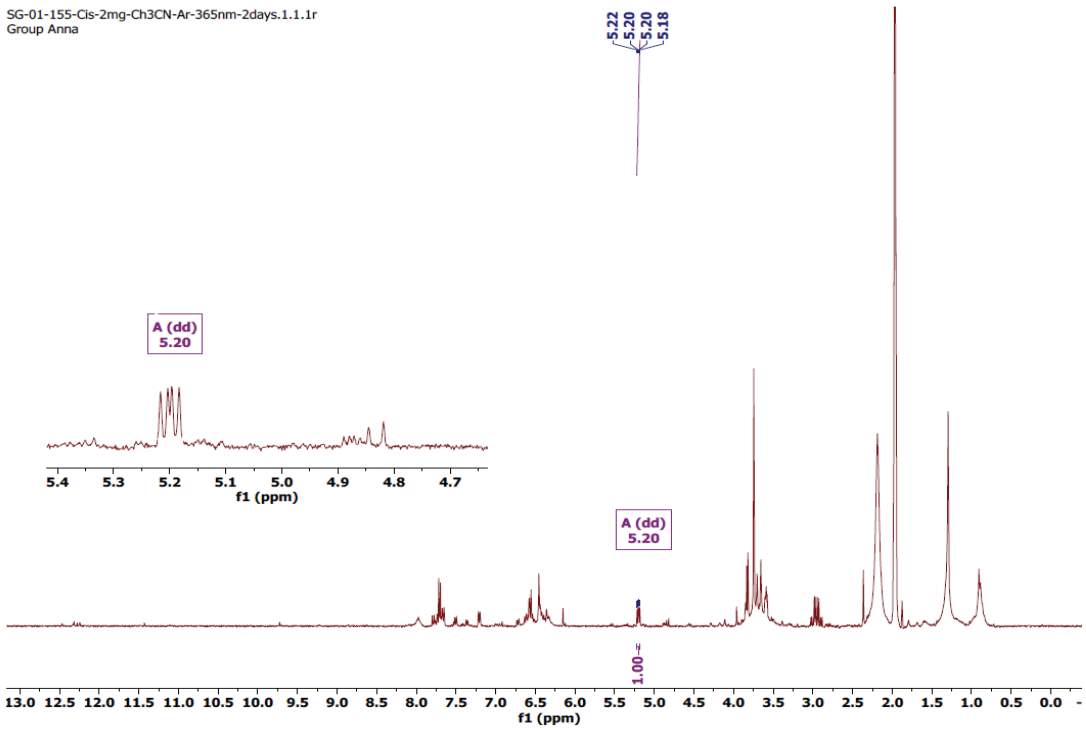

Figure S118. ^{1}H NMR spectrum of the reaction mixture of 0.6 mM *cis*-**1** after irradiation for 2 days using 365 nm LED

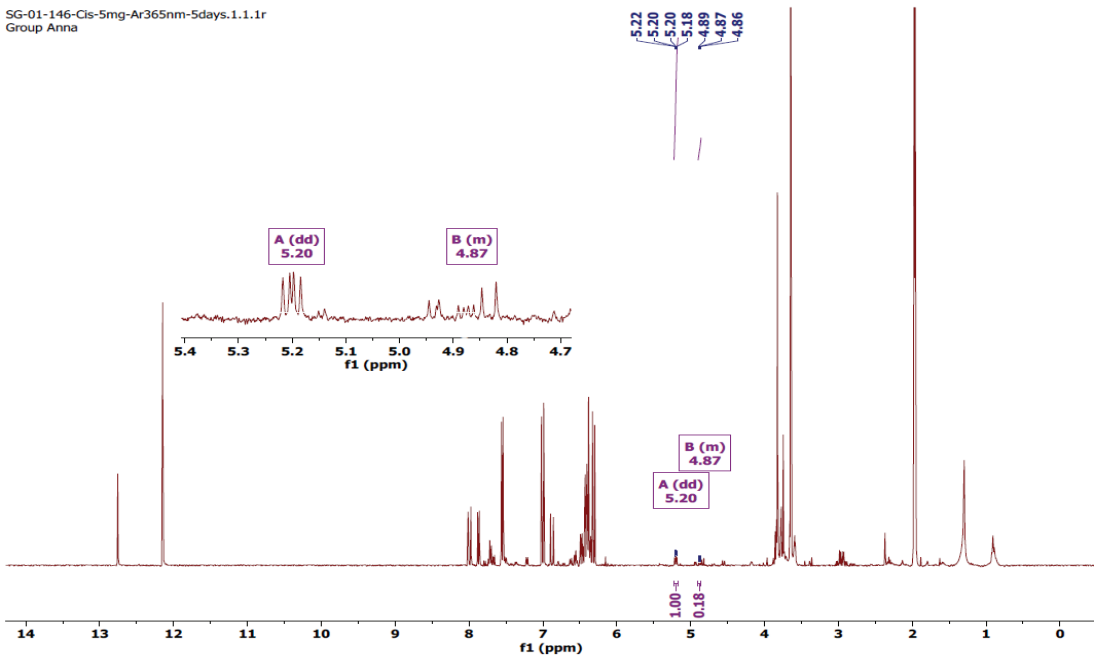

Figure S119. ^{1}H NMR spectrum of the reaction mixture of 1.5 mM *cis*-**1** after irradiation for 5 days using 365 nm LED

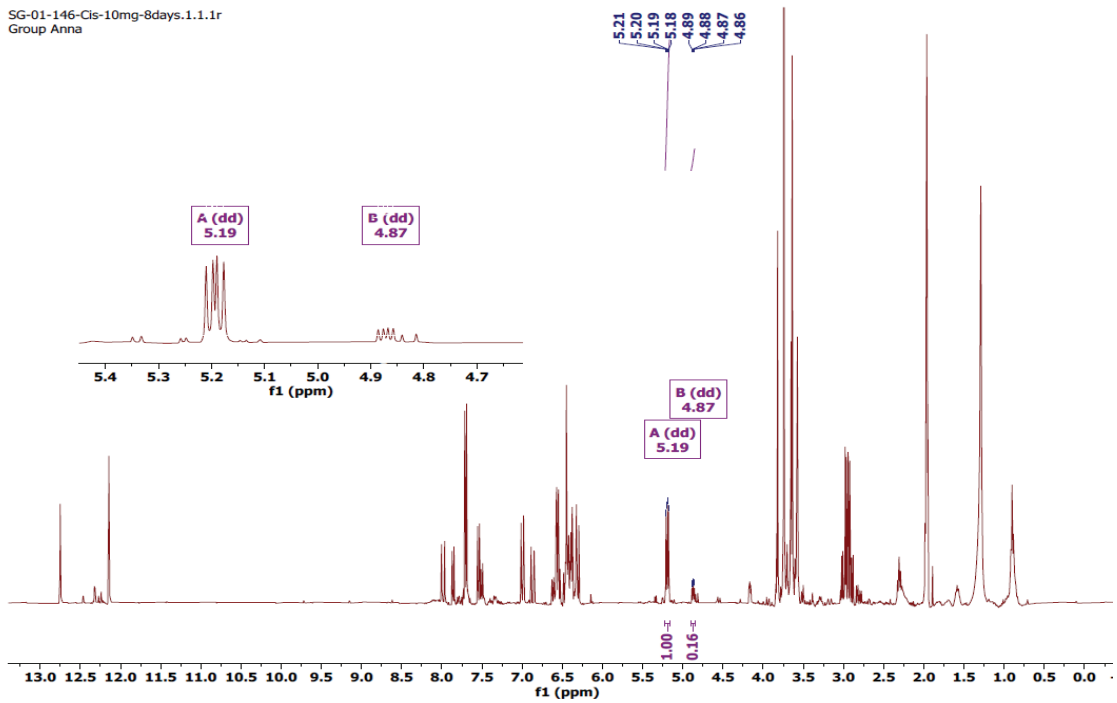

Figure S120. ^{1}H NMR spectrum of the reaction mixture of 3.0 mM *cis*-**1** after irradiation for 8 days using 365 nm LED

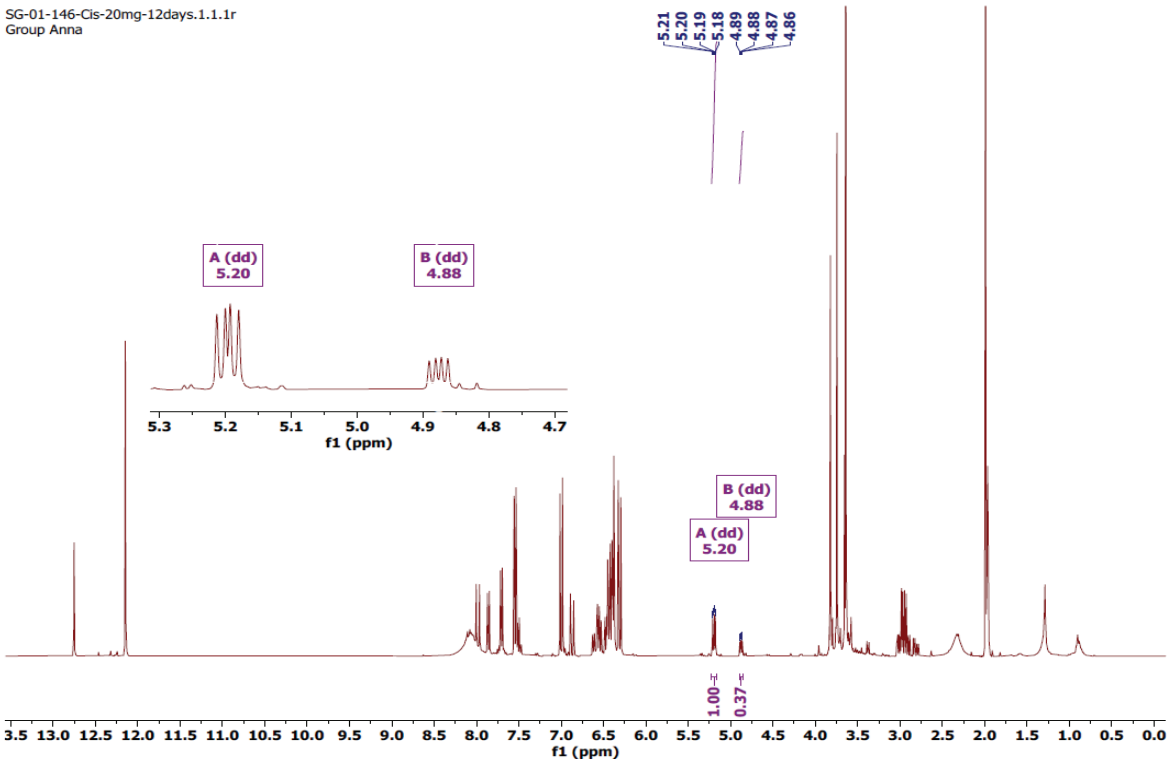

Figure S121. ^{1}H NMR spectrum of the reaction mixture of 6.0 mM *cis*-**1** after irradiation for 12 days using 365 nm LED

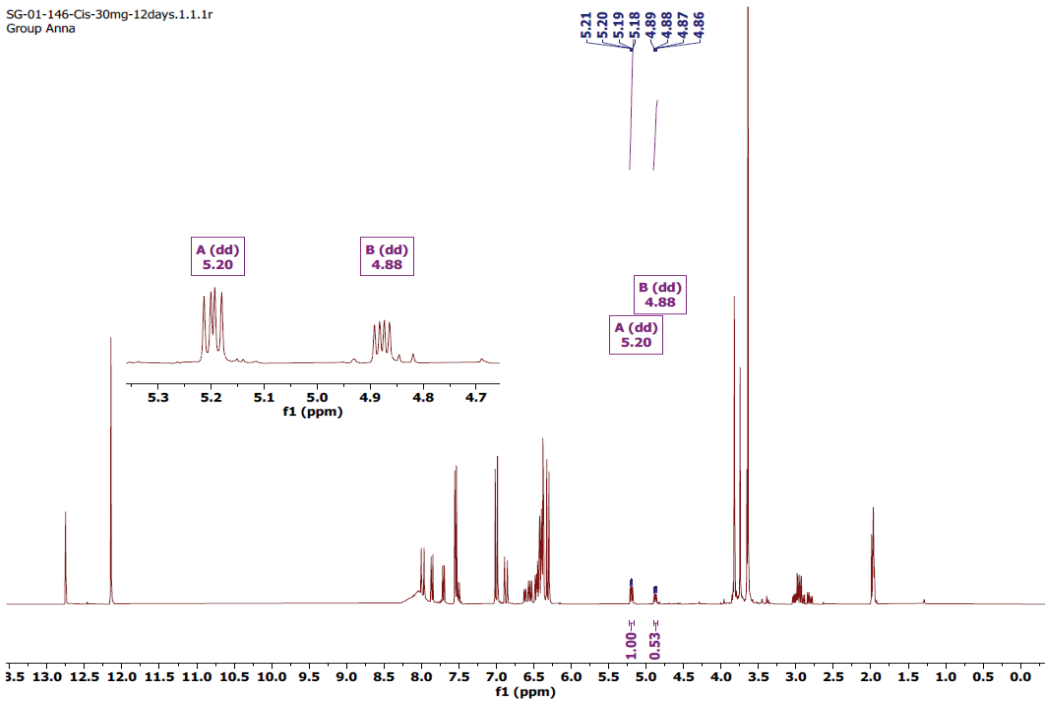

Figure S122. ^{1}H NMR spectrum of the reaction mixture of 9.0 mM *cis*-**1** after irradiation for 12 days using 365 nm LED

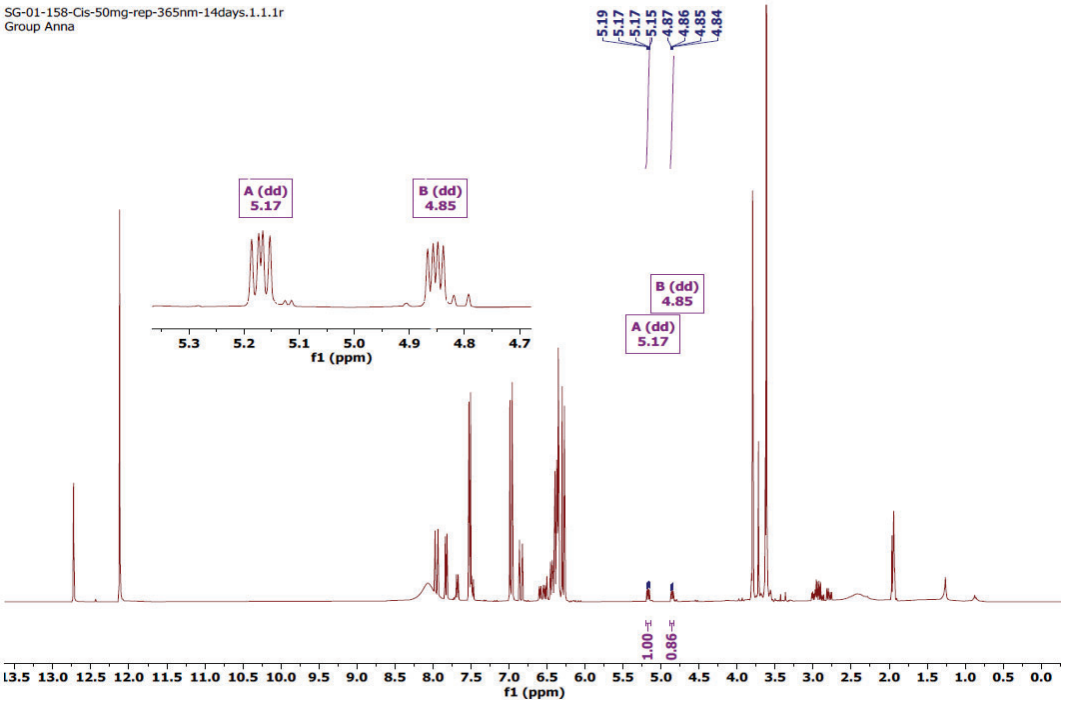

Figure S123. ^{1}H NMR spectrum of the reaction mixture of 15.0 mM *cis*-**1** after irradiation for 14 days using 365 nm LED

ii. Concentration dependent photoreactivity of trans-1 in argon saturated acetonitrile

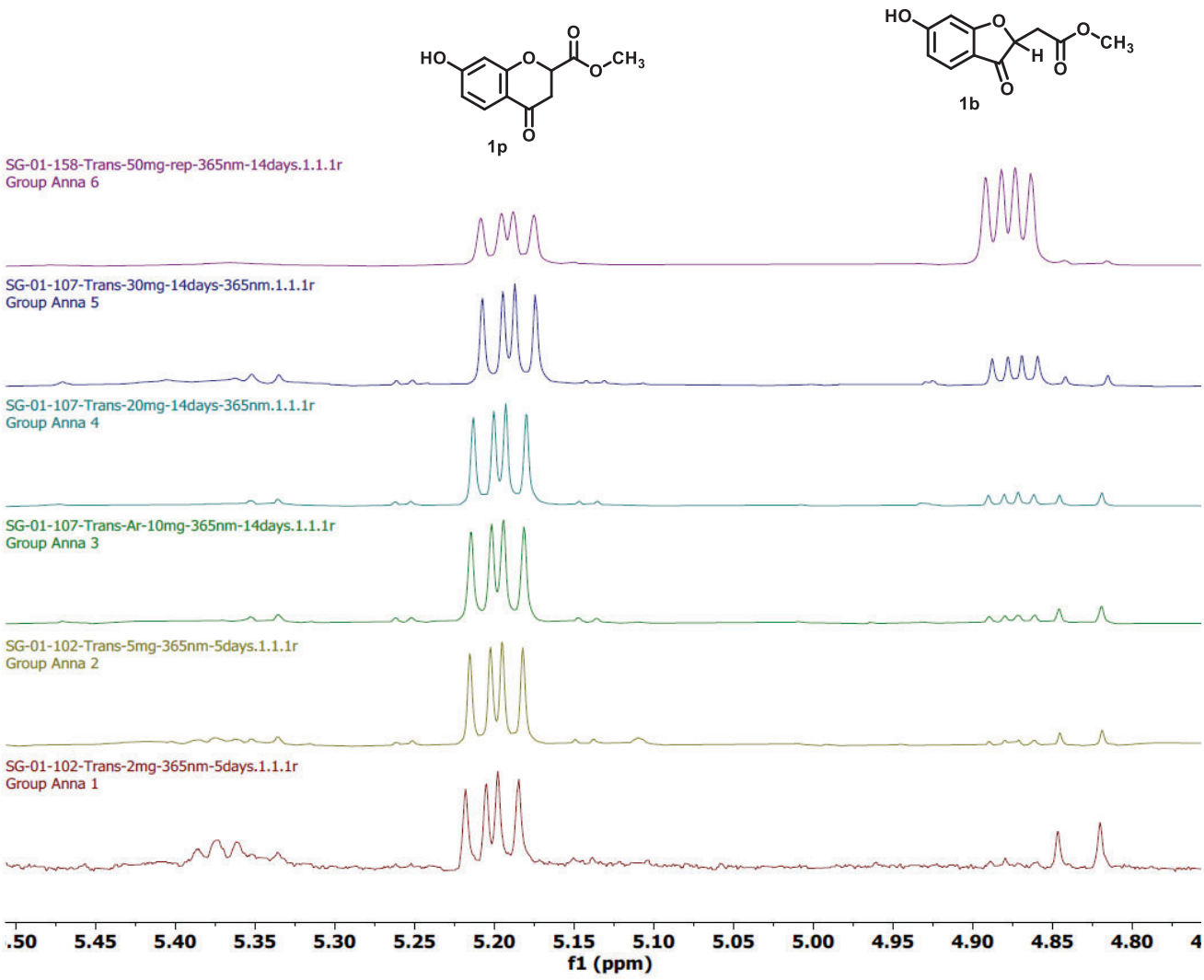

Figure S124. Overlaid ^{1}H-NMR spectra of *trans*-**1** in argon saturated acetonitrile solution with varying concentration

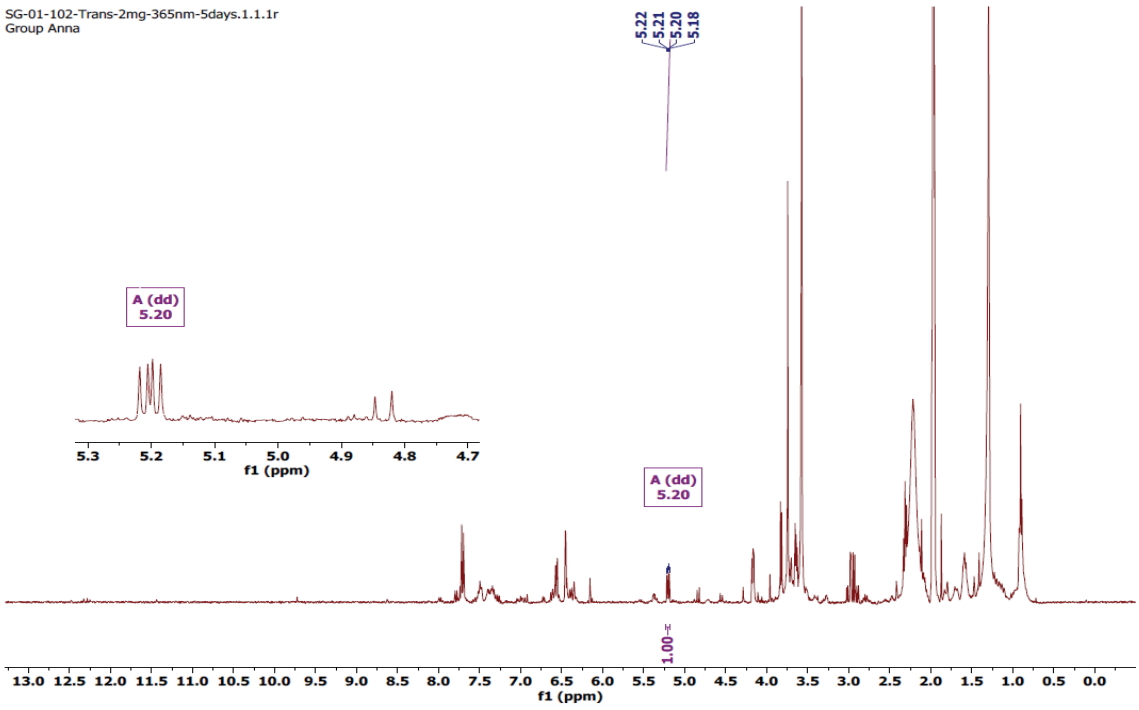

Figure S125. ^{1}H NMR spectrum of the reaction mixture of 0.6 mM *trans*-**1** after irradiation for 5 days using 365 nm LED

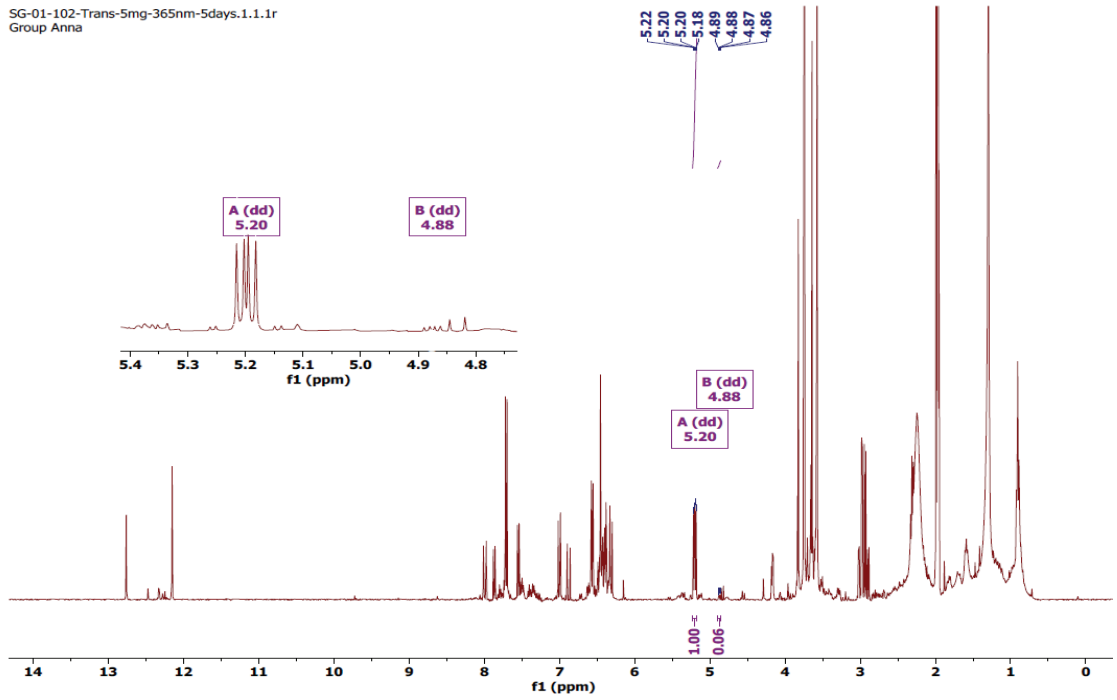

Figure S126. ^{1}H NMR spectrum of the reaction mixture of 1.5 mM *trans*-**1** after irradiation for 5 days using 365 nm LED

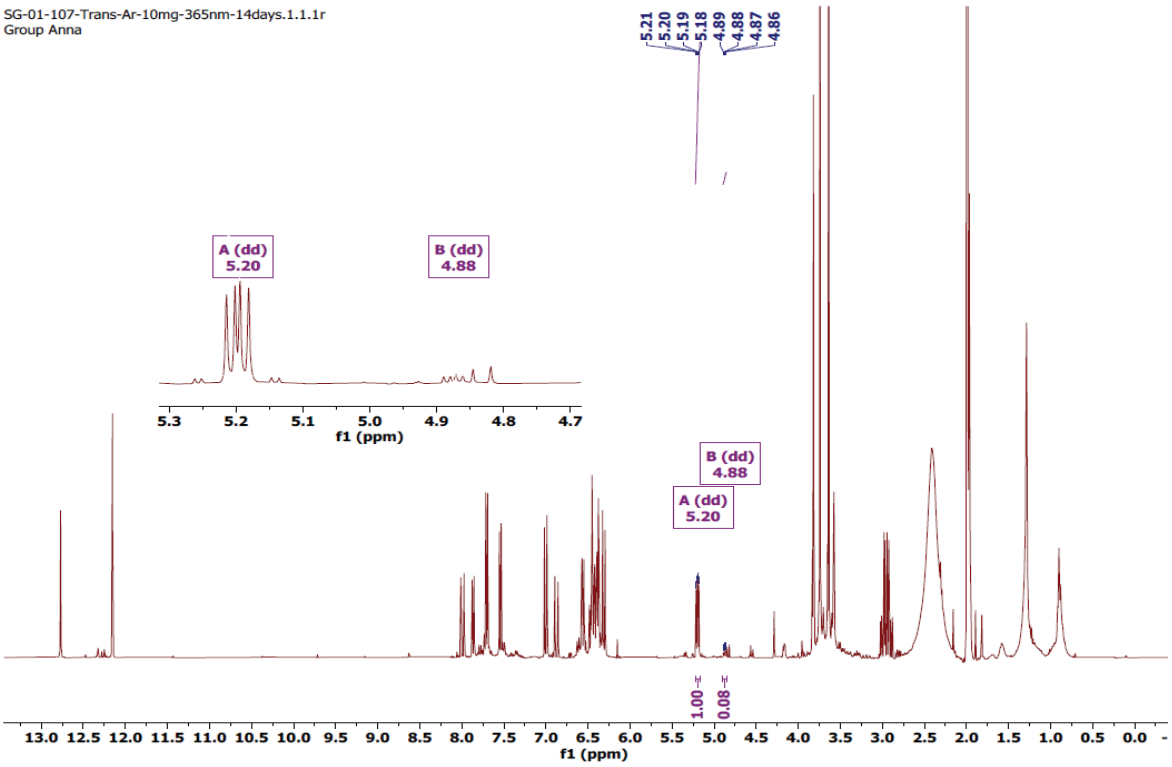

Figure S127. ^{1}H NMR spectrum of the reaction mixture of 3.0 mM *trans*-**1** after irradiation for 14 days using 365 nm LED

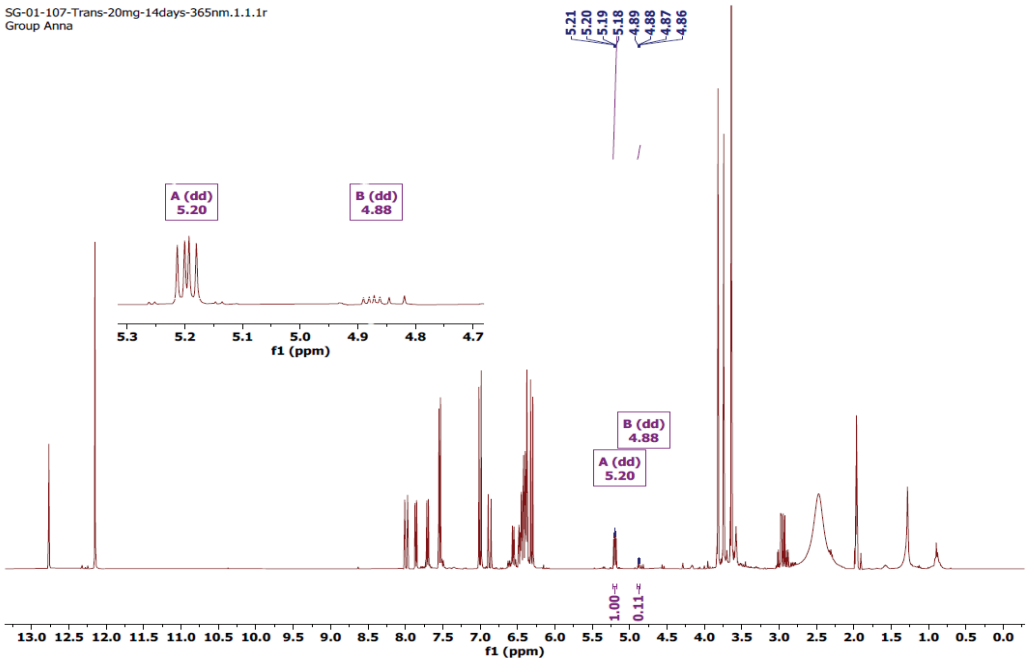

Figure S128. ^{1}H NMR spectrum of the reaction mixture of 6.0 mM *trans*-**1** after irradiation for 14 days using 365 nm LED

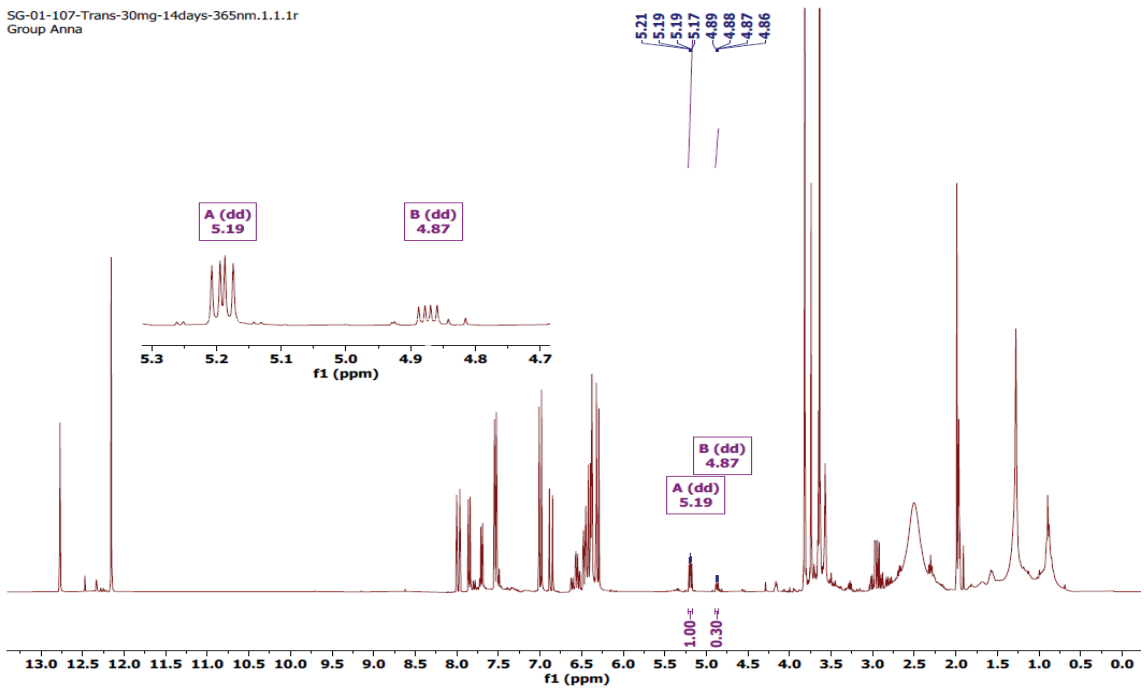

Figure S129. ^{1}H NMR spectrum of the reaction mixture of 9.0 mM *trans*-**1** after irradiation for 14 days using 365 nm LED

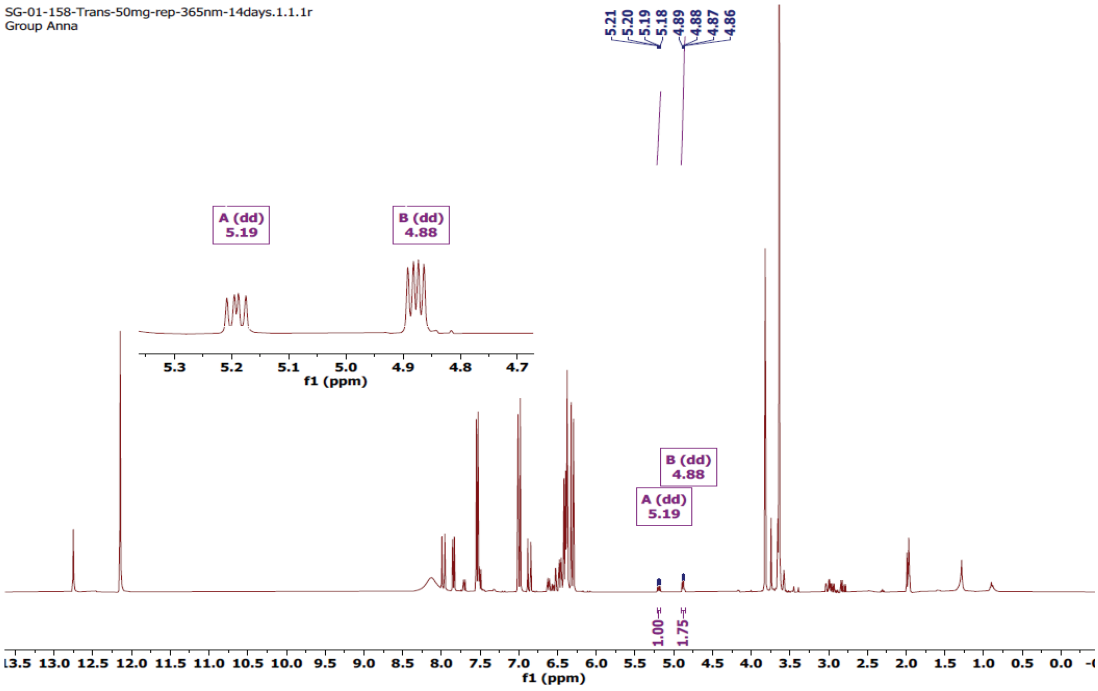

Figure S130. ^{1}H NMR spectrum of the reaction mixture of 15.0 mM *trans*-**1** after irradiation for 14 days using 365 nm LED

VII. Photoreactivity of trans-1 under continuous flow method

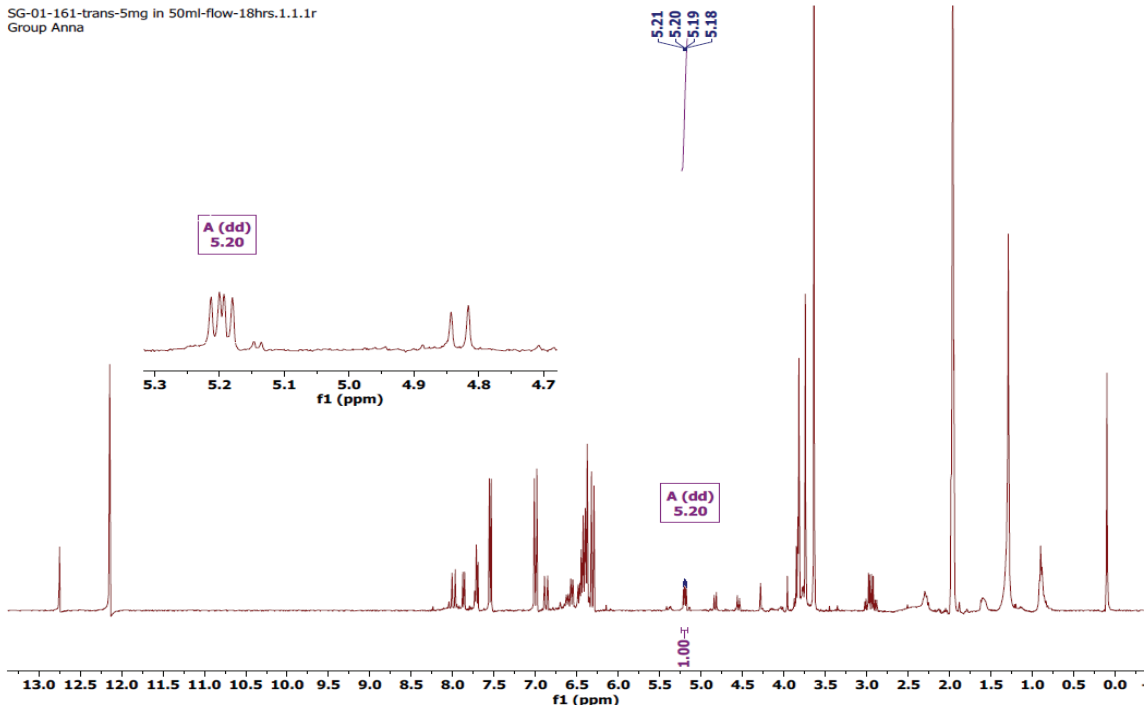

Figure S131. ^{1}H NMR spectrum of the reaction mixture of 0.45 mM *trans*-**1** after irradiation for 18 h using 365 nm LED under the continuous flow

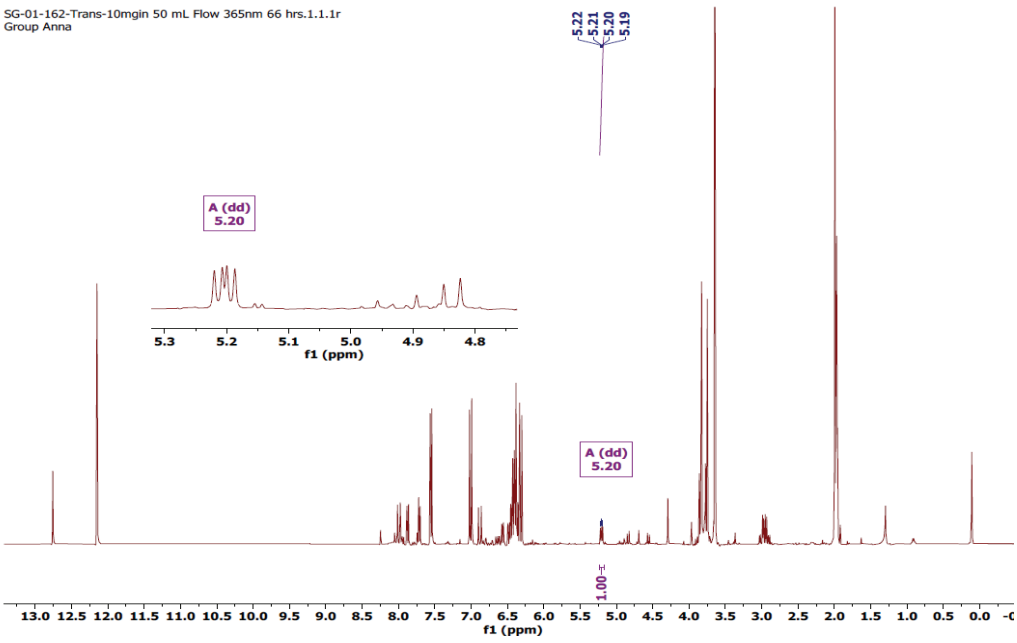

Figure S132. ^{1}H NMR spectrum of the reaction mixture of 0.9 mM *trans*-**1** after irradiation for 66 h using 365 nm LED under the continuous flow

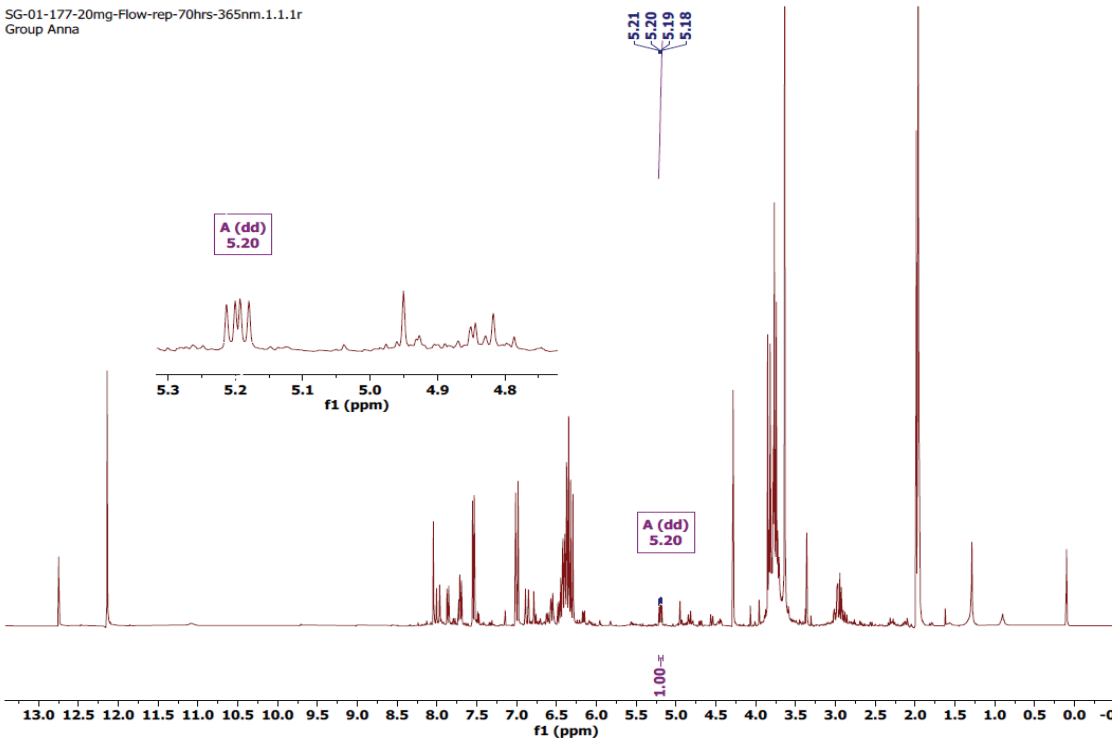

Figure S133. ^{1}H NMR spectrum of the reaction mixture of 1.8 mM *trans*-**1** after irradiation for 70 h using 365 nm LED under the continuous flow

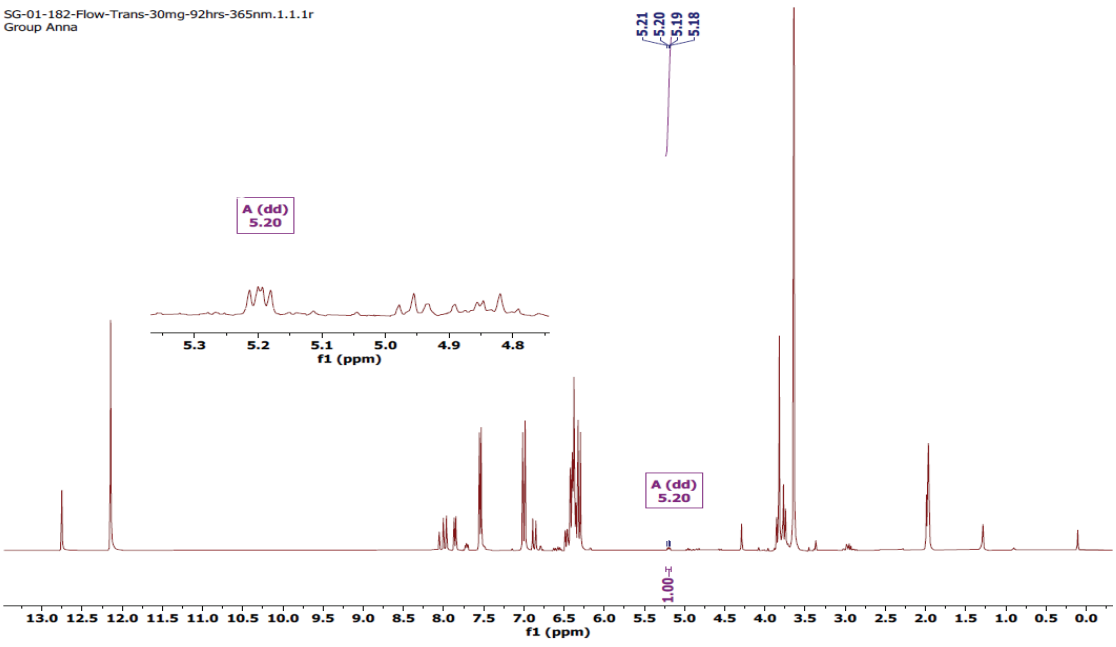

Figure S134. ^{1}H NMR spectrum of the reaction mixture of 2.7 mM *trans*-**1** after irradiation for 92 h using 365 nm LED under the continuous flow

VIII. Trapping Studies of 2- hydroxy chalcones with Tris(trimethylsilyl)silane [TTMSS]

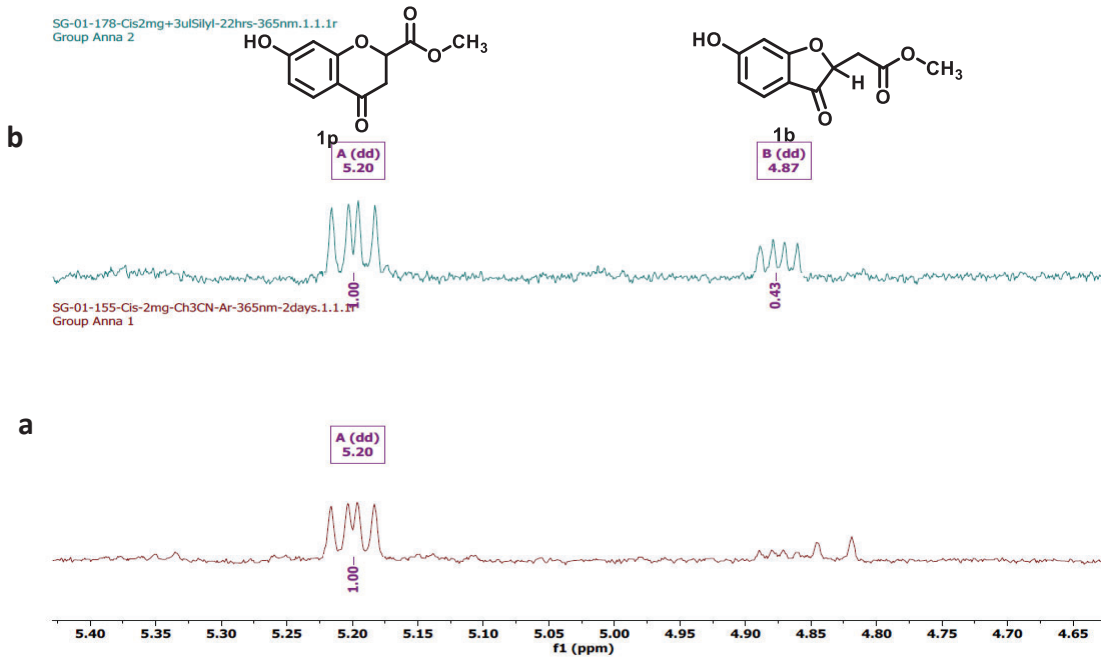

Figure S135. Overlaid ^{1}H NMR spectra of 0. 6 mM solution of *cis*-**1** irradiated with (b) and without (a) TTMSS using 365 nm LED

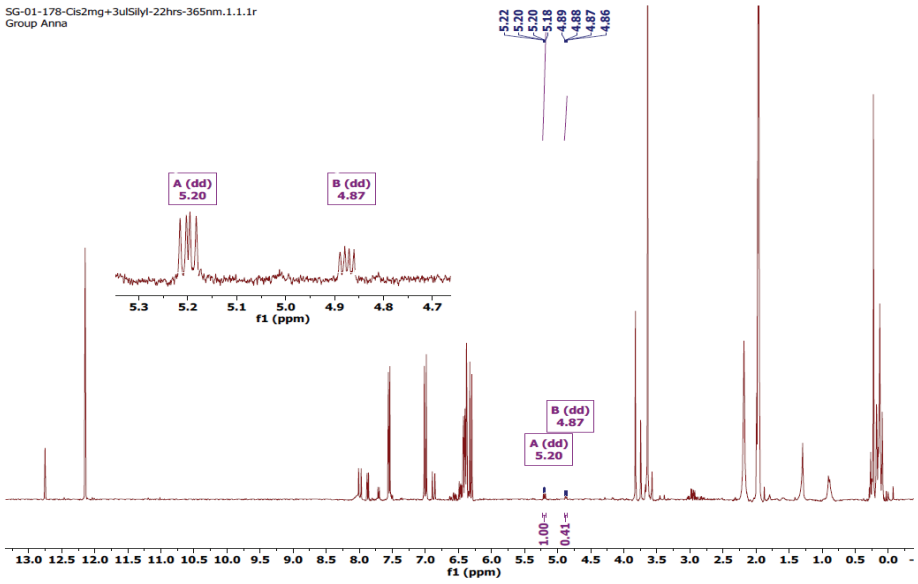

Figure S136. ^{1}H NMR spectrum of 0. 6 mM solution of *cis*-**1** irradiated with TTMSS for 22 h using 365 nm LED

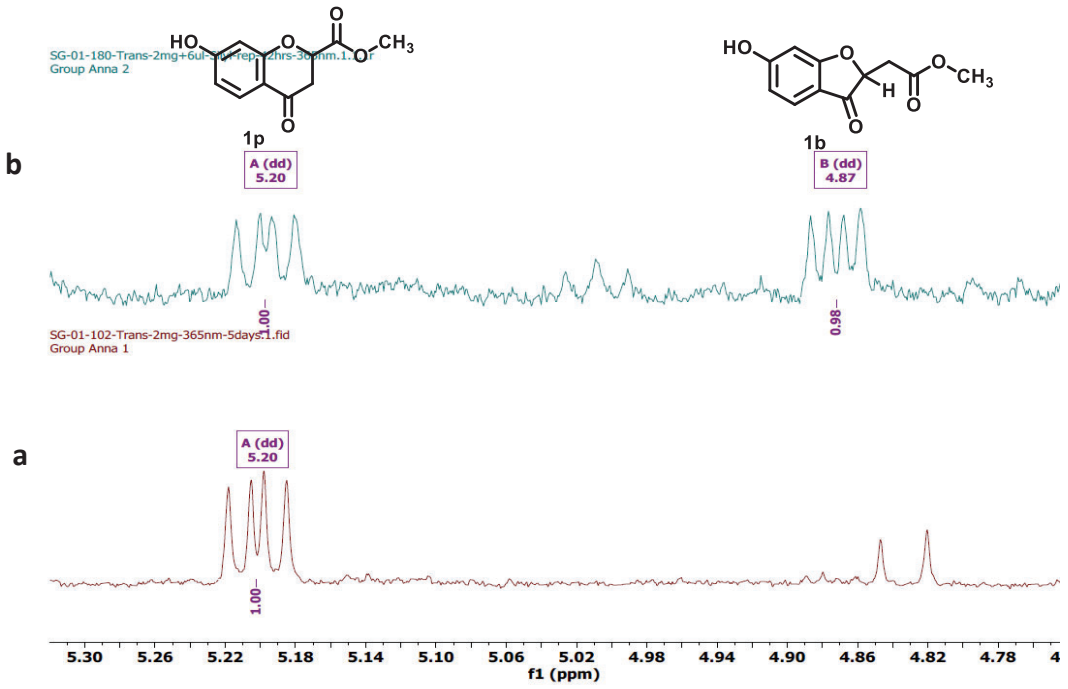

Figure S137. Overlaid ^{1}H NMR spectra of 0. 6 mM solution of *trans*-**1** irradiated with (b) and without (a) TTMSS using 365 nm LED

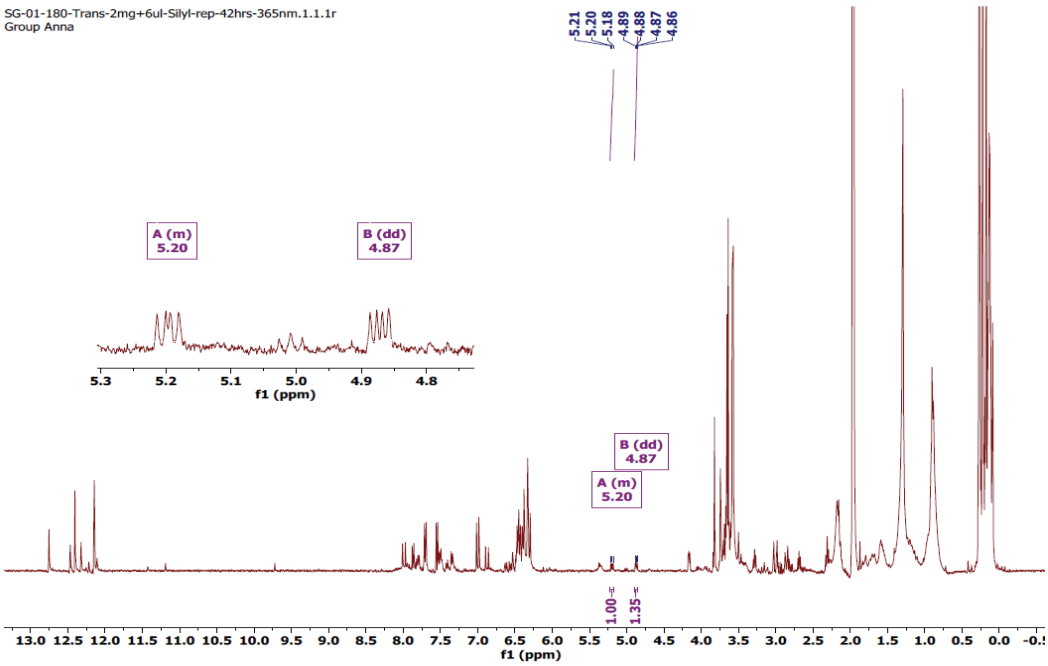

Figure S138. ^{1}H NMR spectrum of 0. 6 mM solution of *trans*-**1** irradiated with TTMSS for 42 h using 365 nm LED

IX. Photoreactivity of 2-hydroxy chalcones in protic solvents

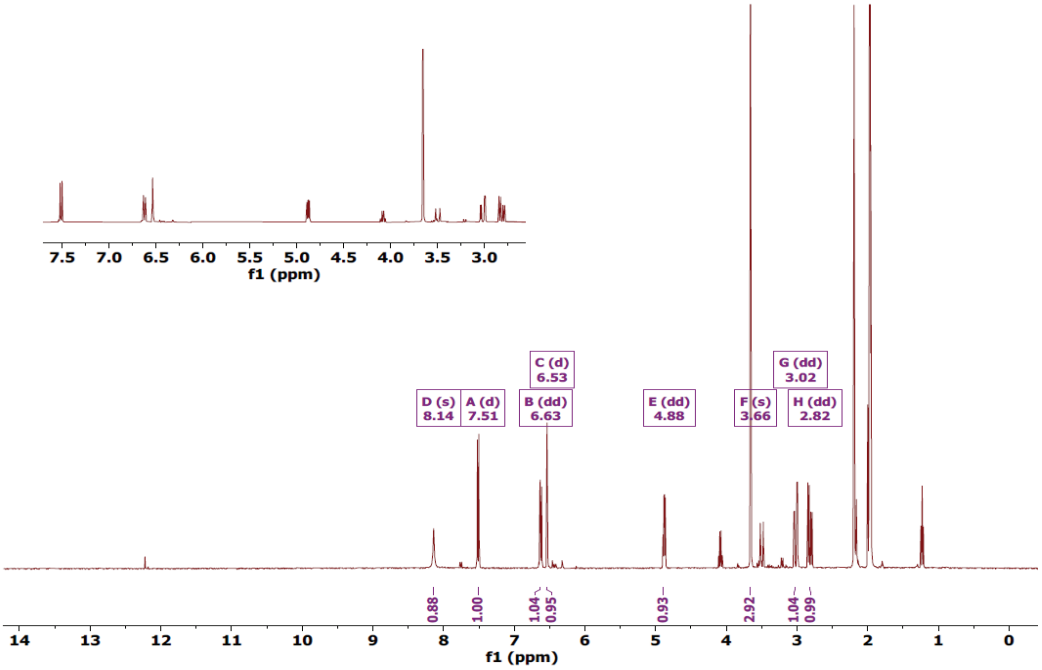

Figure S139. [1]HNMR spectrum of diluted solution < 1.5 mM of *cis*-**1** in MeOH upon irradiation at 365 nm

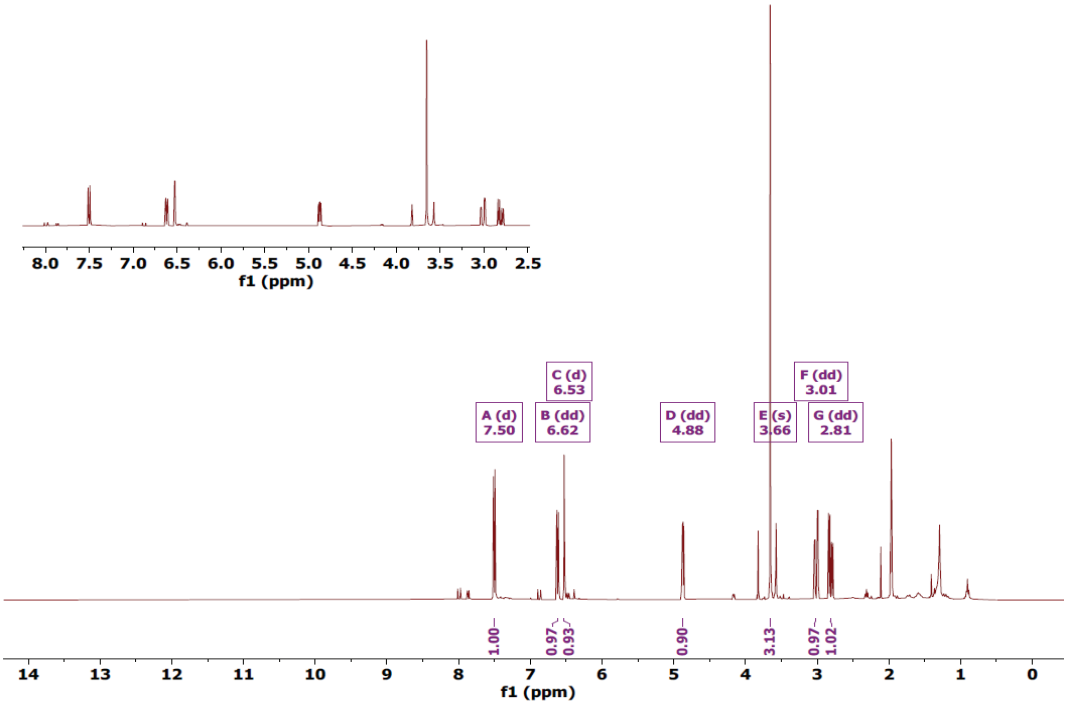

Figure S140. [1]HNMR spectrum of diluted solution < 1.5 mM of *trans*-**1** in MeOH upon irradiation at 365 nm

X. Quantum chemical calculations

S_0 of Non-H bonded *cis*-1B

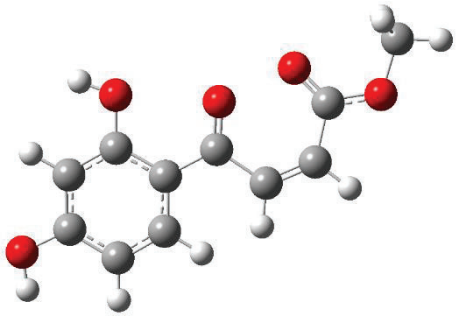

DFT/B3LYP 6-31+G(d), E = -801.309637 a.u

Center Number	Atomic Number	Atomic Type	Coordinates (Angstroms) X	Y	Z
1	6	0	-1.96239	0.871089	-0.57214
2	6	0	-0.8905	0.610148	0.323016
3	6	0	-0.9551	-0.57543	1.077157
4	6	0	-2.01046	-1.47234	0.980831
5	6	0	-3.05287	-1.1904	0.087345
6	6	0	-3.02693	-0.02816	-0.68289
7	1	0	-2.025	-2.37837	1.582305
8	1	0	-3.84658	0.165363	-1.37073
9	8	0	-1.93456	1.998622	-1.32348
10	6	0	0.250356	1.53365	0.495009
11	8	0	0.339109	2.641793	-0.01721
12	6	0	1.365143	1.177366	1.462371
13	6	0	2.45934	0.438691	1.224209
14	6	0	2.684388	-0.30053	-0.0394
15	8	0	1.913308	-0.36373	-0.9787
16	8	0	3.891336	-0.91749	-0.02233
17	6	0	4.2341	-1.65452	-1.20947
18	1	0	5.22679	-2.06337	-1.01906
19	1	0	3.511107	-2.45666	-1.38158
20	1	0	4.248248	-0.99018	-2.0777
21	1	0	3.252317	0.376851	1.964347
22	1	0	1.303006	1.714164	2.409009
23	8	0	-4.12699	-2.01621	-0.07637
24	1	0	-4.03858	-2.79262	0.498721
25	1	0	-0.14278	-0.79852	1.761455

26	1	0	-2.71658	2.022005	-1.89839

S_0 of H-bonded *cis*-1B

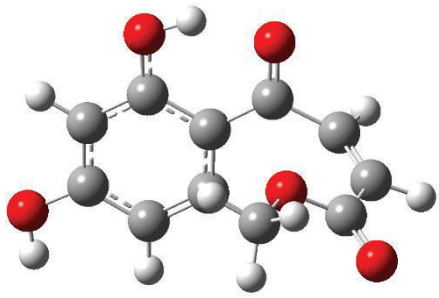

DFT/B3LYP 6-31+G(d), E = -801.329867 a.u

Center Number	Atomic Number	Atomic Type	Coordinates (Angstroms) X	Y	Z
1	6	0	-1.98281	0.899132	-0.52583
2	6	0	-0.90055	0.536245	0.333785
3	6	0	-0.98154	-0.69368	1.020238
4	6	0	-2.06982	-1.53568	0.881664
5	6	0	-3.12379	-1.15358	0.025636
6	6	0	-3.08407	0.049983	-0.67082
7	1	0	-2.11251	-2.48021	1.419232
8	1	0	-3.89921	0.333541	-1.32753
9	8	0	-1.98758	2.049648	-1.21633
10	6	0	0.235414	1.433375	0.48793
11	8	0	0.3056	2.53442	-0.08664
12	6	0	1.339053	1.128422	1.470122
13	6	0	2.452468	0.416306	1.250123
14	6	0	2.726552	-0.28505	-0.02808
15	8	0	1.98282	-0.32365	-0.9899
16	8	0	3.935707	-0.89016	0.010165
17	6	0	4.324189	-1.592	-1.186
18	1	0	5.312745	-1.99907	-0.97292
19	1	0	3.612772	-2.39315	-1.40354
20	1	0	4.362184	-0.90256	-2.03349
21	1	0	3.220358	0.34624	2.015179
22	1	0	1.227622	1.63978	2.426221

23	8	0	-4.22228	-1.93961	-0.15616
24	1	0	-4.14145	-2.75189	0.368323
25	1	0	-0.1638	-0.9863	1.67189
26	1	0	-1.14342	2.527498	-1.00512

S_0 of Non-H bonded *trans*-1B

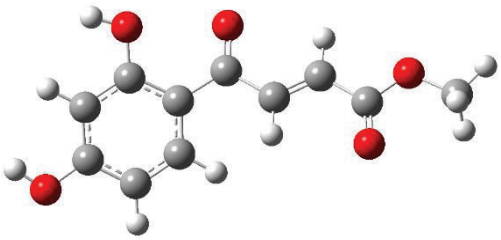

DFT/B3LYP 6-31+G(d), E = -801.316760 a.u

Center Number	Atomic Number	Atomic Type	Coordinates (Angstroms) X	Y	Z
1	6	0	-3.74877	0.399255	0.232246
2	6	0	-3.86928	-0.96993	-0.01732
3	6	0	-2.7353	-1.73764	-0.30861
4	6	0	-1.49753	-1.11168	-0.33652
5	6	0	-1.33078	0.269153	-0.10534
6	6	0	-2.49577	1.022646	0.182755
7	1	0	-4.63323	0.991106	0.467748
8	1	0	-2.8424	-2.79882	-0.5058
9	6	0	0.012509	0.902191	-0.21515
10	6	0	1.208009	0.035683	0.065507
11	6	0	2.4524	0.464817	-0.18998
12	6	0	3.631715	-0.38176	0.118585
13	8	0	-2.37412	2.349503	0.442748
14	8	0	0.166774	2.081533	-0.51463
15	8	0	4.77766	0.259187	-0.20518
16	8	0	3.599804	-1.50188	0.59553
17	6	0	5.996302	-0.46251	0.050006
18	1	0	6.084469	-0.69317	1.115152
19	1	0	6.012962	-1.39343	-0.52327
20	1	0	6.798132	0.203425	-0.26947

21	1	0	1.072754	-0.94489	0.512885
22	1	0	2.626078	1.444744	-0.62464
23	1	0	-3.24	2.717892	0.679583
24	8	0	-5.07113	-1.6139	0.012501
25	1	0	-5.78557	-0.99085	0.219311
26	1	0	-0.62623	-1.71287	-0.57629

S_0 of H-bonded *trans*-1A

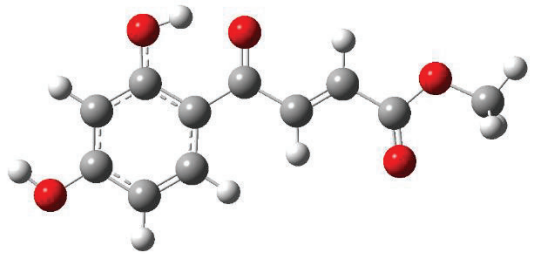

DFT/B3LYP 6-31+G(d), E = -801.339871 a.u

Center Number	Atomic Number	Atomic Type	Coordinates (Angstroms) X	Y	Z
1	6	0	3.770035	0.491941	-2E-06
2	6	0	3.937457	-0.88914	0.000048
3	6	0	2.823979	-1.75367	0.000066
4	6	0	1.555509	-1.21051	0.000016
5	6	0	1.329484	0.189799	-5.4E-05
6	6	0	2.481293	1.040694	-4.6E-05
7	1	0	4.619406	1.170355	0.000008
8	1	0	2.984153	-2.82637	0.00012
9	6	0	-0.00213	0.793469	-0.00014
10	6	0	-1.2182	-0.06628	-7.3E-05
11	6	0	-2.44856	0.468944	-0.00011
12	6	0	-3.65298	-0.39988	-4.5E-05
13	8	0	2.382538	2.37586	-4.4E-05
14	8	0	-0.14761	2.036749	-0.00015
15	8	0	-4.77912	0.345908	0.000268
16	8	0	-3.64897	-1.61748	-0.00029
17	6	0	-6.01965	-0.3854	0.000328
18	1	0	-6.08823	-1.01409	-0.89148

19	1	0	-6.08816	-1.01403	0.892178
20	1	0	-6.80156	0.374045	0.000346
21	1	0	-1.12656	-1.1465	-0.00002
22	1	0	-2.59296	1.544771	-0.00017
23	8	0	5.165	-1.47492	0.000089
24	1	0	5.861261	-0.7983	0.000101
25	1	0	0.712759	-1.89203	0.000033
26	1	0	1.407739	2.593339	0.000006

S_1 of Non-H bonded *cis*-1B

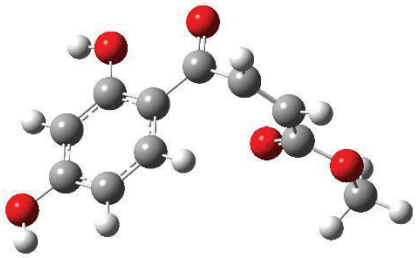

DFT/B3LYP 6-31+G(d), E = -801.194444 a.u

Center Number	Atomic Number	Atomic Type	Coordinates (Angstroms) X	Y	Z
1	6	0	-1.96239	0.871089	-0.57214
2	6	0	-0.8905	0.610148	0.323016
3	6	0	-0.9551	-0.57543	1.077157
4	6	0	-2.01046	-1.47234	0.980831
5	6	0	-3.05287	-1.1904	0.087345
6	6	0	-3.02693	-0.02816	-0.68289
7	1	0	-2.025	-2.37837	1.582305
8	1	0	-3.84658	0.165363	-1.37073
9	8	0	-1.93456	1.998622	-1.32348
10	6	0	0.250356	1.53365	0.495009
11	8	0	0.339109	2.641793	-0.01721
12	6	0	1.365143	1.177366	1.462371
13	6	0	2.45934	0.438691	1.224209
14	6	0	2.684388	-0.30053	-0.0394
15	8	0	1.913308	-0.36373	-0.9787
16	8	0	3.891336	-0.91749	-0.02233
17	6	0	4.2341	-1.65452	-1.20947
18	1	0	5.22679	-2.06337	-1.01906

19	1	0	3.511107	-2.45666	-1.38158
20	1	0	4.248248	-0.99018	-2.0777
21	1	0	3.252317	0.376851	1.964347
22	1	0	1.303006	1.714164	2.409009
23	8	0	-4.12699	-2.01621	-0.07637
24	1	0	-4.03858	-2.79262	0.498721
25	1	0	-0.14278	-0.79852	1.761455
26	1	0	-2.71658	2.022005	-1.89839

S_1 of H-bonded *cis*-1B

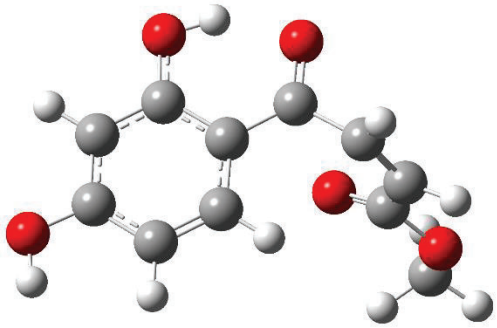

DFT/B3LYP 6-31+G(d), E = -801.217033 a.u

Center Number	Atomic Number	Atomic Type	Coordinates (Angstroms) X	Y	Z
1	6	0	-1.98281	0.899132	-0.52583
2	6	0	-0.90055	0.536245	0.333785
3	6	0	-0.98154	-0.69368	1.020238
4	6	0	-2.06982	-1.53568	0.881664
5	6	0	-3.12379	-1.15358	0.025636
6	6	0	-3.08407	0.049983	-0.67082
7	1	0	-2.11251	-2.48021	1.419232
8	1	0	-3.89921	0.333541	-1.32753
9	8	0	-1.98758	2.049648	-1.21633
10	6	0	0.235414	1.433375	0.48793
11	8	0	0.3056	2.53442	-0.08664
12	6	0	1.339053	1.128422	1.470122
13	6	0	2.452468	0.416306	1.250123
14	6	0	2.726552	-0.28505	-0.02808

15	8	0	1.98282	-0.32365	-0.9899
16	8	0	3.935707	-0.89016	0.010165
17	6	0	4.324189	-1.592	-1.186
18	1	0	5.312745	-1.99907	-0.97292
19	1	0	3.612772	-2.39315	-1.40354
20	1	0	4.362184	-0.90256	-2.03349
21	1	0	3.220358	0.34624	2.015179
22	1	0	1.227622	1.63978	2.426221
23	8	0	-4.22228	-1.93961	-0.15616
24	1	0	-4.14145	-2.75189	0.368323
25	1	0	-0.1638	-0.9863	1.67189
26	1	0	-1.14342	2.527498	-1.00512

S_1 of Non-H bonded *trans*-1A

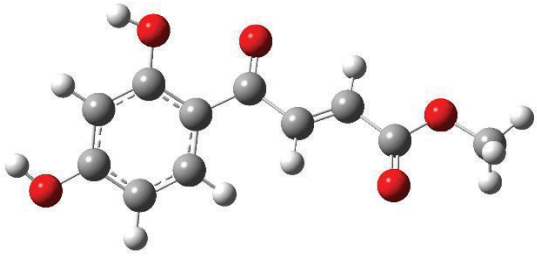

DFT/B3LYP 6-31+G(d), E = -801.222633 a.u

Center Number	Atomic Number	Atomic Type	Coordinates (Angstroms) X	Y	Z
1	6	0	-3.75092	0.395033	0.223002
2	6	0	-3.8657	-0.97502	-0.02429
3	6	0	-2.72738	-1.74007	-0.30567
4	6	0	-1.49127	-1.11059	-0.32644
5	6	0	-1.33027	0.271385	-0.09775
6	6	0	-2.49938	1.022006	0.180631
7	1	0	-4.6386	0.984877	0.451349
8	1	0	-2.83	-2.80203	-0.50103
9	6	0	0.011893	0.907564	-0.20206
10	6	0	1.208025	0.043201	0.082348
11	6	0	2.451304	0.466299	-0.18814
12	6	0	3.631243	-0.37878	0.12219

13	8	0	-2.38355	2.34992	0.4377
14	8	0	0.165132	2.087041	-0.50162
15	8	0	4.775662	0.252892	-0.22443
16	8	0	3.600945	-1.49079	0.617842
17	6	0	5.994662	-0.46883	0.028956
18	1	0	6.094697	-0.68105	1.096888
19	1	0	6.001147	-1.40975	-0.52797
20	1	0	6.795015	0.188333	-0.31169
21	1	0	1.073562	-0.93121	0.543373
22	1	0	2.623779	1.439812	-0.63745
23	1	0	-3.25239	2.716628	0.666091
24	8	0	-5.06573	-1.62254	-0.00145
25	1	0	-5.78372	-1.00108	0.197748
26	1	0	-0.61649	-1.70992	-0.55833

S_1 of H-bonded *trans*-1A

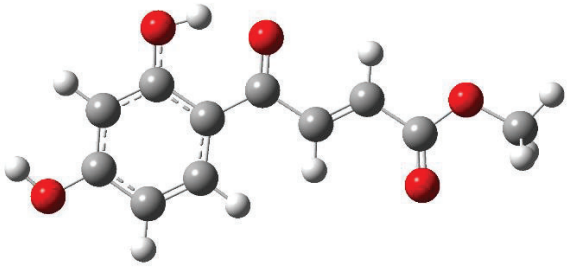

DFT/B3LYP 6-31+G(d), E = -801.247375 a.u

Center Number	Atomic Number	Atomic Type	Coordinates (Angstroms) X	Y	Z
1	6	0	3.769956	0.492827	0.000018
2	6	0	3.93853	-0.88809	0.000082
3	6	0	2.82569	-1.7534	0.000161
4	6	0	1.556808	-1.21115	0.000149
5	6	0	1.329632	0.188962	0.000058
6	6	0	2.480841	1.040703	-1.9E-05
7	1	0	4.618773	1.171954	-9E-06
8	1	0	2.986588	-2.82599	0.000248
9	6	0	-0.00236	0.791869	0.000009

10	6	0	-1.2183	-0.06801	-7.5E-05
11	6	0	-2.44848	0.467708	-0.00018
12	6	0	-3.6536	-0.40015	-0.00024
13	8	0	2.381492	2.375846	-0.00015
14	8	0	-0.14838	2.035048	-3.5E-05
15	8	0	-4.77907	0.346634	0.00039
16	8	0	-3.65076	-1.61774	-0.00075
17	6	0	-6.02018	-0.38366	0.000425
18	1	0	-6.08934	-1.01211	-0.8915
19	1	0	-6.08913	-1.01238	0.892186
20	1	0	-6.80145	0.376445	0.000649
21	1	0	-1.12678	-1.14826	-7.8E-05
22	1	0	-2.59218	1.543631	-0.00019
23	8	0	5.166593	-1.47276	0.000072
24	1	0	5.862069	-0.79534	0.000062
25	1	0	0.714555	-1.89331	0.000215
26	1	0	1.406696	2.593497	-0.00015

T_1 of Non-H bonded *cis*-1B

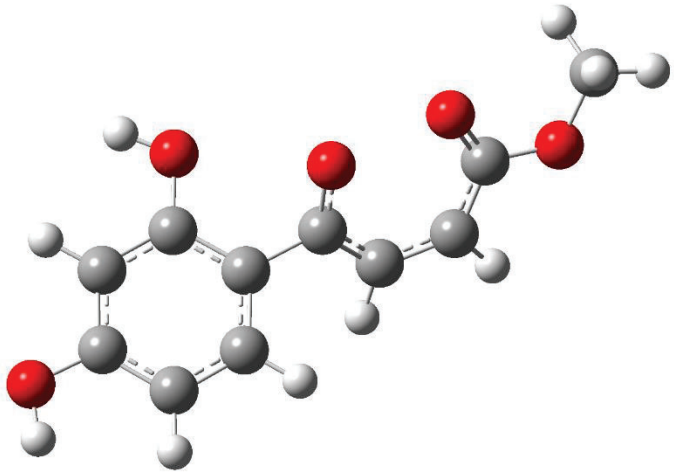

DFT/B3LYP 6-31+G(d), E = -801.233293 a.u

Center Number	Atomic Number	Atomic Type	Coordinates (Angstroms) X	Y	Z
1	6	0	-1.98991	1.010309	-0.23465
2	6	0	-1.20377	-0.13086	0.051013
3	6	0	-1.87039	-1.324	0.370076
4	6	0	-3.26023	-1.41428	0.38248
5	6	0	-4.01592	-0.27317	0.087115
6	6	0	-3.38356	0.933056	-0.22252
7	1	0	-3.74847	-2.35376	0.63132
8	1	0	-3.99252	1.802551	-0.4575
9	8	0	-1.34531	2.164062	-0.5605
10	6	0	0.285095	-0.08734	0.043923
11	8	0	0.781179	0.859783	0.780272
12	6	0	1.041673	-1.03642	-0.66048
13	6	0	2.429383	-1.14013	-0.72772
14	6	0	3.3402	-0.24145	-0.08244
15	8	0	3.034565	0.745551	0.61
16	8	0	4.644082	-0.55455	-0.2972
17	6	0	5.617675	0.310333	0.311133
18	1	0	6.585312	-0.10238	0.023259
19	1	0	5.509645	1.333044	-0.06129
20	1	0	5.507256	0.308658	1.399304
21	1	0	2.874068	-1.9339	-1.31805
22	1	0	0.457222	-1.75143	-1.23224
23	8	0	-5.383	-0.27068	0.084019
24	1	0	-5.7162	-1.15204	0.314884
25	1	0	-1.27885	-2.19957	0.621488
26	1	0	-1.99106	2.859231	-0.76154

T_1 of H-bonded *cis*-1B

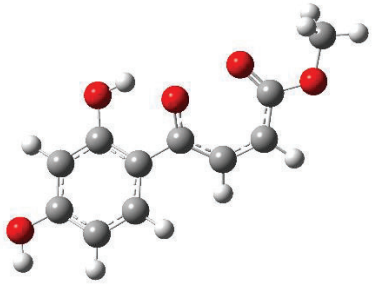

DFT/B3LYP 6-31+G(d), E = -801.243998 a.u

Center Number	Atomic Number	Atomic Type	Coordinates (Angstroms) X	Y	Z
1	6	0	-1.93901	1.028718	-0.10446
2	6	0	-1.20761	-0.17617	0.112147
3	6	0	-1.94326	-1.36353	0.304438
4	6	0	-3.32764	-1.39176	0.22744
5	6	0	-4.02173	-0.19679	-0.03231
6	6	0	-3.33246	1.002001	-0.19496
7	1	0	-3.86736	-2.32404	0.377881
8	1	0	-3.872	1.924155	-0.38135
9	8	0	-1.34923	2.235072	-0.27441
10	6	0	0.267902	-0.18149	0.126871
11	8	0	0.805707	0.934358	0.553254
12	6	0	1.034972	-1.2879	-0.2737
13	6	0	2.42419	-1.36895	-0.32084
14	6	0	3.312102	-0.27886	-0.06916
15	8	0	2.984919	0.898527	0.202186
16	8	0	4.620991	-0.60522	-0.17208
17	6	0	5.573921	0.451106	0.048185
18	1	0	6.550202	-0.01937	-0.07103
19	1	0	5.439041	1.248634	-0.68778
20	1	0	5.464565	0.862011	1.055554
21	1	0	2.89259	-2.30388	-0.6086
22	1	0	0.476149	-2.15728	-0.60402
23	8	0	-5.38352	-0.14917	-0.12177
24	1	0	-5.75695	-1.03331	0.019512
25	1	0	-1.41188	-2.28315	0.529376
26	1	0	-0.39355	2.15946	-0.06886

T_1 of Non-H bonded *trans*-1A

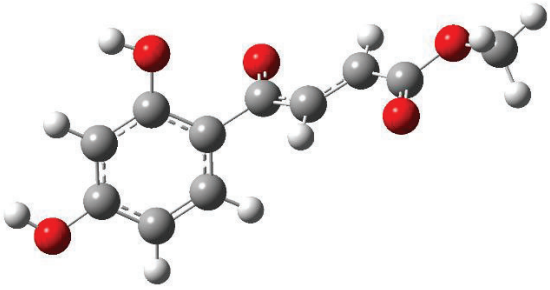

DFT/B3LYP 6-31+G(d), E = -801.233693 a.u

Center Number	Atomic Number	Atomic Type	Coordinates (Angstroms) X	Y	Z
1	6	0	-3.51121	0.622055	0.666074
2	6	0	-4.03079	-0.59896	0.222727
3	6	0	-3.23792	-1.49757	-0.51638
4	6	0	-1.92963	-1.15314	-0.80652
5	6	0	-1.35949	0.050418	-0.34072
6	6	0	-2.18815	0.958819	0.369182
7	1	0	-4.13353	1.308181	1.239104
8	1	0	-3.66915	-2.43721	-0.84439
9	6	0	0.049721	0.405095	-0.67314
10	6	0	1.206675	-0.06825	-0.06846
11	6	0	2.501574	0.257175	-0.461
12	6	0	3.645353	-0.28816	0.250463
13	8	0	-1.6298	2.12261	0.775094
14	8	0	-0.05299	1.209546	-1.6967
15	8	0	4.823556	0.149626	-0.28708
16	8	0	3.605817	-1.04755	1.21304
17	6	0	6.013384	-0.33626	0.347474
18	1	0	6.043398	-0.03079	1.397806
19	1	0	6.061545	-1.42815	0.293763
20	1	0	6.841076	0.11113	-0.20525
21	1	0	1.073207	-0.73185	0.782437
22	1	0	2.690191	0.918014	-1.30067
23	1	0	-2.27396	2.663536	1.258888
24	8	0	-5.30965	-0.97877	0.476028

25	1	0	-5.77964	-0.2965	0.9821
26	1	0	-1.30555	-1.82741	-1.38509

T_1 of H-bonded *trans*-1A

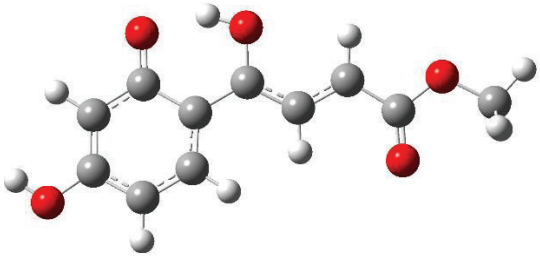

DFT/B3LYP 6-31+G(d), E = -801.269911 a.u

Center Number	Atomic Number	Atomic Type	Coordinates (Angstroms) X	Y	Z
1	8	0	2.384862	2.332881	0.134987
2	1	0	0.710983	2.524896	-0.09392
3	8	0	5.197586	-1.51199	0.064757
4	1	0	5.912004	-0.86331	0.17002
5	8	0	-0.18558	2.108919	-0.17309
6	8	0	-3.59268	-1.60643	0.128959
7	8	0	-4.81571	0.302905	-0.00877
8	6	0	1.318795	0.197541	-0.06231
9	6	0	2.498918	1.070097	0.069831
10	6	0	3.813098	0.480607	0.117861
11	1	0	4.647969	1.16833	0.225041
12	6	0	3.986852	-0.8857	0.026866
13	6	0	2.854879	-1.71338	-0.12418
14	1	0	2.998831	-2.78628	-0.20682
15	6	0	1.556492	-1.1654	-0.17334
16	1	0	0.730221	-1.85498	-0.30471
17	6	0	-0.04556	0.771306	-0.08324
18	6	0	-1.20575	-0.00124	-0.01555
19	1	0	-1.11656	-1.07812	0.076111
20	6	0	-2.49444	0.513091	-0.047

21	1	0	-2.67741	1.578034	-0.1308
22	6	0	-3.64082	-0.38496	0.034181
23	6	0	-6.00744	-0.49303	0.064457
24	1	0	-6.83384	0.217452	0.017525
25	1	0	-6.03645	-1.05628	1.001892
26	1	0	-6.05374	-1.19373	-0.77446

trans-1BR

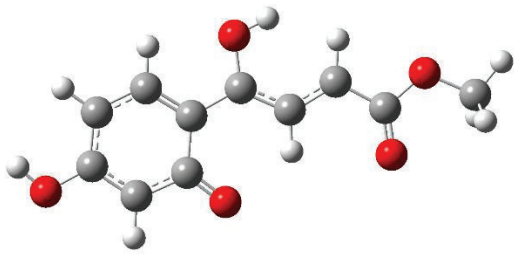

DFT/B3LYP 6-31+G(d), E = -801.257896

Center Number	Atomic Number	Atomic Type	Coordinates (Angstroms) X	Y	Z
1	6	0	-1.78162	-0.9635	-0.00277
2	6	0	-1.41035	0.464096	0.00001
3	6	0	-2.44371	1.387096	0.003218
4	6	0	-3.8116	1.011164	0.003679
5	6	0	-4.18113	-0.3364	0.00092
6	6	0	-3.18473	-1.30712	-0.00234
7	1	0	-4.57212	1.789428	0.006153
8	1	0	-3.43532	-2.36268	-0.00475
9	8	0	-0.93355	-1.89467	-0.0063
10	6	0	-0.0218	0.934435	-0.00078
11	8	0	0.053538	2.300014	-0.00321
12	6	0	1.133531	0.146318	0.000813
13	6	0	2.432974	0.633109	-0.00218
14	6	0	3.577465	-0.27596	0.001695
15	8	0	3.531048	-1.49628	0.008828
16	8	0	4.751401	0.420622	-0.00333
17	6	0	5.945182	-0.37734	0.00001
18	1	0	6.770812	0.335546	-0.00529

19	1	0	5.983808	-1.00564	0.894591
20	1	0	5.981619	-1.01639	-0.887
21	1	0	2.685437	1.691786	-0.0086
22	1	0	0.99311	-0.92772	0.004463
23	8	0	-5.48034	-0.75793	0.001069
24	1	0	-6.08389	0.001818	0.003645
25	1	0	-2.20734	2.444678	0.005487
26	1	0	0.98184	2.579742	0.001168

Cis-1BrA

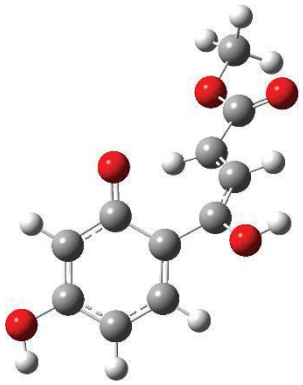

DFT/B3LYP 6-31+G(d), E = -801.254046 a.u

Center Number	Atomic Number	Atomic Type	Coordinates (Angstroms) X	Y	Z
1	6	0	1.394117	-0.51224	0.810658
2	6	0	1.279183	0.740744	0.049571
3	6	0	2.331798	1.108517	-0.77335
4	6	0	3.472999	0.297924	-0.92923
5	6	0	3.58388	-0.92826	-0.24235
6	6	0	2.568476	-1.33011	0.605224
7	1	0	4.274406	0.626404	-1.58822
8	1	0	2.641338	-2.25649	1.165068
9	8	0	0.518456	-0.86474	1.643627
10	6	0	0.111145	1.628956	0.187699
11	8	0	0.490375	2.941514	0.306151
12	6	0	-1.23223	1.290755	0.126941
13	6	0	-1.78894	0.037666	-0.1101
14	6	0	-3.23935	-0.1071	-0.15904

15	8	0	-4.05698	0.793127	-0.00433
16	8	0	-3.60111	-1.39541	-0.40939
17	6	0	-5.01292	-1.64624	-0.46884
18	1	0	-5.10911	-2.71401	-0.67006
19	1	0	-5.48839	-1.3893	0.48223
20	1	0	-5.47434	-1.05995	-1.26901
21	1	0	-1.18871	-0.85143	-0.25138
22	1	0	-1.94995	2.104302	0.249098
23	8	0	4.672897	-1.74262	-0.37625
24	1	0	5.315343	-1.35425	-0.99069
25	1	0	2.279687	2.046281	-1.31772
26	1	0	-0.2984	3.509728	0.329126

Cis-1BrB

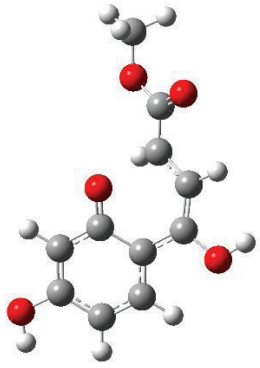

DFT/B3LYP 6-31+G(d), E = -801.235511 a.u

Center Number	Atomic Number	Atomic Type	Coordinates (Angstroms) X	Y	Z
1	6	0	0.998623	-0.54901	0.349029
2	6	0	1.307163	0.835489	-0.02288
3	6	0	2.634926	1.165658	-0.32617
4	6	0	3.638154	0.201147	-0.31353
5	6	0	3.33562	-1.15183	-0.01156
6	6	0	2.039984	-1.52852	0.278834
7	1	0	4.661522	0.483803	-0.55324
8	1	0	1.798449	-2.55751	0.521653
9	8	0	-0.16709	-0.87386	0.752883
10	6	0	0.252048	1.817243	-0.01979

11	8	0	0.689492	3.115044	0.072224
12	6	0	-1.09523	1.508533	-0.05915
13	6	0	-1.62264	0.2349	-0.38575
14	6	0	-3.00496	-0.05895	-0.04068
15	8	0	-3.73534	0.652756	0.642728
16	8	0	-3.41292	-1.2465	-0.56868
17	6	0	-4.75624	-1.63812	-0.25284
18	1	0	-4.89691	-2.60668	-0.73474
19	1	0	-4.88592	-1.7244	0.829951
20	1	0	-5.47233	-0.90762	-0.64124
21	1	0	-1.15298	-0.42109	-1.10584
22	1	0	-1.8151	2.281692	0.214594
23	8	0	4.303151	-2.11593	-0.00852
24	1	0	5.165274	-1.73145	-0.23211
25	1	0	2.879095	2.191348	-0.58144
26	1	0	-0.06412	3.720585	-0.01576

Cis-1BrC

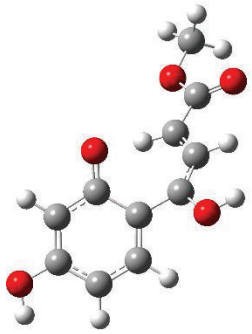

DFT/B3LYP 6-31+G(d), E = -801.219182 a.u

Center Number	Atomic Number	Atomic Type	Coordinates (Angstroms) X	Y	Z
1	6	0	1.394117	-0.51224	0.810658
2	6	0	1.279183	0.740744	0.049571
3	6	0	2.331798	1.108517	-0.77335
4	6	0	3.472999	0.297924	-0.92923
5	6	0	3.58388	-0.92826	-0.24235
6	6	0	2.568476	-1.33011	0.605224
7	1	0	4.274406	0.626404	-1.58822
8	1	0	2.641338	-2.25649	1.165068

9	8	0	0.518456	-0.86474	1.643627
10	6	0	0.111145	1.628956	0.187699
11	8	0	0.490375	2.941514	0.306151
12	6	0	-1.23223	1.290755	0.126941
13	6	0	-1.78894	0.037666	-0.1101
14	6	0	-3.23935	-0.1071	-0.15904
15	8	0	-4.05698	0.793127	-0.00433
16	8	0	-3.60111	-1.39541	-0.40939
17	6	0	-5.01292	-1.64624	-0.46884
18	1	0	-5.10911	-2.71401	-0.67006
19	1	0	-5.48839	-1.3893	0.48223
20	1	0	-5.47434	-1.05995	-1.26901
21	1	0	-1.18871	-0.85143	-0.25138
22	1	0	-1.94995	2.104302	0.249098
23	8	0	4.672897	-1.74262	-0.37625
24	1	0	5.315343	-1.35425	-0.99069
25	1	0	2.279687	2.046281	-1.31772
26	1	0	-0.2984	3.509728	0.329126

Cis-1BrD

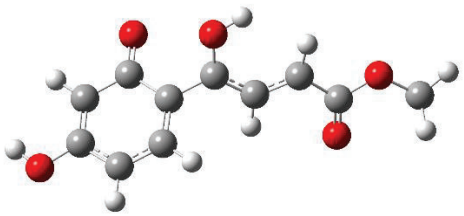

DFT/B3LYP 6-31+G(d), E = -801.256598 a.u

Center Number	Atomic Number	Atomic Type	Coordinates (Angstroms) X	Y	Z
1	8	0	2.023912	2.088505	1.026489
2	1	0	-0.93868	2.337731	-1.0353
3	8	0	5.227554	-1.34729	0.189175
4	1	0	5.825066	-0.76855	0.689449
5	8	0	-0.04631	1.954401	-1.07673
6	8	0	-3.4802	-1.44821	0.781435
7	8	0	-4.7863	0.168942	-0.13754

8	6	0	1.346622	0.217828	-0.28243
9	6	0	2.331396	1.000763	0.481235
10	6	0	3.666492	0.455815	0.61774
11	1	0	4.379125	1.047101	1.187523
12	6	0	3.993856	-0.77201	0.081498
13	6	0	3.023067	-1.51752	-0.62711
14	1	0	3.30288	-2.48303	-1.0367
15	6	0	1.722508	-1.009	-0.80253
16	1	0	1.003494	-1.59553	-1.36771
17	6	0	-0.02105	0.744989	-0.4671
18	6	0	-1.15982	0.046267	-0.08192
19	1	0	-1.00448	-0.88872	0.449377
20	6	0	-2.47833	0.434734	-0.30055
21	1	0	-2.74975	1.337427	-0.84219
22	6	0	-3.58369	-0.38918	0.17707
23	6	0	-5.9442	-0.56468	0.290943
24	1	0	-6.79972	0.025171	-0.04045
25	1	0	-5.94838	-0.67247	1.379401
26	1	0	-5.95984	-1.55789	-0.16706

E-Enol noH-bonded

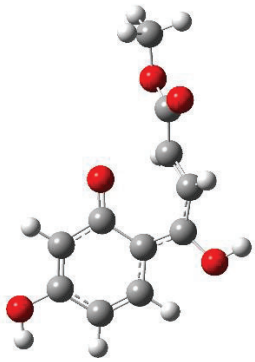

DFT/B3LYP 6-31+G(d), E = -801.281191 a.u

Center Number	Atomic Number	Atomic Type	Coordinates (Angstroms) X	Y	Z
1	6	0	0.940295	-0.67537	0.051402
2	6	0	1.249641	0.75192	-0.26827
3	6	0	2.617243	1.123652	-0.49314
4	6	0	3.644425	0.238952	-0.33678

5	6	0	3.358897	-1.09139	0.115245
6	6	0	2.074851	-1.51092	0.350388
7	1	0	4.672484	0.537538	-0.53109
8	1	0	1.8782	-2.5315	0.659754
9	8	0	-0.21728	-1.17161	0.077599
10	6	0	0.301241	1.754353	-0.04352
11	8	0	0.761433	3.025635	0.104197
12	6	0	-1.07751	1.490967	0.21302
13	6	0	-1.6829	0.416503	-0.36644
14	6	0	-3.02354	-0.02157	0.117816
15	8	0	-3.57286	0.390398	1.122664
16	8	0	-3.5541	-0.94229	-0.70941
17	6	0	-4.83218	-1.47756	-0.31932
18	1	0	-5.08612	-2.20659	-1.08883
19	1	0	-4.75548	-1.95728	0.659989
20	1	0	-5.58008	-0.68107	-0.27567
21	1	0	-1.3596	0.010471	-1.31171
22	1	0	-1.58533	2.039001	1.00597
23	8	0	4.374468	-1.98013	0.314422
24	1	0	5.22628	-1.56723	0.10213
25	1	0	2.825508	2.147312	-0.78691
26	1	0	0.007946	3.636079	0.168106

E-Enol H-bonded

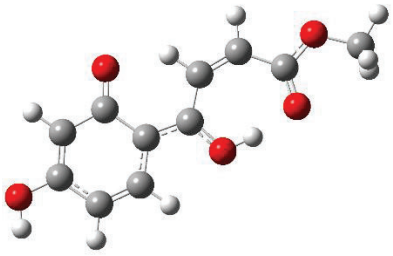

DFT/B3LYP 6-31+G(d), E = -801.309323 a.u

Center Number	Atomic Number	Atomic Type	Coordinates (Angstroms) X	Y	Z
1	6	0	-2.0111	1.1354	0.000742
2	6	0	-1.24381	-0.16103	0.000316
3	6	0	-1.99601	-1.39363	0.000666

4	6	0	-3.35515	-1.41739	0.000514
5	6	0	-4.09547	-0.1788	-3.2E-05
6	6	0	-3.45787	1.02569	-9.3E-05
7	1	0	-3.89184	-2.36432	0.000756
8	1	0	-4.0202	1.953089	-0.00025
9	8	0	-1.47694	2.261764	0.001849
10	6	0	0.151199	-0.26181	-0.00076
11	8	0	0.675214	-1.4913	-0.00121
12	6	0	1.006508	0.922725	-0.00185
13	6	0	2.357109	1.07144	-0.00168
14	6	0	3.413318	0.047645	-0.00025
15	8	0	3.26031	-1.17672	0.000631
16	8	0	4.6306	0.606236	0
17	6	0	5.756739	-0.29601	0.0013
18	1	0	6.635596	0.347936	0.00123
19	1	0	5.733916	-0.92489	0.89467
20	1	0	5.734828	-0.92633	-0.89108
21	1	0	2.739638	2.087947	-0.00266
22	1	0	0.419382	1.837438	-0.00256
23	8	0	-5.45895	-0.20662	-0.00041
24	1	0	-5.77623	-1.12338	-0.00031
25	1	0	-1.44312	-2.32564	0.000904
26	1	0	1.673267	-1.47412	-0.00081

Z-Enol noH-bonded

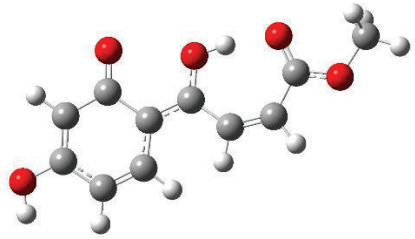

DFT/B3LYP 6-31+G(d), E = -801.293659 a.u

Center Number	Atomic Number	Atomic Type	Coordinates (Angstroms) X	Y	Z
1	6	0	2.137157	1.17132	-0.01561
2	6	0	1.237681	-0.04373	0.032632
3	6	0	1.877508	-1.33575	0.092076

4	6	0	3.23047	-1.48528	0.075428
5	6	0	4.091993	-0.33218	-0.00477
6	6	0	3.57323	0.923819	-0.05088
7	1	0	3.669193	-2.47947	0.135125
8	1	0	4.217602	1.794813	-0.1022
9	8	0	1.702109	2.328541	-0.03885
10	6	0	-0.15885	0.096699	0.014109
11	8	0	-0.68486	1.309922	0.06007
12	6	0	-1.02902	-1.07979	-0.08163
13	6	0	-2.38041	-1.23044	-0.09939
14	6	0	-3.44029	-0.21327	-0.01944
15	8	0	-3.29186	1.006962	0.045935
16	8	0	-4.65387	-0.78316	-0.03082
17	6	0	-5.78477	0.111748	0.038538
18	1	0	-6.6604	-0.53613	0.015208
19	1	0	-5.75064	0.68932	0.965457
20	1	0	-5.77875	0.791654	-0.81682
21	1	0	-2.76155	-2.24353	-0.18618
22	1	0	-0.49864	-2.01836	-0.16976
23	8	0	5.448057	-0.50058	-0.03094
24	1	0	5.670485	-1.4436	0.011858
25	1	0	1.286903	-2.24017	0.178394
26	1	0	-1.67902	1.29311	0.039258

E-enol TS

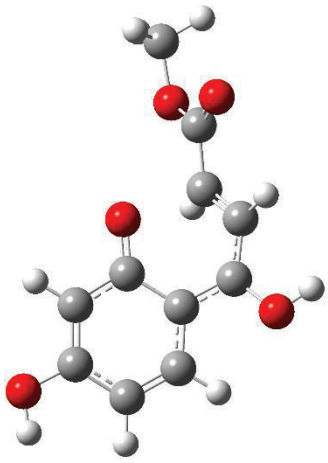

DFT/B3LYP 6-31+G(d), E = -801.279632 a.u

Center Number	Atomic Number	Atomic Type	Coordinates (Angstroms) X	Y	Z
1	6	0	0.871245	-0.61479	0.083841
2	6	0	1.232996	0.771283	-0.28673
3	6	0	2.605125	1.078251	-0.52889
4	6	0	3.600236	0.149794	-0.37039
5	6	0	3.259306	-1.14742	0.112321
6	6	0	1.954674	-1.49855	0.38055
7	1	0	4.637556	0.400109	-0.58178
8	1	0	1.717925	-2.50046	0.720868
9	8	0	-0.32222	-1.06518	0.166183
10	6	0	0.31592	1.820289	-0.04697
11	8	0	0.844165	3.054017	0.16741
12	6	0	-1.05597	1.591266	0.162609
13	6	0	-1.60912	0.448952	-0.38453
14	6	0	-2.94568	-0.01979	0.095794
15	8	0	-3.51358	0.400189	1.085528
16	8	0	-3.4403	-0.97119	-0.71592
17	6	0	-4.702	-1.54211	-0.32122
18	1	0	-4.92684	-2.294	-1.07759
19	1	0	-4.61351	-1.99982	0.66751
20	1	0	-5.47634	-0.77054	-0.29675
21	1	0	-1.31049	0.097063	-1.36244
22	1	0	-1.60309	2.15981	0.912139
23	8	0	4.224724	-2.08962	0.31619
24	1	0	5.094131	-1.73203	0.076478
25	1	0	2.853921	2.088772	-0.8372
26	1	0	0.124004	3.702286	0.245264

IRC:

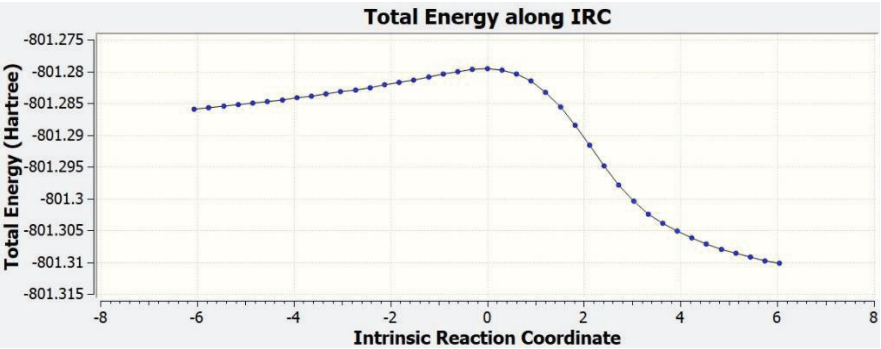

6-Ring (5)

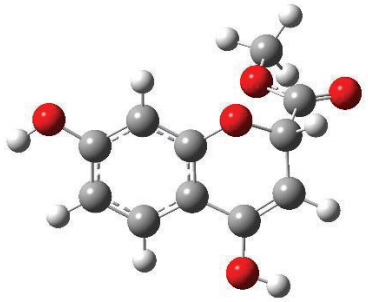

DFT/B3LYP 6-31+G(d), E = -801.316227 a.u

Center Number	Atomic Number	Atomic Type	Coordinates (Angstroms) X	Y	Z
1	6	0	0.709146	0.168962	-0.69259
2	6	0	0.853802	-0.99575	0.089742
3	6	0	2.048247	-1.18048	0.795844
4	6	0	3.075088	-0.24031	0.730434
5	6	0	2.908525	0.903895	-0.06145
6	6	0	1.726372	1.112891	-0.77733
7	1	0	3.997877	-0.39649	1.285165
8	1	0	1.600706	2.000493	-1.38752
9	8	0	-0.40657	0.387466	-1.45238
10	6	0	-0.24227	-1.95854	0.070888
11	8	0	0.039858	-3.15089	0.679391
12	6	0	-1.4083	-1.66497	-0.53381
13	6	0	-1.62292	-0.29147	-1.12405
14	6	0	-2.52144	0.540422	-0.18931
15	8	0	-3.72724	0.394245	-0.15571
16	8	0	-1.83287	1.381196	0.594175
17	6	0	-2.60837	2.147299	1.538588
18	1	0	-1.8837	2.762555	2.071698
19	1	0	-3.33513	2.770935	1.011824
20	1	0	-3.13277	1.478717	2.226319
21	1	0	-2.17236	-0.36487	-2.0673
22	1	0	-2.23749	-2.36509	-0.58447
23	8	0	3.875061	1.867323	-0.17289
24	1	0	4.644019	1.624525	0.366187
25	1	0	2.170545	-2.07578	1.396392
26	1	0	-0.74491	-3.72138	0.659182

Flavanone-1a

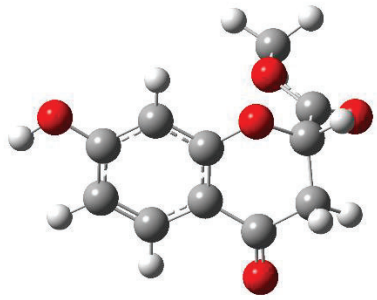

DFT/B3LYP 6-31+G(d), E = -801.342313 a.u

Center Number	Atomic Number	Atomic Type	Coordinates (Angstroms) X	Y	Z
1	6	0	0.707321	0.077323	-0.73891
2	6	0	0.708069	-1.01864	0.153108
3	6	0	1.849194	-1.22913	0.949073
4	6	0	2.954839	-0.40033	0.8576
5	6	0	2.933099	0.673309	-0.05476
6	6	0	1.814493	0.917747	-0.84995
7	1	0	3.833723	-0.57745	1.473998
8	1	0	1.796989	1.758543	-1.53449
9	8	0	-0.35364	0.361866	-1.5499
10	6	0	-0.42551	-1.95761	0.187199
11	8	0	-0.48326	-2.92254	0.94023
12	6	0	-1.51591	-1.6882	-0.84285
13	6	0	-1.61986	-0.19902	-1.19624
14	6	0	-2.34224	0.591515	-0.09111
15	8	0	-3.45383	0.281232	0.285748
16	8	0	-1.64506	1.636789	0.368345
17	6	0	-2.28791	2.419273	1.397782
18	1	0	-1.57659	3.20778	1.642089
19	1	0	-3.22312	2.840457	1.020688
20	1	0	-2.49398	1.795067	2.2707
21	1	0	-2.23561	-0.07572	-2.09217
22	1	0	-1.26045	-2.25041	-1.75171
23	8	0	3.98965	1.524289	-0.19659
24	1	0	4.705318	1.269643	0.407135
25	1	0	1.842955	-2.07544	1.629547
26	1	0	-2.47363	-2.06304	-0.47415

TS of *cis*-**1** T_{1k} and *cis*-**1** So H transfer

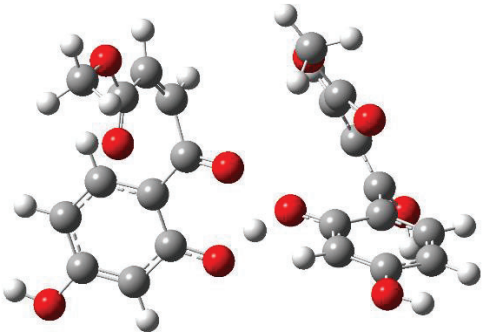

DFT/B3LYP 6-31+G(d), E = -1602.554985 a.u

Center Number	Atomic Number	Atomic Type	Coordinates (Angstroms) X	Y	Z
1	8	0	1.583406	-0.89771	-0.30353
2	1	0	5.406523	-1.86586	-1.11138
3	8	0	3.141368	-0.18851	4.100903
4	1	0	3.951761	0.023602	4.58969
5	8	0	5.173185	-1.27951	-1.85024
6	8	0	2.740669	2.158502	-0.36409
7	8	0	1.099601	2.840702	-1.77126
8	6	0	3.874858	-0.37776	-0.0297
9	6	0	2.548654	-0.60093	0.511831
10	6	0	2.334763	-0.51053	1.913875
11	1	0	1.333256	-0.64476	2.307353
12	6	0	3.398581	-0.25765	2.762034
13	6	0	4.699517	-0.07897	2.244369
14	1	0	5.530321	0.129776	2.915165
15	6	0	4.917663	-0.14207	0.863564
16	1	0	5.917105	0.045872	0.479848
17	6	0	4.133963	-0.46114	-1.47455
18	6	0	3.482321	0.165056	-2.53352
19	1	0	3.764434	-0.23674	-3.50586
20	6	0	2.543913	1.193348	-2.55305
21	1	0	2.062916	1.414481	-3.50077
22	6	0	2.173241	2.065451	-1.44599
23	6	0	0.65585	3.741201	-0.74026
24	1	0	-0.16272	4.308289	-1.18611
25	1	0	1.46791	4.410209	-0.44173
26	1	0	0.30566	3.175222	0.126811
27	8	0	-0.16872	-2.17241	0.68478

28	1	0	0.653865	-1.36581	0.211474
29	8	0	-3.60184	-5.10597	-0.54537
30	1	0	-4.46646	-5.13492	-0.98428
31	8	0	-0.85321	0.599574	0.62868
32	8	0	-4.17672	1.065675	1.207076
33	8	0	-5.04993	3.036657	0.509166
34	6	0	-2.12803	-1.17809	-0.34789
35	6	0	-1.35267	-2.29032	0.166287
36	6	0	-1.91035	-3.5973	0.093082
37	1	0	-1.33114	-4.42451	0.488849
38	6	0	-3.14064	-3.82068	-0.50289
39	6	0	-3.86963	-2.74864	-1.05518
40	1	0	-4.83399	-2.92225	-1.52772
41	6	0	-3.3532	-1.45826	-0.96614
42	1	0	-3.94262	-0.63664	-1.35966
43	6	0	-1.71929	0.228282	-0.15583
44	6	0	-2.31497	1.297629	-1.05161
45	1	0	-1.73036	1.47015	-1.95601
46	6	0	-3.34914	2.111632	-0.7953
47	1	0	-3.58915	2.926472	-1.4728
48	6	0	-4.20363	1.983065	0.408038
49	6	0	-5.92427	3.029254	1.652173
50	1	0	-6.51513	3.941875	1.5696
51	1	0	-5.34045	3.027354	2.576524
52	1	0	-6.56944	2.146605	1.631976

IRC:

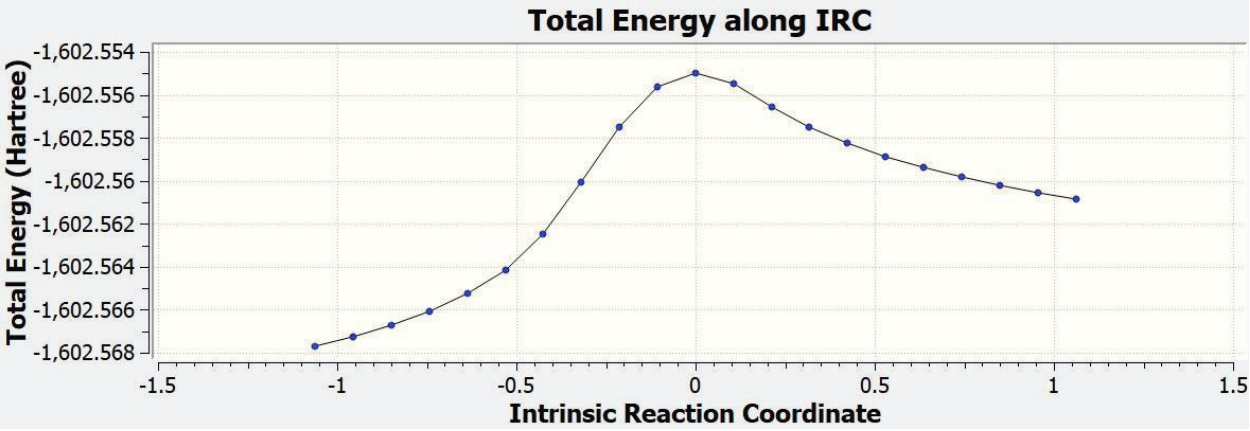

cis-**1** ketyl radical (**7**)

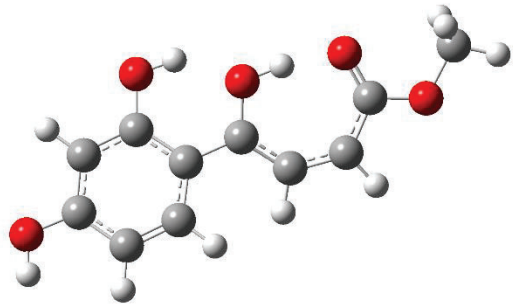

DFT/B3LYP 6-31+G(d), E = -801.922937 a.u

Center Number	Atomic Number	Atomic Type	Coordinates (Angstroms) X	Y	Z
1	6	0	-2.08999	1.039287	-0.0815
2	6	0	-1.25894	-0.11834	0.059562
3	6	0	-1.92425	-1.35995	0.19684
4	6	0	-3.30331	-1.48022	0.166274
5	6	0	-4.08747	-0.32534	-0.0013
6	6	0	-3.48225	0.920356	-0.12022
7	1	0	-3.7711	-2.45479	0.286839
8	1	0	-4.08416	1.814548	-0.24053
9	8	0	-1.60762	2.295758	-0.21345
10	6	0	0.199189	-0.03563	0.055019
11	8	0	0.694654	1.19973	0.285771
12	6	0	1.031601	-1.13989	-0.19122
13	6	0	2.423088	-1.27075	-0.22964
14	6	0	3.425139	-0.25564	-0.03307
15	8	0	3.233291	0.956723	0.192509
16	8	0	4.680175	-0.74466	-0.12583
17	6	0	5.751316	0.199275	0.045897
18	1	0	6.665542	-0.38444	-0.0649
19	1	0	5.69789	0.981441	-0.71625
20	1	0	5.703016	0.656707	1.03779
21	1	0	2.817881	-2.25749	-0.44756
22	1	0	0.501802	-2.05988	-0.41109
23	8	0	-5.45191	-0.36759	-0.04324
24	1	0	-5.75842	-1.28266	0.055485
25	1	0	-1.34011	-2.25934	0.358775
26	1	0	-0.63745	2.276923	-0.07618
27	1	0	1.711541	1.210287	0.251712

cis-**1** phenoxy radical (**6**)

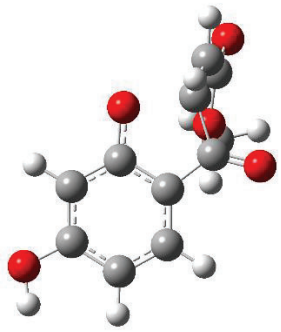

DFT/B3LYP 6-31+G(d), E = -800.662446 a.u

Center Number	Atomic Number	Atomic Type	Coordinates (Angstroms) X	Y	Z
1	6	0	1.033348	0.324148	0.86091
2	6	0	0.842703	0.796822	-0.45584
3	6	0	1.822063	0.587082	-1.43592
4	6	0	2.983829	-0.0923	-1.1037
5	6	0	3.159622	-0.56745	0.217735
6	6	0	2.195982	-0.37503	1.208035
7	1	0	3.756809	-0.26711	-1.84891
8	1	0	2.355251	-0.74671	2.214047
9	8	0	0.07193	0.586853	1.752412
10	6	0	-0.44107	1.456843	-0.60838
11	8	0	-0.91796	1.993935	-1.59786
12	6	0	-1.17864	1.480329	0.740789
13	6	0	-2.40299	0.773312	0.976692
14	6	0	-2.82309	-0.47715	0.334003
15	8	0	-3.90149	-1.00331	0.563762
16	8	0	-1.90779	-0.97164	-0.52215
17	6	0	-2.26966	-2.1863	-1.206
18	1	0	-1.41945	-2.41781	-1.84721
19	1	0	-2.44299	-2.98839	-0.48368
20	1	0	-3.17356	-2.02842	-1.80007
21	1	0	-1.11173	2.447355	1.236641
22	8	0	4.286283	-1.24296	0.584269
23	1	0	4.890522	-1.31951	-0.17104
24	1	0	1.656195	0.956206	-2.44422
25	1	0	-3.09147	1.139468	1.730991

TS Ketyl radica(**7**) Intramolecular H-transfer

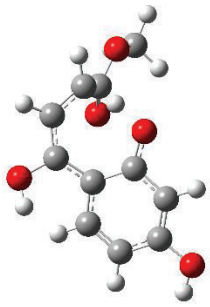

DFT/B3LYP 6-31+G(d), E = -801.858831 a.u

Center Number	Atomic Number	Atomic Type	Coordinates (Angstroms) X	Y	Z
1	8	0	0.073901	-0.7037	1.672374
2	8	0	-4.08708	-1.92863	-0.04095
3	1	0	-4.73717	-1.69931	-0.72368
4	8	0	-0.3784	3.13088	-0.29738
5	8	0	1.854901	-0.34862	-1.29144
6	8	0	3.526826	-0.97882	0.097953
7	6	0	-0.88266	0.788659	-0.02437
8	6	0	-0.87361	-0.39003	0.848848
9	6	0	-2.01757	-1.2367	0.829163
10	1	0	-2.03174	-2.08149	1.508761
11	6	0	-3.05357	-1.04018	-0.05763
12	6	0	-3.0324	0.047666	-0.97197
13	1	0	-3.82329	0.164962	-1.70925
14	6	0	-1.98109	0.930712	-0.92353
15	1	0	-1.95248	1.73176	-1.65862
16	6	0	0.035733	1.886996	0.094008
17	6	0	1.325974	1.885997	0.623834
18	1	0	1.711274	2.860181	0.918569
19	6	0	2.104022	0.70335	0.889368
20	1	0	2.961065	0.868326	1.541388
21	6	0	2.448386	-0.22891	-0.23801
22	6	0	3.926352	-1.9662	-0.86919
23	1	0	4.786588	-2.46979	-0.42681
24	1	0	4.202424	-1.48762	-1.81278
25	1	0	3.112775	-2.67463	-1.04747
26	1	0	-1.34707	3.155607	-0.36374
27	1	0	1.198949	-0.02515	1.446017

IRC:

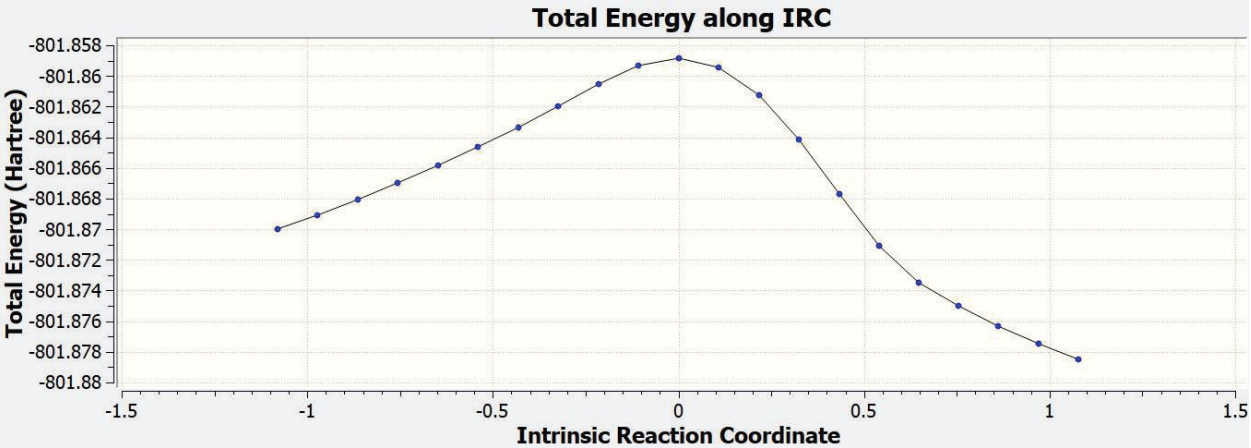

Radical (**9**)

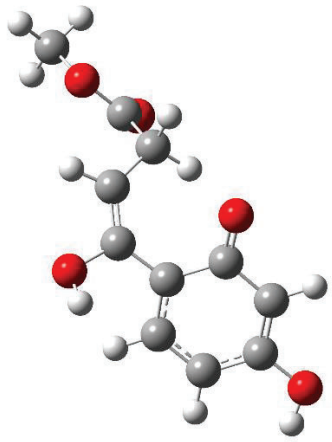

DFT/B3LYP 6-31+G(d), E = -801.882826 a.u

Center Number	Atomic Number	Atomic Type	Coordinates (Angstroms) X	Y	Z
1	8	0	-0.87383	-0.85508	1.907757
2	8	0	-4.81178	-1.25314	-0.63271
3	1	0	-5.28783	-0.81407	-1.3548
4	8	0	0.067018	2.784641	0.18216
5	8	0	2.970805	-1.51634	-1.24425
6	8	0	4.045679	-0.10316	0.154039
7	6	0	-1.14682	0.702572	0.118073
8	6	0	-1.55879	-0.46121	0.934725
9	6	0	-2.81262	-1.1072	0.605906

10	1	0	-3.0999	-1.97494	1.18994
11	6	0	-3.6294	-0.61588	-0.38148
12	6	0	-3.24337	0.537186	-1.12306
13	1	0	-3.88724	0.907564	-1.91857
14	6	0	-2.03569	1.175166	-0.85997
15	1	0	-1.75156	2.030651	-1.46668
16	6	0	0.110486	1.406277	0.350126
17	6	0	1.337778	0.891657	0.612293
18	1	0	2.13034	1.622814	0.75497
19	6	0	1.75534	-0.55016	0.626266
20	1	0	2.031171	-0.84049	1.649951
21	6	0	2.962576	-0.79214	-0.2707
22	6	0	5.24293	-0.25722	-0.63217
23	1	0	5.99108	0.367879	-0.14401
24	1	0	5.068739	0.076651	-1.65852
25	1	0	5.558814	-1.30375	-0.64101
26	1	0	-0.79579	3.119448	0.474995
27	1	0	0.964525	-1.22151	0.29766

TS of radical (**9**) to form radical (**10**)

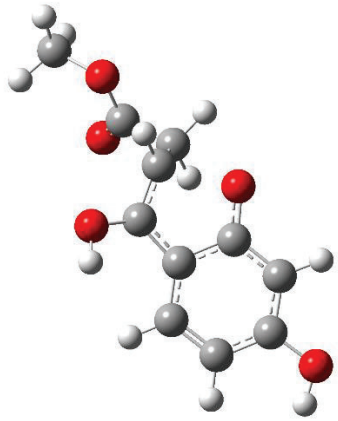

DFT/B3LYP 6-31+G(d), E = -801.861701 a.u

Center Number	Atomic Number	Atomic Type	Coordinates (Angstroms) X	Y	Z
1	8	0	0.542773	-1.29739	-1.22376
2	8	0	4.94932	-0.87318	0.473252
3	1	0	5.509775	-0.2421	0.95139
4	8	0	-0.50573	2.274485	-0.93012

5	8	0	-3.15238	-0.26864	1.824251
6	8	0	-3.85412	-0.39279	-0.32165
7	6	0	1.131232	0.662959	-0.06802
8	6	0	1.466594	-0.64794	-0.57437
9	6	0	2.775245	-1.13872	-0.3772
10	1	0	3.059125	-2.11596	-0.75217
11	6	0	3.699627	-0.34952	0.295145
12	6	0	3.376908	0.943496	0.783433
13	1	0	4.12489	1.523795	1.319057
14	6	0	2.10091	1.443928	0.592193
15	1	0	1.839871	2.422767	0.990195
16	6	0	-0.16888	1.02095	-0.52013
17	6	0	-1.01602	-0.05689	-0.89141
18	1	0	-1.62402	0.102558	-1.78214
19	6	0	-1.60233	-1.02676	0.109143
20	1	0	-1.77358	-1.99062	-0.38313
21	6	0	-2.9324	-0.52004	0.658464
22	6	0	-5.15146	0.085009	0.085736
23	1	0	-5.74218	0.129885	-0.82942
24	1	0	-5.06451	1.075159	0.540591
25	1	0	-5.6011	-0.60588	0.803678
26	1	0	0.28986	2.836346	-0.94977
27	1	0	-0.93348	-1.17467	0.957936

IRC:

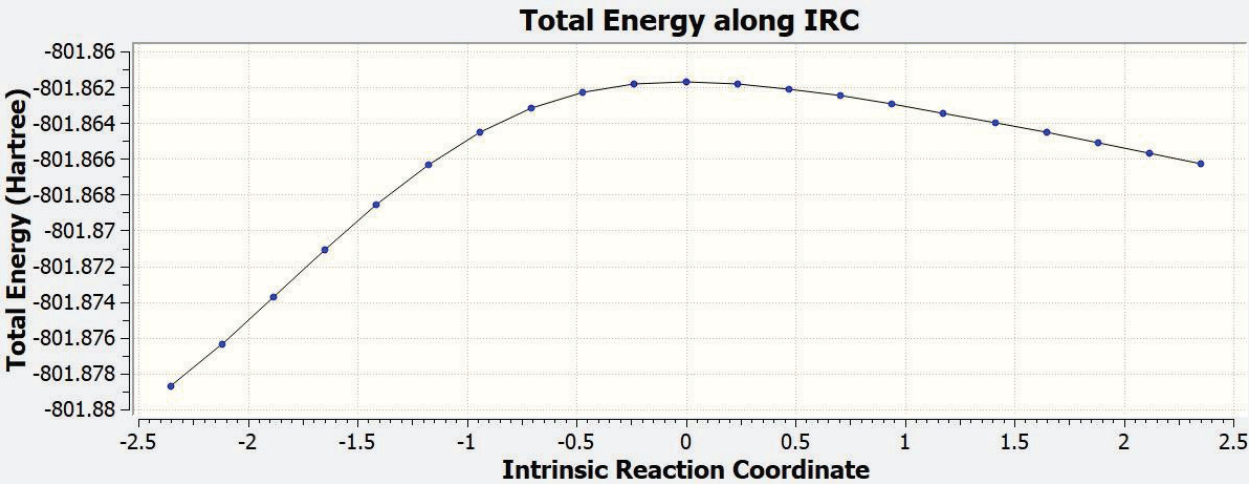

Radical (**10**)

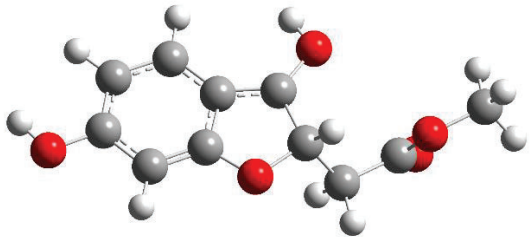

DFT/B3LYP 6-31+G(d), E = -801.895366 a.u

Center Number	Atomic Number	Atomic Type	Coordinates (Angstroms) X	Y	Z
1	8	0	0.431266	-1.46126	-0.44737
2	8	0	5.118996	-0.68403	0.156737
3	1	0	5.741234	0.044389	0.307866
4	8	0	-1.04839	1.825089	-0.26362
5	8	0	-3.59733	0.065062	1.602027
6	8	0	-3.6232	-0.3703	-0.61721
7	6	0	1.192176	0.702921	-0.11917
8	6	0	1.533318	-0.67922	-0.23626
9	6	0	2.821543	-1.14855	-0.14728
10	1	0	3.06279	-2.20159	-0.24098
11	6	0	3.839952	-0.19286	0.071936
12	6	0	3.549207	1.173145	0.191683
13	1	0	4.357644	1.882732	0.357384
14	6	0	2.232271	1.63601	0.098195
15	1	0	2.027663	2.699807	0.189523
16	6	0	-0.19605	0.763731	-0.26564
17	6	0	-0.75061	-0.61529	-0.47897
18	1	0	-1.21644	-0.73472	-1.46707
19	6	0	-1.73096	-1.11683	0.602406
20	1	0	-1.91552	-2.18163	0.411848
21	6	0	-3.06702	-0.4	0.615051
22	6	0	-4.89618	0.296054	-0.7194
23	1	0	-5.17397	0.227345	-1.77147
24	1	0	-4.80024	1.340194	-0.41096
25	1	0	-5.6375	-0.2027	-0.08946
26	1	0	-0.57889	2.632642	-0.00056
27	1	0	-1.28337	-1.01764	1.593955

TS to form radical (**8**) from phenoxy radical (**6**)

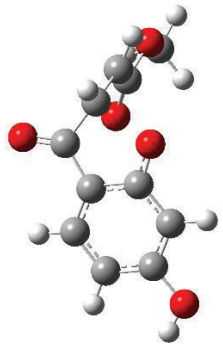

DFT/B3LYP 6-31+G(d), E = -800.657602 a.u

Center Number	Atomic Number	Atomic Type	Coordinates (Angstroms) X	Y	Z
1	8	0	-0.27046	0.367481	1.902876
2	8	0	-4.09589	-1.79944	0.152908
3	1	0	-4.6779	-1.78203	-0.62323
4	8	0	0.526079	2.59186	-1.08048
5	8	0	1.661992	-0.57569	-0.97772
6	8	0	3.56862	-1.03434	0.165772
7	6	0	-0.99487	0.932268	-0.24315
8	6	0	-1.12057	0.139799	0.934764
9	6	0	-2.15057	-0.82099	1.036833
10	1	0	-2.24545	-1.44212	1.920463
11	6	0	-3.08328	-0.89709	0.005708
12	6	0	-2.97668	-0.08715	-1.14876
13	1	0	-3.70469	-0.19345	-1.95028
14	6	0	-1.9225	0.816281	-1.27327
15	1	0	-1.80084	1.411885	-2.17351
16	6	0	0.222527	1.746056	-0.25232
17	6	0	1.102977	1.502431	0.972635
18	1	0	1.065675	2.297164	1.713283
19	6	0	2.20861	0.671764	0.983221
20	1	0	2.918452	0.717561	1.802353
21	6	0	2.419847	-0.35021	-0.04504
22	6	0	3.870646	-2.06322	-0.79341
23	1	0	4.825913	-2.48172	-0.47573
24	1	0	3.948326	-1.63614	-1.79701
25	1	0	3.090919	-2.82983	-0.78642

IRC:

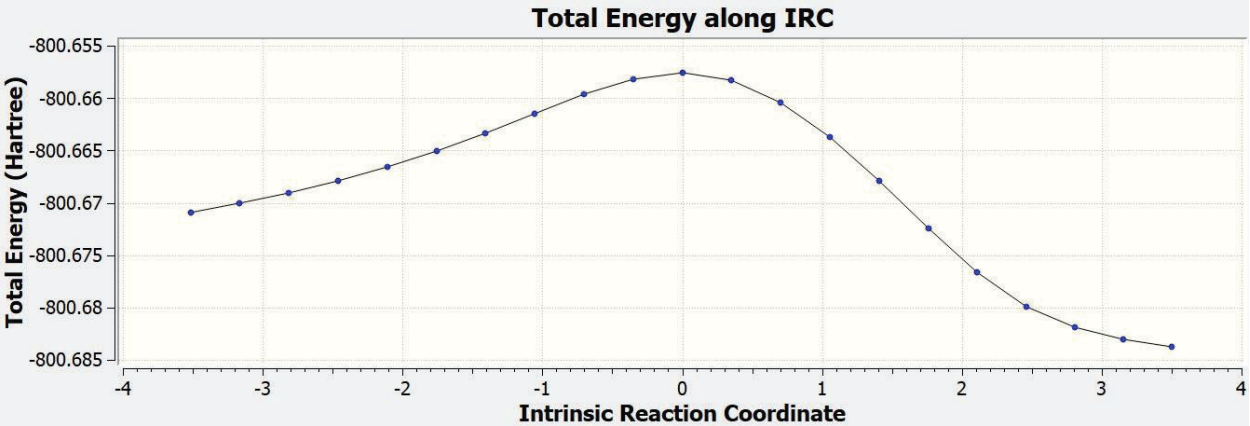

Radical (**8**)

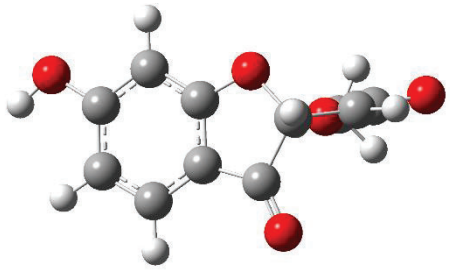

DFT/B3LYP 6-31+G(d), E = -800.685687 a.u

Center Number	Atomic Number	Atomic Type	Coordinates (Angstroms) X	Y	Z
1	6	0	0.926806	-0.1429	-0.79391
2	6	0	0.893682	-0.99378	0.319743
3	6	0	1.968722	-1.01967	1.216482
4	6	0	3.05833	-0.19332	0.977456
5	6	0	3.066898	0.655269	-0.15501
6	6	0	2.002686	0.694589	-1.06168
7	1	0	3.908767	-0.19209	1.655943
8	1	0	2.028548	1.351729	-1.92361
9	8	0	-0.1794	-0.21915	-1.57937
10	6	0	-0.36852	-1.7172	0.294953
11	8	0	-0.82292	-2.55248	1.053462
12	6	0	-1.07556	-1.22282	-1.0215
13	6	0	-2.45329	-0.69728	-0.84836
14	6	0	-2.81396	0.509354	-0.1186

15	8	0	-3.95367	0.954942	-0.07907
16	8	0	-1.76473	1.081541	0.52109
17	6	0	-2.06266	2.269001	1.276028
18	1	0	-1.11392	2.575413	1.717156
19	1	0	-2.45378	3.04929	0.617345
20	1	0	-2.79907	2.050419	2.054252
21	1	0	-1.08575	-2.0648	-1.72329
22	8	0	4.120361	1.478807	-0.41742
23	1	0	4.805737	1.374765	0.261605
24	1	0	1.942045	-1.67736	2.080595
25	1	0	-3.2886	-1.26413	-1.2431

TS of H transfer from radical (**10**) to radical (**8**)

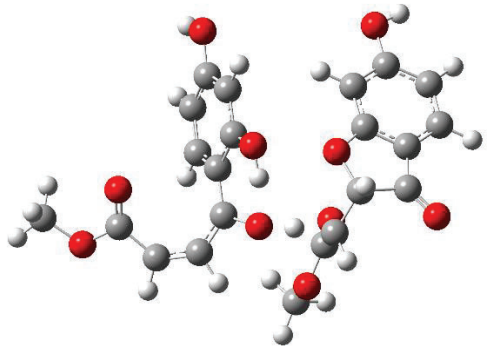

DFT/B3LYP 6-31+G(d), E = -1602.554180 a.u

Center Number	Atomic Number	Atomic Type	Coordinates (Angstroms) X	Y	Z
1	8	0	1.910732	0.041176	0.771414
2	8	0	4.360454	3.298969	-1.69668
3	1	0	5.230395	3.423092	-2.10807
4	8	0	4.241167	-2.6532	1.024696
5	8	0	1.436144	-1.94205	-1.42992
6	8	0	0.099521	-3.60805	-0.67213
7	6	0	4.075757	-0.41036	0.096301
8	6	0	3.008703	0.499619	0.119245
9	6	0	3.084288	1.75346	-0.4735
10	1	0	2.259311	2.456237	-0.45238
11	6	0	4.287276	2.070686	-1.1109
12	6	0	5.378971	1.170223	-1.15031
13	1	0	6.295735	1.460051	-1.65928

14	6	0	5.274054	-0.07435	-0.54595
15	1	0	6.09882	-0.78067	-0.56846
16	6	0	3.656168	-1.611	0.799034
17	6	0	2.202296	-1.27134	1.304097
18	1	0	2.25851	-1.17453	2.395753
19	6	0	1.15175	-2.27078	0.93864
20	1	0	1.200482	-3.17627	1.547926
21	6	0	0.934823	-2.55816	-0.50627
22	6	0	-0.1806	-3.9797	-2.03534
23	1	0	-0.85111	-4.83653	-1.96722
24	1	0	0.743685	-4.25192	-2.55164
25	1	0	-0.66209	-3.15193	-2.56287
26	8	0	-0.72134	0.957421	2.891453
27	8	0	-0.87011	4.609914	-0.04083
28	1	0	-1.16159	4.874056	-0.92834
29	8	0	-1.09829	-1.43247	1.870429
30	8	0	-4.66828	0.765496	0.148078
31	8	0	-6.00405	-0.53888	-1.14315
32	6	0	-1.66615	0.56234	0.677956
33	6	0	-1.05004	1.411402	1.66956
34	6	0	-0.80862	2.760225	1.410592
35	1	0	-0.3643	3.382929	2.17922
36	6	0	-1.13713	3.292385	0.168737
37	6	0	-1.70614	2.478419	-0.84069
38	1	0	-1.92993	2.897644	-1.81918
39	6	0	-1.96815	1.150757	-0.57235
40	1	0	-2.38889	0.524285	-1.35
41	6	0	-1.92029	-0.84137	0.937128
42	6	0	-2.86317	-1.70774	0.346048
43	1	0	-2.58884	-2.75255	0.490865
44	6	0	-4.06715	-1.51796	-0.32222
45	1	0	-4.5405	-2.40355	-0.73557
46	6	0	-4.88049	-0.31294	-0.39274
47	6	0	-6.92886	0.553567	-1.22101
48	1	0	-7.75085	0.194535	-1.84224
49	1	0	-6.4572	1.429178	-1.67751
50	1	0	-7.29058	0.824587	-0.22456
51	1	0	-0.0317	-1.78465	1.391646
52	1	0	-0.8208	-0.02488	2.878738

IRC:

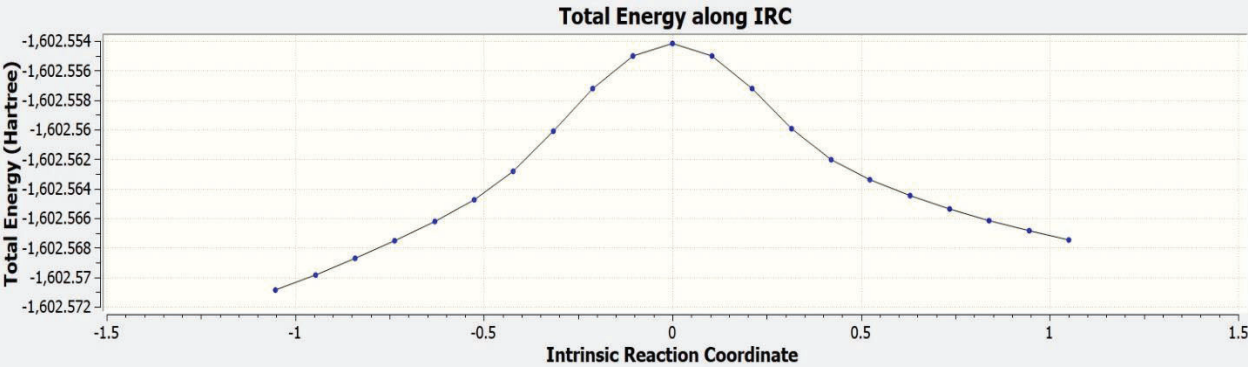

5-Ring **1b**

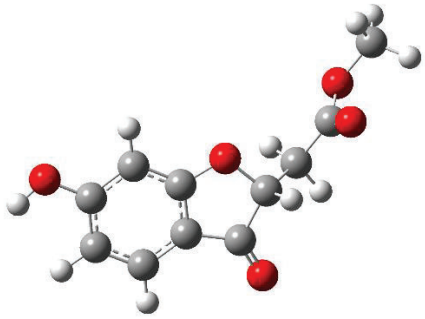

DFT/B3LYP 6-31+G(d), E = -801.348607 a.u

Center Number	Atomic Number	Atomic Type	Coordinates (Angstroms) X	Y	Z
1	6	0	-3.48471	-1.05386	0.07342
2	6	0	-3.84498	0.287352	0.347335
3	6	0	-2.88086	1.285206	0.313287
4	6	0	-1.5602	0.938	0.002372
5	6	0	-1.22862	-0.40111	-0.26133
6	6	0	-2.17173	-1.42222	-0.23572
7	1	0	-4.87956	0.527692	0.582822
8	1	0	-3.13762	2.320188	0.52071
9	6	0	-0.33497	1.717976	-0.10253
10	6	0	0.751982	0.699324	-0.50679
11	8	0	0.08812	-0.59494	-0.53563
12	6	0	1.930171	0.676146	0.454496
13	6	0	3.114795	-0.10054	-0.09125
14	8	0	3.398558	-0.20247	-1.26688
15	8	0	3.845301	-0.63815	0.906146
16	6	0	5.032533	-1.35243	0.505803

17	1	0	5.717163	-0.68335	-0.02196
18	1	0	4.767993	-2.1891	-0.14569
19	1	0	5.479007	-1.70975	1.433832
20	1	0	-1.9167	-2.45555	-0.44236
21	1	0	1.100399	0.904516	-1.52516
22	1	0	2.253135	1.715441	0.607631
23	1	0	1.633795	0.279486	1.430035
24	8	0	-4.40822	-2.05577	0.098644
25	8	0	-0.13307	2.909764	0.078505
26	1	0	-5.28365	-1.70007	0.319289

Chapter 3: Supporting Information

I. Characterization of stating materials and photoproducts using different spectroscopy

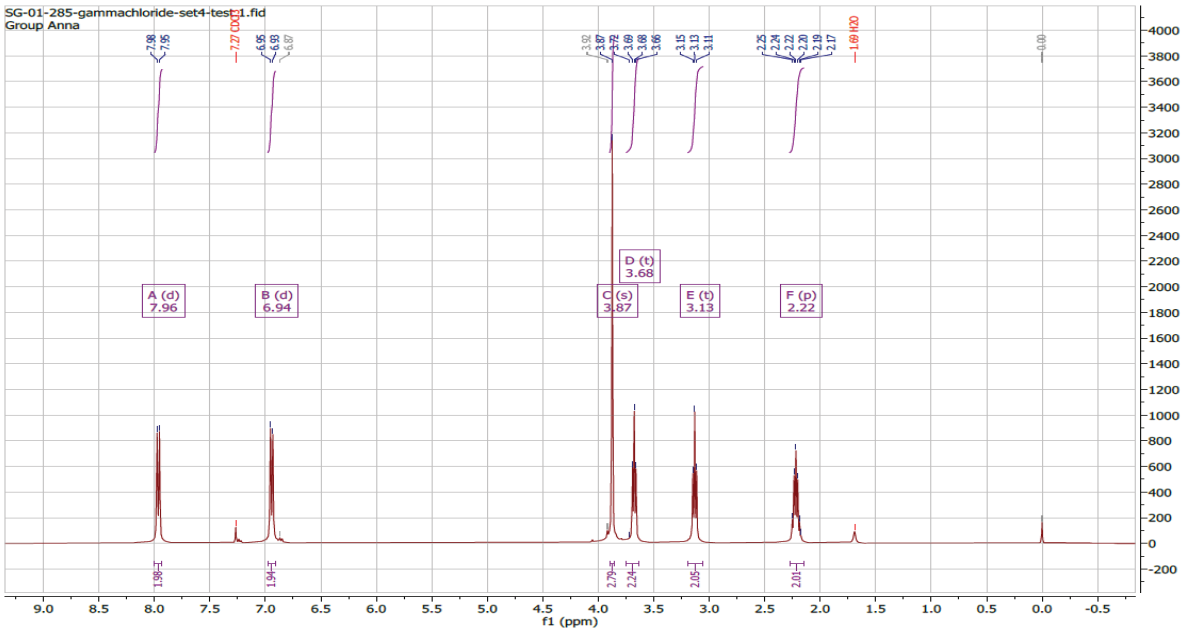

Figure S141.^{1}H NMR of Methoxy Gamma Chloride

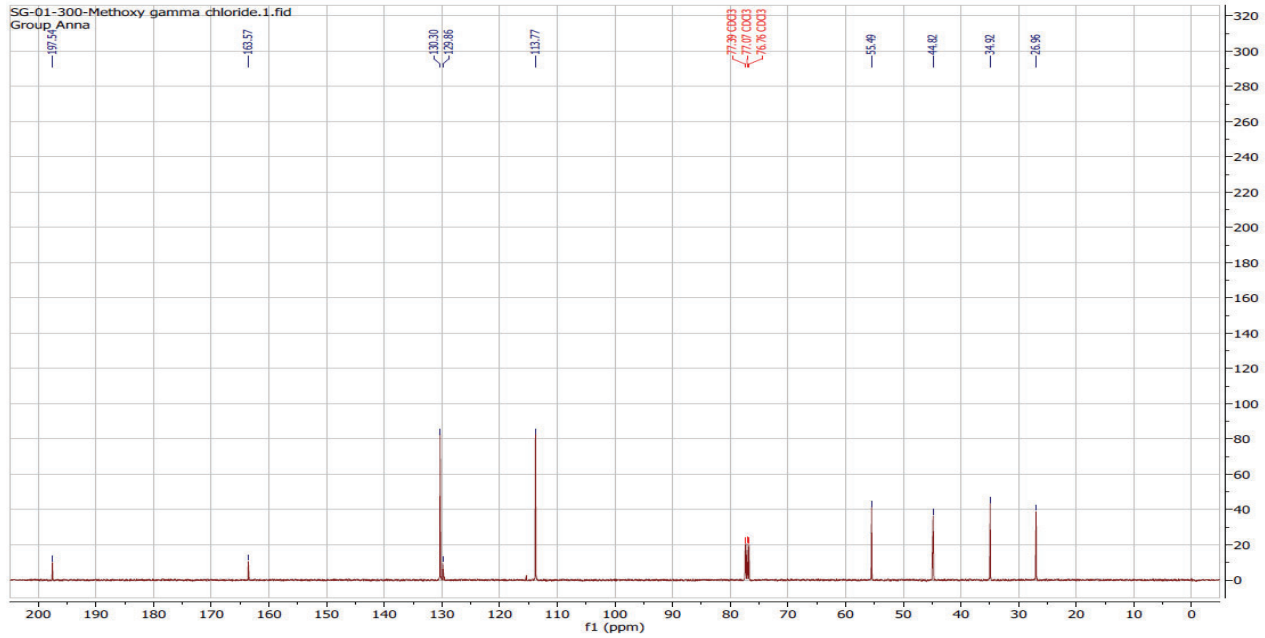

Figure S142. ^{13}C NMR of Methoxy Gamma Chloride

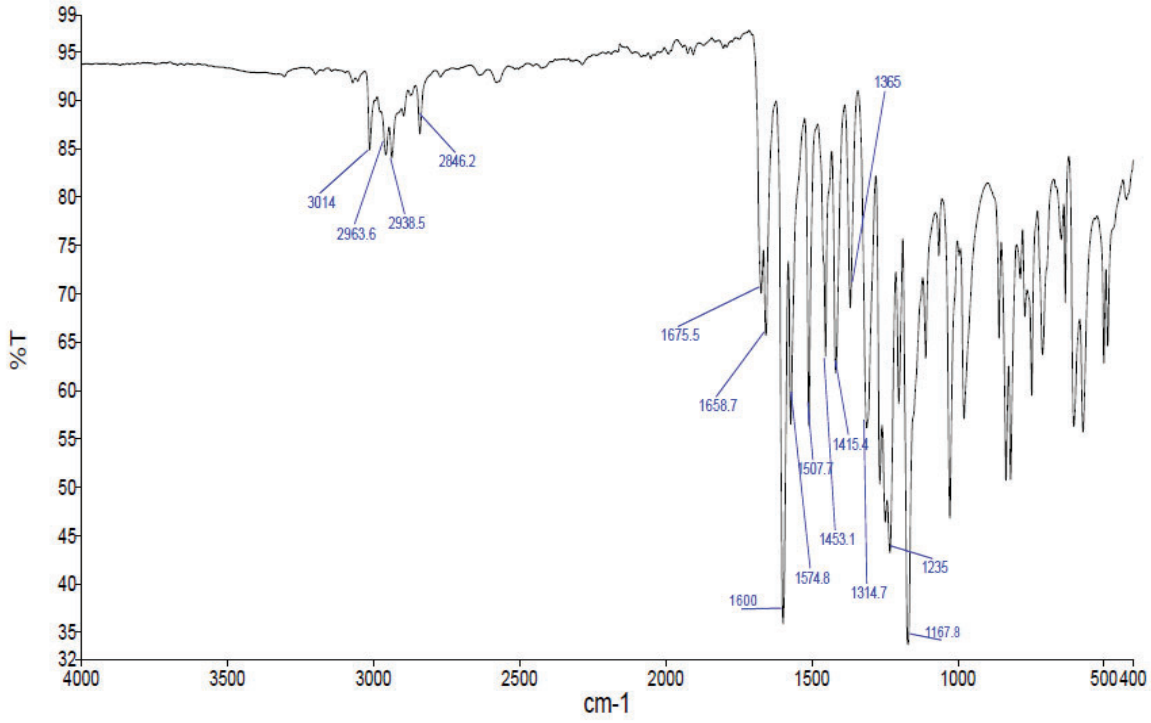

Figure S143. FTIR Spectrum of Methoxy gamma chloride

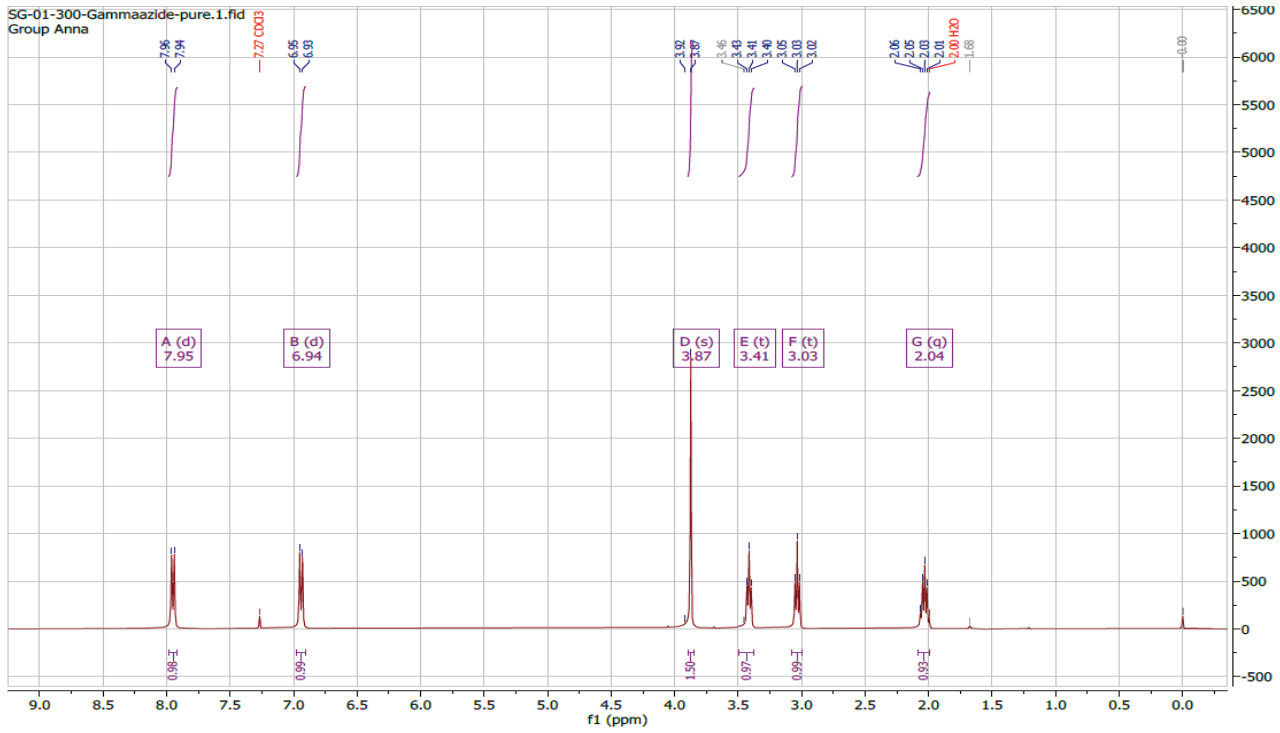

Figure 144. ^{1}H NMR of Methoxy Gamma Azide

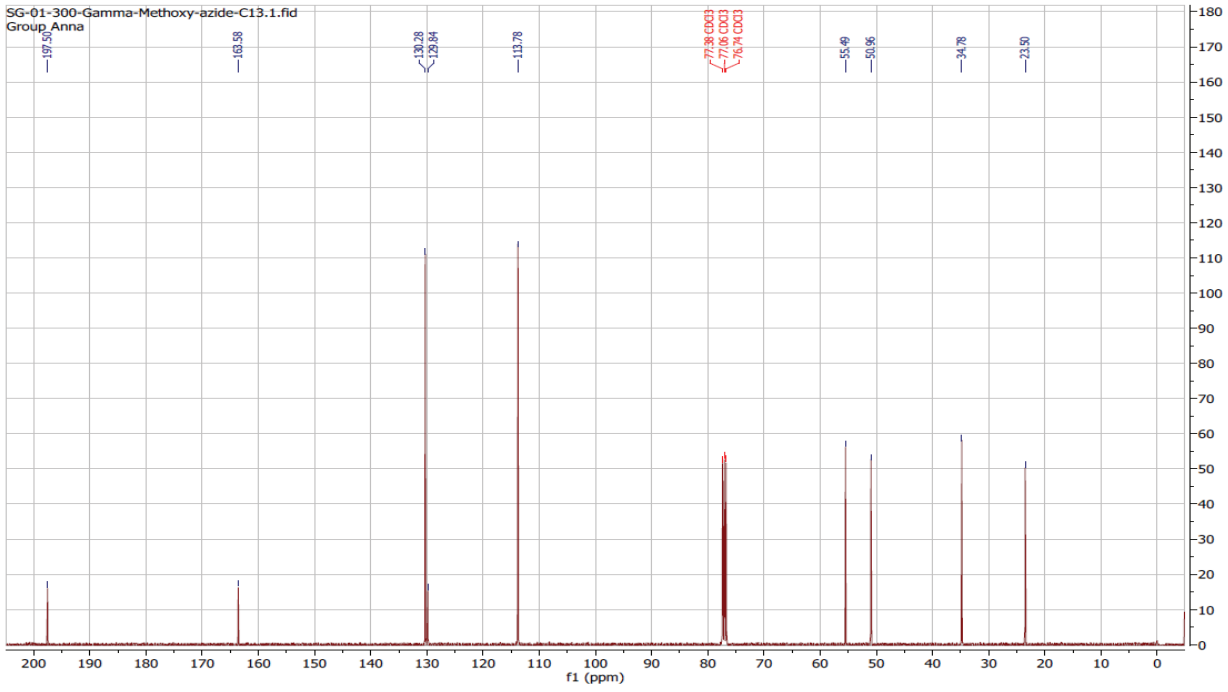

Figure S145. ^{13}C NMR of Methoxy Gamma Azide

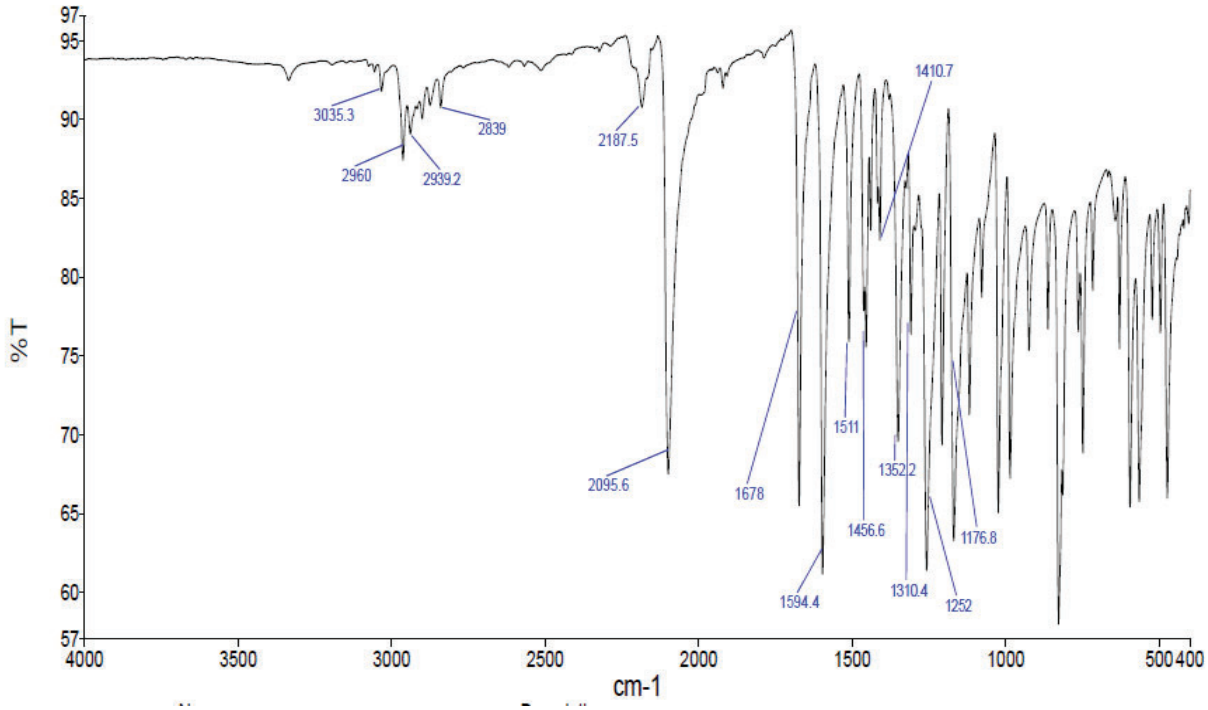

Figure S146. FTIR Spectrum of Methoxy Gamma Azide

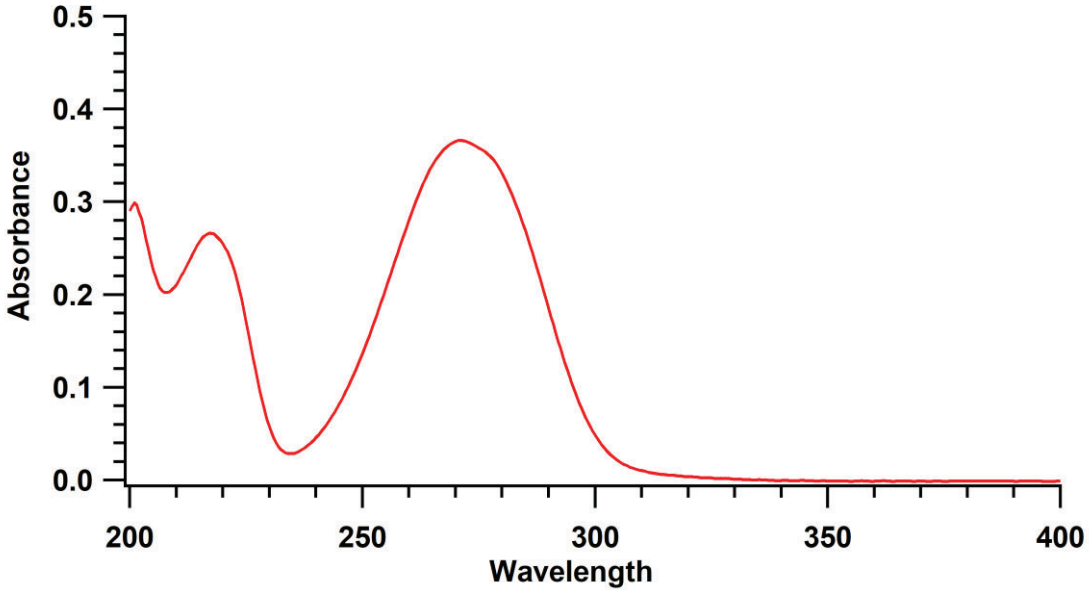

Figure S147. UV-Vis Spectrum of Methoxy Gamma Azide

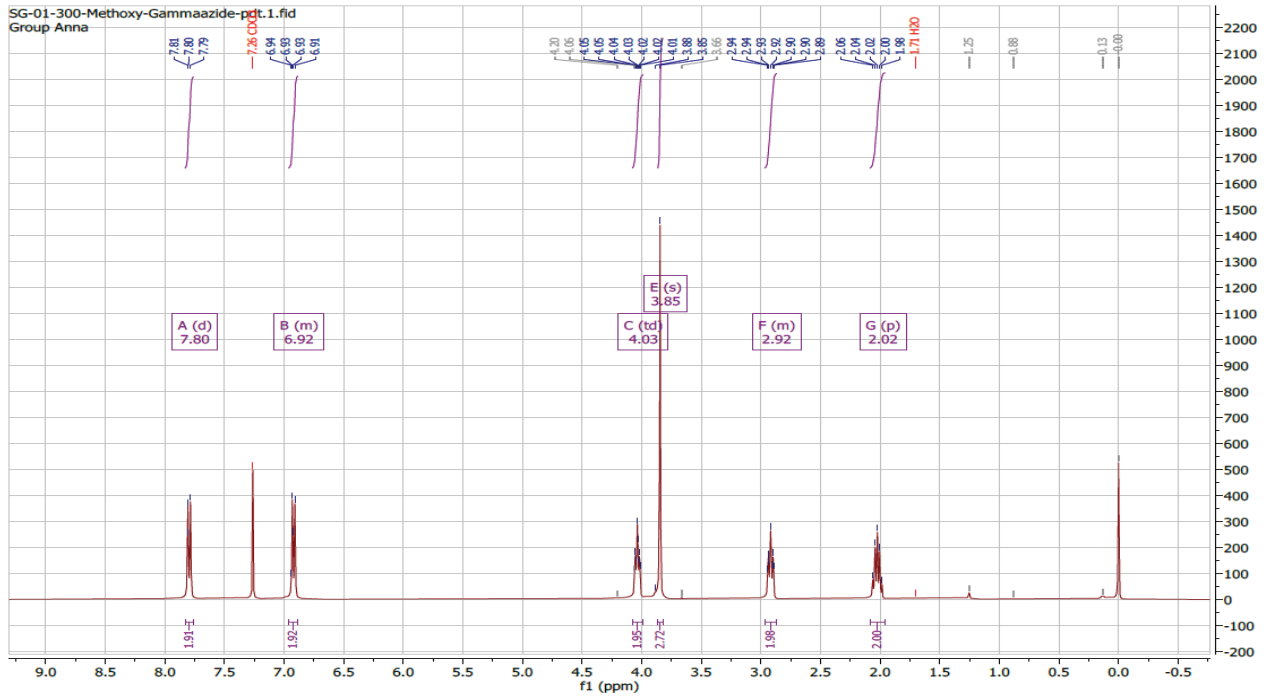

Figure S148. ^{1}H NMR of Methoxy Heterocyclic product

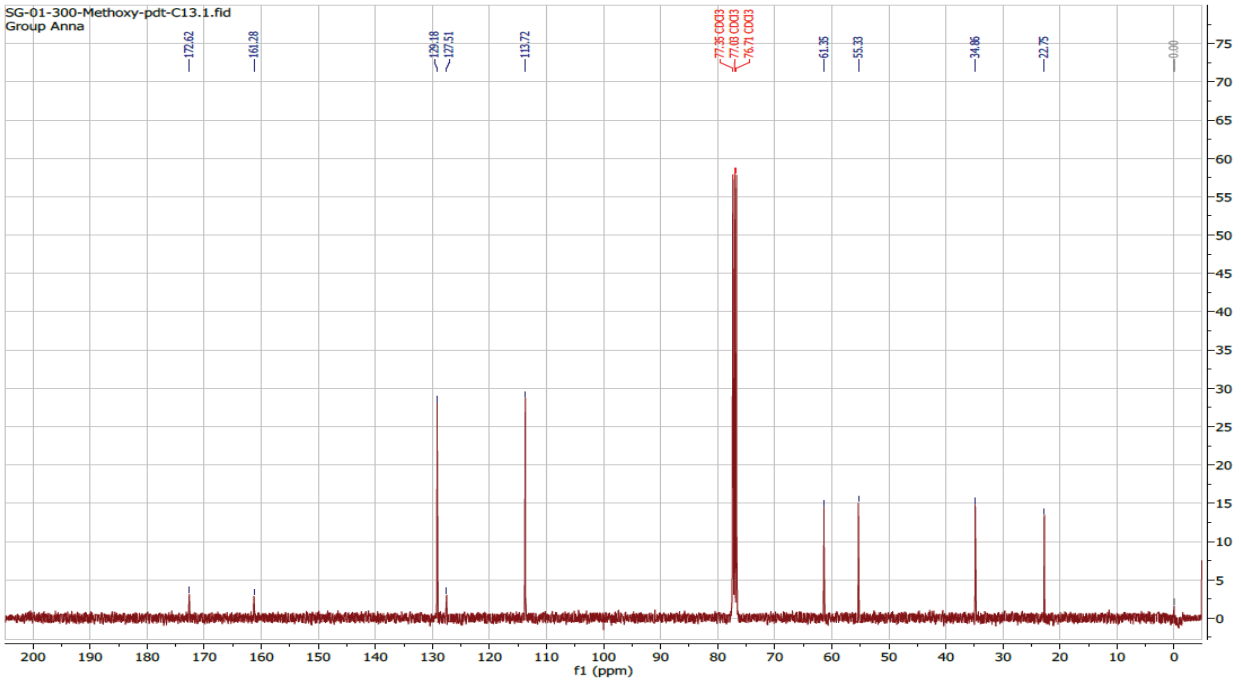

Figure S149. ^{13}C NMR of Methoxy Heterocyclic product

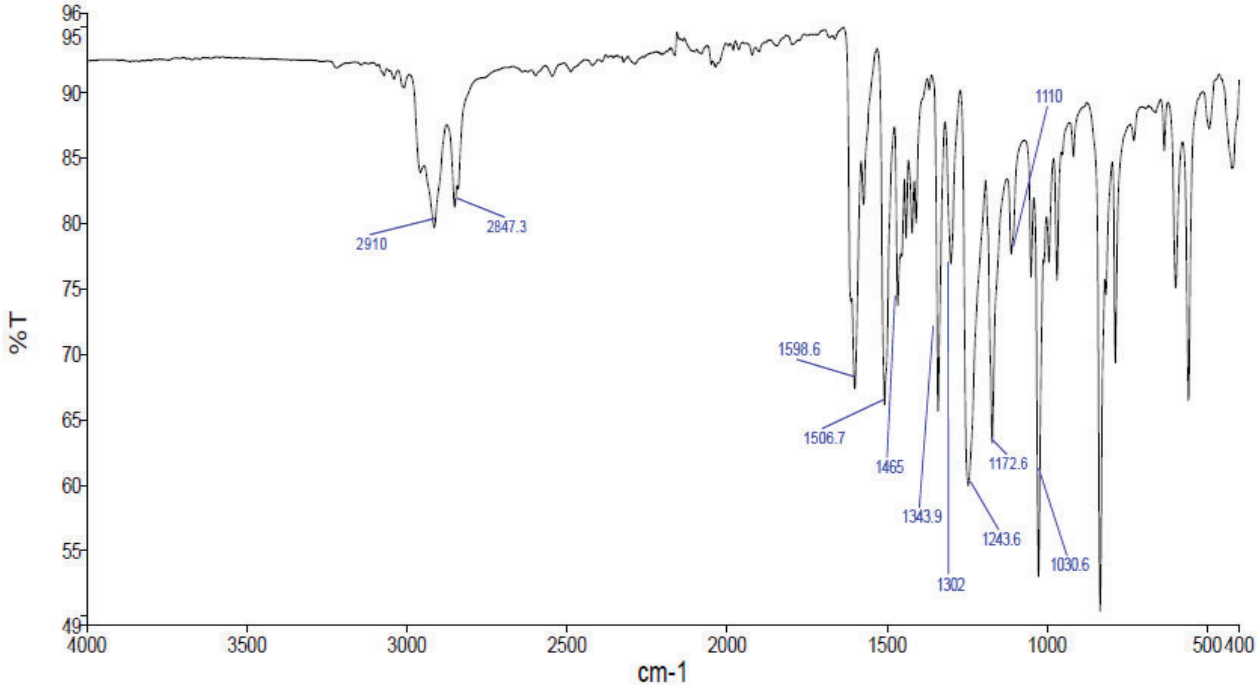

Figure S150. FTIR Spectrum of Methoxy Heterocyclic product

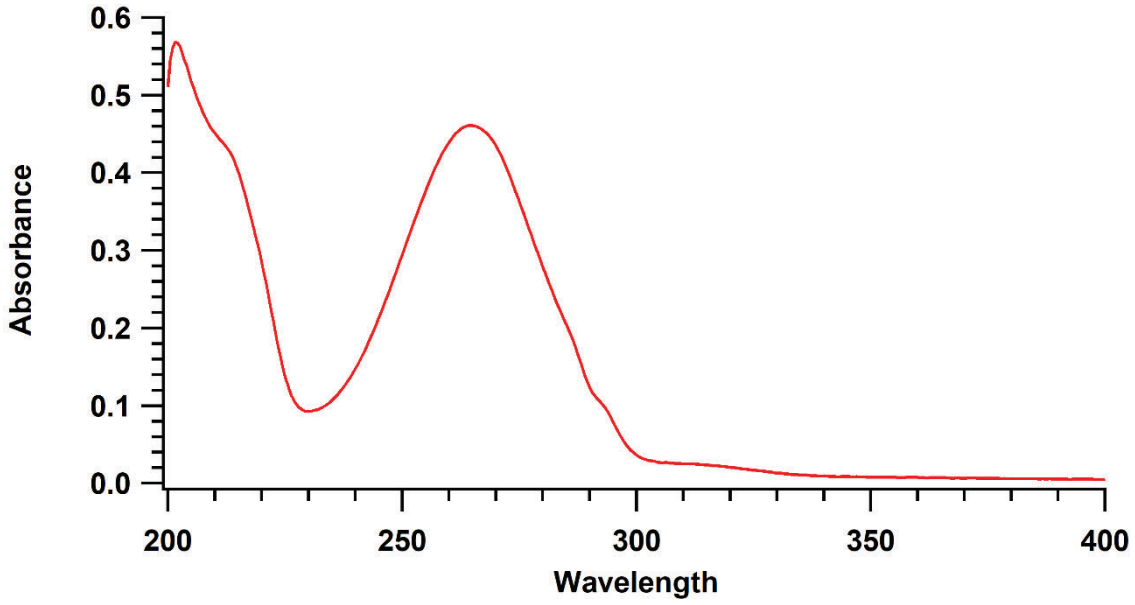

Figure S151. UV-Vis Spectrum of Methoxy Heterocyclic product

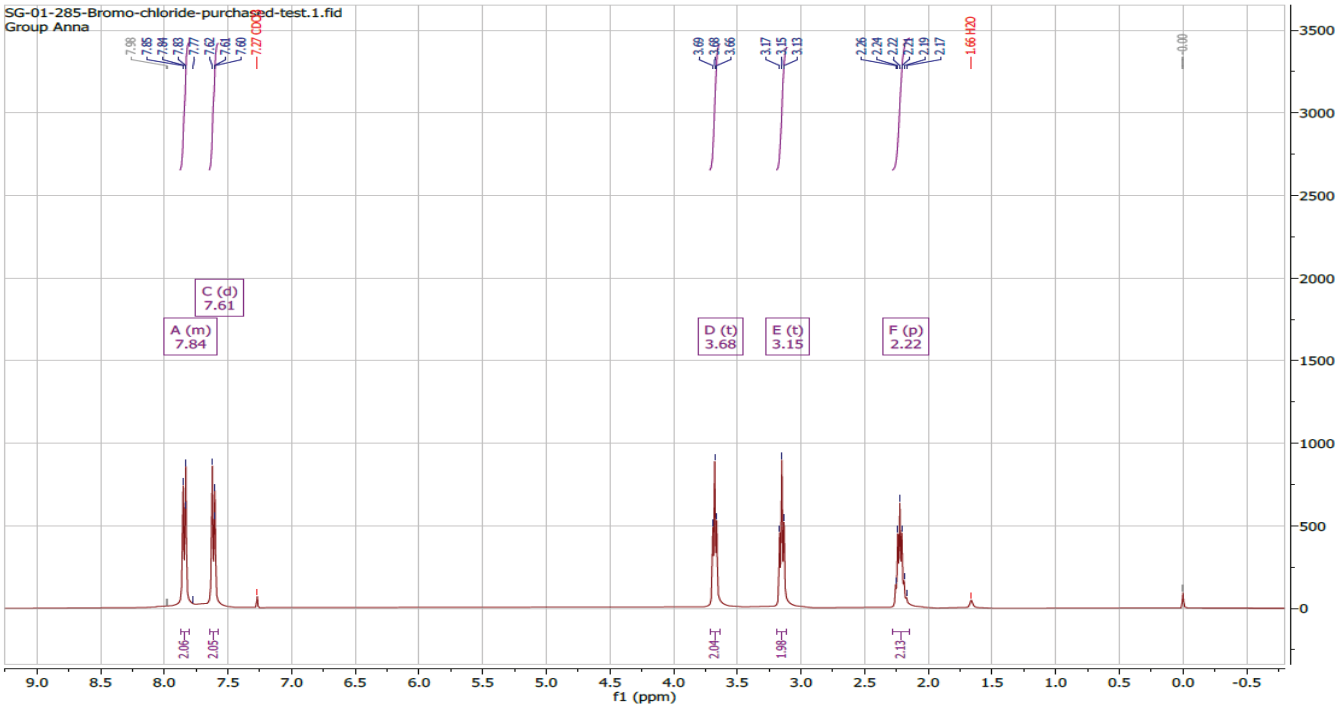

Figure S152. ^{1}H NMR of Bromo Gamma Chloride

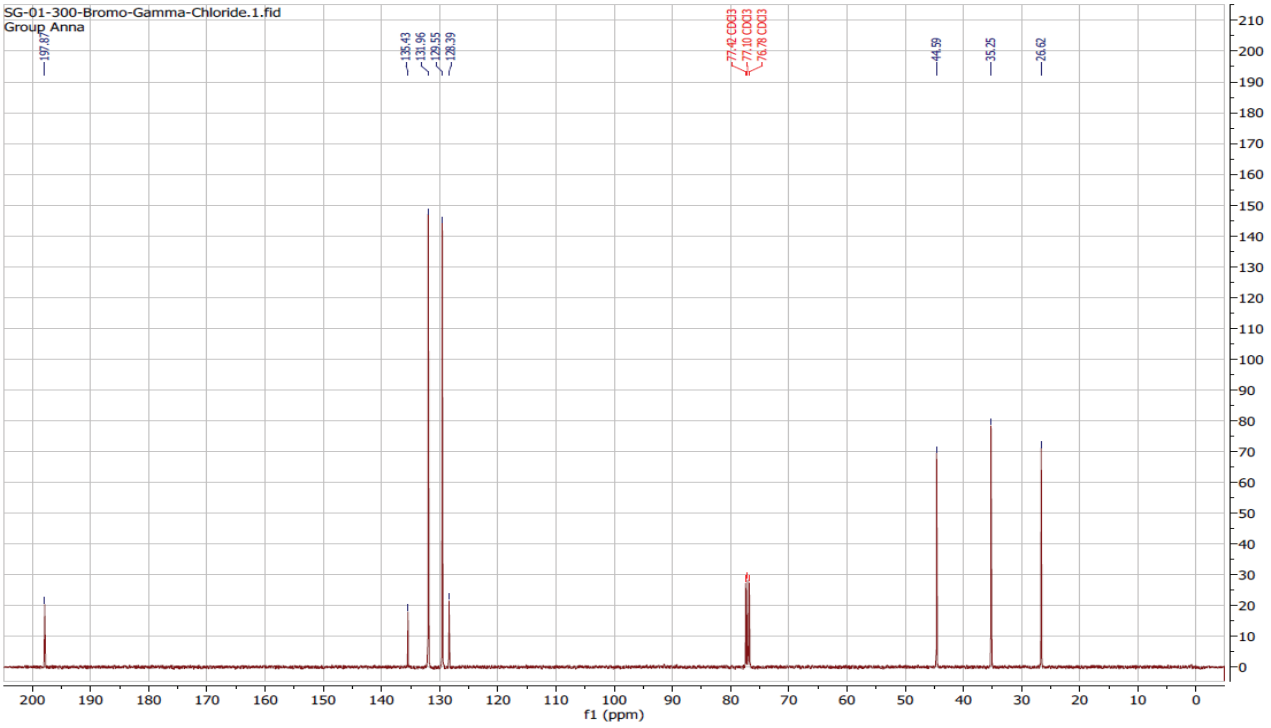

Figure S153. ^{13}C NMR of Bromo Gamma Chloride

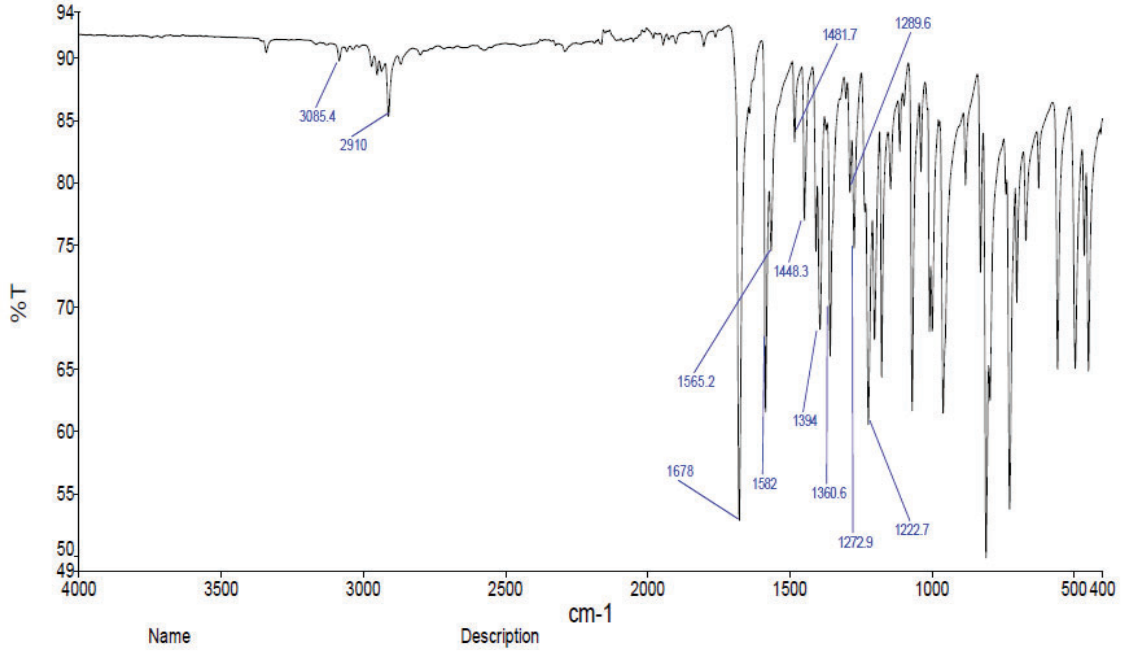

Figure S154. FTIR Spectrum of Bromo Gamma chloride

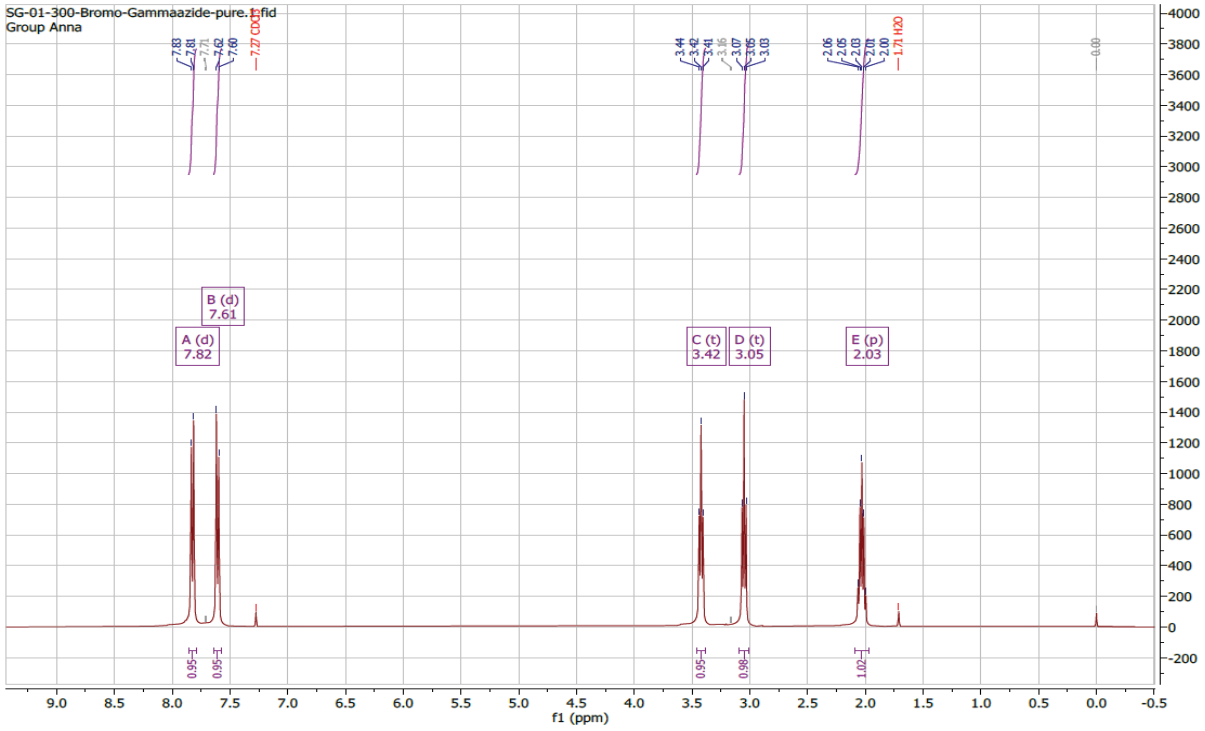

Figure S155. ^{1}H NMR of Bromo Gamma azide

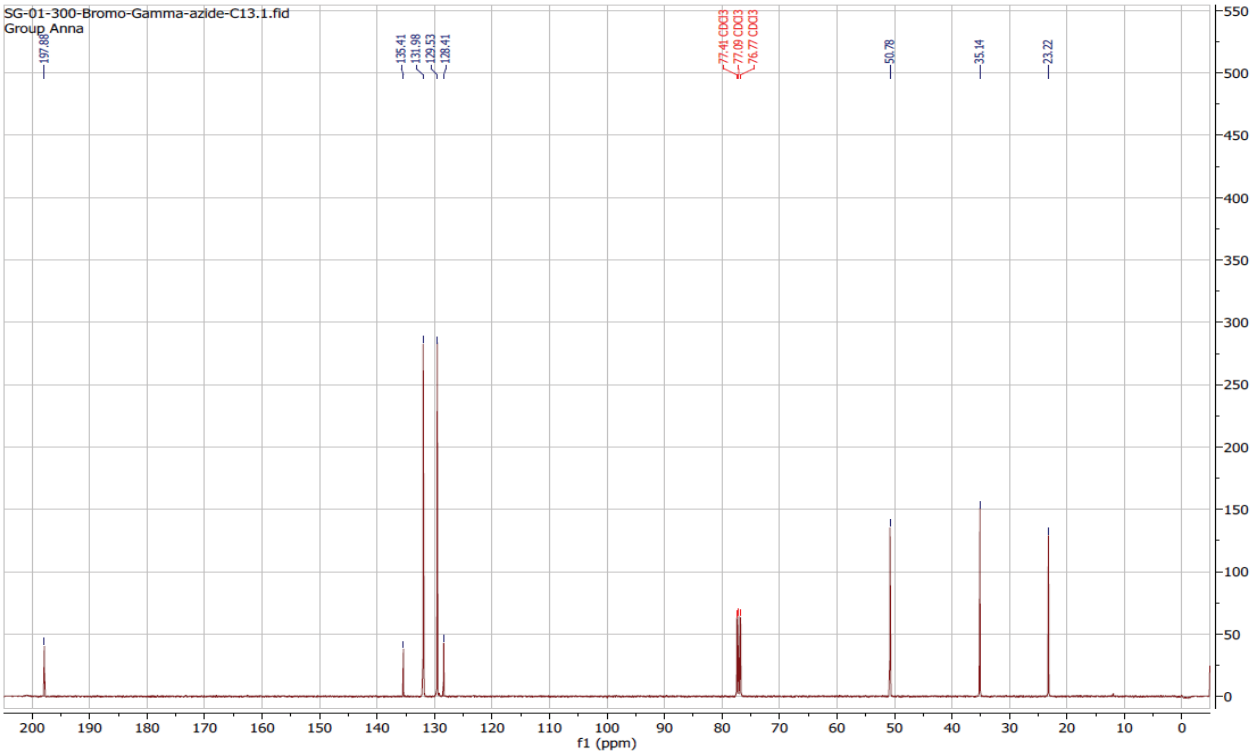

Figure S156. ^{13}C NMR of Bromo Gamma azide

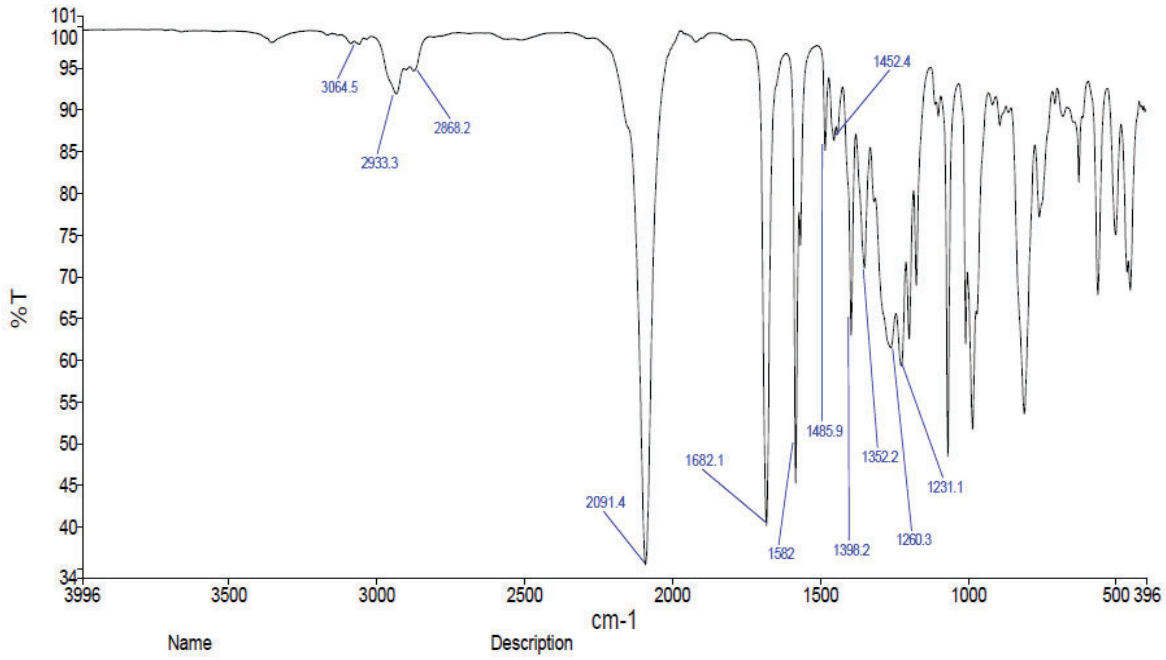

Figure S157. FTIR Spectrum of Bromo Gamma Azide

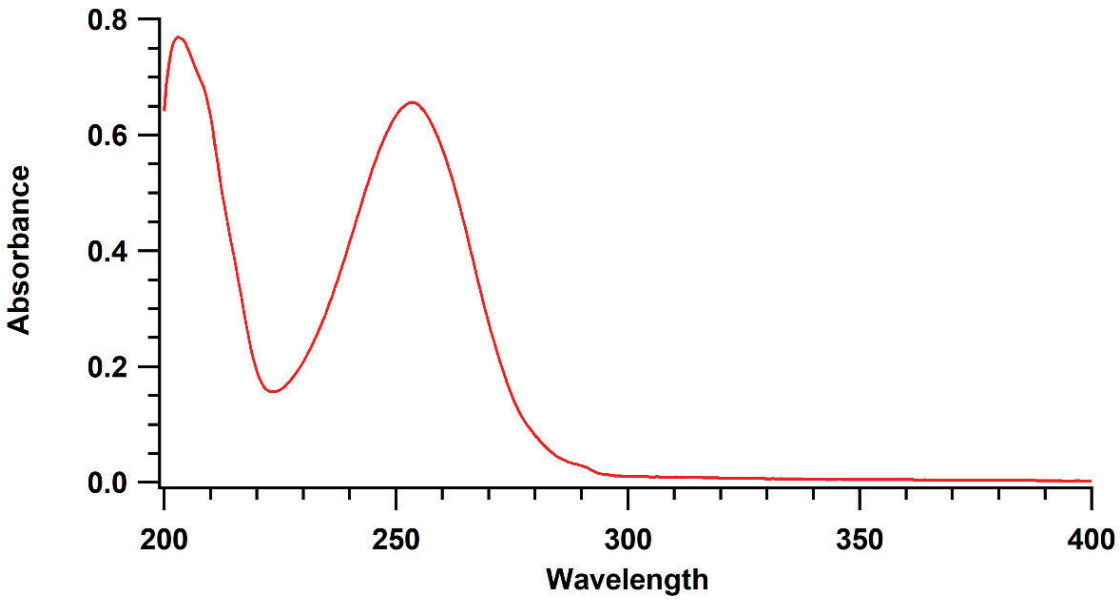

Figure S158. UV-Vis Spectrum of Bromo Gamma Azide

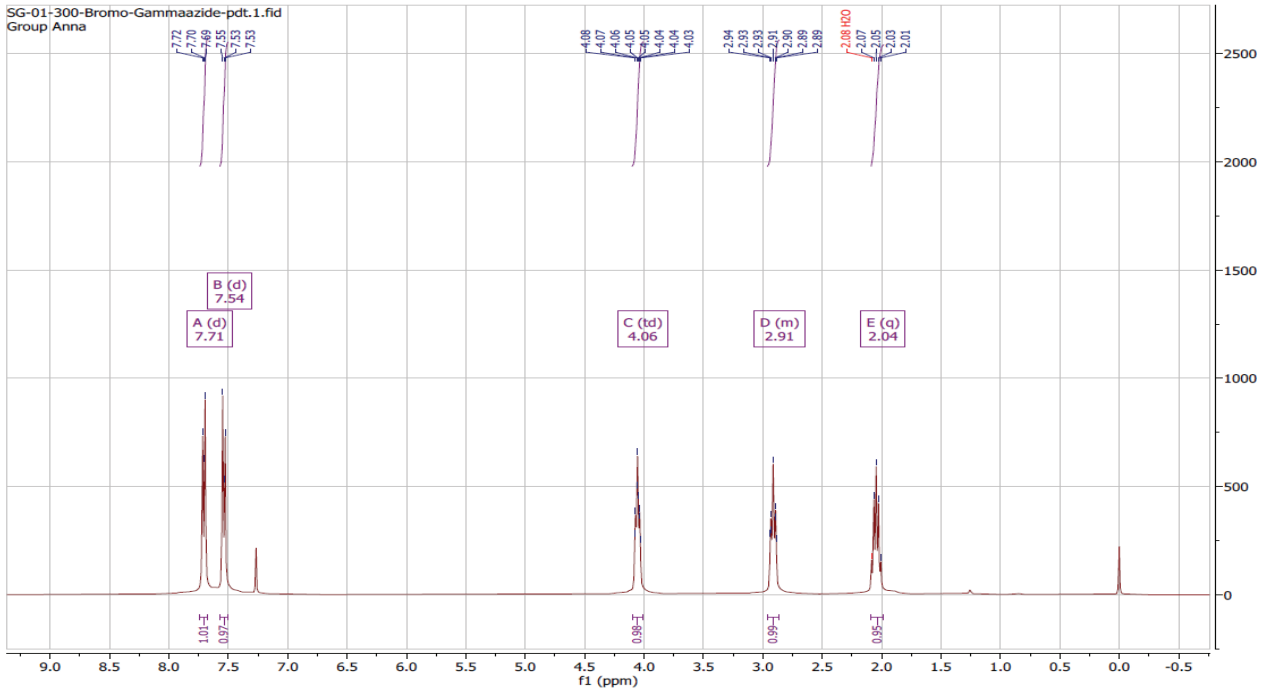

Figure S159. ^{1}H NMR of Bromo Heterocyclic product

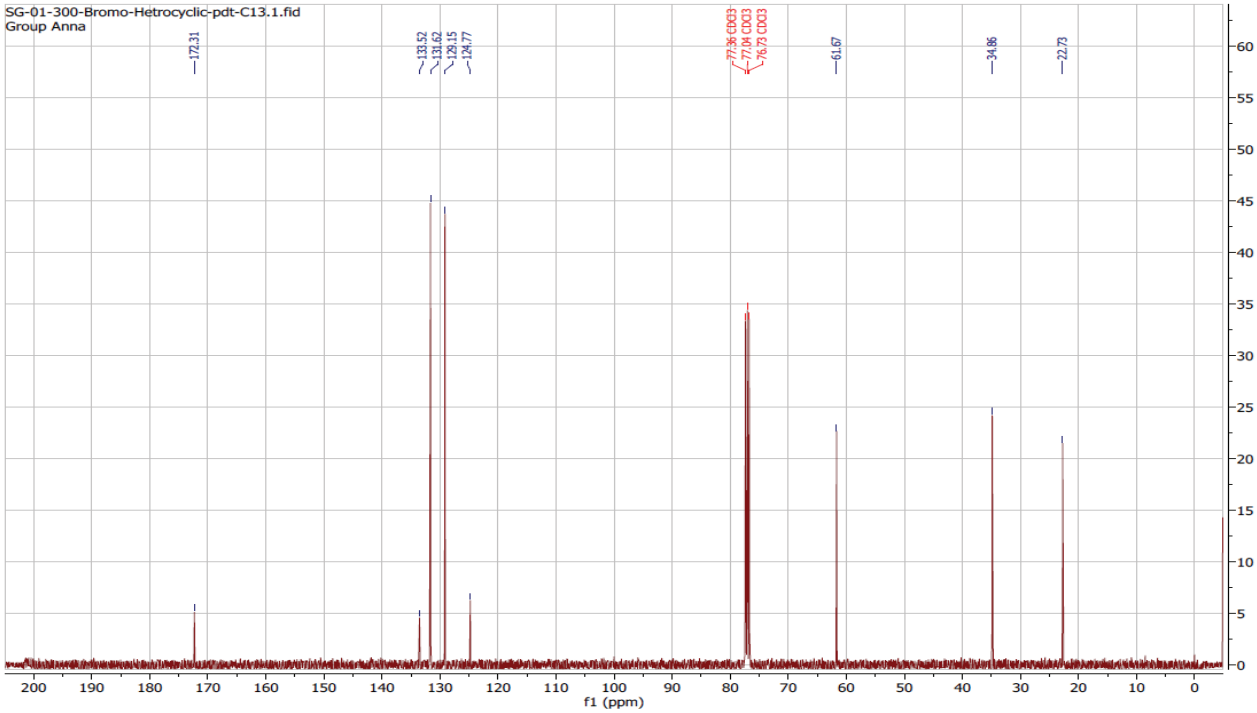

Figure S160. ^{13}C NMR of Bromo Heterocyclic product

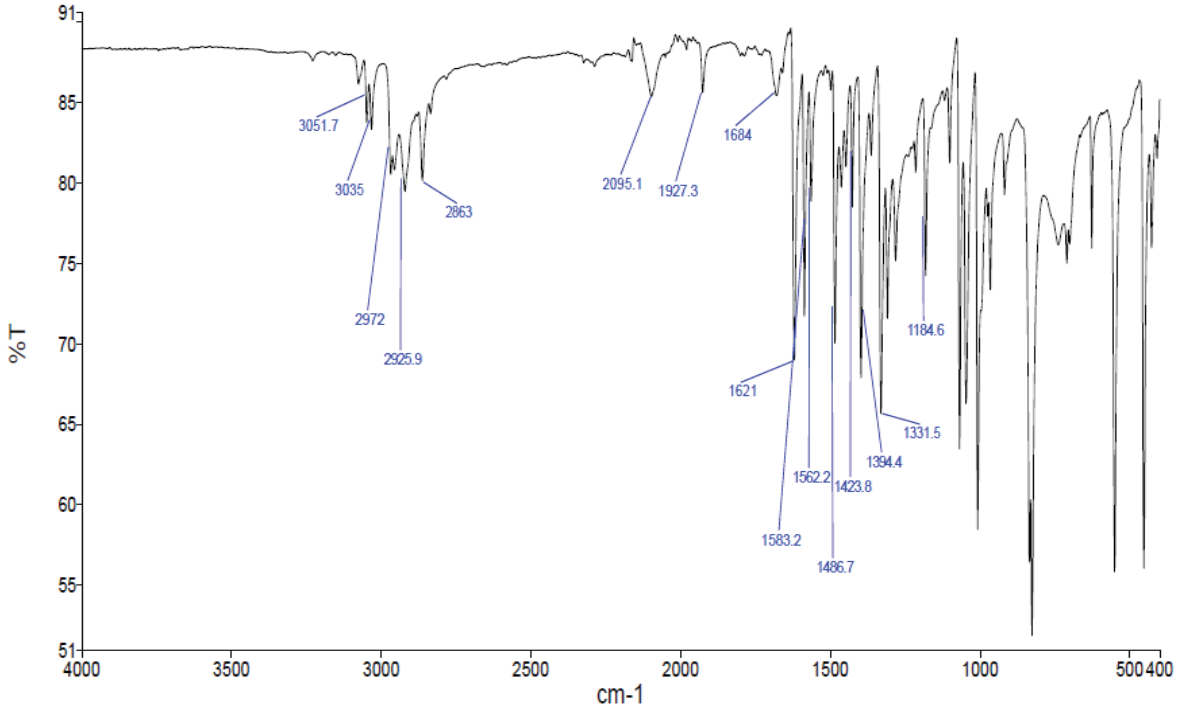

Figure S161. FTIR Spectrum of Bromo heterocyclic product

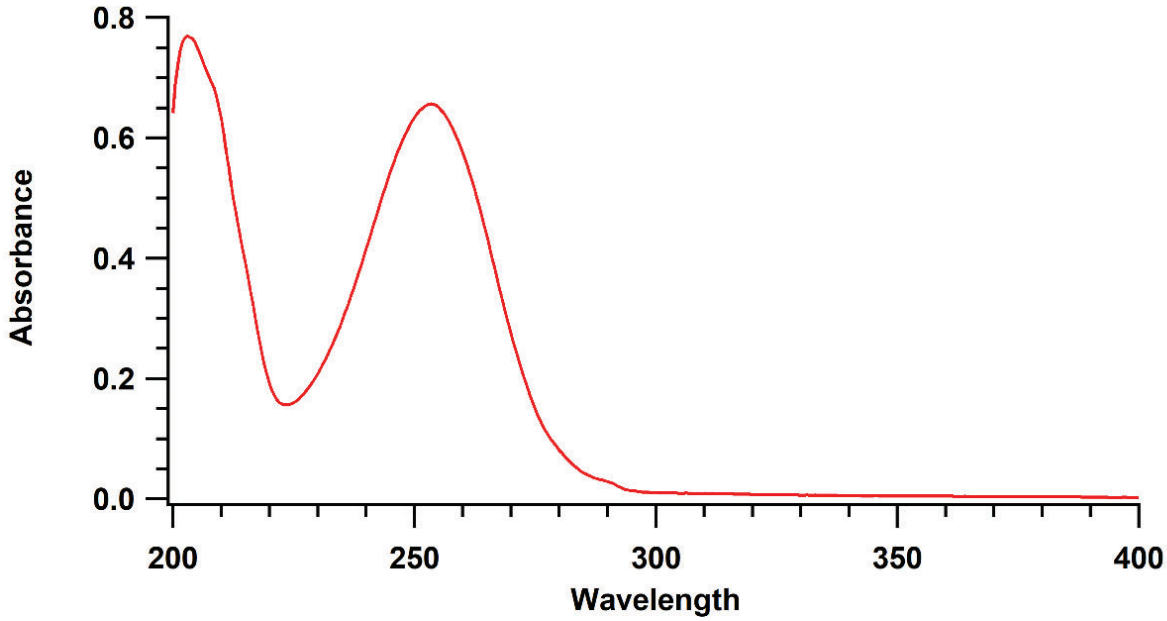

Figure S162. UV-Vis Spectrum of Bromo heterocyclic product

II. Photolysis of **1a** and **1b** monitored without TTMSS

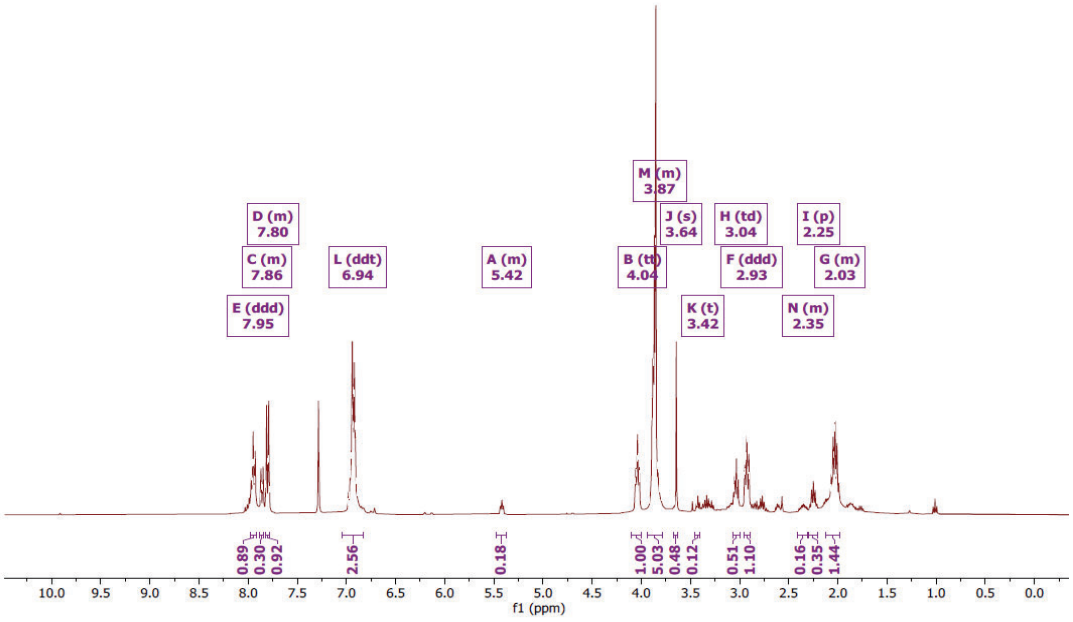

Figure S163. ^{1}H-NMR of argon saturated MeOH solution of **1a** after 18 h of irradiation using 340 nm LED.

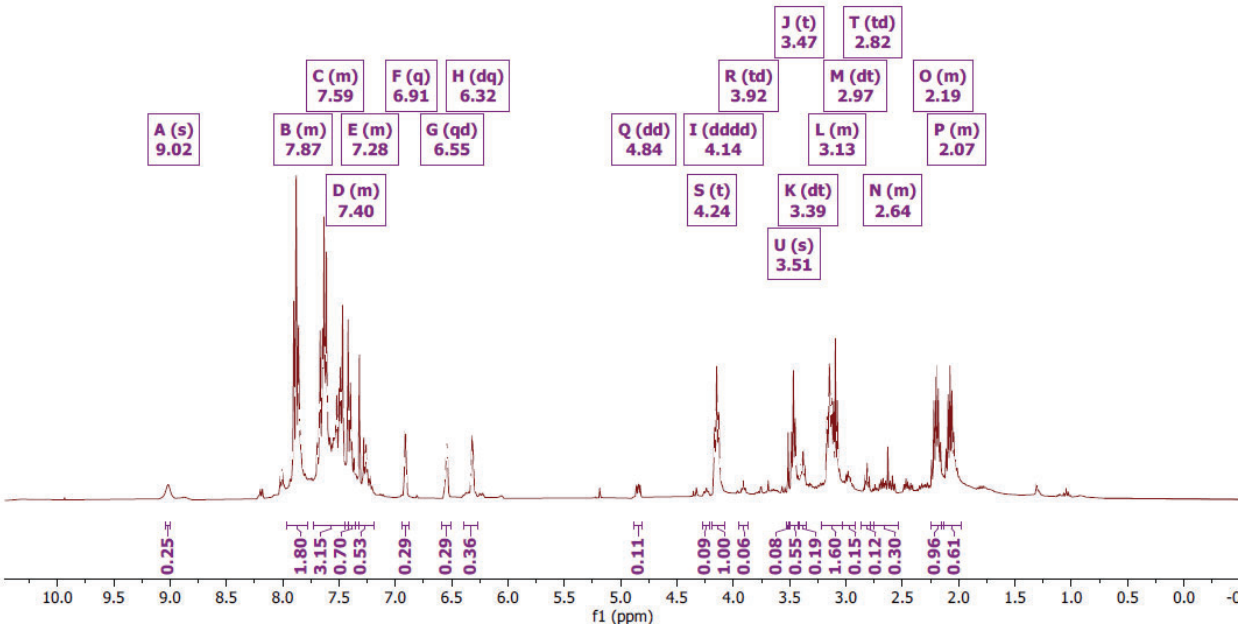

Figure S164. ^{1}H-NMR of argon saturated MeOH solution of **1a** after 18 h of irradiation using 340 nm LED.

III. Reaction progress monitored using Proton NMR in the presence of TTMSS

a) Photolysis of 1a with TTMSS

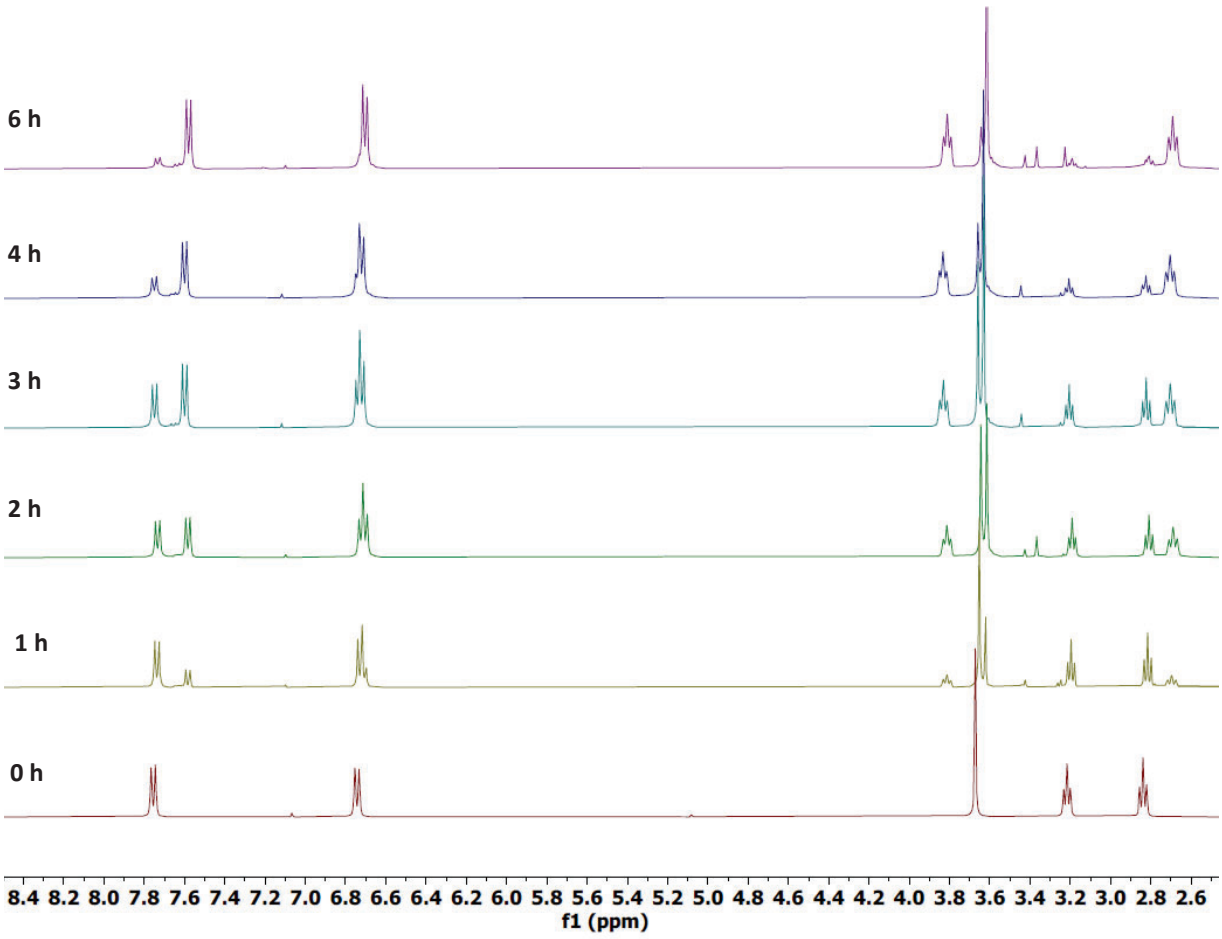

Figure S165. Progress of the reaction of Methoxy Azide with TTMSS in argon saturated MeOH upon irradiation at 340 nm

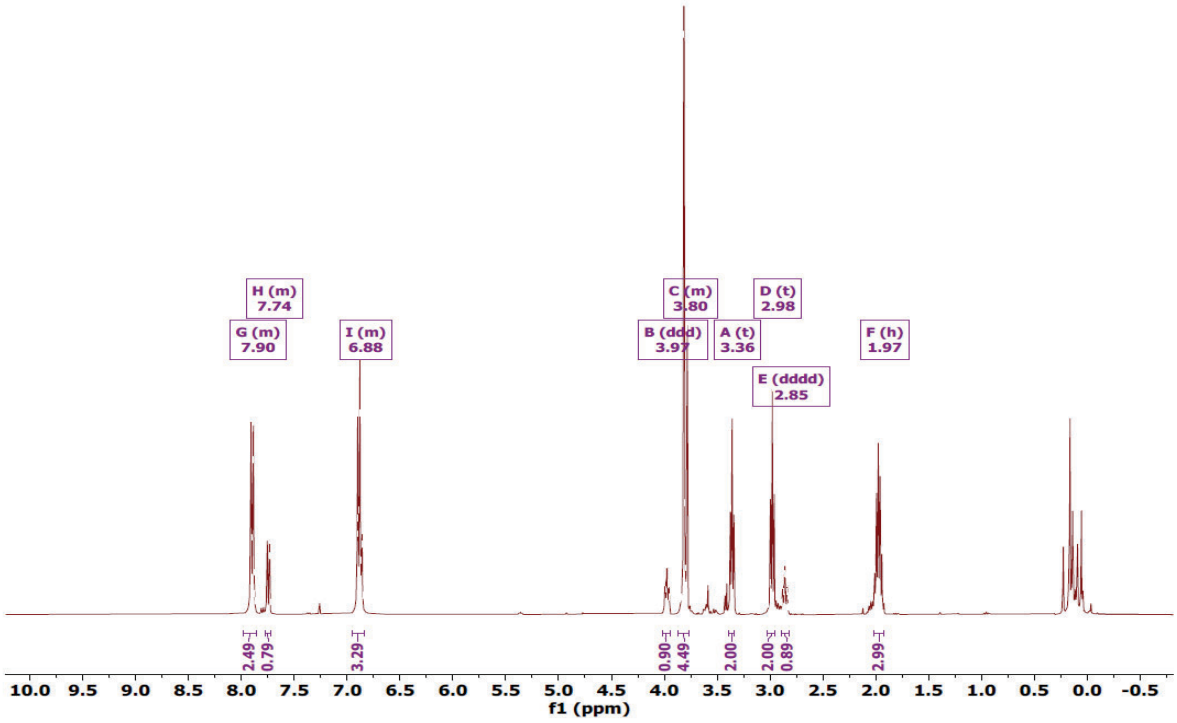

Figure S166. Methoxy Azide with TTMSS in argon saturated MeOH at 0 h irradiation at 340 nm

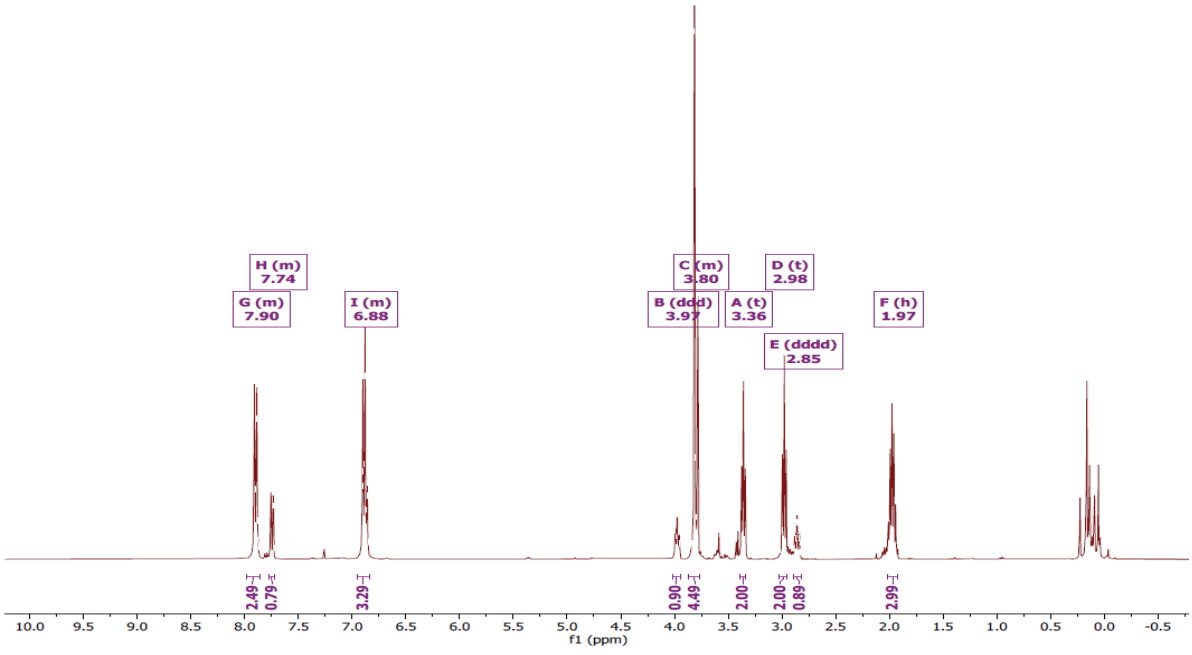

Figure S167. Methoxy Azide with TTMSS in argon saturated MeOH at 1 h irradiation at 340 nm

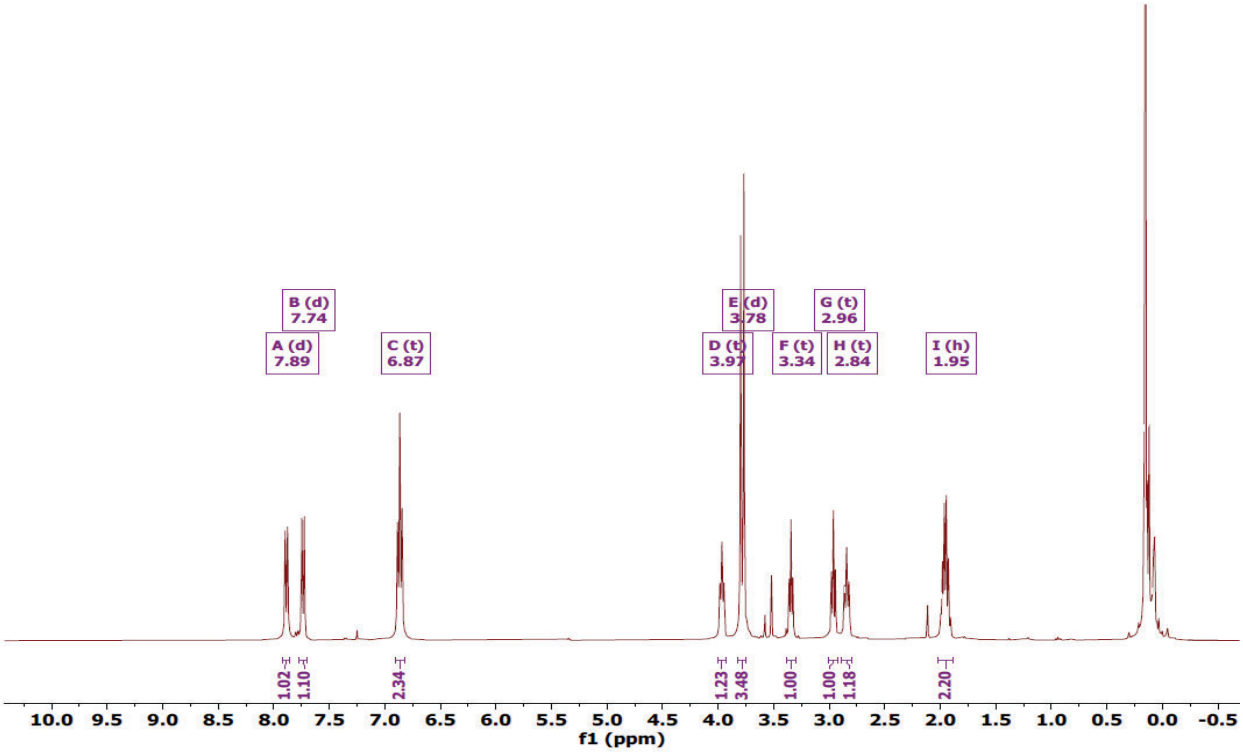

Figure S168. Methoxy Azide with TTMSS in argon saturated MeOH at 2 h irradiation at 340 nm

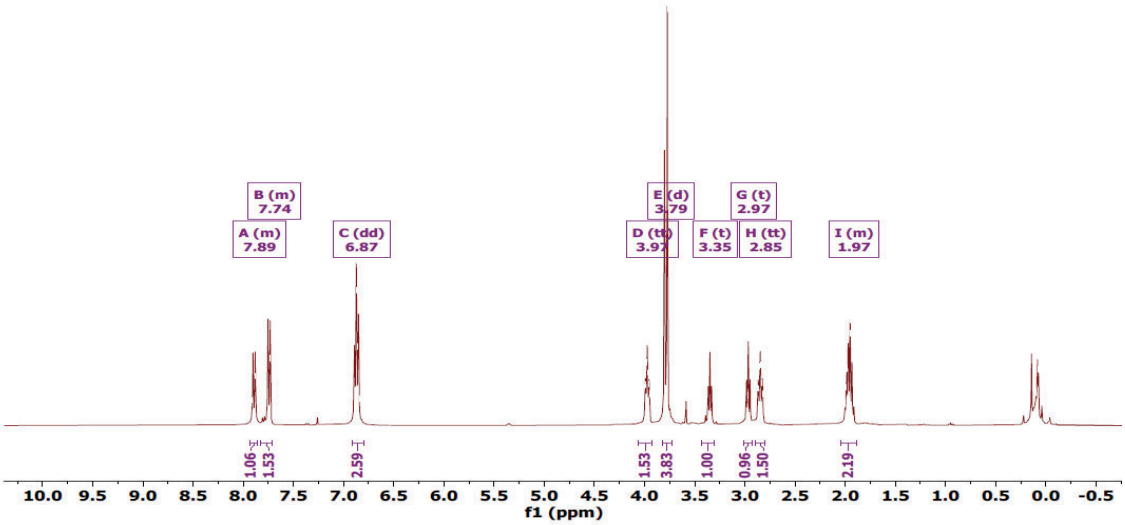

Figure S169. Methoxy Azide with TTMSS in argon saturated MeOH at 2 h irradiation at 340 nm

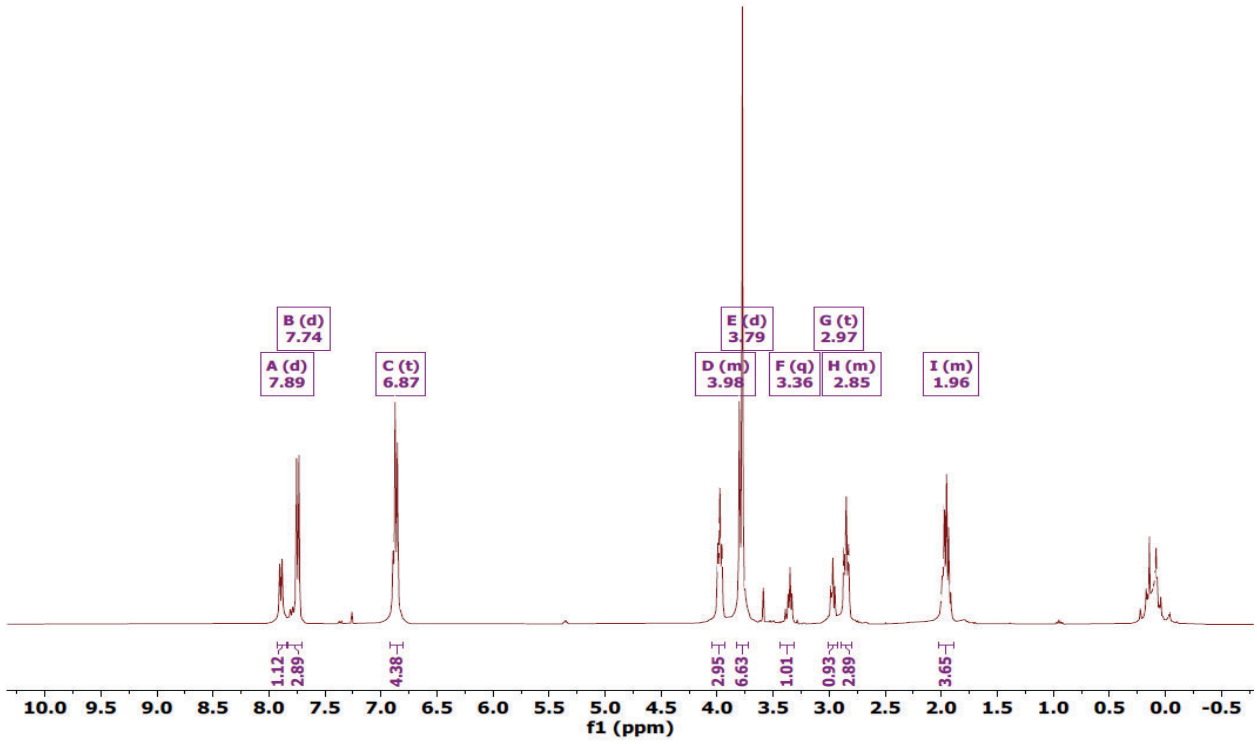

Figure S170.. Methoxy Azide with TTMSS in argon saturated MeOH at 2 h irradiation at 340 nm

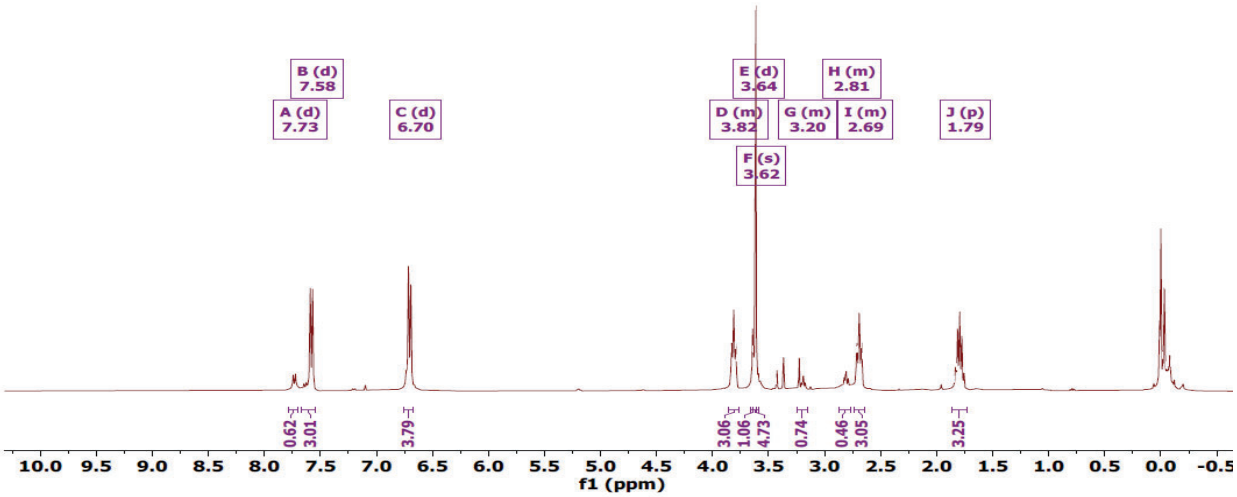

Figure S171. Methoxy Azide with TTMSS in argon saturated MeOH at 2 h irradiation at 340 nm

b) Photolysis of 1b with TTMSS

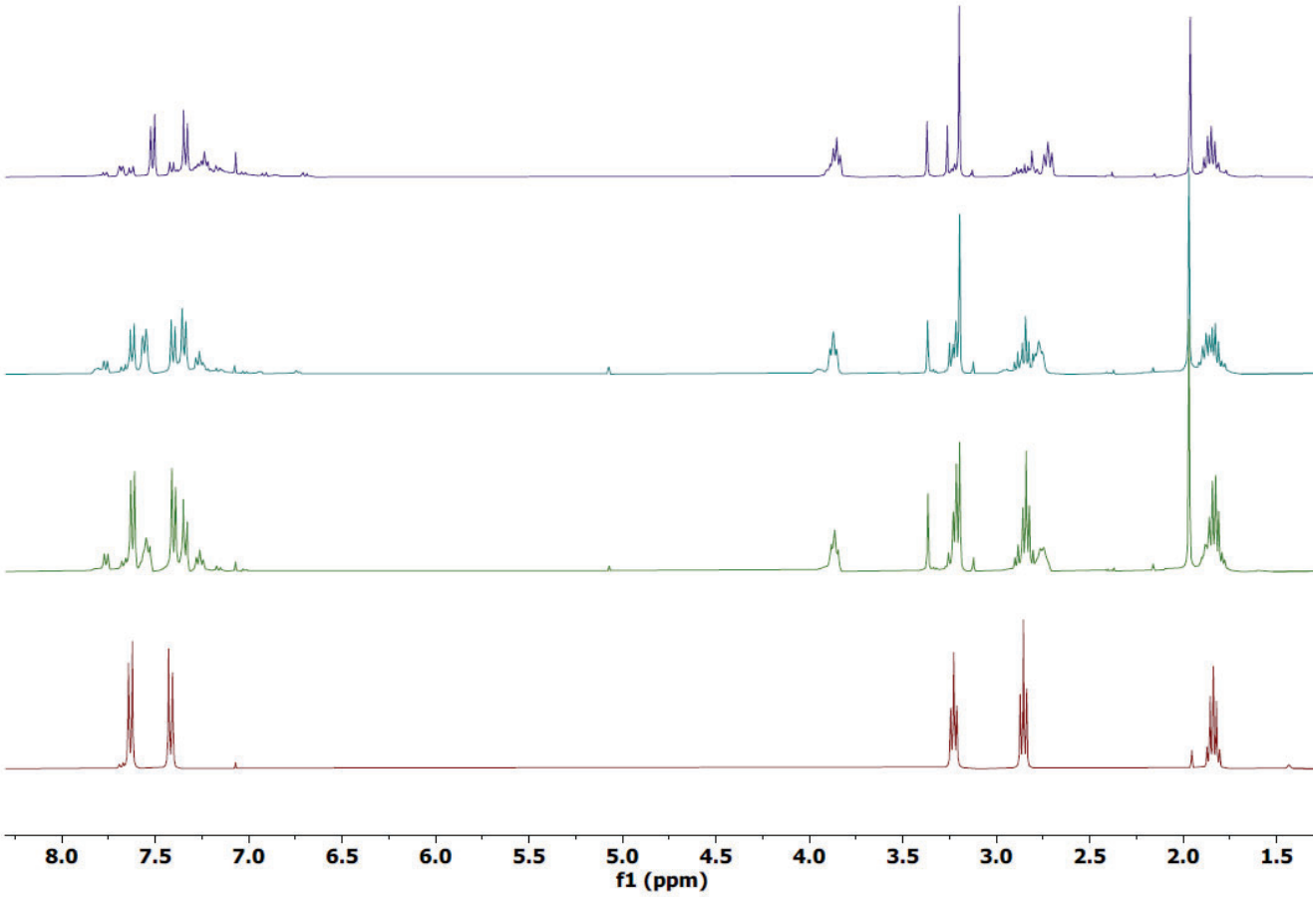

Figure S172.. Progress of the reaction of Methoxy Azide with TTMSS in argon saturated MeOH upon irradiation at 340 nm

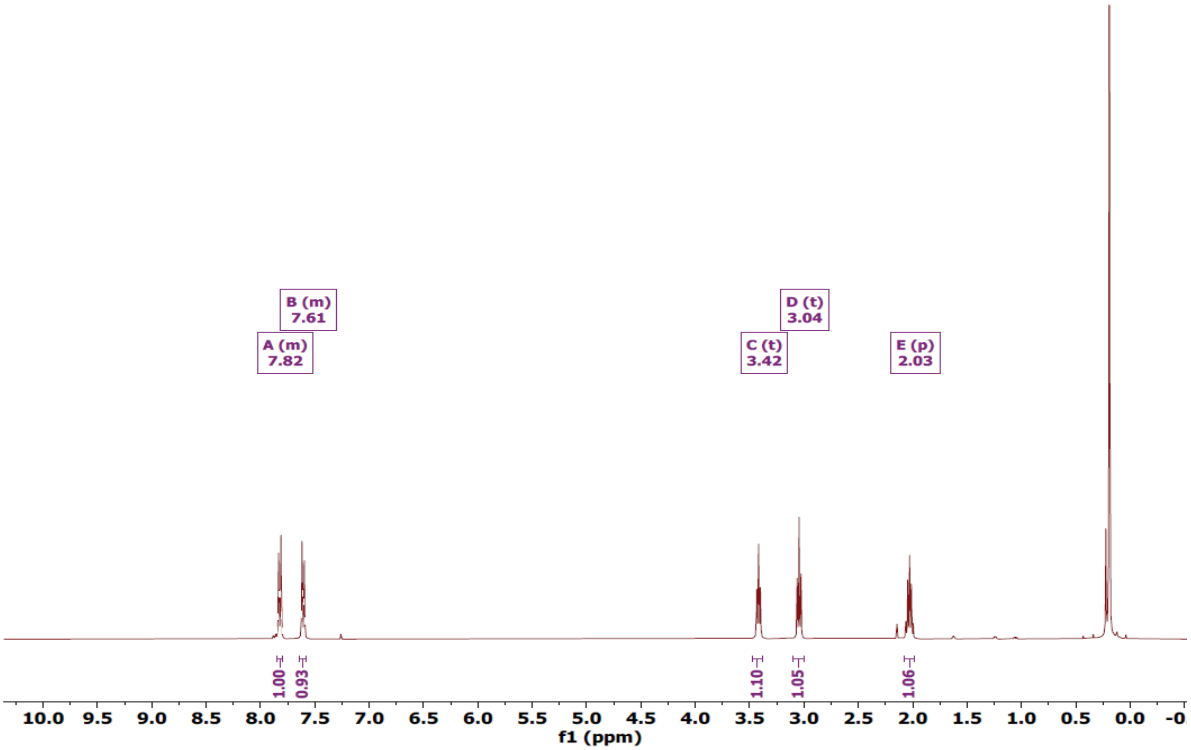

Figure S173. Bromo Azide with TTMSS in argon saturated MeOH at 0 h irradiation at 340 nm

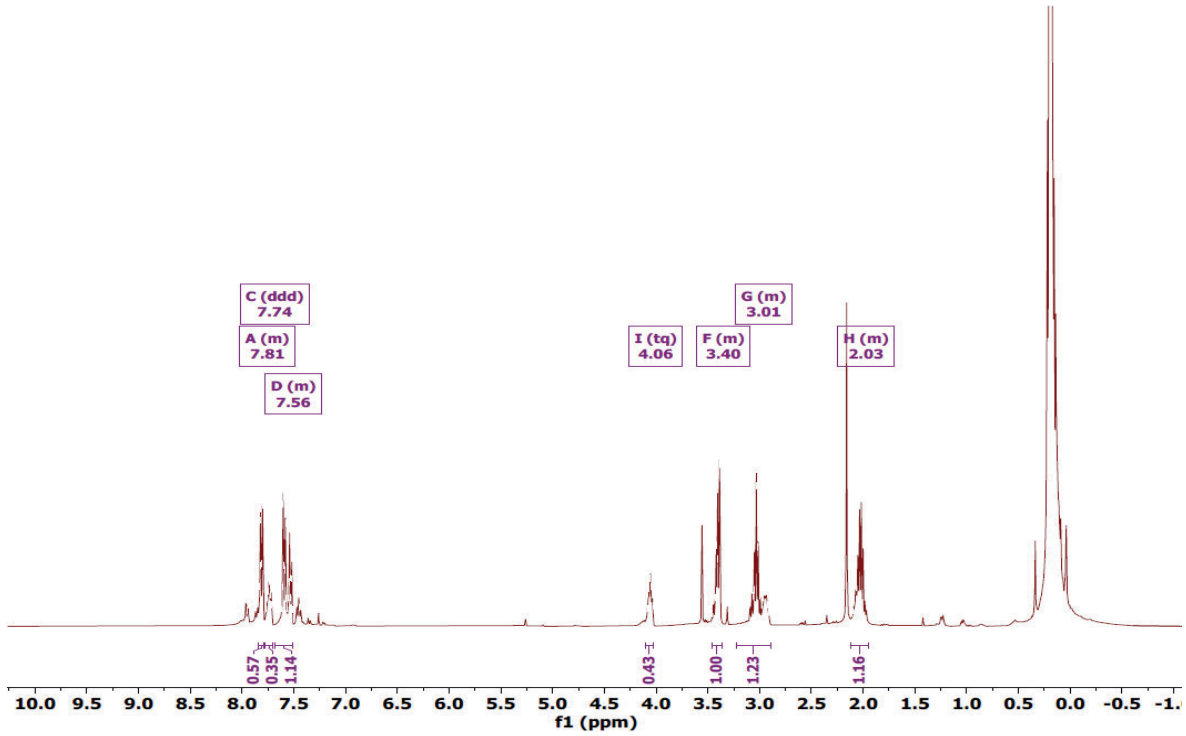

Figure S174. Bromo Azide with TTMSS in argon saturated MeOH at 1 h irradiation at 340 nm

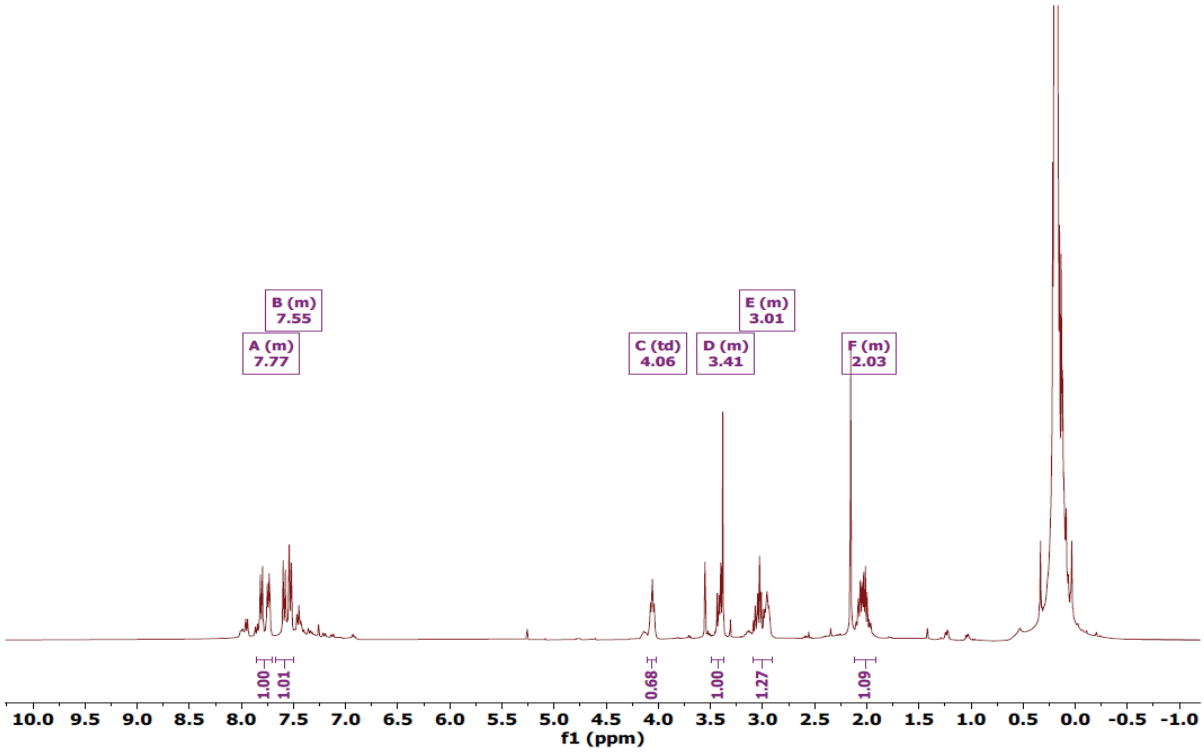

Figure S175. Bromo Azide with TTMSS in argon saturated MeOH at 2. h irradiation at 340 nm

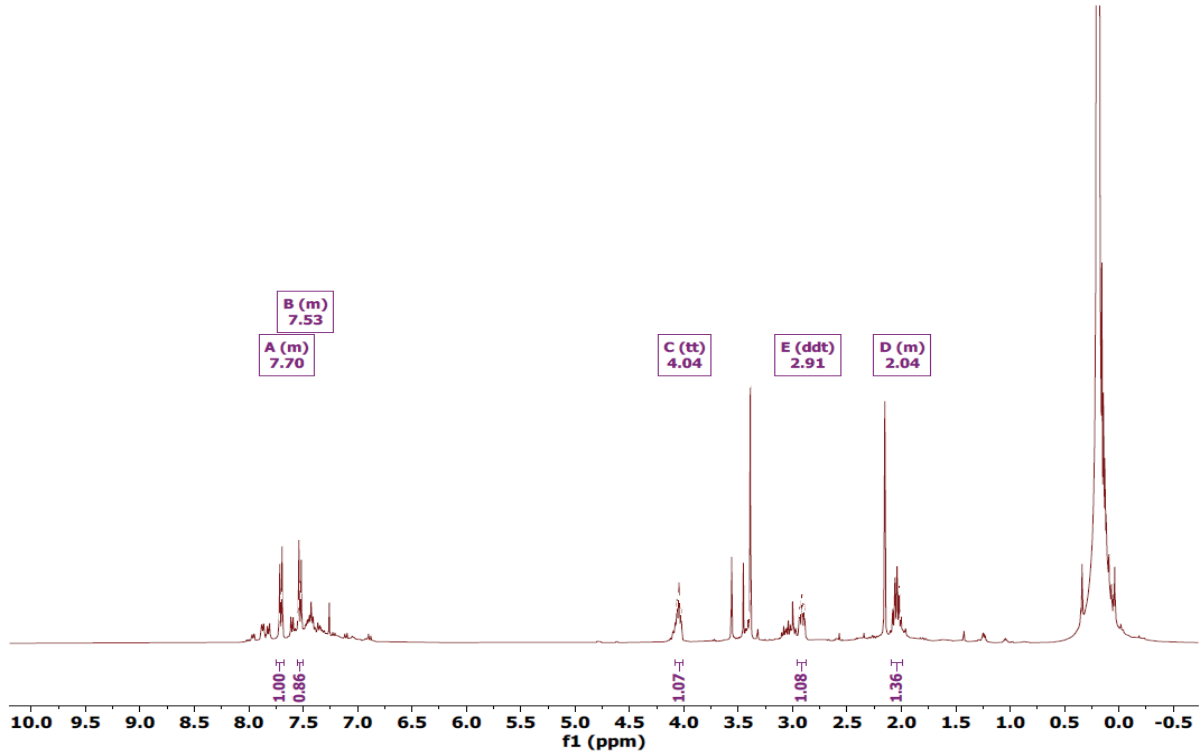

Figure S176. Bromo Azide with TTMSS in argon saturated MeOH at 2. h irradiation at 340 nm

IV. Quantum chemical calculations

I. Optimizations

S_0 of 1a

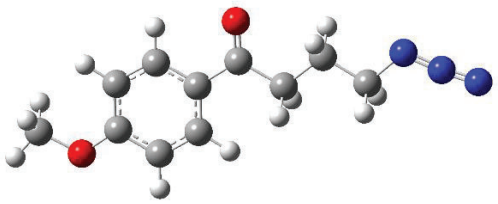

DFT/B3LYP 6-31+G(d), E = -741.655473 a.u

Standard Orientation:

Center Number	Atomic Number	Atomic Type	Coordinates (Angstroms) X	Y	Z
1	6	0	-3.56916	0.846196	-7E-06
2	6	0	-2.243133	1.272828	-5E-05
3	6	0	-1.177863	0.359306	-3E-05
4	6	0	-1.482908	-1.016543	7.2E-05
5	6	0	-2.798703	-1.4584	0.00014
6	6	0	-3.852958	-0.529269	0.00012
7	1	0	-4.365667	1.581801	-8E-05
8	1	0	-2.012394	2.333708	-0.0001
9	1	0	-0.689265	-1.757479	7.7E-05
10	1	0	-3.038055	-2.517459	0.0002
11	6	0	0.217615	0.889479	-7E-05
12	8	0	0.433276	2.095834	-0.0002
13	6	0	1.380781	-0.103769	-0.0002
14	1	0	1.275519	-0.76004	-0.8771
15	1	0	1.275211	-0.76104	0.87587
16	6	0	2.751735	0.575561	0.00048
17	1	0	2.847957	1.226435	-0.875
18	1	0	2.847821	1.22494	0.87712
19	6	0	3.882212	-0.44885	-0.0002
20	1	0	3.82183	-1.093944	-0.8893
21	1	0	3.82155	-1.095531	0.88762
22	8	0	-5.105785	-1.057842	0.00024

23	6	0	-6.226052	-0.177134	-0.0003
24	1	0	-7.1061	-0.821801	-0.0002
25	1	0	-6.233986	0.454448	0.89684
26	1	0	-6.233636	0.453866	-0.8978
27	7	0	5.178487	0.274767	0.00064
28	7	0	6.186725	-0.435475	5.4E-05
29	7	0	7.189058	-0.986189	-0.0005

S_0 of 1b

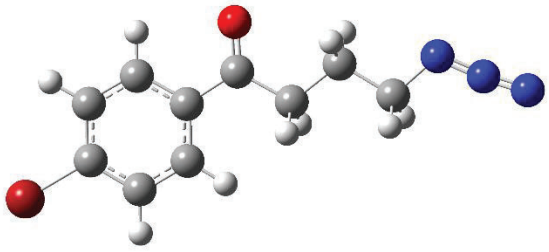

DFT/B3LYP 6-31+G(d), E = -3198.254656 a.u

Standard Orientation:

Center Number	Atomic Number	Atomic Type	Coordinates (Angstroms) X	Y	Z
1	6	0	2.745594	1.260713	-0.000169
2	6	0	1.396789	1.603956	-0.000052
3	6	0	0.400409	0.613557	0.000072
4	6	0	0.787874	-0.735729	0.000105
5	6	0	2.135628	-1.09477	-0.000083
6	6	0	3.10325	-0.090055	-0.000272
7	1	0	3.511438	2.029258	-0.000176
8	1	0	1.09374	2.646265	-0.000058
9	1	0	0.043506	-1.525741	0.000199
10	1	0	2.428902	-2.139176	-0.000014
11	6	0	-1.036143	1.048018	-0.000025
12	8	0	-1.324548	2.236534	0.000216
13	6	0	-2.126243	-0.021018	-0.000303
14	1	0	-1.974719	-0.66912	0.875956

15	1	0	-1.97486	-0.668564	-0.876995
16	6	0	-3.540856	0.561677	0.000021
17	1	0	-3.681922	1.203027	0.876465
18	1	0	-3.682113	1.203545	-0.876015
19	6	0	-4.597451	-0.538963	-0.000186
20	1	0	-4.49151	-1.179197	0.888129
21	1	0	-4.491688	-1.178691	-0.888888
22	7	0	-5.938781	0.095048	0.000124
23	7	0	-6.896706	-0.682563	0.000043
24	7	0	-7.859118	-1.2998	0.000147
25	35	0	4.944707	-0.572771	0.000081

T1 of 1a

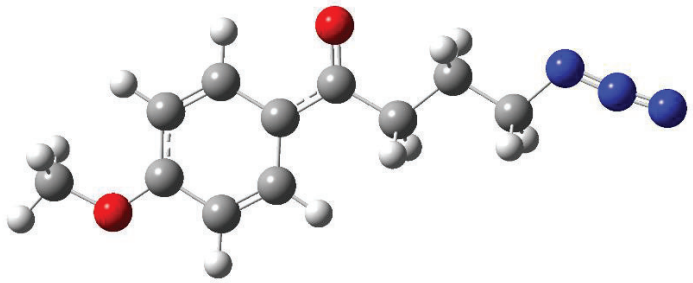

DFT/B3LYP 6-31+G(d), E = -741.543692 a.u

Standard Orientation:

Center Number	Atomic Number	Atomic Type	Coordinates (Angstroms) X	Y	Z
1	6	0	3.55865	0.89795	-0.000088
2	6	0	2.256072	1.311914	-0.000156
3	6	0	1.13501	0.334619	-0.000024
4	6	0	1.488536	-1.081289	0.000205
5	6	0	2.788743	-1.472658	0.00027
6	6	0	3.865115	-0.492716	0.000121
7	1	0	4.354913	1.635562	-0.000193
8	1	0	1.991806	2.361961	-0.000312
9	1	0	0.703224	-1.829387	0.000323
10	1	0	3.067279	-2.522716	0.000437

11	6	0	-0.206767	0.822828	-0.000122
12	8	0	-0.412865	2.073923	-0.000288
13	6	0	-1.381806	-0.155982	0.000021
14	1	0	-1.30546	-0.818649	0.877355
15	1	0	-1.305417	-0.818958	-0.877076
16	6	0	-2.74029	0.550405	-0.000136
17	1	0	-2.822572	1.203289	0.875365
18	1	0	-2.822528	1.202984	-0.875869
19	6	0	-3.890685	-0.450829	0.000009
20	1	0	-3.843346	-1.097644	0.888608
21	1	0	-3.843295	-1.097958	-0.888359
22	8	0	5.106002	-1.030855	0.000203
23	6	0	6.245101	-0.167634	0.000095
24	1	0	7.113062	-0.827439	0.000207
25	1	0	6.255356	0.460708	-0.897868
26	1	0	6.255325	0.460974	0.897872
27	7	0	-5.175675	0.294986	-0.000165
28	7	0	-6.195563	-0.397265	-0.000041
29	7	0	-7.207264	-0.931567	0.000066

T1 of 1b

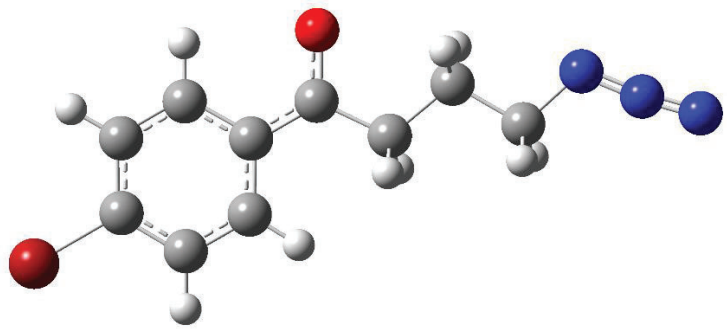

DFT/B3LYP 6-31+G(d), E = -3198.142444 a.u

Standard Orientation:

Center Number	Atomic Number	Atomic Type	Coordinates (Angstroms) X	Y	Z
1	6	0	-2.739412	1.264314	0.002095
2	6	0	-1.395465	1.603394	0.00174
3	6	0	-0.384954	0.595295	-0.000395
4	6	0	-0.804919	-0.766243	-0.002697
5	6	0	-2.152823	-1.096969	-0.002061
6	6	0	-3.118834	-0.084212	0.000319
7	1	0	-3.496196	2.042369	0.003959
8	1	0	-1.108166	2.65107	0.003642
9	1	0	-0.071871	-1.566711	-0.004815
10	1	0	-2.455603	-2.139201	-0.003545
11	6	0	0.993452	0.94051	-0.000553
12	8	0	1.372507	2.207168	-0.003968
13	6	0	2.141722	-0.065523	-0.002318
14	1	0	2.020289	-0.709207	-0.887169
15	1	0	2.018151	-0.714003	0.878641
16	6	0	3.548759	0.550904	0.000985
17	1	0	3.69002	1.189827	-0.877755
18	1	0	3.687975	1.184941	0.883598
19	6	0	4.618094	-0.53855	-0.000826
20	1	0	4.517553	-1.17567	-0.891718
21	1	0	4.515514	-1.180654	0.886249
22	7	0	5.947642	0.115357	0.00253
23	7	0	6.918088	-0.648156	0.001607
24	7	0	7.890617	-1.248023	0.001257
25	35	0	-4.966453	-0.548339	0.000719

T1 Azide of 1a

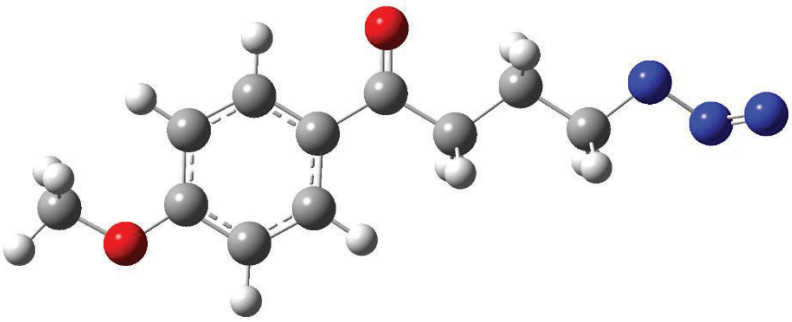

DFT/B3LYP 6-31+G(d), E = -741.586449 a.u

Standard Orientation:

Center Number	Atomic Number	Atomic Type	Coordinates (Angstroms) X	Y	Z
1	6	0	3.572392	0.847752	-0.018448
2	6	0	2.247031	1.276075	-0.013401
3	6	0	1.180714	0.363742	0.001881
4	6	0	1.484012	-1.012542	0.012218
5	6	0	2.799152	-1.455978	0.007421
6	6	0	3.85453	-0.528105	-0.007964
7	1	0	4.369778	1.582277	-0.030343
8	1	0	2.017661	2.337211	-0.021395
9	1	0	0.689629	-1.752613	0.024264
10	1	0	3.037292	-2.515258	0.015364
11	6	0	-0.213492	0.895297	0.006551
12	8	0	-0.429343	2.101689	-0.003367
13	6	0	-1.378339	-0.096287	0.024348
14	1	0	-1.269631	-0.744757	0.906464
15	1	0	-1.2818	-0.762083	-0.846265
16	6	0	-2.747923	0.587188	0.026966
17	1	0	-2.833612	1.24681	0.896992
18	1	0	-2.845964	1.229812	-0.854268
19	6	0	-3.884171	-0.43629	0.047771
20	1	0	-3.829342	-1.098294	0.928137
21	1	0	-3.834657	-1.101837	-0.832744
22	8	0	5.106389	-1.058149	-0.011558
23	6	0	6.228052	-0.179101	-0.02686
24	1	0	7.106995	-0.825223	-0.026871

25	1	0	6.230773	0.44398	-0.929866
26	1	0	6.242625	0.460079	0.864709
27	7	0	-5.17021	0.238705	0.050113
28	7	0	-6.201061	-0.743552	0.259423
29	7	0	-7.209853	-0.697857	-0.357777

T1 Azide of 1b

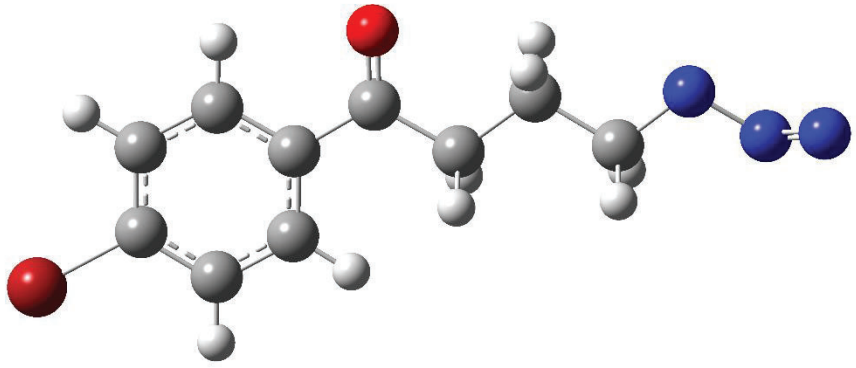

DFT/B3LYP 6-31+G(d), E = - 3198.185499 a.u

Standard Orientation:

Center Number	Atomic Number	Atomic Type	Coordinates (Angstroms) X	Y	Z
1	6	0	-2.748743	1.26192	0.020099
2	6	0	-1.40044	1.606709	0.016469
3	6	0	-0.403069	0.61736	-0.001392
4	6	0	-0.78897	-0.732384	-0.015638
5	6	0	-2.136329	-1.092732	-0.01213
6	6	0	-3.105097	-0.089133	0.005766
7	1	0	-3.515393	2.029552	0.033822
8	1	0	-1.098535	2.649291	0.027419
9	1	0	-0.044004	-1.521748	-0.029684
10	1	0	-2.428466	-2.137387	-0.023211
11	6	0	1.032235	1.053421	-0.004351
12	8	0	1.32065	2.241947	0.009438

13	6	0	2.124449	-0.013749	-0.025104
14	1	0	1.970026	-0.651117	-0.908577
15	1	0	1.981734	-0.673142	0.844147
16	6	0	3.537804	0.573798	-0.027088
17	1	0	3.66833	1.22778	-0.895805
18	1	0	3.680398	1.205803	0.855738
19	6	0	4.600595	-0.525765	-0.050989
20	1	0	4.50052	-1.179171	-0.933712
21	1	0	4.505514	-1.188797	0.82751
22	7	0	5.92919	0.060995	-0.052061
23	7	0	6.891048	-0.990481	-0.259011
24	7	0	7.900157	-1.011122	0.358586
25	35	0	-4.945791	-0.573401	0.010297

Triplet Nitrene of 1a

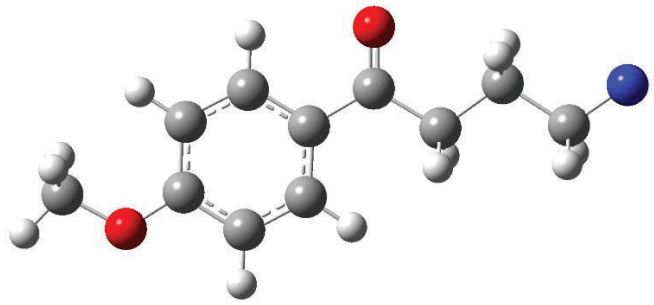

DFT/B3LYP 6-31+G(d), E = -632.110003 a.u

Standard Orientation:

Center Number	Atomic Number	Atomic Type	Coordinates (Angstroms) X	Y	Z
1	6	0	2.595999	0.935062	0.000011
2	6	0	1.244481	1.272335	0.00003
3	6	0	0.242575	0.289713	0.00002
4	6	0	0.638628	-1.062737	-0.00001
5	6	0	1.980969	-1.415826	-0.000025
6	6	0	2.970866	-0.418403	-0.000016

7	1	0	3.341626	1.722183	0.000018
8	1	0	0.943513	2.315461	0.000054
9	1	0	-0.103834	-1.854948	-0.000017
10	1	0	2.290437	-2.456552	-0.000047
11	6	0	-1.185233	0.725329	0.000051
12	8	0	-1.481574	1.914641	0.000062
13	6	0	-2.279345	-0.343485	-0.000009
14	1	0	-2.132963	-0.991909	0.876519
15	1	0	-2.132816	-0.992001	-0.876438
16	6	0	-3.693135	0.242547	-0.000166
17	1	0	-3.834079	0.88275	0.876475
18	1	0	-3.83415	0.882099	-0.877278
19	6	0	-4.768239	-0.872164	0.000283
20	1	0	-4.640304	-1.521393	0.888107
21	1	0	-4.639983	-1.522445	-0.886729
22	8	0	4.256175	-0.862056	-0.000037
23	6	0	5.314862	0.09176	-0.000009
24	1	0	6.236069	-0.492577	-0.000016
25	1	0	5.280359	0.722157	-0.897307
26	1	0	5.280347	0.722119	0.897315
27	7	0	-6.089372	-0.357202	-0.000259

Triplet Nitrene of 1b

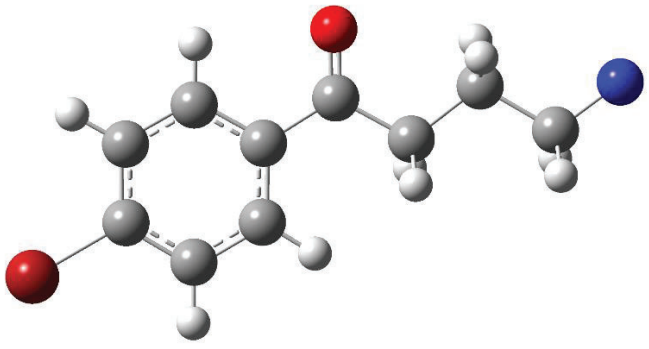

DFT/B3LYP 6-31+G(d), E = -3088.709132 a.u

Standard Orientation:

Center Number	Atomic Number	Atomic Type	Coordinates (Angstroms) X	Y	Z
1	6	0	1.78961	1.297963	0.000026
2	6	0	0.418197	1.535087	0.000015
3	6	0	-0.497832	0.469892	-0.000024
4	6	0	-0.006419	-0.845156	-0.000061
5	6	0	1.365207	-1.097932	-0.000053
6	6	0	2.251549	-0.020767	-0.000011
7	1	0	2.493264	2.123852	0.000063
8	1	0	0.034688	2.550563	0.000045
9	1	0	-0.686951	-1.690804	-0.000089
10	1	0	1.73905	-2.116273	-0.000076
11	6	0	-1.963779	0.790608	-0.000019
12	8	0	-2.344712	1.952998	0.000013
13	6	0	-2.967063	-0.360373	-0.000037
14	1	0	-2.768168	-0.994824	0.876486
15	1	0	-2.768132	-0.994817	-0.876555
16	6	0	-4.423407	0.109842	-0.000075
17	1	0	-4.615236	0.736367	0.876838
18	1	0	-4.615286	0.736059	-0.877199
19	6	0	-5.405136	-1.087575	0.000151
20	1	0	-5.225852	-1.724727	0.887755
21	1	0	-5.225743	-1.725161	-0.887122
22	7	0	-6.762953	-0.678095	-0.000036
23	35	0	4.12489	-0.357916	0.000015

Triplet Nitrene of 1a and TTMSS

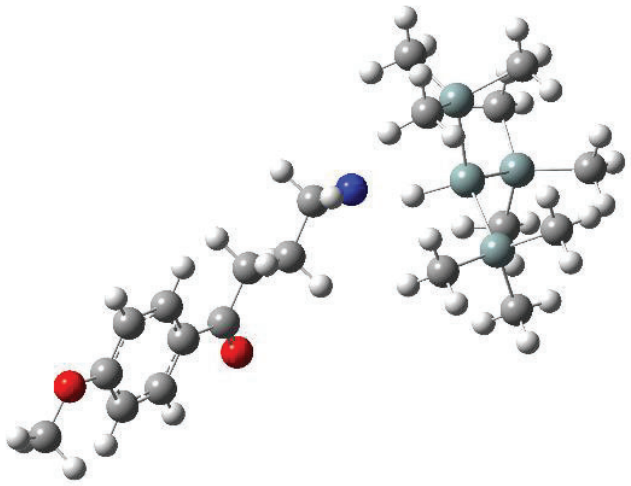

DFT/B3LYP 6-31+G(d), E = -2150.045435 a.u

Standard Orientation:

Center Number	Atomic Number	Atomic Type	Coordinates (Angstroms) X	Y	Z
1	6	0	-7.434757	0.118474	0.716416
2	6	0	-6.381313	-0.778871	0.875852
3	6	0	-5.249371	-0.736921	0.047473
4	6	0	-5.201166	0.245125	-0.962113
5	6	0	-6.242274	1.146861	-1.134278
6	6	0	-7.368174	1.090202	-0.29536
7	1	0	-8.293062	0.055172	1.375828
8	1	0	-6.422221	-1.534001	1.654834
9	1	0	-4.34396	0.313199	-1.624999
10	1	0	-6.208941	1.905276	-1.910538
11	6	0	-4.158911	-1.730351	0.277174
12	8	0	-4.245487	-2.565553	1.170183
13	6	0	-2.925122	-1.688745	-0.625392
14	1	0	-2.475556	-0.687242	-0.556188
15	1	0	-3.253942	-1.794783	-1.669859
16	6	0	-1.890226	-2.76204	-0.280104
17	1	0	-1.561214	-2.644901	0.757293
18	1	0	-2.341906	-3.756561	-0.352394
19	6	0	-0.6611	-2.6849	-1.219482
20	1	0	-0.193757	-1.683774	-1.150747

21	1	0	-0.98012	-2.815235	-2.27193
22	8	0	-8.335028	2.014334	-0.541268
23	6	0	-9.506521	2.019447	0.269902
24	1	0	-10.123285	2.834858	-0.11064
25	1	0	-10.054341	1.072998	0.181062
26	1	0	-9.259168	2.206999	1.322233
27	7	0	0.319605	-3.661995	-0.91696
28	14	0	3.044637	0.306922	0.011482
29	1	0	1.638002	-0.135683	-0.294529
30	14	0	3.82244	1.343647	-1.98138
31	14	0	4.256159	-1.663115	0.571571
32	14	0	2.840582	1.831523	1.824036
33	6	0	4.644707	-2.690362	-0.981097
34	1	0	5.271935	-2.142319	-1.694732
35	1	0	5.184535	-3.605262	-0.700661
36	1	0	3.727531	-2.99566	-1.498844
37	6	0	5.901335	-1.201135	1.41236
38	1	0	5.741408	-0.661872	2.354266
39	1	0	6.475247	-2.108166	1.646248
40	1	0	6.528198	-0.570249	0.770069
41	6	0	3.237908	-2.744067	1.756036
42	1	0	2.317495	-3.09635	1.275017
43	1	0	3.816285	-3.630257	2.051655
44	1	0	2.959486	-2.208029	2.671041
45	6	0	4.430274	2.858432	2.029386
46	1	0	4.334877	3.542996	2.883196
47	1	0	5.305752	2.223072	2.211501
48	1	0	4.640699	3.467133	1.141293
49	6	0	2.507807	0.916013	3.458887
50	1	0	2.36253	1.637424	4.274746
51	1	0	1.604923	0.295953	3.400231
52	1	0	3.342362	0.262638	3.740611
53	6	0	1.385078	3.017472	1.512533
54	1	0	1.284091	3.727277	2.345048
55	1	0	0.437891	2.470827	1.425644
56	1	0	1.518843	3.599067	0.592845
57	6	0	3.036467	3.062004	-2.217203
58	1	0	3.323369	3.757701	-1.4193
59	1	0	3.361646	3.500575	-3.170678
60	1	0	1.940943	3.007763	-2.233986
61	6	0	3.360014	0.28003	-3.489772

62	1	0	3.790908	-0.726211	-3.429781
63	1	0	2.272357	0.169799	-3.581434
64	1	0	3.726373	0.746408	-4.414667
65	6	0	5.71335	1.557127	-1.941398
66	1	0	6.060723	2.059489	-2.854438
67	1	0	6.037665	2.163269	-1.086555
68	1	0	6.230813	0.591911	-1.879205

Methoxy Nitrene-H of 1a and Silyl Radical

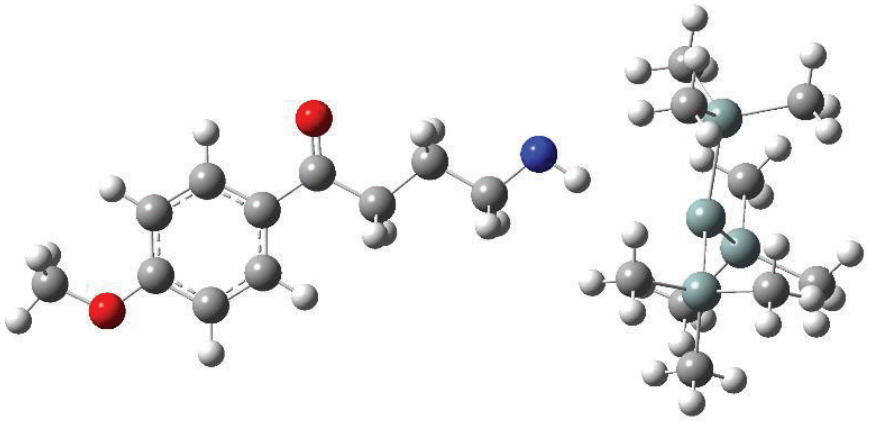

DFT/B3LYP 6-31+G(d), E = -2150.051922 a.u

Standard Orientation:

Center Number	Atomic Number	Atomic Type	Coordinates (Angstroms) X	Y	Z
1	6	0	-8.525511	-0.563223	0.030867
2	6	0	-7.295192	-1.216827	0.050261
3	6	0	-6.085565	-0.50598	0.050166
4	6	0	-6.143446	0.901692	0.029837
5	6	0	-7.360905	1.568742	0.010383
6	6	0	-8.56227	0.84032	0.010732
7	1	0	-9.439152	-1.147068	0.031552
8	1	0	-7.254821	-2.301685	0.065917
9	1	0	-5.231294	1.490525	0.029055
10	1	0	-7.409503	2.653373	-0.005337

11	6	0	-4.803657	-1.274931	0.071539
12	8	0	-4.80954	-2.500322	0.088908
13	6	0	-3.484702	-0.503453	0.071332
14	1	0	-3.482137	0.175104	0.938169
15	1	0	-3.468772	0.151865	-0.813046
16	6	0	-2.247054	-1.402328	0.092509
17	1	0	-2.269036	-2.049611	0.976231
18	1	0	-2.256311	-2.073066	-0.773775
19	6	0	-0.946695	-0.596133	0.090925
20	1	0	-0.915835	0.091792	0.959291
21	1	0	-0.904654	0.069189	-0.794541
22	8	0	-9.70315	1.581807	-0.009202
23	6	0	-10.960028	0.9114	-0.010355
24	1	0	-11.713588	1.700143	-0.027731
25	1	0	-11.071272	0.278475	-0.899726
26	1	0	-11.086334	0.303613	0.894406
27	7	0	0.219297	-1.447772	0.107822
28	14	0	3.919293	0.169493	0.005605
29	1	0	1.048742	-0.830047	0.10965
30	14	0	3.941116	1.73378	-1.768549
31	14	0	4.478395	-2.075024	-0.506953
32	14	0	4.392204	0.979177	2.177422
33	6	0	3.958301	-2.481462	-2.29019
34	1	0	4.462167	-1.841676	-3.024896
35	1	0	4.217255	-3.522748	-2.526194
36	1	0	2.8763	-2.371078	-2.428753
37	6	0	6.358894	-2.344679	-0.354109
38	1	0	6.716022	-2.147825	0.664136
39	1	0	6.612792	-3.385503	-0.599513
40	1	0	6.919907	-1.694004	-1.035823
41	6	0	3.593106	-3.271418	0.670964
42	1	0	2.50327	-3.180587	0.59301
43	1	0	3.86289	-4.307484	0.423279
44	1	0	3.873085	-3.09744	1.716684
45	6	0	6.071247	1.878373	2.225052
46	1	0	6.276501	2.247759	3.239603
47	1	0	6.894246	1.212363	1.939048
48	1	0	6.090419	2.740814	1.547799
49	6	0	4.446532	-0.453046	3.426838
50	1	0	4.637382	-0.063716	4.436347
51	1	0	3.498872	-1.003753	3.456356

52	1	0	5.243022	-1.170025	3.193782
53	6	0	3.046006	2.204474	2.731851
54	1	0	3.272607	2.591379	3.73494
55	1	0	2.060538	1.724788	2.774604
56	1	0	2.971008	3.06246	2.053278
57	6	0	3.618364	3.492291	-1.116965
58	1	0	4.39223	3.817353	-0.411117
59	1	0	3.610976	4.207156	-1.95122
60	1	0	2.649218	3.565951	-0.608913
61	6	0	2.587722	1.316005	-3.038826
62	1	0	2.711285	0.307732	-3.451029
63	1	0	1.587222	1.372186	-2.592699
64	1	0	2.619467	2.025854	-3.876909
65	6	0	5.621462	1.72949	-2.666182
66	1	0	5.615679	2.457887	-3.489143
67	1	0	6.442154	1.996018	-1.989304
68	1	0	5.850119	0.746239	-3.095015

Nitrene-H Rotated of 1a

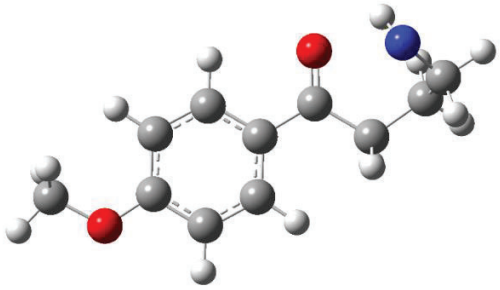

DFT/B3LYP 6-31+G(d), E = -632.750328 a.u

Standard Orientation:

Center Number	Atomic Number	Atomic Type	Coordinates (Angstroms) X	Y	Z
1	6	0	-2.319613	0.978083	-0.148037
2	6	0	-0.947644	1.107099	-0.349778
3	6	0	-0.089171	-0.001821	-0.292627
4	6	0	-0.653605	-1.265334	-0.025235
5	6	0	-2.019111	-1.411585	0.175078
6	6	0	-2.863161	-0.289657	0.116156
7	1	0	-2.950552	1.858453	-0.196567
8	1	0	-0.517213	2.082281	-0.555129
9	1	0	-0.026286	-2.149648	0.027314
10	1	0	-2.457974	-2.383182	0.380637
11	6	0	1.368638	0.211484	-0.522929
12	8	0	1.801089	1.327654	-0.797983
13	6	0	2.311373	-0.990861	-0.443809
14	1	0	2.023411	-1.676083	-1.255092
15	1	0	2.121313	-1.540219	0.488524
16	6	0	3.801935	-0.640916	-0.562205
17	1	0	4.345139	-1.535945	-0.893183
18	1	0	3.935085	0.122453	-1.33762
19	6	0	4.450171	-0.167318	0.755847
20	1	0	5.521807	0.031038	0.553055
21	1	0	4.434681	-0.979254	1.497877
22	8	0	-4.184192	-0.532651	0.328175
23	6	0	-5.100734	0.557749	0.290617
24	1	0	-6.081735	0.123328	0.488213
25	1	0	-4.865682	1.29977	1.063814

26	1	0	-5.104561	1.03865	-0.695541
27	7	0	3.914268	1.022539	1.374009
28	1	0	3.653049	1.669032	0.615633

Nitrene-H Rotated of 1b

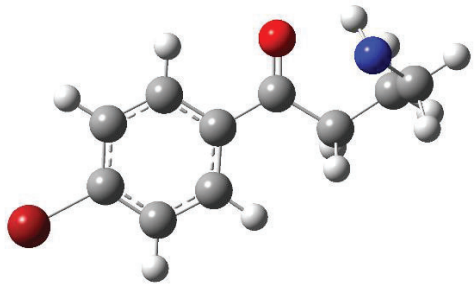

DFT/B3LYP 6-31+G(d), E = -3089.349682 a.u

Standard Orientation

Center Number	Atomic Number	Atomic Type	Coordinates (Angstroms) X	Y	Z
1	6	0	-1.530406	1.24584	-0.175347
2	6	0	-0.150027	1.30351	-0.340667
3	6	0	0.62751	0.133219	-0.33884
4	6	0	-0.013121	-1.104675	-0.170215
5	6	0	-1.396883	-1.178382	-0.009988
6	6	0	-2.14251	0.000351	-0.013064
7	1	0	-2.125809	2.152824	-0.173245
8	1	0	0.349009	2.258397	-0.471547
9	1	0	0.557342	-2.027874	-0.164775
10	1	0	-1.887324	-2.137612	0.117198
11	6	0	2.108682	0.264223	-0.530072
12	8	0	2.607016	1.36536	-0.732058
13	6	0	2.971126	-0.996084	-0.507029
14	1	0	2.669019	-1.603303	-1.37374
15	1	0	2.716323	-1.595207	0.37782
16	6	0	4.483047	-0.732673	-0.555641
17	1	0	4.982966	-1.636026	-0.92843
18	1	0	4.689837	0.070467	-1.272308

19	6	0	5.107663	-0.38944	0.81452
20	1	0	6.193801	-0.235518	0.658857
21	1	0	5.017218	-1.248864	1.494084
22	7	0	4.599209	0.781235	1.490004
23	35	0	-4.031095	-0.090881	0.2098
24	1	0	4.484849	1.516703	0.777586

Nitrene-H Cyclized of 1a

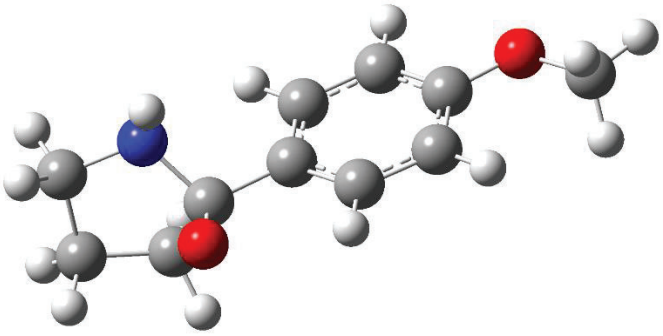

DFT/B3LYP 6-31+G(d), E = -632.746269 a.u

Standard Orientation:

Center Number	Atomic Number	Atomic Type	Coordinates (Angstroms) X	Y	Z
1	6	0	-2.132303	0.973945	-0.026431
2	6	0	-0.747168	1.185604	-0.023054
3	6	0	0.150401	0.118419	-0.000943
4	6	0	-0.36729	-1.187806	0.027091
5	6	0	-1.737872	-1.416318	0.031281
6	6	0	-2.631354	-0.332795	0.000254
7	1	0	-2.798834	1.829246	-0.043928
8	1	0	-0.357706	2.199287	-0.027402
9	1	0	0.310452	-2.037376	0.063983
10	1	0	-2.141327	-2.424364	0.060953
11	6	0	1.64999	0.382387	-0.030627
12	8	0	1.999799	1.680766	0.229293
13	6	0	2.407953	-0.194271	-1.248087
14	1	0	2.264558	0.446875	-2.122824
15	1	0	2.024784	-1.193018	-1.489113

16	6	0	3.869971	-0.249783	-0.769993
17	1	0	4.460077	-1.00157	-1.303767
18	1	0	4.346646	0.72305	-0.916334
19	6	0	3.771043	-0.555099	0.743091
20	1	0	4.466427	0.049007	1.335798
21	1	0	3.97258	-1.612872	0.962901
22	8	0	-3.960396	-0.659	0.003699
23	6	0	-4.916381	0.391942	-0.023637
24	1	0	-5.893102	-0.095222	-0.016262
25	1	0	-4.824424	1.038923	0.858831
26	1	0	-4.817716	0.998438	-0.933713
27	7	0	2.369139	-0.277328	1.090915
28	1	0	2.186439	0.149404	1.996859

Nitrene-H Cyclized of 1b

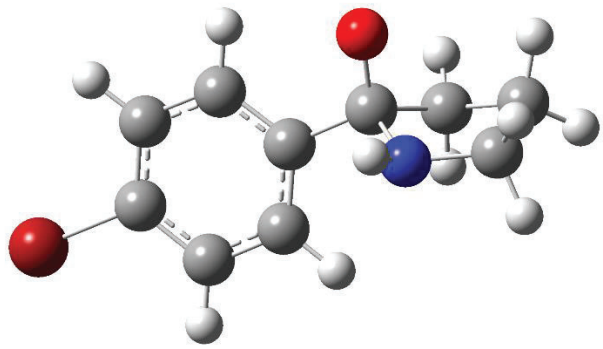

DFT/B3LYP 6-31+G(d), E = -3089.348963 a.u

Standard Orientation:

Center Number	Atomic Number	Atomic Type	Coordinates (Angstroms) X	Y	Z
1	6	0	-1.361757	1.268741	-0.021885
2	6	0	0.032014	1.371813	-0.008403
3	6	0	0.834601	0.227671	0.023182
4	6	0	0.221353	-1.031679	0.053339
5	6	0	-1.168573	-1.151837	0.049412
6	6	0	-1.94766	0.005212	0.0057

7	1	0	-1.980113	2.160078	-0.04892
8	1	0	0.505582	2.348883	-0.011841
9	1	0	0.831267	-1.930506	0.097047
10	1	0	-1.639111	-2.129216	0.079492
11	6	0	2.351591	0.371097	-0.006405
12	8	0	2.803598	1.623244	0.309338
13	6	0	3.044516	-0.207262	-1.261049
14	1	0	2.945753	0.483625	-2.103421
15	1	0	2.577064	-1.158771	-1.54146
16	6	0	4.501122	-0.40484	-0.805139
17	1	0	5.022881	-1.173065	-1.384367
18	1	0	5.053705	0.532655	-0.907949
19	6	0	4.389539	-0.779426	0.69087
20	1	0	5.139418	-0.270165	1.305328
21	1	0	4.498573	-1.860705	0.853326
22	7	0	3.019908	-0.399018	1.072726
23	35	0	-3.851168	-0.148963	-0.018234
24	1	0	2.887249	0.00111	1.999461

NH Cyclized of 1a with TTMSS

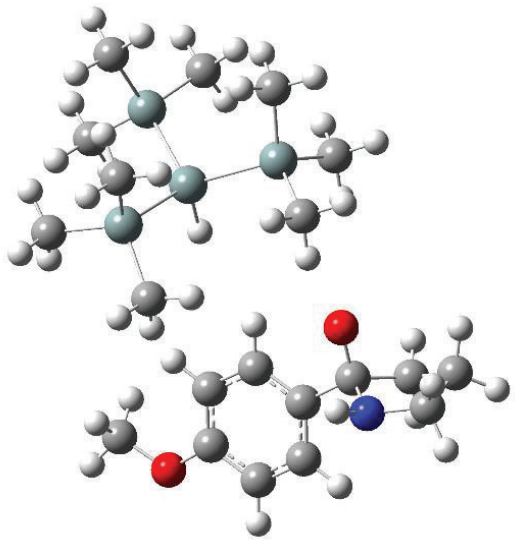

DFT/B3LYP 6-31+G(d), E = -2150.682069 a.u

Standard Orientation:

Center Number	Atomic Number	Atomic Type	Coordinates (Angstroms) X	Y	Z
1	6	0	-2.784517	-2.314196	0.408774
2	6	0	-2.638174	-0.921201	0.37293
3	6	0	-3.733439	-0.081853	0.169439
4	6	0	-4.99849	-0.667099	-0.010627
5	6	0	-5.160531	-2.046898	0.014716
6	6	0	-4.050961	-2.881131	0.230042
7	1	0	-1.908861	-2.933207	0.570364
8	1	0	-1.652028	-0.483683	0.495961
9	1	0	-5.866139	-0.036572	-0.19009
10	1	0	-6.135466	-2.502851	-0.131598
11	6	0	-3.547312	1.429292	0.168328
12	8	0	-2.243427	1.838914	0.073703
13	6	0	-4.324553	2.201994	1.258146
14	1	0	-3.806397	2.127281	2.218685
15	1	0	-5.327554	1.775064	1.376514
16	6	0	-4.46885	3.466392	-0.823717
17	1	0	-3.824232	4.171386	-1.359684
18	1	0	-5.494532	3.598924	-1.195733
19	8	0	-4.311787	-4.224305	0.242244
20	6	0	-3.231225	-5.122597	0.454557
21	1	0	-3.667272	-6.122825	0.426854
22	1	0	-2.474883	-5.031976	-0.336275
23	1	0	-2.759732	-4.956541	1.432202
24	7	0	-4.074698	2.070768	-1.064838
25	6	0	-4.383574	3.63955	0.71091
26	1	0	-3.465551	4.174423	0.968201
27	1	0	-5.230728	4.207597	1.108238
28	1	0	-3.524289	1.871902	-1.897629
29	14	0	2.272068	-0.063266	0.074772
30	1	0	0.949472	-0.631695	0.508976
31	14	0	2.568656	-0.785148	-2.169934
32	14	0	2.087104	2.29931	0.278842
33	14	0	3.869855	-1.005169	1.560159
34	6	0	1.066376	3.036928	-1.144099
35	1	0	0.046686	2.63448	-1.140034
36	1	0	0.995838	4.127572	-1.028184

37	1	0	1.515869	2.837296	-2.124589
38	6	0	1.224165	2.741129	1.913465
39	1	0	1.742312	2.321862	2.78406
40	1	0	1.184715	3.83192	2.040532
41	1	0	0.192874	2.368568	1.917125
42	6	0	3.818323	3.09506	0.257387
43	1	0	4.363574	2.864262	-0.666335
44	1	0	3.734499	4.188293	0.326979
45	1	0	4.43476	2.758371	1.100171
46	6	0	3.773932	-0.191324	3.278774
47	1	0	4.477538	-0.676925	3.969011
48	1	0	4.029019	0.874791	3.242847
49	1	0	2.770072	-0.278874	3.71221
50	6	0	5.640507	-0.781449	0.896551
51	1	0	6.369873	-1.198792	1.604126
52	1	0	5.783675	-1.292385	-0.06367
53	1	0	5.890121	0.276623	0.749761
54	6	0	3.535606	-2.866268	1.780891
55	1	0	3.602147	-3.41082	0.831568
56	1	0	4.266749	-3.308272	2.471764
57	1	0	2.535859	-3.043544	2.196436
58	6	0	0.97018	-0.506184	-3.162348
59	1	0	0.685093	0.552045	-3.186763
60	1	0	1.099885	-0.843569	-4.200029
61	1	0	0.129724	-1.063715	-2.731435
62	6	0	2.988398	-2.641411	-2.247053
63	1	0	3.944167	-2.866613	-1.758307
64	1	0	2.215142	-3.251693	-1.764366
65	1	0	3.065946	-2.969986	-3.292667
66	6	0	3.98317	0.173824	-3.009696
67	1	0	4.12575	-0.179292	-4.040145
68	1	0	3.773763	1.249672	-3.056016
69	1	0	4.935392	0.043735	-2.480716

NH Cyclized ketyl radical of 1a with Silyl radical

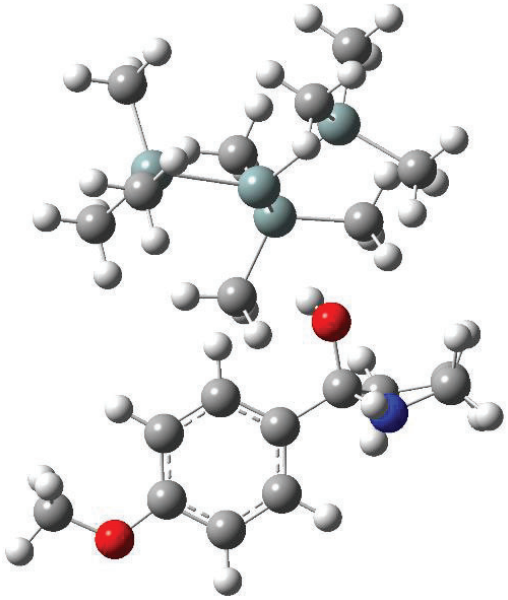

DFT/B3LYP 6-31+G(d), E = -2150.703170 a.u

Standard Orientation:

Center Number	Atomic Number	Atomic Type	Coordinates (Angstroms) X	Y	Z
1	6	0	-3.718626	-1.51935	-0.504831
2	6	0	-2.832273	-0.439253	-0.629452
3	6	0	-3.163993	0.837172	-0.17513
4	6	0	-4.433693	1.016566	0.405802
5	6	0	-5.324136	-0.040561	0.5386
6	6	0	-4.969772	-1.322008	0.085653
7	1	0	-3.420428	-2.493068	-0.877922
8	1	0	-1.875663	-0.605457	-1.113952
9	1	0	-4.730152	2.007498	0.737537
10	1	0	-6.30455	0.102782	0.983801
11	6	0	-2.206386	2.023309	-0.287875
12	8	0	-1.029614	1.674567	-1.062363
13	6	0	-1.766622	2.638761	1.063378
14	1	0	-0.924838	2.086136	1.494659
15	1	0	-2.593795	2.580144	1.776963

16	6	0	-2.001604	4.337317	-0.699843
17	1	0	-1.187313	4.414673	-1.434384
18	1	0	-2.612052	5.244541	-0.770499
19	8	0	-5.91313	-2.298272	0.260678
20	6	0	-5.616705	-3.613594	-0.186265
21	1	0	-6.496716	-4.213811	0.05202
22	1	0	-5.441179	-3.637673	-1.270087
23	1	0	-4.742088	-4.025477	0.334833
24	7	0	-2.846136	3.152467	-0.922801
25	6	0	-1.425183	4.112037	0.722938
26	1	0	-0.346059	4.290879	0.734731
27	1	0	-1.876557	4.793973	1.45076
28	1	0	-3.044625	2.969825	-1.904441
29	14	0	2.130296	-0.434054	0.038671
30	1	0	-0.448839	1.088202	-0.543472
31	14	0	1.880128	-2.584402	-0.919451
32	14	0	3.280018	1.196689	-1.240267
33	14	0	2.337691	-0.325506	2.394915
34	6	0	3.048337	0.861457	-3.096708
35	1	0	1.989338	0.881619	-3.379776
36	1	0	3.564403	1.633746	-3.683499
37	1	0	3.460804	-0.109954	-3.395192
38	6	0	2.613358	2.932953	-0.854592
39	1	0	2.736662	3.192529	0.203662
40	1	0	3.153604	3.684761	-1.446511
41	1	0	1.54789	3.011102	-1.100868
42	6	0	5.144483	1.16079	-0.847377
43	1	0	5.589879	0.184754	-1.074798
44	1	0	5.671766	1.916833	-1.445959
45	1	0	5.341205	1.378692	0.209461
46	6	0	2.633637	1.468567	2.953731
47	1	0	2.707366	1.513336	4.048975
48	1	0	3.564815	1.877825	2.543579
49	1	0	1.814671	2.131409	2.649696
50	6	0	3.801066	-1.386372	2.997493
51	1	0	3.88829	-1.326203	4.091391
52	1	0	3.673139	-2.443042	2.732769
53	1	0	4.751473	-1.048081	2.567421
54	6	0	0.754268	-0.961885	3.232954
55	1	0	0.542653	-2.004001	2.966407
56	1	0	0.857673	-0.911899	4.325677

57	1	0	-0.122069	-0.364851	2.953543
58	6	0	0.871305	-2.489637	-2.528311
59	1	0	1.351558	-1.845173	-3.273662
60	1	0	0.768737	-3.490733	-2.969513
61	1	0	-0.137498	-2.096798	-2.354118
62	6	0	0.982368	-3.751329	0.285183
63	1	0	1.551008	-3.901572	1.210929
64	1	0	-0.00866	-3.370244	0.55919
65	1	0	0.844074	-4.737051	-0.180043
66	6	0	3.580155	-3.341567	-1.328511
67	1	0	3.455071	-4.341572	-1.766952
68	1	0	4.133275	-2.729455	-2.051308
69	1	0	4.204837	-3.445183	-0.433117

NH Cyclized OH of 1a

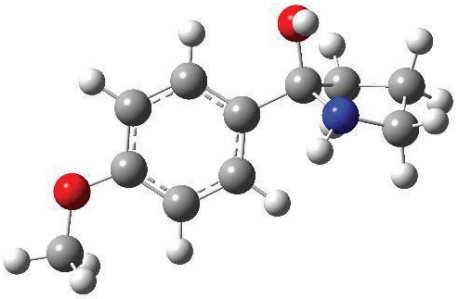

DFT/B3LYP 6-31+G(d), E = -633.404918 a.u

Standard Orientation:

Center Number	Atomic Number	Atomic Type	Coordinates (Angstroms) X	Y	Z
1	6	0	1.872411	-0.987617	0.009317
2	6	0	0.476537	-0.895469	-0.014103
3	6	0	-0.182025	0.339606	-0.038437
4	6	0	0.60562	1.50098	-0.027509
5	6	0	1.995614	1.428914	-0.002538
6	6	0	2.639959	0.184281	0.014133
7	1	0	2.339654	-1.966167	0.024939

8	1	0	-0.099308	-1.819452	-0.008613
9	1	0	0.112005	2.466457	-0.038354
10	1	0	2.602457	2.32984	0.004193
11	6	0	-1.710218	0.412432	-0.04999
12	8	0	-2.136734	1.779465	-0.213401
13	6	0	-2.380733	-0.110719	1.242476
14	1	0	-2.450286	0.681712	1.992471
15	1	0	-1.788416	-0.932883	1.662415
16	6	0	-3.366754	-1.270648	-0.602336
17	1	0	-4.211912	-1.317742	-1.298714
18	1	0	-3.002042	-2.299718	-0.44699
19	8	0	4.007809	0.216583	0.0355
20	6	0	4.716116	-1.014534	0.061478
21	1	0	5.77436	-0.747785	0.078285
22	1	0	4.472793	-1.59736	0.959923
23	1	0	4.5062	-1.616081	-0.833103
24	7	0	-2.303305	-0.390321	-1.126064
25	6	0	-3.737056	-0.630089	0.744297
26	1	0	-4.429246	0.205375	0.591602
27	1	0	-4.20743	-1.342703	1.429798
28	1	0	-2.427454	1.845678	-1.137782
29	1	0	-1.613675	-0.868121	-1.695145

NH Cyclized OH of 1b

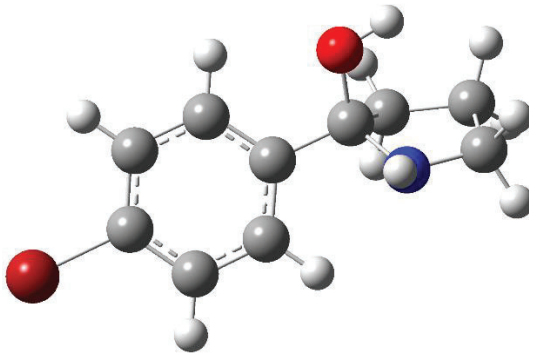

DFT/B3LYP 6-31+G(d), E = - 3090.005776 a.u

Standard Orientation:

Center Number	Atomic Number	Atomic Type	Coordinates (Angstroms) X	Y	Z
1	6	0	1.366334	1.258655	-0.012212
2	6	0	-0.026065	1.357634	-0.067207
3	6	0	-0.826014	0.209197	-0.129601
4	6	0	-0.203425	-1.045918	-0.139946
5	6	0	1.186839	-1.159924	-0.086485
6	6	0	1.95974	-0.001804	-0.020498
7	1	0	1.978865	2.15325	0.0343
8	1	0	-0.494759	2.335132	-0.070733
9	1	0	-0.816256	-1.93971	-0.203586
10	1	0	1.660122	-2.136432	-0.09773
11	6	0	-2.347245	0.305825	-0.129371
12	8	0	-2.657057	1.629138	-0.634689
13	6	0	-2.986918	0.09157	1.263398
14	1	0	-2.885781	0.984027	1.887474
15	1	0	-2.47801	-0.73666	1.767557
16	6	0	-4.445674	-0.282973	0.932818
17	1	0	-4.891933	-0.927799	1.695901
18	1	0	-5.076235	0.613698	0.874449
19	6	0	-4.355631	-0.982773	-0.4502
20	1	0	-5.096032	-0.57206	-1.152388
21	1	0	-4.547313	-2.060205	-0.373303
22	7	0	-2.966388	-0.757096	-0.894589
23	35	0	3.862955	-0.145403	0.070228
24	1	0	-2.854561	-0.63106	-1.896614
25	1	0	-3.611996	1.776578	-0.547845

Heterocyclic ring of 1a

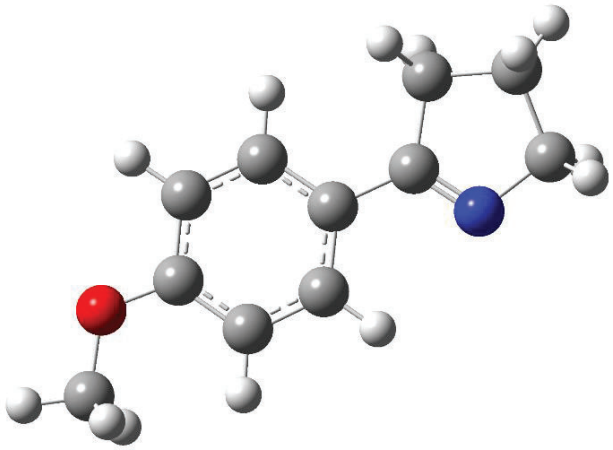

DFT/B3LYP 6-31+G(d), E = -556.979416 a.u

Standard Orientation:

Center Number	Atomic Number	Atomic Type	Coordinates (Angstroms) X	Y	Z
1	6	0	1.848487	-0.998189	-0.032026
2	6	0	0.457856	-1.092596	-0.024728
3	6	0	-0.355461	0.05136	0.013742
4	6	0	0.277984	1.308257	0.047387
5	6	0	1.664001	1.418807	0.044216
6	6	0	2.46018	0.265085	0.003156
7	1	0	2.441179	-1.905742	-0.064354
8	1	0	-0.019605	-2.067067	-0.049134
9	1	0	-0.316225	2.216972	0.080793
10	1	0	2.151071	2.388968	0.072393
11	6	0	-1.826164	-0.073258	0.024665
12	6	0	-2.763652	1.132669	0.041942
13	1	0	-2.498023	1.8866	-0.707502
14	1	0	-2.716863	1.627744	1.023025
15	6	0	-3.870485	-1.017673	0.10511
16	1	0	-4.360869	-1.704777	-0.594251
17	1	0	-4.218968	-1.291728	1.112
18	8	0	3.809561	0.471863	0.00024

19	6	0	4.674168	-0.657003	-0.039948
20	1	0	5.687802	-0.252736	-0.034573
21	1	0	4.532157	-1.299386	0.838761
22	1	0	4.520006	-1.244918	-0.954034
23	7	0	-2.417794	-1.21415	0.054532
24	6	0	-4.1339	0.474859	-0.219555
25	1	0	-4.412584	0.58938	-1.273601
26	1	0	-4.939097	0.90691	0.383066

Heterocyclic ring of 1b

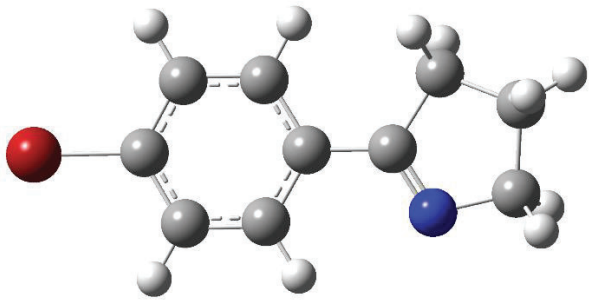

DFT/B3LYP 6-31+G(d), E = -3013.580477 a.u

Standard Orientation:

Center Number	Atomic Number	Atomic Type	Coordinates (Angstroms) X	Y	Z
1	6	0	-1.06321	-1.227332	0.045106
2	6	0	0.328044	-1.23351	0.031455
3	6	0	1.057031	-0.031597	-0.023469
4	6	0	0.349409	1.179165	-0.070102
5	6	0	-1.046829	1.20072	-0.060632
6	6	0	-1.74041	-0.005494	-0.000513
7	1	0	-1.618218	-2.158662	0.090261
8	1	0	0.872537	-2.171646	0.065623
9	1	0	0.884037	2.123346	-0.116321

10	1	0	-1.583957	2.142574	-0.098933
11	6	0	2.535873	-0.054015	-0.027788
12	6	0	3.388061	1.211603	-0.023073
13	1	0	3.076447	1.925938	0.747316
14	1	0	3.299831	1.727334	-0.990346
15	6	0	4.803299	0.643861	0.214774
16	1	0	5.565523	1.124588	-0.406021
17	1	0	5.095881	0.78268	1.261749
18	6	0	4.635408	-0.86538	-0.10072
19	1	0	5.158248	-1.516699	0.608945
20	1	0	5.008441	-1.12753	-1.10138
21	7	0	3.197622	-1.153544	-0.063601
22	35	0	-3.646348	0.008994	0.013545

Transition state and IRC

Triplet Azide to triplet Nitrene of 1a

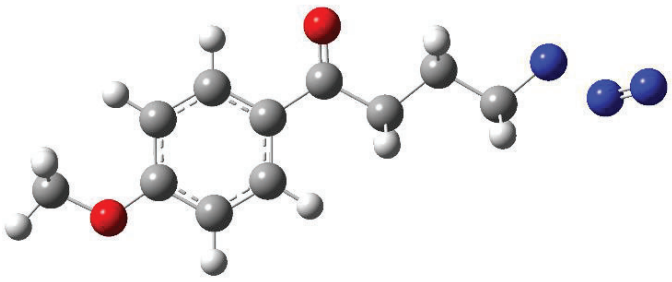

DFT/B3LYP 6-31+G(d), E = -741.586359 a.u

Imaginary frequency = 1 (-316.42)

Standard Orientation:

Center Number	Atomic Number	Atomic Type	Coordinates (Angstroms) X	Y	Z
1	6	0	3.577582	0.842881	-0.020773
2	6	0	2.253771	1.275976	-0.015467
3	6	0	1.1842	0.367509	0.002207
4	6	0	1.482555	-1.009838	0.014705
5	6	0	2.796091	-1.458005	0.00966
6	6	0	3.854783	-0.533959	-0.008131
7	1	0	4.377591	1.574517	-0.03454
8	1	0	2.028206	2.337915	-0.025128
9	1	0	0.685518	-1.747019	0.02864
10	1	0	3.030429	-2.518119	0.019258
11	6	0	-0.208112	0.90407	0.006973
12	8	0	-0.419617	2.111226	-0.004787
13	6	0	-1.376438	-0.08334	0.027162
14	1	0	-1.269599	-0.730917	0.910125
15	1	0	-1.283193	-0.750679	-0.842597
16	6	0	-2.74376	0.605106	0.029984
17	1	0	-2.826199	1.265934	0.899379
18	1	0	-2.83979	1.247025	-0.851951
19	6	0	-3.884409	-0.415439	0.052843
20	1	0	-3.827564	-1.077244	0.933614

21	1	0	-3.837243	-1.082544	-0.826966
22	8	0	5.104735	-1.068504	-0.011752
23	6	0	6.229529	-0.193518	-0.029394
24	1	0	7.106149	-0.84279	-0.028943
25	1	0	6.23382	0.428001	-0.933471
26	1	0	6.247063	0.447137	0.861063
27	7	0	-5.164404	0.26394	0.05844
28	7	0	-6.225517	-0.784914	0.246996
29	7	0	-7.224491	-0.722118	-0.361834

IRC:

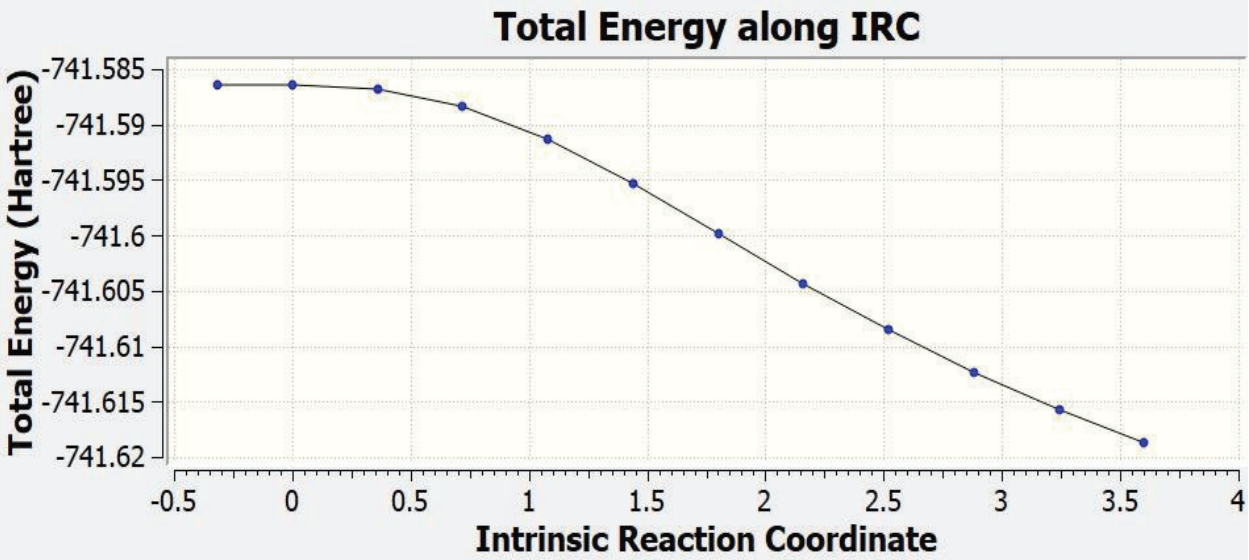

Triplet Azide to triplet Nitrene of 1b

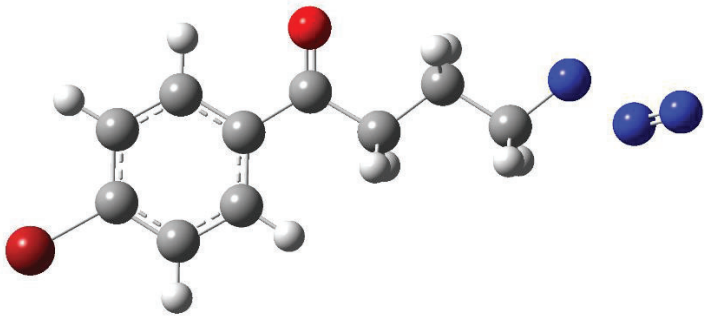

DFT/B3LYP 6-31+G(d), E = -3198.185413 a.u

Imaginary frequency = 1 (-314.67)

Standard Orientation:

Center Number	Atomic Number	Atomic Type	Coordinates (Angstroms) X	Y	Z
1	6	0	2.754095	1.260121	-0.022681
2	6	0	1.406908	1.609237	-0.018782
3	6	0	0.406388	0.623122	0.00174
4	6	0	0.787986	-0.727817	0.018411
5	6	0	2.134188	-1.092473	0.014672
6	6	0	3.106151	-0.092027	-0.005878
7	1	0	3.523182	2.025271	-0.038535
8	1	0	1.108334	2.652756	-0.031626
9	1	0	0.040507	-1.514762	0.034522
10	1	0	2.422985	-2.138036	0.027581
11	6	0	-1.027535	1.063782	0.004841
12	8	0	-1.312121	2.253216	-0.010783
13	6	0	-2.123084	0.000115	0.028095
14	1	0	-1.970683	-0.635909	0.912864
15	1	0	-1.982936	-0.661507	-0.839838
16	6	0	-3.534758	0.592163	0.02934
17	1	0	-3.662797	1.24801	0.896986
18	1	0	-3.675225	1.223022	-0.854624
19	6	0	-4.60158	-0.50519	0.055462
20	1	0	-4.499343	-1.158019	0.938757
21	1	0	-4.508039	-1.170106	-0.822149

22	7	0	-5.924982	0.085345	0.058877
23	7	0	-6.911227	-1.033303	0.247736
24	7	0	-7.911974	-1.038836	-0.361485
25	35	0	4.945306	-0.582145	-0.010997

IRC:

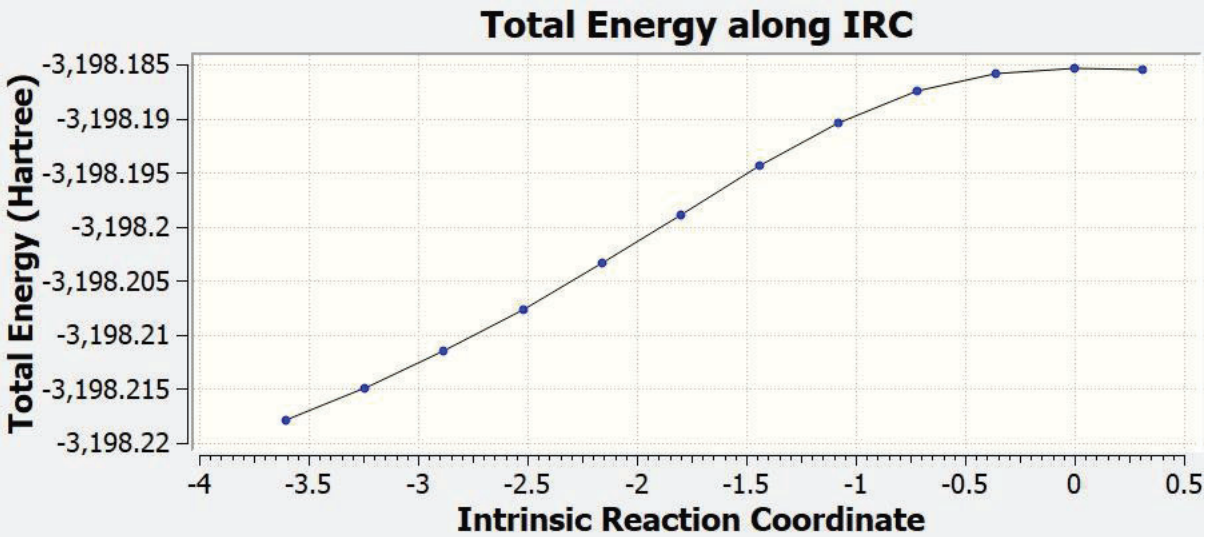

Triplet nitrene of 1a with TTMSS H-Transfer

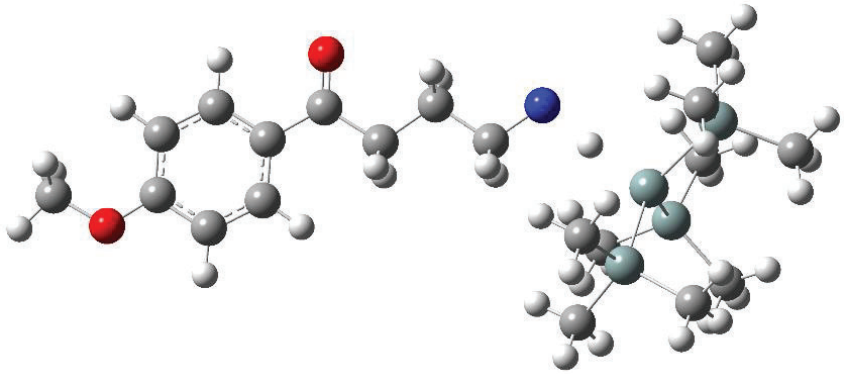

DFT/B3LYP 6-31+G(d), E = -2150.028455 a.u

Imaginary frequency = 1 (-1395.64)

Standard Orientation:

Center Number	Atomic Number	Atomic Type	Coordinates (Angstroms) X	Y	Z
1	6	0	-7.957513	-0.702595	-0.000245
2	6	0	-6.739343	-1.378243	-0.02153
3	6	0	-5.517233	-0.688931	-0.031966
4	6	0	-5.549635	0.719739	-0.020204
5	6	0	-6.754781	1.408471	0.001047
6	6	0	-7.969032	0.701583	0.011155
7	1	0	-8.881452	-1.269908	0.00728
8	1	0	-6.718572	-2.463719	-0.030464
9	1	0	-4.627184	1.292302	-0.027452
10	1	0	-6.783945	2.493846	0.010203
11	6	0	-4.250079	-1.480356	-0.054576
12	8	0	-4.275982	-2.705672	-0.064015
13	6	0	-2.917042	-0.732284	-0.065277
14	1	0	-2.881268	-0.075633	0.817099
15	1	0	-2.904849	-0.057888	-0.93478
16	6	0	-1.698725	-1.65877	-0.091114
17	1	0	-1.718854	-2.326521	0.776692
18	1	0	-1.73877	-2.304764	-0.974536
19	6	0	-0.378131	-0.867462	-0.095836
20	1	0	-0.322155	-0.209243	0.791783

21	1	0	-0.342708	-0.189088	-0.969816
22	8	0	-9.096066	1.463275	0.031878
23	6	0	-10.365054	0.815792	0.043112
24	1	0	-11.103954	1.618274	0.058954
25	1	0	-10.50655	0.204835	-0.857214
26	1	0	-10.483446	0.190689	0.93704
27	7	0	0.759787	-1.742565	-0.124943
28	14	0	3.30007	0.036123	-0.002318
29	1	0	1.898671	-0.884539	-0.074981
30	14	0	2.966192	1.989399	-1.312068
31	14	0	4.887975	-1.47349	-0.919527
32	14	0	3.630608	0.493601	2.305454
33	6	0	4.663861	-1.611151	-2.804192
34	1	0	4.861382	-0.660056	-3.3136
35	1	0	5.360268	-2.355913	-3.213453
36	1	0	3.647382	-1.92856	-3.066397
37	6	0	6.67271	-0.904758	-0.572475
38	1	0	6.880792	-0.848755	0.503151
39	1	0	7.389304	-1.613047	-1.010876
40	1	0	6.8777	0.083305	-1.002574
41	6	0	4.630901	-3.197137	-0.163225
42	1	0	3.607171	-3.552813	-0.329413
43	1	0	5.319735	-3.921201	-0.619785
44	1	0	4.811904	-3.201203	0.918086
45	6	0	4.955591	1.839929	2.551601
46	1	0	5.111558	2.02935	3.622623
47	1	0	5.920906	1.543841	2.123081
48	1	0	4.66347	2.789906	2.08733
49	6	0	4.185986	-1.068856	3.236972
50	1	0	4.273089	-0.857787	4.311705
51	1	0	3.468027	-1.888795	3.115415
52	1	0	5.16307	-1.426851	2.890599
53	6	0	2.007372	1.09906	3.094716
54	1	0	2.165445	1.339694	4.155007
55	1	0	1.22833	0.328367	3.043674
56	1	0	1.620815	1.999894	2.603293
57	6	0	1.870921	3.2529	-0.399783
58	1	0	2.336402	3.602995	0.529624
59	1	0	1.699699	4.132845	-1.035032
60	1	0	0.89013	2.83382	-0.143282
61	6	0	2.111332	1.554762	-2.956063

62	1	0	2.698673	0.842049	-3.546642
63	1	0	1.121373	1.111003	-2.793531
64	1	0	1.974062	2.459413	-3.564286
65	6	0	4.627822	2.831566	-1.708347
66	1	0	4.461448	3.743145	-2.298836
67	1	0	5.166581	3.119259	-0.797357
68	1	0	5.286812	2.176164	-2.290829

IRC:

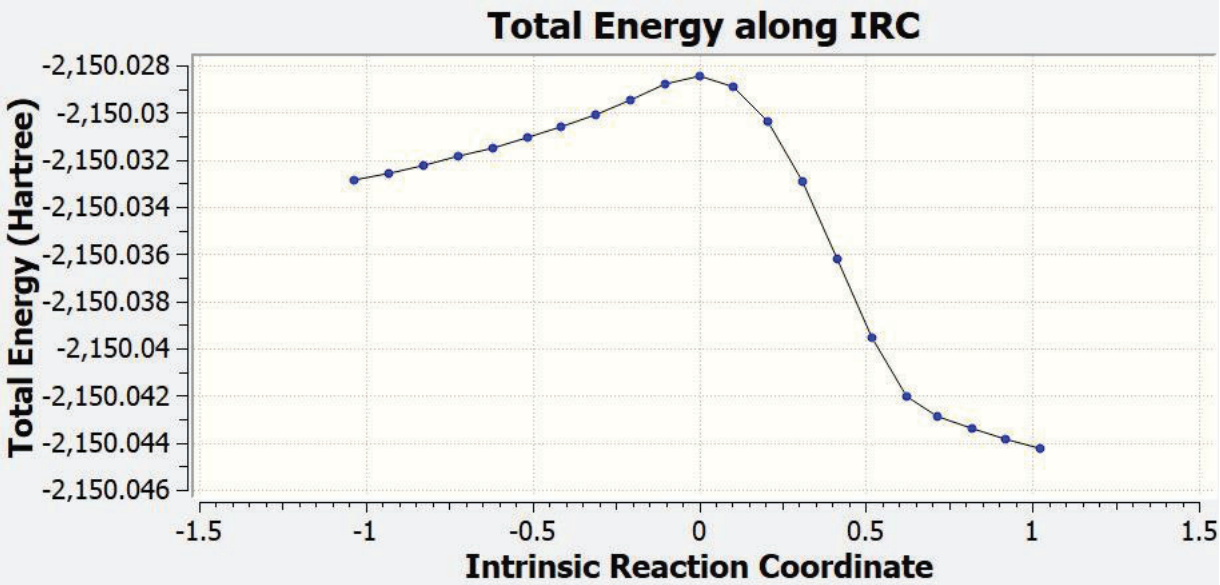

TS Intramolecular Cyclization of 1a

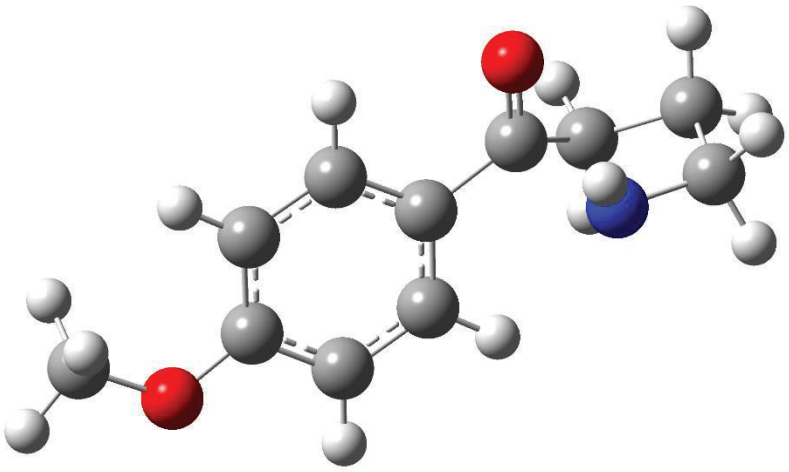

DFT/B3LYP 6-31+G(d), E = -632.733149 a.u

Imaginary frequency = 1 (-400.26)

Standard Orientation:

Center Number	Atomic Number	Atomic Type	Coordinates (Angstroms) X	Y	Z
1	6	0	-2.172269	0.978969	-0.001598
2	6	0	-0.796353	1.218545	-0.076436
3	6	0	0.124348	0.170543	-0.165147
4	6	0	-0.367676	-1.146679	-0.167901
5	6	0	-1.729964	-1.403423	-0.086935
6	6	0	-2.643966	-0.339431	-0.007333
7	1	0	-2.855054	1.819361	0.058537
8	1	0	-0.422711	2.237909	-0.067514
9	1	0	0.320071	-1.986411	-0.205101
10	1	0	-2.111883	-2.42011	-0.07833
11	6	0	1.591596	0.505638	-0.268407
12	8	0	1.962422	1.700221	-0.045543
13	6	0	2.490327	-0.343289	-1.181697
14	1	0	2.44925	0.078833	-2.193166
15	1	0	2.133057	-1.376689	-1.23784

16	6	0	3.906943	-0.275736	-0.601363
17	1	0	4.589741	-0.981209	-1.086771
18	1	0	4.303107	0.734591	-0.737207
19	6	0	3.77881	-0.564286	0.918429
20	1	0	4.549167	-0.040425	1.495895
21	1	0	3.89286	-1.644792	1.09928
22	8	0	-3.961752	-0.693554	0.062167
23	6	0	-4.938816	0.335219	0.154794
24	1	0	-5.902404	-0.175122	0.201344
25	1	0	-4.799529	0.936988	1.062409
26	1	0	-4.914031	0.989495	-0.726466
27	7	0	2.418979	-0.222303	1.308922
28	1	0	2.372274	0.51394	2.021044

IRC:

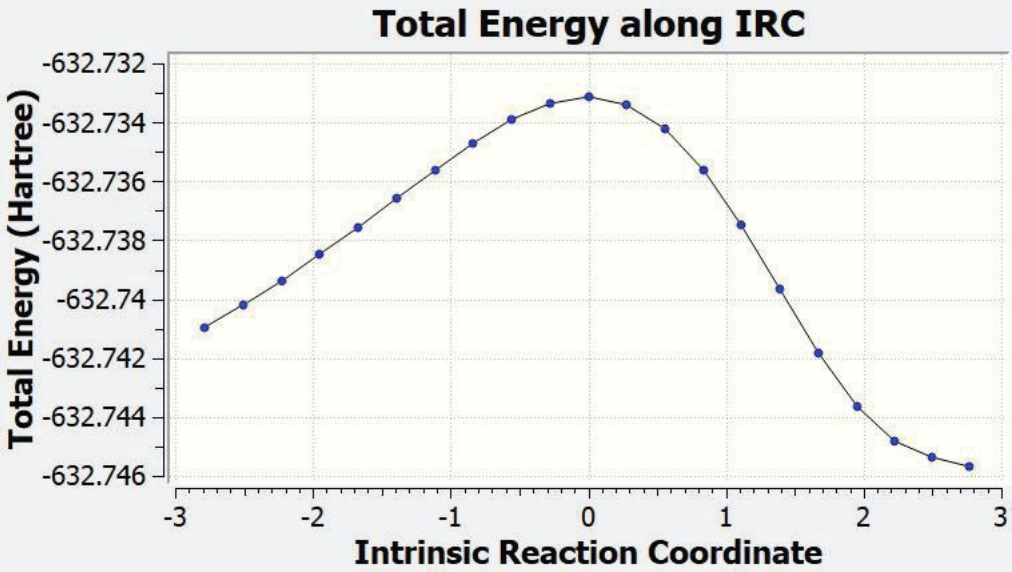

TS: TTMSS and Ketone H Transfer of 1a

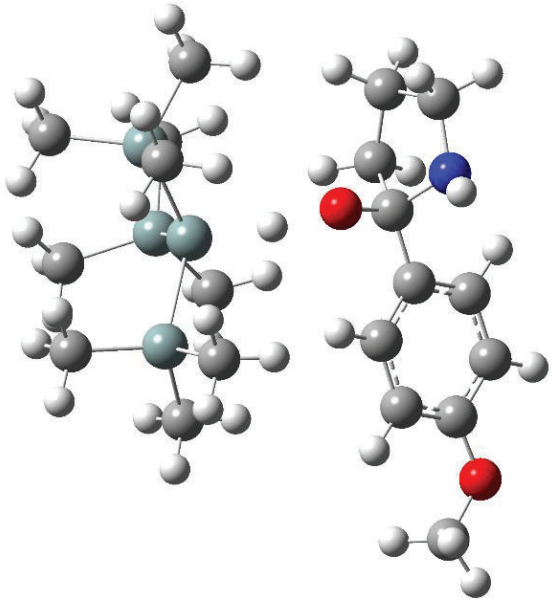

DFT/B3LYP 6-31+G(d), E = -2150.668218 a.u

Imaginary frequency = 1 (-1117.97)

Standard Orientation:

Center Number	Atomic Number	Atomic Type	Coordinates (Angstroms) X	Y	Z
1	6	0	-3.628447	-1.150452	-0.549921
2	6	0	-2.575024	-0.234268	-0.683313
3	6	0	-2.683684	1.078653	-0.228557
4	6	0	-3.900665	1.470275	0.360045
5	6	0	-4.955192	0.577883	0.502766
6	6	0	-4.824207	-0.7452	0.049848
7	1	0	-3.501743	-2.161287	-0.922277
8	1	0	-1.655833	-0.546805	-1.165226
9	1	0	-4.03194	2.496591	0.69193
10	1	0	-5.894143	0.884088	0.955037
11	6	0	-1.538254	2.078586	-0.389808
12	8	0	-0.445041	1.566026	-1.116253
13	6	0	-1.077584	2.776465	0.910099
14	1	0	-0.403483	2.134416	1.481961

15	1	0	-1.947437	2.995576	1.538263
16	6	0	-1.090198	4.38514	-0.940812
17	1	0	-0.34673	4.515327	-1.737419
18	1	0	-1.701257	5.296129	-0.902385
19	8	0	-5.916803	-1.549034	0.234538
20	6	0	-5.849095	-2.89573	-0.212281
21	1	0	-6.815436	-3.339476	0.034245
22	1	0	-5.689118	-2.949468	-1.297454
23	1	0	-5.051799	-3.448409	0.302384
24	7	0	-1.973302	3.232116	-1.185334
25	6	0	-0.407391	4.075047	0.416488
26	1	0	0.664545	3.919994	0.269611
27	1	0	-0.52699	4.894169	1.133153
28	1	0	-2.114781	2.994424	-2.164791
29	14	0	1.621487	-0.380254	0.011243
30	1	0	0.396766	0.612569	-0.435431
31	14	0	1.220011	-2.481721	-1.033923
32	14	0	3.529073	0.71329	-0.896802
33	14	0	1.656705	-0.532931	2.385801
34	6	0	3.559588	0.537968	-2.790274
35	1	0	2.641234	0.931643	-3.242024
36	1	0	4.40629	1.099114	-3.209101
37	1	0	3.667863	-0.506845	-3.105523
38	6	0	3.491398	2.567085	-0.48086
39	1	0	3.475414	2.748595	0.600353
40	1	0	4.378721	3.068709	-0.890896
41	1	0	2.604619	3.042966	-0.915244
42	6	0	5.1361	-0.033042	-0.195903
43	1	0	5.215303	-1.107056	-0.403318
44	1	0	6.008889	0.457639	-0.64841
45	1	0	5.208797	0.102426	0.890283
46	6	0	2.281014	1.082368	3.176411
47	1	0	2.260521	0.996266	4.271542
48	1	0	3.313537	1.307139	2.882585
49	1	0	1.661988	1.944572	2.901332
50	6	0	2.830041	-1.934383	2.923654
51	1	0	2.870121	-1.991925	4.020167
52	1	0	2.495214	-2.911391	2.554446
53	1	0	3.853094	-1.774356	2.56233
54	6	0	-0.076582	-0.908942	3.069154
55	1	0	-0.460535	-1.865492	2.695888

56	1	0	-0.046366	-0.966615	4.165985
57	1	0	-0.803614	-0.135636	2.795162
58	6	0	0.595013	-2.236346	-2.812823
59	1	0	1.330742	-1.706636	-3.429213
60	1	0	0.402884	-3.209934	-3.284588
61	1	0	-0.335334	-1.657591	-2.845872
62	6	0	-0.066487	-3.502984	-0.072286
63	1	0	0.29843	-3.779361	0.924569
64	1	0	-1.009242	-2.95932	0.058641
65	1	0	-0.287253	-4.434496	-0.611764
66	6	0	2.830708	-3.497442	-1.105066
67	1	0	2.636434	-4.478729	-1.559712
68	1	0	3.600407	-3.0015	-1.708808
69	1	0	3.250927	-3.672213	-0.107193

IRC:

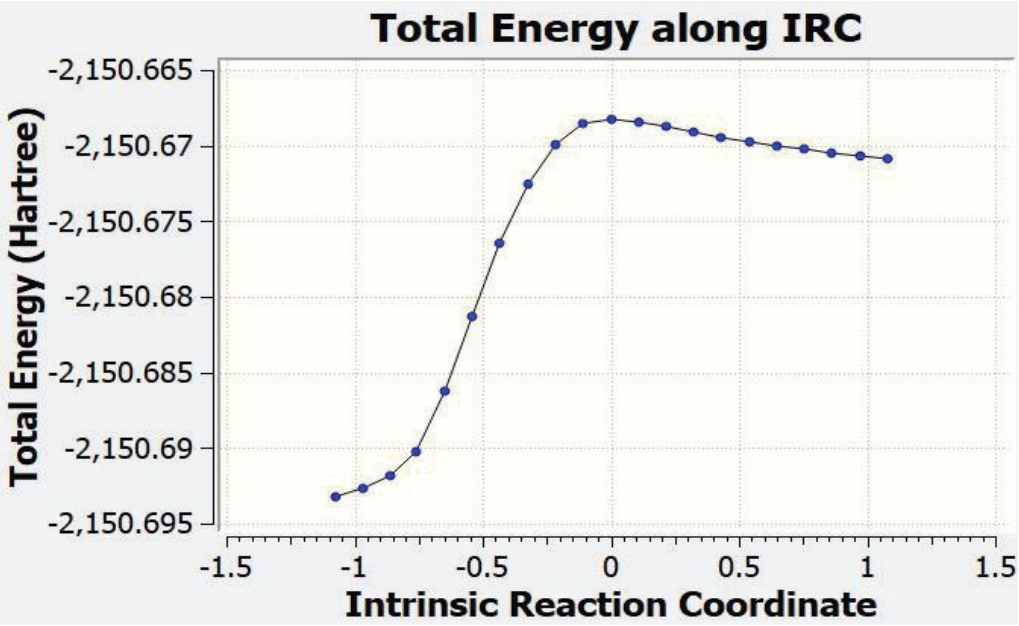

Chapter 4: Supporting Information

I. Spectroscopic characterization of the compounds

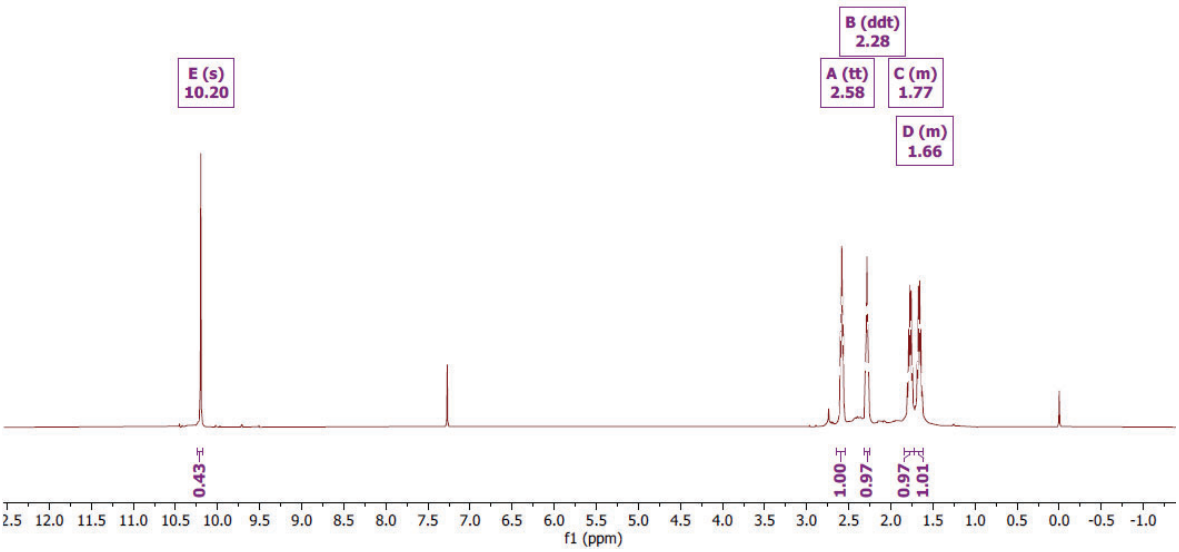

Figure S177. ^{1}H NMR spectrum of compound (i-**b**)

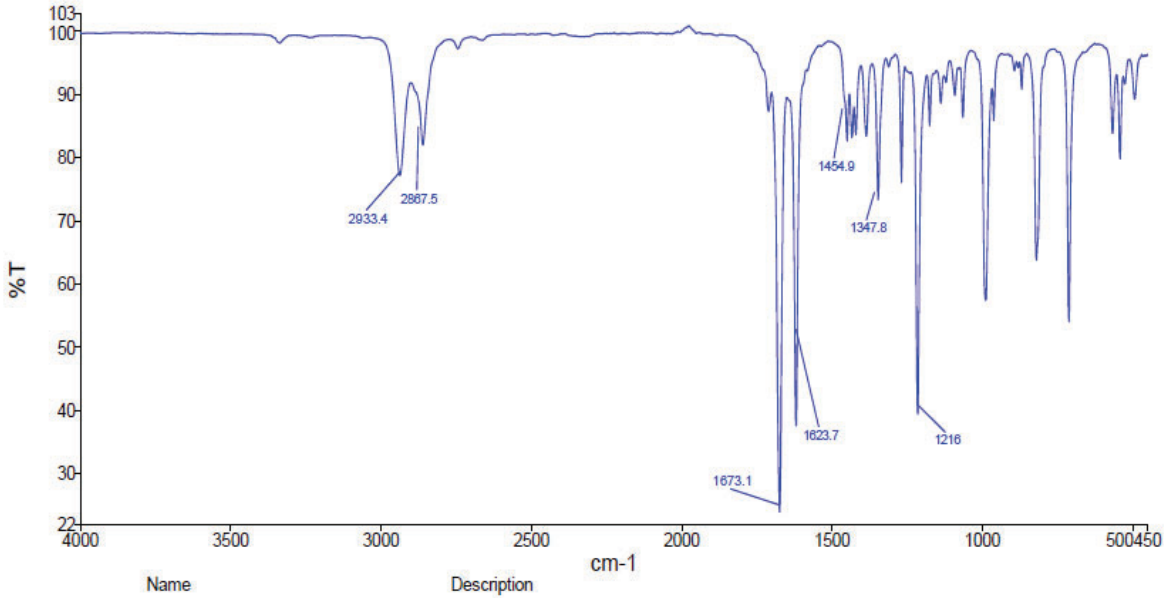

Figure S178. FTIR spectrum of compound (i-b)

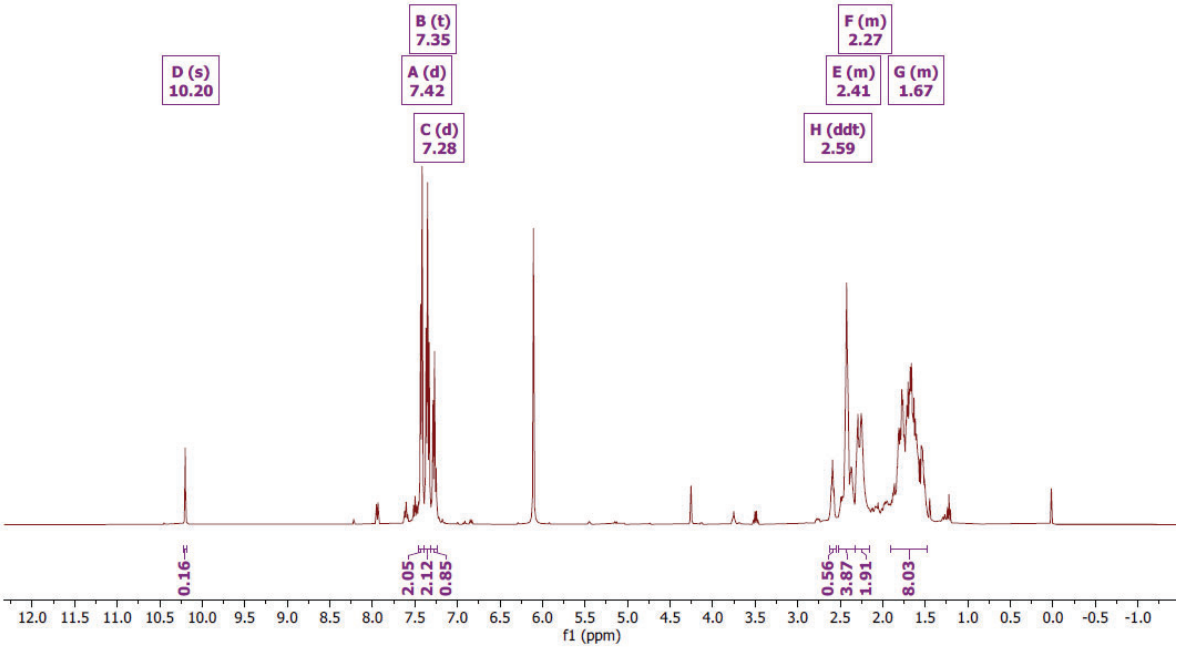

Figure S179. ^{1}H NMR spectrum of crude (ii-**b**)

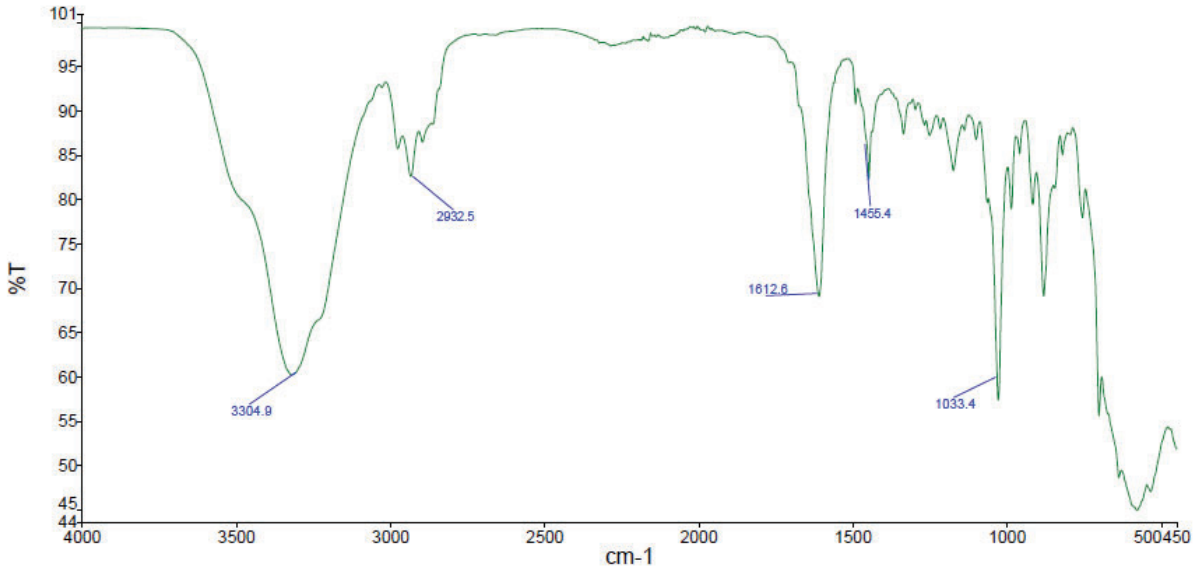

Figure S180. FTIR spectrum of crude (ii-b)

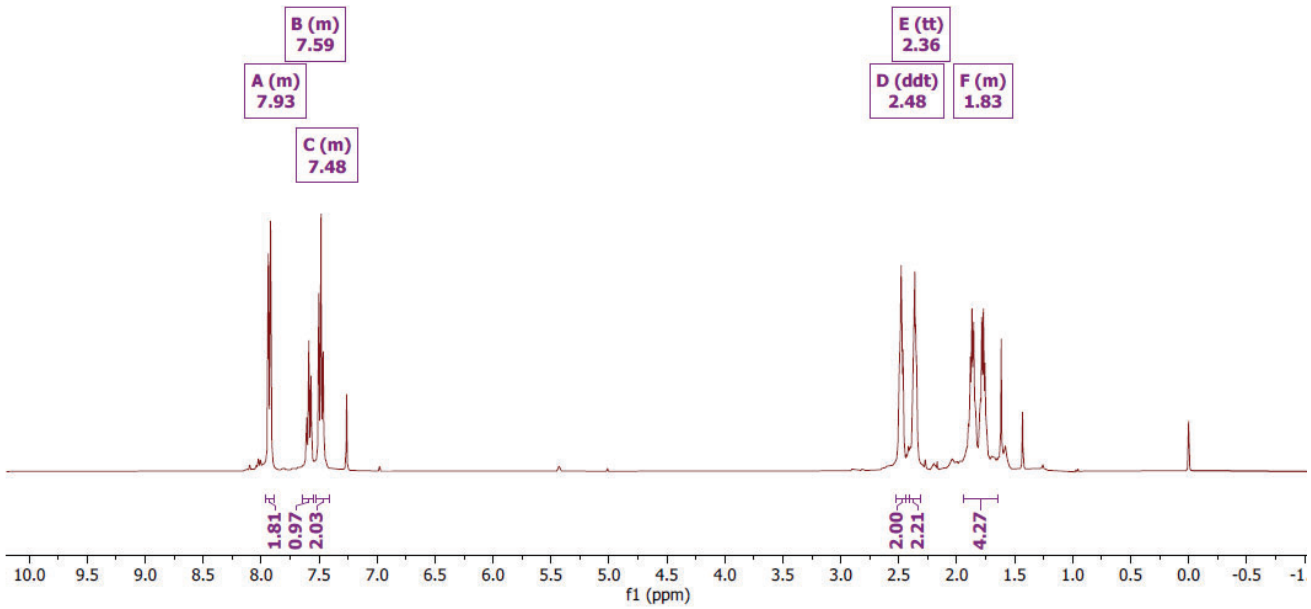

Figure S181. ^{1}H NMR spectrum of compound (iii-**b**)

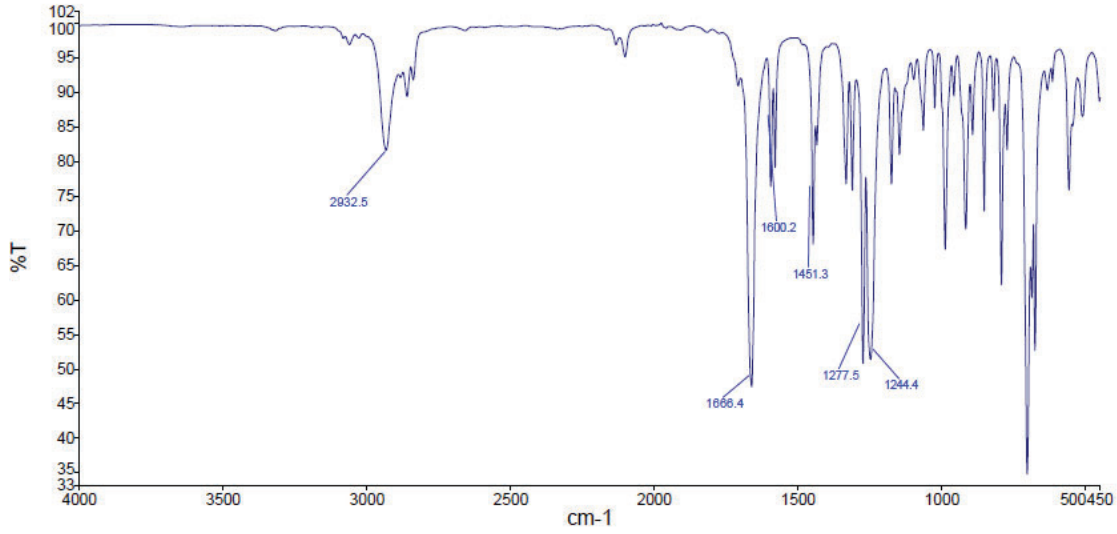

Figure S182. FTIR spectrum of compound (iii-**b**)

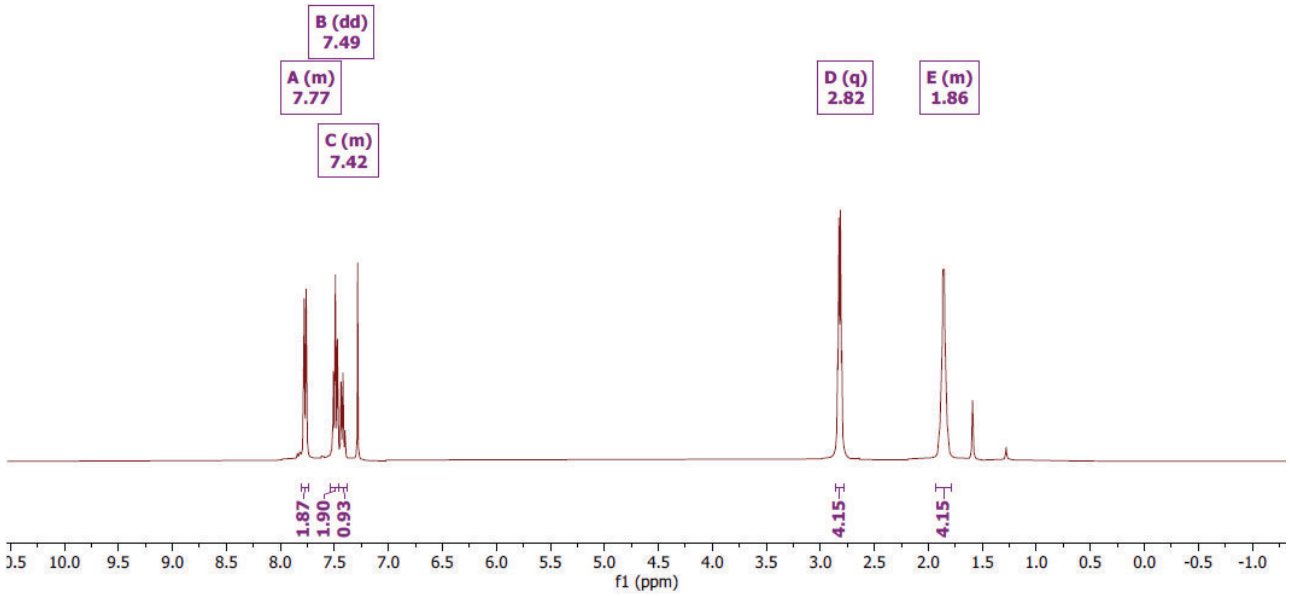

Figure S183. ^{1}H NMR spectrum of isoxazole-**2**

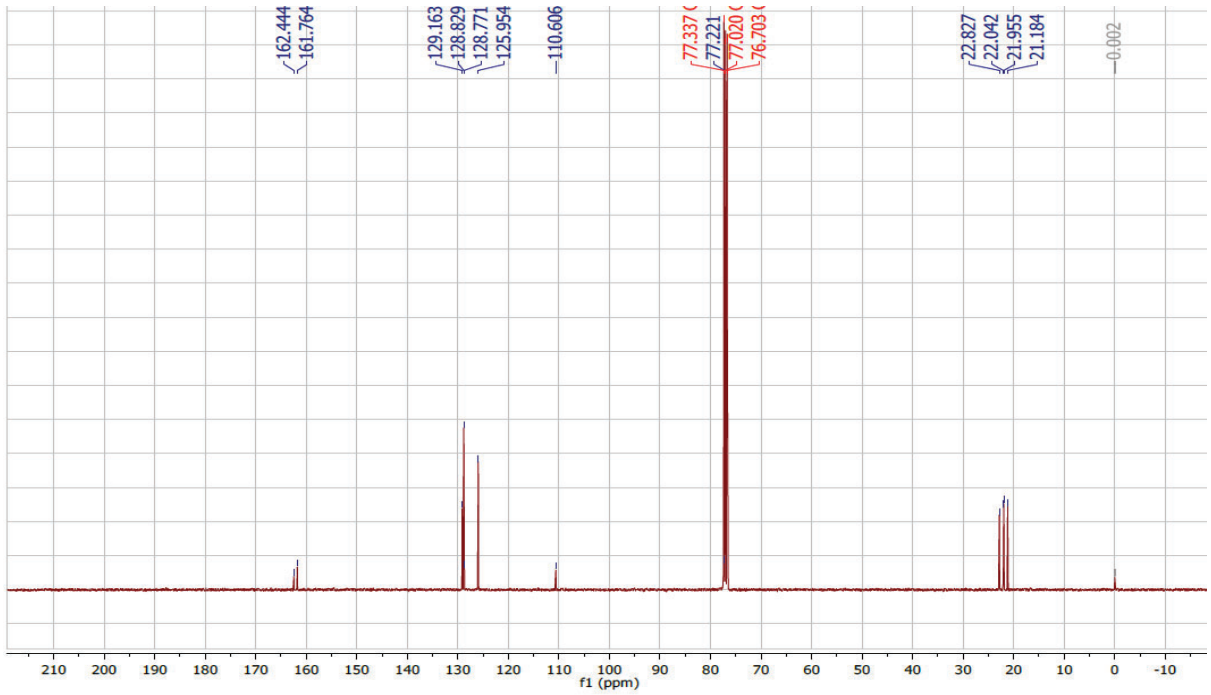

Figure S184. ^{13}C NMR spectrum of isoxazole-**2**

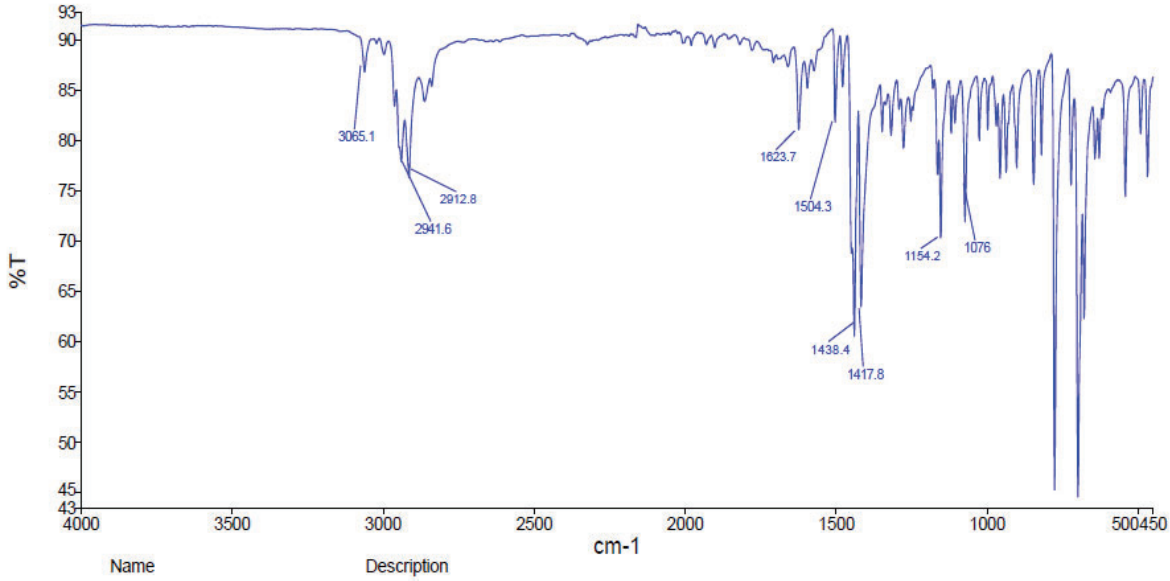

Figure S185. FTIR spectrum of isoxazole-**2**

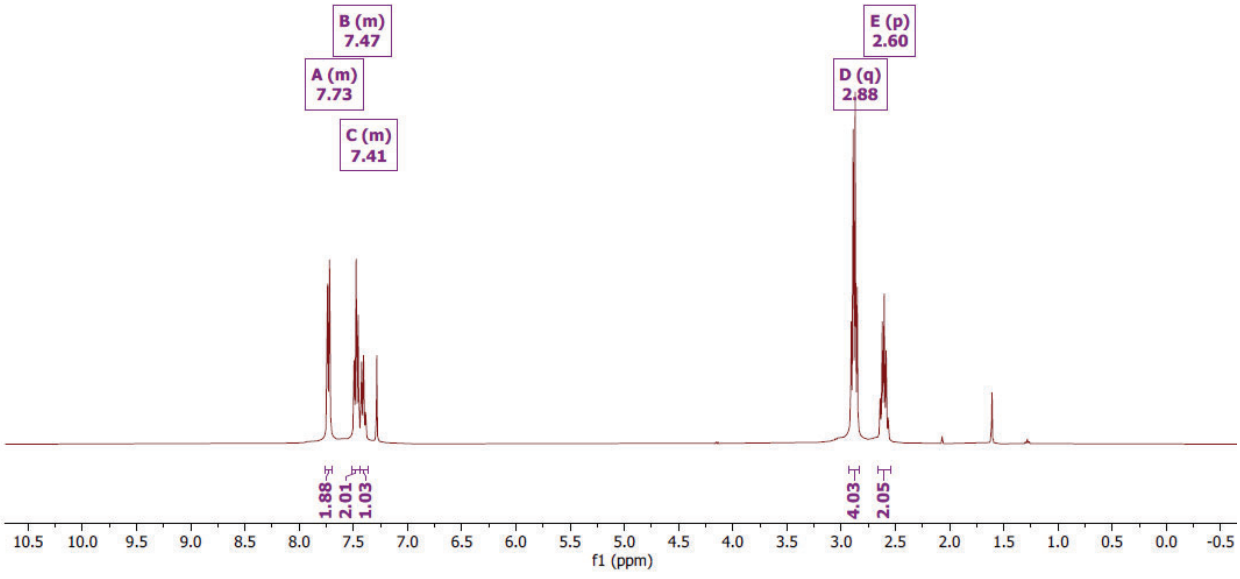

Figure S186. ^{1}H NMR spectrum of isoxazole-**1**

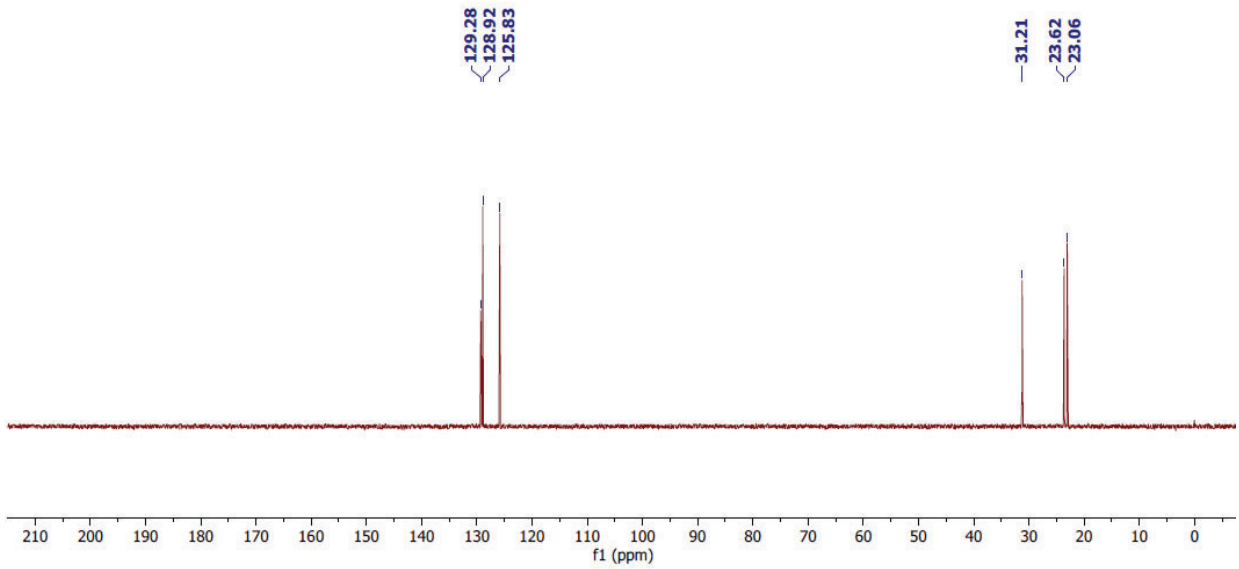

Figure S187. ^{13}C NMR spectrum of isoxazole-**2**

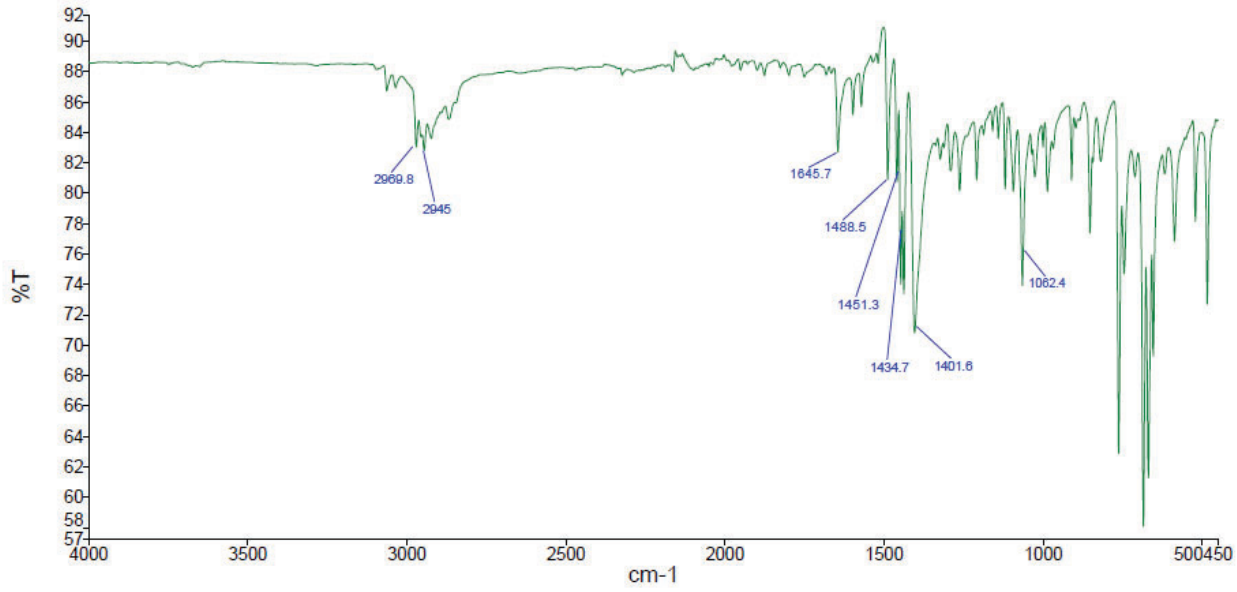

Figure S188. FTIR spectrum of isoxazole-**1**

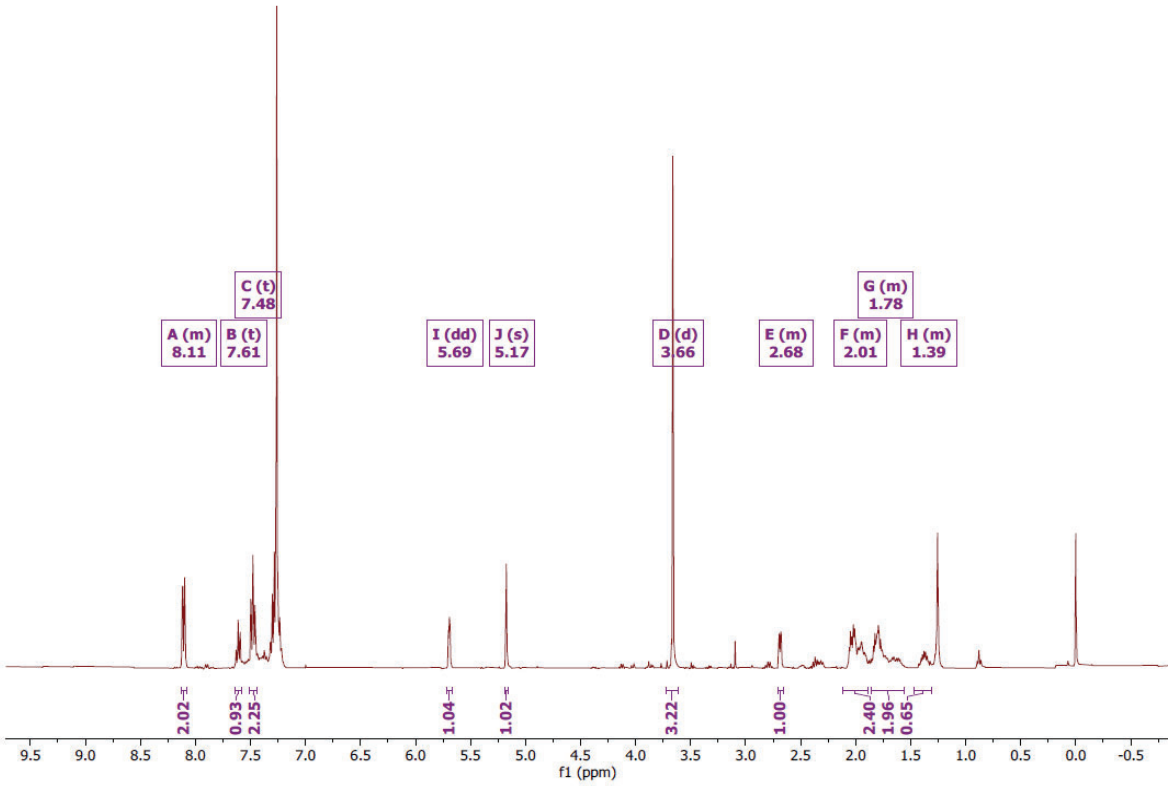

Figure S189. ^{1}H NMR spectrum of photoproduct **3**

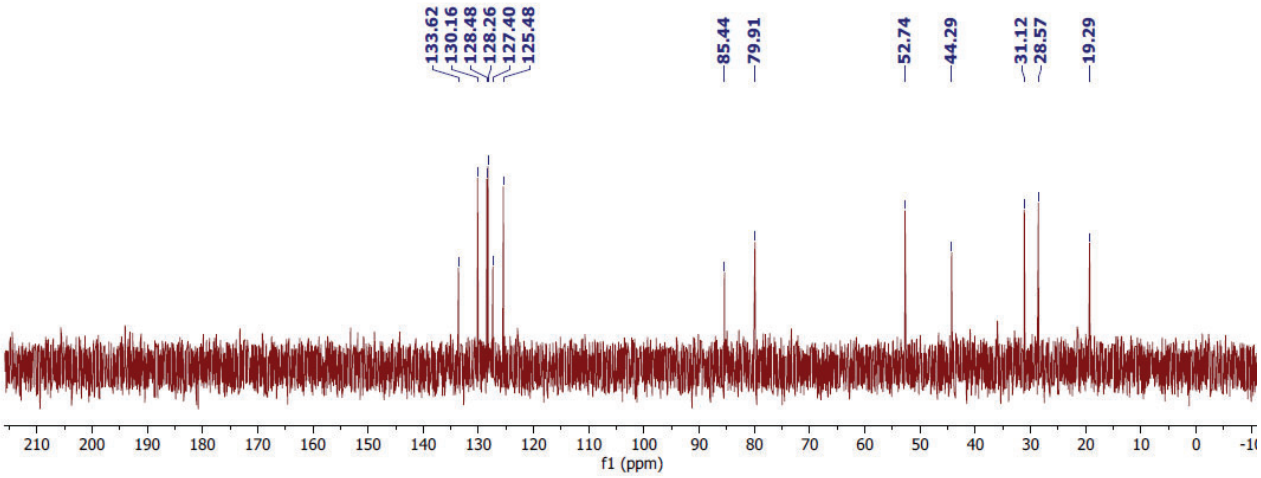

Figure S190. ^{13}C NMR spectrum of photoproduct **3**

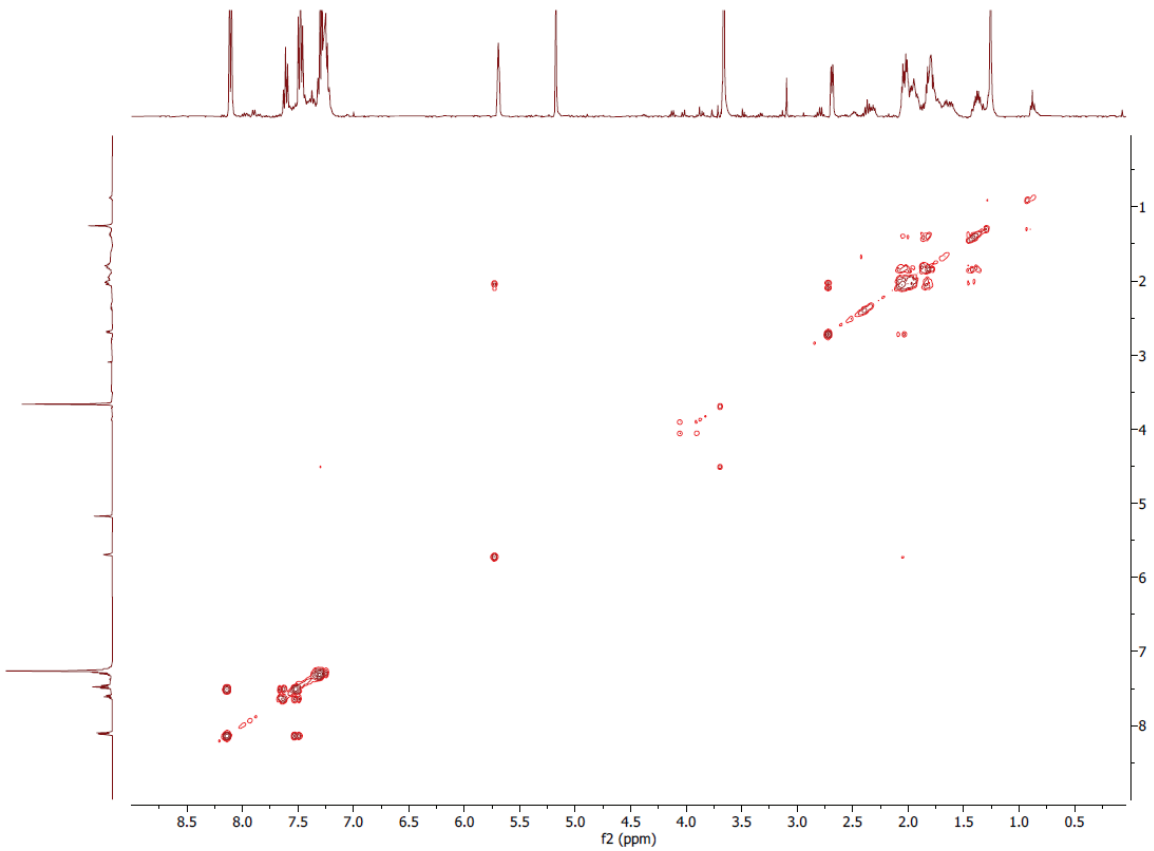

Figure S191. COSY-2D spectrum of photoproduct 3

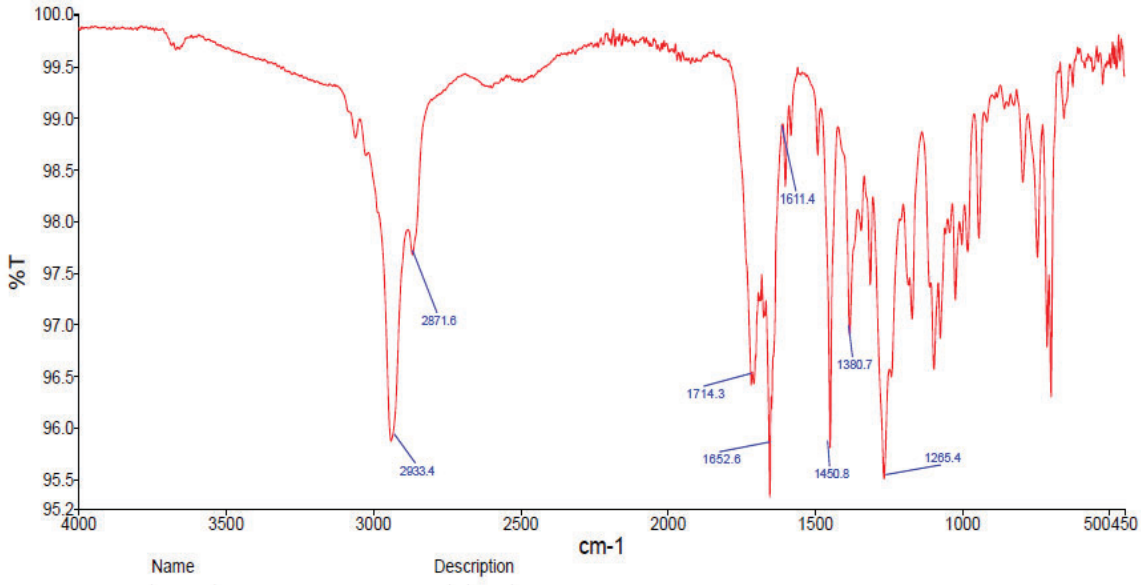

Figure S192. FTIR spectrum of photoproduct 3

II. GCMS characterization of compounds

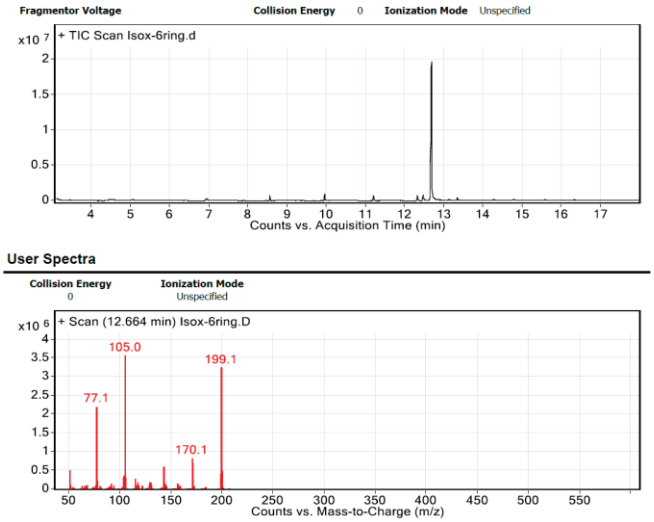

Figure S193. GCMS spectrum of isoxazole-**2**

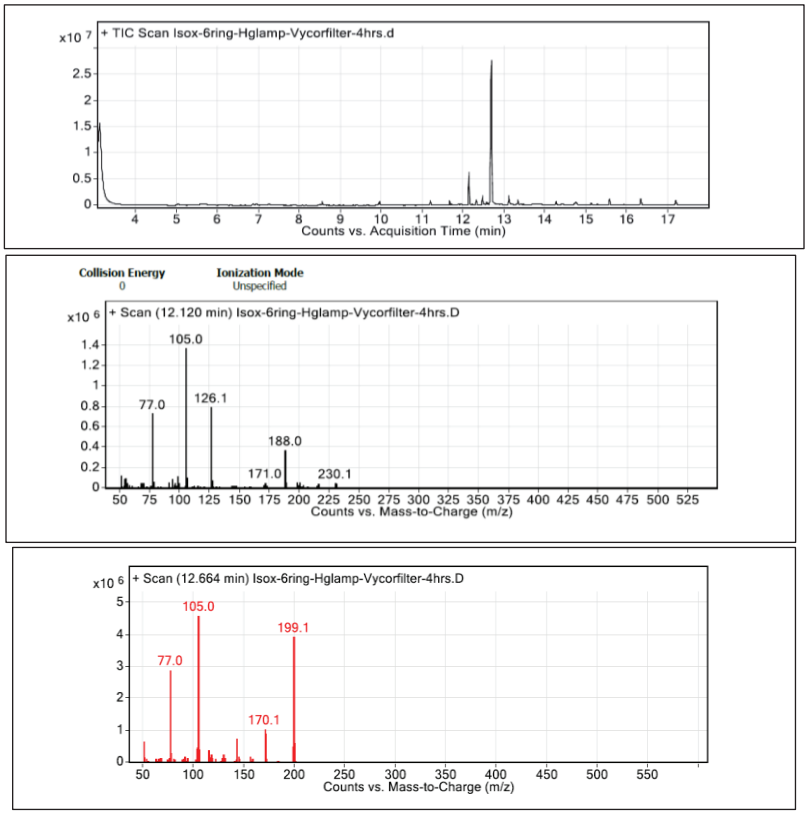

Figure S194. GCMS spectrum of argon saturated MeOH solution of isoxazole-2 after irradiation of 4 h using Hg lamp.

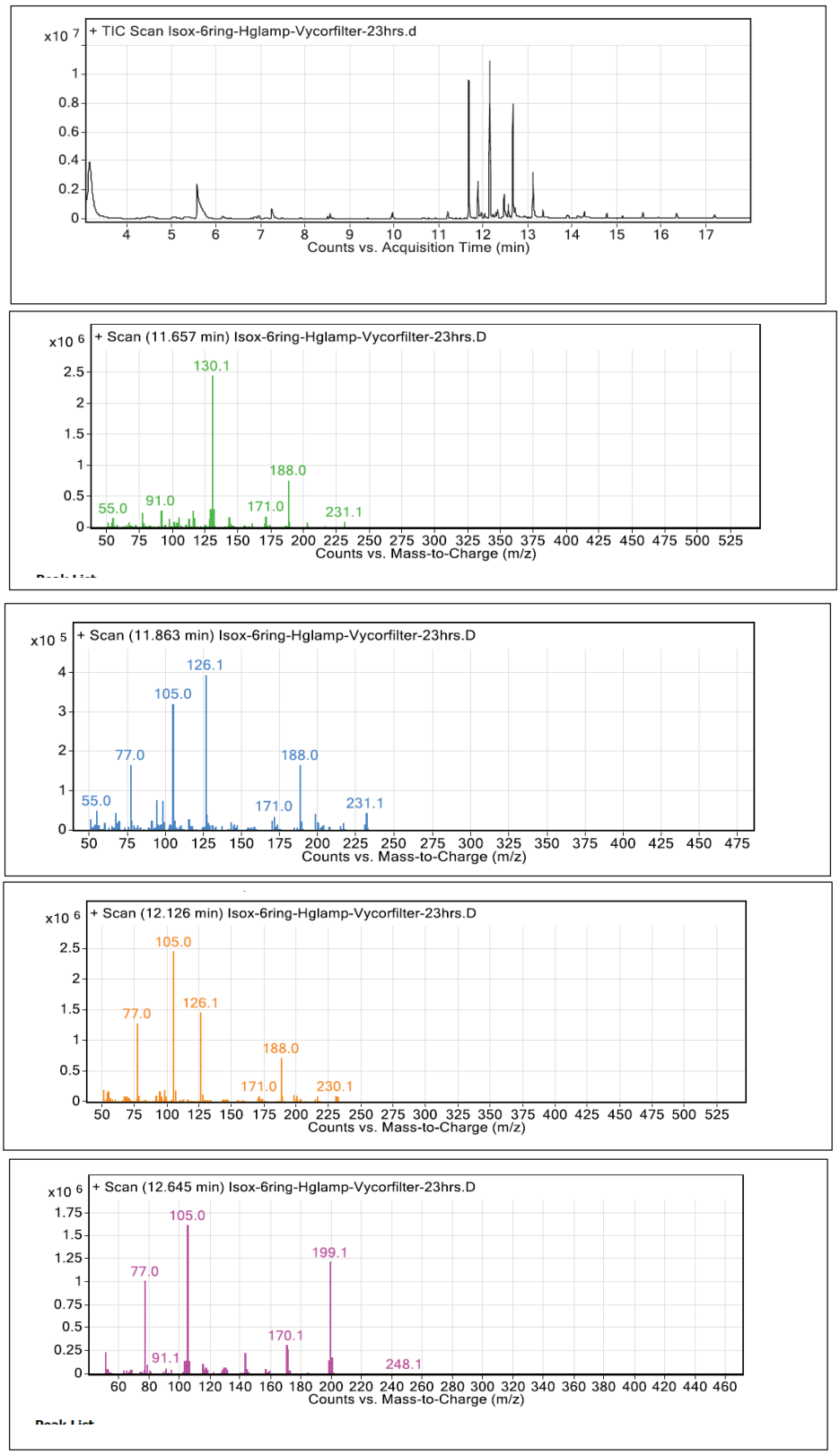

Figure S195. GCMS spectrum of argon saturated MeOH solution of isoxazole-2 after irradiation of 23 h using Hg lamp.

III. Quantum modelling data

S_0 of isoxazole-**2**

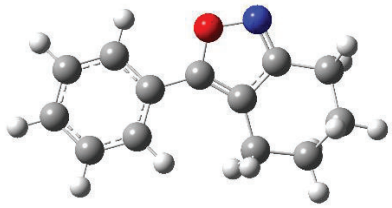

DFT/B3LYP 6-31+G(d), E = -633.179398 a.u

Center Number	Atomic Number	Atomic Type	Coordinates (Angstroms) X	Y	Z
1	6	0	-4.27711	-0.61704	-0.01326
2	6	0	-3.28064	-1.56421	0.237813
3	6	0	-1.93817	-1.18491	0.261747
4	6	0	-1.56872	0.153078	0.029428
5	6	0	-2.58051	1.101505	-0.21653
6	6	0	-3.92	0.716601	-0.23731
7	1	0	-5.32237	-0.91434	-0.03093
8	1	0	-3.54776	-2.60159	0.422471
9	1	0	-1.17899	-1.92893	0.477632
10	1	0	-2.30791	2.136697	-0.39378
11	1	0	-4.68806	1.46098	-0.43095
12	6	0	-0.16299	0.559624	0.043376
13	6	0	1.037053	-0.1099	-0.0071
14	6	0	2.008735	0.935252	0.038496
15	7	0	1.461288	2.127259	0.110219
16	8	0	0.080051	1.895855	0.110309
17	6	0	1.410703	-1.56525	-0.09313
18	1	0	1.24785	-2.05348	0.880287
19	1	0	0.773396	-2.09407	-0.81334
20	6	0	2.894498	-1.72195	-0.49061
21	1	0	3.007078	-1.51548	-1.56483
22	1	0	3.202653	-2.763	-0.33549
23	6	0	3.808005	-0.77093	0.301814
24	1	0	4.86027	-0.97777	0.072934
25	1	0	3.676614	-0.95274	1.378431
26	6	0	3.493089	0.704186	-0.0158
27	1	0	3.855871	0.947889	-1.02445
28	1	0	4.00823	1.381829	0.674265

S_0 of isoxazole-**2**

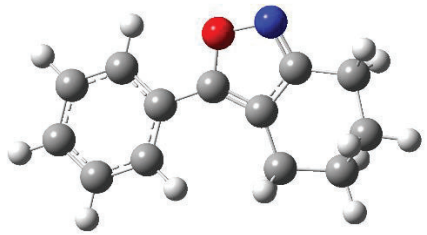

DFT/B3LYP 6-31+G(d), E = -633.012058 a.u

Center Number	Atomic Number	Atomic Type	Coordinates (Angstroms) X	Y	Z
1	6	0	-4.27711	0.617042	0.013256
2	6	0	-3.28064	1.564213	-0.23781
3	6	0	-1.93817	1.184905	-0.26175
4	6	0	-1.56872	-0.15308	-0.02943
5	6	0	-2.58051	-1.10151	0.216528
6	6	0	-3.92	-0.7166	0.237308
7	1	0	-5.32237	0.914335	0.030926
8	1	0	-3.54776	2.601586	-0.42247
9	1	0	-1.17899	1.928926	-0.47763
10	1	0	-2.30791	-2.1367	0.39378
11	1	0	-4.68806	-1.46098	0.430945
12	6	0	-0.16299	-0.55962	-0.04338
13	6	0	1.037053	0.109902	0.007098
14	6	0	2.008735	-0.93525	-0.0385
15	7	0	1.461288	-2.12726	-0.11022
16	8	0	0.080051	-1.89586	-0.11031
17	6	0	1.410703	1.565248	0.093125
18	1	0	1.24785	2.053477	-0.88029
19	1	0	0.773396	2.094071	0.813337
20	6	0	2.894498	1.721952	0.490605
21	1	0	3.007078	1.515479	1.564829
22	1	0	3.202653	2.762996	0.335487
23	6	0	3.808005	0.770929	-0.30181
24	1	0	4.86027	0.977774	-0.07293
25	1	0	3.676614	0.952744	-1.37843
26	6	0	3.493089	-0.70419	0.0158
27	1	0	3.855871	-0.94789	1.024449
28	1	0	4.00823	-1.38183	-0.67427

T_1 of isoxazole-**2**

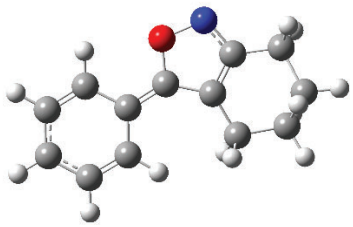

DFT/B3LYP 6-31+G(d), E = -633.080009 a.u

Center Number	Atomic Number	Atomic Type	Coordinates (Angstroms) X	Y	Z
1	6	0	-4.28661	0.639081	-0.04404
2	6	0	-3.25889	1.615845	-0.06573
3	6	0	-1.9329	1.254012	-0.04384
4	6	0	-1.54501	-0.1463	0.004143
5	6	0	-2.62039	-1.12974	0.016955
6	6	0	-3.93748	-0.73105	-0.00493
7	1	0	-5.32944	0.941033	-0.06005
8	1	0	-3.52354	2.669915	-0.10287
9	1	0	-1.16786	2.021238	-0.0691
10	1	0	-2.35975	-2.18147	0.04643
11	1	0	-4.72239	-1.48349	0.007685
12	6	0	-0.22973	-0.55588	0.033898
13	6	0	1.077275	0.111857	0.042871
14	6	0	1.998912	-0.90861	0.027228
15	7	0	1.430743	-2.14546	0.025814
16	8	0	0.035335	-1.93354	0.048243
17	6	0	1.453322	1.562266	0.049927
18	1	0	1.20515	2.015257	-0.92385
19	1	0	0.86808	2.115028	0.796147
20	6	0	2.95958	1.737215	0.342293
21	1	0	3.131294	1.618687	1.421499
22	1	0	3.261072	2.759933	0.085908
23	6	0	3.82496	0.718484	-0.41753
24	1	0	4.888098	0.917655	-0.23764
25	1	0	3.659	0.832638	-1.49832
26	6	0	3.488375	-0.7254	0.000999
27	1	0	3.902271	-0.93801	0.997443
28	1	0	3.941654	-1.45252	-0.68341

^{1}2N

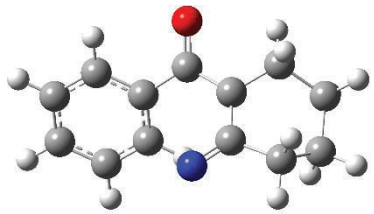

DFT/B3LYP 6-31+G(d), E = -633.110894 a.u

Center Number	Atomic Number	Atomic Type	Coordinates (Angstroms) X	Y	Z
1	6	0	1.124417	0.521608	0.170685
2	6	0	1.355882	-0.77562	0.802845
3	6	0	2.355961	1.306834	-0.17289
4	1	0	2.076956	2.224062	-0.69651
5	1	0	2.828333	1.633845	0.768981
6	6	0	3.390295	0.483244	-0.98739
7	1	0	3.151249	0.563806	-2.05401
8	1	0	4.373834	0.948937	-0.85551
9	6	0	2.814832	-1.25889	0.801666
10	1	0	2.84058	-2.31739	1.075542
11	1	0	3.361228	-0.70745	1.579582
12	6	0	3.441516	-1.01196	-0.57967
13	1	0	4.475804	-1.37552	-0.58066
14	1	0	2.900298	-1.62072	-1.31496
15	6	0	-0.19464	1.179541	0.071283
16	6	0	-1.47069	0.408029	-0.04786
17	6	0	-1.55226	-0.80429	-0.7508
18	6	0	-2.6411	0.973046	0.484473
19	6	0	-2.78262	-1.44221	-0.91431
20	1	0	-0.65965	-1.24505	-1.18315
21	6	0	-3.86534	0.322331	0.34207
22	1	0	-2.57346	1.922007	1.007559
23	6	0	-3.93869	-0.88608	-0.36008
24	1	0	-2.83722	-2.37533	-1.46875
25	1	0	-4.76334	0.758116	0.772269
26	1	0	-4.89465	-1.39036	-0.47714
27	8	0	-0.2212	2.417052	0.087915
28	7	0	0.466321	-1.4927	1.366168

^{3}2N

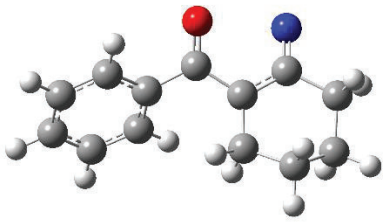

DFT/B3LYP 6-31+G(d), E = -633.117616 a.u

Center Number	Atomic Number	Atomic Type	Coordinates (Angstroms) X	Y	Z
1	6	0	-4.10758	-0.80438	-0.24972
2	6	0	-3.05577	-1.24973	-1.05516
3	6	0	-1.78237	-0.69434	-0.91187
4	6	0	-1.55339	0.325128	0.024833
5	6	0	-2.62251	0.785669	0.810407
6	6	0	-3.88809	0.214343	0.684258
7	1	0	-5.09654	-1.24326	-0.35481
8	1	0	-3.22708	-2.0255	-1.79699
9	1	0	-0.97583	-1.03319	-1.55612
10	1	0	-2.44528	1.595718	1.511639
11	1	0	-4.70598	0.568141	1.306617
12	6	0	-0.22203	1.01144	0.154581
13	6	0	1.06486	-1.22702	0.491645
14	6	0	2.449554	-1.69286	0.967532
15	6	0	3.521485	-1.32207	-0.06058
16	6	0	3.606923	0.200199	-0.21735
17	6	0	2.234066	0.873528	-0.40006
18	6	0	1.03363	0.22056	0.054637
19	1	0	4.502613	-1.70952	0.240903
20	1	0	2.68786	-1.22565	1.933524
21	1	0	2.426156	-2.77638	1.135456
22	1	0	0.758451	-1.86952	-0.35012
23	1	0	0.310421	-1.39394	1.270133
24	1	0	4.053636	0.637324	0.686457
25	1	0	4.251341	0.483673	-1.05532
26	1	0	3.281227	-1.78753	-1.02744
27	8	0	-0.18403	2.218029	0.393443
28	7	0	2.225512	2.027504	-0.97862

TS of ^{3}2N

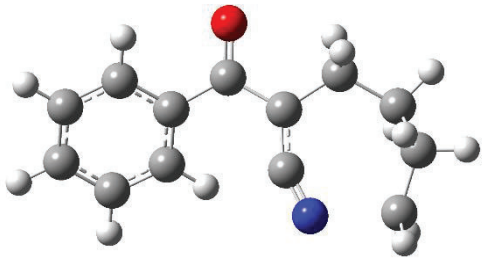

DFT/B3LYP 6-31+G(d), E = -633.069032 a.u

Center Number	Atomic Number	Atomic Type	Coordinates (Angstroms) X	Y	Z
1	6	0	4.187688	-1.01631	0.030988
2	6	0	3.062317	-1.60544	0.612602
3	6	0	1.839423	-0.93086	0.61629
4	6	0	1.734851	0.349078	0.046592
5	6	0	2.878414	0.942927	-0.51604
6	6	0	4.093019	0.26085	-0.5339
7	1	0	5.136158	-1.54744	0.021159
8	1	0	3.133504	-2.59117	1.064476
9	1	0	0.978214	-1.39926	1.080373
10	1	0	2.794945	1.940304	-0.93637
11	1	0	4.967068	0.724071	-0.98425
12	6	0	0.47288	1.154564	0.058302
13	6	0	-2.06795	1.408651	0.221833
14	6	0	-3.38446	0.744552	0.667413
15	6	0	-4.07132	-0.18109	-0.3668
16	6	0	-3.70917	-1.63574	-0.27912
17	6	0	-1.04404	-0.84214	-0.27278
18	6	0	-0.86291	0.516498	0.043339
19	1	0	-5.1635	-0.09575	-0.2271
20	1	0	-3.22715	0.197	1.607029
21	1	0	-4.07087	1.565823	0.907797
22	1	0	-2.23542	1.933146	-0.73439
23	1	0	-1.78826	2.203592	0.924018
24	1	0	-3.78115	-2.11129	0.697749
25	1	0	-3.9916	-2.27816	-1.10908
26	1	0	-3.88097	0.191914	-1.38358
27	8	0	0.523724	2.390554	0.047993
28	7	0	-1.69046	-1.83578	-0.46915

IRC:

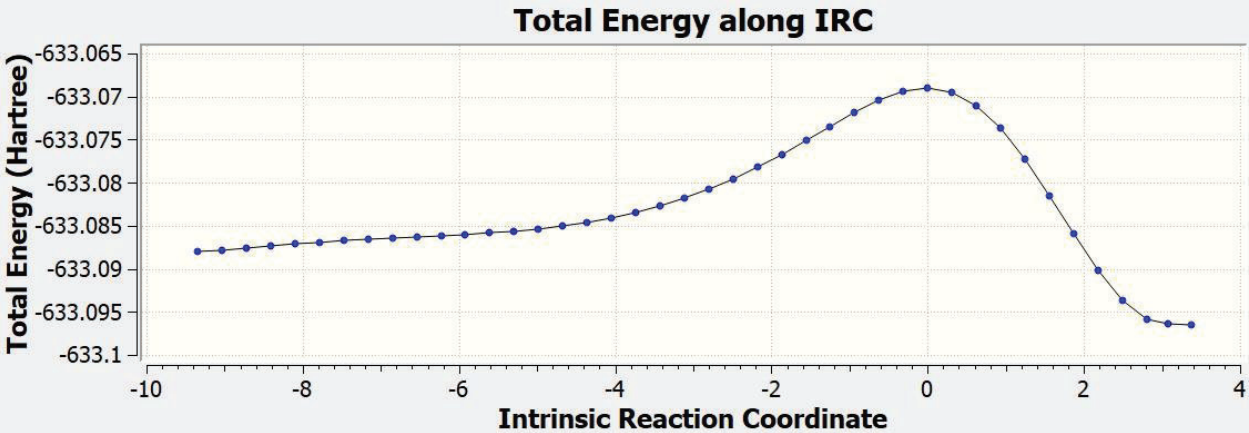

2K

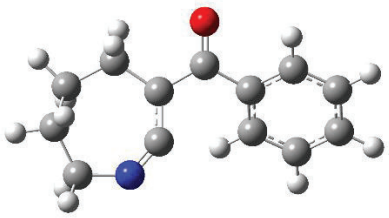

DFT/B3LYP 6-31+G(d), E = -633.096540 a.u

Center Number	Atomic Number	Atomic Type	Coordinates (Angstroms) X	Y	Z
1	6	0	3.0561	-1.58312	-0.65259
2	6	0	1.827713	-0.9186	-0.64109
3	6	0	1.710826	0.345548	-0.03979
4	6	0	2.848409	0.933211	0.540329
5	6	0	4.068629	0.260184	0.545361
6	6	0	4.17544	-1.0008	-0.05235
7	1	0	3.13654	-2.55634	-1.12969
8	1	0	0.968358	-1.38023	-1.11496
9	1	0	2.75651	1.919349	0.984894
10	1	0	4.937544	0.718471	1.010686
11	1	0	5.128206	-1.52448	-0.05363
12	6	0	0.443039	1.144353	-0.04273
13	6	0	-0.89319	0.500376	-0.03328
14	6	0	-1.02804	-0.86597	0.336224
15	6	0	-2.07553	1.408708	-0.27073

16	1	0	-2.24657	1.982351	0.655969
17	1	0	-1.78078	2.165036	-1.00839
18	6	0	-3.39033	0.735013	-0.69203
19	1	0	-3.25311	0.212346	-1.64999
20	1	0	-4.11494	1.536178	-0.8838
21	6	0	-3.98206	-0.234	0.346075
22	1	0	-5.0607	-0.34783	0.170226
23	1	0	-3.87752	0.193408	1.353651
24	6	0	-3.37455	-1.63893	0.319764
25	1	0	-3.59708	-2.13139	-0.63894
26	1	0	-3.82397	-2.26961	1.095997
27	7	0	-1.92185	-1.72552	0.488052
28	8	0	0.495217	2.380691	-0.02342

---

^{3}2N to **2K** TS

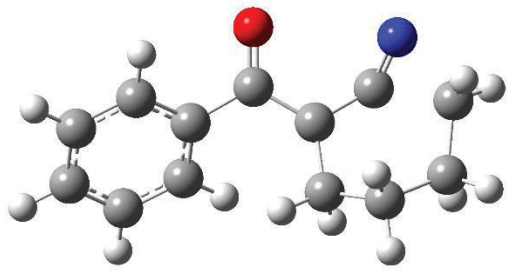

DFT/B3LYP 6-31+G(d), E = a.u

Center Number	Atomic Number	Atomic Type	Coordinates (Angstroms) X	Y	Z
1	6	0	-4.24326	-0.68906	-0.00089
2	6	0	-3.2618	-1.31674	-0.77285
3	6	0	-1.96052	-0.80922	-0.7985
4	6	0	-1.62922	0.339234	-0.06235
5	6	0	-2.6286	0.977173	0.691257
6	6	0	-3.92276	0.459879	0.731125
7	1	0	-5.25434	-1.08762	0.024018
8	1	0	-3.50975	-2.19717	-1.36041
9	1	0	-1.21151	-1.29333	-1.41922

10	1	0	-2.37337	1.881187	1.23597
11	1	0	-4.68484	0.955967	1.326852
12	6	0	-0.26226	0.961589	-0.09635
13	6	0	1.035485	-1.32893	0.178862
14	6	0	2.34269	-1.57771	0.961833
15	6	0	3.595207	-1.20477	0.156252
16	6	0	3.848175	0.310485	-0.07564
17	6	0	2.155008	0.687305	-0.74841
18	6	0	0.923347	0.111826	-0.2375
19	1	0	4.489458	-1.55984	0.690386
20	1	0	2.319957	-1.01547	1.905547
21	1	0	2.397478	-2.64064	1.226546
22	1	0	1.039843	-1.97868	-0.71271
23	1	0	0.170943	-1.62049	0.781423
24	1	0	4.200511	0.747262	0.863657
25	1	0	4.561663	0.468279	-0.8801
26	1	0	3.569367	-1.71328	-0.8144
27	8	0	-0.14405	2.194745	-0.02261
28	7	0	2.784007	1.709919	-0.3211

IRC:

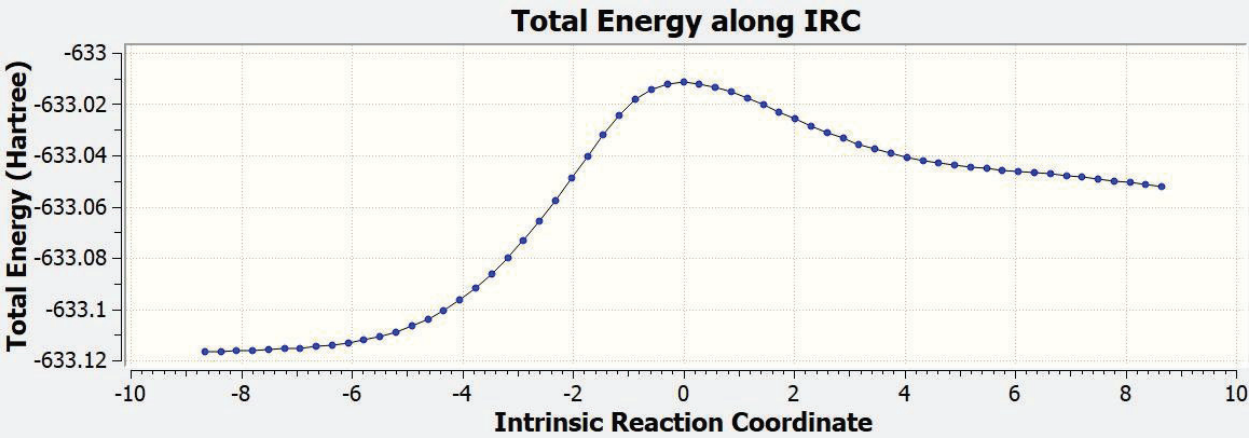

Azirene of **2**

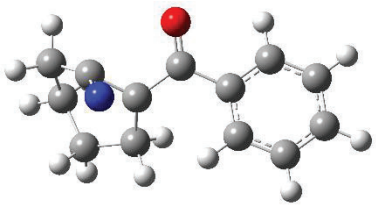

DFT/B3LYP 6-31+G(d), E = -633.137878 a.u

Center Number	Atomic Number	Atomic Type	Coordinates (Angstroms) X	Y	Z
1	6	0	3.803221	0.562879	-0.80112
2	6	0	4.155816	-0.6387	-0.17527
3	6	0	3.205132	-1.34446	0.567427
4	6	0	1.898637	-0.86159	0.669311
5	6	0	1.537671	0.342826	0.045125
6	6	0	2.505471	1.056616	-0.68151
7	1	0	4.54283	1.115282	-1.37505
8	1	0	5.170187	-1.02006	-0.26215
9	1	0	3.480785	-2.26858	1.068873
10	1	0	1.169673	-1.40596	1.261567
11	1	0	2.22128	1.997861	-1.14246
12	6	0	0.166601	0.927919	0.182778
13	8	0	0.001288	2.143059	0.114557
14	6	0	-1.01875	0.028691	0.401423
15	6	0	-2.30261	0.668503	0.650976
16	7	0	-1.81509	0.275293	1.740289
17	6	0	-3.55074	0.774542	-0.13211
18	1	0	-3.63217	1.735039	-0.65155
19	1	0	-4.42166	0.656893	0.523606
20	6	0	-1.17886	-1.35271	-0.23561
21	1	0	-0.59952	-1.37345	-1.16831
22	1	0	-0.78912	-2.16196	0.396131
23	6	0	-2.67785	-1.62683	-0.5573
24	1	0	-3.19524	-1.94545	0.357777
25	1	0	-2.74268	-2.46784	-1.25777
26	6	0	-3.41551	-0.40351	-1.15403
27	1	0	-4.41437	-0.69511	-1.49782
28	1	0	-2.86405	-0.04325	-2.03196

MeOH trapped **2K** (**3)**

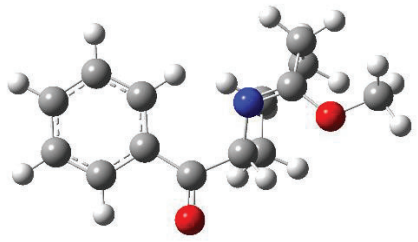

DFT/B3LYP 6-31+G(d), E = -748.893111 a.u

Center Number	Atomic Number	Atomic Type	Coordinates (Angstroms) X	Y	Z
1	6	0	-4.31271	1.307879	0.382372
2	6	0	-3.01558	1.798122	0.545302
3	6	0	-1.91514	0.944716	0.422415
4	6	0	-2.10357	-0.41826	0.131252
5	6	0	-3.41788	-0.9015	-0.02651
6	6	0	-4.51103	-0.0485	0.095983
7	1	0	-5.16564	1.975382	0.480226
8	1	0	-2.85589	2.848725	0.775834
9	1	0	-0.91072	1.318096	0.575043
10	1	0	-3.55672	-1.95475	-0.24791
11	1	0	-5.51827	-0.43753	-0.03103
12	6	0	-0.99123	-1.41677	-0.0348
13	7	0	0.925431	0.075173	0.736369
14	8	0	-1.26892	-2.59511	-0.24038
15	6	0	0.973867	-0.67899	-1.52394
16	1	0	1.877172	-1.25816	-1.75075
17	1	0	0.215557	-0.99965	-2.24802
18	6	0	1.271896	0.836066	-1.76474
19	1	0	0.412295	1.436477	-1.44497
20	1	0	1.342428	0.960899	-2.85417
21	6	0	2.57972	1.457987	-1.18381
22	1	0	2.709275	2.45419	-1.62695
23	1	0	3.435152	0.856897	-1.52327
24	6	0	2.659254	1.612603	0.375853
25	1	0	1.94728	2.368234	0.716072
26	1	0	3.666705	1.907818	0.685803
27	6	0	0.50612	-1.07124	-0.05751

28	6	0	2.18246	0.258668	0.829064
29	8	0	3.061331	-0.79269	0.798679
30	1	0	0.994374	-2.01073	0.22048
31	6	0	4.453323	-0.56364	1.035423
32	1	0	4.902086	-1.55436	1.126916
33	1	0	4.922138	-0.03006	0.200469
34	1	0	4.608388	-0.00817	1.967058
